Recent Progress and Prospects in Catalytic Water Treatment

Vasile I Parvulescu, Florence Epron, Hermenegildo Garcia, Pascal Granger

▶ To cite this version:

Vasile I Parvulescu, Florence Epron, Hermenegildo Garcia, Pascal Granger. Recent Progress and Prospects in Catalytic Water Treatment. Chemical Reviews, 2021, 122 (3), pp.2981-3121. 10.1021/acs.chemrev.1c00527 . hal-03525107

HAL Id: hal-03525107

https://hal.science/hal-03525107

Submitted on 13 Jan 2022

Recent progress and prospects in catalytic water treatment

Vasile I. Parvulescu,[†,*] Florence Epron,[#,*] Hermenegildo Garcia,[○,*] Pascal Granger[¥,*]

[†]*University of Bucharest, Department of Organic Chemistry, Biochemistry and Catalysis, B-dul Regina Elisabeta 4-12, Bucharest 030016, Romania.*
[#]*Université de Poitiers, CNRS UMR 7285, Institut de Chimie des Milieux et Matériaux de Poitiers (IC2MP), 4 rue Michel Brunet, TSA 51106, 86073 Poitiers Cedex 9, France*
[○]*Instituto Universitario de Tecnología Química, Universitat Politecnica de Valencia-Consejo Superior de Investigaciones Científicas, Universitat Politencia de Valencia, Av. de los Naranjos s/n, 46022 Valencia, Spain*
[¥] *Univ. Lille, CNRS, Centrale Lille, Univ. Artois, UMR 8181 - UCCS - Unité de Catalyse et Chimie du Solide, F-59000 Lille, France*

Corresponding authors:

Vasile I. Parvulescu	Email : vasile.parvulescu@chimie.unibuc.ro
	Phone number+ 40745502052
Florence Epron	Email: florence.epron@univ-poitiers.fr
	Phone number : +33 549 454 832
Hermenigildo Garcia	Email : hgarcia@upv.es
	Phone number : +34 963 877 807
Pascal Granger	Email: pascal.granger@univ-lille.fr
	Phone number: +33 320 434 938

TABLE CONTENT

Abstract

Presently, conventional technologies in water treatment are not enough efficient to completely mineralize refractory water contaminants. In this context, the implementation of catalytic processes could be an alternative. Despite the advantages provided in terms of kinetics of transformation, selectivity and energy saving, the numerous attempts have not lead yet to implementation at industrial scale. This review examines at different scales of investigations which controversies and limitations must be solved to bridge the gap between fundamentals and practical developments. Particular attention has been paid to the development of solar-driven catalytic technologies and some other emerging processes, such as microwave assisted catalysis, plasma-catalytic processes or biocatalytic remediation taking into account their specific advantages and the drawbacks. Challenges for which a better understanding related to the complexity of the systems and the coexistence of various solid-liquid-gas interfaces have been identified.

TOC
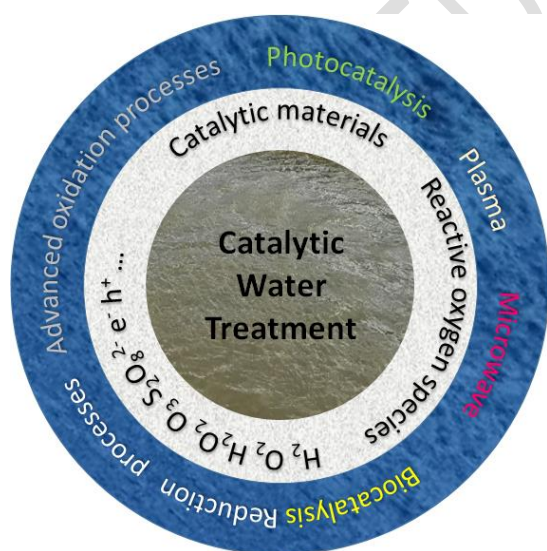
Keywords: Catalytic water treatment; Microwave catalysis; Plasma catalysis; bio- and photobiocatalysis; Sonophotocatalysis; Photoelectrocatalysis; Solid-liquid-gas interface.

1. Introduction

Today the growing need of water in diverse utilizations offers today new paradigms shifts in hydric resource management.[1] Water treatment and recycling will be one of the major environmental concern in the near future, with implication also in energy consumption and carbon footprint. Important social challenges also lie in the access of basic sanitation, especially to prevent infectious diseases. This right is still not universal all over the World and significant investments must be programmed, taking the population growth worldwide into account, especially in Asia and Africa. In this context, a huge amount of investigations has been published in the past two decades, according to databases taking the water treatment as keyword. In the area of water treatment, catalysis represents a minor contribution, but a fairly clear trend has been emerging, exhibiting an exponential growth in the past decades (Figure 1).[2-5] They tackled different challenges related to: – The identification of source of wastewater – the assessment of wastewater composition – the removal of trace amount of organic or mineral contaminants. In some extent, important advances both on water resource recovery and circularity imply to bridge the gap between concepts and practice.[6] This review will focus on the three items dedicated to the removal of refractory soluble pollutants, but an important aspect will be focused on the existing link between the chemical nature of the contaminant and the infrastructure implemented for its removal.
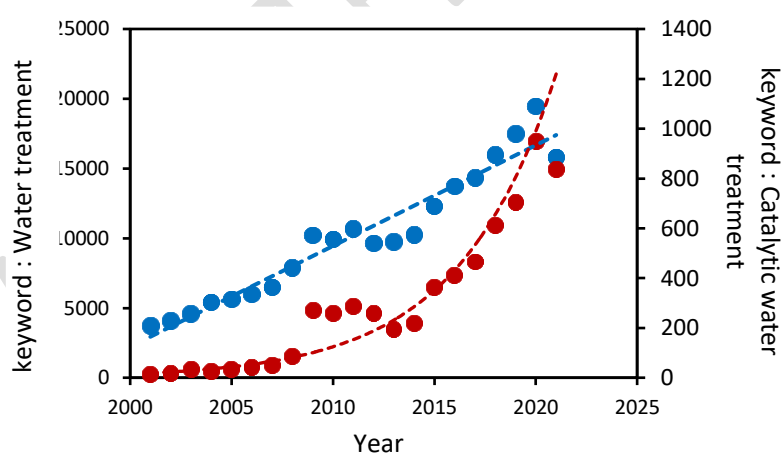
Figure 1. Evolution of published data from the Scopus database in the past two decade (2001 to 2021) – Water treatment (blue symbol); catalytic water treatment (red symbol).

Treated wastewater can be classified in different categories from drinking to reclaimed water determined by their degree of potability. Reclaimed water is currently used for irrigation,

industry and various non-potable uses. In the particular case of drinking water, nitrates and pesticides are recognized as major sources of pollution. Nevertheless, the removal of micropollutants even at extremely low concentration is a growing issue because of potential risk due to prolonged exposures. These finding have stimulated certain initiatives around the world in terms of stricter regulations taking the assessment of the risks of effects on human health into account.

The reuse of drinking water implies wastewater treatment able to deal with microorganisms, pharmaceutical and personal care products, etc. In a general way, classical successive oxidation pretreatment, coagulation flocculation, sedimentation, filtration and disinfection processes are implemented. However, current technologies to treat contaminated water could not be enough efficient and can generate secondary waste streams. By way of illustration, prechlorination of contaminated water for their oxidation can lead to the formation of carcinogenic, mutagenic and genotoxic chlorinated byproducts. The efficiency of ozone as substitute is also questionable with the formation of pathogens. Heterogeneous catalysis can offer an alternative for a faster degradation and improved mineralization. In addition, unique options may emerge, this is particularly true for the reduction of chlorinated micropollutants with catalytic hydrodechlorination processes preferred over catalytic ozonation[7]. In this context, a question emerges on the specificity of a catalytic process, on its flexibility in the context of assisted or hybrid systems.

As illustrated in Figure 2, various advanced oxidation processes (AOPs), operating at full scale and based on the generation of hydroxyl radicals utilizing ozonation treatment, Fenton or UV irradiation, have been developed. Different categories have arise more recently with various degrees of development from the lab- to pilot- and full scale. In most cases, a two steps process is involved starting from the generation of the active oxidant intermediates and their subsequent reaction with the targeted undesired contaminant.

Diverse strategies have been inventoried providing new opportunities in the development of hybrid systems to treat poorly biodegradable organic compounds. For instance, the relevance in coupling adsorption and enzymatic degradation has been highlighted. Recently catalytic technologies emerged as an alternative with a remarkable growing interest in parallel to the sharp development of AOPs for waste water and drinking water treatment. It has been found that coupling technologies including a catalytic step can be an appropriate approach especially for the development of continuous flow catalytic reactor and for facing important issues related to the abatement at ambient working temperature of ultra-low concentration of persistent pollutants. Presently, the development of single or hybrid heterogeneous catalytic systems is

not trivial and must face to significant challenges inherent to the complexity of gas-liquid-solid interfaces. New advances in the integration of nanotechnologies have taken place with the aim of getting convergence between green chemistry and manufacturing in connection with social welfare.[8]
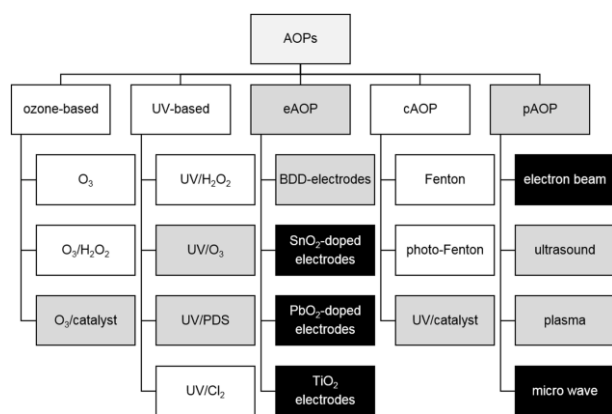
Figure 2. Broad overview and classification of different AOPs. Individual processes are marked as established at full-scale (white), investigated at lab- and pilot scale (grey) and tested at lab-scale (black) – Reproduced with permission from Ref. [9]. Copyright 2018 Elsevier.

Why this review article?

Up to now, catalytic technologies for water treatment are not widespread at the industrial level. Future breakthrough that could make this one more realistic at larger scale lies in better understanding of the catalyst functionalities at the nanoscale and its better integration in the reactor design. Such requirements need the implementation of a multiscale approach. In addition, all technical developments must insure complete mineralization of the effluent, which means that the degradation of intermediates must be characterized in order to evaluate the kinetics of their transformation with respect to their potential toxicity. Indeed, this latter point is probably a major concern in the development of efficient novel technologies and usually requires complex chemical analysis of the solutions.

Accordingly, one of the objectives of the present review paper is to tackle from fundamental to practical issues with the aim to elaborate integrated and sustainable combined approaches involving a catalytic step to remove trace amounts of pollutants under smooth operating conditions, *i.e.* ambient pressure and temperature and more severe reaction treatments for refractory soluble pollutants. Particular attention for developments in nanoengineered catalytic materials and *in-situ* characterization closer to reaction conditions are presently needed. Molecular modelling of gas/liquid/solid interface and *operando* spectroscopic characterization in working conditions are important tools that should lead to the

development of new generation of catalysts with structure, texture and surface properties adjusted to the type of catalysis and reactor design. Presently, most of investigations deal with the removal of single pollutants while real waste water contains complicate pollutant mixtures. The need of efficient prediction tools that able to take this complexity into account are needed. This could be embodied by emerging branch of computer sciences and artificial intelligence.

To the best of our knowledge, critical reviews yet published most often dealt with restricted domains of investigation such as ozonation and biodegradation of chlorophenol,[10] the development of membrane process for water treatment,[11] the detection and investigation of reactive oxygen species in heterogeneous catalytic ozonation,[12] the degradation of organic pollutants in wastewaters by photoelectrocatalysis,[13] the benefit of cavitation combined with advanced oxidation process,[14] the state of the art in combining microwave to catalysis for the degradation of organics,[15] or the challenges of photocatalysis in water treatment technologies. This list is not exhaustive. As a matter of fact, a huge number of review papers can be found dealing with a specific point in the wide area of catalytic water treatment. On the other hand, there is no document providing a critical overview at different discussion levels from nanoscale to chemical engineering, of the various single and couple catalytic technologies. Presently, different attempts for developing hybrid technologies can be limited by several factors especially by the description and the monitoring of the gas-liquid-solid interface, which will depend on the chemical composition of the solid and the reactor design. The complexity also lies in specific requirements toward the development of nanoengineered materials. It is true that important questions arise to link fundamental to practical issues for developing integrated and sustainable combined approaches involving a catalytic step to remove trace amount of pollutant in smooth operating conditions. Accordingly, further knowledge coming from theoretical studies and *in-situ* spectroscopic investigation to assist the investigators involved in water treatment to apprehend more accurately the role of the water-solid interface and the nature of intermediates as useful information to elaborate more efficient catalytic technologies. Based on this, the content of this review paper covers different fields of study at the boundaries of material sciences, kinetic and chemical engineering and physical chemistry.

Chapter 2 will give an overview of useful kinetic insight and related reaction mechanisms which drive the formation and the reactivity of intermediates. From this the main question lies in how to improve the production of more active radical intermediates from the decomposition of oxidant mostly recognized as non-selective. This assertion on the importance of the reaction mechanism is not limited to oxidation processes and can be extended to numerous

heterogeneous catalyzed reactions involving non-radical intermediates such as reduction reactions.

In practice, direct oxidation by the oxidant (O_3, H_2O_2, persulfates) and catalytic oxidation by more reactive oxygen species may occur simultaneously on heterogeneous catalysts and several controversies have arisen likely due to the absence of knowledge on the catalyst functionality and also due to valence change of active elements in working conditions. Hence, more robust practical and theoretical approaches are needed to quantify and calculate rate constant for the production of $^\bullet OH$ intermediate. The development of reliable quenching methodologies jointly with the use of advance physicochemical techniques such as EPR spectroscopy are probably a necessary to depict more accurately catalyst functionality that could offer new directions in the catalysts preparation. *In-situ* production of reactive intermediate is not restricted to oxidation processes, some examples for reduction reactions will also be given as illustration that water can be a useful reservoir for the production of hydrogen and oxygen through water splitting.

The optimization of multiphase reactors with improved performances is a challenging task. A key point lies in the contact between the different phases and further improvements need to find strategies able to reduce the interfacial tensions. Among different concepts and ideas, the wettability can be an important parameter that can drive the catalyst efficiency through the minimization of diffusion limitations. New prospect towards the development of miniaturized technologies will be envisioned with the aim to get more efficiency.

Chapter 3 will illustrate different existing technologies at different development levels. A particular focus will be paid toward their ability to face to the emergence of recalcitrant contaminants. Biocatalytic processes are widespread because enzymes are intrinsically highly active at low temperature. The implementation of such biocatalytic process is quite flexible leading to high level of remediation. But they can suffer from drawbacks with the emergence of refractory molecules and significant inhibitory effects that can drastically alter their efficiency. Presently, the strategies which could make bioremediation industrially, environmentally, and economically more relevant are in some extent questionable. The steric hindrance of refractory molecules, their very low residual concentrations can represent an important technical issue for the development of an effective technology.

Alternative technologies such as Plasma catalysis have been extensively investigated in water treatment. Fragmentation processes through physicochemical process that lead to smaller reactive intermediates can be useful. However, the most important potentiality of plasma has

been regarded as generator of reactive species thanks to an electric field. This technology can be potentially powerful but depends on many parameters such as reactor configuration according to the type of discharge and operating conditions making its optimization challenging. The different existing scenarios will be reviewed in terms of advantages and drawbacks.

The use of energetic radiations from microwaves is conceptually an attractive approach. When metal or semiconductor is irradiated by microwaves, a local increase of the temperature can occur leading to plasmas and hot spots that can speed up the rate of contaminant transformation. The concept is attractive and could open innovative architectures for catalytic materials allowing a local heating of active sites thanks to nano-heaters at their vicinity.

Chapter 4 describes innovative combined light-assisted technologies. Photocatalytic processes attracted considerable attention in the past two decades. But their exploration is not so widespread for liquid phase applications. In addition, limitations are to a restricted range of solar spectrum utilization still remain to be solved. Future trends lie in the development of a new variety of materials that can produce more efficiently $^{\bullet}$OH hydroxyl radicals. In combination to new varieties of photocatalysts, efficient hybrid photocatalytic/ultrafiltration process and photocatalytic/biological treatment could be a powerful approach for water purification using visible light. Important limitations will be tackled in this review inherent to the distribution of the active materials and photoreactor design. Particular attention will be paid to synergy effects promoted by combining photocatalysis with biocatalysis, sonocatalysis and well as electrocatalysis. An important aspect lies in the efficiency of such coupling with the aim of getting synergistic effects and cost savings, while reaching high pollutant removal efficiency. In practice, optimization is not trivial and can imply as pre-requisite significant improvements of each single technology.

The coupling between photocatalysis and biodegradation is an emerging technology that breaks with preconceived ideas and usual concepts that photocatalytic reaction and biodegradation must be performed in two separate reactors to preserve high efficiency. Particular attention will be paid to check if recent insights into biodegradation mechanism may allow future improvements..

Sono-photocatalysis is also an emerging technology which can provide huge advantages due to the creation of cavitation in the reaction media with formation, growth and collapse of microbubbles creating high local temperature and pressure. In these extreme conditions, dissolved oxygen and water can be activated to produce reactive radicals. Accordingly,

contaminant oxidation and reduction in water can be enhanced. However, the benefit of ultrasounds also lies in the reduction of recombination of photoregenerated charge and improvement in mass transfer diffusion of the organic pollutant from the liquid phase to the catalyst surface. The coupling with photocatalysis will be illustrated.

Finally, photoelectrocatalysis as an emerging technology will be illustrated being an effective approach to inhibit the recombination of photogenerated charge carrier and enhance oxidation ability. Significant improvements were obtained thanks to novel designs of photoelectrodes developing 3D hierarchical heterostructures leading to full spectrum light absorption, a decrease of the photocarrier recombination rate and a lower transmission resistance at the catalyst/electrolyte interface. Some illustrations will be given regarding new varieties of materials and the efficiency of doping especially for improving light absorption and electrical conductivity

The last chapter will provide some guidelines with the aim to open new areas of expertise in the field of catalytic water treatment. Some of them refer to strategies for predicting or investigating the catalyst at nanoscale close to real working conditions. Presently, the role of the gas-liquid-solid interface in most of the applications where a solid catalyst is in contact with liquid and gaseous reactants is quite unknown with various chemical and physical phenomena which probably govern the stability and reactivity of intermediates by modifying their energies and entropies. To date, the literature concerning these specific aspects in catalytic systems under three-phase conditions is scarce. Advanced *in-situ* physicochemical characterizations coupled to molecular modeling can be a powerful approach to clarify the complexity induced by various interactions between the solvent, the solid and the reactant giving rise to dispersion forces, hydrogen bonding and chemical bonding. From this approach the identification of relevant descriptors and the management of big data through the implementation of artificial intelligence algorithms could be powerful to speed up discovery in efficient integrated catalytic approaches.

2. From kinetics and reaction mechanisms to reactor design in catalytic water treatment

The catalytic conversion of pollutants in water is a wide topic, since it refers to many kinds of catalytic processes using mainly oxidizing, but also reducing agents, with the common major objective of converting pollutants into innocuous products for the environment and

human health. The major challenges when referring to wastewater treatment by heterogeneous catalysis are to ensure that 1) it is an actual heterogeneous process, which means that it may really occurs at the surface of the catalyst and not in water either by direct reaction between the active oxidizing or reducing species or by homogeneous catalysis by reaction involving solubilized elements of the catalysts in the case of oxidizing treatment, 2) the active sites of the catalyst do not need to be externally regenerated and 3) the conversion into harmless compounds is complete, with no formation of other toxic compounds.

Wet air oxidation (WAO) and AOPs are the two main types of oxidative water treatment for which heterogeneous catalysts can be used. WAO is operated in severe conditions, *i.e.* at high temperature, usually between 125 and 320 °C under high air or O_2 pressure, between 0.5-20 MPa; it is more appropriate for high pollutant concentrations for energy saving, and can be applied at high flow rates. It implies thermally initiated free-radical chain reactions involving organic radicals •R of the organic pollutant RH as well as inorganic radicals, among which hydroxyl radicals (•OH) are the most oxidizing ones.[16] A wide range of metal oxides have been tested as catalysts of catalytic WAO (CWAO) under amenable conditions.

AOPs were defined in 1987 as water treatment processes operating at near-ambient temperature and pressure and based on the generation of •OH by chemical or photochemical decomposition of O_3 or H_2O_2.[17] The definition of AOPs was later on extended to physical-chemical processes such as photo(cata)lysis, sonolysis, electrolysis and ionizing radiation, and also to techniques involving other strong oxidizing agents ($SO_4•^-$ and Cl•).[18-19] The standard redox potential of the main oxidizing species involved in the WAO process and AOPs are summarized in Table 1.

Table 1. Redox potential of the main oxidizing species used in AOPs. Adapted from refs [20] and [21].

Oxidant	Half reaction	Redox potential (V/NHE)
HO•	$HO• + e^- + H^+ \rightleftharpoons H_2O$	+ 2.73
$SO_4•^-$	$SO_4•^-_{(aq)} + e^- \rightleftharpoons SO_4^{2-}_{(aq)}$	+ 2.43
Cl•	$Cl•_{(aq)} + e^- \rightleftharpoons Cl^-_{(aq)}$	+ 2.43
$S_2O_8^{2-}$	$S_2O_8^{2-} + 2H^+ + 2e^- \rightleftharpoons 2\ HSO_4^-$	+ 2.08
O_3	$O_3 + 2H^+ + 2e^- \rightleftharpoons O_2 + H_2O$	+ 2.07
HSO_5^-	$HSO_5^- + 2\ H^+ + 2\ e^- \rightleftharpoons HSO_4^- + H_2O$	+ 1.81
H_2O_2	$H_2O_2 + 2H^+ + 2e^- \rightleftharpoons 2\ H_2O$	+ 1.78
O_2	$O_2 + 4\ H+ + 4\ e^- \rightleftharpoons 2\ H_2O$	+ 1.23

Catalytic water treatment using reducing agents is by far less widespread than oxidizing treatment and is reserved to convert specific pollutants, such as nitrate into molecular nitrogen,[22] or for removing chlorine of organochlorinated compounds.[23] Catalytic nitrate removal from drinking water is usually performed at room temperature and under atmospheric pressure in the presence of supported noble metal-based bimetallic catalysts and a reducing agent, the most frequently H_2. The main challenge concerns the selectivity into N_2 since the over reduction may lead to other toxic molecules, such as ammonia.[22] Catalytic hydrodechlorination consists in removing Cl by hydrogenolysis, *i.e.* bond cleavage, of the C-Cl bond of very toxic chlorinated species by H_2 in the presence of metallic supported catalysts, generally based on palladium. It is used for wastewater detoxification making it possible either its post treatment by biological or chemical way or its recycling or for microcontaminants. The main difficulty of this process relates to the deactivation of the catalyst due to the poisoning by HCl. Reduction reactions are classically performed under ambient conditions.[23]

2.1. Strategies for *in-situ* production of reactive intermediates

2.1.1. Advanced oxidation processes

Fenton reaction

The oldest AOP is the Fenton process, originally consisting of activating H_2O_2 by Fe^{2+} ions, a homogeneous catalytic process, to produce strong oxidizing reactive oxygen species (ROS) HO• according to the following reactions:[24]

$$Fe^{2+} + H_2O_2 \rightarrow Fe^{3+} + HO\bullet + OH^- \qquad (1)$$
$$Fe^{3+} + H_2O_2 \rightarrow Fe^{2+} + HO_2\bullet + H^+ \qquad (2)$$
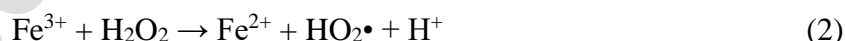
In addition to HO• and HO_2•, other reactive intermediates, especially short-living radical species, are produced as organic radicals from the pollutant (R•) or other ROS (O_2^-•, RO_2•).[25] The main drawbacks of this process are (i) an important consumption of costly H_2O_2, a part of which being converted into molecular oxygen and then lost for the process, (ii) an optimum pH value below 3, (iii) a low reaction rate, the rate-limiting step being the reduction of Fe^{3+} (reaction (2)) and (iv) the need of neutralizing the reaction medium at the end of the process

for recovering iron species in the form of sludge.[24] Immobilization of the active species on a solid results in heterogeneous Fenton catalysts that were developed to overcome some of these limitations. A large variety of Fe(III) containing heterogeneous catalysts, based on iron minerals (magnetite, ferrihydrite, hematite, goethite etc.), modified clays (intercalated or pillared, clay-supported catalysts), mixed oxides or exchanged zeolites have been used for heterogeneous Fenton-like process, as summarized in Table 2 from the review of Zhu et al.[24] In addition to a better recovery, the advantage of heterogeneous Fenton-like catalysts over homogeneous Fenton catalysts is that they can be used in a wide range of pH values, between 2 and 10, although the H_2O_2 excess can be very large when their pH value is not very acidic. However, the main difficulty encountered is the unavoidable iron leaching due to the presence of strongly oxidizing species. The presence of complexing agents in the wastewater may accelerate the leaching process. Even if toxicity of Fe in water is relatively low, its presence is detrimental to the quality due to the undesirable coloration that it produces. A way to limit the leaching consists in immobilizing iron oxides catalyst in other matrix, like in core-shell structures or in carbon matrix. An example of the effect of the immobilization of ferrihydrite in multiwalled carbon nanotubes (CNTs), not only on the removal of the pollutant, Bisphenol A (BPA), but also on the Fe leaching is presenting in Figure 3.[26] It can be seen that the presence of CNTs enhances the BPA disappearance and limits the iron leaching, although it does not completely avoid it. As a consequence, it can be difficult to discriminate the homogeneous from the heterogeneous catalytic process. Even if it is proposed that the amount of dissolved iron may be negligible compared to that of iron immobilized in the catalyst, this phenomenon is detrimental for the long stability of the catalyst.[24]
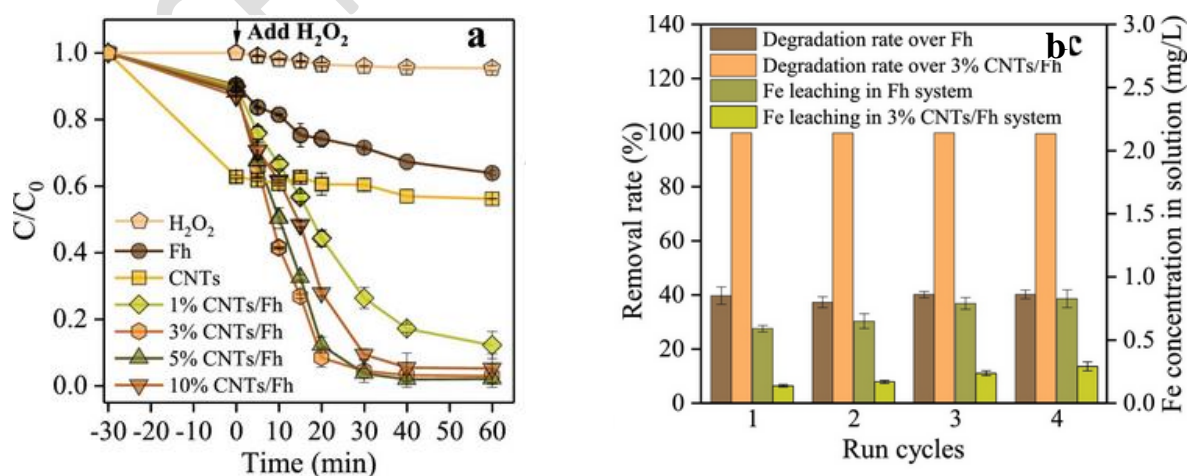
Figure 3. Relative concentration of BPA in solution versus time before and after introduction of H_2O_2 at t = 0 in the reaction medium, in the presence of ferrihydrite (Fh), multiwalled CNTs (CNTs), and Fh

immobilized in various amounts of CNTs (a) and BPA conversion (removal or degradation rate) and Fe concentration in solution after 60 min of reaction in the presence of Fh and CNTs/Fh, after successive run cycles (b). Adapted from ref [26]. Copyright 2020 Elsevier.

Metal-organic frameworks (MOFs), and especially those containing iron cations such as MILs, and their derivatives are promising catalysts for Fenton-like water treatment due to their high adsorption properties and the easy control of the design and of the number of active sites. However, Fe MOFs must be still improved to overcome the problem of low Fe(II)/Fe(III) cycle efficiency and slow mass transfer of pollutants. Nevertheless, they can be a promising strategy to remove trace of organic pollutants by concentrating micropollutants inside the pores near the active sites.[27]

Table 2. Examples of heterogeneous Fenton catalysts. Adapted from ref [24].

Type of Fe species	Catalysts
Magnetite Fe_3O_4	Zn/Co/Mo-Fe_3O_4, Fe^0/Fe_3O_4, graphene oxide (GO)/Fe_3O_4, Fe_3O_4@void@TiO_2
Ferrihydrite (Fh), natural hydrous ferric oxide	CNTs/Fh, Ag/AgX(X = Cl, Br)/Fh, $BiVO_4$/Fh, Citrate/Fh
Hematite Fe_2O_3	α-Fe_2O_3/Bi_2WO_6, shape-controlled hematite, Ag/α-Fe_2O_3
Goethite α-$Fe^{III}O(OH)$	Cu-α-FeOOH, reduced GO-α-FeOOH, Cu-Fe_3O_4@FeOOH, FeOOH/g-C_3N_4
Pyrite FeS_2	FeS_2/SiO_2
Fe(III) in clays	Layered double hydroxides, pillared clays, clay supported catalysts
Nanoscale zerovalent iron (nZVI)	Biochar/nZVI, CNTs-Fe0, Fe@Fe_2O_3, nZVI-diatomite
Other type of oxides or hybrid materials	$Bi_{25}FeO_{40}$, $BiFeO_3$/g-C_3N_4, Ag/ZnO/$ZnFe_2O_4$Transition metal-exchanged zeolites, Fe^0@C@$MnFe_2O_4$, Pt/$LaFeO_3$, $CuFeO_2$, $CuFe_2O_4$@graphite carbon, GO/$FePO_4$, NCNTs-$FePO_4$, $Co_xFe_yO_4$-BiOBr, $CoFe_2O_4$/g-C_3N_4, FeOCl/SiO_2, MOFs

As the slow kinetics of Fe(III) reduction to Fe(II) determines the global kinetics of the heterogeneous Fenton process, strategies have been developed to accelerate the regeneration rate of Fe(II) active species necessary for producing the most active HO• species (Reaction (1)). Some of these strategies are based on introducing additional electrons in the catalyst. This can be done by application of an external electron source, by combining heterogeneous Fenton process with an electrochemical process (electro-assisted Fenton process) or a photocatalytic process (photo-Fenton process) or by combining the Fenton catalyst with electron-rich materials. The photo-Fenton process consists in combining semi-conductors (TiO_2, $BiVO_4$, g-C_3N_4) with the heterogeneous Fenton-like catalyst. The photogenerated electrons on the semiconductor are transferred to heterogeneous Fenton catalyst for the reduction of Fe(III), with the possibility of direct degradation of the organic pollutants by photocatalysis too. The electro-assisted Fenton process presents also many advantages such as (i) the regeneration of not only the iron species immobilized in the catalytic material but also leached Fe^{3+} and (ii) the *in-situ* generation of H_2O_2, according to the following reactions:

$$Fe^{3+} + e^- \rightarrow Fe^{2+} \tag{3}$$
$$2e^- + 2H^+ + O_2 \rightarrow H_2O_2 \tag{4}$$

On the other hand, the photo-Fenton process allows the direct photolysis of H_2O_2 in addition to the reduction of Fe^{3+} or Fe(III) species:[24]

$$Fe^{3+} + H_2O \rightarrow Fe(OH)^{2+} + H^+ \tag{5}$$
$$Fe(OH)^{2+} + h\nu \rightarrow Fe^{2+} + HO• \quad (\lambda < 580nm) \tag{6}$$
$$H_2O_2 + h\nu \rightarrow 2\ HO• \quad (\lambda < 310nm) \tag{7}$$
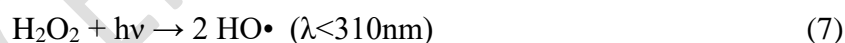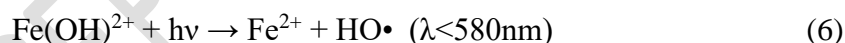
Photo-Fenton process is the most effective strategy when the iron species are associated with photosensitive materials.

Electrons can also be provided by introducing electron-rich species in the catalytic material, such as nZVI (Table 2), carbon materials (biochars, CNTs, GO), metal sulphides (MoS_2, WS_2, Cr_2S_3, CoS_2). The design of composite materials for enhancing the Fe(II)/Fe(III) cycle will be commented in more detail in paragraph 2.4.

Finally, other combinations like microwave-Fenton and ultrasound-Fenton processes lead to encouraging results in terms of pollutant removal efficiency in the presence of heterogeneous catalysts.[24,26]

One can note that hydroxyl radicals are the reactive species that are usually invoked for Fenton-based heterogeneous catalytic processes, while nonradical mechanisms have been frequently evidenced in the presence of carbon materials and in some cases with metal oxides for processes based on the use of ozone or persulfates. However, a nonradical pathway, based on the production of singlet oxygen $^1O_2$ was for the first time proposed in 2021 to explain the enhanced degradation of sulfamethoxazole using a g-C_3N_4/MgO composite for activating H_2O_2 activation (Figure 4).[28]
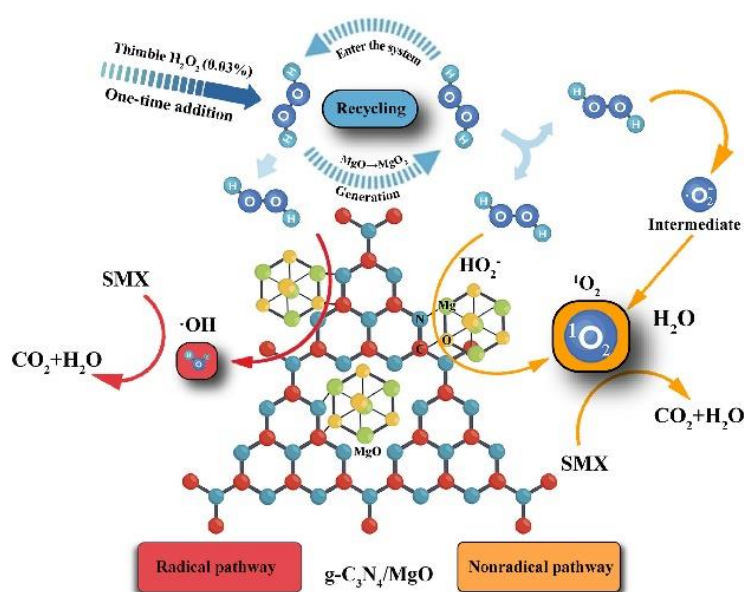
Figure 4. Mechanism of degradation of sulfamethoxazole using a g-C_3N_4/MgO catalyst for H_2O_2 activation. Reproduced with permission from Ref. [28]. Copyright 2021 Elsevier.

Ozonation

With high redox potential (Table 1), O_3 can be directly used to degrade water contaminants, especially those with unsaturated carbon bonds. However, due to its high generation cost and moderate efficiency to reach alone a complete mineralization of recalcitrant contaminants, ozone is often combined with other water treatment technologies, such as H_2O_2, UV irradiation or with an increase in pH to favor •OH generation. It was shown in the late 1940s that the addition of transition metal ions such as Co^{2+} in water can catalyze the decomposition of O_3 into more oxidizing hydroxyl radicals HO• species[29], according to a mechanism similar to that of the Fenton process. Also, as for Fenton reaction, the pH value is of major importance, but ozonation reaction is possible in the wide range of pH. The pH value controls, however, the type of reactive oxygen species formed. At pH<4, direct ozonation

occurs preferentially, while catalyzed ozonation is dominant at pH>9, both mechanisms being involved in between[30]. Various metal ions have proven their efficiency for promoting the pollutant mineralization, such as Mn^{2+}, Fe^{2+}, Co^{2+}, Ni^{2+}, Zn^{2+}, Fe^{3+}, Ce^{3+}, etc.[30], not only by favoring the production of hydroxyl radicals but also by forming complexes with pollutants, especially low-molecular weight acids, thus favoring their degradation[30]. Many types of heterogeneous catalysts have been efficiently applied to the catalytic ozonation of various pollutants Most of them are based on the use of metal oxides or oxyhydroxides, as for example MnO_2, the most studied, Fe_2O_3, $FeOOH$, Fe_3O_4, Al_2O_3, $AlOOH$, MgO, CeO_2, TiO_2, ZnO, Co_3O_4, or mixed metal oxides, as spinel ferrites MFe_2O_4 (M = Mn, Cu, Ni, Co etc.)[30] or perovskites $LaMO_3$ (M = Mn, Fe etc.). Theses oxides can be used alone or supported or incorporated in another oxide to improve their surface exposed to the reactants and their stability. For example, manganese and cerium oxides supported on mesoporous Fe-MCM-41 were demonstrated to be efficient for the mineralization of oxalic acid, a recalcitrant pollutant requiring harsh conditions to decompose[31]. Also, a wide range of zeolites, alone or modified by addition of metal oxides have been found to be efficient for pollutant removal by catalytic ozonation, due to a combination of parameters, including their high surface area, the possibility of adjusting hydrophilicity/hydrophobicity, the acidity by the silica to alumina ratio and the pore size. Metals, in the metallic state, supported on metal oxides are also active catalysts for ozonation by either favoring the production of •OH and/or the adsorption of the organic pollutant[32]. Some examples of the reaction mechanisms will be detailed in paragraph 2.2. Basically there are 3 types of mechanisms to explain the interaction of the catalyst with organic pollutants and O_3.

- adsorption of O_3 onthe catalyst surface where it is decomposed into reactive radicals that react with pollutants in water;

- adsorption of organic pollutants on the catalyst surface where they react with O_3 in water.

- adsorption of both O_3 and organic pollutants on the catalyst surface where they react.

Given that these 3 mechanisms are reported independently of the type of catalyst, the literature does not provide a clear strategy to select the appropriate catalyst. Of course, a high surface area must be favored for maximizing the adsorption, but other parameters are reported to play a role in the ozone activation and/or pollutant adsorption. Some of them are: (i) surface hydroxyl groups for promoting •OHs generation (ii) the point of zero charge (pzc) of the oxide determining the charge of the hydroxyl group as a function of pH and consequently the adsorption of ionized pollutant molecules, (iii) structural defects and (iv) surface

functionalities[12]. Lewis acid sites (LAS), characterized in gas phase, are also frequently invoked as important for adsorbing the O_3 Lewis base or anions such as carboxylic anions. However, as LAS mainly react with water molecules under the reaction conditions, their beneficial effect on the catalytic activity is not evident and could be linked to the formation of hydroxyl groups in water. Surprisingly, the redox behavior of the metal oxides is often neglected, while it is a key point in the catalytic activity of metal oxides in other oxidation reactions. The challenge for the catalytic ozonation process consists in being able to stabilizie mixed valences of the active species and favor M^{n+}/M^{n+1} cycles, while decreasing the particle size for increasing their accessibility to reactants[33]. For non-polar molecules, some hydrophobic functions may be incorporated on the surface of the catalyst for their adsorption. In the case of zeolites, solids with high silica content can be used[34]. Another key point is the efficiency of the immobilization of the active phase to avoid its leaching in the reaction conditions. However, as for Fenton reaction, some solubilisation of the active phase often occurs, even if recent progress in catalytic formulation has allowed limiting this adverse phenomenon. For example, only ca. 0.8 wt% of the total Cu in highly dispersed Cu(I)/Cu(II) catalyst supported onto defect-rich mesoporous alumina was leached after one cycle of phenol conversion during 60 min with no modification of the structure and porosity of the used catalyst[33]. Metal leching complicates determination of the mechanism, since both heterogeneous and homogeneous active species present in the reaction medium can participate in the reaction[34].

Carbon-based materials as activated carbon, (N, S or F-doped) carbon nanotubes, graphitic carbon nitride or (N or P-doped reduced) graphene oxides are other type of active catalysts for ozonation process. As for metal oxides, many types of mechanisms have been proposed, implying surface functionalities (oxygen functional groups) or dopants, which have been demonstrated as key parameters, more important than the surface area. One surprising point is that in some cases basic sites are proposed to be responsible for high reactivity, which seems in contradiction with the mechanisms proposed for metal oxide catalysts for which acidic sites play a major role. The advances of heterogeneous catalytic ozonation based on the use of nanocarbon materials are reported in a recent comprehensive critical review[35].

Whatever the heterogeneous catalyst studied, hydroxyl radical HO• and/or superoxide radicals $O_2^{\bullet-}$ species produced from O_3 are the most often proposed active species However, nonradical oxidation process can also occur by oxidation of the pollutant by O_3 due to its high redox potential (Table 1), not only directly in homogeneous phase but also indirectly, through the catalyst. In the latter case, the catalyst may favor either (i) the electron mobility and thus

the electron transfer from molecules to ozone or (ii) the adsorption of O_3 and the organic molecule favoring the intermolecular electron transfer without O_3 dissociation. The formation of highly reactive singlet oxygen $^1O_2$ from the catalytic dissociation of O_3 has also been proposed as an alternative pathway in the oxidation of pollutants in water[12]. The advantage of non-radical oxygen active species is their strong resistance to scavengers present in water matrixes. Figure 5 summarizes various ozonation reaction pathways.
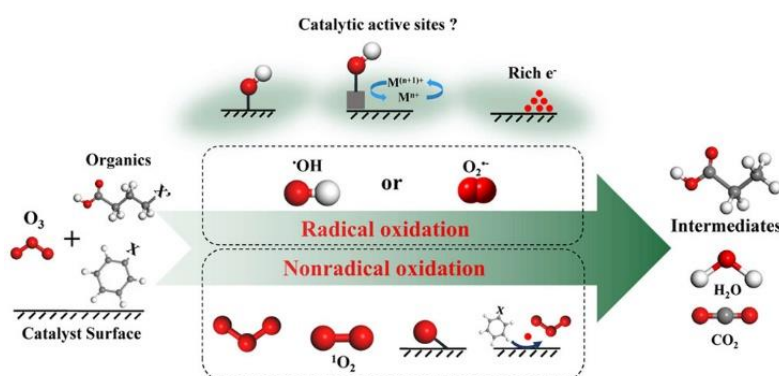
Figure 5. Scheme of the various reactive oxygen species involved in catalytic ozonation process for water treatment. Reproduced with permission from ref [12]. Copyright 2020 American Chemical Society.

Sulfate radicals

Production of highly oxidizing sulfate radicals ($SO_4{}^{\bullet-}$) from peroxymonosulfate (PMS) or peroxydisulfate (PDS) through homolytic or heterolytic cleavage of the O–O bond emerged in the 1990's as an environmental and cost-effective alternative to the use of H_2O_2 reactant due in part to its high redox potential (Table 1) and low cost[36]. One major advantage of PMS and PDS is that they exhibit lesser pH dependency tha H_2O_2. It should be noted that at pH above 8.5, OH^- are oxidized by $SO_4{}^{\bullet-}$ giving rise to $HO\bullet$ and $HSO_4{}^-$ species, and $HO\bullet$ becomes the predominant oxidizing species[36]. $SO_4{}^{\bullet-}$ reacts with organic compounds similarly to $HO\bullet$ but, contrary to $HO\bullet$ that may oxidize a wide range of organic pollutants, $SO_4{}^{\bullet-}$ is more selective and its reactivity depends on the substrate.

For water treatment, the O-O bond dissociation can be promoted using physical techniques, such as UV irradiation or ultrasound application, or by chemical activation, by electron transfer as in Fenton reaction, using transition metal ions M^{n+} in homogeneous phase (equation (8)) for PDS and (9) for PMS. Heterogeneous catalysts based on metals (Fe, Ni), metal oxides (Co_3O_4, MnO_x), either alone, supported (supports = TiO_2, Al_2O_3, SiO_2, MnO_2, MgO, graphene oxide, zeolite ZSM-5, SBA-15) or as mixed oxides (spinel ferrites MFe_2O_4 with M = Co, Cu, Mn, Ni, Mg; etc.) have also been reported for O-O bond breaking[21].

$$S_2O_8^{2-} + M^{n+} \rightarrow M^{n+1} + SO_4^{2-} + SO_4^{\bullet-} \cdot \qquad (8)$$

$$HSO_5^- + M^{n+} \rightarrow M^{n+1} + OH^- + SO_4^{\bullet-} \cdot \qquad (9)$$
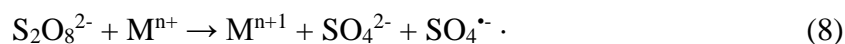
Metal-organic frameworks (MOF) such as MILs, containing transition metal cations such as Fe^{2+} and dicarboxylic acids, or ZIFs composed of cations such as Co^{2+} or Zn^{2+} and imidazolate, present also interesting properties as catalysts for SO_4^- generation. They include large surface area, high porosity, capability to adsorb pollutants and accessibility to unsaturated metal sites that can activate persulfates into strong oxidizing species[37].

Carbon-based materials (activated carbon, graphene oxides, or carbon nanotubes) constitute also another range of heterogeneous catalysts active for the mineralization of organic pollutants in the presence of PMS or PDS. Studies on the performance of carbon-based materials asa heterogeneous catalysts for the removal of a wide range of pollutants using PMS and PDS have been recently reported [38].

Due to their high redox potential (Table 1) persulfates as PMS and PDS can also oxidize organic pollutants either directly, or via a catalytic material playing the role of electron shuttle without any change in its oxidation state. On one hand, clear evidence of direct interaction between non-activated persulfate and organic molecules, has been given. For example, a direct interaction between PMS and a micro-pollutant, trimethoprim, an antibiotic with amino groups on heterocyclic rings, has been recently proven [39]. The degradation pathway leads selectively to hydroxylamines that are less toxic intermediates than nitroso- and nitro-products obtained by deeper oxidation. On the other hand, evidence in support of nonradical mechanisms in the presence of carbon materials (Carbon nanotubes, graphitized nanodiamond), CuO or noble metals (Pd, Au, for example) favoring the electron transfer from the contaminant to the persulfate has been provided [36,40-41]. Figure 6a shows the evolution of 2,4-dichlorophenol (2,4-DCP) in water in the presence of PMS or PDS and Co^{2+} in CuO in similar concentrations. It can be seen that the conversion rate is much higher for CuO, and it was demonstrated that CuO plays the role of electron shuttle as illustrated in Figure 6b [42].
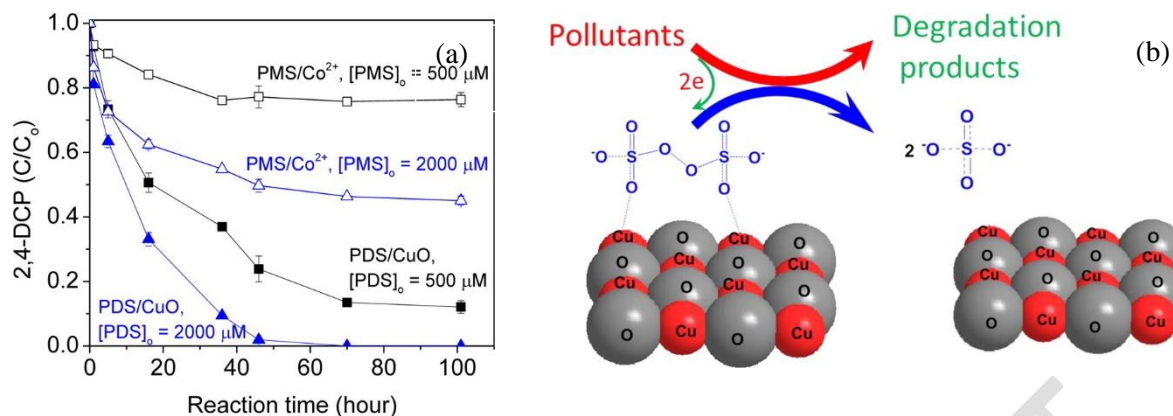
Figure 6. Evolution of 2,4-DCP (C0 = 500 μmol L^{-1}) in the presence of PMS/Co^{2+} and PDS/CuO at 20 °C (a) and proposed mechanism of catalytic reaction in the presence of CuO (b). Adapted with permission from ref [42]. Copyright 2014 American Chemical Society.

It was also proposed that singlet oxygen, $^1O_2$, generated by self-decomposition of persulfates, or on some Fe-based materials along with superoxide radical (O_2•$^-$) should also be an oxidizing species originating from persulfate, $^1O_2$ could be produced in parallel to radical species, even if its clear identification is still subject to discussion and this reaction route should continue to be investigated [36,40,43].

Other advanced oxidation processes

Reactive oxygen species can also be generated by photocatalysis, microwaves and non-thermal plasma, which will be treated in sections 4.1, 3.1 and 3.2, respectively. Apart from electrochemical oxidation which is a mature process already extensively applied to water treatment [44], two other technologies emerged recently, namely sonocatalysis and radiolysis.

In sonocatalysis water treatment, the ultrasonic irradiation through the liquid modifies the local pressure in time and space creating bubbles that expand and collapse. This phenomenon is accompanied by an increase in temperature, up to 4500°C, and in pressure, up to 10^2 MPa, inside bubbles, generating •H and HO• via water decomposition. Ultrasounds alone are not sufficiently efficient for allowing the complete mineralization of organic pollutants. Hence, the efficiency of this process may be increased by coupling with other oxidation processes such as electrochemical oxidation, Fenton-like or iron-activated persulfate processes or by using a catalyst[45]. The role of the catalyst is to act as (i) a nucleus for bubble formation, especially on hydrophobic surfaces and (ii) favor the formation of reactive oxygen species through the interaction of the acoustic field with the surface of the catalyst. The catalytic effect depends on the conditions of sonication, the nature of the gas dissolved in water and the physicochemical properties of the catalyst, such as roughness, porosity and particle size[46]. Catalytic materials

reported in the literature are mainly semi-conductors, such as TiO_2 and ZnO. In this case, the local high temperature may create a thermal excitation of the semi-conductor, corresponding to photons in the 200-700 nm wavelength range, leading to the creation of electron-hole pairs like in photocatalysis. In this way, reactive oxygen species (ROS), and especially HO•[46] can also be generated. Other solid materials as Al_2O_3, glass beads and carbons are also used to reduce the energy needed to obtain cavitation bubbles. More details are reported elsewhere [46].

Radiolysis, based on the use of gamma sources (^{60}Co or ^{137}Cs) or less costly, more effective and safe, electron beam, is another way to generate highly active species from water, either strongly oxidizing, such as HO•, or strongly reducing, such as e[-]. This type of treatment is particularly adapted to degrade pharmaceuticals and personal care products at trace levels, and especially highly recalcitrant pollutants as antibiotics and hormones. Its efficiency may also be improved by combining radiolysis with O_3 or H_2O_2 or by using catalysts, such as TiO_2, Al_2O_3, SiO_2 or activated carbon, but examples of radiocatalysis are scarce. Details on this kind of process may be found in ref. [47].

2.1.2. WAO and CWAO

Wet air oxidation is a hydrothermal process operated at elevated temperatures and pressures under oxygen aimed at oxidizing organic or inorganic pollutants in aqueous solution at medium loadings (chemical oxygen demand COD typically between 20 and 200 g(O_2) L[-1]) for which incineration is not possible. It is a low cost process due to the possibility of energy recovery from the exothermicity of the oxidation reaction, a very efficient process. WAO allows the conversion of refractory pollutants. WAO is a mature technology, with industrial units installed worldwide, principally for the treatment of sewage sludge[48]. Since high pressures (0.5 – 20 MPa) and temperatures (125 – 320 °C) are applied in this process, a high amount of O_2 is solubilized in water leading to the formation of free radicals, highly active oxygen species as hydroxyl radical included, that will play a role in the formation of products. The use of transition metal catalysts, mainly based on copper salts, allowes to relax somewhat the harsh operating reaction conditions, at the expense of an additional processing step to recover the catalyst. This drawback can be solved by using a heterogeneous catalyst. The solids used as catalysts must be mechanically and chemically robust not only to high temperature and air pressure, but also to the corrosive environments encountered due to the formation of refractory carboxylic acids as intermediate products of the (C)WAO process. Consequently, the leaching of the active species is a major concern for this process. For this reason, even if

non-noble transition metals should be preferred due to their lower cost, noble metal based catalysts continue to be developed for this process. Due to their high activity for CWAO, Pt, Pd and Ru were the most studied noble metals, supported on various oxides such as Al_2O_3, CeO_2, $Ce_xZr_{1-x}O_2$, TiO_2, MnO_x-CeO_x, TiO_2-CeO_x, etc. Carbon supports have also been used resulting in very active catalysts even if the resistance under the reaction conditions could be limited, leading to the loss of carbon[49]. The choice of the support can be also governed by its ability to favor the oxygen transfer, such as CeO_2-based supports with redox properties[50]. Noble metal based heterogeneous catalysts have been efficiently used for the removal of organic pollutants, as model molecules, of which phenol was studied in depth[51] as well as carboxylic acids (succinic acid, benzoic acid, or small refractory acids such as acetic acid etc.) and nitrogen compounds [49,52]. Besides model molecules, industrial wastewaters from pulp and paper mill or dyes effluents for example, have also been submitted to CWAO with noble metal catalysts. While metal leaching could be limited, this kind of catalysts is nevertheless subject to deactivation due to their sensitivity to sulphur and halogens that can be present in the effluents and to the blockage of the active sites by carbonaceous deposit, either carbonates or coke, a polymeric carbon. Due to their lower cost and better availability, non-noble metal based catalysts have also been the subject of numerous studies on CWAO. Various catalysts were tested, not only based on copper oxides but also on other metal oxides MOx (M = Bi, Fe, Co, Ni, Mn, Cr, V, Zn etc.), alone or supported on the same type of support as for noble metals. Generally higher metal loadings are necessary to reach reasonable activities, compared to noble metals. The current trend is to decrease the temperature and pressure of reaction to increase catalyst stability, since non-noble metals are subject to leaching in the highly corrosive classical CWAO conditions. In that case, a complete mineralization into CO_2 of the organic matter is not always possible, but pollutants can be converted into biodegradable compounds, making the process still of interest. For example, it was shown that non-biodegradable industrial organic wastes, containing pyridine and derivatives, can be converted by CWAO into biodegradable compounds using MnO_x/Al_2O_3 promoted by CeO_2 at atmospheric pressure and temperature as low as 70°C[53].

Another trend in CWAO concerns the valorization of organic pollutants. For example by adapting the process, valuable gases such as biogas (CO + H_2), H_2 and/or alkanes can be obtained instead of carbon dioxide only. This can be achieved by coupling CWAO process with aqueous phase reforming (APR), operated in similar conditions. In that case, the objective is to achieve a partial oxidation of the pollutants and to valorize the oxidation products by converting them into H_2 and/or alkanes. For example, while the direct APR of aromatic

compounds such as phenol, yields CO_2, their prior treatment by CWAO produces carboxylic acids that are then more easily converted into valuable gases by APR. Thus, it was demonstrated that the APR of phenol yields 96.4% CO_2, the CWAO-APR coupling leads to a mixture of CO_2 (77.6%) and CH_4 (22.4%)[54].

2.1.3. Reducing processes

For nitrate reduction reactions, two kinds of active species can be used, depending on the pollutant to reduce: either chemisorbed hydrogen, or metallic species. The choice of the reducing agent depends on the molecule to convert.

Thus, nitrate are highly oxidizing species that can be directly reduced by metallic species such as zero-valent iron, leading to metal ions in solution or metal oxides inhibiting further reduction[55]. This concept was the basis of the proposed mechanism of catalytic nitrate reduction on bimetallic supported catalysts. These catalysts consist of an oxidizable metal, such as Cu, Fe or Sn, associated with a noble metal able to chemisorb hydrogen, such as Pd or Pt. The process is carried out under dihydrogen flow and to maintain the oxidizable metal in the metallic state.[56] For example on the bimetallic Pd-Cu catalyst, nitrate can be reduced to nitrite, or even to molecular nitrogen or ammonia by direct redox reaction (Figure 7) with metallic copper, leading to its oxidation into Cu^{n+} (with n = 1 or 2), which returns to the zerovalent state by reduction via the H atoms chemisorbed onto Pd, allowing the catalytic cycling. Then, intermediate nitrite may be reduced either by hydrogen chemisorbed onto Pd or, as for nitrate, by direct redox reaction with copper (Figure 7).
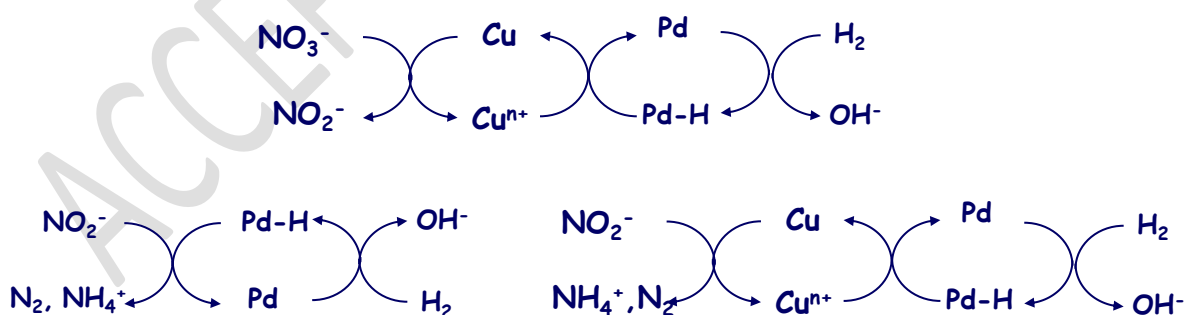
Figure 7: Schematic representation of nitrate and nitrite reduction onto a Pd-Cu bimetallic catalyst.

Of course, chemisorbed hydrogen is the most used reducing species for pollutant removal in water by reduction using a heterogeneous catalyst, as for nitrate reduction and/or hydrodechlorination reactions[57]. Most often H_2 gas is introduced in the reaction medium, but in some cases it also could be generated *in-situ*. For example, formic acid HCOOH has been

used as a hydrogen precursor since it can be easily decomposed into H_2 and CO_2 at the surface of noble metals. For nitrate reduction, the same catalyst can be used for the conversion of the pollutant and formic decomposition, and the production of CO_2 allows buffering the reaction medium[58].

Table 3. Main active species identified for oxidizing pollutants in water using heterogeneous catalysts

Type of treatment	Oxidant	Active species	Main types of heterogeneous catalysts
Fenton	H_2O_2	$HO\bullet$, $^1O_2$	Fe-based catalysts
Ozonation	O_3	$HO\bullet$, $^1O_2$	MO_x or $MM'O_x$ (M or M' = Fe, Al, Ti, Mg, Ce, Zn, Co etc.) alone or supported Carbon materials
Persulfates	$S_2O_8^{2-}$, HSO_5^-	$SO_4\bullet^-$, $HO\bullet$, $O_2\bullet^-$ $^1O_2$, $S_2O_8^{2- -}$	M^0 (M = Fe, Ni, Pt, Pd etc.) MO_x or $MM'O_x$ (M or M' = Co, Cu, Mn etc.)
Sonocatalysis	(O_2)	$HO\bullet$ $(H\bullet)$	Semi-conductors (TiO_2, ZnO) Al_2O_3
Radiolysis	(O_2)	$HO\bullet$ (e-)	TiO_2, Al_2O_3, SiO_2
Wet air oxidation	O_2	$HO\bullet$	Supported noble metals (Pd, Ru, Pt) MO_x (M = Bi, Fe, Co, Ni, Mn, Cr, V, Zn etc.

2.2. From kinetics and reactions mechanisms to reactor design in catalytic water treatment

2.2.1. First considerations on radical mechanisms in catalyzed and non-catalyzed homogeneous systems.

Regarding AOPs of organic contaminants in aqueous phase, a major concern is their poor efficiency with incomplete mineralization in case of emergent refractory water contaminants. Recent examples on the degradation of phthalate esters by HO• and $SO_4^{•-}$ radicals and N-containing aromatic and heterocyclic contaminants have been published [59-61]. Experimental and theoretical studies have provided important kinetic and thermodynamic data sometimes coupled with ecotoxicity. Most of the reported treatment can be useful but incomplete, providing only information on the initial stage and the preferential bond breakage initiated by reactive HO• radicals thanks to a first H-abstraction at the phenyl and $-CO_2C_4H_9$ groups for the degradation of phthalate esters to catechol.[59] For N-containing heterocyclic compounds, their sluggish reactivity can be related to the position of N atoms in the heterocyclic ring.[61] DFT calculations coupled to kinetic measurements on the ozonation of benzotriazole, benzimidazole, indazole and indole found an enhanced mineralization for substitution in ortho position of the N atom compared to meta position. The apparent preferential first order kinetics with respect to the organic contaminant according to Eq. (10) in ozonation has also been a point of discussion. Let us note that the apparent rate constant k_{obs} depends on the concentration of reactive oxygen species [ROS] as well as their reactivity reflected by the rate constant k_{ROS}. In practice, an accurate estimation of these two parameters is not an easy task. DFT calculations can rationalize the k_{ROS} values, particularly when electron redistribution in conjugated systems can facilitate the attack of the active oxygen species at certain preferential positions.

$$\frac{d[C]}{dt} = -k_{obs}[C] = -(k_{O3}[O_3] + k_{ROS}[ROS])[C] \qquad (10)$$

Equation (10) also reflects the existence of parallel and consecutive processes with combined effects of a direct oxidation pathway with ozone regarded as non-selective reagent and an indirect pathway involving reactive oxygen species from the self-decomposition of ozone recognized as the major route. This latter step is non-selective and essential to insure complete mineralization process.[62]

The toxicity of by-products from incomplete oxidation must be carefully considered because a high toxicity makes AOP inefficient for refractory contaminants. Another important aspect is related to the residual concentration of ozone in the reaction media which can decompose into ROS according to Eqs. (11)-(14):

$$O_3 + OH^- \rightarrow O_2\bullet^- + HO_2\bullet \tag{11}$$

$$O_3 + HO\bullet \rightarrow O_2 + HO_2\bullet \tag{12}$$

$$O_3 + HO_2\bullet \rightarrow 2O_2 + HO\bullet \tag{13}$$

$$2H^+ + 2e^- + 2HO_2\bullet \rightarrow {}^1O_2 + 2H_2O \tag{14}$$
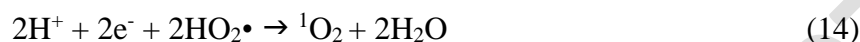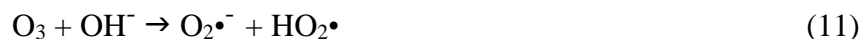
Radicals generated from ozone will be commented in the following paragraphs. Ozone decomposition depends on the pH conditions. This reaction occurs much faster in alkaline conditions[63] becoming significant over pH = 7 corresponding to half-time in the time scale 15-25 min[50]. Acidic conditions are detrimental for the production of ROS and will induce lower mineralization rates.[51] A key point lies in the production of ROS more reactive than ozone. Indeed, the involvement of hydroxyl radicals has been found to promote the major degradation route. The presence of N atoms leads to higher complexity in the mineralization process because nitrates and ammonium species can form ultimately. The compounds represent a serious drawback in terms of ecotoxicity[64]. Among the different contaminants in aquatic environment, amino acids such as glycine, serine, aspartic acid and glutamic acid are the most representative and currently considered as model compounds. For instance, it was found that glycine ozonation leads to ammonia production through a HO• reaction pathway. On the other hand, a direct ozone attack leads to nitrate formation[65-66]. As exemplified in scheme 1, a parallel pathway can explain the formation of nitrates and ammonia after O_3 addition. For nitrates, the intermediate production of hydroxyl-amine and its subsequent oxidation produces an oxime that forms nitrates ultimately. On the other hand, ammonia would result from an electron transfer producing $HO_3^{-\bullet}$, C-centered and imine intermediates further hydrolyzed to NH_4^+.
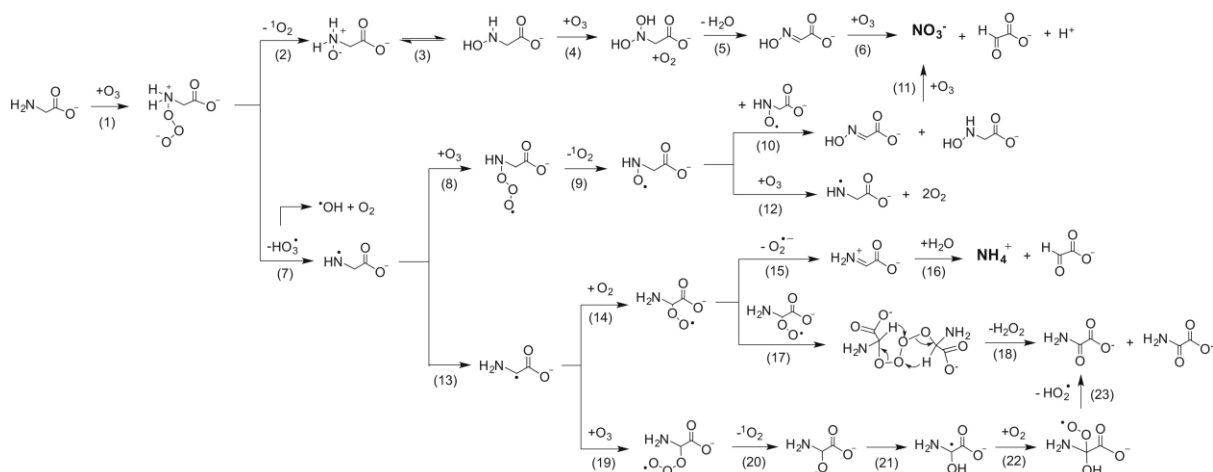
Scheme 1. Proposed mechanism of nitrate and ammonium formation from the ozone-glycine. Reproduced with permission from ref. [64]. Copyright 2017 Elsevier.

According to their respective oxidizing potentials (2.07 V for O_3 vs. 2.73 V for HO•), it is obvious that strategies accelerating the decomposition of ozone into HO• can be efficient. Numerous investigations were aimed at developing homogeneous processes by adding soluble transition metals as catalysts [67-68]. The assistance of H_2O_2 incorporation as source of HO• as well as UV radiations has been also extensively explored [69-70] demonstrating that their combination can be efficient to convert O_3 into HO•. Significant studies comparing the removal of terephtalic acid by ozonation in wastewater by combining Fe^{2+}, H_2O_2 and UV light (Figure 8) have been reported[71]. Photolysis of ozone under UV irradiation at $\lambda = 254$ nm produces H_2O_2 as precursor for the formation of HO• [72]. Under optimal alkaline conditions the consumption of OH$^-$ according to Eq. (17) induces lowering of pH that could led to a gradual loss of efficeincy.

$$O_3 + H_2O + h\nu \rightarrow H_2O_2 + O_2 \tag{15}$$

$$H_2O_2 + h\nu \rightarrow 2 \text{ HO•} \tag{16}$$

$$H_2O_2 + OH^- \rightarrow HO_2^- + H_2O \tag{17}$$

When iron cations are introduced, the following set of reactions can occur [67,71,73].

$$Fe^{2+} + O_3 \rightarrow Fe^{3+} + O_3^- \tag{18}$$

$$O_3^- + H^+ \leftrightarrows HO_3 \rightarrow \text{HO•} + O_2 \tag{19}$$

$$Fe^{2+} + O_3 \rightarrow (FeO)^{2+} + O_2 \tag{20}$$

29

$$(FeO)^{2+} + H_2O \rightarrow Fe^{3+} + \cdot OH + OH^- \qquad (21)$$

Additional undesired side reactions can take place then lowering the pH:

$$HO\bullet + Fe^{2+} \rightarrow Fe^{3+} + OH^- \bullet \qquad (22)$$

$$(FeO)^{2+} + Fe^{2+} + 2H^+ \rightarrow 2Fe^{3+} + H_2O \qquad (23)$$
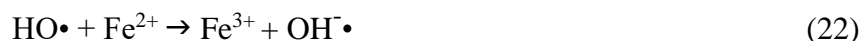
Returning to Eq. (10) a major point of concern is related to the estimation of the contribution on the overall rate of O_3 and ROS. In other words, which experimental method can be implemented to calculate accurately the pseudo first order rate constants $k_{mol} = k_O[O_3]$ and $k_{rad} = k_{ROS}[ROS]$. Ter-butyl alcohol can be used as HO• scavenger[74]. Accordingly, the indirect oxidation can be rapidly deactivated due to a much higher rate constant for HO• scavenging in comparison with a slow process for ozone ($k_{OH,TBA} = 3.6 \times 10^{10}$ L.mol^{-1}.min^{-1} vs. $k_{O3,TBA} = 0.18$ L.mol^{-1}.min^{-1}). Consequently, it has been possible to calculate and compare k_{mol} (direct molecular oxidation process) and k_{rad} (indirect radical oxidation process). Based on this, the efficiency of different scenarios can be compared. Figure 8 shows that irradiation of UV has no significant impact likely due to absorption process. Clearly, the conjunction of UV irradiation and H_2O_2 addition improves the contribution of k_{rad}. In the absence of UV and H_2O_2, the total rate measured in the presence of Fe^{2+} clearly underlines a catalytic effect which becomes magnified in the presence of UV and H_2O_2. Hence, a synergistic effect in the promotion of HO• radicals clearly appears in the combination of O_3 with Fe^{2+}, UV and H_2O_2 (Figure 8).
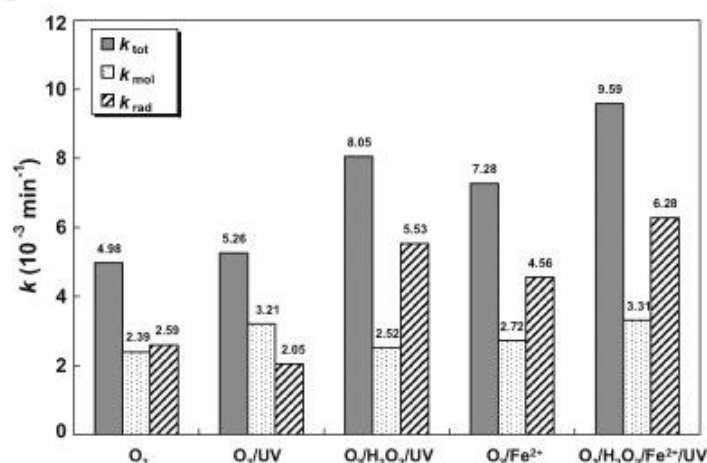
Figure 8. Rate constants of individual contributions, molecular reaction (k_{mol}) or radical reaction (k_{rad}), and overall reaction (k_{tot}) for the optimized ozonation systems. Reproduced with permission from ref. [71]. Copyright 2009 Elsevier.

Improving the efficiency of ozonation process implies increased production of reactive oxygen species, *i.e.* HO•. Further extrapolation must keep in mind the related cost-efficiency by using external energy sources or by adding costly reactants such H_2O_2 to promote the formation of HO• species. The balance between these strategies and those consisting in *in-situ* generation of reactive oxygen species, without any input of external energy could make latter preferable, as discussed in the previous chapter. The decomposition of hydrogen peroxide in the pre3sence of soluble iron species leading to the formation of HO• has been investigated. In adition to HO•, iron species stabilized in unusual Fe(IV) oxidation state are also suited to oxidize a limited variety of organic compounds [75]. The distribution of HO• and iron species varies according to the pH conditions and a shift to lower pH values induces the predominance of Fe(IV). As a consequence, a loss of the overall efficiency can be assigned to a lower production of hydroxyl radicals. Previous studies also revealed that Cu(I) can play the same role as Fe^{2+} leading at neutral pH to ac tive Cu(+III) oxidant and the generation of HO• from H_2O_2 [76-77]. The restoration of Cu(I) is insured by the use hydroxylamine which is, however, problematic from an ecotoxicity point of view. In fact, the potential environmental risk is assumed limited because they are mitigated by complete decomposition of hydroxylamine into inert gases. On the other hand, some restrictions on the maximum Cu^{2+} concentration of 1.3 mg/L set by the U.S. Environmental Protection Agency would imply the installation of costly nanofiltration devices. The use of heterogeneous copper catalysts could represent an alternative to avoid high concentration of soluble ionic copper species.

Previous investigation by using nanomolar concentrations of Cu(I) and Cu(II) with H_2O_2 led to the set of reactions 24-28[78].

$$H_2O_2 \leftrightarrows H^+ + HOO^- \tag{24}$$

$$Cu(II) + HOO^- \rightarrow Cu(I) + HO_2\bullet \tag{25}$$

$$HO_2^{\cdot} \leftrightarrows H^+ + O_2\bullet^- \tag{26}$$

$$Cu(I) + H_2O_2 \rightarrow Cu(II) + HO\bullet + OH^- \tag{27}$$
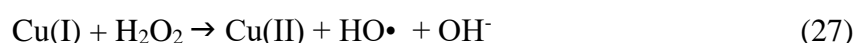
However, the rate expression (28) corresponding to step (27) for HO• production has been invalidated.

$$d[HO\bullet])/dt = -k[Cu(I)][H_2O_2] \tag{28}$$

As the matter of fact, it has been found that step (27) would be insignificant. On the other hand, the reaction between Cu^{2+} and hydrogen peroxide would stabilize copper at higher oxidation state, since in that case HO• would act as oxidizing agent. At pH = 8, the dominant oxidizing Cu(III) species would be $Cu(OH)_3$. While a reasonable agreement between predicted and experimental data was found, some limitations persist. The limitations are related to the negligible participation of HO• and also the extension of this model to more complex and realistic compositions. As an example, the presence of chloride would modify the rate constant values in the kinetic model and then their recalculation is necessary.

$$Cu^{2+} + HO• \leftrightarrows Cu(OH)^{2+} \hspace{3cm} (29)$$

$$Cu(OH)^{2+} + 2H_2O \rightarrow Cu(OH)_3 + 2H^+ \hspace{2cm} (30)$$
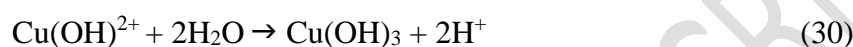
A key point in catalytic ozonation in the presence of Fe^{2+} is also related to the Fe^{2+}/ Fe^{3+} ratio which must be maintained at its highest level during the catalytic cycle. This condition has been verified in the oxidation of L-Rhodamine in the presence of molybdenum powder[79]. In practice, a solution must be found to lower the rate of Equation (22). The beneficial effect of molybdenum powder acting as cocatalyst can be due to the aforementioned high Fe^{2+}/ Fe^{3+} ratio. Indeed, metallic Mo^0 species can promote the reduction of Fe^{3+} to active Fe^{2+} further dispersed in the bulk of the solution whereas Fe^{3+} exhibiting a lower solubility remains at the surface. Jointly, Mo^{6+} oxidizes $O_2•^-$ to $^1O_2$. Further insights on the reaction mechanisms were obtained inthis study by using coumarin and benzoic acid for trapping HO• at the surface of Mo powder and in the aqueous solution. They found that in the absence of trapping agent, HO• can be preferentially reduced on the surface by metallic Mo species to $O_2•^-$. Its subsequent transformation to $^1O_2$, having longer lifetime, poses the question on the effective role played by $^1O_2$.

2.2.2. Implication of heterogeneous catalysts: Consequences on the kinetics and reaction mechanisms.

Many examples have used solid catalysts to promote the removal of organics in catalytic ozonation [35,80], CWAO [81-82], catalytic wet peroxidative oxidation [83], catalytic hydrodechlorination through wet peroxide oxidation[84]. Heterogeneous catalysts have also been employed to deal with mineral contaminants in water such as abatement of nitrates [46,85].

Reaction mechanisms involve nonradical intermediates adsorbed on the surface. Alternatively, heterogeneous catalysts can also activate the production of ROS. In this particular case heterogeneous and homogeneous catalytic processes can coexist and the prevalence of a reaction route will intimately depend on the operating conditions.

Impact of heterogeneous catalysts on ROS generation

Heterogeneous catalysts can generate reactive intermediates in higher selectivity through *in-situ* O_3 decomposition [86]. As a matter of fact, the advantages related to the introduction of heterogeneous catalysts are often related to faster generation of HO•. Heterogeneous catalysts also face significant drawbacks, such as in efficient ozone mass transfer in the porous of some solid catalysts[87]. It is also obvious that ozone activation and the overall degradation pathways of the organic contaminants by heterogeneous systems is more complex. Three general reaction mechanisms can be . Mechanism 1 considers the adsorption of ozone and subsequent production of ROS, while mechanism 2 assumes the adsorption of the organic contaminant with subsequent reactions with ozone and/or ROS and, finnaly, mechanism 3 would occur through coadsorption of ozone and the organic contaminants, competition for the same sites then inducing subsequent surface reactions.

For the catalytic ozonation of BPA by Fe_3O_4–MnO_2 magnetic composite[88], the authors suggested a weak adsorption of BPA in agreement with mechanism 1. They suggested water adsorption on Fe_3O_4–MnO_2 (M) with heterolytic dissociation leading to OH^- and H^+ which promotes the formation of hydroxyl groups at the surface. Ozone can further interact through adsorption leading to the production of reactive HO• radicals according to the following sequence:

$$M + H_2O \rightarrow M\text{-}OH^- + H^+ \tag{30}$$

$$M\text{-}OH^- + 2O_3 \rightarrow M\text{-}O_2\bullet^- + HO_3\bullet + O_2 \tag{31}$$

$$HO_3\bullet \rightarrow HO\bullet + O_2 \tag{32}$$

$$M\text{-}O_2\bullet^- + O_3 + H_2O \rightarrow M\text{-}OH^- + HO_3\bullet + O_2 \tag{33}$$
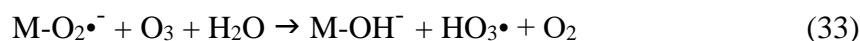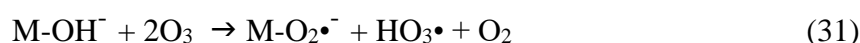
The superiority of heterogeneous catalytic processes over homogeneous counterpart in this specific case is related to a much higher concentration of HO• reaching 67.3 μmol/L after 30

min, whereas the concentration of HO• in the absence of heterogenous catalyst is 7.6 μmol/L. Even though the contribution of homogeneous process has been found insignificant for heterogeneously catalyzed systems, these authors mentioned that the presence of soluble Fe^{3+}/Fe^{2+} and Mn^{4+} can also activate the decomposition of ozone. It is worth notting that this sequence seems to support previous assumptions suggesting that $O_2^{\bullet-}$ could contribute to the production of hydroxyl radicals[61]. In the particular case of heterogeneous catalysts, $O_2\bullet$ would restore the $M-OH^-$ species.

In line with previous examples, a kinetic model for the catalytic ozonation of formic acid over iron oxide deposited on activated carbon considers the following steps: (i) formic acid adsorbed on the surface, (ii) O_3 interacts with the activated carbon leading to surface reactive oxygen species capable to oxidize adsorbed formic acid species, (iii) iron oxide at the surface favors the decomposition of ozone and (iv) the kinetics is not limited by the extent of adsorption of formic acid and then can involve equally the solid-liquid interface and/or the bulk solution[89]. In fact, it was found that pH conditions were a key parameter which can modify the chemistry of the catalyst surface and influence the homogeneous decomposition of ozone to ROS : (i) in acidic conditions the catalytic oxidation of formic acid is promoted, while (ii) at pH >7.5 the solid catalyst has no impact on the rate of oxidation. All the reaction pathways suspected of taking place in a wide range of pH are summarized in Figure 9.
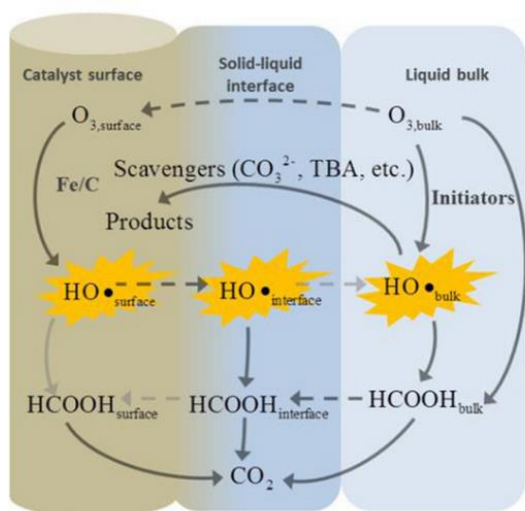
Figure 9. Reaction scheme depicting the mechanism of formate oxidation during catalytic ozonation. Reproduced with permission from ref [89]. Copyright 2020 Elsevier.

In a recent critical review [11], various scenarios for ozonation reactions have been envisioned when both the organics and O_3 become co-adsorbed and react according to a

Langmuir-Hinshelwood mechanism. An alternative considers an Eley-Rideal mechanism in which organic molecules adsorbed on the catalyst surface react with free solubilized ozone. The reverse configuration can also be assumed, adsorbed ozone reacting with organics in solution. In some case, more complex features must be taken into account. First adsorbed ozone on the catalyst functionalities can decompose to form $O_2^{\bullet-}$ and $HO^{\bullet}$ that can further react with ozone in solution and/or adsorb on the catalyst[90]. In addition, partial lixiviation of the heterogeneous catalyst releasing active elements in solution can also occur.

Let us continue with the removal of ibuprofen on Fe_2O_3/Al_2O_3@SBA-15[90]. In that case, mineralization involves predominantly reaction on the catalyst surface. The combination of *in-situ* ATR-FTIR and Raman spectroscopy, with EPR measurements led the authors to the conclusion that ozone preferentially chemisorbs on strong Lewis acid sites of alumina and becomes transformed into surface bounf $O_2^{\bullet-}$ and $HO^{\bullet}$ on Fe^{3+} Lewis acid sites. Subsequent attack of ibuprofen still occurs on the surface. Let us note that this proposal can be criticized. Indeed, in aqueous medium, Lewis acid sites can be easily hydrolyzed as earlier discussed in the Chapter 2.1. Hence, the debate can be opened regarding the real implication of Lewis acid sites as well as the accurate identification of reactive intermediates among all observed adsorbates.

Another example is given by the catalytic ozonation of oxalate coming from the degradation of organics in water and usually recognized as refractory molecule even in the presence of highly reactive $HO^{\bullet}$ radicals [91]. Palladium oxide supported on CeO_2 as catalyst provided interesting catalytic features with preferential adsorption of O_3 on PdO and oxalate on CeO_2, which means that the PdO interface with CeO_2 must be properly optimized to promote the subsequent reaction between surface O_{ads} and, surface adsorbed peroxide $O_{2,ads}$. Importantly, lattice oxygen vacancy at the surface of CeO_2 strengthens the stabilization of Pd^{2+} as evidenced by Raman spectroscopy.

Previous examples emphasize the relevance of adding H_2O_2 in the reaction medium to increase the concentration of active ROS. In practice, several investigations have reported the *in-situ* production of H_2O_2 in aqueous phase via the reduction of dissolved gaseous oxygen instead of direct use of expensive hydrogen peroxide. The higher efficiency of copper phosphide (Cu_xP) compared ro CoP for the removal of 4-chlorophenol in batch conditions has been proposed as evidence that Cu_xP acts as catalyst producing ROS [86].

Catalytic wet air oxidation

Catalytic wet air oxidation, operating at high partial oxygen pressure and temperature, differs from AOPs such as catalytic ozonation process. Basically, the efficiency of WAO involves as pre-requisite to enhance the solubility of oxygen. For phenol removal in the absence of catalyst, HO• radicals still represent the active ROS coming from the dissociation of hydrogen peroxide produced by reaction between phenol and oxygen. The addition of homogeneous catalysts allows to work under milder operating conditions. Phenol removal is a benchmark process that and can be achieved in the presence of copper [92] in the temperature range 40-110°C with oxygen partial pressure in the range 0.6-1.9 MPa. Suggested mechanisms still involve free radicals initiated by an electron transfer from Cu to phenol. However, in this specific case hydroxyl radicals do not participate, being replaced by ROH•$^-$ and ROOH•$^-$ as reaction intermediates.

Interesting mechanistic insights have been reported for the abatement of acetaminophen in water in the presence of ferrous ions and CuO [93]. A peculiarity is related to the relative efficiency of such system in acidic conditions, while most of examples report a deactivation in these pH range. It was found that 30% of the acettaminophen is mineralized at pH = 3. These authors related this result to the synergistic effect between CuO and Fe(II) which led them to the conclusion that Fe(II) adsorbed on CuO are more active than Fe(II) in the bulk solution. The proposed mechanism scheme for the production of HO• radicals is presented in Figure 10.
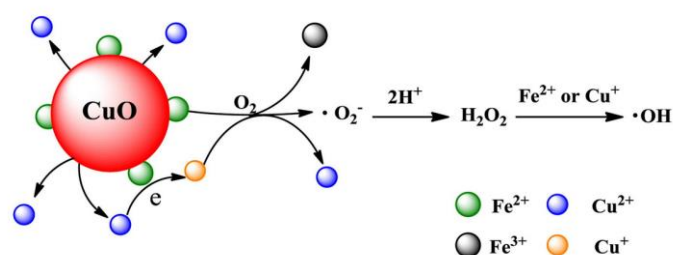
Figure 10. Schematic illustration of the ROS generation by Fe(II)/CuO resulting in the degradation of acetaminophen in acid pH. Reproduced with permission from ref. [93]. Copyright 2017 Elsevier.

Adsorbed Fe^{2+} is able to reduce O_2 to •O_2^- and Cu(II) (in CuO) to Cu(I). Once formed Cu(I) can play the role of electron mediator in the production of H_2O_2 and subsequent decomposition to HO•.

Copper-based catalysts have attracted the attention of many investigators due to their redox properties comparable to that exhibited by iron. Generation of radicals from the decomposition

of H_2O_2 has been widely studied, where using Cu^{2+} stabilized in different matrixes as active sites.[69] In some cases, Cu and Fe can be combined in the same MCM-41 matrix[94].

2.2.2.2. Impact of heterogeneous catalysts with alternative reaction pathways involving exclusively neutral adsorbed intermediates

Compared to catalytic wastewater treatments involving the generation of ROS as major intermediates reacting in adsorbed phase or in the bulk solution, it appears that heterogeneous catalysts in which reactive intermediates are only neutral adsorbed species are less studied. Among, the most investigated, the CWAO of ammonia and the reduction of nitrates can serve as relevant examples because these two inorganic pollutants are undesirable in water and cause environmental concerns. Nitrates comes from intensive usage of fertilizers. Also, different direct and indirect ammonia streams can be identified coming from industry, agriculture and also from the abatement of N-containing as illustrated in scheme 2 [64] Accordingly, particular attention was paid to ammonia oxidation and nitrate reduction.

Numerous investigations dealt with nitrates reduction especially in drinking water [95-100]. Hydrogen is useful to convert nitrates selectively to nitrogen. In practice, a major drawback lies in the over reduction leading to the formation of undesired ammonia as exemplified in scheme 2.
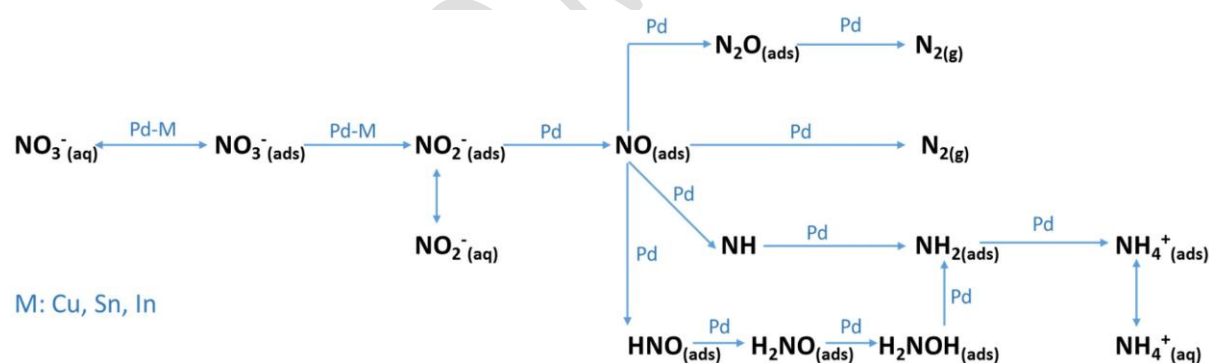
Scheme 2. Mechanism of the catalytic nitrate reduction over bimetallic catalysts. Reproduced with permission from ref.[100]. Copyright 2017 Elsevier.

Earlier kinetics investigations of nitrate reduction by hydrogen on Pd-Cu/γ-Al$_2$O$_3$ in the range 7-20°C led to the suggestion of a Langmuir-Hinshelwood mechanism where nitrate and hydrogen adsorption are at equilibrium and noncompetitive. Afterwards, a bimolecular surface reaction between adsorbed nitrates and hydrogen species was proposed. The following rate equation (34) can be established leading to a good agreement between experimental and predicted rates [101].

$$r = -\frac{d[NO_3^-]}{m\,dt} = \frac{kK_{H2}^n P_{H2}^n K_{NO3}[NO_3^-]}{(1+K_{NO3}[NO_3^-])(1+K_{H2}^n P_{H2}^n)} \qquad (34)$$

where k stands for the rate constant, K the equilibrium constant, $[A_i]$ the concentration of the reactant A_i, m the mass of catalyst and n refers to the number of adsorbed hydrogen molecules.

On the other hand, some contradictions have arisen with other investigations on the same reaction studied on monolith reactor washcoated with alumina containing 2.0 wt% Pd and 1.4 wt% Cu. In that case an Eley-Rideal mechanism has been privileged which neglects nitrate adsorption whereas dissociative adsorption of hydrogen has been assumed in the kinetic model[102].

Finally, recent kinetic investigation of nitrites on Pd/γ-Al$_2$O$_3$ [103] performed in a semi-batch slurry reactor at atmospheric pressure in wide operating conditions led to reaction order values with respect to the concentration of hydrogen and nitrites varying respectively in the range 0.3-2 and -0.4-0.9. A predominant production of nitrogen in comparison to ammonia was observed. Such results have been explained according to a Langmuir-Hinshelwood mechanism assuming competitive reactions on palladium sites and the formation of NH via dissociative hydrogenation of HNOH as rate-determining step. The formation of nitrogen would occur predominantly through a bimolecular reaction between NH and NO, NOH or HNOH whereas dimerization of adsorbed NO or adsorbed N would not be significant.

Ammonia is produced in various applications and can form as undesired side product during the mineralization processes[104]. Thermodynamic considerations of the equilibrium between soluble/gas ammonia and speciation in liquid phase is an important issue and is a preliminary step before establishing reliable kinetic model[105]. It has been found that the fraction of solubilized ammonia largely exceeds that ammonium ions which could explain the high efficiency of catalytic wet oxidation reaction process because ammonia in its molecular form is more reactive than NH_4^+. As already indicated, CWAO needs more severe conditions compared to ozonation conditions with temperature in the range 150-320°C and higher pressure in the range 0.5-20 MPa to increase oxygen dissolution in water and fulfill coverage conditions in terms of adsorbed oxygen species[104]. The kinetics of this reaction is favored on transition metal oxides. The plot of ammonia conversion as a function of the heat of formation of the oxides (Figure 11) exhibits a typical volcano-type curve highlighting Ru/Al$_2$O$_3$ as a benchmark for ammonia oxidation[106]. Such evolution emphasizes the importance of the rate of ammonia conversion according to the Metal-O bond strength depending on the surface O concentration

and the reactivity of O species decreasing when the surface becomes more stable. Both activity and selectivity exhibit the same volcano-type curves emphasizing $NH^{\star}$ as key intermediate in the formation of N_2 according to the following suggested mechanism:

$$O_2 + 2\star \rightarrow 2O^{\star} \qquad (35)$$

$$NH_3 + O^{\star} \rightarrow NH^{\star} + H_2O \qquad (36)$$

$$NH^{\star} + O^{\star} \leftrightarrows HNO^{\star} + \star \qquad (37)$$

$$NH^{\star} + HNO^{\star} \rightarrow N_2 + H_2O + 2\star \qquad (38)$$

$$HNO^{\star} + O^{\star} \leftrightarrows HNO_2^{\star} + \star \qquad (39)$$

$$HNO_2^{\star} \leftrightarrows NO_2^- + H^+ + \star \qquad (40)$$

$$NO_2^- + O^{\star} \leftrightarrows NO_3^- + \star \qquad (41)$$
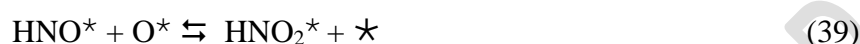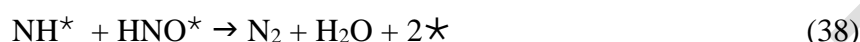
Let us note that the production of undesired nitrates would be also favored at high surface oxygen concentration. In practice, significant evolution takes place in the course of the reaction due to the generation of H^+ through step (40). Accordingly, the dissociation equilibrium between NH_3 and NH_4^+ shifts toward the production of NH_4^+ which contradicts previous explanations and emphasizes a predominant stabilization of ammonium ions. It is also obvious, that this explanation disagrees with the above-mentioned reaction sequence emphasizing ammonia as reactive species with alkaline conditions as pre-requisite to stabilize this species[106].
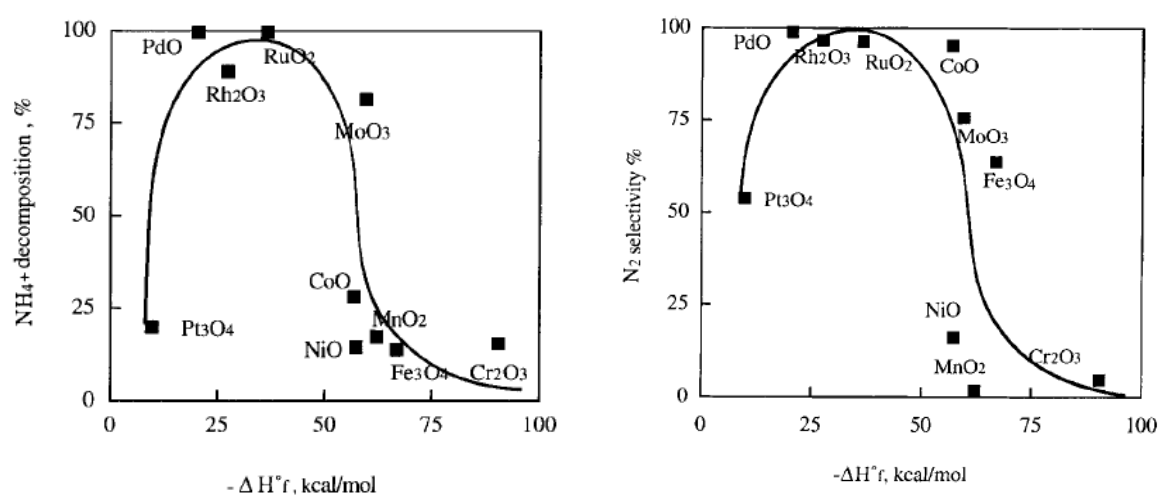
Figure 11. Plot of percentage decomposition of ammonia and selectivity to nitrogen production versus the heat of formation of metal oxide of the most stable oxidation state per gram atom of oxygen ($-\Delta_f H^0$. $[NH_4^+]$ = 1500 ppm (pH = 12.3), air feed pressure = 1.5 MPa (at 25°C), M/Al$_2$O$_3$ = 4 g, reaction temperature = 230°C. Reproduced with permission from ref [106]. Copyright 1998 Elsevier.

It is worthwhile to notice that the above-mentioned mechanism has been criticized. Indeed, the formation of nitrogen from catalytic wet oxidation of ammonia on Ru/TiO_2 has been predominantly ascribed to a reaction in aqueous phase between NO_2^-/NO_3^- and NH_4^+ according to steps (42) and (43)[107]. Such steps have been further confirmed in slightly acidic conditions[108].

$$NO_2^- + NH_4^+ \rightarrow N_2 + 2H_2O \tag{42}$$

$$3NO_3^- + 5NH_4^+ \rightarrow 4N_2 + 9H_2O + 2H^+ \tag{43}$$
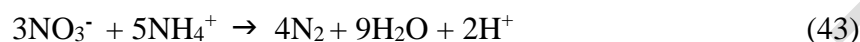
As a matter of fact, it was recently found that step (38) at the surface of the catalyst and the reaction between NO_2^- and NH_4^+ to produce N_2 coexist but this latter one becomes more predominant when pH decreases[109].

2.2.3. Strategies and methodologies for the identification of unstable reactive species in the bulk solution and at the surface of heterogeneous catalysts

2.2.3.1. Detection and quantification of reactive radical oxygen species.

As exemplified in Equation (10) accurate kinetics modeling implies a correlation between the rate of degradation of the contaminant and the evolution of the concentration of the reactive oxygen species in aqueous phase. In practice, the direct quantification of HO• is not feasible. Up to now spectroscopic techniques or other analytical techniques provide only indirect information when HO• radicals are trapped into neutral and stabilized adducts[110-111]. EPR technique has been widely used for the identification of reactive oxygen species among those produced from the decomposition of ozone, *i.e.* $O_2 \bullet^-$, $HO_2 \bullet$, HO• and $^1O_2$ [79,112-113]. This technique is characterized by a high selectivity and sensibility with limit of detection for concentration in the range 10^{-14} mol/L. In practice HO• has been recognized as the most efficient oxygen species. Spin trapping agents are currently used due to the fast reaction of HO• leading to more stable species compatible with the EPR time-scale detection. The contribution of $HO_2 \bullet$ on the EPR signal can be differentiated in the presence of methanol for quenching DMPO-OOH. $HO_2 \bullet$ in equilibrium with $O_2 \bullet^-$ is in principle less reactive with a lower oxidation potential (~0.6 V vs. 2.73 V for HO•) but could play an essential role for the production of HO•[61]. Nevertheless, some interferences might perturb the EPR signals especially in the presence of O_2 and O_3 which can partly oxidize the trapping agent to generate electron spinning

signals and then leading to misleading quantifications[61]. A recent review paper emphasized improper methods for quenching tests related competitive undesired reactions between the spin trapping agent and radicals[12]. Among the panel of spin trapping agents, 5,5-dimethyl-1-pyrroline-N-oxide (DMPO) is widely used containing β-hydrogen and nitroxide nitrogen which can react to form DMPO-OH adduct. The kinetics of the formation appears as a key parameter to obtain reliable EPR measurements and must be accelerated in the presence of much larger DMPO concentration and fast spin trapping[113]. Theoretical models have been developed to investigate the reactivity and stability of DMPO-OH which must be improved[114]. A mechanism scheme has been derived which explains the different steps involved in the degradation of DMPO and DMPO-OH leading to the production of diamagnetic intermediates species (3) and (4) in Scheme 3. In fact, reliable EPR measurements can be obtained when the DMPO concentration is 20 and 200 times than the concentration of H_2O_2 and Fe^{2+} respectively. Disturbances of the EPR spectra appear in case of such conditions are not fulfilled with the superimposition of a triplet signal assigned to paramagnetic dimers in comparison to the characteristic quartet signature assigned to DMPO-OH.
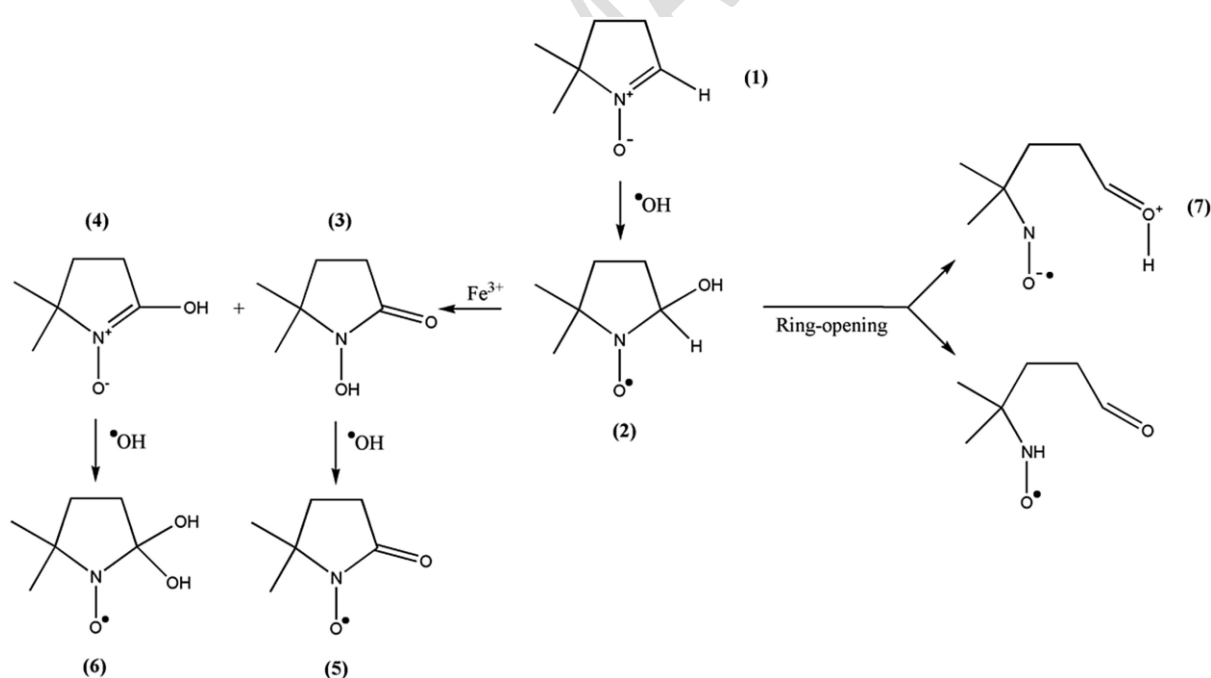
Scheme 3: General oxidation and degradation pathways of DMPO (1) and DMPO-OH (2). Reproduced with permission from ref [114]. Copyright 2016 Elsevier.

While numerous papers proved the relevance of EPR measurements, due to its sensitivity and selectivity, most of them deal with qualitative approaches in the detection of ROS. Only a few of them tackle quantitative methodologies [112,115]. The combination of EPR technique, rapid

data acquisition systems and stopped flow system allow the investigation of the direct generation of HO• radicals and the accurate calculation of k_{ROS} in Eq. (1). Such methodology has been implemented in the course of the abatement of 3-chlorophenol by ozone[112]. The initial rate for the formation of DMP-OH is given by the following expression:

r_0 (10^{-6} mol/L/s) = (9.7×[3-chlorophenol(10^{-9} mol/L)] + 0.0005) ×exp(57×[ozone(10^{-9} mol/L)]

In practice, this allows to optimize a dosage strategy for ozone introduction.

Recent advances have been pointed out in the particular case of the development of heterogeneous catalytic ozonation processes for water treatment emphasizing several technical problems in the detection of reactive intermediate from *operando* techniques related to the adaptation of the reactor design to the spectroscopic techniques[12]. Also, the coexistence of radical- and non-radical processes occurring in the bulk of the solution and at the surface of the catalysts leads to more complexity in the development of reliable strategies to relate the rates of organics degradation to the functional groups on the surface of the catalysts. Another drawback has been recently pointed out related to fact that EPR cannot detect and differentiate HO• at the surface compared to HO• dispersed in solution[79]. Nevertheless, this technique is still extensively used in case of heterogeneous catalytic ozonation to identify HO• and $O_2^{\bullet-}$ on graphene doped with N, P, B and S[116]. Recent investigations of the electroreduction of oxygen on Pt nanoparticles also identified HO• as unique reaction intermediates by coupling spin-trap EPR and electrochemical analysis[117].

In-situ EPR measurements have been also implemented to clarify the heterogeneously catalyzed decomposition of hydrogen peroxide on cobalt and copper hydrogel containing Cu(II) and Co(II) active centers coordinated to aliphatic amine, N-heterocycle, and/or carboxylic acid ligands. Reactive oxygen species from H_2O_2 have been characterized by spin trapping with DMPO. On the Co(II) system the main detection of O_2, $O_2^{\bullet-}$ associated to pH lowering can be explained by step (44) whereas step (45) takes place on Cu(II) system[118]. It was also observed that the ligand -NH_2 combined with high density of copper centers represents the best compromise in terms of production of HO•. On the other hand, at low density -COO^- outperforms all the other systems.

$$2\ H_2O_2 \leftrightarrows O_2^{\bullet-} + O_2 + 4H^+ + 3e^- \qquad\qquad (44)$$

$$4\ H_2O_2 \leftrightarrows O_2 + 2OH^\bullet + 2H_2O_2 + 2H^+ + 2e^- \qquad\qquad (45)$$
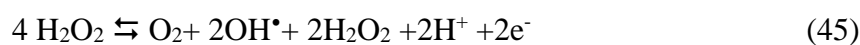
Other investigations also pointed out the relevance in the generation of HO• radicals from oxygen instead of H_2O_2 assisted by nanoporous activated carbon as heterogeneous catalyst. The thermodynamics and kinetics were investigated. A first order kinetic is observed with optimal conditions at pH = 6 and 20°C leading to a rate constant of 8.9×10^2 min^{-1} and activation energy of 8.67 kJ/mol. This process was found slightly thermodynamically favored with Δ_rH and Δ_rS values of respectively 17.73 kJmol^{-1} and 61.01 J mol^{-1}K^{-1} [119].

In-situ investigation of adsorbed species on catalyst functionality: Implication of these ad-species in the reaction mechanism and related catalyst functionalities

Few studies investigated the response of catalytic surface in the course of ozonation reaction. For instance, IR observations reported significant exchange between O_3 and OH groups resulting in significant attenuation of the signal assigned to surface OH groups of the catalyst. Such perturbations have been assigned to O_3 adsorption on Lewis acid sites compared to experiments performed in gas phase[120]. Such information can be complemented by *in-situ* Raman observations since the presence of O atomic species coming from ozone decomposition can originate Raman lines near 913 and 938 cm^{-1}.[91]

ATR-FTIR experiments can be useful in the identification of adsorbed species on heterogeneous catalysts. Even though, *in-situ* investigations are scarcer for liquid-solid systems compared to gas-solid systems relevant information can be obtained. Some relevant mechanistic insights were obtained from the characterization of NO_2^-, NO, NH_2 and NH_4^+ species and their evolution under reaction conditions [121-122]. First important information is related to the differentiation of NO_2^- adsorbed at the surface and in the bulk solution. Subsequent reduction of NO_2^- to NO adsorbed[123-124] on Pd is characterized by a blue shift 1705-1720 cm^{-1} which reflects the coverage dependency of the strength of adsorption bond[121]. Separate experiments from hydroxylamine adsorption complement the reaction mechanism showing a fast disproportionation to detectable IR active NH_3 and N_2O species[122]. Appropriate methodologies for conducting these *in-situ* experiments led the authors to the conclusion that NO_{ads} is not involved in the production of N_2 which would occur predominantly according to step (18) while ammonia production would involve step (19) leading to a revised version of reaction in scheme 4.
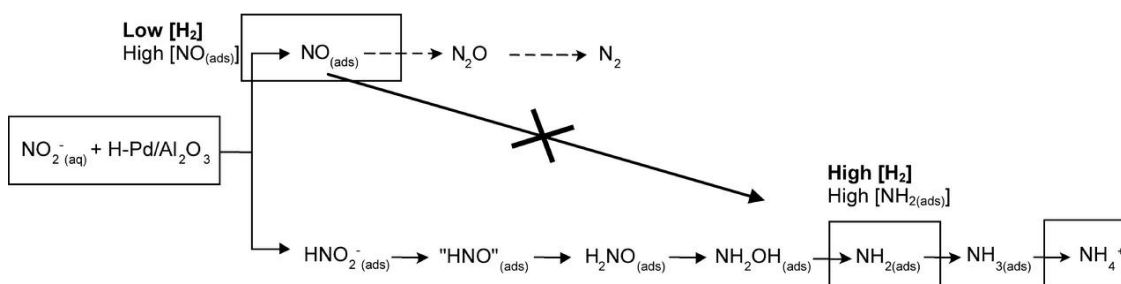
Scheme 4. Improved reaction scheme of the catalytic hydrogenation of nitrite over Pd/Al$_2$O$_3$. The reactions in the boxes are based on the findings in the present paper. The dotted lines represent possible reaction pathways for N$_2$O and N$_2$ formation. Reproduced with permission from ref [121]. Copyright 2008 Elsevier.

2.2.3. Implementation of DFT calculations

Many examples in heterogeneous catalysis emphasized the usefulness of theoretical calculations especially from the Density Functional Theory. We must also point out that their relevance is proven and credible when they are preferentially combined to experimental approaches[61]. Presently, most of the developments are focused on the electronic properties of catalyst surfaces and electron distribution in connection with the calculation of adsorption energies[125]. Such calculations can be useful to check if set of atomic orbitals and their related orientation can properly activate the reaction. One question derived from these theoretical investigations is if they are able to provide new guidelines for developing active surface or guide experiment design?[126-127]

It has been found that the catalytic activity of α-MnO$_2$ is intimately related to the concentration of surface defects.[128] DFT calculations of adsorption energy on (110) surface does not provide decisive arguments for preferential ozone adsorption energy compared to those computed for O$_2$ and H$_2$O adsorption of respectively -0.44 eV, -0.71 and -0.59 eV respectively. On the other hand, the inclusion of oxygen vacancies sharply decreases the adsorption energy of ozone while they remain quasi-unchanged for O$_2$ and H$_2$O. In practice, the level of formation of surface anionic vacancies can be monitored by the ratio Mn^{3+}/Mn^{4+} which could be a good criterion for the selection of appropriate preparation method.

Theoretical calculations can also explain synergistic effects on the reaction rate when two metals are combined. The catalytic reduction of nitrophenol in aqueous phase reveals enhanced activity on 2wt.%Ag@Pt/sepiolite core-shell structure compared to single metal Ag/sepiolite and Pt/sepiolite ascribed to an electron redistribution from Ag to Pt. [129]

Despite the reaction scheme for nitrate reduction being quite simple with a two-step reduction involving the intermediate formation of nitrites, the detailed reaction mechanism illustrated in scheme 4 appears more complex involving a large number of adsorbed intermediates some of them not yet experimentally identified. DFT calculations can provide the most probable pathways through the stability of active intermediates. This is illustrated in Figure 12 where two intermediates from the hydrogenation of adsorbed NO can be equally envisioned via the O and N atom. The route involving NOH* corresponds to a much higher energy revealing its instability and leading the authors to privilege the pathway with *HNO. The power of DFT calculations is to verify from these energetic profiles possible reaction intermediates. So, a parallel pathway for explaining ammonia formation would involve the dissociation of NO* to N* and O* energetically favorable (see Figure 13)[130].
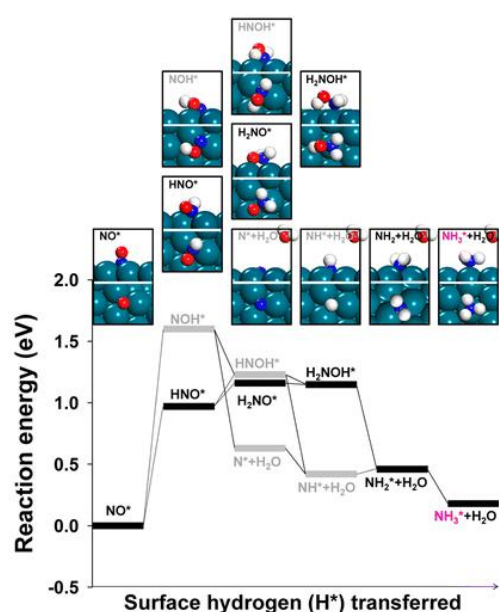
Figure 12. Reaction energy diagram for the hydrogenation pathways of NO* on the Pd(111) surface. This pathway preferentially yields NH₃. Reproduced with permission from ref [131]. Copyright 2014 American Chemical Society.
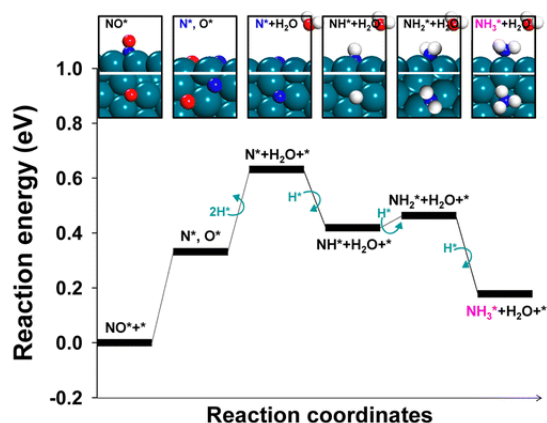
Figure 13. Reaction energy diagram for the decomposition of NO* followed by sequential hydrogenation on the Pt(111) surface. Although the direct combination of N* can yield N_2, the hydrogenation of N* to yield NH_3 is more plausible because the migration barrier is substantial. Reproduced with permission from ref [131]. Copyright 2014 American Chemical Society.

DFT calculations also offer some guidelines through the examination of the thermodynamics and kinetics providing prospects for optimizing catalytic processes. A representative example can be given illustrating the potential interest in using $CO_2^{\bullet-}$ instead of hydrogen to reduce nitrates in water and avoid undesired ammonia production. Up to now most of catalytic abatement processes privilege hydrogen as green reducing agent. Recent investigation pointed out an alternative route free of ammonia production using $CO_2^{\bullet-}$ as reducing agent produced from HCOOH under UV irradiation. However, starting from nitrates, the reduction to N_2 is incomplete and stopped to NO and N_2O [85]. Calculations of Gibbs free energies and activation energies showed that the first step is not thermodynamically favored and exhibits a high activation barrier. From, these information, the authors changed their strategy by using Zn/Ag bimetal to reduce nitrates and then a quasi-complete reduction of nitrites to nitrogen was insured by $CO_2^{\bullet-}$. Another example illustrating the potentialities of DFT calculations provides rationalization about the role of Cu^+ in supported bimetallic Pd-Cu particles. Calculations indicate that nitrate adsorption occurs preferentially on Cu^+ due to a stronger adsorption than on Pd^0. By contrast, H_2 dissociates on Pd^0 which insures the reduction of nitrates[134]. During the catalytic cycle, Cu^+ transformed to Cu^{2+} can be restored through reduction with H_{ads} on Pd.

In a last example, theoretical calculations based on the frontier molecular orbital theory clarified the controversies arising in the steps involved in the production of nitrogen in the catalytic wet oxidation of ammonia showing that the symmetry of the HOMO for NH_4^+ matches with the LUMO of NO_2^- leading to the production of nitrogen[108].

2.2.5. Kinetic modelling of complex media

Most of kinetic models are developed at lab-scale in simulated conditions taking simple reaction media into account far from the compositions of real wastewater stream containing several unstable contaminants and/or refractory molecules. In such case the study of the individual kinetics for each contaminant is not easy. Indeed, a large number of reactions and intermediates must be considered. The robustness of simplified kinetic model must be verified in various conditions, *i.e.* batch or continuous reactors running in a large range of operating conditions such as subcritical or supercritical water conditions. A lumped kinetics has been examined starting from a generalized lumped kinetic model and including the specificities of the surface catalytic functionalities thanks to Langmuir-Hinshelwood-Hougen-Watson mechanism. [132] Accordingly, fitted kinetic and equilibrium constant are physically and chemically consistent and in good agreement between predicted and experimental measurements. Nevertheless, it is sometimes not easy to generalize such kinetic approaches because the real implication of the catalyst functionalities can be questionable. For instance, the kinetics of the catalytic ozonation on MnO_2 of six emergent contaminants showed some difference in their reactivity towards ozone, *i.e.* gemfribrozil, diclofenac acid, benzafibrate, dichlorophenoxyacetic acid, ibuprofen, clofibric acid and *p*-clorobenzoic acid. [133] A general kinetic model has been developed based on a second order kinetics with O_3 and HO• which correspond to previous Eq. (10). In case of significant contribution of heterogeneous catalysis, a third terms should be in principle added to this equation corresponding to $k_{catal}[C]$. Preliminary observations were reported on synthetic water where the introduction of MnO_2 speeds up the decomposition of ozone thanks to the presence of surface hydroxyl group bonded to Mn^{3+}. In this study, the catalyst is seen as a HO• promoter by accelerating the decomposition of O_3 rather than a promoter of active adsorbed intermediate from the adsorption of the contaminant on a catalytic functionality, which led the authors to neglect $k_{catal}[C]$ in the overall rate equation. Such assumption seems to be in reasonable agreement with earlier observations which consider the catalyst as a promoter of ROS[128]. Nevertheless, in case of porous catalytic materials exhibiting high adsorption capacity this simplified model could largely underestimate the removal efficiency. The remaining question is related to the preservation or saturation of this adsorption capacity after extended operation and if a reasonable assumption in neglecting $k_{catal}[C]$ matches with experimental data. Clearly, more sophisticated models should be taken

into account in the former case including adsorption, surface reaction and diffusion. The use of a non-porous catalysts of which functions would be mainly to promote the decomposition of ozone would probably give a better fit in the particular case of the selected example, but cannot be generalized to all heterogeneous catalytic systems. Other examples of catalytic wet air oxidation examples, performed in batch conditions using Ru/TiO_2 demonstrated a much higher mineralization compared to non-catalyzed system[134]. An interesting dissertation is reported on the opportunity to include true kinetics in typical lumped kinetic model with high complexity, which finally could represent a weak practical interest. In their model, Pintar *et al.* studied the kinetic of the total organic carbon based on a simplified triangular lumped kinetic model which accounts for a direct mineralization of the organic matter to CO_2 and H_2O and a sequential pathway involving the intermediate formation of acetic acid further transformed to CO_2 and H_2O. A set of second order differential equations was found to correctly model the concentration profile vs. time which account for the temperature dependency of the rate constants.

An important consideration is often neglected in most of studies, *i.e.*, the impact of deactivation and how to integrate this deactivation in the calculations of the rate constant values. As reported, poisoning and active sites overcoat by precipitation can be more detrimental on the catalyst activity than mass transfer phenomena[135].

2.3 Challenges and new concepts in the development of multiphase Gas-Liquid-Solid reactors

This chapter deals with the development of homogeneous and heterogeneous reactors in line with chapter 2.2. The evolution in the implementation of structured reactors based on new conceptual ideas is also described which account for inherent drawbacks related to three-phase reactors. The technologies related to the development of more complex hybrid reactors for combined treatment processes will be mostly described in dedicated sections of the following chapters 3 and 4.

2.3.1. Current reactor technologies: advantages and drawbacks in the particular case of triphasic systems

The optimization of multiphase catalytic reactors for improving their efficiency is a challenging task. Improving the intrinsic surface properties of the catalyst is insufficient. A key point lies in the contact between the different phases and further improvements are needed to find strategies able to reduce the interfacial tensions. Minimization of mass transfer by advanced mixing technologies and shorter diffusion pathways in porous structure is of prime importance. These criteria can serve as guidance in future developments of more efficient catalytic technologies based on smaller reactors and the combination of functionalities in the reactor. The development of new generation of catalysts and reactors more efficient in the removal of recalcitrant water pollutants could help in scaling down industrial units with smaller size reactors. Such opportunity could ease the transfer of technology from lab-scale reactors to macro-scale reactors. Presently, lab-scale does not give an exact replica of the operation of pilot and/or industrial reactor. Hence, the opportunity to develop smaller industrial units could contribute to lower the existing limitations to replicate comparable performances and to speed up the development of efficient systems for recalcitrant contaminants.

Generally, in most cases fixed-bed flow reactors and fluidized-bed reactors are widespread in petrochemical and bulk industry[136]. In the particular case of catalytic abatement of water contaminants the debate in the selection of the best technical approach, three-phase batch vs. continuous flow reactors is still unclear even though the treatment of large flow volume at industrial scale gives *a priori* some advantages to flow reactors. Some examples are illustrated in the literature showing the superiority of continuous flow reactors in the catalytic hydrodechlorination of 2,4-dichlorophenol on Pd/Al_2O_3[137] (Figure 13). This superiority was attributed to (i) rate and selectivity enhancement to phenol due to a better H_2 transfer related to an extended gas-liquid interface and (ii) faster release of HCl at the surface improving catalyst lifetime.

Despite the advantages provided by fixed bed flow reactors in terms of activity, selectivity, and stability and the disadvantage for batch reactors linked to higher liquid-to-catalyst ratio[16], there is no systematic consensus likely due to the complexity associated to the control of hydrodynamics of pilot continuous flow reactors, which governs their global efficiency. Investigations at different scales notably at lab-scale can show significant deviations in their behavior with unexpected CSTR behavior for plug flow reactors which diverge from usual behavior of macro-scale reactors[138]. Operating parameters such as liquid flow rate, *i.e.* time residence of the contaminant, reactor design, and aeration directly influence the hydrodynamic behavior of the reactor. The liquid flow rate was found to be a critical parameter. One can expect at lab-scale that a rise in liquid flow rate in continuous flow reactor could shift the behavior from CSTR to a plug flow reactor. Additional constraints also appear inherent to the small size of lab-scale reactors which implies catalyst

particles very small to fit the ratio between the reactor diameter and grain size diameter currently encountered in pilot and industrial catalytic reactors. Similarly, some deviations can appear regarding the length of the catalyst bed-to-the grain size diameter. The current lower speed velocity of liquid flow in lab-scale reactors to meet the residence time of industrial ones can allow backmixing of the liquid phase which deviate from typical plug flow reactor behavior. Different behaviors also characterize down-flow or upflow mode for trickle-bed flow reactors with poor wetting of the catalyst and backmixing in the former case. On the other hand, the upflow mode insuring a quasi-complete wetting can lead to the formation of stagnant zone that could seriously alter the chemical kinetics. The non-uniformity for liquid distribution inside packed bed can affect the reaction rate for catalytic wet oxidation of phenolic contaminants.[139] Their prediction by using an Eularian CFD model in unsteady state operating conditions led to the detection of backmixing phenomena and validated with good confidence experimental observations preferentially at high temperature. A solution connected to the functioning mode of reactor, *i.e.* upflow vs. downflow mode, has been suggested to overcome such limitations consisting in dilution technique by using smaller size of diluent[140-141].
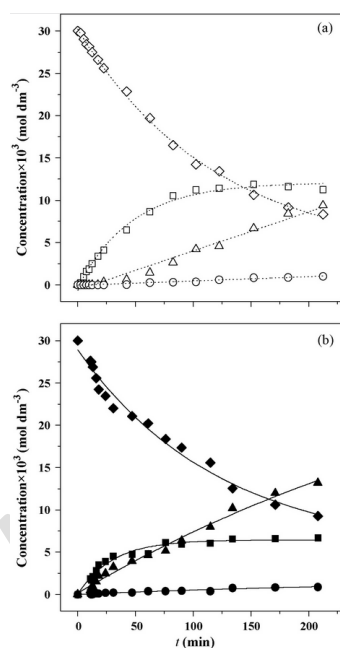
Figure 14. Concentration profiles on Pd/Al$_2$O$_3$ vs. times for 2,4-DCP (♦,◊), 2-CP (□,■), phenol (△,▲) and cyclohexanone (○,●)) in (a) discontinuous (open symbols) and (b) continuous (solid symbols) operation. Reprinted with permission from ref [137]. Copyright 2011 Elsevier.

The choice of the best technology lies in various criteria related to intimate contact between the different reactants in liquid and gaseous phase with the catalyst surface. Indeed, they can

drive the efficiency in terms of conversion and selectivity. Other parameters must be also kept in considerations related to the treatment of concentrated industrial wastewater which can contain particulate leading to catalyst fouling [142-144].

The abatement of mineral and organic contaminants must be effective with the absence of inherent toxicity for the reaction products. In practice, several parameters must be considered in the selection of the best available technology which account several drawbacks and advantages: – Separation of catalyst from the reaction products is uneasy for suspension reactors – Intensive mixing is also needed for this type of reactor to hinder mass transfer limitations, *i.e.* diffusion on the gas in the aqueous phase and also diffusion of the reactants at the surface of the catalysts. This implies for heterogeneous catalysts to develop a high mechanical shear force – The size of the catalyst grain must be also lowered to minimize internal mass transfer phenomena. Batch reactors and stirred tank reactors present significant advantages with homogeneous distribution of the reactivity and high residence time to ensure complete conversion of the water contaminants characterized by low concentrations and slow kinetics. This type of reactor is usually privileged in case of systems homogeneously catalyzed due to the absence of diffusion processes. For heterogeneously catalyzed systems, fixed bed reactor, *i.e.* trickle bed reactor, with catalyst bed immobilized inside the reactor can be more efficient then requiring lower volume.

2.3.2. Impact of wettability on catalyst efficiency

Mass transport of the reactants in triphasic catalytic systems is of major concern to optimize their performance in terms of activity and selectivity. Indeed, the solubility of gaseous hydrogen or oxygen in water is usually much lower than soluble ionic/organic species which means that gradient concentrations can occur at the vicinity of the active sites which may lower their efficiency. As previously presented, optimal conditions are sometimes needed because of opposite effects can occur when hydrogen diffusion is improved for reduction reactions[145]. It is particularly true for nitrates reduction by hydrogen because a faster hydrogen diffusion will increase the turn-over number of active sites, but jointly will inevitably deteriorate the selectivity behavior with enhanced production of undesired ammonia. As the selectivity is governed by the N/H ratio, *i.e.* by the residual hydrogen pressure[146], then an optimal concentration of nitrates and hydrogen must be found. In a first attempt, slight increase of the turn-over frequency was observed on Pd/γ-Al$_2$O$_3$ partly hydrophobized. In practice, Pd/γ-Al$_2$O$_3$ was mixed with γ-Al$_2$O$_3$ silylated by perfluorinated octyltrichlorosilane[146]. This result can be

rationally explained when the H_2 gas bubbles directly in contact with a surface partly hydrophobized diffuse more easily, while the hydrophilic part of the catalyst would favor the transport of nitrates species. However, an alteration of the selectivity with improved production of ammonia instead of nitrogen can occur resulting from this faster hydrogen diffusion. Nonetheless, an alternative was found by working at lower partial hydrogen pressure ahich allowed to reach the optimal N/H ratio to minimize ammonia formation [147].

This concept of wettability through the promotion of hydrophobicity has been previously verified on Pd/SiO$_2$ with selectivity improvement on silylated catalysts in the hydrogenation of aromatic ketones by preventing the consecutive production of saturated alcohol[148]. While the resistance of mass transfer phenomena can be still minimized, the authors privileged an alternative explanation which refers more to the impact of silylation on the adsorptive properties of Pd particles with ease of weakly bonded unsaturated alcohol to desorb from the Pd surface. It is worthwhile to note that this explanation could not completely match the changes observed on the selectively in the course of nitrate reduction on Pd/γ-Al$_2$O$_3$ if we agree that the subsequent hydrogenation of N$_{ads}$ to ammonia from a fast NO dissociation requires a strong adsorption on Pd sites.

2.3.3. Development of structured reactors

Catalytic Membrane reactor

The use of membrane reactors can be an alternative particularly to improve the diffusion of one reactant compared to each other. The inclusion of membrane can improve the efficiency by favoring the contact between the reactant and the active sites and also preventing undesired reactions. But to take advantage of this strategy particular attention to specific pre-requisites in terms of pores, thickness of the membrane, and stability in the reaction medium must be paid. By way of illustration, in case of polymer membranes a deterioration can be related to oxidation and polymeric chain scission which can induce a loss of its mechanical properties[149]. As aforementioned, the regulation of hydrogen through a careful monitoring of the gradient pressure across the catalytic thickness could be a relevant approach[150]. The example of Figure 15 illustrates a reactor composed of a porous steel membrane as substrate for the growth of carbon nanofibers encapsulated in a gas permeable coating. These microreactors develop high mechanical strength and specific surface area. The authors found high efficiency to reduce nitrites in the presence and in the absence of precious metals. They also demonstrated that the supply of hydrogen was not needed the carbon material acting as reducing agent.
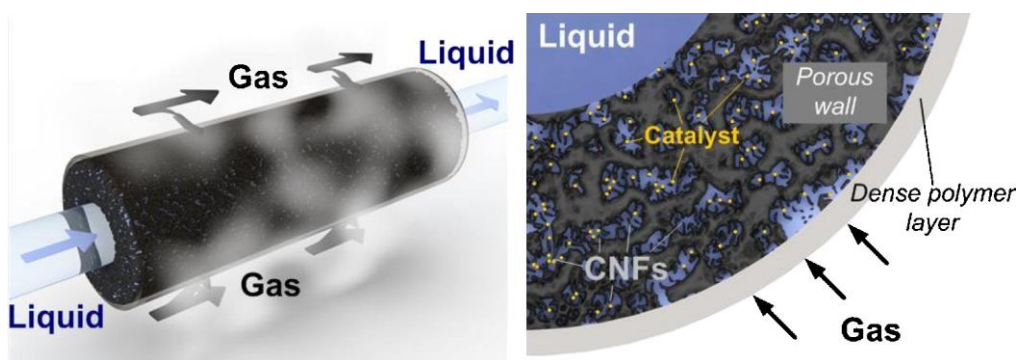
Figure 15. Porous metallic membrane microreactors for multiphase nitrate reduction reaction. Porous stainless steel membrane as support decorated with carbon nanofibers (CNFs). The reactor is encapsulated with a selective, gas permeable PDMS layer. Reproduced with permission from ref [151]. Copyright 2011 Elsevier.

Two-stage membrane bioreactors were found efficient at 20°C avoiding the production of nitrite and ammonia during nitrate abatement with low membrane fouling[152]. Better efficiency of porous ceramic membrane was also proved by displacing liquid phase outside the pores of the membrane and monitoring the position of the gas-liquid interface to minimize the diffusion path of the gas reactant [153]. Recent investigation reports successful developments of catalytic hydrogel membrane reactor protecting Pd particles from deactivation compared to batch reactor and a good stability of the hydrogel structure for pH > 4. Optimization of the hydrogel thickness is envisioned thanks to 1-D model able to predict the reactivity across the membrane thickness [154].

As a matter of fact, membrane reactors are already widespread in catalytic water treatment due to different advantages related to simple reactor design and ensuring a better control of the G-L-S interface which undoubtedly can provide significant advantages in catalytic water treatment [150,153,155-156]. By opposition to reduction processes, sensitive to the concentration of hydrogen and nitrates at the vicinity of active sites, oxidation processes can be in some extent weakly dependent of oxygen partial changes [148]. Accordingly, such kinetic features can attract the development of membrane reactors to get complete mineralization and retain undesired molecules. A critical review recently published emphasized the relevance of such technology in single and hybrid systems[149]. A renewed interest is linked to the development of bioreactors. As earlier mentioned the most important featured is linked to a shift of equilibrium to improve yields. Preferential permeation can also avoid undesired side-reaction and prevent deactivation. In practice different strategies can be implemented. Indeed,

the membrane can be set up upstream the catalytic oxidation process corresponding to a sequential approach or can be combined with the catalyst according to a one pot approach. Most of the examples described in the literature illustrate this option, but some benefits can be obtained in the former case thanks to the improvement in the distribution of ozone and the separation from water which speeds up the rate of ozone mass transfer [157].

The efficiency of membrane has been already demonstrated for various catalytic reactions such as the abatement of trichloroethylene according to a single-stage approach on Pd-loaded polypropylene porous hollow fibers which allows a quasi-complete removal ensuring the release of chorine as HCl and stability over 50 cycles [158]. Cu-ZSM-5 zeolite membranes on paper-like sintered stainless fibers has been investigated in catalytic wet peroxide oxidation of phenol in a fixed bed flow reactor at 40°C revealing high performances related to the 3D structure and large pores which can enhance mass and heat transfer and improve the contact between the reactants [159]. Catalytic membranes doped with palladium and iron exhibit a bifunctional behavior related to *in-situ* production of H_2O_2 and subsequent phenol oxidation[160]. A recent review provides an update of the investigations pointing out the coupling filtration on organic and ceramic membrane and catalytic ozonation. A benefit of nanofiltration to retain small molecules is observed and this coupling also permits to lower catalyst fouling. The literature is scarce regarding the use of polymer membrane because of the sensitivity to ozone oxidation. Ceramic membranes are often preferred despite their poorer cost-efficiency likely due to the ease to disperse the catalytic active layer [161].

Monolithic reactors

Different reactor designs have been explored especially monolithic reactors for the photo-Fenton oxidation of acetic acid. Some attempts revealed different performances when $LaFeO_3$ as active phase was wash-coated on corundum or cordierite. The reusability was proved in the absence of significant leaching. Co-adsorption of hydrogen peroxide and acetic acid may take place at the surface of the catalyst. Nevertheless, the competitive adsorption largely in favor of acetic acid makes uneasy the adsorption and decomposition of H_2O_2. As a matter of fact, the authors privileged an Eley-Rideal mechanisms which account for adsorption of acetic acid at equilibrium further reacting with photo-generated $HO^{\bullet}$ radicals. Some issues remain regarding the continuous feed of H_2O_2 to maintain the efficiency, the impact of the composition of the monolith substrate which influences the catalytic properties of the washcoat and the efficiency related to the diffusion insight the reactor structure of the light in case of photocatalytic applications [162-164]. The development of monolithic reactors has been earlier envisioned as an

54

attracting alternative to batch and trickle-bed reactors related to rate enhancement due to a continuous wetting of the catalyst surface which lowers mass transfer perturbation, lowers pressure losses and improved resistance to pore plugging. However, such technology can face to significant difficulties to find an optimal balance between high performances and cost-efficiency[48].

2.3.4. Towards miniaturization: Development of microreactors

As a general trend, the development of smaller and more efficient catalytic processes for water treatment being more energy-efficient also refers to safer and sustainable technological developments. Interesting arguments in the emergence of the so-called process intensification have been put forward.[165] Several criteria have been selected which account for the integration of several functionalities, improved heat and mass transfer by novel mixing technologies, shorter diffusion pathways, miniaturization, with the aim of maximizing synergistic effects and get high activity and better selectivity. Indeed, the high surface to volume ratio in micro-scale reactors is much less perturbed by heat and mass transfer than macro-scale reactors[166-168]. First of all, it must be said that microreactors are suitable for homogeneous reactions as well as for heterogeneous reactions. Nevertheless, in the first case, the issue linked to the recovery of the catalyst is a limiting parameter. From a fundamental viewpoint, such reactors facilitate the difficult optimization of tri-phase reactors related to complex hydrodynamics. Indeed, according to the size of microchannel reactor of the order of 1 mm, the diffusion path decreases and can make mixing time very fast, of the order of microseconds instead of seconds or longer for classical reactors, thanks to a much higher surface-to-volume ratio[169]. Accordingly, a better monitoring of hydrodynamics could provide appropriate operating conditions to obtain more reliable kinetic information useful for catalyst optimization[170]. Several architectures can be envisioned regarding these small reactors. Particular attention is generally paid to the strategy implemented for the introduction of catalyst, homogeneous catalysts are simply dissolved in the reaction medium. On the other hand, different approaches can be envisioned for heterogeneous catalysts: (i) immobilized in the microchannels and then mimicking a catalytic packed bed flow reactors. As earlier discussed the grain size must be adapted to the scale of the channels which inevitably will lead to a detrimental pressure drop[171] – (ii) The catalyst can be coated on the inner wall of the channel with the advantage to overcome significant pressure drop. In that case the

catalyst anchorage is a crucial parameter and can suffer from instabilities. An apparent drawback associated to this methodology is related too much lower amount of catalyst loaded in the microreactor and related lower rate of conversion. Different strategies are currently implemented to stabilize the nanoparticles thanks to physical or chemical interaction and/or the modification of the micro channel surface. Let us note that such type of micro-reactors can be adapted for the immobilization of enzymes as catalysts[172]. As example, a facile fabrication (Figure 15) in mild conditions of glass catalytic microreactor with Ag nanoparticles immobilized in microchannels overcomes the inherent inconvenience associated with this technology, *i.e.* low stability and conversion[173]. A quasi-complete and stable conversion of 4-nitrophenol (4-NP) to 4-aminophenol (4-AP) at 25°C at flow rate 100 μmoL/h was achieved with Ag NP remaining immobilized. In general, a better gas-liquid mixture is obtained from packed bed approach compared to planar metal films, but the resulting efficiency gain by minimizing resistance to mass transfer should not be annihilated by increasing the pressure drop. Gas and liquid reactants are co-fed providing relevant quantitative comparisons based on a simple model given by Equation (46) which accounts for the contribution of the solubility of the gas reactant A_i in the liquid [A,i], the intrinsic rate constant k, the mass transfer linked to the gas diffusion in the liquid, $k_1 a_i$, the diffusion of the dissolved substrate from the bulk to the catalyst surface $k_c a_s$ and finally the diffusion of the solubilized species in the porous structure of the grain represented by the effectiveness factor η. In practice poor accuracy in the separate estimation of $k_1 a_i$ and $k_c a_s$ leads to Equation (47) with $K_L a$ which stands as a global mass transfer coefficient.

$$R = \frac{[A_i]}{\frac{1}{k_1 a_i} + \frac{1}{k_c a_s} + \frac{1}{nk}} \tag{46}$$

$$R = \frac{[A_i]}{\frac{1}{K_L a} + \frac{1}{nk}} \tag{47}$$

The estimation of the $K_L a$ in conventional fixed bed flow reactor and on microfabricated multiphase packed-bed reactor found that the values in this latter case are two order of magnitude larger than that estimated on the conventional reactor emphasizing strong acceleration of diffusion rates.[174]

It is also worthwhile to note that these microreactors can be well suited in case of hybrid technology. Their development for photocatalytic application can provide additional benefit and gain in efficiency thanks to a better spatial distribution of light irradiation (Figure 17)[182].
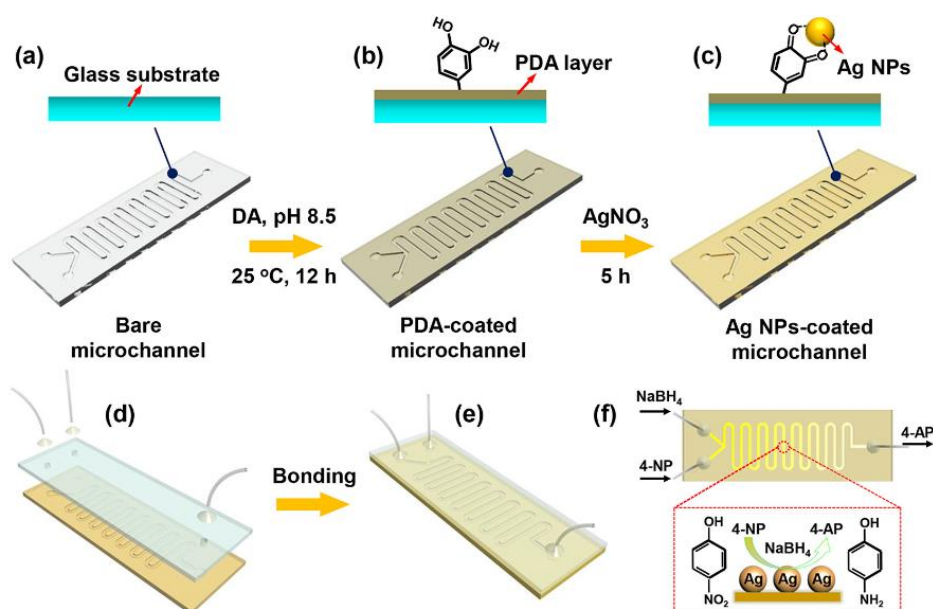
Figure 16. Steps for the fabrication of glass catalytic microreactor with Ag NPs on microchannel surface (a-e) and the catalytic reduction of 4-NP to 4-AP in the catalytic microreactor (f). (a) Bare glass serpentine microchannel fabricated by wet chemical etching. (b) Polydopamine (PDA) is coated onto glass microchannel by immersing the glass into DA solution under weak alkaline conditions. (c) Ag NPs are reduced an in-situ immobilized on the surface of microchannels by catechol groups in PDA coating. (d-e) The Ag NPs-coated glass microchannel is bonded with cover glass containing drilled holes by using UV curable glue (d) to form a glass catalytic microreactor (e). Reproduced with permission from ref [173]. Copyright 2017 Elsevier.
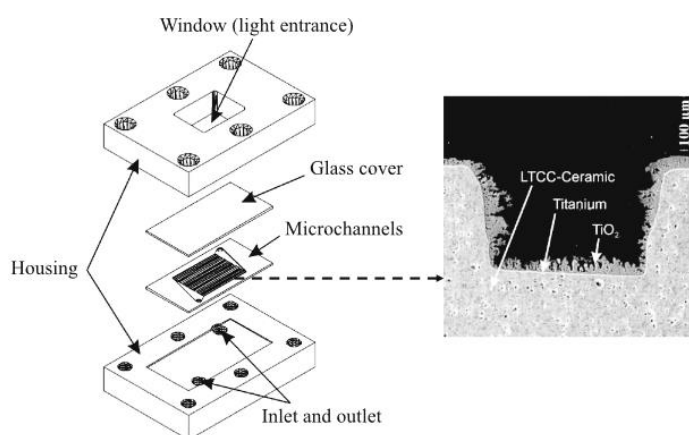
Figure 17. Microreactor and images showing the cross-section microchannel wall. Reproduced with permission from ref [175]. Copyright 2004 Elsevier.

2.4 New guidelines in catalyst design and functionalities

2.4.1. Control of the redox cycles M(n)/M(n+1)

All the oxidation processes based on the use of metal oxides as heterogeneous catalysts have in common the fact that metals involved in the process are submitted to redox reactions and one of the issues of an efficient heterogeneous catalyst for water treatment by AOPs concerns the kinetics of this redox cycle. For heterogeneous Fenton-like catalysts, the reduction of Fe(III) to Fe(II) is less effective than in the traditional homogeneous Fenton process, and it was shown that the enhancement of the Fe(II)/Fe(III) redox cycle may improve not only the activity of the catalyst but also its stability, limiting the possibility of the formation of deactivating $Fe(OH)_3$ species[176].

One strategy to improve the redox cycle consists in adding electron-rich donors able to facilitate charge transport, either externally, as carboxylic acids or other reducing agents, or as a part of the catalyst itself. Carboxylic acids were mainly used as chelating agents to favor the charge transfer for Fenton and photo-Fenton like reaction; their beneficial effect may be explained either by their ability to increase the dissolution of Fe species through the formation of more active soluble Fe complexes, then the homogeneous catalytic reaction, or by their ability of modifying the surface of the catalyst without leaching of the iron species. In the latter case, more sustainable for heterogeneous catalysis, the chelation of Fe(III) species at the surface was demonstrated to decrease the Fe^{3+}/Fe^{2+} redox potential from 0.77 V to less than 0.4 V depending on the ligand, increasing the thermodynamic driving force for the Fenton reaction and the reduction rate of the Fe^{3+} species.[177] Reducing agents, such as hydroxylamine, may also be used to reduce Fe(III) into Fe(II) at the surface.[178]

While the chemical modification of the catalytic surface could be an interesting way, but difficult, to apply due to the limited recyclability of the catalysts,[26] one can play with the composition and/or the design of the catalyst by itself. For example, the adjunction of metal species as zero-valent iron in $Fe@Fe_2O_3$ core-shell nanoparticle favors the reduction of Fe(III) into Fe(II) active species, via a mechanism involving molecular oxygen, for producing highly reactive hydroxyl radicals from H_2O_2 (Figure 18).[179] In this configuration, all the active sites Fe(II)/Fe(III) are at the outer shell, while the reducing species are in the core, protected from oxidation.
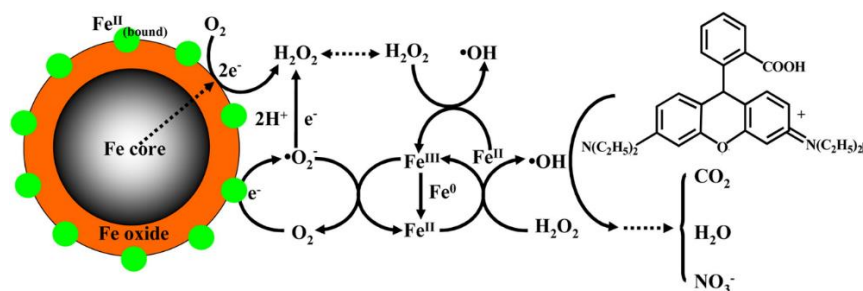
Figure 18. Mechanism of Fenton oxidation in the presence Fe@Fe$_2$O$_3$ core-shell nanoparticle. Reproduced with permission from ref [179]. Copyright 2014 Elsevier.

Carbon materials such as activated carbon, carbon nanotubes, graphene oxides and more recently biochar and hydrothermal carbon (HTC) are classically used for AOPs due to their ability to activate oxidants as H$_2$O$_2$, persulfate or O$_2$[24]. For Fenton-like reaction, carbon nanomaterials have also demonstrated their ability to enhance the reduction of Fe(III) into Fe(II). For example, great interaction between CNTs and Fh, with formation of Fe-O-C bonds, can be simply obtained by mixture of the two solids dispersed in water under sonication, due to initial electrostatic interactions between positively charged surface of small nanoparticles of Fh and the negatively charged oxidized multiwalled CNT[26]. This coupling favored the degradation rate of BPA by heterogeneous Fenton-like process due to an acceleration of the electron transfer from H$_2$O$_2$ to Fh and a lowering the Fe^{3+}/Fe^{2+} redox potential[26].

Doping by metal sulphides may also be used to accelerate the Fe(II)/Fe(III) cycling. It was shown that WS$_2$ can be used to increase the decomposition efficiency of H$_2$O$_2$ by accelerating the redox cycle in solution leading to an efficient degradation of phenol by oxidation, with the ability to reduce simultaneously Cr(VI) present in wastewater[180]. Various MS$_x$ (M = W, Mo, Fe, Zn) were also efficiently used for the degradation of iron activated persulfate decomposition for pollutant degradation[181]. It was shown that both surface active metallic sites and reducing sulphur species contribute to the reduction of Fe(III) to Fe(II) necessary for persulfate decomposition (Figure 19). Recently, Fe^0/FeS hydride materials have been developed for the efficient simultaneous removal of Cr(VI) and phenol from water in the presence of peroxydisulfate[182]. Other systems coupling other metal sulphides and iron species for heterogeneous AOPs are promising ways to explore.
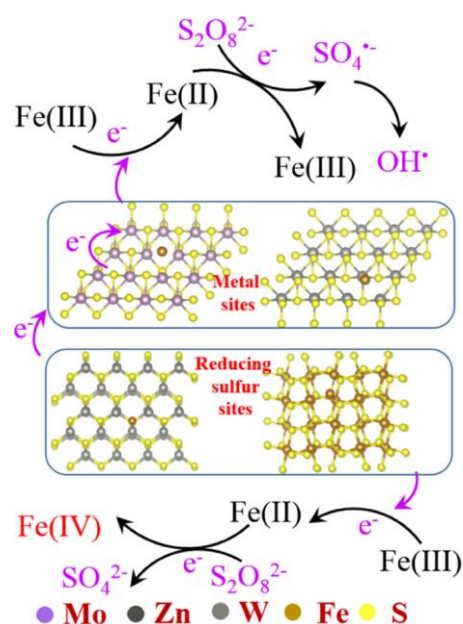
Figure 19. Proposed mechanism of persulfate activation by Fe(III)/Fe(II) in the presence of metal sulphide. Reproduced with permission from ref [181]. Copyright 2021 Elsevier.

The lattice oxygen-rich materials, based on metals with multivalent state such as Ce (III/IV), with facile redox cycle, have demonstrated interesting properties for catalytic oxidation reactions not only for catalytic wet air oxidation, as invoked in paragraph 2.1. but also for AOPs. Oxygen vacancies were proposed to be active sites for H_2O_2 or persulfate activation to ROS due to the back donation of localized electrons to the hydrogen peroxide or persulfate molecule[126,183]. Similarly, oxygen vacancies favor ozone decomposition and the production of ROS, not only HO• species but also $O_2^{•-}$, $^1O_2$ and surface O^{184}. The control of the redox cycles and thus of the ROS produced could be also a way to control the formation of undesirable products by highly oxidizing HO• species. The inhibition of bromate formation is one of the critical issues for the application of ozonation for the removal of organic pollutants from wastewater containing bromide[184]. It was shown that in the presence of a high density of oxygen vacancies, $O_2^{•-}$, as the other ROS produced, is able to (i) promote the pollutant degradation and (ii) reduce Ce(IV) into Ce(III) able to reduce bromate species[185]. Therefore, all the means available to favor the formation of oxygen vacancies at the surface of catalysts with redox properties could be interesting ways for developing efficient oxidation processes for water treatment.

The faceting of metal oxides at the nanoscale favors not only the presence of oxygen vacancies but also the adsorption of the organic molecules depending on their charge and their nature, facilitating their degradation. Thus, MnOOH nanorods[184] or faceted CeO_2[185], with

specific facets exposed for enhancing the amount of high-mobility lattice oxygen were successfully applied to the selective catalytic oxidation of organic pollutants such as 4-nitrophenol or sulfamethoxazole by ozonation in wastewater containing bromide, while inhibiting bromate formation.

The control of the morphology is another interesting way to increase the number of oxygen vacancies. Co_3O_4 mesoporous hollow nanospheres with high amount of oxygen vacancies are very efficient for the degradation of BPA by peroxymonosulfate activation[186]. Hollow $NiCo_2O_4$ spinel microspheres (Figure 20) with hierarchical architectures present high redox properties and numerous active oxygen species at the surface able to mineralize humic substance by catalytic wet air oxidation at atmospheric pressure according to a Mars- van Krevelen mechanism[187].
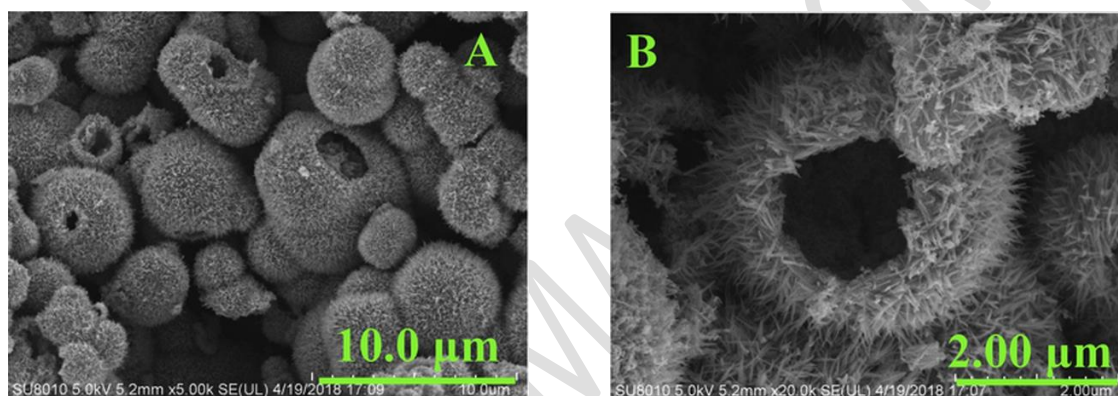
Figure 20. Scanning electron microscopy images of Hollow $NiCo_2O_4$ spinel microspheres active for humic acid mineralization by CWAO at atmospheric pressure. Reproduced with permission from [187]. Copyright 2019 Elsevier.

Doping is another way to enhance the formation of oxygen vacancies. For example, the introduction of Cu(II) in the B-site of $LaCoO_3$ perovskite increases the number of oxygen vacancies accelerating the Co(III)/Co(II) and Cu(I)/Cu(II) redox cycles involved in PMS activation, leading to very efficient degradation of phenol (Figure 21)[188]. Other examples of efficient increase of the number of oxygen vacancies in catalysts for catalytic water treatment can be found in the literature, as the doping of silver ferrite $AgFeO_2$ by Ni for BPA conversion using PMS[189].
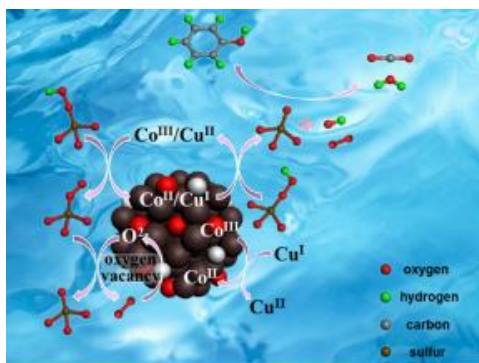
Figure 21. Proposed mechanism of PMS activation over $LaCo_{1-x}Cu_xO_3$. Reproduced with permission from ref [188]. Copyright 2018 Elsevier.

2.4.2. Enhancement of the stability

All the oxidation processes have in common that they favor the lixiviation of the active phase, the oxidizing species necessary to mineralize pollutants being also prone to oxidize metal active species. This is a major concern not only for the catalyst lifetime but also because the solubilisation of the metals degrades the quality of the treated water. A way to limit this problem consists in separating the active metal species from the solution by encapsulation or confinement of the catalyst in porous substrates of various structures or by synthesizing core-shell structures.

The confinement of the active species consists in restricting the space where the reaction occurs, *i.e.* the distance between the catalytic surface and the reactants. This could be achieved using inorganic membranes, porous assembly and hierarchical porous materials to immobilize the catalytic active phases[190-191]. Various host materials have been evaluated for a long time for their capacity of immobilizing efficiently the active phase such as carbon materials, clays, pillared clays, microporous materials such as zeolite, mesoporous materials, polymers etc.[191]. These host materials can be structured to form porous membranes to couple filtration to oxidation (see paragraph 2.3.3).

Core-shell or yolk-shell structures with the active catalyst in the core or yolk and a carbon shell have attracted attention these last years due not only to the capability of carbon to enhance the adsorption and activation of the oxidizing agent and the pollutant, and to favor the redox properties of the catalyst as seen in paragraph 2.4.1 but also to protect the catalyst from leaching and sintering. For example, carbon coated iron-based Fenton-like catalysts present both high activity and stability for the degradation of phenol in the presence of H_2O_2, as illustrated in Figure 22[192]. However, there is a carbon loss and a degradation of the absorptive properties of

the carbon shell during the repeated test, leading to a little loss of the catalytic performance, which can be compensated by the ease of regeneration of such systems[192]. Yolk-shell structure (Figure 23) was also proven to enhance in addition the mass transfer efficiency of a hydrophobic molecule, octane, favoring its efficient oxidation[193]. Manganese ferrite (MnFeO$_4$) is a highly efficient catalyst for oxidation in the presence of ozone, persulfates or H$_2$O$_2$. Its encapsulation by a carbon shell functionalized by amino groups allowed obtaining active catalysts for antibiotic removal by AOP with enhanced stability compared to the bare MnFeO$_4$ nanoparticles[194]. The encapsulation by N-doped porous carbon of metal-based nanoparticles can be easily obtained by pyrolysis of MOF; for example, Fe/Fe$_3$C@N-doped carbon hybrids derived from nano-scale MOFs demonstrated high activity and stability for PMS activation and 4-chlorophenol removal[195]. MOFs can also be directly used for obtaining very efficient core-shell structures for water treatment[37].
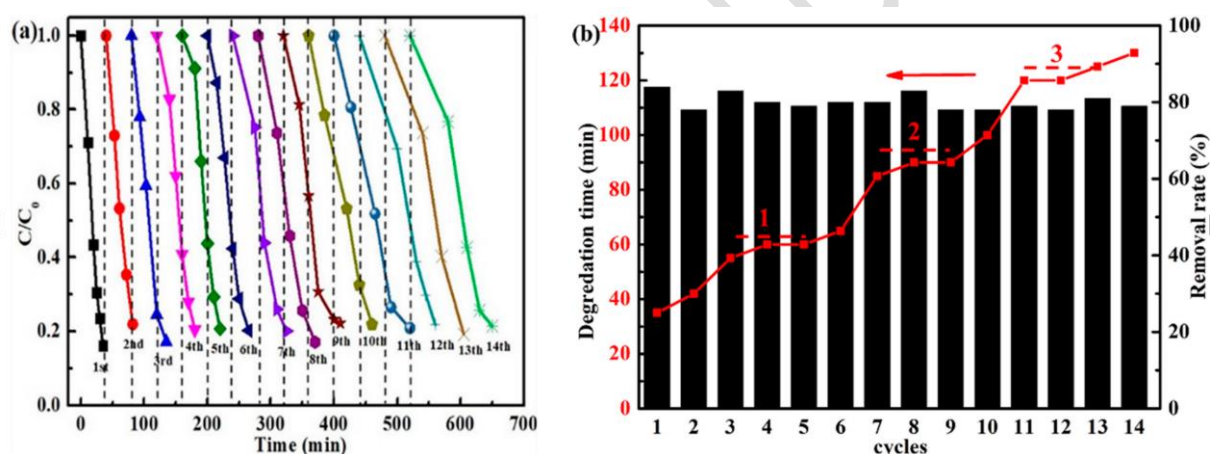
Figure 22. Cyclability of carbon coated iron-based Fenton-like catalysts for phenol degradation in the presence of H$_2$O$_2$ during 14 cycles. Reproduced with permission from ref [192]. Copyright 2020 MDPI.
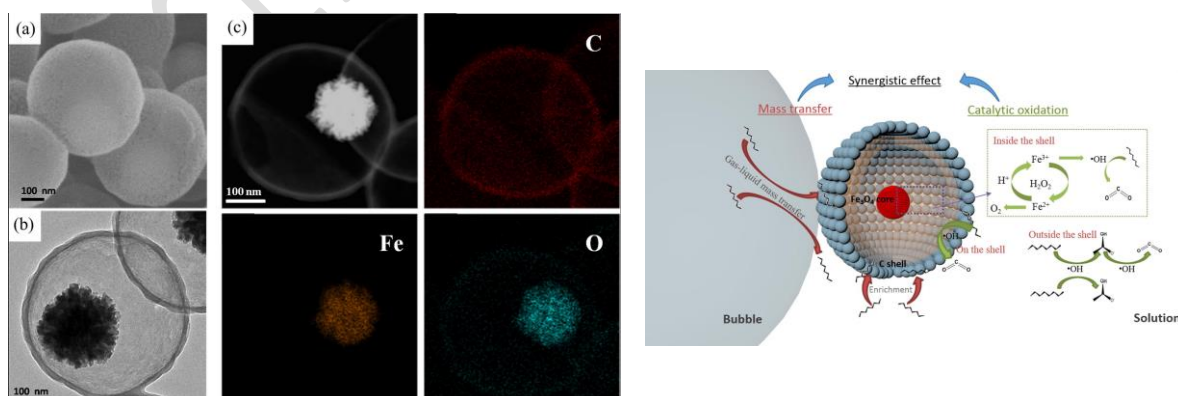
Figure 23. Scanning electron microscopy (a) and transmission electron microscopy image (b) and EDS elemental mapping of Fe$_3$O$_4$@C yolk-shell structures (Left side) and scheme of the reaction mechanism (right side). Reproduced with permission from ref [193]. Copyright 2020 Elsevier.

To the best of our knowledge, core-shell structures without carbon materials are by far less explored. One of the few examples found in the literature demonstrated that the stability of Cu/SiO$_2$ catalysts was enhanced by alumina overcoating using atomic layer deposition, with a reduction of copper leaching by *ca.* 90% while maintaining a high activity for catalytic ozonation for pollutant removal in water[196]. The encapsulation by metal oxides, metals, or metal sulphides, and especially those that have demonstrated to promote the redox cycles for enhancing pollutants degradation, or by other porous oxides with a better resistance towards oxidation than carbon, is a general way to open for improving the stability of catalysts for the oxidation of pollutants in water. Examples of the deposition of protective layers around nanocatalyst for application in catalytic reaction in water, such as biomass valorization, can be found in the literature. Also, methods of encapsulation and examples of core-shell structures can be found in a recent review[197].

2.4.3. Materials with hierarchical porosity

The design of hierarchical porous materials, containing at minimum two levels of interconnected pores, is an efficient strategy that emerged to combine large surface area of 3D catalysts with high accessibility of the reactants to the active sites due to the reduction of steric limitations and facilitated mass transportation in the porous structure, minimizing internal diffusion limitation, which is a major drawback for catalytic reaction in water. It was demonstrated by a computational approach that an optimized bimodal pore size distribution may improve the catalyst efficiency by at minimum one order of magnitude compared to a monomodal pore size distribution[198]. In the case of photocatalysts, 3D ordered hierarchical structures improve light absorption efficiency due to the macrochannels allowing the transportation of the photons to the internal surface of the semiconductor and to the "slow photon" effect, improving the harvesting of light and thus accelerating the formation of electron–hole pairs in the semiconductor [199-200]. In the following, we will give some examples on the use of hierarchical materials for non-solar driven water remediation.

Various types of hierarchical materials may be developed for water treatment. Among them zeolites, various inorganic supports, such as silica-based structures, or carbonaceous materials yielded promising results for pollutant catalytic removal. Depending on the material and the structures needed, various chemical strategies can be applied, which are detailed in reference[201], consisting in either creating holes in the synthesized structures (Top-down

approach) or synthesizing the materials in the presence of templates, for example (Bottom-up approach).

Carbonaceous materials

As carbonaceous materials have demonstrated their efficiency for AOPs, the development of hierarchical porous carbon structures with interconnected micro, meso- and macropores may improve their catalytic properties for wastewater treatment by combining high surface area and a facilitated access to the micropores. Hierarchical porous carbon materials can be directly obtained by pyrolysis-activation of biomass, such as wood, chitosan, grass or nut shells, which present a naturally organized hierarchical structure[202]. They can also be synthesized using various carbon sources in the presence of templates. For example, 3D hierarchically-ordered porous carbon materials (HOPC) with high sp^2-hybridized C and N species and uniform network of pores, obtained by polymerizing 2,6-diaminopyridine on a SiO_2 template, demonstrated a rapid substrate adsorption followed by an efficient oxidation in the presence of persulfate of a wide range of micropollutants. The adsorption capacities of HOPC for aromatic compounds such as BPA were much higher than those of carbon nanotubes (CNTs) and reduced graphene oxide (rGO), which was explained by the high surface area and the uniform pore size, as well as by strong π-π stacking and hydrophobic effects. A complete and rapid mineralization of pollutants was obtained in the presence of HOPC when persulfate was added while on CNTs and rGO a part of pollutants remained physisorbed and not degraded[203].

A very original approach consisting in using directly organic contaminants accumulated on minerals as source of carbon was recently reported in the literature.[204] The authors used double mineral templates, namely montmorillonite and goethite (FeOOH) to synthesize hierarchical porous N-doped graphene-like materials (Figure 24) very efficient for the degradation of BPA by PMS activation.
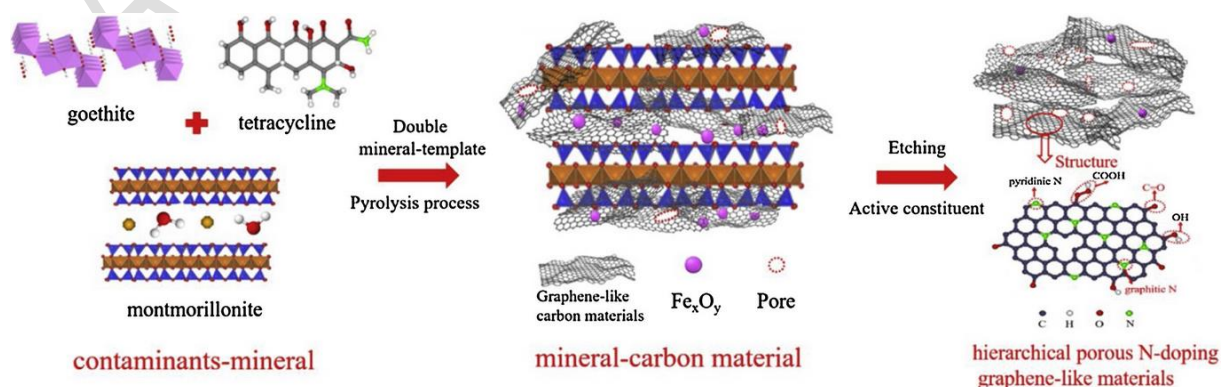
Figure 24. Scheme of the use of double mineral-template for synthesizing hierarchical porous N-doped graphene-like materials. Reproduced with permission from ref [204]. Copyright 2020 Elsevier.

Salt templating is a facile approach to generate hierarchical structures without residual template. Thus, N- doped hierarchical porous carbon structures, with ultrahigh surface area and uniform dispersed macropores, mesopores and micropores, were simply obtained using polyacrylamide as N and C precursor and sodium nitrate salt as template. They outperformed homogeneous catalysts for oxidation of phenol in the presence of PMS[205].

Ice-templating is another innovative approach for obtaining hierarchical structures. Nitrogen-self doped hierarchical porous carbon was synthesized form chitosan, a N-rich natural polymer, by rapid-freezing of the hydrogel obtained by addition of acetic acid deepened in liquid nitrogen, followed by the carbonization-KOH activation of the resulting aerogel assisted by rapid-freezing. The resulting catalyst demonstrated high performance for PMS activation and high adsorption ability of BPA yielding an excellent catalytic activity for mineralization of this pollutant, due to the hierarchical structure associated with a high electron transfer capacity[206].

Zeolites

The microporosity of zeolites, with pore dimensions generally in the 0.2-1 nm range, is the main obstacle to their use for catalytic oxidation of organic substrates with high molecular weight, which remain on the external surface of the zeolite, while the catalytic sites are mainly located inside the pores[207]. Hierarchical zeolitic structures may be obtained by (i) the bottom-up approach, using hard templates (polymers, carbon particles or nanotubes, etc.) that can be easily removed by calcination leading to poor interconnectivity micro- and mesopores, or by grafting organosilanes or (ii) the top-down approach by demetallation[208]. Contrary to dealumination, the desilication by alkaline treatment presents the advantage of creating mesopores in the zeolitic framework without modifying the Brønsted acidity, favoring the adsorption of large organic molecules such as mesosulfuron-methyl, a pesticide, via acido-basic interaction compared to the non-modified zeolite[217]. Hierarchical Fe-ZSM-5, synthesized by hydrothermal treatment in the presence of polystyrene microspheres as macropore-generating agent, was also used as a heterogeneous Fenton-like catalyst. While the hierarchical zeolite was less efficient for mineralizing small phenol molecules in the presence of H_2O_2 than a conventional Fe-ZSM-5 zeolite, the trend is reversed in the presence of lignin, of *ca.* 20 nm diameter, or Na_2EDTA. This better activity of the hierarchical zeolite for large molecule

oxidation was explained by the higher specific surface area accessible to organic molecules at the proximity of iron-containing catalytic site[209]. However, these promising results seem to be insufficient since very few examples are reported in the literature on the use of hierarchical zeolites for water remediation.

Other metal oxides

Among metal oxides, ordered mesoporous silica SBA-15 is by far the most used for wastewater treatment, not only for adsorption, its main utilization, but also as support for immobilizing active phases and controlling their size. The use of SBA-15 for catalytic water treatment has been summarized in a recent review[210]. However, other metal oxides, which can be by themselves active for AOPs or can be used as support for active phase, may be hierarchized to enhance their catalytic performance for water remediation. This field could experience a strong expansion in the coming years.

For example, cobalt oxides-based catalysts have demonstrated their efficiency for PMS activation, but they often suffer from a lack of accessible active sites, which can be improved by synthesizing hierarchical structures. Cobalt titanate spinel (Co_2TiO_4) with very nice 3D flower-like hierarchical structure presented a higher activity in PMS activation for the antibiotic ofloxacin oxidation than conventional heterogeneous cobalt-based catalysts thanks to its high surface area associated with a highly open porous structure and to the promoting effect of Ti[211].

Mass transport phenomenon may have a direct impact not only on the conversion of reactants but also on the selectivity, *i.e.* on the distribution of reaction products. In the case of nitrite reduction, the pH value is of major importance, the presence of OH^- ions competing with NO_2^- favoring the formation of undesired ammonia. Hence, the accumulation of the OH^- produced during the reaction in the vicinity of the active sites and the internal diffusion limitation of NO_2^- inside the catalytic grains are then detrimental to nitrite conversion and to the selectivity towards N_2. Pt catalysts supported on 3D ordered macroporous alumina synthesized by macrostructuration routes in the presence of monodispersed polymer spheres presented a superior activity and selectivity to N_2 than those supported on classical mesoporous Al_2O_3 support due to the open structuration and high degree of interconnectivity of the structure favoring the elimination of the OH^- produced outside the pores[212]. The same enhancement of nitrite conversion was observed using Pt supported on 3D-ordered macroporous mesoporous silica prepared using dual templating methods[198]. These studies demonstrate that not only the choice of the active phase and the optimization of its dispersion, but also the engineering of the

pore architecture of the inert support around the active sites are of major importance for developing efficient catalysts for water treatment.

In conclusion, materials with hierarchical porosity can be advantageously used for water treatment since they favor the accessibility of the reactants to the active sites as well as the desorption and diffusion of the products outside the pores, thus influencing not only the activity but also the selectivity. However, and especially for carbonaceous structures that suffer a lack of stability in the presence of strong oxidizing species, the harsh conditions of industrial water treatment may cause the collapse of these hierarchical structures thus limiting the possibility of application, even if such phenomena has not been observed at the laboratory scale. Consequently, the hydrothermal and mechanical stability of such structures should be evaluated in addition to their recyclability.

2.4.4. Emerging nanomaterials for water treatment

Single atoms for catalytic water treatment

Recently, the development of single atom catalysts (SACs) has attracted attention since it is a way to increase the accessibility to the active sites and increase the metal-support interaction, thus optimizing the specific activity, while decreasing the use of metals. For AOPs, the increase in mineralization rate may also be attributed to the suppression of the HO• quenching occurring on adjacent transition metal atoms[213-214]. The challenge consists in atomically dispersing the metal atoms in the support and more importantly in maintaining this high dispersion during the process, the lack of stability being the main bottleneck for SACs application. SACs were reported for the first time as efficient catalysts for AOPs in 2018[215]. Single cobalt atoms, anchored in porous N-doped graphene demonstrated high reactivity and stability for the catalytic oxidation of recalcitrant BPA in the presence of PMS. This high activity was explained by a dual site reaction, with the activation of PMS on Co atoms and the adsorption of organic molecules on the adjacent pyrrolic N site. Similarly, single Cu atoms incorporated in graphitic carbon nitride (C_3N_4) are able to generate HO• from H_2O_2 and efficiently convert Rhodamine Blue molecules into CO_2 and NH_4^+ without strong deactivation [213]. For this catalyst, it was demonstrated that Cu(I)/Cu(II) redox cycle was involved in the catalytic process. Even if SACs applied to water treatment are mainly focused on carbon-based materials, more prompt to anchor metals, one can note that single Fe atoms, with high activity

for Fenton-like catalytic oxidation of p-hydroxybenzoic acid and phenol, were easily obtained on SBA-15[216].

Even if promising results were obtained in catalytic water treatment with SACs their stability and reusability, their low metal loading and the difficulty of synthesis are for the moment strong limitations to their development at the industrial scale.[213]

MXene-based catalysts

MXenes are 2D transition metal carbide/nitride materials composed of $M_{n+1}X_n$ octahedral layers (M = transition metal, X = C and/or N, n = 1 to 3), with surface termination groups T (-OH, -F, =O) giving high hydrophilicity[217-218]. MXenes, such as $Ti_3C_2T_x$ have demonstrated high adsorption capability for organic pollutants, such as methylene blue, in wastewater due to the strong electrostatic interaction between the MXene material and the dye molecules[219]. These high adsorption capabilities due to strong electrostatic interaction can be also used to favor the dispersion of metal cations and insert metal nanoparticles between MXene layers. Thus, Co_3O_4/MXene, α-Fe_2O_3/MXene and $CoFe_2O_4$/MXene were very efficient catalysts for the degradation by AOP of BPA, salicylic acid, and naproxene, respectively, in water[220-222]. In all these examples, a $Ti_3C_2T_x$ MXene, the most studied MXene, was used. However, one has to take into account that under oxidizing conditions the catalyst should be more in the form of metal oxide/TiO_2/C nanocomposite[223]. However, due to the wide range of composition and the possibility of controlling the surface chemistry of such 2D compounds, MXene are promising materials for enhancing the catalytic properties of catalysts for AOPs in water as well as for water treatment by catalytic reduction[223].

For the moment, the applicability of MXene as catalytic materials is strongly limited by their synthesis route: they are obtained by etching in HF medium to remove the A element (A = group 13 and 14 element) of MAX phases, as the latter cannot be synthesized in large amounts at a high purity level. For these emerging nanomaterials, it is also necessary to rationalize the effect of the nature of M and X on the catalytic properties as well as to study their stability and recyclability. Finally, while MXene are classically characterized in gas phase, it is important to study the influence of some parameters such as the surface composition and the interlayer spacing in water, i.e. in the reaction conditions, in order to go beyond the proof-of-concept level. The photoresponsive properties of those materials have been pointed out and will be briefly depicted in the chapter 4.1.

2.4.5. Towards green catalysts for water treatment

One point that has to be better taken into account when developing catalysts for environmental remediation, and especially for water treatment, is non-toxicity of the catalysts and the development of sustainable routes for their synthesis integrating the principles of green chemistry[224]. Chemical synthesis methods, considered as bottom-up approaches, are the most used for catalyst synthesis. They are based on the use of precursors, solvents, in some cases surfactants, and necessitate the most often thermal process, hydrothermal, solvothermal, and thermal decomposition included[225]. Eco-friendly approach necessitates to use (i) low impact chemicals, (ii) green solvents, water being the best one due to its low cost and large availability, (iii) biobased surfactants and (iv) limit the energy consumption. Biological synthesis, based on the use of uni- or multi-cellular organisms to transform inorganic metal ions into nanomaterials can be considered as green process, but suffers from a slow rate of production[225-226].

Another way towards sustainable development of catalysts concerns the use of catalytic materials from biomass or wastes. Carbon nanotubes or graphene may be highly toxic for animals, plants and microbial diversity and they have been recently proposed as not adapted for remediation processes[227]. They can be advantageously replaced by bio-based carbon materials. For example, carbon nanomaterials, synthesized from cactus using an easy one-pot hydrothermal route, were successfully used without any metal addition as Fenton-like systems for dye decolorization in the presence of H_2O_2[228]. Even if their performance were lower than their classical counterparts containing metals (Cu, Fe, Au, Zn), they present the advantage of lower cost and much lower environmental impact. Other carbonaceous materials, graphitic biochar catalysts, produced by pyrolysis of sludge, were demonstrated to activate PDS to decompose organic pollutants by electron transfer, with the additional property of bacteria inactivation[229]. In addition, sludge-derived biochar can contain minerals with a positive role on the catalytic performance, such as Fe or Mn[230]. Natural biopolymers, especially polysaccharides, with adsorption and ion exchange capacity can also be used to replace carbon nanomaterials as supports or to encapsulate metal and metal oxides nanoparticles for application in wastewater treatment[231]. Another way to explore is the valorization of metal-accumulating plants used for the rehabilitation of mining sites. Eco-CaMnOx catalysts were recently obtained by controlled thermal treatment of Mn-rich biomass without chemical treatment. These mixed calcium-manganese catalysts ($Ca_2Mn_3O_8$ and $CaMnO_3$) demonstrated high efficiency for epoxidation of biosourced terpenes and lipids using $H_2O_2/NaHCO_3$ and could be interesting catalysts for Fenton-like or WAO water treatment[232]. For these green

catalysts, originating from biomass or waste, a specific attention may be paid to improve their stability in the reaction medium, especially in the presence of strong oxidizing species.

3. From fundamentals to practical improvements in catalytic processes for the removal of persistent water contaminant

This chapter will be dedicated to non-solar driven catalytic processes, *i.e.* biocatalysis and combined plasma and microwave catalytic systems. The utilization of enzymes produced from microorganisms is a mature technology likely due to their remarkable high turnover number and remarkable regioselectivity. Their immobilization will be discussed as a means to improve their reusability. In addition, it will be shown that the catalytic performance of enzymes can be modified according to the strategy employed for their immobilization. While this technology is mature, important evolution can derive from the development of new enzyme synthesis especially by genetically modified bacteria to treat emergent non-biodegradable pollutants.

Plasma assists wastewater catalytic treatment through the production of more reactive species than oxygen in the former case, *i.e.* ozone, hydroxyl radicals, H_2O_2, peroxide, peroxynitrites, ozone, hydrogen peroxide, etc. which degrade the organic contaminants in water. Their *in-situ* production can be achieved by electrical discharge and consequently suppress external use of costly oxidizing agents. By itself this technology is not operative but better efficiency can be obtained with heterogeneous catalysts. The mode of operation of microwaves differs from plasma, but it still needs the presence of catalysts and also the use of oxidizing agents. In this specific case microwave irradiation can induce a local and selective heating which can speed up any chemical transformation. Principles and adaptation to the reactor design will be discussed in terms of advantages and drawbacks based on fundamentals and concepts developed in the previous chapters.

3.1. Microwave assisted catalysis for water treatment

3.1.1. Generalities

Microwave (MW) radiation is an electromagnetic wave in the 0.3-300 GHz frequency range corresponding to 1-0.001 m wavelength. To avoid interference with radar and telecommunications, MW generators are always operated in the range from 2450 MHz of 915

MHz for non-military applications[233]. The heating by microwave is more efficient than conventional heating leading to higher heating rates, and consequently increased reaction rates with reduced apparent activation energies, different thermodynamic functions and enhanced energy efficiency. For these reasons, MW irradiation is more and more used in chemistry for many applications such as inorganic and organic synthesis, extraction for chemical analysis, polymerization processes, catalytic processes, and soil, air and water remediation[233]. The penetration, reflexion and absorption of MW irradiation depend on the medium. The complex permittivity ε^* (Equation (48)) of a non-magnetic material allows describing the level of heat that can be generated under microwave interaction with a medium or a material[234-235].

$$\varepsilon^* = \varepsilon' - j\,\varepsilon'' \qquad\qquad (48)$$

Where the real part of the complex permittivity ε' is the relative dielectric constant (F m^{-1}), related to the amount of electric energy that can be stored in the material, ε'', the imaginary part, is the dielectric loss factor (F m^{-1}), expressing the ability of the material to dissipate microwave energy, and j is the imaginary unit. Absorbing molecules, also named lossy molecules, because of their polarity, can rapidly convert MW energy into thermal energy, and thus can be heated. The capacity of a material or a medium to convert the MW irradiation into thermal energy at a given frequency and temperature can be evaluated using the dielectric loss tangent (tanδ), describing the energy dissipation of a dielectric material, according to Equation (49)[236] :

$$\mathrm{Tan}\delta = \frac{\varepsilon''}{\varepsilon'} \qquad\qquad (49)$$

Lossy medium with the highest Tanδ value can be considered as the best MW absorbers[237]. For example, H_2O_2 (Tanδ = 0.260 at 2.45 GHz and 25 °C) is a better absorber than water (Tanδ = 0.123 at 2.45 GHz and 25 °C)[233]. The microwave absorption by the lossy medium causes the rotation of the polar molecules following approximately the high-frequency alternating electric field of the microwaves, with a delay in time leading to thermal energy.

At the opposite of lossy materials, there are transparent materials, with low values of Tanδ, as polystyrene (Tanδ = 0.0004 at 2.45 GHz and 25 °C), quartz (Tanδ = 0.00025 at 2.45 GHz and 20 °C), or alumina (Tanδ = 0.0010 at 2.45 GHz and 25 °C), while composites or multi-phase materials composed of at minimum a lossy material and a transparent material, allow the absorption of MW by localized energy conversion[235]. Charged molecules such as ions behave

similarly to polar molecules under microwave, increasing their movement under microwave electric field generating heating.

The dielectric loss is not the only way of heating under MW. Metals, metal-based materials and semiconductors were initially considered as impossible to heat using MW energy due to their ability to reflect MW and to the development of electron clouds due to the limited penetration of MW in this type of materials. At the early 2000's, it was demonstrated that MW induced magnetic field is responsible for the movement of electrons in the oscillating electric field generating volumetric and uniform heating in the material[237]. The last type of heating under MW can be attributed to magnetic loss occurring in magnetic materials, as Fe, Ni and Co, affected by both electric field and magnetic field, and some metal oxides such as ferrites or nickel oxides[237]. Finally, it was demonstrated that there can be a positive, but non-thermal, effect of microwaves on the intra-particle diffusion and mass transfer coefficients in surface modified porous silica due to the molecular excitation of organic molecules with a higher dielectric loss than the aqueous solution[238].

Consequently, MW irradiation can be an efficient way for wastewater treatment, due not only to the heating of water or polar pollutants, but more importantly to possible beneficial interactions with oxidants and catalysts. In fact, the direct treatment of wastewater under MW irradiation leads to an increase in temperature, which causes the removal from water of volatile or semivolatile pollutants by evaporation, but is not sufficient for breaking chemical bonds and decompose organic pollutants. For this reason, MW water treatment is always used in combination with other processes, using oxidants and/or catalysts or absorbing materials such as carbonaceous materials[233].

3.1.2. MW associated with oxidants

When associating MW with oxidants for water treatment, the increase in temperature favors their decomposition into efficient ROS species. The two main oxidants commonly used with MW are hydrogen peroxide and persulfates, which are decomposed by homolytic O-O bond cleavage into $HO\bullet$ and $SO_4\bullet^-$, respectively, with a beneficial effect of heating. However, it was demonstrated that the decomposition rate of persulfate into sulfate radicals is 3 to 4 times higher under MW than under conventional heating, for the same temperature in the 60 to 80°C range, proving that the action of MW is both thermal and non-thermal. From the calculation of the Arrhenius equation parameters, it was shown that the pre-exponential factor is much higher when MW is applied, compared to conventional heating (CH), which was explained by an

increase in the molecular mobility induced by MW.[239] However, due to the different heating way of the medium, from an external source for the conventional heating and from the medium for the microwave heating with a rapid and uniform heating, it is not obvious to rationalize this non-thermal effect according to the various explanations that can be found in the literature. For this reason, this phenomenon needs to be studied more in depth, for instance by controlling the rates of heating in real-time.[233]

MW combined with persulfate lead to an improvement of its efficiency, as exemplified in Figure 25 where it is clear that the removal rate of p-nitrophenol (PNP), one of the most important intermediates in the production of pesticides and pharmaceuticals, is particularly high when both peroxydisulfate (PDS) and MW are applied, while PDS alone is unable to convert PNP, evidencing the beneficial effect of MW heating.[240] Thus, PDS/MW has exhibited high efficiency for degrading in a short time various pollutants such as dyes (acid orange 7), other phenols or pesticides (imidachloprid).[241] An advantage of the use of combined persulfate/MW system is that the presence of anions, such as Cl^-, CO_3^{2-}, NO_3^- and PO_4^{3-}, cations, as Mg^{2+}, Ca^{2+}, K^+ and Na^+, and natural organic matter, as humic acid, has no negative effect on its performance for degrading pollutants. [241]
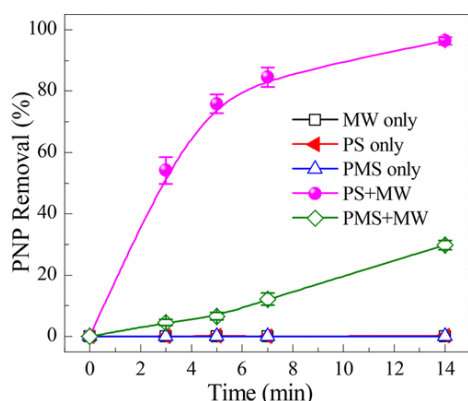
Figure 25. p-nitrophenol (PNP) removal vs. time under MW activation or not, and in the presence of various oxidants (Peroxydisulfate (PDS, here PS) and peroxymonosulfate (PMS)). ([oxidant]/PNP = 15, [PNP] = 20 mg L^{-1}, MW power = 300 W. Reproduced with permission from ref.[240]. Copyright 2019 American Chemical Society.

PMS may be more difficult to activate under MW than PDS as illustrated in Figure 25, but generally persulfates/MW have demonstrated better efficiency compared to H_2O_2/MW, as in the case of BPA removal, where even the combination of PMS/CH is more efficient than that of H_2O_2/MW (Figure 26).
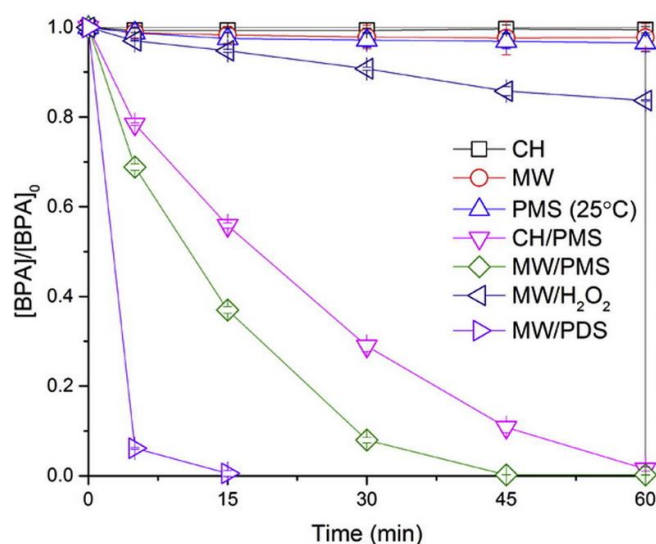
Figure 26. Conversion of BPA under conventional heating (CH) or microwave (MW) associated or not with various oxidants: Hydrogen peroxide (H_2O_2), Peroxymonosulfate (PMS) and peroxydisulfate (PDS) at 80°C when the temperature is not specified. Reproduced with permission from ref [242]. Copyright 2017 Elsevier.

Thus, the efficiency of oxidant/MW systems decreases in the order PDS/MW > PMS/MW > H_2O_2/MW, which follows the dissociation enthalpies of the peroxide bond[243]. The generation of $SO_4\bullet^-$ and $HO\bullet$ from PMS/MW has been proven to be the main ROS in this process, thanks to the use of hydroxyl radical scavenger (tert-butyl alcohol) and a scavenger for both radical species (ethanol). The PMS/MW process demonstrated high performance for degrading various organic contaminants such as dyes (Acid orange 7, methylene blue), a herbicide (Atrazine) or drugs (Ibuprofen, sulfamethoxazole)[244].

The efficiency of the oxidant/MW system for wastewater treatment depends strongly on many parameters such as energy intensity and pH, in addition to the obvious effect of the concentration of the oxidant and the pollutant as well as that of the presence or not of radical scavengers in the medium. The amount of energy needed to reach the optimal performance of the system depends on the reactants and the presence of other species in the reaction medium, but in a general way, an increase in microwave power will increase the removal efficiency. As far as the effect of pH is concerned, the oxidant/MW systems are efficient in acidic or neutral conditions. Alkaline medium does not favor the formation of active radicals from H_2O_2, which is mainly decomposed into O_2 at high pH value, but it has no negative effect on persulfate/MW system[233,242].

3.1.3. MW associated with materials

The irradiation of catalytic or non-catalytic materials by MW can increase their ability for degrading pollutants in water according to various kinds of interactions.

For non-catalytic MW absorbing materials, *i.e.* materials with dielectric properties but not able to activate contaminants degradation, such as carbonaceous materials, MW irradiation may induce polarization, heating and hot spots able to generate ROS by thermal decomposition of water, which, combined with their strong adsorption capacity, favor the mineralization of organic pollutants[233,237]. In other words, the association of MW with MW-absorbing materials with no intrinsic catalytic properties may transform them into catalysts.

For intrinsic catalysts, the interaction with MW depends on the presence of metals or transition metals oxides, with magnetic and/or semiconducting properties. As already discussed, conducting materials such as metals and magnetic materials can be directly heated under microwave irradiation. For intrinsic catalysts with semiconducting properties, MW irradiation can generate e^-/h^+ pairs, by excitation of the e^- of the valence band (VB), able to react with water and O_2 generating ROS as very active hydroxyl radical species, according to the following reaction equations[237]:

$$MW + catalyst \rightarrow h^+ + e^- \tag{50}$$

$$h^+ + H_2O \rightarrow HO\bullet + H^+ \tag{51}$$

$$h^+ + OH^- \rightarrow HO\bullet \tag{52}$$

$$e^- + O_2 \rightarrow \bullet O_2^- \tag{53}$$

$$\bullet O_2^- + H_2O \rightarrow HOO\bullet + OH^- \tag{54}$$

$$2\ HOO\bullet \rightarrow O_2 + H_2O_2 \tag{55}$$

$$e^- + HOO\bullet + H_2O \rightarrow H_2O_2 + OH^- \tag{56}$$

$$e^- + H_2O_2 \rightarrow HO\bullet + OH^- \tag{57}$$

$$\bullet O_2^- + H_2O_2 \rightarrow HO\bullet + OH- + O_2 \tag{58}$$

$$HO\bullet + contaminants \rightarrow H_2O + CO_2 \tag{59}$$
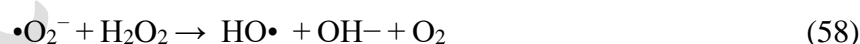
For supported metal or metal oxides nanoparticles, the catalytic properties under MW irradiation is also conditioned by the nature of the support, and its own interaction with microwaves. In addition, for supported metal catalysts, where the metal is dispersed at the surface of a carbon or metal oxide support, MW radiation can penetrate metallic nanoparticles if the size of nanoparticles is lower than the depth of penetration[244], determined by the following equation:

$$\delta = \sqrt{\frac{2}{\omega \mu_0 \sigma}} \tag{60}$$

Where δ is the depth of penetration, also called skin depth, ω is the angular frequency, μ_0 is the permeability of free space ($\mu_0 = 4\pi \ 10^{-7}$ H m^{-1}) and σ is the electric conductivity. For example, for copper ($\sigma = 5.81 \ 10^7 \ \Omega^{-1} \ m^{-1}$), a MW radiation at the frequency of 2.45 GHz, the depth of penetration will be of 1.3 μm, much larger than the common size of supported Cu nanoparticles.

Microwave with non-catalytic materials

MW associated with lossy materials such as carbonaceous materials is a powerful and simple process for treating organic pollutants in aqueous solution. Thus activated carbon (AC) and granular AC (GAC) with large surface area, chemical inertness and thermal stability are able to adsorb and then degrade organic compounds under MW irradiation due to the creation of hot spots. It was demonstrated that the presence of O_2 may play a beneficial role in the generation of hydroxyl radicals in the presence of this kind of materials, by using hydroxybenzoic acid conversion into 2,3-dihydroxybenzoic acid as a probe of HO• formation (Figure 27)[245].

Most often, the association of MW with carbonaceous materials is applied in conditions such that both adsorption and pollutants conversion take place at the same time, which can be a drawback for efficient treatment since hot spots may hinder the pollutant mass transfer to the surface [233]. This problem may be solved by decorrelating adsorption from degradation processes, which in that case can be seen as a regeneration process.
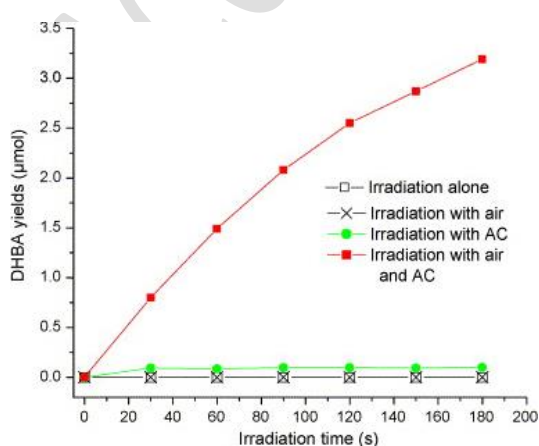
Figure 27. Amount of 2,3-dihydroxybenzoic acid (DHBA) resulting from reaction of salicylic acid with hydroxyl radical. Reproduced with permission from ref.[245]. Copyright 2007 Elsevier.

Other carbonaceous materials as biochar, derived from biomass, or carbon nanotubes (CNT) have also demonstrated their ability to adsorb high amounts of organic pollutants in water[246-247]. For CNT, which possesses one-dimensional and hollow structure, it was demonstrated that their diameter has a strong influence on the catalytic degradation efficiency under MW[248].

Many examples of water treatment coupling MW with carbonaceous materials can be found in the literature and were reviewed in refs. [233,237]. So, high catalytic efficiencies were demonstrated for converting detergents (sodium dodecyl benzene sulfonate), dyes (Congo red, methyl orange, and methylene blue), insecticides (Methylparathion) or plastic additives (Bisphenol A).

Microwave with catalytic materials

Ferrites (MFe_2O_4, with $M = Co$, Zn or Ba) are among the most promising catalyst for coupling with MW due to their high efficiency for the degradation of organic contaminants in water due to the easy synthesis protocol, the low cost of the precursors, their semiconductivity, their high structural stability, especially under hot spots generated by MW radiation, and the ease of recycling due to their magnetic properties[249-250].

While Bi_2O_3 semiconductor could be a good candidate for photocatalysis thanks to its band gap energy in the visible region (2.8 eV), allowing generation of ROS in water for degrading organic pollutants, its efficiency is not satisfactory without the addition of dopants or heterojunctions. On the contrary, Bi_2O_3 is highly efficient for degrading PNP in water under MW irradiation allowing the generation of e^-/h^+ pairs efficient for producing ROS[251], opening the way to the development of various derived Bi-based oxides for this kind of application.

Recently, new layered composite catalysts composed of perovskite ($LaCu_{0.5}Co_{0.5}O_3$) intercalated between layers of a natural clay, montmorillonite, demonstrated a high activity and stability for BPA degradation under MW heating[252]. It was proposed that hot spots were formed at the surface of the perovskite, but that the crucial factor for the high activity was the formation of e-/h+ pairs in the perovskite generating ROS, while the clay plays a positive role in the adsorption of the pollutant. The most important parameters controlling the activity are the Co^{3+}/Co^{2+} ratio and the amount of adsorbed oxygen species against lattice oxygen, obtained for the smallest perovskite particle size[252]. A possible BPA degradation mechanism was proposed, illustrated in Figure 28.
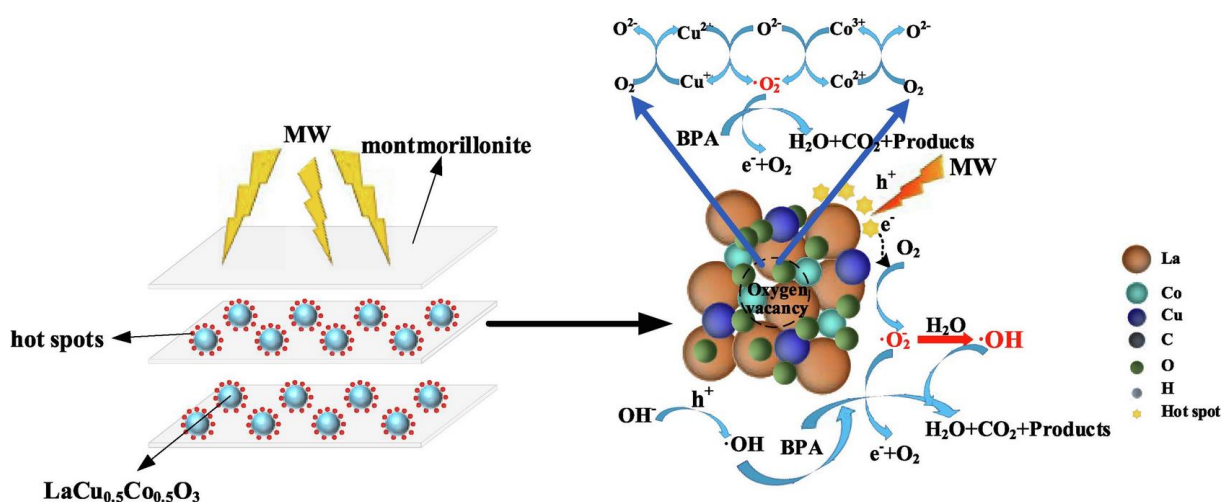
Figure 28. Proposed mechanism of BPA degradation under MW irradiation in the presence of a perovskite, $LaCu_{0.5}Co_{0.5}O_3$, intercalated into a montmorillonite clay. Adapted with permission from ref. [252]. Copyright 2020 Elsevier.

As far as supported catalysts are concerned, their properties under MW heating strongly depend on the support. Metal oxides supports, such as Al_2O_3, that are not able to absorb microwaves, only favor the dispersion of the active phase, and for this reason very few examples of their use as catalytic support for MW/Catalyst wastewater treatment are reported in the literature. For instance, CuO_x/Al_2O_3 catalysts were used for MW-induced treatment of phenol in aqueous solution but associated with chlorine dioxide[253]. In fact, only metal oxides with high adsorption properties, as zeolites, can be able to help converting pollutants. For example, Y zeolite is transparent to microwave, but microwave irradiation can interact with the high amount of polar species in the micropores, such as adsorbed water and cations, and possibly with the adsorbed organic molecule if it is polar, creating hot spots able to break chemical bonds by thermolysis. As a consequence, the rate of microwave-induced degradation strongly depends on the density and type of surface cations and on the amount of water trapped in the micropores[254-255]. The cation-exchange properties of zeolites can be used to incorporate transition metal ions with redox properties, enhancing the adsorption and catalytic properties of zeolites under microwave. Thus, Hu and Cheng[255] demonstrated that Cu^{2+} and Fe^{3+} exchanged into the micropores of a dealuminated Y zeolite increases the amount of the adsorbed pollutant, atrazine, and accelerates its degradation under microwave.

Contrary to metal oxide supports, the catalytic properties of the active phases supported on lossy materials such as carbonaceous materials or SiC (Tanδ = 1.71 at 2.45 GHz and 25 °C[256]) may be directly enhanced under MW irradiation since the support can play a direct role in the reaction. For example, copper oxides alone or associated with cerium oxides and deposited on AC by simple impregnation ($CuO@AC$ and $CuO-CeO_2@AC$) demonstrated high

efficiency for the removal of crystal violet wastewater when associated with microwave irradiation without adding any oxidant.[257] A clear beneficial effect of CuO and CuO-CeO$_2$ was highlighted compared to MW associated with AC, as exemplified in Figure 28. In fact, MW radiation will mainly interact with the AC support to generate hot spots able to dissociate water into ROS species and the role of the Cu dopant was attributed to the Cu^{+I}/Cu^{+II} redox properties favoring the oxygen mobility and electron transfer, with an additional effect of CeO$_2$ redox properties[233,257].
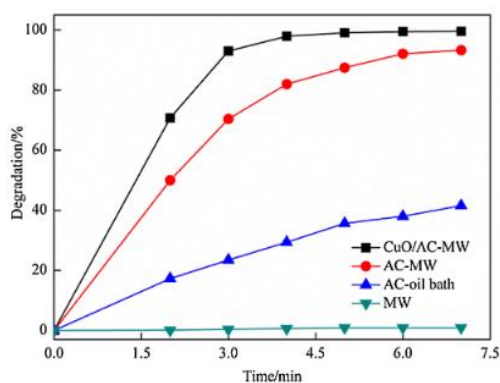
Figure 29. Comparison of the degradation of crystal violet in the presence of CuO/AC or AC associated with MW or oil bath heating, compared to MW treatment alone. Reproduced with permission from ref. [257]. Copyright 2016 Elsevier.

SiC is also an interesting support for active phases since it is not only a lossy material able to create hot spots but also a semiconductor. CuO deposited onto SiC displayed a very high catalytic activity under MW for PNP degradation due to the combined effect of hot spots able to accelerate the formation of e$^-$/h$^+$ pairs and water decomposition[258].

MW associated with Fenton and Fenton like heterogeneous catalysts

Fenton process, associating Fe(II) soluble species and H$_2$O$_2$ in acidic medium, is an efficient way for degrading pollutants in water. As already seen, MW irradiation favors the formation of hydroxyl radicals from H$_2$O$_2$. This enhancement is also important for the Fenton process for which it was shown that the amount of HO• for the MW-Fenton process is 2.8 times higher than for the classical Fenton process without MW after 7 min of reaction[259]. However, for the same reasons as for the development of heterogeneous catalysts for Fenton-like process, studies on wastewater treatment by MW-Fenton process are mostly focused on the use of heterogeneous catalysts. As it was inferred that both MW/H$_2$O$_2$ and MW/catalytic material are both able to generate ROS species in water with a positive effect on pollutants removal rate, it

is obvious that coupling these two processes in a single one, MW/H$_2$O$_2$/catalytic material, and even more when the catalytic material is associated with a lossy material such as carbonaceous material, is a very efficient process for the degradation of pollutants in wastewater, and numerous examples are found in the literature. For example, copper ferrite associated with reduced graphene oxide revealed to be an efficient and reusable catalyst, able to degrade more than 95% of a dye, rhodamine blue, in 1 min in optimal conditions (30 mg L^{-1} of rhodamine blue, 15 mg of catalyst, 600 μL of H$_2$O$_2$ and 500W of MW power (2.45 GHz)). It was shown, using radical trapping, that the active species were HO•, •O$_2^-$ and h$^+$.[260]

In the same way, persulfate oxidant was used associated with MW and catalysts and exhibited high performance for degrading pollutants. Thus, Rhodamine Blue was degraded within 1.5 min using 10 mg of catalyst (2D porous NiCoO$_4$), 10 mg of peroxymonosulfate and 300 W of MW power (2.45 GHz) at 70°C[261].

3.1.4. MW associated with photochemical process

It is possible to have simultaneously both UV–Vis and MW radiations generated *in-situ* using microwave discharge electrodeless lamps, composed of a glass cavity filled with an inert gas and an excitable substance, a metal usually, such as MW-powered Hg/Ne lamp that produces wavelength in the UV-Vis region as well as MW radiation making it easy to combine MW/UV-Vis treatment of wastewater [262]. At minimum three kinds of photochemical processes, namely the UV-H$_2$O$_2$ process, UV-Fenton process and photocatalytic process that can be coupled with MW irradiation are described in the literature.

Publications on MW/UV/H$_2$O$_2$ process are scarce, and are mostly dedicated to the removal of dyes, such as rhodamine blue[263] using the experimental apparatus displayed in Figure 30.
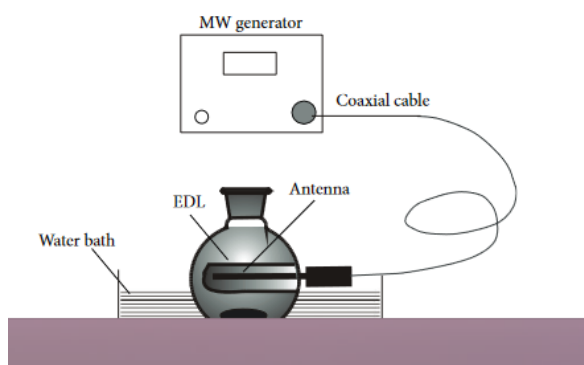
Figure 30. MW-UV photoreactor used for the MW/UV/H_2O_2 removal of rhodamine blue from water. Reproduced with permission from ref. [263]. Copyright 2013 Hindawi.

Photo-Fenton reaction coupled with MW irradiation was studied in 2007 and compared with the MW/Fenton treatment for the removal of pesticides from water, demonstrating a clear advantage of using additional UV in the MW/Fenton process, since only 45% of pesticide degradation was reached without UV, while the addition of UV allowed degrading 80% of the pesticide in the same conditions[264]. In spite of these promising results, this approach was not followed very much afterwards, and researches were a little more focused on the combination of MW and photocatalysts, since the coupling of MW and UV light may be an efficient way for improving the quantum efficiency of the photocatalytic process. Of course, TiO_2 was the most studied as photocatalyst in this process, and the addition of MW helped degrading dyes compared to UV alone[265]. The doping of TiO_2 by metals is a way to increase the e^-/h^+ separation and then the photocatalytic efficiency that was also explored under combined MW/UV. It was shown using Ag/TiO_2 that, under MW irradiation, the presence of silver can increase the adsorption of organic pollutants at the surface of TiO_2 in addition to the promotion of the charge separation process, with a clear beneficial effect of the combination of UV and MW compared to UV and conventional heating, for the degradation of 4-chlorophenol and methyl orange. [266]

3.1.5. MW associated with other physical processes

MW irradiation has also been efficiently combined with many other physical processes, such as electrochemical or ultrasonic processes, allowing a lot of possible combinations that remain to be explored.

In electrochemical water treatment, one of the main drawback is the deactivation of the electrodes due to the blocking of the active sites by the pollutants or intermediates[259]. For example, some aromatic species, and especially phenolic intermediates may be polymerized at the surface of the electrodes decreasing the accessibility of the electrode to the reactants and thus its efficiency[267]. Also, carbonyl intermediates can be strongly adsorbed onto Pt electrodes leading to surface passivation. MW irradiation is a way to overcome this limitation. As the azo bond in methyl orange is not completely removed by electrochemical oxidation using Pt electrode, the addition of MW radiation allows its complete mineralization due to the rapid degradation of aromatic intermediates such as dinitrophenol, nitrophenol, hydroquinone,

benzoquinone and small organic acids (maleic and oxalic acids)[267]. Few other examples may be found in ref. [259].

Some examples have been reported showing a beneficial effect of combining MW and high-intensity ultrasound (US) for mineralizing organic pollutants. A synergetic effect was shown when applying MW/US radiations for phenol degradation, even if this effect is more marked when H_2O_2 is present in the reaction medium[268].

3.2. Plasma-catalytic processes utilized in the decontamination of waste waters

As part of water remediation and sustainability, advanced oxidation processes (AOP) promo[269-270]ted by atmospheric pressure plasmas are very promising in the field of wastewater treatment, especially with the aim of their reuse for irrigation, district cooling, process heating/cooling, landscaping, etc.[271-275] In this respect, the decontamination of waste waters through low-temperature plasma induced liquid phase chemistry has received a great interest. [276-278] This interest derives from the efficiency of plasma to generate reactive species such electrons, ions, radicals and photons with an electric field that can further produce reactive oxygen and nitrogen species together with UV light and/or pulsed electric field.[272] Such a chemically aggressive environment at near room temperature both at reduced and at ambient pressures may enable a unique condition promoting degradation of pollutants.

However, only plasma is not enough effective to produce sufficient water purification. The species produced by plasma may induce a certain level of oxidation, but not enough to correspond to a complete mineralization (decontamination) of wastewaters (Figure 31). Atmospheric-pressure dielectric-barrier discharge plasma has proven to be a promising technology for removing priority pollutants from water. However, their efficiency declines when the solution to be treated contains a high concentration of organic matter and mineral salts, which can originate an inhibition or competition effect for the plasma-generated oxidant species.[279] Therefore, coupling plasma with a catalyst is expected to produce a more efficient pollutant degradation[280] with the condition that the catalyst is not affected/damaged by plasma-generated reactive species. Therefore, the dosage of the key species, such as the O atom and quite oxidizing species such as HO^-, O_2^- or HO_2^- generated by direct discharges in water (Figure 31) affording an advanced liquid oxidation, rather than less aggressive O_2, O_3 or NO, obviously also part of the plasma activated oxygen, might be optimized by the presence of catalysts.

Very specific for plasma, the oxidation reactions in aqueous solutions may occur after the switching-off of the plasma reactor as a post-discharge effect due to the relative high lifetime of radicals such as NO or HONOO. [281-283] Figure 32 depicts different discharges used in plasma-liquid treatments. To be effective, the plasma process should be adapted to the envisaged application.
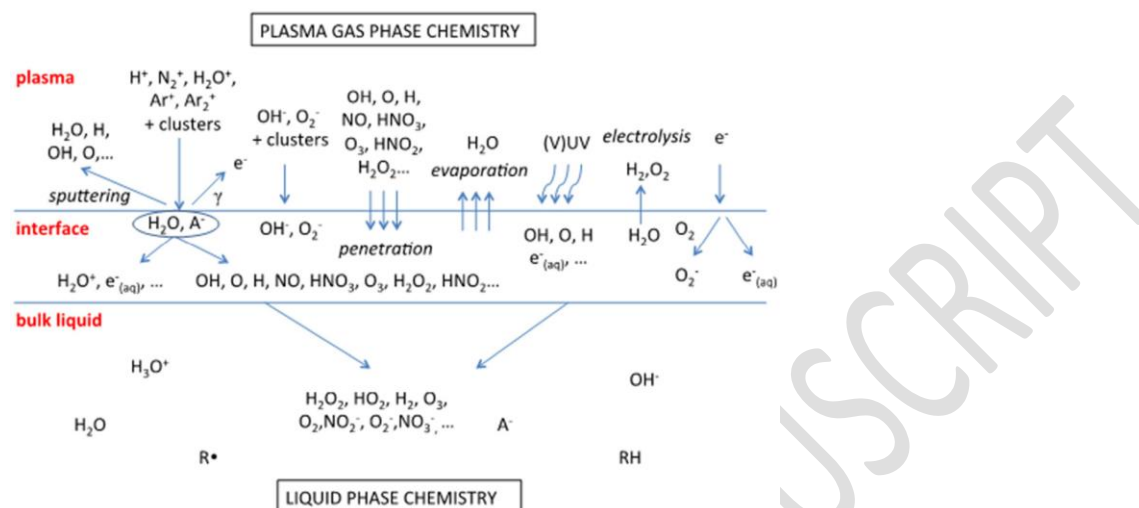
Figure 31. Schematic diagram of some of the most important species and mechanisms for an argon/humid air plasma in contact with water. Reproduced with permission from ref [272]. Copyright 2016 IOP Publishing.
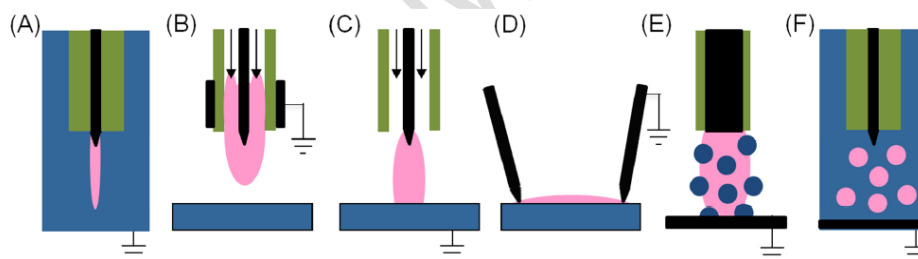
Figure 32. Schematic of different discharges used in plasma-liquid interactions: (a) Direct discharge in liquid, (b-d) gas phase discharges and (e-f) multiphase discharges. In more detail: (b) plasma jet without direct contact with liquid, (c) gas phase plasma with liquid electrode, (d) surface discharge, (e) gas phase plasma with dispersed liquid phase (aerosols) and (f) discharges in bubbles. Blue=liquid, pink=plasma, green=dielectric, black=metal electrodes. Reproduced with permission from ref [272]. Copyright 2016 IOP Publishing.

3.2.1 Plasmas considered for the decontamination of waste waters

Non-thermal plasma, also named cold plasma or non-equilibrium plasma is a non-thermodynamic equilibrium plasma where the electron temperature is much hotter than the temperature of heavier species such as ions and neutral atoms and radicals.[284] Non-equilibrium gas discharges at low pressure, with gas temperatures close to room temperature require a high

electric field to initiate the breakdown that may follow two mechanisms, *i.e.* a) the *Townsend breakdown* that can be generated such as in micro-discharge or special dielectric barrier discharge (DBD) and b) the *streamer breakdown* where the glow regime can also exit in well-controlled corona discharge. At atmospheric pressure a streamer discharge tends to become into a spark discharge, in particular at high current density, which leads to heating of the gas (Figure 33). For the specific case of the water purification by plasma such a situation is not preferred. Therefore, from the technical point of view, it is necessary to avoid the transition of streamer into spark, either by limiting the current density or by controlling the streamer development time.[285]
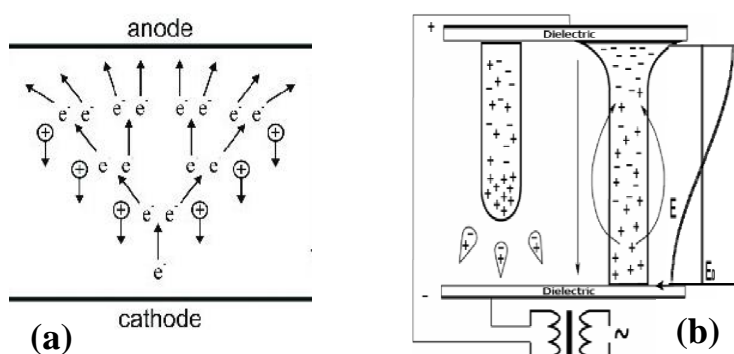
Figure 33. Townsend (a) and streamer (b) breakdown in non-equilibrium gas discharges. Reproduced with permission from ref [286]. Copyright 2020 Wiley-VCH GmbH.

Dielectric-barrier discharge (DBD)

DBD plasma dates since 1857 when it was firstly reported by Ernst Werner von Siemens.[287] DBD plasma is produced at atmospheric pressure and above through the electrical discharge between two electrodes separated by an insulating dielectric barrier without having the extremely high temperatures as in an electric arc (Figure 34).
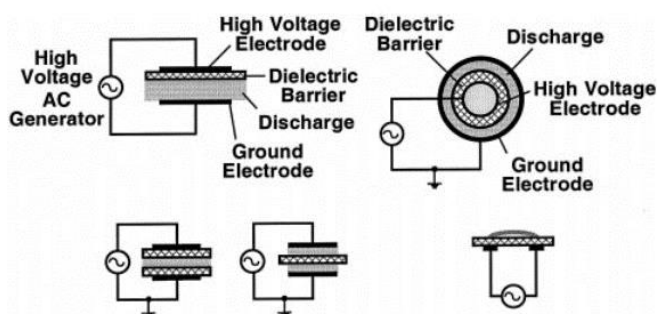
Figure 34. Different DBD configurations. Reproduced with permission from ref [288]. Copyright 2001 Royal Society of Chemistry.

The DBD can be easily applied in water where it may generate ozone that can further initiate the unselective oxidation of organic molecules. The electrons generated in DBDs have mean energies in the range of 1 to 10 eV.[289] Therefore, the combination of non-thermal atmospheric pressure streamer and DBD directly in water is one of the most widely used electric discharge types for water decontamination. Many DBDs have been found to exhibit regular structures depending on their electrode configurations, gas properties, and operation parameters.

Corona discharge (DC)

A DC is a local, non-equilibrium discharge, which occurs only when the field is highly non-uniform. This is produced by electrodes with a small curvature radius, such as a sharp point or a thin wire affording an ionization process confined to a local region in the vicinity of the high voltage corona electrode (Figure 35).

Figure 35. Corona discharge set-up. Adapted with permission from ref [290]. Copyright 2020 IOP Publishing.

DC coronas are not continuous steady-state discharges, as the corona current has a pulsed nature in time with different pulse widths depending on the discharge parameters. In recent decades *pulsed corona discharge* has been widely studied with the aim to increase the corona current.

Glow discharge plasma (GDP)

GDP is an electrical process where the glow discharge in and in contact with liquids can dissociate the water molecule into hydroxyl radical (HO•) and hydrogen atom (•H) as active species for the degradation of the water pollutants (Figure 36a). [291-292]

Microwave-UV plasma (MPUVL)

MPUVL is another technology for generating a high-intensity UV light and that can be also controlled to operate at a certain length by producing ozone (Fig. 36b). The microwave power is injected into a resonant cavity and the surface wave excitation takes place within the cavity through that part of the discharge tube (fused silica) protruding inside it.[293] This plasma has the advantages of controlling the power per unit length of tubes of any shape, length or diameter.
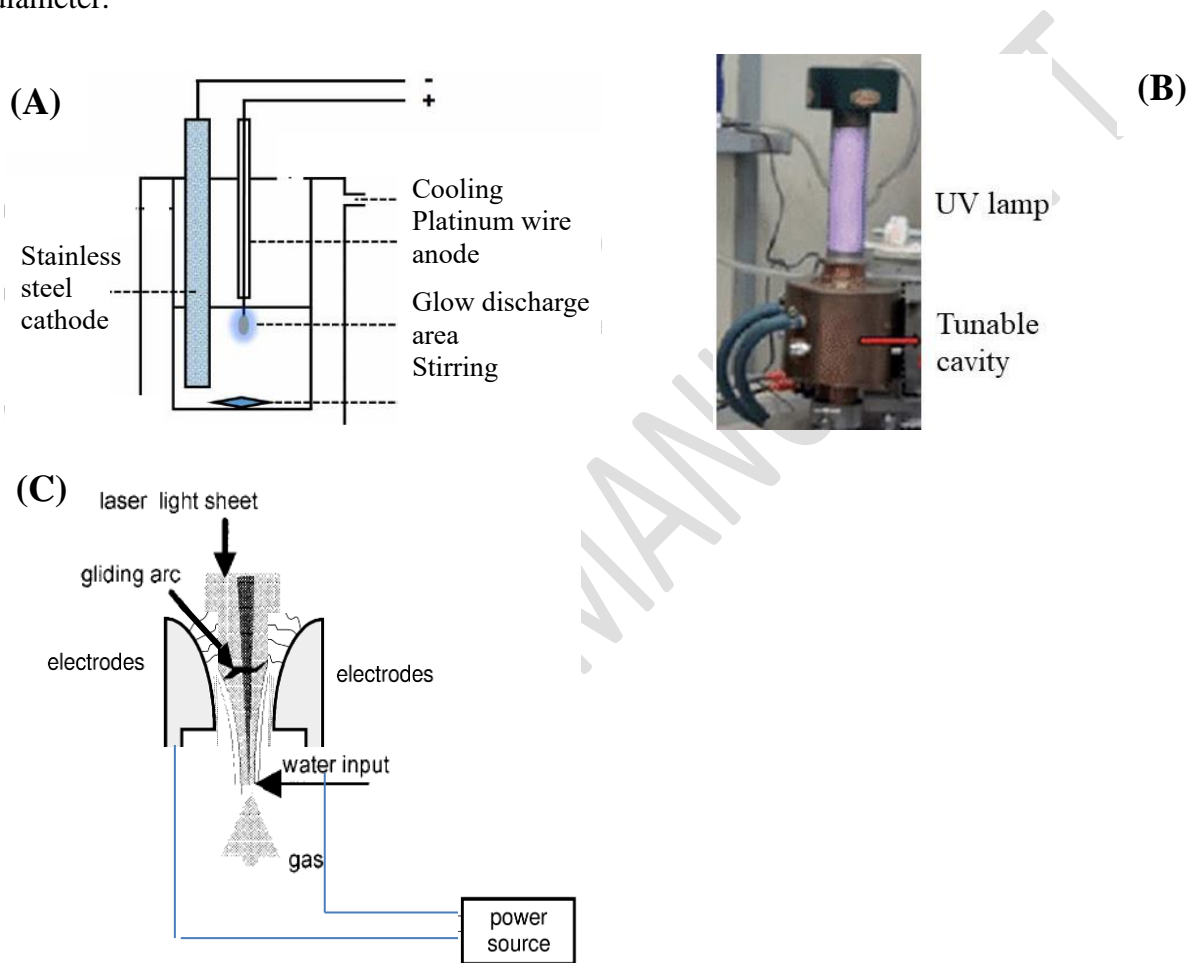
Figure 36. (A) Set-up of a GDP electrical process. Reproduced with permission from ref [294]. Copyright 2016 IWA Publishing. (B) Set-up of a MPUVL system. Adapted from ref [293]. Copyright 2001 IOP Publishing. (C) Set-up of gliding arc discharge plasma system. Adapted from ref [295]. Copyright 1996 IAP Publishing.

Gliding arc discharge plasma (GADP)

GADP is a type of non-equilibrium plasma near atmospheric pressure, in between the thermal plasma and cold plasma. Accordingly, it is enough selective and efficient in the

stimulation of chemical reactions, generally for limited power and low pressure, and may serve in environmental applications (Figure 36c).

3.2.2. The combination of plasma with catalysis

The combination of plasma with catalysis is expected to produce a cumulative enhancement of the AOP efficiency.[296] Plasma generated in electrical discharge already afforded some promising results in environmental applications working at atmospheric pressure and nearby room temperature. Aqueous discharge plasma technologies and their applications for water decontamination have achieved many valuable results during the past 30 years, and some papers and books have comprehensively reviewed and discussed the development of aqueous plasma chemistry, electric discharge mechanisms and water treatment applications. Furthermore, since plasma chemical processes are rather unselective their association with catalysis may generate an improved selectivity for the total oxidation.[297]

Plasma has been associated with both homogeneous and heterogeneous catalysis.[296] Homogeneous catalysis is limited to reactions involving cations of transition metal elements (Fe^{n+}, Mn^{n+}, Co^{n+}, etc.) and the Fenton reaction as well.[298] Except for the TiO_2 which was the most often plasma catalyst the rest are mainly oxides of the same transition metal elements utilized in homogeneous catalysis coupled plasma.[308,309] Immobilized catalysts have been reported as well.[299]

3.2.3. Catalytic treatment of water under the plasma exposure

DBD-plasma catalytic systems for wastewater treatment

The DBD configuration allows a suitable positioning of the catalyst very close to the discharge zone.[300] In this way, the interaction between the electric field and the catalyst surface is enhanced, and the interaction between the UV rays generated by the plasma and its oxidizing species with those generated by the catalyst generates a synergy. However, such a configuration is less suitable for a powder catalyst but is proper for a structured catalyst. It also gives the possibility of an easy catalyst separation at the end of the treatment.[300]

High voltage electrical discharges in and in contact with liquids involve combinations of AOPs and produce high-energy electrons, UV light, and shock waves. The electrons produced by electrical discharge are highly energetic with a typical mean energy of 1–10 eV, which can collide with background molecules and induce secondary reactions to generate other reactive

species, such as those presented in Figure 31. However, different types of discharge exhibit different characteristics in terms of both the nature of the reactive species and extent of water purification. For example, H_2O_2 can be formed in water via either DBD or microwave plasma jets.[301-302]

Degradation of plasticizers from water

Electric discharge plasma can efficiently degrade aqueous pollutants by its *in-situ* generated strong oxidative species (HO•, O•, H_2O_2, O_3, etc.) and other physicochemical effects (UV irradiation, shockwaves, local high temperature, etc.), but a high energy consumption limits its application in water treatment.[276] The contribution of the catalysts in such processes is related to their capability to activate molecular species such as O_3 and H_2O_2. Thus, the combination of the participation of the radical oxidative mechanism with that of the catalyst activated species should enhance the total oxidation process.

The spectral emission intensities of the reactive species generated by plasma are stronger in water compared to air.[273] However, under flow conditions this intensity decreases along with the flow speed. Also, the reaction kinetics was found to be diffusion-controlled when the solution flow speed was low and activation-controlled under high solution flow speed. This is obviously translated in an enhanced degradation efficiency with increasing flow speed, which increased the discharge voltage and temperature of the solution and changed the initial pH value.

Such a behavior may associate to a photocatalytic process as it has been demonstrated for the degradation of phenols and *p*-nitrophenols generated from petrochemicals, resins, papermaking, plastics, synthetic fibers, oil refineries, coking plants, medical industries, and many other industries.[273] The bandgap value of anatase TiO_2, around 3.2 eV, enables the activation of the catalyst through irradiation produced by plasma. However, such a combination of plasma with the TiO_2 catalyst does not produce a complete, but only an advanced oxidation of the phenols. High phenol removal yields by electrical discharge were reported in combination with a less acidic catalyst such as FeZSM-5.[303] The addition of NH_4ZSM-5 and HY zeolites afforded only a very small increase in the phenol removal respect to Fe-exchanged zeolite. For FeZSM5, the phenol removal yield was almost doubled.

Degradation of bisphenol A in water has been carried out on rGO-WO_3 nanocomposite with superior results respect to sole DBD as well as to DBD/WO_3 systems, as demonstrated by the degradation rate constant.[304] Also, the measurement of the evolution of the O_3 and the H_2O_2

concentrations in the reaction system proved the catalytic behavior of rGO-WO$_3$ for the HO•
formation, while its combination with GO led to a positive enhancement of the catalytic effect
(Figure 37).
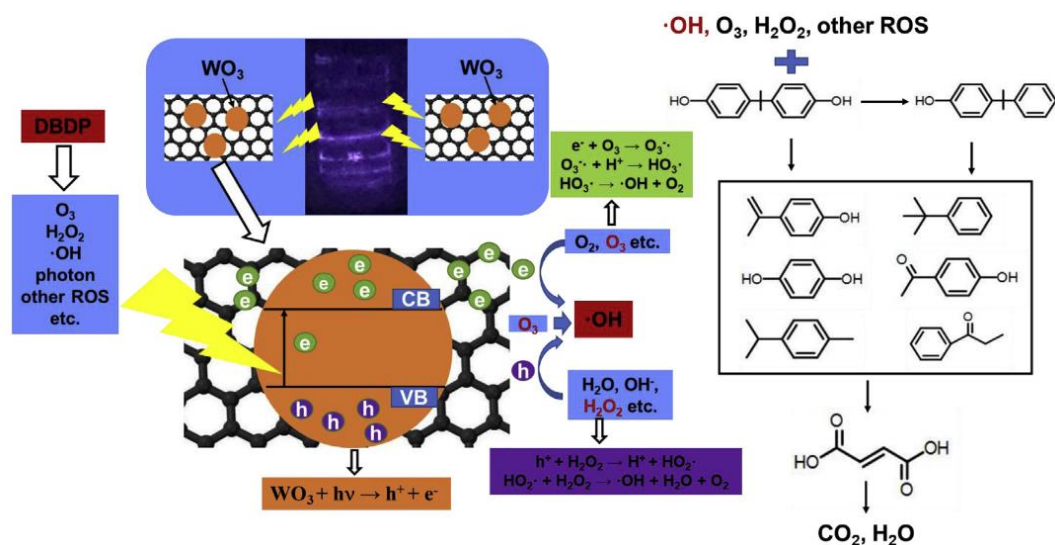
Figure 37. Catalysis and degradation procedure of the BPA in the DBDP/rGO-WO$_3$ system Reproduced
with permission from ref [304]. Copyright 2021 Elsevier.

Decontamination of waters polluted with pharmaceuticals by plasma coupled with catalysis

Trans-ferulic acid is an important part of *γ*-oryzanol utilized as ingredient in various
medicines, and one of the main organic component of olive oil mill wastewaters. The
degradation of this compound in water was reported using DBD plasma coupled with a CoOOH
catalyst where the synergistic effect of plasma and catalyst has been attributed to the catalytic
conversion of plasma-produced O$_3$ and H$_2$O$_2$ into OH on the active sites of CoOOH surface,
i.e. Lewis acid sites offered by the lattice.[305]Figure 38 illustrates routes and reactions involved
in the catalytic process.
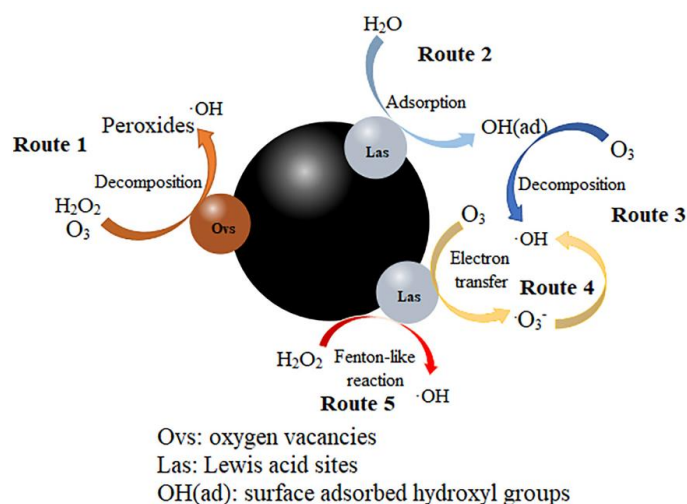
Figure 38. Routes involved in the plasma coupled catalytic degradation of *Trans* -ferulic acid. Reproduced with permission from ref [305]. Copyright 2019 Elsevier.

Methylene blue, also known as methylthioninium chloride, and "the first fully synthetic drug used in medicine".[306] is a medication and dye.[307] It is also extensively used as synthetic dye in various industries such as textile, paper and plastics to impart aesthetic color to the materials. The effluents of these industries generate wastewaters representing a dramatic source of non-aesthetic pollution, eutrophication and perturbations in the aquatic life.[308] Due to these negative effects, methylene blue has been often considered as a probe molecule for the plasma-catalysis degradation experiments. Its degradation by plasma-coupled catalysis using Cu, W or Fe electrodes as source of the corresponding metal nanoparticles has been proposed to occur *via* both homogeneous (release of dissolved metal ions) and heterogeneous (on the surface of the particles) catalytic processes.[308] Both are associated with either the production of radical OH·according to equation (61) or the steps illustrated in Figure 38.

$$H_2O_2 + Cu^+ + H^+ \rightarrow HO\bullet + Cu^{2+} + H_2O \qquad (61)$$
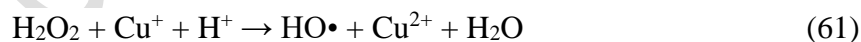
By association with the radicals generated during the decomposition of the species generated by plasma, the degradation of pharmaceuticals in water has also been investigated using heterogeneous photocatalysts like TiO_2 derived materials. Thus, the removal of triclocarban (TCC, an antimicrobial and antifungal compound) in aqueous solution has been reported using DBD plasma combined with TiO_2-coated activated carbon fibers (TiO_2/ACFs) catalysts at atmospheric pressure and room temperature.[309] Equation (62) indicates that TiO_2 and ACF can decompose ozone and the resultant O• radical would contribute to an advanced

removal process of organic pollutants through the production of •OH radicals (Figure 39). Further addition of gold enhances the rate of the processes, however, with a still incomplete mineralization.[310]

$$O_3 + TiO_2 \ (TiO_2/ACFs) \rightarrow O\bullet + H_2O \rightarrow 2 \ HO\bullet \tag{62}$$
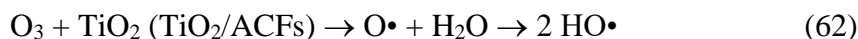
The role of ACF has also been confirmed from its combination with Ag_3PO_4 in the degradation of quinolone antibiotic levofloxacin in water. The synergetic effect induced by the addition of Ag_3PO_4/ACFs led to a four times increase of the mineralization rate.[311]
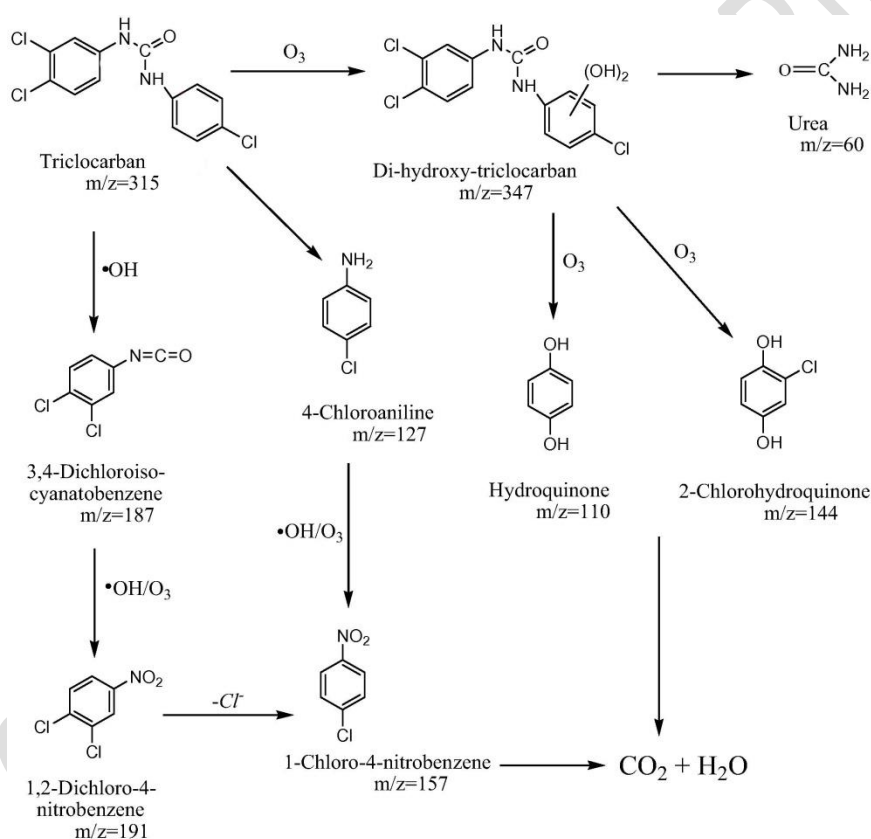
Figure 39. The proposed degradation pathway of TCC in DBD/TiO$_2$/ACFs system. Reproduced with permission from ref [309]. Copyright 2016 Elsevier.

High degradation effects on penicillin antibiotics (ampicillin and amoxicillin) were also reported upon DBD plasma exposure,[312] while further enhancement was achieved by the addition of a homogeneous catalyst (salts of Fe^{2+}, Co^{2+}, Mn^{2+}, or H_2O_2, etc.). The same effect was observed in the case of another penicillin (norfloxacin) or methylene blue.[313-314]Other complex molecules as nicotine ((S)-3-(1-methylpyrrolidin-2-yl)pyridine ($C_{10}H_{14}N_2$)), an agonist at most nicotinic acetylcholine receptors, or ibuprofen ((**N**-[2-cyclohexyloxy-4-

nitrophenyl] methanesulfonamide)), an analgesic and anti-inflammatory drug, were as well partially degraded in similar conditions (Figure 40).[315-316]
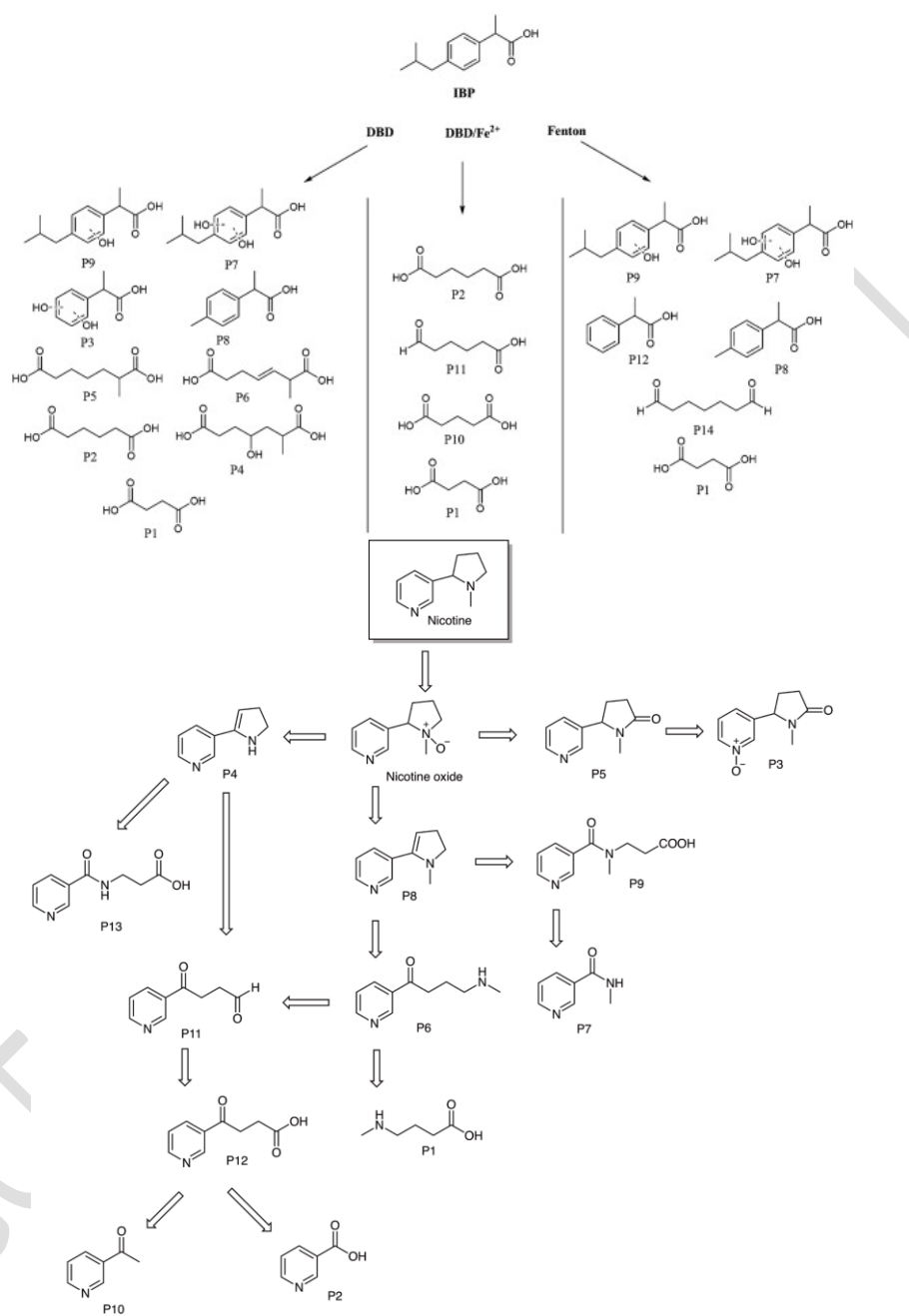
Figure 40. Proposed mechanism for the ibuprofen and nicotine degradation in the DBD reactor. Reproduced with permission from refs [315] and [316]. Copyright 2018 IOP Publishing and 2015 Elsevier.

These results confirmed the importance of soluble metal species in the process. Other more reactive additives such as CaO_2, acting as promoter, were also found to enhance the degradation rate compared to H_2O_2.[317] In all these cases, the homogeneous cation catalyst promotes a

Fenton reaction with the plasma-generated H_2O_2, thus enhancing the aqueous HO• concentration.

Heterogeneous catalysts containing the same active species, *i.e.* supported iron and manganese oxides on granular activated carbon, showed similar performance under DBD plasma for the degradation of oxytetracycline in water.[280] Compared to individual oxides it has been concluded that the supported oxides could better catalyze the O_3 decomposition into active HO•, HO_2• and O^{2-} radicals responsible for the enhanced degradation of oxytetracycline, even though the oxidation is leading to a mixture of degradation compounds in the final treated water.

In-situ decomposition of ozone produced in plasma with the formation of atomic oxygen may also be achieved taking a metal oxide catalyst. This has been confirmed with CeO_2, Fe_2O_3/CeO_2, and ZrO_2/CeO_2 for the degradation of sulfamethoxazole, an antibiotic for bacterial infections,[318] and of phenol, and associated to the presence of the oxygen vacancies.[319] The acid/base properties of the support exert only a limited effect, the main role being assumed to the supported cation. As a confirmation, the mineralization of paracetamol in water via a plasma-catalyst coupling process using a neutral glass fiber supported Fe^{3+} catalyst led to a mineralization rate of 54% for a full conversion of paracetamol.[320] The synergetic effects of the plasma-catalysis combination improved the energy yield by a factor of two.

Graphene-Fe_3O_4 nanocomposites fit even better for such applications. Their introduction into discharge plasma system, which made full use of the light and H_2O_2 to induce a photo-Fenton reaction, would promote the formation of ·OH. Meanwhile, the magnetism endowed by catalyst allows an easy separation from the aqueous solution and avoids secondary pollution caused by the catalyst. Figure 40 shows the concentration of reactive HO• in three different configurations: plasma, plasma and Fe_3O_4 and plasma reduced graphene-Fe_3O_4.[321] In accordance to this behavior, the degradation efficiency of ofloxacin, an antibiotic whose presence in aquatic environment causes renal dysfunction, allergic reaction and central symptoms, is increased from 65 to 99.9 %.

Fe(0) has also been reported as effective in the plasma-catalytic degradation of pharmaceutical wastes.[322] The results with a nano- zero-valent Fe^0-CeO_2 nanocomposite catalyst in the degradation of diclofenac (a nonsteroidal anti-inflammatory drug used to treat pain and inflammatory diseases) showed that it significantly enhanced the removal of this pharmaceutical, with a synergistic factor DBD/catalyst of 3.7 and a great reusability. It significantly promotes the generation of reactive oxygen species in the DBD system with both O_3 and H_2O_2.

The effect of the oxide crystal phase on the degradation activity of antibiotics in wastewater was checked for α-MnO$_2$, β-MnO$_2$ and γ-MnO$_2$ catalysts for ciprofloxacin.[323] Higher levels of Mn^{3+} were observed for α-MnO$_2$ probably due to an enhanced population of defects prone to interact with the species produced by plasma irradiation. The combination of DBD with α-MnO$_2$ showed the highest ciprofloxacin degradation efficiency (ca 93%) Besides the crystal phase, the process is influenced by the peak voltage, air flow rate, concentration and pH.
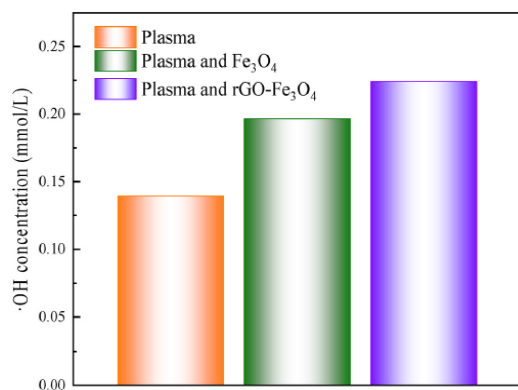
Figure 41. Formation of ·OH under various systems. Reproduced with permission from ref [321]. Copyright 2021 Elsevier.

Decontamination of waters polluted with pesticides

The degradation of thiamethoxam, a systemic insecticide from the neonicotinoids class, was investigated by coupling plasma with a TiO$_2$ catalyst.[324] The degradation process was promoted by the addition of homogeneous Fe^{2+} and Cu^{2+} sulfates as catalysts due to an additional production of radicals.[314] The mechanism is described in Figure 42.[324]

The DBD degradation of pesticide nitenpyram has been investigated with both homogeneous (FeSO$_4$, Fe$_2$(SO$_4$)$_3$) and heterogeneous (MnO$_2$) catalysts. The degradation tests indicated that basic conditions (pH = 11, associated to the reaction of ozone with water followed by decomposition of H$_2$O$_2$ to HO• at high pH values), homogeneous catalysts and higher applied voltages favored the degradation of this pesticide.[325] The reaction mechanism is, however, doubtful, since at basic pH values •OOH are the preferred radicals formed from H$_2$O$_2$.
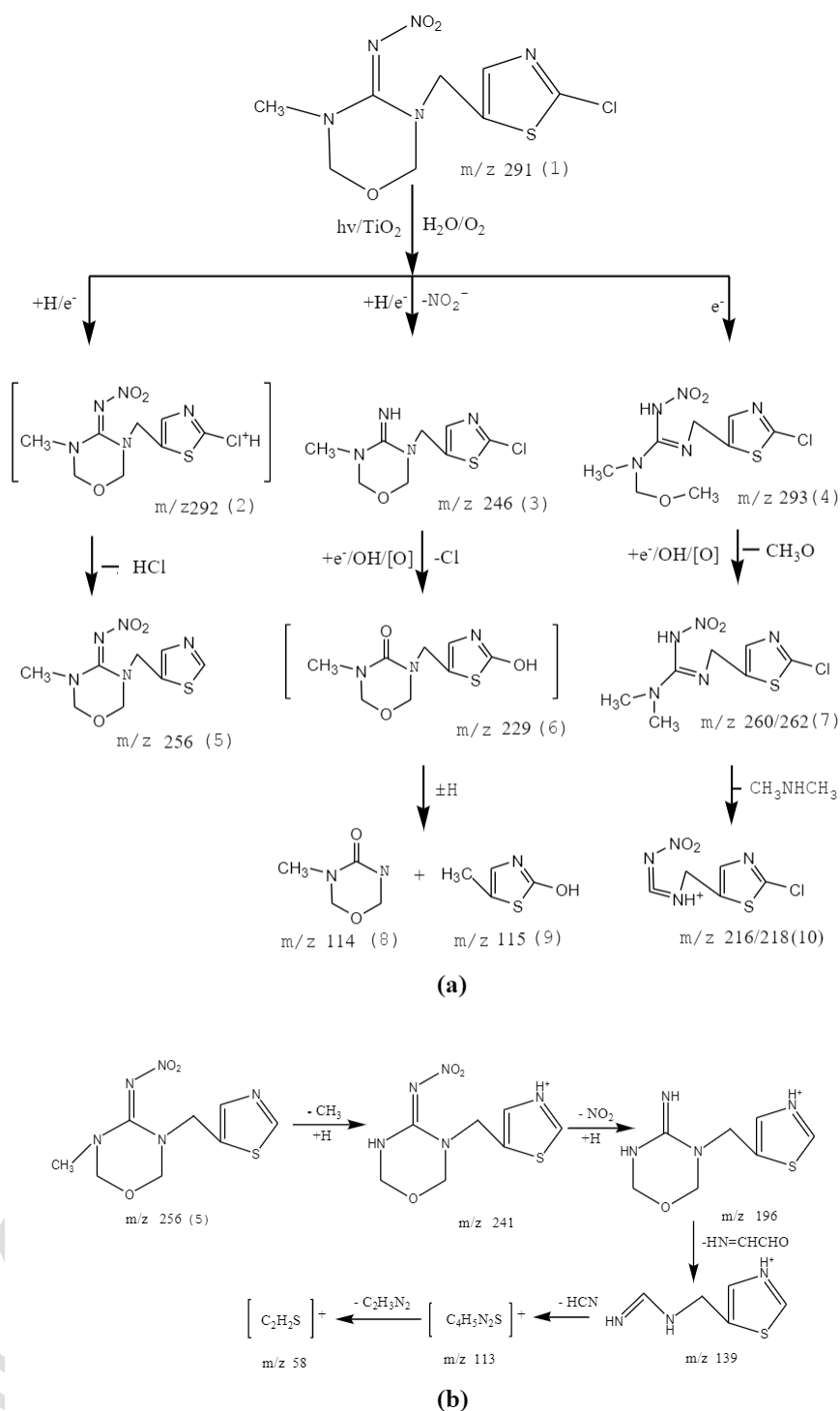
Figure 42. (a) Degradation process of thiamethoxam; (b) Probable degradation pathway. Reproduced with permission from ref [324]. Copyright 2016 De Gruyter.

Decontamination of waters polluted with organic dyes from the textile industry

The degradation of the organic dyes has also been investigated by coupling plasma with both heterogeneous and homogeneous catalysts. By association with photocatalysis, TiO$_2$ powders have been also investigated as catalysts under plasma exposure. The use of TiO$_2$ has

the advantage of utilizing ultraviolet radiation in the discharge process with TiO_2 and the capacity of the defects to interact with species produced under plasma.[272] Thus, TiO_2 improves the overall energy efficiency and degradation performance. However, working with TiO_2 powders generate operational difficulties. To avoid this, TiO_2 powders can be replaced by titanium anodic electrodes. Taking a high voltage to generate plasma it may produce dissolution of the cathode and the formation of TiO_2 particles onto the electrode. The presence of these TiO_2 particles in the electrolyte increases the degradation of Rhodamine B dye through a photocatalytic mechanism.[326] Foils containing titanium and gold exhibit a superior effect than Ti alone, while the coverage with Cu and Ta leads to less effective catalysts due to the fact that oxide particles produced from the Cu or Ta electrodes during plasma discharge have no photocatalytic performance.[326]

Collective effects also resulted from combining a hetero-structured Ag/TiO_2 nanocomposite catalyst with the O_3 produced in an atmospheric pressure plasma jet generated in a DBD system for the degradation of methyl orange. Accordingly, the Ag quantum dots dispersed on a commercially available TiO_2 photocatalyst (Evonik P25) afforded a catalytic advanced oxidation of methyl orange leading to a fast cleavage (over 90 % within 15 min).[327]

The discoloration and mineralization of "acid orange 7" azo dye was studied with a structured catalyst consisting of Fe_2O_3 immobilized on glass spheres. Experiments carried out in a DBD reactor led to a complete discoloration and even a mineralization of 80 % of the dye, working with a voltage equal to 12 kV.[328] Tests with radical scavengers evidenced that the species that contributes the most for the degradation of this dye was $O_2\bullet^-$ generated according to the mechanism described in Fig. 43.

Fe-MOFs have also been investigated for the degradation of methyl orange in a DBD plasma/Fenton-like system in which the electron (e^-) photogenerated by plasma promotes the Fe(II)/Fe(III) cycle.[329] The proposed reaction mechanism consisted mainly in a coordinated oxidation process of hydroxyl radicals (HO$\bullet$), photo-generated holes (h^+) and superoxide radicals ($\bullet O_2^-$). In addition, these Fe-MOFs showed stability and reusability in several consecutive degradation processes.

The degradation via homogeneous catalysts has been demonstrated for 4-chlorophenol, a precursor of the quinizarin dye, in a rather expensive and less applicable system consisting in hydrogen peroxide and Fe^{2+} with a significant decrease in the toxicity.[330] A significant enhanced rate of crystal violet degradation has been reported as well.[331]

The presence of iron catalyzes the decomposing of H_2O_2 in Fenton-type reactions and provides an additional source of •OH radicals according to equation (63).

$$Fe^{2+} + H_2O_2 \rightarrow HO\bullet + OH^- + Fe^{3+} \tag{63}$$
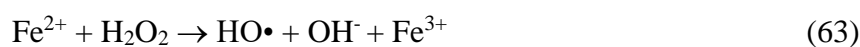
Degradation of surfactants from fresh waters

Dielectric barrier discharge under atmospheric pressure associated to heterogeneous catalysts has also been considered for the decomposition of sulfonol (alkylphenylsulfonate, $C_{12}H_{25}C_6H_4SO_3Na$) and sodium lauryl sulfate ($C_{12}H_{25}SO_4Na$) surfactants in water solution.[332] Among the investigated catalysts (NiO, TiO$_2$, Ag$_2$O and NiO/TiO$_2$) Ag$_2$O demonstrated the best catalytic behavior. These catalysts caused not only changes in decomposition rates, but also in the formation rates of intermediate and final degradation products, consisting in a mixture of carboxylic acids, aldehydes, carbon dioxide and phenol.

Degradation of toxic pollutants from fresh waters

Microcystins are hepatotoxic cyclic heptapeptide toxins produced by cyanobacteria that affect the nerve system and liver in human body. These are found in freshwater.[333] and their degradation has been reported by combining plasma irradiation with Mn/Ti-doped carbon xerogel catalysts,[334] *i.e.,* solid materials able to activate species produced by plasma. As for the other complex molecules the degradation is limited to compounds whose presence in water is still not innocuous (Figure 43).
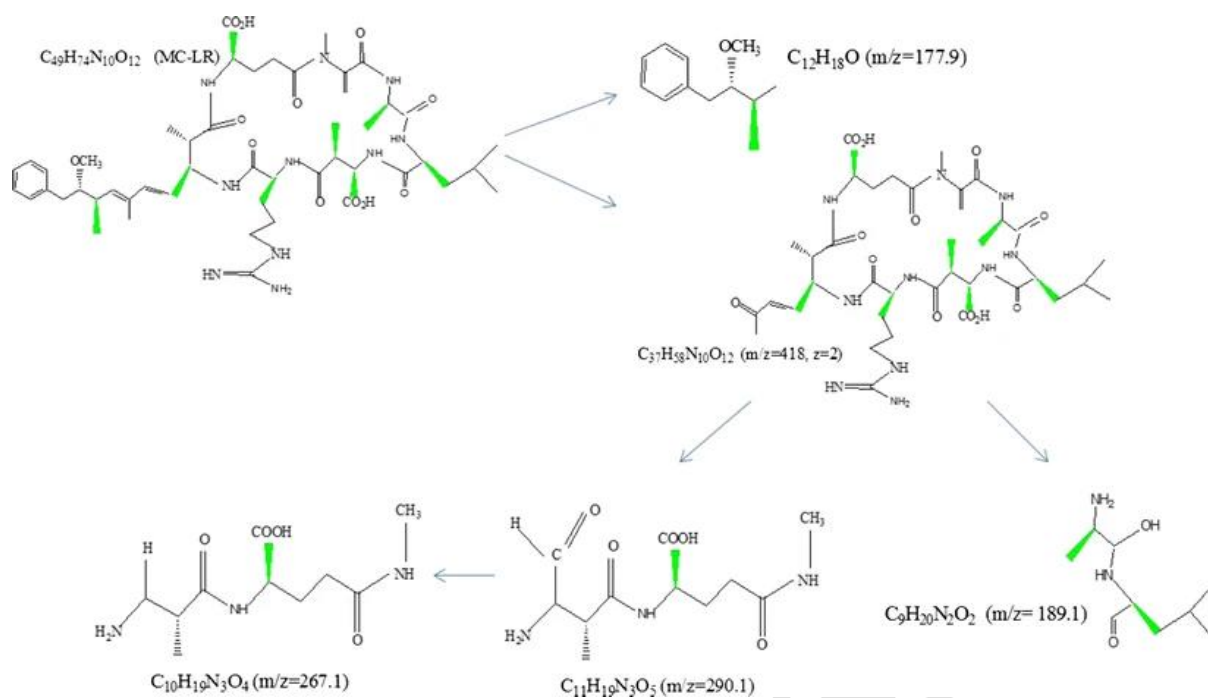
Figure 43. Proposed degradation pathway of microcystins by water surface discharge with Mn/Ti-doped carbon xerogel catalysts. Reproduced with permission from ref [334]. Copyright 2015 Springer Nature.

Decontamination of waters polluted with organic dyes under DC

Pulsed discharge plasma produced underwater is an attractive method to treat wasted water based on some physical effects, such as an intense electric field at a tip of discharge plasma, ultraviolet radiation, chemically radical formation and shockwave generation.[335] However, so far the method has been merely considered for the degradation of the dyes and pharmaceuticals from waters. The water treatment by bipolar pulsed discharge plasma brings some additional advantages compared to cold plasma. Besides the chemical effects, physical effects such as the optical radiation allows association with a photocatalyst such as TiO_2 nanoparticles. This synergistic model has been demonstrated for the degradation of an Indigo Carmine dye in aqueous solution.[336] Multi-walled carbon nanotubes (MWCNT)-TiO_2 supported on γ-Al_2O_3 composites were investigated in pulsed discharge plasma for the degradation of azo dye acid orange II with a total degradation (but not mineralization).[337] The activation of oxygen in these reactions was suggested to occur as a synergetic process through a photoinduced electron absorption on titania and electron transfer on MWCNT (scheme 5).

$$MWCNTs + (e^-) + O_2 \rightarrow \bullet O_2^- + MWCNTs \xrightarrow{H_2O} \bullet OH + MWCNTs$$
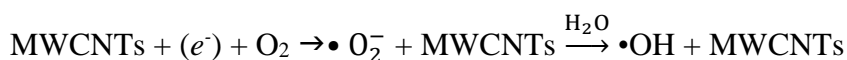
Scheme 5. The activation of oxygen under DC plasma catalytic conditions

Homogeneous catalysis combined with pulsed electrical discharge plasma considered ferrous ion as catalyst and methylene blue as a liquid phase hydroxyl radical scavenger. The non-homogeneous nature of the plasma discharge favored the production of hydrogen peroxide in the plasma-liquid interface over the chemical oxidation of the organic in the bulk liquid phase, while post-plasma reactions with the Fenton catalyst led to a complete utilization of the plasma-formed hydrogen peroxide.[338]

The degradation of methylene blue by pulsed corona discharge has been investigated in the presence of a $FeCl_2$ catalyst.[282] These experiments evidenced the role of the pH and the concentration of H_2O_2 generated in water during the plasma time. Post-plasma chemical reactions of methylene blue and its degradation products with active species which persisted in the aqueous solution were evidenced by their continuous decrease and by H_2O_2 concentration as well after the discharge have been stopped.

Decontamination of waters polluted with pharmaceuticals under DC

DC catalytic systems was as well considered for the degradation of pharmaceutical compounds.[339] Tetracycline has been degraded in the presence of suspended nanoparticles of flake-like Bi_2MoO_6 catalyst, but merely without the disruption of the condensed cycles (Figure 44).
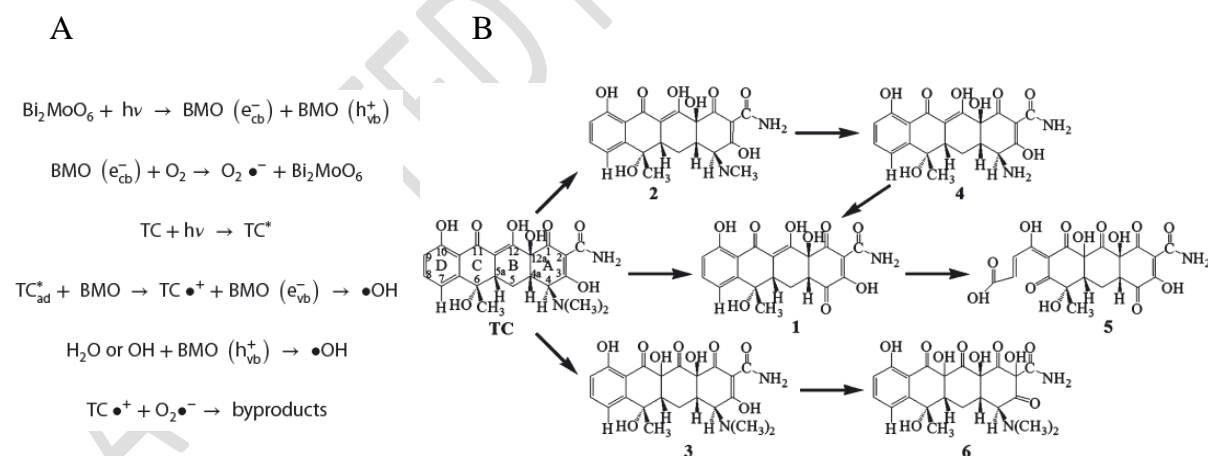
Figure 44. (A) Catalytic involvement of the Bi_2MoO_6 catalyst and (B) the proposed degradation pathway of tetracycline under corona discharge plasma. Adapted from ref. [339]. Copyright 2014 Wiley.

Degradation in water of flumequine, a synthetic fluoroquinolone antibiotic used to treat bacterial infections, has been investigated by coupling pulsed discharge plasma with reduced graphene oxide (rGO)/TiO_2 nanocomposites. Compared with the individual rGO and TiO_2, their association provided a synergetic behavior affording an increased consumption of O_3 with

the production of additional •OH radicals, thus accelerating the degradation of the antibiotic. Mineralization of the antibiotic into CO_2 and H_2O is, however, only partial. Besides, the effect of the catalyst dosage, plasma (peak voltage, air flow rate) and chemical (solution pH) parameters are important factors controlling the process efficiency.[340]

Other nanocomposites comprised of reduced graphene oxides and Fe_3O_4[341] or WO_3 were investigated for the degradation of ofloxacin and enrofloxacin by pulsed discharge plasma. The degradation of these therapeutic drugs followed the same mechanism as for the (rGO)/TiO_2 nanocomposites, and due to the complexity of the targeted molecules, took place only with a rather small mineralization degree (Figure 45).[342]
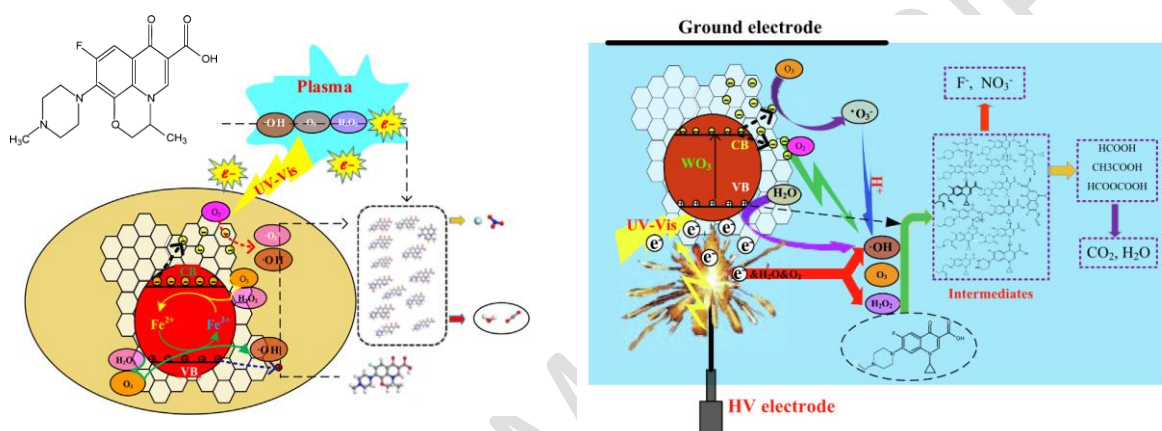
Figure 45. Schematic illustration of ofloxacin degradation mechanism by discharge plasma coupled with rGO-Fe_3O_4. Adapted from refs [341] and [342]. Copyright 2021 and 2019 Elsevier.

Composites of different oxides as TiO_2/WO_3 were as well associated to pulsed discharge plasma to increase the degradation of chloramphenicol.[343] As in the previous examples, the composites accelerated the interfacial charge transfer process leading to •OH, O_3, O_2^-, h^+ and high-energy electrons that contributed to the degradation process (Figure 46). Cycling degradation experiments confirmed a good reusability as well as stability of the TiO_2/WO_3 composite.
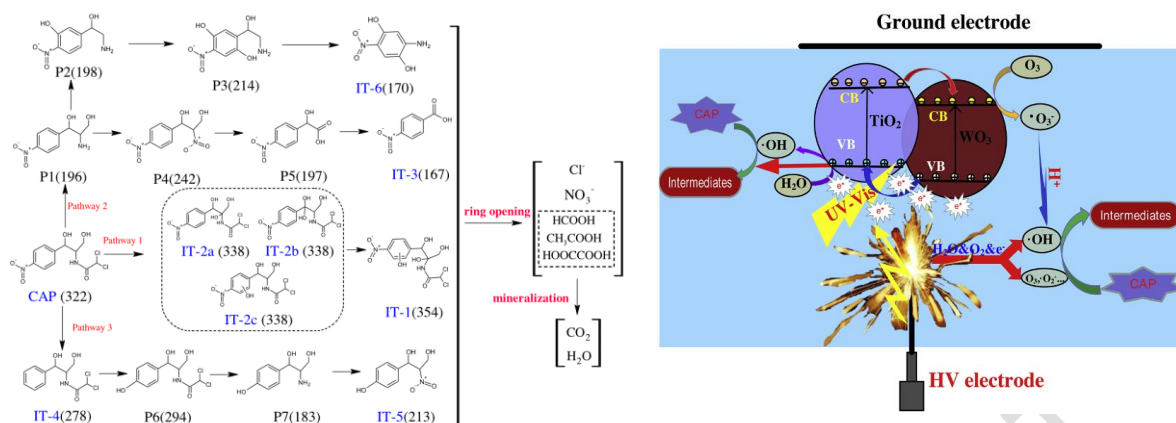
Figure 46. Proposed pathway of chloramphenicol degradation in pulsed discharge plasma TiO_2/WO_3 system and schematic illustration of the degradation mechanism. Adapted from ref [343]. Copyright 2019 Elsevier.

GDP catalytic systems for waste water treatment

GDP has been considered for the degradation of phthalates, i.e. compounds integrated in the plasticizers group, in an aqueous solution, by association with pyrite as a heterogeneous iron source in the Fenton catalytic reaction.[294] Phthalate derivatives as 4-hydroxyphthalic acid, 4-methylphthalic acid and 4-tert-butylphthalic anhydride were degraded in this way with efficiencies over 99% in a rather short range of time. The degradation is sustained by the continuous formation of •OH and the inhibition of the quenching reaction in the pyrite Fenton system due to the constant dissolution of Fe(II). However, the increasing concentration of SO_4^{2-} anions in water according to reaction steps (64)-(67) is not beneficial.

$$2FeS_2 + 7O_2 + 2H_2O \rightarrow 2Fe^{2+} + 4SO_4^{2-} + 4H^+ \qquad (64)$$

$$2FeS_2 + 15H_2O_2 \rightarrow 2Fe^{3+} + 4SO_4^{2-} + 2H^+ + 14H_2O \qquad (65)$$

$$2FeS_2 + 14Fe^{3+} + 8H_2O \rightarrow 15Fe^{2+} + 2SO_4^{2-} + 16H^+ \qquad (66)$$

$$Fe^{2+} + H_2O_2 \rightarrow Fe^{3+} + OH^- + HO• \qquad (67)$$
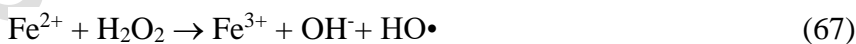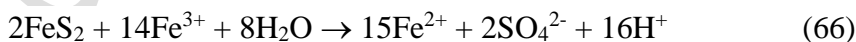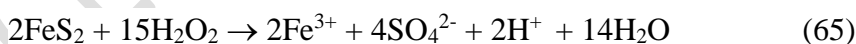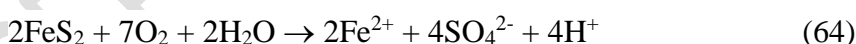
GADP catalytic systems for the water treatment of surfactants and dyes

The degradation of perfluorinated non-ionic surfactant (Forafac) in the gliding arc in humid air is accelerated by the presence of titanium dioxide powders as catalysts.[344] The gliding arc discharge in association to TiO_2 enhanced the production of the OH• radicals. The use of anatase and rutile led to different results and like in most photocatalytic processes, anatase was more efficient.

The degradation of a cocktail of azo and/or anthraquinonic dyes has also been studied by non-thermal gliding arc coupled to titanium dioxide as photocatalyst. The process merely consisted in decolorization of water that still contain residues of organic molecules and chloride, sulphate and phosphate ions.[345]

3.2.4. Plasma reactors for waste waters treatment

Technologies involving plasma discharges in water as advanced oxidation techniques makes not any more necessary the addition of external reagents such as strong oxidants (O_3 or H_2O_2, these being produced *in-situ*). This saving of chemicals makes plasma treatments very attractive. However, application of such technologies in practice demands high energy yields that largely depend on the reactor configuration and the operational conditions.[346] Further combination of these technologies with catalysis requires the implementation of specific plasma catalytic reactors for optimal decontamination of which design and operatory conditions at an applicative level are not trivial.

The discharge in the treatment of liquid solutions is typically realized: i) above the liquid surface, ii) direct in liquid, and iii) in bubbles/vapor in liquid.[347] As commented above, these discharges produce specific radical species with high oxidative potential such as hydroxyl groups, singlet oxygen (Scheme 6).

$$H_2O + e \rightarrow HO\bullet + H\bullet + e \quad (68)$$

$$H_2O + e \rightarrow H_2O^+ + 2e \quad (69)$$

$$H_2O + H_2O^+ \rightarrow H_3O^+ + {}^\bullet OH \quad (70)$$

$$H_2O + e \rightarrow H_2O^* + e \quad (71)$$

$$H_2O + H_2O^* \rightarrow H_2O + HO\bullet + H\bullet \quad (72)$$

$$H_2O + H_2O^* \rightarrow H_2O + {}^\bullet O + H_2 \quad (73)$$

$$H_2O + H_2O^* \rightarrow H_2O + {}^\bullet O + 2H\bullet \quad (74)$$

$$2H_2O \rightarrow H_2O_2 + H_2 \quad (75)$$

$$H_2O_2 + e^-_{aq} \rightarrow HO\bullet + OH^- \quad (76)$$

$$H_2O_2 + H\bullet \rightarrow H_2O + HO\bullet \quad (77)$$

$$H_2O_2 + O_3 \rightarrow HO_2{}^\bullet + O_2 + HO\bullet \quad (78)$$

$${}^\bullet O + H_2O \rightarrow 2HO\bullet \quad (79)$$

$${}^\bullet O + O_2 \rightarrow O_3 \quad (80)$$

$$HO\bullet^- + O_3 \rightarrow HO_2{}^\bullet + O_2{}^- \quad (81)$$

$$O_2{}^- + H^+ + O_3 \rightarrow HO_3{}^\bullet + O_2 \quad (82)$$

$$HO_3{}^\bullet \rightarrow HO\bullet + O_2 \quad (83)$$
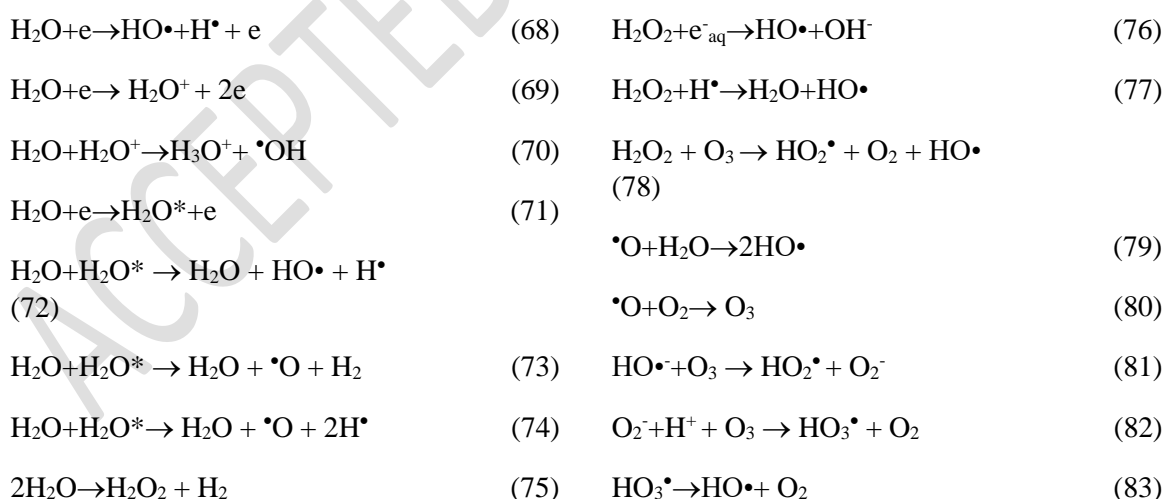
Scheme 6. Radical species produced under plasma catalytic treatment of wastewaters

Each type of discharge requires specific reactors [298,348-349]. Plasma catalytic bubble column reactor is a potential solution for such applications. Experiments carried out with red azo dye

azophloxine in the presence of the CeO_2 catalysts indicate a multistep process with intermediate byproducts that cannot completely be mineralized. Noteworthy, the performance and durability of CeO_2 were further improved via plasma preactivation.[350] Using a DBD reactor bubbled with zero air (*i.e.* less than 0.1 ppm of hydrocarbon impurities) allows an advanced oxidation process (reported for the mineralization of model pesticides and dye pollutants) from aqueous medium with a good control of the effect of various parameters like applied voltage, gas flow rates, concentrations of waste, or addition of the catalyst.[331,351]

Versatile possibilities to enhance the degradation of the wastes in water are also provided by a loop reactor. It allows water recirculation between the plasma reactor and the reservoir by a pump. The gas discharge can be operated either in a continuous or in a pulsed mode and the time exposure depends on both the discharge voltage and recycle number.[352]

The association of plasma with catalysis offers indeed a powerful tool for the purification/decontamination of wastewaters containing organic compounds/biomolecules. However, even though some progress has been reported, technical difficulties still exist for the successful application at industrial scale. In most of the cases, the mineralization of complex molecules as pharmaceuticals, pesticides or insecticides is not complete and the reaction intermediates are not innocuous. In addition, the presence of a persistent homogeneous catalyst in water is not desirable and the cost for additives like CaO_2 is too high for a current application.

Also, very important, such procedures cannot be applied to waters where such compounds and their metabolized products can cause damage to the aquatic ecosystem, such lakes or rivers. Especially wastes from hospitals, but also from textile industry, domestic utilization and hotels (mainly care products) or agriculture, are difficult to be treated in this way. For the first types there is still possible to collect these in pools where a combined treatment by plasma and catalysis could be considered. However, some of the untransformed intermediates are even more dangerous than the initial ones and in these cases other strategies have to be adopted for the degradation/mineralization. For the wastes produced from agriculture (insecticides, pesticides, etc.) such a treatment is still not feasible if catalysts cannot be separated from treated waters.

Also important, the dominant species generated by plasma (O_3, and H_2O_2), but also $\bullet O$ or HO$\bullet$ radicals, may affect the long-term activity and stability of utilized catalyst and operation time is also an important factor to be controlled.

3.3. Biocatalytic remediation of water

Bioremediation is an alternative to traditional physical and chemical remediation technologies. Biocatalysts refer to enzymes produced by microorganisms found in nature, where they may already be doing what is also desired for a specific application. Microorganisms may produce a very broad structural diversity of enzymes with very diverse activity and selectivity. Thus, these enzymes offer a huge potential that may allow an advanced degradation of both inorganic and organic compounds.

Many biological methods have been applied to the remediation of sediments thereby decreasing or eliminating environmental contamination present in water, wastewater, sludge, soil, aquifer material, or gas streams [353-354]. Actually, these methods can be divided into *in-situ* remediation including immobilization [355-356], burying [357], phytoremediation[358] and amendment [359-360] and *ex-situ* remediation including washing [33,361], electrochemical remediation [362], ultrafiltration [363] and solvent extraction [364]. *In-situ* bioremediation causes less dust dispersion and hence better degradation of the contaminant. It can be enhanced via bio-augmentation (*i.e.* by the introduction of more archaea or bacterial cultures to enhance the contaminant degradation), bioventing (*i.e.* by stimulating the natural *in-situ* biodegradation of contaminants by providing enough air or oxygen to existing microorganisms to sustain the microbial activity), bio-sparging (*i.e.* an *in-situ* remediation technology that uses indigenous microorganisms to biodegrade organic constituents in the saturated zone; in biosparging, air (or oxygen) and nutrients (if needed) are directly injected into the saturated zone to increase the biological activity of the indigenous microorganisms) [365]. Genetic and metabolic engineering protocols have been recently proposed as well [366]. These considered the use of transcription-activators like effector nucleases, clustered regularly interspaced short palindromic repeats, or zinc finger nucleases as major gene editing tools used.

All these methods are based on multiple metabolic pathways promoted by enzymes [367] where the enzymatic systems are often compared with conventional chemical micro-/nanomotors. In this respect, they are particularly attractive because their activity is associated to the presence of pollutants denoted as biocompatible fuels, such as glucose, urea, glycerides, and peptides, commonly found in waters that can be conveniently treated by bioremediation [368]. In accordance enzymes have been utilized as such or designed with functional material constituents to efficiently perform tasks related to water remediation, and environmental monitoring.

3.3.1 Bioremediation of the metals

Divalent and heavy metals play an important role in the aquatic ecological environment [369]. Table 4 shows the allowed limits of these pollutants. With the development of modern technology and the process of urbanization, heavy metal pollution in sediments has become a serious problem. Heavy metals in sediments can accumulate through the food chain, and cause great damage to the ecology because of their persistence, bioaccumulation and high toxicity.

Bacteria have been extensively investigated for the biomineralization of the metals [370-372]. However, they have certain limitations in regard to biomineralization in terms of immobilizing metals. Therefore a possible utilization of fungi has been as well emphasized [373-374]. Fungi have higher tolerance to metals compared to bacteria and could serve as efficient candidates for the sequestration of divalent ions and also to remove high valence and polyatomic ions that cannot directly precipitate as carbonates [375].

Table 4. Priority pollutants limits (according to Electronic Code of Federal Regulations and The World Health Organization. Adapted from refs [376] and [377].

Toxic Metals and Oxides	Maximum concentration (mg/L)	Average concentration (mg/L)
Antimony	20×10^{-3}	
Arsenic	11×10^{-3}	8×10^{-3}
Barium	2	
Beryllium	1×10^{-3}	
Cadmium	5×10^{-3}	
Chromium	0.2	0.2
Copper	1.0	1.0
Iron	1.0	1.0
Lead	10×10^{-3}	
Mercury	39×10^{-6}	24×10^{-6}
Nickel	228×10^{-6}	
Selenium	23×10^{-3}	12×10^{-3}
Silver	0.1	
Strontium	25	
Thallium	2×10^{-3}	

Zinc	1.0	1.0
Uranyl	3.5×10^{-3}	
Asbestos	7 millions fibers	

The mechanism of the bioremediation of the metals also depends on their nature. The metals in the (II) oxidation state are mainly precipitated by the released CO_2, while high valent metals as Cr(VI) or Se (IV) are bioremediated through the reduction to an inferior oxidation state as Cr(III) or Se(0) [378-380] and low valent pollutants such as As(III) via oxidation of to less toxic species as As(V) [381-382]. The bioremediation of mixtures of high valent reducible cations and low valent oxidizable cations may occur simultaneously. Thus, Cr(III) can easily precipitate to Cr(III)-hydroxide at higher pH in the presence of coagulants such as $FeCl_3$ followed by conversion of soluble As species into insoluble products [383].

3.3.1.1. Microbially induced carbonate precipitation

Microbially induced carbonate precipitation (MICP) is a bio-mediated approach to treat contaminated media, including water and soil, with potential applications in civil and environmental engineering. Although MICP is not only an ureolytically driven process, it can lead to calcite precipitation by microbial enzymes, which catalyzes the hydrolysis of urea to increase the pH, resulting in greater mineral saturation with respect to calcium carbonates [384]. Thus, MICP is initiated through *i)* ureases catalyzed reactions [385-386]; *ii)* carbonic anhydrase catalyzed reactions [387] and *iii)* other enzymes catalyzed reactions.

Bioremediation through ureases catalyzed reactions

Ureases constitute a large family of amido-hydrolases and phosphor-triesterases with homologous sharing more than 50 percent sequence identity [388]. They are found in certain plants, in numerous bacteria, fungi, algae, and some invertebrates, as well as in soils, as a soil enzyme [389]. Urease, the first crystallized enzyme [390], is an assembly of protein metallocenters that catalyzes the hydrolysis of urea to form ammonia and carbonic acid. It is a nickel-containing metallo-enzyme of high molecular weight of which structure corresponds to a tightly associated trimer of ($\alpha\beta\gamma$)-units in a triangular arrangement with extensive contacts (Figure 47). Nickel ions exist in two different coordinations *i.e. i)* Ni-1 coordinated by three ligands (with low occupancy of a fourth ligand) and *ii)* Ni-2 coordinated by five ligands [391.] This structure is compatible with a catalytic mechanism whereby urea ligates Ni-1 to complete

its tetrahedral coordination and a hydroxide ligand of Ni-2 attacks the carbonyl carbon. A carbamylated lysine provides an oxygen ligand to each nickel, explaining why carbon dioxide is required for the activation of urease apo-enzyme [392]. In the proposed mechanism urea is hydrolyzed into NH_4^+ and CO_2 by urease secreted by the ureolytic bacteria leading to a release of CO_3^{2-} causing the precipitation of a large family of cations such as Ca^{2+}, Ba^{2+} and radio-nucleide contaminants such as Sr^{2+} [393] or mixtures of these like Sr^{2+} and UO_2^{2+} [394] and a rise of pH from 7.5 to 9.1. MICP is also effective to heavy elements such as Cd^{2+}, Pb^{2+}, Ni^{2+}, Co^{2+}, Cu^{2+}, Zn^{2+}, etc. [395-398]. Carbonate mineralization by bacteria also affords the production of biomimetic materials with specific structural properties including unique size, crystallinity, isotopic and trace element compositions [399] and specific porous properties [400].

   This mechanism was also confirmed by X-ray absorption spectroscopic analysis (EXAFS) [401]. *In vivo* assembly of the metallo-center in K. aerogenes [389] involves the participation of four accessory gene products, among which one has been postulated to function as a molecular chaperone that stabilizes a urease apo-protein conformation that is competent for nickel incorporation, and a second serves as a nickel donor for urease activation on the basis of its ability to bind approximately six nickel ions per dimer with rather high specificity. Although mandatory, the role of the other two genes is less defined.
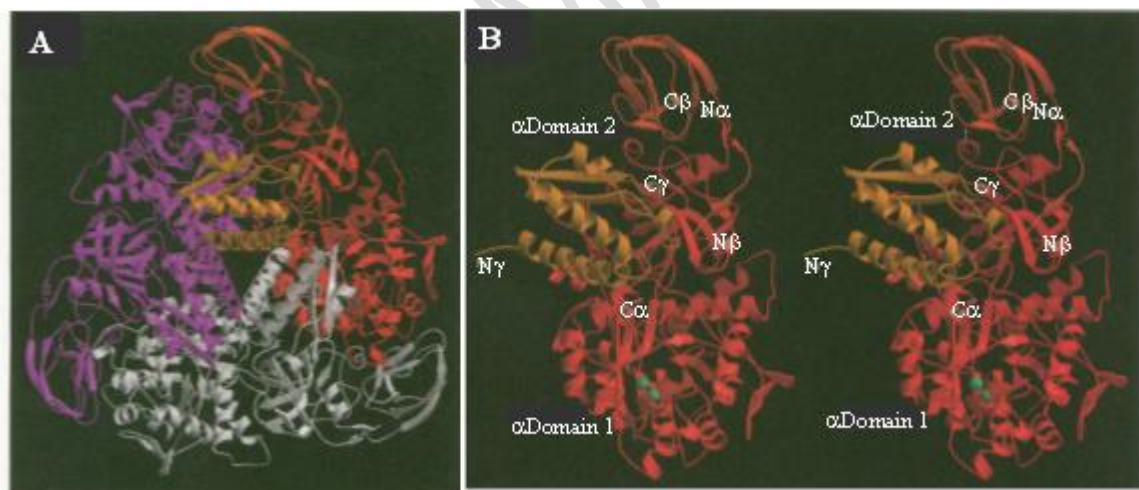
Figure 47. The structures of the urease $(\alpha\beta\gamma)_3$ trimer and the $(\alpha\beta\gamma)_4$-unit. (**A**) A ribbon diagram of the $(\alpha\beta\gamma)_3$ trimer of urease, as viewed down the crystallographic threefold axis with one $(\alpha\beta\gamma)$-unit in violet, one in white, and the third colored according to the individual subunits: α (red), β (orange), and γ (yellow). The nickel ions at each active site are shown as cyan spheres. The overall shape of the trimer is triangular with approximate dimensions of 110 by 110 by 80 Å. The nickel centers are located approximately 50 Å from one another in the α subunits of each $(\alpha\beta\gamma)$-unit. (**B**) A stereo ribbon diagram highlighting the secondary structural elements in the three subunits, α (red), β (orange), and γ (yellow) of urease. This $(\alpha\beta\gamma)$-unit was chosen such that the proximity of the termini corresponds with equivalent residues in the one subunit urease from jack bean. The nickel ions (cyan) are located at the carboxyl termini of the strands in the $(\alpha\beta_8$ barrel of the α subunit. Reproduced with permission from [391]. Copyright 1995 American Association for the Advancement of Science.

The presence of toxic cations such as Pb has only a marginal effect on bacterial growth and associated urease activity at its typical concentrations in water. Even more, the calcium source and initial bacteria concentration were found to remarkably influence Pb immobilization efficiency in terms of Pb removal percentage [398]. Supplementary geochemical simulation results indicate that the Pb immobilization mechanisms include abiotic precipitation, biotic precipitation and bio-sorption [398].

The precipitation of carbonates is governed by a series of parameters such as the calcium and M (HMs) concentration, dissolved concentration of carbon dioxides, pH, and the presence of nucleation sites [402]. Studies working with bacterial cells have been shown that they can function as well as nucleation sites, carbonates being deposited onto the bacterial cell surfaces [403-404].

Subsurface ureolysis rates can be accelerated through a combination of relative contributions of biomass and mineral precipitation. In this respect, the addition of dilute molasses has been demonstrated to promote the overall microbial growth with several orders of magnitude. The addition of cysteine to the medium also significantly improved bacterial Cr(VI) reduction rate [405]. As such an effect, the estimated ureolysis rates in recovered ground waters may increase with at least two orders of magnitude [406]. The ammonium concentration can be easily quantified from the following equations (84)-(87). At time t it is given by:

$$[NH_4^+]_{total} = 2[urea]_0(1-e^{-kt}) + [NH_4^+]_0^{total} \tag{84}$$

where $[NH_4^+]_0^{total}$ is the total ammonium concentration at time 0. In the subsurface, ammonium can exchange with cations on the aquifer matrix and only a fraction of the total ammonium remains in solution:

$$f_{aq} = [NH_4^+]/[NH_4^+]^{total} = [NH_4^+]/([NH_4^+] + [NH_4^+]^{rock})[\,NH_4^+]^{total} = [NH_4^+]/f_{aq} \tag{85}$$

where f_{aq} is the fraction of ammonium that remains in solution. In subsurface media, the fraction of a sorbing constituent that remains in solution is related to the retardation factor R_f by [406]:

$$R_f = 1/f_{aq} \tag{86}$$

that allows to calculate the concentration of ammonium as following [406]:

$$[NH_4^+] = 2[urea]_0(1 - e^{-kt})/R_f \qquad (87)$$

Differently to the divalent cations, high valent cations as Cr(VI) are sequestrated as coatings of segments of mycelia representing a quite complex calcium chromium oxide carbonate ($Ca_{10}Cr_6O_{24}(CO_3)$) species [374]. However, compared to the divalent cations for which the decrease of the concentration of soluble cations is almost total for high valent cations as Cr(VI), the percentage of removal is only below 65%. Considering the need for calcium sources in the bioremediation process of waters containing such high valent cations it was suggested that the combination with ureolytic bacteria may have a better immobilization effect in soil [374]. Due to this enzymatic reaction, soil pH increases and carbonate is more effectively produced [396].

A mechanism for the removal of Cr (VI) in the presence of cultured bacteria is described in Figure 48 [407]. The contaminant firstly binds to the surface via reversible or irreversible interactions (an extracellular mechanism). This is followed by an active transport to engulf the surface bound moieties (*i.e.* an intracellular mechanism). The bacterial cell wall is primarily composed of peptidoglycan, teichoic acid (a polymer of glycopyranosyl glycerol phosphate) and teichuronic acid (in which the phosphate functional groups are replaced with carboxyl groups). These surface groups act as charge carriers for the surface adsorption and sites for cellular ingestion. The other charge carrying species are the phosphates, esters, phenols and metals. Thus, Fe_3O_4 from the matrix or present in active surface channels can also reduce the Cr(VI) to Cr (III) according to equation (88) that further can immobilize the cell surface [407].

$$8H^+ + Cr_2O_7^{2-} + 6Fe_3O_4 \rightarrow 2Cr^{3+} + 9Fe_2O_3 + 4H_2O \qquad (88)$$
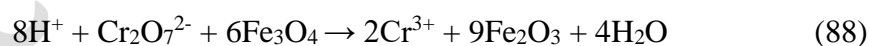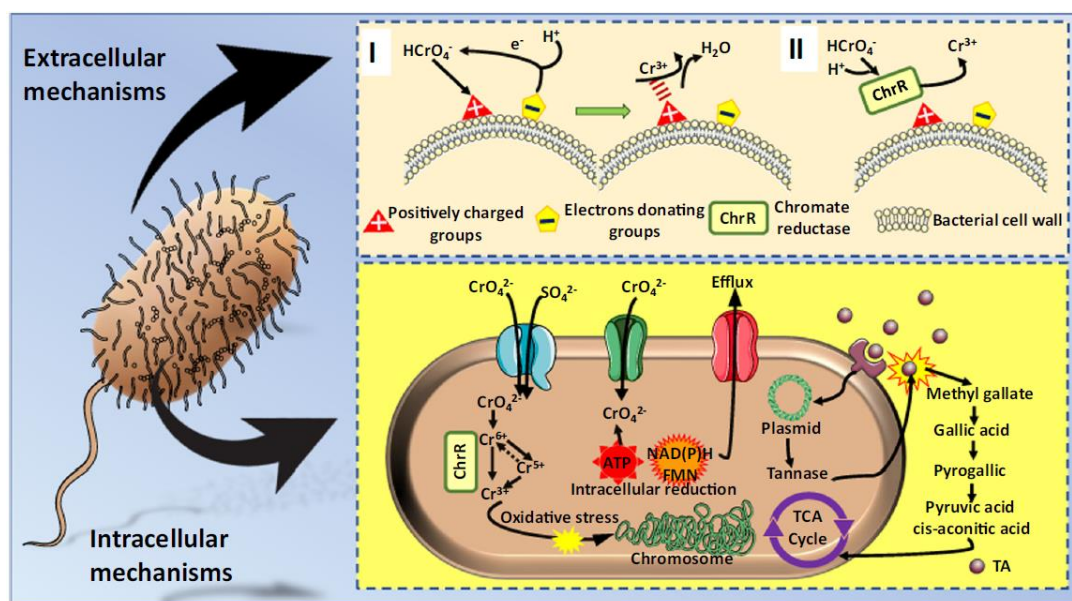
Figure 48. Schematic diagram showing the proposed extracellular and intracellular mechanisms for the degradation and stabilization of Cr(VI) and tartaric acid (TA) in bacterial environment. Reproduced with permission from [407]. Copyright 2021 Elsevier.

Apart from electrostatic interactions, other means of extracellular degradation of Cr(VI) emerges in bacterial cultures. ChrR-chromate reductase is a soluble flavin mononucleotide-binding and NADH-dependent reductase enzyme that can reduce Cr(VI) to Cr(III) (Figure 48) (and references inside) [407]. During the Cr(VI) reduction, reactive oxygen species are generated which can cause oxidative damage to the cells. ChrR enzyme has a quinone reductase activity during Cr reduction which can neutralize the generated reactive oxygen species [408-409]. Other component molecules such as ATP, NAD(P)H and FMN may also reduce the Cr (VI). However, this cannot protect the bacteria from the oxidative damage [407].

Some reports have also indicated that precipitates produced from acid mine drainage, as a major source of heavy metal contamination, could be transformed into a catalyst for heavy metal remediation through diverse microbial interactions [410]. The produced catalysts can be effective in the remediation of other heavy metals as well leading to a double remedial effect: *i)* the combination of environmental catalysts resulted from an environmental waste with *ii)* the remediation of the contaminated groundwater. The concept proved the efficiency for Cr(VI) reducing/immobilizing capacity [410].

Literature reported various strains for an efficient remediation of calcium (Bacteria Bacillus pasteurei, Bacillus subtilis, Bacillus safensis [407], Sporosarcina pasteurii, Terrabacter tumescens [393], etc.), reducing of Cr(VI) , (Bacillus cereus SJ1 [378], Lysinibacillus fusiformis ZC1 [379], Rhizopus sp. LG04 [411] and Alishewanella sp. WH16-1 [380], etc.) and As(III)-oxidizing

bacteria (Agrobacterium tumefaciens 5A and GW4 [412-413], Rhizobium sp. NT-26 [414], Hydrogenophaga sp. NT-14 and H1 [382,415], Herminiimonas arsenicoxydans ULPAs1 [416] and Halomonas sp. HAL1 [381]).

Bioremediation through carbonic anhydrase catalyzed reactions

Carbonic anhydrase together with ribulose-1,5-bisphosphate carboxylase/oxygenase (affording the carbon fixation) are enzymes hosted by polyhedral protein shells of bacterial microcompartments carboxysomes merely of the *ccm*, which appears to be limited to cyanobacteria, and *cso*-types, which occurs in non-photosynthetic autotrophs and in some cyanobacteria [417-419]. The active site of most carbonic anhydrases contains a zinc ion.

Shell carbonic anhydrase isolated from homogeneous carboxysome preparations from various sources (such as Halothiobacillus neapolitanus, Citrobacter freundii, Bacillus megaterium, Bacillus sp. and Bacillus simplex [420], microalgal bacterial flocs containing Desmodesmus sp., unidentified coccal microalgal sp., diatoms (Nitzchia sp.), and cyanobacteria (Phormidium sp., Oscillatoria sp) [421]) demonstrated efficiency in bioremediation of various metals. Further engineering of the cyanobacteria through transformation by genomic homologous recombination with plasmid DNA vectors enhances the secretion of carbonic anhydrases and, as consequence, their efficiency [422].

Carbonic anhydrase may also catalyze the biomineralization in synergism with urease showing efficiency for the bioremediation and bio-recovery of cations such as calcium, lead and strontium [423].

Other enzymes catalyzing bioremediation of metals

Oil contamination by heavy metals in combination with elevated atmospheric CO_2 has important effects on the rhizosphere microenvironment by influencing plant growth. With R. pseudoacacia rhizosphere in the presence of cadmium and lead, free amino acids, or organic acids showed that, in rhizosphere soils, the enzyme activity (i.e., dehydrogenase, invertase, or *β*-glucosidase) increased significantly relative to ambient CO_2; differently to these the L-asparaginase activity decreased [424]. The behavior of the enzyme is thus correlated to the soil matrix. Contrarily, the presence of phenolic acids inhibits the bioremediation of heavy metals. L-Asparaginase enzymes catalyze the hydrolysis of L-asparagine to L-aspartate and ammonia, thus favoring reactions requiring a base media [424].

3.2.1.2 Operational conditions

The identification of the strategies affording better understanding of industrially, environmentally, and economically applicable biomineralization routes is still challenging. For ureolytic biomineralization leading to the formation of solid calcium carbonate, porous media reactors emerged as more promising. This has been confirmed by real-time stereomicroscopy observations carried out using quasi-2D porous media reactors constructed from polycarbonate plates (Figure 49).
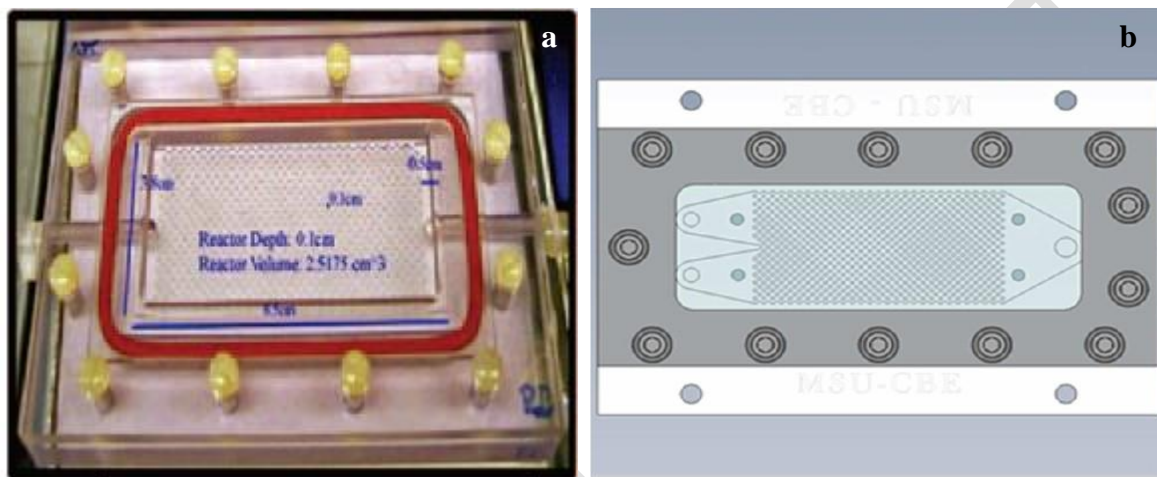
Figure 49. Single inlet (a) and (b) pulsed injection of calcium mineralization medium systems for the biomineralization of divalent cations. Reproduced with permission from refs [393,425]. Copyright 2013 American Chemical Society and 2011 Cambridge University Press.

Following the distribution of calcite precipitates, the overall immobilization of dissolved calcium, and the solubility of precipitates as a function of position demonstrated that single inlet [425] and pulsed injection of calcium mineralization medium systems [393] led to some differences. Mineralization and growth media following the pulsed strategy promoted $CaCO_3$ precipitation in a large extent while sustaining the ureolytic culture over the time (Figure 49). The pulsed injection strategy precipitated 71−85% of calcium and 59% of strontium, while the continuous injection was less efficient (61% precipitated and 56% calcium strontium.

3.3.1.3 Combined metal bioremediation approaches

Microbial fuel cells (MFCs) define bio-electrochemical devices that synergistically combine electrochemical and microbial biocatalytic reactions and harness the power of microorganisms as biocatalysts to convert organic substrates directly into electrical energy via substrate oxidation [426-427]. This approach has been inspired by the early work of Potter reporting electrical effects accompanying the decomposition of organic compounds and accounts to the

excellent abilities of these microorganisms to produce electricity and remove pollutants simultaneously [428]. The produced electrons promote the reduction/mineralization of the polluting multivalent heavy cations (copper, hexavalent chromium, mercury, silver, thallium) into harmless species [429]. Equation (10) presents the anodic reaction taking acetate as an example of sacrificial species. The remediation of divalent and heavy metal-contaminated environments may also occur via the precipitation with released CO_2. Cathodic reduction of selected heavy metals is exemplified by equations (89)-(95) [429].

Anodic reaction:

$$CH_3COO^- + 2H_2O \longrightarrow 2CO_2 + 7H^+ + 8e^- \tag{89}$$

Cathodic reduction:

$$Cr_2O_7^{2-} + 14H^+ + 6e^- \longrightarrow 2Cr^{3+} + 7\,H_2O \quad E^0 = 1.33\text{ V} \tag{90}$$
$$Cu^{2+} + 2e^- \longrightarrow Cu \quad E^0 = 0.337\text{V} \tag{91}$$
$$2Cu^{2+} + H_2O + 2e^- \longrightarrow Cu_2O + 2H^+ \quad E^0 = 0.207\text{V} \tag{92}$$
$$Cu_2O + 2e^- + 2H^+ \longrightarrow 2Cu + H_2O \quad E^0 = 0.059\text{V} \tag{93}$$
$$2Hg^{2+} + 2e^- \longrightarrow Hg_2^{2+} \quad E^0 = 0.911\text{ V} \tag{94}$$
$$Hg_2^{2+} + 2e^- \longrightarrow 2Hg \quad E^0 = 0.796\text{ V} \tag{95}$$
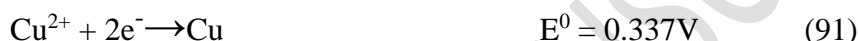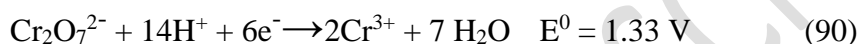
3.3.1.4 Bioremediation of metals through catalysis by supported enzymes and immobilized bacteria

The immobilization of bacteria may enhance the microbial potential pretreatment for bioremediation of heavy metals in wastewater as it has been demonstrated for Cr(VI) and As(III) [405]. However, the stability of these composites is limited and after a number of cycles the cells might leach out. Indeed, immobilization of strains via embedding with sodium alginate produced biobeads that exhibited a stable Cr(VI) reduction (91.8%) and As(III) oxidation (29.6%) for around five continuous cycles of wastewater [405].

The denitrification genes taking narG, nirK, nirS, nosZ as references and the activities of their relevant enzymes (S-NiR, S-NR) were investigated in heavy-metals (Hg) polluted soils with different remediation strategies. Their association with compost, biochar or their combination generated a behavior specific to supported enzymes [430]. As an important parameter, the pH have a notably impact on their metabolism. Thus, the activity and stability and also the dissociation state of these enzymes increase jointly. Also important, the abundance

of the genes significantly changed under the Hg stress, indicating nirS gene was more sensitive to Hg pollution than nosZ gene [431].

3.3.2 Bioremediation of organic compounds

It is appreciated that approximately 60% of all industrial chemicals exhibit no specific toxicity [432]. However, where they are persistent and bio-accumulating, generate a hazard to the environment by acting as baseline toxicants.

Organic compounds include a very large number of chemicals produced from various segments of the chemical industry. These include the production of solvents, pharmaceuticals, polymers and plastics, colorants, pesticides, personal care products, etc. Among these pharmaceuticals, pesticides, and personal care products have a strong pollutant influence for waters. Chemicals such as endocrine disrupting compounds can interfere with endocrine (or hormonal) systems where their accumulation may cause cancerous tumors and other developmental disorders. These compounds mimic or antagonize the effects of endogenous hormones and consequently alter the synthesis and metabolism of natural hormones, or modify hormone receptor levels, disrupting endocrine and reproductive functions, which ultimately affect the health of humans and wildlife [433]. Pharmaceuticals, dioxin and dioxin-like compounds, polychlorinated biphenyls, pesticides, and plasticizers such as bisphenol A and phthalates are other compounds that can produce such effects.

3.3.2.1 Bioremediation of antibiotics, antiviral, anticonvulsants and anti-inflammatory drugs

The prioritization of these wastes considers different criteria like sale, physico-chemical properties, toxicity, degradability and resistant towards treatment [434]. Drugs residue characterization revealed their presence in effluents and soil well associated to different therapeutic categories. This type of compounds covers the highest percentage in terms of analgesics, anti-bacterial, and anti-infective, contrast media and minor as anti-epileptics, anti-inflammatories, and β-blockers. The consumption of antibiotics and antivirals continued to exceedingly increase and, as a consequence, they are enhancing the water and soil contamination. Finally the uncomplete metabolism of these complex molecules results in complicate matrices combining both unreacted organic molecules and metabolites [435]. Over the time rather high levels of antibiotic residuals were accumulated in wastewaters environments that can be related to antibiotic resistance genes in bacteria as well. In addition to these,

antibiotics residues excreted from agricultural activities, industrial and domestic wastes contribute as well to the water and soil contamination [436-437]. Further, the partial degradation in the aquatic ecosystem and an inappropriate disposal induce the appearance of diverse antibiotic resistant genes and bacteria, hence it is imperative to devise strategies to remediate/mitigate spreading antibiotics to the environment.

Biodegradation of antibiotics and antivirals strongly depends on their chemical structure and in most of the reported examples occurs with selectivities smaller than 80%. There are only few recent examples in which the degradation reached or exceeded this level using Chrysopogon zizanioides and Leptosphaerulina sp. [438-439]. Even more, the biodegradation of these compounds results in a multitude of relative complex compounds of which further decomposition is difficult [440].

Sources of antibiotics and antivirals are multiple and include domestic, hospital and pharmaceutical wastes. High metropolitan hospitals discharge every day more than 1400 different antibiotics/metabolites which, depending on the mass load of drugs, the geographic location and the type of healthcare facility are in the range of about 1.5-310 g/day [441]. Among these, the penicillin (amoxicillin, ampicillin, bacampicillin, epicillin, metampicillin) is one of the most important groups of antibiotics used in medicine and veterinary as a feed additive representing more than 70 % of the antibiotics consumed in various countries [442].

For the moment, the wastewater treatment plants are generally not designed to remove antibiotics from collected waste, and many of the currently proposed methods are unsafe for environmental use [443]. However, various bioremediation strategies are recognized as potent removal solutions [444].

At this moment, the conventional methods including wastewater treatment plants are found ineffective for the complete removal of the recalcitrant antibiotics [444]. Antibiotic residues could influence the biomass and activity of microbial, and induce generations of resistance genes in the environment [445]. At another level, ecotoxicity studies have demonstrated that pharmaceutical pollutants could affect the growth, reproduction and behavior of birds, fishes, invertebrates, plants and bacteria [446]. Therefore, the bioremediation of wastewaters containing antibiotics and antivirals deserves a special interest. Along a very large number of publications, this topics constituted the subject of a series of reviews [443-444,447-451] analyzing the efficiency of the specific biocatalysts by direct association with various microorganisms, type of the reactor, processing conditions and selected strategies, etc.

The use of individual lipases or cellulases or an association of these enzymes can permit the inactivation of antibiotics in wastewater effluents, thus preventing the pollution of the

environment [452]. Following such a pathway, antibiotics like tetracycline, chlortetracycline, doxycycline or oxytetracycline have been degraded without adding any other chemicals by a percentage of 16, 48, 34 and 14%, respectively, in a rather short range of time (4 h of reaction) [453]. Working with peroxidases between 70% and 99% of tetracycline antibiotics can be eliminated during a 4 h treatment [453-454].

Sulfamethoxazole is an antibiotic used for bacterial infections such as urinary tract infections, bronchitis, and prostatitis and its presence in aquatic environments is another source of health concern [455]. Bioremediation with the laccase activity of Pycnoporus sanguineus is significantly inhibited by its presence occurring with a lower removal efficiency of sulfamethoxazole. However, the association of this laccase with 2,20-azino-bis-(3-ethylbenzothiazoline-6-sulfonic acid) produced a rather fast degradation of sulfamethoxazole, but this sulfonic acid *per se* also rises a serious environmental issue. An efficient alternative is the co-culture with Alcaligenes faecalis. Actually, the laccase production by the co-culture effectively inhibited the accumulations of *N*-4-acetyl-sulfamethoxazole and *N*-hydroxy-sulfamethoxazole and alleviated the cytotoxicity of sulfamethoxazole transformation products also leading to a very small concentration of sulfamethoxazole in the treated water [455]. Alcaligenes faecalis strains may also efficiently degrade vitamin B3 (Nicotinic acid) under convenient conditions (1 g L^{-1} within 3 days at 30 °C and pH=7.0) [456].

It is also important to notice that these wastes may produce important changes in the structure of bacteria [457]. Trace amount of antibiotics (piperacillin and erythromycin) present in a wastewater matrix led to a shift in the population of bacteria in favor of a sensitive subtype, presumably on account of triggering protective biochemical processes in the resistant mutant, conferring no selective advantage since the sensitive strain remains unaffected in this concentration range. Such an impact on the population dynamics can be diminished by using advanced oxidation treatments, considering that degradation products from the wastewater matrix constituents (such as humic acid) might also have an effect [457]. Also, the presence of trace amount of antibiotics makes the bacteria more sensitive towards the attack of free radicals during an advanced oxidation treatment. Amoxicillin piperacillin and erythromycin can been degraded by several bacteria (Figure 50) [458]. However, some bacteria such as Staphylococcus aureus, Escherichia coli, Acinetobacter sp., Vibrio sp., Micrococcus sp., or Helicobacter pylori are resistant to amoxicillin, and therefore offer a big challenge to remove antibiotics from the environment. Studies carried out in the biodegradation of this antibiotic confirmed the complexity of the process and a limited fragmentation process.

Enzymatic biodegradation of antibiotics and antivirals by degrading enzymes produced by microorganisms such as bacteria, fungi, algae and biocatalysts follows specific mechanisms showing certain advantages and disadvantages in the efficient antibiotics removal. These processes are controlled by temperature, pH, and complexity of the antibiotics and consist mainly in the modification or hydrolysis of labile functional groups of the structure. Such biodegradation pathways are usually predominant in wastewaters [459-460].

The biodegradation of antibiotics depends on various environmental parameters such as temperature, pH, nitrogen and carbon sources, solid retention time, and microbial activity [461]. Recent progress in isolation of new bacteria opens new conditions in which the biodegradation of antibiotics may proceed. Arthrobacter nicotianae OTC-16, as a novel tetracycline-degrading bacterium, could degrade oxytetracycline/tetracycline into by-products with less toxicity to bacteria and algae at ambient temperature, both in acidic and alkaline environments at concentrations in the range of 25–150 mg L^{-1} [462].
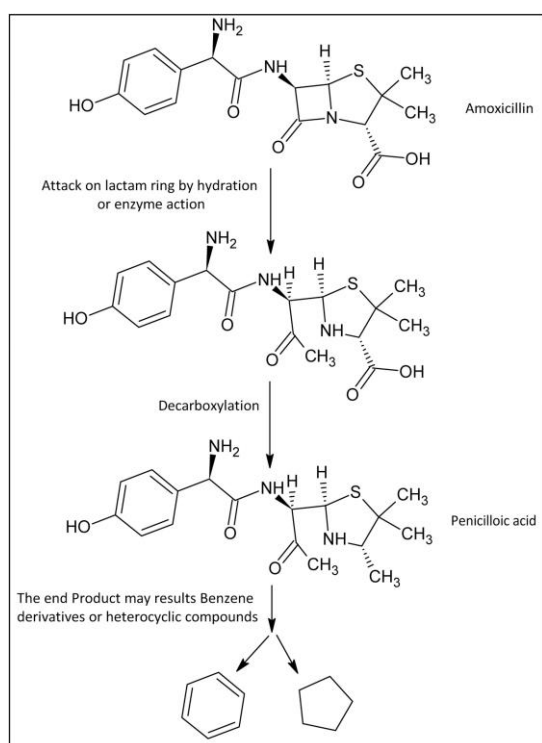
Figure 50. A generalized degradation of amoxicillin along with its metabolites Reproduced with permission from [458]. Copyright 2021 Elsevier.

In addition to antibiotics (tetracyclines) [463], peroxidases proved activity for removal of anticonvulsant (carbamazepine) and inflammatory (diclofenac) drugs [464] although with a limited degradation capability compared to laccases. Margot et al.[465] indicated that 25% of diclofenac and 95% of mefenamic acid could be depleted in 20 h with laccase from Trametes

versicolor, whereas Lloret *et al.* [466]. reported that laccase from Myceliophthora thermophila could degrade up to 65% of the diclofenac, but was ineffective towards naproxen. The addition of redox mediator such as 1-hydroxybenzotriazole (HBT) may even enhance the degradation of such drugs almost doubling the rate [467]. However, mass spectrometric analyses demonstrated that two degradation products of carbamazepine, 10,11-dihydro-10,11-epoxycarbamazepine and 9(10H)-acridone, were formed via repeated treatment with laccase and HBT.

To sum up, besides hormones and phenolic pollutants [468-469], with equivalent results, laccases and peroxidases can successfully remove antibiotics, antiviral, anticonvulsants and anti-inflammatory drugs from wastewaters. Laccases seem more attractive, because they do not need the addition of H_2O_2 and are less affected by other organic pollutants in wastewater [470].

One of the advantages of such a bioremediation approach is that it may provide a dual function as that of antibiotic elimination and CO_2 fixation simultaneously [471]. This has been demonstrated in an algal treatment of two widely used antibiotics, cefradine and amoxicillin for which a significant improvement in the removal efficiency of the antibiotics occurred when CO_2 was added into the treatment. Changes in the content of photosynthetic pigments and the activities of ribulose-1,5-bisphosphate carboxylase-oxygenase (RuBisCO - an enzyme present in plant chloroplasts, involved in the fixation atmospheric carbon dioxide during photosynthesis) and carbonic anhydrase secreted by Psychrobacter species occurred as algal responses to the treatment conditions.

3.3.2.2. Biodegradation of steroids

Estrogens are a category of sex hormone responsible for the development and regulation of the female reproductive system and secondary sex characteristics. They have high estrogenic potency as endocrine-disrupting compounds and, as consequence, its presence in the environment may cause male reproductive dysfunction to wildlife [472]. Estrogens correspond mainly to four major endogenous structures: estrone, estradiol, estriol and estetrol [473]. Besides these four types, a range of synthetic and natural substances that possess estrogenic activity have been also identified in the water environment. These are commonly referred as xenoestrogens and include: *i)* synthetic substances such as bisphenol A and homologous, *ii)* plant products with estrogenic activity called phytoestrogens containing natural organic

compounds such as coumestrol, daidzein, genistein, miroestrol, etc., and *iii)* products of fungi known as mycoestrogens and containing compounds as zearalenone [429].

The biodegradation of steroidal estrogens, including estrone, 17β-estradiol and estriol, and synthetic replica including 17α-ethinylestradiol and 3-methyl ether of ethinylestradiol mainly focused on laccases. They showed, indeed, potential for inhibition of endocrine-disrupting potency in the aqueous environment. Such family of enzymes contains copper atoms at a trinuclear site and an ensemble of N-glycosylation and carbohydrate centres and disulfide bridges with various forms and size of the substrate-binding pocket (Figure 51) [474]. The presence of copper in such a unique configuration induces a high oxidative behavior as shown for 17β-estradiol. Thus, hormones can be degraded by anaerobic bacteria, but only to some extent. Indeed, although endocrine disruptors, such as 17β-estradiol, could be converted to estrone or 17α-estradiol, the decrease of the estrogenicity of the water can only suggest that those compounds would accumulate in anoxic environments [475]. Enzymatic oxidation by fungal laccases was also considered a promising alternative for efficient and sustainable removal of such organic pollutants in water. This includes laccases from the Pycnoporus sanguineus CS43 fungus [476].

Etherification and the oxidative polymerization of phenolic fragments lead to heavier molecules. These processes are favored by the catalytic contribution of the copper trinuclear sites [477-478]. Thus, instead of total oxidation of these molecules, that is very hard or even not possible, the transformation of the estrogenic compounds like 17β-estradiol into insoluble polymers appears as a more feasible route. Laccases like Coriolopsis gallica were able to do partially this job with a significant reduction of its effects [479].

Such reactions demand however relatively long reaction times. In addition to natural estrogens, Carballa et al. reported an anaerobic transformation of estrogens and other pharmaceuticals, like antibiotics and naproxen by these enzymes of musks [480]. Overall, most of the studies focused on the bioenzymatic endocrine disruptors removal showed that the transformation of these compounds is not entirely possible and more than 10% remains untransformed even after a prolonged reaction time [480]. Noteworthy, with less complicate compounds such as bisphenol-A or triclosan such a polymerization treatment efficiently eliminated the endocrine activity [479].
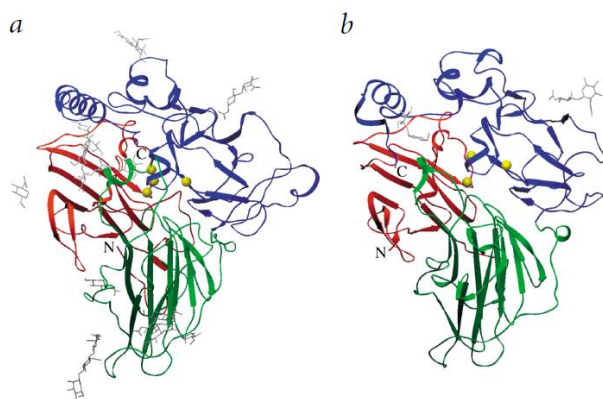
Figure 51. Three-dimensional structures of a) *Melano-carpus albomyces laccase* (MaL) and b) *Coprinus cinereus laccase* (CcL). Carbohydrates are shown as gray sticks. Domain A (red) includes residues that participate in the binding of coppers at the trinuclear site. Domain B (green) contains residues that take part in the substrate binding. Domain C (blue) contains residues that participate in the binding of coppers at the mononuclear and the trinuclear site, as well as in substrate binding. The mononuclear site is located entirely in domain C, and the trinuclear site is located at the interface between domains A and C. The diphenolic substrate-binding site is located in the cleft between domains B and C. Reproduced with permission from ref [474]. Copyright 2002 Springer Nature.

Oxidoreductase enzymes such as dehydrogenases extracted from a marine bacterium Rhodococcus sp may as well degrade typical steroids such as estradiol or testosterone, [481] but like for laccases this is not enough to ensure an effective bioremediation.

Aromatic ring-hydroxylating dioxygenases, also called Rieske dioxygenases, are multicomponent systems comprised of an oxygenase component that catalyzes the aerobic degradation of many aromatic compounds though the introduction of the hydroxyl groups on the aromatic substrate and a reductase component (consisting of either one or two proteins) that carries electrons from nicotinamide adenine dinucleotide (NADH) through a flavin adenine dinucleotide (FAD) and an iron–sulfur $Cys_4[2Fe–2S]$ cluster cofactor to the oxygenase $Cys_2His_2[2Fe–2S]Fe^{2+}$ component (Scheme 7 and Figure 52) [482]. All these structural details were well established through the exhaustive X-ray and EXAFS characterizations [483-485].
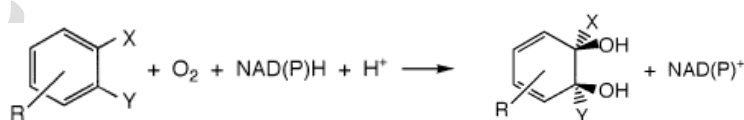
Scheme 7. Aerobic oxidation of aromatic compounds by Rieske dioxygenases. NAD(P)H is an anionic hydrogen donor [485]. Copyright 2002 Elsevier.

Besides the properties of the molecule proposed to be degraded, the efficiency of biodegradation is determined by the factors influencing the microbial growth such as water temperature, pH, oxygen, phosphorus, and nitrogen concentrations [486-488].

Phytosterols were as well identified as contributors to endocrine disruption in aquatic species. Fish exposed to phytosterols have displayed altered sexual development, changes in hormone production, decreased egg production and decreased spawning frequency [489-490]; endocrine disruption has also been observed in some small mammals exposed to phytosterols [490]. Several microorganisms have been reported for their ability to degrade3 phytosterols under aerobic conditions, but except the very preliminary steps little is known about the biotransformation pathways and nature/multitude of intermediate compounds. These microorganisms (Nocardia rhodocrous, Rhodococcus erythropolis, Mycobacterium smegmatis, etc) mostly contain two types of enzymes: cholesterol oxidases, which use oxygen as an electron acceptor, and cholesterol dehydrogenases/isomerases [491-492]. Because of their structural similarity, phytosterols are expected to follow a pathway similar to cholesterol, which has been studied in more detail. Thus, under aerobic conditions, cholesterol is first oxidized to cholest-5-en-3-one, followed by isomerization to cholest-4-en-3-one (Figure 53) [493].
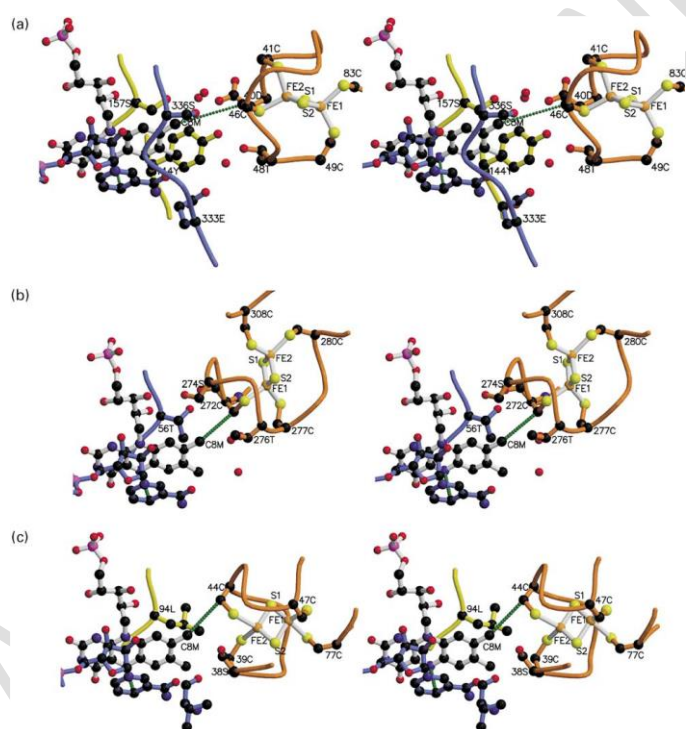
Figure 52. Possible routes of electron transfer (shown as dotted green lines) from NAD(P)H through the flavin onwards to [2Fe–2S] center in (a) BenC, (b) *oxidoreductase* (PDOR), and (c) the ferredoxin *reductase* complex from maize leaf. In all three structures, the distance between the C8M on the isoalloxazine ring of the flavin and the closest iron atom is short enough for direct electron transfer. Another possible pathway for electron transfer from the flavin to the [2Fe–2S] center is through the Cb of one of the iron-ligating cysteine residues. The FAD in BenC and the ferredoxin *reductase* complex from maize leaf has been truncated at the position connecting the two phosphorus atoms for clarity. Reproduced with permission from ref [485]. Copyright 2002 Elsevier.
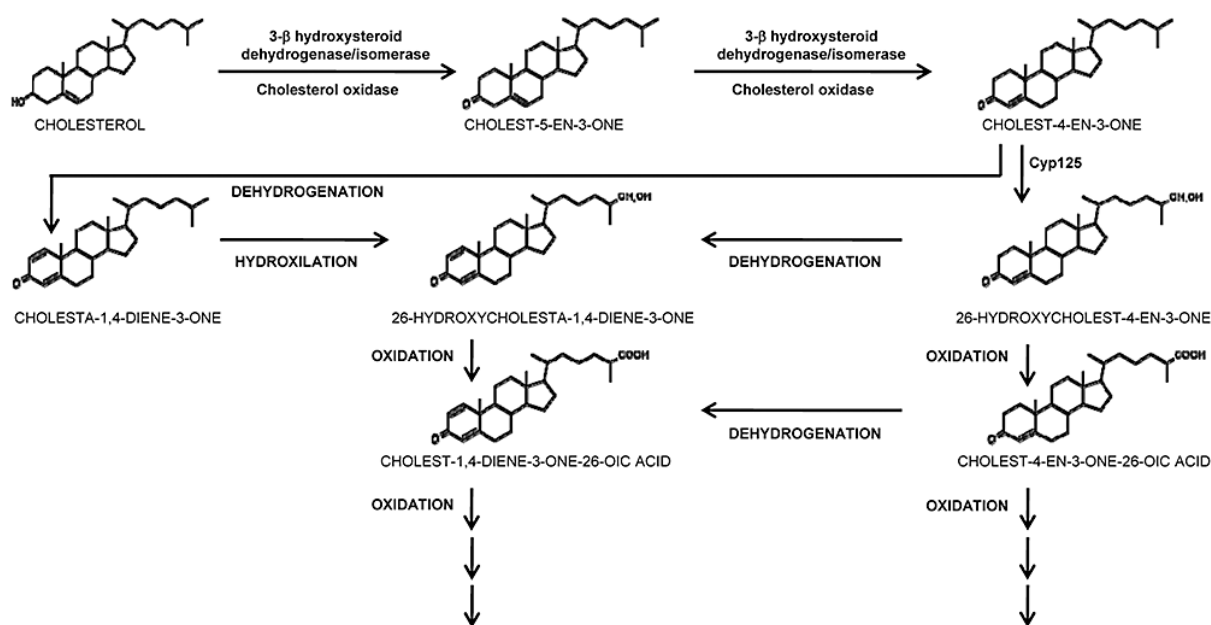
Figure 53. Bioremediation of cholesterol. Reproduced with permission from ref [493]. Copyright 2011 Wiley-VCH GMBH.

Peroxidases may also be effective for the degradation of steroids, but differently to laccases, which catalyze the oxidation of phenolic constituents by the dissolved O_2 as the electron acceptor, they demand the addition of H_2O_2 to initiate these reactions [468-469]. Under proper conditions (optimal pH, temperature, H_2O_2 concentration, enzyme/substrate ratio, etc.) these may also achieve 80 % or higher removal of natural and synthetic hormones from synthetic waters in a short range of time [468-469,494]. The presence of additional organic compounds in wastewaters may generate lower degradation rates because of an inhibiting effect on the enzyme activity or of a competition for H_2O_2 [495].

Engineering of such enzymes may enhance the performance of biocatalysts for bioremediation. This has been well demonstrated for a laccase produced in the yeast, *Pichia pastoris*, engineered by site-directed mutagenesis where the rate of the electron transfer from the copper-containing active site of laccase has been increased [496].

3.3.2.3 Biodegradation of pesticides

Pesticides are substances that are meant to control pests. The term pesticide includes a large group of chemicals such as herbicides (which may include chemicals to treat weeds and other unwanted vegetation), fungicides (used to prevent the growth of molds and mildew), insecticides (which may include insect growth regulators, termiticides, etc.), nematicide,

molluscicide, piscicide, avicide, rodenticide, bactericide, insect repellent, animal repellent, antimicrobial, and disinfectants for preventing the spread of bacteria, and compounds used to control mice and rats. Ecological risk of such chemicals to aquatic-phase amphibians and fish is high and directly related to their high diversity [497-498]. The pesticide biodegradation can be carried out under aerobic or anaerobic conditions [488].

Pesticides are monitored in water resources and treated waters and the hierarchization is based on three criteria: *i)* use of parent molecule, *ii)* toxicity, and *iii)* environmental fate of parent molecule [499]. These criteria are divided in subcriteria and combined using a scoring system to provide a final ranking of molecules. Thus, four subcriteria were proposed for toxicity [499]: (a) The carcinogenic, mutagenic, reprotoxic character of molecules and, accordingly, the selected molecules were subclassified in categories 1A, 1B, or 2; (b) The acceptable daily intake (refers to the amount of substance that may be ingested daily by the consumer throughout his or her life, with no adverse effect on health. The lower this dose, the more toxic the molecule; (c) The lethal dose (that corresponds to the quantity of an active substance, administered at one time, which causes the death of 50% of a group of test animals) and (d) The endocrine disrupting character, *i.e.* the capacity to alter the functions of the endocrine system and thereby induces adverse effects on an intact organism. For environmental fate criterion the proposed subcriteria for the pesticides classification [499] are (a) the log K_{ow} (octanol-water partition coefficient) that estimates the hydrophilic or lipophilic nature of a substance. It gives an overall estimation of the distribution of a compound in the environment. Low values reflect high affinity for water; (b) the organic carbon-water partition coefficient (K_{oc}) representing the retention potential of a substance on soil organic matter and estimates its mobility; (c) the solubility in water. The mobility of a pesticide is related to its solubility (the higher the solubility, the higher the score); (d) the half-life in soil (DT50soil) that expresses the potential for degradation of a substance and its rate of degradation in soil. DT50 is the time required for 50% of the mass of the substance to disappear from soil subsequently to transformations. Fosetyl, mancozebe, malathion, azametiphos, benfuracarb, thiophanate-methyl, thiodicarb and fenamiphos degrade very quickly (in less than one day) in soil; (e) photolysis. The action of photolysis is evaluated by the degradation time of 50% of the active substance; and (f) hydrolysis that is evaluated by the degradation time of 50% of the active substance in water. Formothion is the compound that hydrolyses the fastest ($\approx$ 4 h), while furathiocarb and propham degrade very slowly (10,000 days or more).

Biodegradation of herbicides

Worldwide herbicide use in agriculture, whilst safeguarding crop yields also presents water quality issues. Typically, the concentrations of herbicides are larger in the stream of the grassland catchment dominated by poorly drained soils than in the arable catchment dominated by well-drained soils [500]. Incidental losses of herbicides during time of application and low flows in summer caused concentrations that exceeded the European Union drinking water standard due to a lack of dilution. However, these are present in the stream throughout the year while the total mass load is higher in winter flows, suggesting a persistence of primary chemical residues in soil and sub-surface environments and restricted degradation.

Herbicides from the phenoxyalkane acid group including derivatives of phenoxyacetic acid (4-chloro-2-methylphenoxyacetic, 2,4-dichlorophenoxyacetic and phenoxypropionic acids derivatives (2,4-D) are the oldest yet still widely applied weed control agents [501-502]. At higher concentrations, phenoxy acids present in these compounds induce rapid and uncontrolled growth of dicotyledonous plants, which leads to plant death. Initially also associated with non-Hodgkin's lymphoma and other cancers, further *in vivo* and *in vitro* studies of 2,4-D toxicity have produced equivocal results [503]. These indicated that an increased proliferation after low 2,4-D exposure may be of importance since proliferation is an important contributor to malignant transformation. Additionally, there were indications that in the presence of 2,4-D, biological responses to other chemicals may be changed resulting in an increased level of mutational events, boasting of enzymatic and non-enzymatic activities and regulation of mineral nutrients under stress conditions [504].

Microorganisms selected for the biodegradation process should contain microbial enzymes able to tolerate the oxidative stresses caused by the herbicides themselves that can be achieved merely via a complex system of enzymatic and non-enzymatic antioxidative stress systems. Many of these response systems are not herbicide specific, but rather triggered by a variety of substances and, collectively, these nonspecific response systems may enhance the survival and fitness potential of microorganisms [505].

Some herbicides contain a substituted aromatic ring linked with a carboxylic acid residue via an ether bond (Table S2 in SI). Carbon-chlorine bonds and carbon-methyl group bonds in the aromatic ring are important structural elements that influence the reactivity and lipophilicity of phenoxy acids. Mecoprop and dichlorprop derivatives are chiral compounds consisting of two isomeric molecules (S and R enantiomers) that differ in the spatial arrangement of atoms. The R enantiomer is the only biologically active enantiomeric form of mecoprop and dichlorprop [506].

Phenoxy acid herbicide degradation is catalyzed by the tfdA gene classes belonging to *β*- and *γ*-proteobacteria [507-508]. These genes encode dioxygenases, *i.e.* the main enzymes that participate in aerobic degradation of aromatic compounds. In the presence of dioxygenases, 2,4-dichlorophenoxyacetic acid is transformed to 2,4-dichlorophenol that is still a toxic compound. Effective proteobacteria whose cells contain a low molecular weight nucleic acid are adapted to oligotrophic waters concentrations and include Achromobacter, Pseudomonas, Variovorax, Cupriavidus, Sphingomonas or Delftia species [501,509].

Differently to 2,4-dichlorophenoxyacetic acid, the atrazine is a persistent pesticide presenting very low degradation rates. Atrazine is the most common herbicide applied in crops of economic relevance, such as sugar cane, soybean, and corn. Atrazine and its derivatives including desethyl (DEA) and desisopropyl-atrazine (DIA) are toxic to the environment, affecting animal and human health [510]. Strong leaching and long residue characteristics of atrazine also caused pollution of groundwater [511] generating multiple toxic effects on fish, algae, aquatic plants and mammals [512]. In addition to an interference with the endocrine of humans and animals, residual atrazine and its related metabolites also threaten the stability of the ecosystem [513].

Herbicides from the Atrazine group

Atrazine is a group of systemic herbicides also called triazines. S-triazine herbicides have been largely used to control broadleaf and grassy weeds in corn, sorghum, and sugarcane crops. The enzymes responsible for the biodegradation of these compounds are those capable to hydrolyze the C-N bond of aromatic structures. Thus, Leucobacter triazinivorans JW-1, a prometryn-degrading bacterium, was found to rapidly degrade s-triazine herbicides. However, these responsible enzymes have not been purified and characterized yet [514]. The structural architecture of such enzymes should resemble that of cytosine deaminase in class III amidohydrolase, with a single Zn^{2+} coordinated by His and Asp that has been assumed to function as a single acid-base catalyst. The activation of water for hydrolysis, as compared to the other amidohydrolases, has not been demonstrated [514].

Enzymes such as hydrolases and peroxidases or cytochrome P450 enzymatic complex present in various fungus and bacteria (Pleurotus ostreatus, Pseudomonas species, Acinetobacter, Burkholderia, Methylobacterium, Rhodococcus, Sphingomonas, Streptomyces, Variovorax or Williamsia) showed a rather high potential in the degradation process of the atrazine group as well. These are as well naturally biodegraded by microbial communities such

as Paenarthrobacter aurescens and their genome scale metabolic models [488,515-517]. Mechanistic studies on the cometabolic biodegradation of atrazine indicated that cytochrome P450 monooxygenases catalyze degradation of this herbicide through several hydroxy-, dechlorinated or dealkylated metabolites. The obtained metabolomics data revealed that atrazine induced oxidative stress and disruption of the carbon and nitrogen metabolism cause an increase in the membrane fluidity and induce lipid peroxidation as well [518]. Pseudomonas aeruginosa secreting dehydrogenases and oxidase enzymes also presented activity for such biodegradation [519].

Arthrobacter species is another efficient bacterial strain for atrazine degradation at 30 °C and slightly basic pH in the range 7.0–9.0 [520]. The metabolic pathway follows firstly a dechlorination into hydroxyatrazine, followed by the dealkylation to N-isopropylammelide, and ultimately deamination to cyanuric acid. Although cyanuric acid has a low level of toxicity without any serious health concern, high-levels of this chemical can induce risk because of the chlorine diminished ability to kill bacteria and viruses.

Atrazine chlorohydrolase, TrzN (triazine hydrolase or atrazine chlorohydrolase), initiates bacterial metabolism of the herbicide atrazine by hydrolytic displacement of a chlorine substituent from the *s*-triazine ring [521]. Differently to dehalogenases, which use water as a co-substrate, and are not metalloenzymes, TrzN requires a divalent metal ion to catalyze hydrolytic dehalogenation and thus differs mechanistically from other well studied halidohydrolases (Figure 54). TrzN is involved in substrate binding, stabilization of the transition state, and possibly protonation of the epoxide oxygen and uniquely positions threonine 325 in place of a conserved aspartate that ligates the metal in most mononuclear members of the amidohydrolases superfamily. These enzymes present an activity nearly constant in the range pH 6.0-10.0, which is consistent with the loss of a proton-donating group [521]. Also, such enzymes show a two-domain structure with the core having the *α/β* hydrolase-fold topology. The catalytic residues, Asp107 and His275, are located in a predominantly hydrophobic environment between the two domains. A tunnel connects the back of the active-site cavity with the surface of the enzyme and provides access to the active site for the catalytic water molecule, which in the crystal structure, has been found at hydrogen bond distance to His275 (Figure 55) [522].
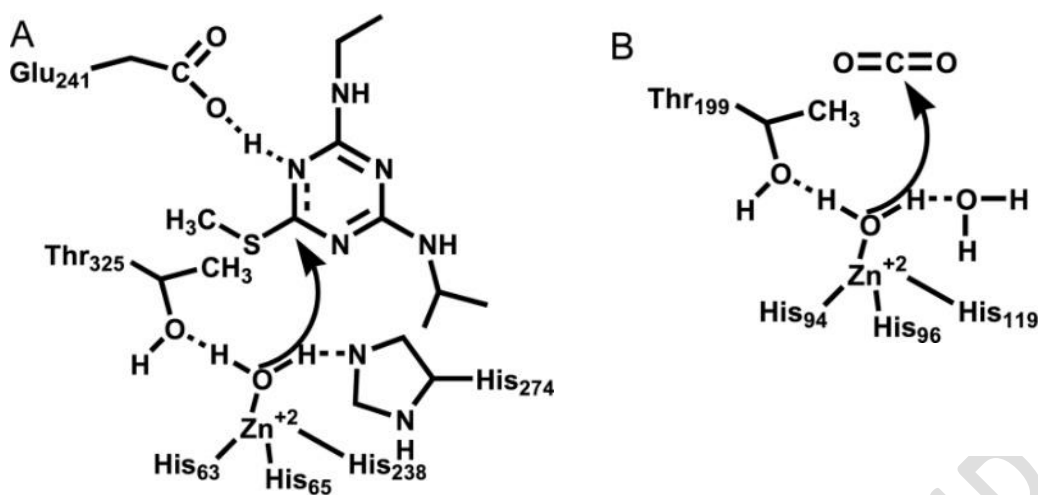
Figure 54. Proposed mechanism for TrzN and comparison with carbonic anhydrase. Reproduced with permission from ref [521]. Copyright 2010 Elsevier.

In vivo removal experiments also suggested that laccases may have a possible role on atrazine biodegradation. These investigations focusing on less explored ligninolytic enzymes and cell-bound mechanisms evidenced key aspects of the atrazine fungal metabolism underlying the role of the nitrogen in this process [523]. Also, the combination of phosphate-solubilizing bacteria with biochar may promote the degradation of atrazine. Following this approach it enables functional bacteria to fully play its environmental functions [524].

A self-immobilization method for microorganisms was also developed based on fungal pellets [525]. Biochar overcomes disadvantages of pellets such as cell leakage, cell loading limitation and low mechanical strength and therefore can be utilized for the immobilization of atrazine biodegrading microorganisms. Thus, the addition of biochar enhances the connection between the microorganisms and pellets-based carrier, affording biodegradation at an accessible pH, *i.e.* between 6 and 10.
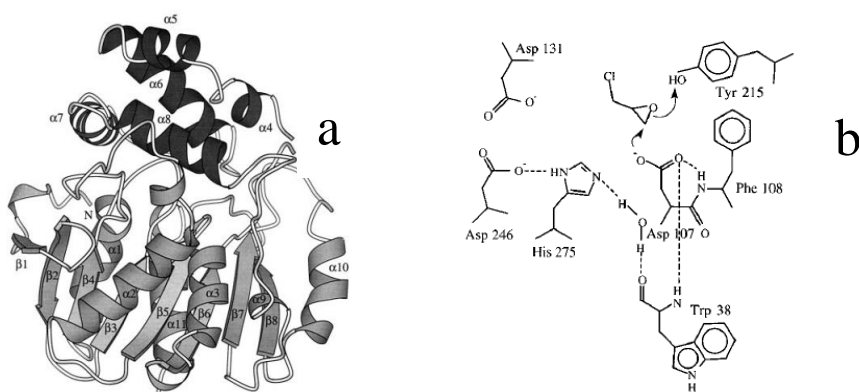
Figure 55. Schematic view of the secondary structure elements of the epoxide hydrolase monomer: α-helices, β-strands, and coils are represented by helical ribbons, arrows, and ropes, respectively; the α-helices of the cap domain are shown in dark gray (a) and representation of the catalytic mechanism of epoxide hydrolase (b); the Michaelis complex with epichlorohydrin is shown before the formation of covalent intermediate, which is indicated by arrows, hydrogen bonds are shown as dashed lines. Reproduced with permission from ref [522]. Copyright 1999 Elsevier.

Metagenomics has also contributed to the biodegradation of atrazine. It provided the discovery of genes and metabolic pathways involved in the degradation of xenobiotics [526]. Thus, some microorganisms like Agrobacterium rhizogenes and Candidatus Muproteobacteria bacterium tree species can metabolize these compounds, where the rhizodegradation accelerates the degradation of atrazine residues, eliminating toxic effects on plants highly sensitive to this herbicide.

Fungi like Bjerkandera adusta producing an ensemble of enzymes with oxidative properties possess pretty high removal efficiency of the xenobiotic atrazine compound at different parameters like pH (2.0-8.0) and temperature (16-32 °C) operating at very low concentrations (25-100 ppm) [527]. In the case of Rhodococcus ruber, the enzymes of β-oxidation consist of a mixture of hydratase, dehydrogenase, 3-oxoacyl-thiolase, 2,3-enoyl-isomerase, 3-hydroxyacyl-epimerase [528].

Some studies have shown that the cooperation of mixed bacteria is more effective for the biodegradation in mineral media than a single strain [529]. Atrazine was faster biodegraded by two strains, Arthrobacter sp. DNS10, utilizing atrazine as the sole nitrogen source for growth, and Enterobacter sp. P1, that is a phosphorus-solubilizing bacterium that releases various kinds of organic acids, but lacks the ability to degrade atrazine [530]. This concept can be expanded to mixtures of pesticide/herbicides from agricultural wastewaters affording a better biodegradation of atrazine and imazalil, metalaxyl and pyrimethanil [531].

Mixing Arthrobacter sp. NJ-1 with Klebsiella variicola Strain FH-1 also enhanced the biodegradability of atrazine and the efficiency depended on the mixing ratio and the culture

medium (addition of sucrose and NH$_4$Cl) that is not easily to be achieved under natural conditions [532].

Chloroacetanilides

Acetochlor is a member of the class of herbicides known as chloroacetanilides. Its mode of action is elongase inhibition, and inhibition of geranyl pyrophosphate cyclization enzymes, as part of the gibberellin pathway. Acetochlor is suspected to be a carcinogenic and endocrine disrupter and has been characterized as a class B-2 agent (probable human-carcinogen) by the United States Environmental Protection Agency (EPA, 2006). Its consecutive application has resulted in the widespread drug resistance of weeds and a high risks to environment and human health [533].

Microorganisms play a significant role in the degradation of chloroacetamide herbicides and for particular case of acetochlor, a rather high number of aerobic-degrading strains (Delftiasp. T3-6, Pseudomonas oleovorans LCa2, Rhodococcussp. B1 and T3-1, Sphingobium quisquiliarum DC-2, Sphingomonads wittichii DC-6, Sphingobium sp. MEA3-1, Sphingobium baderi DE-13) and also anaerobic (genera Sporomusa, Sporobacterium, Dechloromonas, Azotobacter and Methanobacterium) have showed activity [534]. The aerobic degradation pathway of acetochlor in these cases is the result of a concerted process catalyzed by enzymes contained in the microorganisms. This leads initially to N-dealkylated to 2-chloro-N-(2-methyl-6-ethylphenyl) acetamide and is catalyzed by the Rieske non-heme iron oxygenase from Sphingomonads wittichii DC-6 or by the cytochrome P450 from Rhodococcus sp. T3-1; after which the intermediate is hydrolyzed to 2-methyl-6-ethylaniline by an amidase cloned from Sphingobium quisquiliarum that catalyzes the amide bond cleavage [535]. 2-methyl-6-ethylaniline is further hydroxylated by a monooxygenase to 4-hydroxy-2-methyl-6-ethylaniline, which is then hydrolytically deaminated to 2-methyl-6-ethylhydroquinone that is subsequently hydroxylated by the two-component flavin-dependent monooxygenase to 3-hydroxy-2-methyl-6-ethylhydroquinone, which finally is subject to ring cleavage.

The anaerobic acetochlor degradation is also possible [534]. Experiments carried out with Sporomusa, Sporobacterium, Dechloromonas, Azotobacter, Rummeliibacillus, or Methanobacterium showed a significant increase in abundance which corresponded to a positive correlation with the acetochlor degradation capacity. This was also valuable for other chloroacetanilides such as alachlor, propisochlor, butachlor, pretilachlor or metolachlor, where the N-alkoxyalkyl structure of these herbicides significantly affected their biodegradability.

The proposed anaerobic degradation pathway of acetochlor by the acclimated anaerobic sludge is described in Scheme 8 [534].
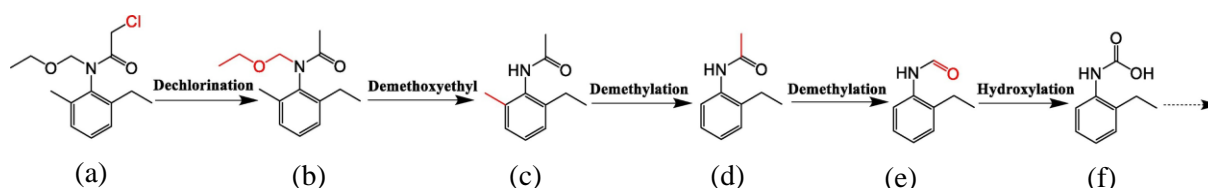
Scheme 8. Proposed anaerobic degradation pathway of acetochlor by the acclimated anaerobic sludge. (a) acetochlor 2-ethyl-N-carboxyl aniline; (b) 2-ethyl-6-methyl-N-(ethoxy- methyl) acetanilide; (c) N-(2-methyl-6- ethylphenyl) acetamide (d) N-2-ethylphenyl acetamide; (e) N-2-ethylphenyl formamide. Reproduced with permission from ref [534]. Copyright 2020 Elsevier.

Changing the microorganism producing enzymes may change the acetochlor degradation pathway as well. Arabidopsis thaliana synthesizing an *oxygenase* component is producing in the first step 2-chloro-N-(2-methyl-6-ethylphenyl)acetamide that is further degraded by the enzymes produced by other indigenous microorganisms in the soil [536]. The surface of the catalytic domain of these enzymes receives the Rieske domain from the adjacent subunit placing the [2Fe-2S] center in the right conformation with respect to the catalytic iron (Figure 56)[537].

This change can also be correlated to the nature of the herbicide. Butachlor-degrading Pseudomonas sp. strain But2 isolated from soil can degrade butachlor regardless its concentration and grows without a lag phase, [538] while during degradation, 2-chloro-N-(2,6-diethylphenyl) acetamide, 2,6-diethylaniline, and 1,3-diethylbenzene were formed, which indicated that deamination occurred. The mixed bacterial culture of Pseudomonas sp. But2 and Acinetobacter baumannii DT showed highly effective biodegradation of both butachlor and propanyl in liquid media and soil as well.
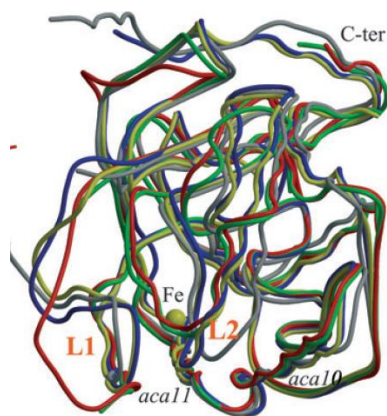
Figure 56. Catalytic domains of oxidases. The two solvent exposed loops LI and LII are shown at the entrance of the catalytic pocket, as well as, the highly conserved consecutive helices, aca 10 and aca11. Reproduced with permission from ref [537]. Copyright 2007 Wiley-VCH GMBH.

Other chloro-derivative herbicides

Diuron is among the selective and the most persistent herbicides. Widespread use of this compound has led to elevated concentrations of diuron in groundwater and wastewater. According to literature there are two main mechanisms involved in the partial degradation of diuron, an abiotic degradation to 3,4-dichloroaniline as the only product, the reaction being catalyzed by OH^- and H^+ and a buffer by the minerals in water, and a biotic degradation that involves the implication of micro-organisms [539-540].

Biodegradation of 3,4-dichloroanilines was first reported using Pseudomonas putida which has been able to mineralize 3,4-dichloroanilines with liberation of carbon dioxide in the presence of aniline as an analogue co-substrate (Scheme 9) [541].

Amongst the microorganisms able to degrade 3-chlorolevulinic acid and 3,4-dichloroanilines degraders, two belong to the *γ*-Proteobacteria and seven to the β-Proteobacteria which are part of to the Pseudomonas genus [542]. In the absence of any other C and N sources enzymes from Pseudomonas fluorescens catalyze a dehalogenation and a hydroxylation of the aromatic ring. These bacteria mainly secrete of hydrolytic enzymes, especially lipases and proteases [543]. These enzymes do not contain metals and their activity is a result of an organocatalytic effect.

Most of the lipases belong to sn-1,3 specific lipase, namely, Fatty acid hydrolysis/esterification specifically at the either/both sn-1 and sn-3 position while lipases from Pseudomonas or Candida families catalyze in a non-regiospecific manner such reactions [544]. Structural analysis and biochemical assays revealed that disulfide bonds and salt bridges

play a vital role in their catalytic behavior（Figure 57）. The catalytic domain includes a central β sheet comprising six parallel β strands, which are surrounded by 12 helices.
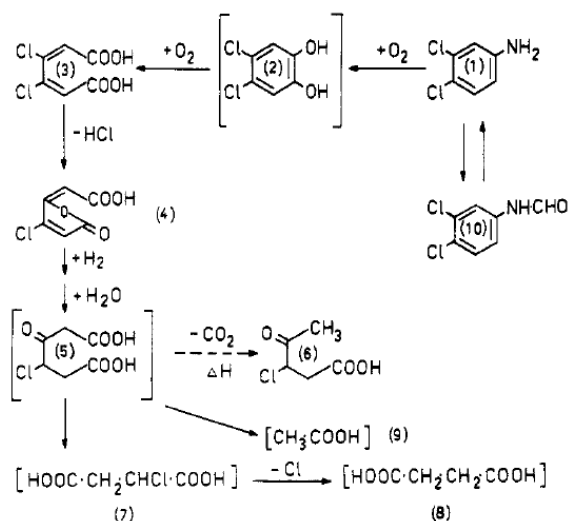
Scheme 9. Suggested pathway of 3,4-Dichloroaniline biodegradation by Pseudomonas putida. (1) 3,4-dichloroaniline ; (2) 4,5-dichlorocatechol; (3) 3,4-dichloromuconate; (4) 3-chloro-4-(carboxymethylene)- but-Zenolide (3-chlorobutenolide); (5) 3-chloro-4-ketoadipic acid; (6) 3-chlorolevulinic acid; (7) 2-chlorosuccinic acid; (8) succinic acid; (9) acetic acid; (10) 3',4'-dichloroformylanilide. The intermediates in brackets were postulated. Reproduced with permission from ref [541]. Copyright 1982 American Chemical Society.
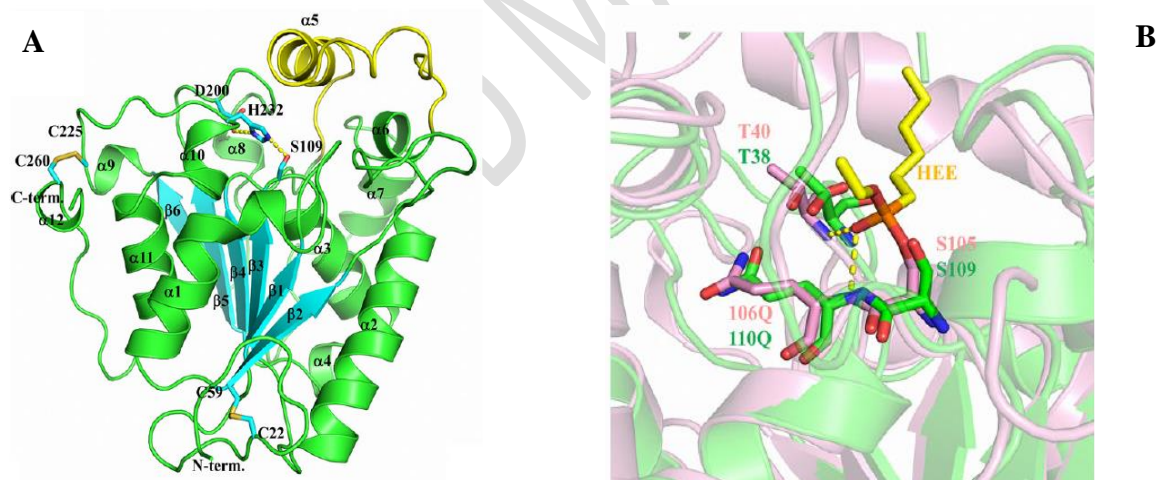
Figure 57. Overall structure of a *lipase*. (A) Cartoon representation of *lipase* showing that the structure has 12 a helices and six β strands. The catalytic triad and disulfide bonds are labelled and shown in stick model representation (B). The superimposition of lipases (green, PDB (Protein Data Bank) code: 5H6B) (pink, PDB code: 1LBS)). Oxyanion holes (threonine and glutamine) and nucleophilic serines are all labelled and shown as sticks. The n-hexyl phosphonate ethyl ester is displayed with yellow stick representation. Reproduced with permission from ref [544]. Copyright 2017 Wiley-VCH GMBH.

Proteases are enzymes catalyzing the proteolysis, i.e. the breakdown of C-N bonds in the presence of water. The degradation of diuron with bacteria secreting such enzymes occurs pretty fast [545]. In the cases of Pseudomonas aeruginosa FN or Streptomyces griseus protease,

133

the evolved degradation product was 3,4-dichloroanilines [546]. Optimal conditions corresponded to a temperature of 25 °C and a concentration of diuron as high as 0.5 mg/L.

The presence of other microorganisms poisoning Cytochrome P450 genes such as bacteria or fungi may transform the diuron degradation products (such as hydroxylated intermediates (3-(3,4-dichlorophenyl)-1-hydroxymethyl-1-methylurea)) to further metabolized N-dealkylated compounds 3-(3,4-dichlorophenyl)-1-methylurea (DCPMU) and 3,4-dichlorophenylurea. This underlines the relevant role of hydroxylation for subsequent N-demethylation [547]. Responsible for these degradation steps are hemes incorporated in the Cytochrome P450 structure (Figure 58).
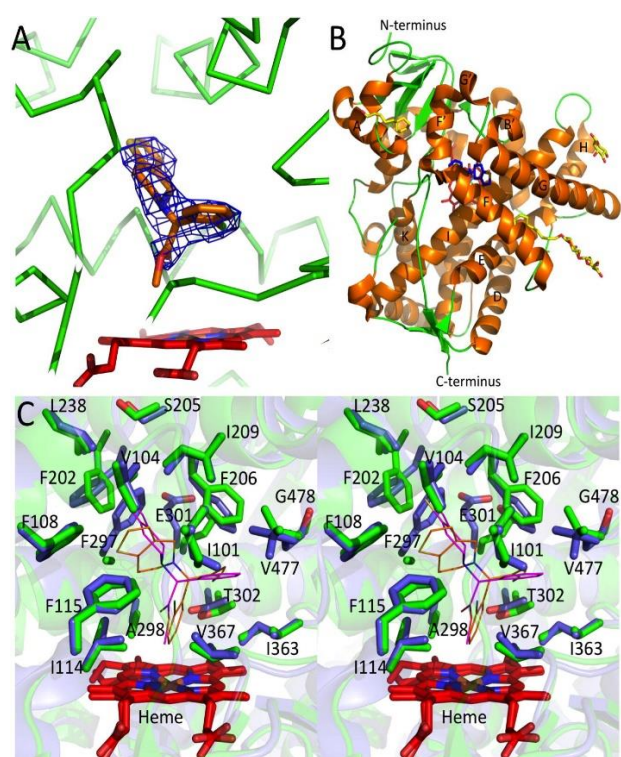
Figure 58. Structure of the cytochrome P450 2B4, F297A, with 2B4 WT structure showing residues within 5 Å from the ligand. A) An unbiased F_o - F_c electron density map determined before inclusion of the ligand in the 2B4 F297A complex contoured at 3σ corresponding to clopidogrel above heme. B) Crystal structure of 2B4F297A clopidogrel complex: α-helices are shown in orange, and β−sheets and loops are shown in green. Three Cymal-5 molecules (two partially occupied molecules) and clopidogrel are shown in yellow and blue sticks, respectively. C) Superimposed structures of 2B4 F297A (green) and 2B4 WT (blue) complexes of clopidogrel in stereo view representing active site residues within 5 Å from the ligand (magenta lines) in 2B4 F297A. The corresponding residue in the 2B4 WT structure in complex with clopidogrel (orange sticks) is also shown. Reproduced with permission from ref [548]. Copyright 2013 Elsevier.

Quinclorac is another effective but environmentally persistent herbicide commonly used in the rice production [549]. Its degradation occurred with a slow rate using Pseudomonas gammaproteobacteria mainly producing *dehydrogenase* enzymes [550] while its combination

with Achromobacter sp., producing oxidoreductases [551] generated a concerted effect with a bioremediation of approximately 92 % of the 50 mg/l after 5 days. Both enzyme families may contain metals as Mo, W and Fe, Mo^{VI}, W^{VI} or Fe^{III} oxidation state may be involved in a redox process [550]. The active oxo-metal center is bound to cofactors (which do not contain metal) and an 4Fe-4S cluster [552-554]. Thus, combining the two classes of enzymes expands the biodegradation capability.

Alachlor and metolachlor are other currently utilized chloroacetanilide herbicides. Their biodegradation was mainly achieved by dechlorination and hydroxylation reactions taking Trichoderma sp as a source of enzymatic catalysts [555]. These cultures produce lysins, also known as endolysins or murein hydrolases, which are hydrolytic enzymes able to cleave and hydroxylate such molecules. This process is typically achieved by the joint action of multiple lysin molecules at a local region of the host cell wall [556] that in fact corresponds to an organosupramolecular catalytic process. Figure 59 presents a stereo view of these enzymes.
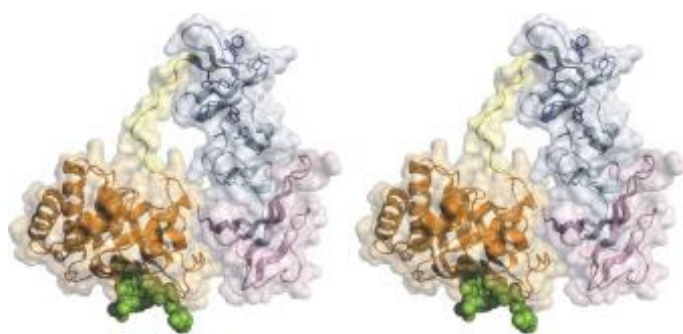
Figure 59. Stereo view of the three-dimensional structure of the complex Cpl-1E94Q-(2S5P)2. The catalytic module of *pneumococcal phage* is in *orange*; the linker is in *yellow*; the choline-binding module is in *blue* (CI domain) and in *magenta* (CII domain). The bound peptidoglycan is drawn in *green* space-filled representation. Reproduced with permission from ref [557]. Copyright 2007 Elsevier.

Linuron (3-(3,4-dichlorophenyl)-1-methoxy-1-methylurea) is a phenylurea herbicide that is used to control the growth of grass and weeds for the purpose of supporting the growth of crops like soybeans and acts as an endocrine disruptor compound in combination with other xenoestrogens such as bisphenol A, ethynylestradiol, and 4-n-nonylphenol [558]. These compounds were either not inoculated or inoculated with the enzymes secreted by fungus Pleurotus ostreatus.

Pentachlorophenol has been introduced into the environment mainly as a wood preservative and biocide [559]. This is a recalcitrant biocide that bioaccumulates in the environment due to its persistent nature and has been listed as a priority pollutant due to its toxicological and health effects. Biodegradation of this molecule can be achieved by the treatment with a common species of crust fungus, namely, Phlebia with a maximum activity

level for Phlebia acanthocystis. This secretes several enzymes such as laccase, lignin peroxidase and manganese peroxidase. In the presence of these enzymes, pentachlorophenol is transformed into pentachloroanisole and *p*-tetrachlorohydroquinone via methylation and oxidation reactions, which are further converted to methylated products including tetrachloro-4-methoxyphenol and tetrachloro-1,4-dimethoxybenzene.

Pentachlorophenol is also degraded in the presence Bacillus cereus, an aerobic spore-forming bacterium able to produce pectinase and mannanase enzymes [560]. Pectinase is an enzyme that breaks down pectin, i.e. structural acidic heteropolysaccharides, while mannanase catalyzes hydrolysis of terminal, non-reducing beta-D-mannose residues in beta-D-mannosides.

Chlorimuron ethyl is a sparingly soluble sulfonylurea herbicidal agent that inhibits actetolactate synthase, an enzyme involved in synthesis of branched chain amino acids including valine, leucine, and isoleucine. Carboxylesterase, a de-esterification enzyme, was reported to catalyze its degradation [561]. It can hydrolyze chlorimuron-ethyl and also produce the cleavage of the NC bond of the sulfonylurea bridge and pyrimidine ring deamination. Additionally, carboxylesterase can hydrolyze the ester bond between hemicellulose and lignin in straw materials or the ester bond connecting the side chains in xylan. Taking genes expressed in R. erythropolis D310-1 open shown a complex degradation pathway including a xenobiotic biodegradation metabolism implying toluene degradation and aminobenzoate degradation pathways that might contribute to its survival in the presence of chlorimuron-ethyl. All these processes follow a supramolecular organo-catalysis mechanism. Figure 60 offers a structural image of the chlorimuron-ethyl-degrading enzyme.

Metal ions are important factors affecting the activity of this enzyme. The reported results showed that the relative activity of carboxylesterase increased slightly in the presence of Cu^{2+} due the capacity to stabilize the binding of the enzyme-substrate complex and the active conformation of the enzyme, while other cations such as Mg^{2+}, Zn^{2+} or Ba^{2+} inhibited the process [561].

An advanced microbial degradation of a compound as chlorimuron-ethyl is, however, a complex process that involves gene regulation of multiple metabolic pathways requiring the presence of a more complex key degradation enzymatic system such as a mixture of cytochrome P-450, carboxylesterase and monooxygenase [562]. Glutathione-S-transferase (Figure 61) is also participating in the degradation of Chlorimuron-ethyl in water due to its ability to catalyze the conjugation of the reduced form of glutathione to xenobiotic substrates [563].
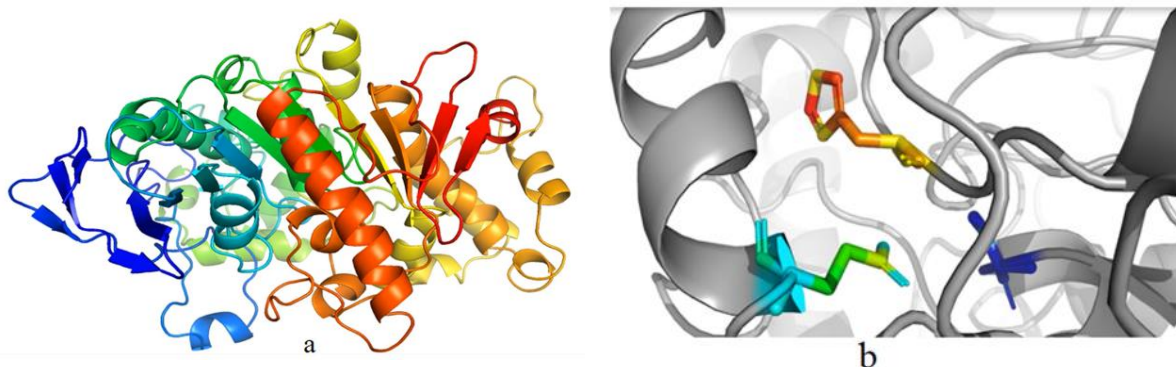
Figure 60. Structural analysis of the chlorimuron-ethyl-degrading enzyme: (a) tertiary structure, and (b) catalytic triad. Reproduced with permission from ref [561]. Copyright 2020 Elsevier.
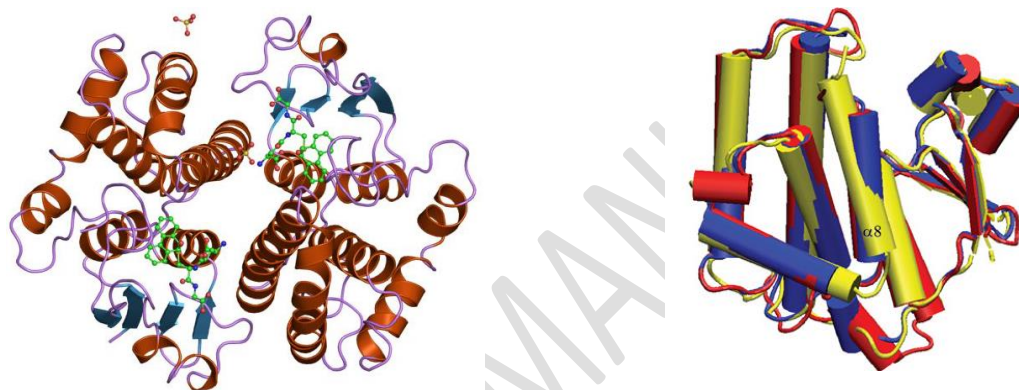
Figure 61. Glutathione-S-transferase with a) the 2-fold axis into the active site, with the glutathione sulphonic acid shown as a ball-and-stick figure; and b) cylinders represent helices, arrows represent strands, and lines represent random coil of Aligned Anopheles glutathione transferases. Reproduced with permission from ref [564]. Copyright 2005 Portland Press.

Trichloroacetic acid is one of the main halogenated compounds that are carcinogenic to humans and animals. Although it is not used as herbicide or in composition of these the ability of various strains to biodegrade it was evaluated as a dehalogenase enzyme assay [565]. Structurally, haloalkane dehalogenases belong to the α/β-hydrolas esuperfamily. Their active site is buried in a predominantly hydrophobic cavity at the interface of the α/β-hydrolase core domain and the helical cap domain, and is connected to the bulk solvent by access tunnels. The reaction is an acid/base catalyzed process that occurs via a nucleophilic substitution with either an amino acid side chain of the enzyme or with an activated water molecule acting as the nucleophile [566].

Chlorobenzoic acids are recalcitrant and toxic materials which enter the environment directly using both herbicides and pesticides, or indirectly through the biodegradation of polychlorinated biphenyl compounds. The biodegradation of 4-chlorobenzoic acid, as an

example, was demonstrated by Lysinibacillus macrolides DSM54T, which resulted as a promising candidate for bioremediation of such compounds [567].

Trifluralin is another widely used dinitroaniline herbicide, which can persist in the environment and has substantial ecotoxicity, especially to aquatic organisms. Instead of chlorine its structure incorporates fluorine and despite the strongly xenobiotic character of some of substituents, biodegradation of trifluralin does occur either by dealkylation or nitro-group reduction [568]. The genes and enzymes responsible for biodegradation are still largely unknown, the relative roles of abiotic processes vs growth-linked biodegradation vs cometabolism are unresolved, and the impact of different environmental factors on the rates and extents of biodegradation are not clear. However, a Candida species gave a certain yield of mineralization even at 14 ºC [568].

Lactofen is a fluoro-chlorinated complex ester of acifluorfen acting as a nitrophenyl ether selective chiral herbicide to control broadleaved weeds in soybean, cereals, potatoes and peanuts [569]. Esterases screted by strain Edaphocola flava HME-24 could degrade via an initial hydrolysis to desethyl lactofen and a subsequent disruption to acifluorfen that is still a large non-innocent fluoro-chlorinated compound. This esterase was also able to transform *p*-nitrophenyl esters, but the activity decreased when the carbon chain length increased. It showed enantioselectivity during the degradation of lactofen, diclofop-methyl, and quizalofop-ethyl, with a higher degradation efficiency of (S)- respect to (R)-enantiomers.

Other herbicides

Isoxaflutole is an herbicide activated in soils and plants to its diketonitrile derivative that is the active form of the herbicide [570]. Laccase enzymes in two fungi, Phanerochaete chrysosporium and T. versicolor, are able to convert this diketonitrile to the inactive benzoic acid analogue [570].

Another member of the Pseudomonas family, Pseudomonas stutzeri, a gram-negative bacterium, is known for its diverse metabolism. It mainly secretes glucan 1,4-α-maltotetraohydrolase that degrades simazine, one of the most used herbicides in maize fields. In addition, Pseudomonas stutzeri-Y2 degraded atrazine and terbuthylazine, and propazine [571]. The functional durability of this bacterium has been prolonged through various immobilization materials and compositional combinations that were designed and compared to enhance of prolong its bacterial functions. In conjunction with it Arthrobacter ureafaciens bacterium secretes deglycosylation enzymes capable of cleaving all non-reducing unbranched N-acetylneuraminic and N-glycolylneuraminic acid residues by hydrolysis. Based on this it can

also degrade simazine [572]. The strain XMJ-Z01 is highly resistant to simazine and can tolerate simazine at a high level.

Nicosulfuron is one of the main sulfonylurea herbicides that have been widely used to protect maize crops. It contains both sulphur and nitrogen functionalities that can induce recalcitrant effects in water requiring its biodegradation. Bacillus velezensis showed a rather high efficiency for the degradation in water of this herbicide. Bacillus velezensis CF57 preserves its efficiency in a wide range of temperature, pH, and a low inoculation amount. This wide activity range allows a broad degradation spectrum of other sulfonylurea herbicides as well [573]. Its catalytic activity is attributed to concerted various lignocellulolytic activities exerted by cellulase (hydrolysis of the 1,4-beta-D-glycosidic linkages), xylanase (breaking down hemicellulose), chitinase (glycosyl hydrolysis of the β-1,4 glycosidic bond of chitin) (Figure 62), α-amylase (hydrolysis of α-bonds of large, alpha-linked polysaccharides, such as starch and glycogen, yielding glucose and maltose) (Figure 63), β-glucanase, and pectinase (breaking down pectin, a polysaccharide found in plant cell walls) [574].

Bentazone is another herbicide of the thiadiazine group of chemicals widely applied in rice and cereal crops, and widespread in the aquatic environment. Experiments carried with Trametes versicolor, a fungus secreting both laccase and cytochrome P450 enzymatic systems, proved efficiency in remediation of this herbicide [575]. The reactions involved in this process included hydroxylations, oxidations, methylations, N-nitrosation, and dimerization. Bacterial contamination is the bottleneck in the implementation of fungal bioreactors and trickle-bed reactors resulted as a solution for the implementation of fungal bioremediation at a real scale.
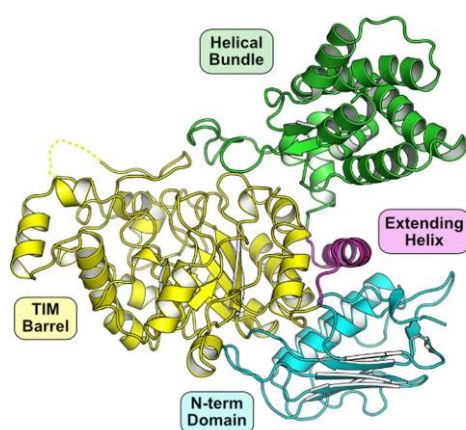
Figure 62. The active site architecture of Chitinase FjGH20. Reproduced with permission from ref [576]. Copyright 2020 Springer Nature.
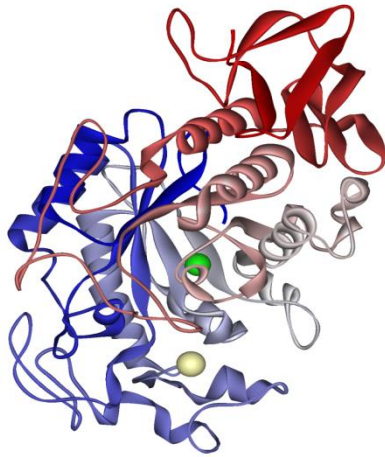
Figure 63. The active site architecture of α-amylase. Reproduced with permission from ref [577]. Copyright 1996 International Union of Crystallography.

Glyphosate, N-(phosphonomethyl) glycine, is one of the most widely broad-spectrum used herbicides that targets broadleaf weeds, grasses, and woody plants [578]. Bradyrhizobium sp are part of the microorganisms that degrade and use herbicide residues as a source of carbon and nitrogen. Their biochemical activity is related to the combination of secreted enzymes: catalase, esterase, oxidase, reductase, and urease [579]. In particular, the Bradyrhizobium sp BR 3901 strain can use products based on diuron, sulfentrazone, and 2,4-dichlorophenoxyacetic acid as a carbon source with a limited toxicity to this bacterial strain, and the oxyfluorfen-based product as a nitrogen source.

The golden mussel Limnoperna fortunei is a freshwater invasive species which has been found to increase glyphosate dissipation in water and to accelerate eutrophication [580]. This mussel generates an increase in the concentration of dissolved nutrients in water (N–NH_4^+ and P-PO_4^{3-}), even higher than that caused by the filtering activity of the mussels, probably resulting from stress or from the degradation of glyphosate and adjuvants. Thus, larger bioavailability of these nutrients due to glyphosate metabolization mediated by mussels may accelerate eutrophication processes in natural water.

Aquifer contamination following herbicide glyphosate has also been considered, quantifying the sensitivity of soil and aquifer to this contamination [581]. Target quantities evaluate its toxic metabolite amino-methyl-phosphonic acid concentrations in the top soil as well as their leaching below the root zone taking as parameters, absolute permeability, air-entry suction, and porosity.

Organophosphonates are molecules that contain a very chemically stable carbon-phosphorus (C-P) bond. Microorganisms can utilize phosphonates as potential source of crucial

elements for their growth, as developed several pathways to metabolize these compounds. One among these pathways is catalyzed by C-P lyase complex, which has a broad substrate specificity, and, therefore, a wide application in degradation of herbicides deposited in the environment, such as glyphosate [582]. The carbon-phosphorus (C-P) lyase complex is essential for the metabolism of inactivated phosphonates to phosphate in bacteria (PhnK), where genes expressing (PhnK) exposes the active site residues PhnH and PhnJ (Figure 64) [583].

This multi-enzyme system has been recognized in Escherichia coli. Genetic studies have demonstrated that the enzymatic system is encoded by Phn operon containing 14 genes (PhnC-PhnP). The ability to degrade phosphonates is also found in other microorganisms, especially those present in soils and marine bacteria that have homologous genes to those in Escherichia coli. Despite the existence of differences in structure and composition of the Phn gene cluster, each of these strains contains genes necessary to promote the C-P bond cleavage [582].
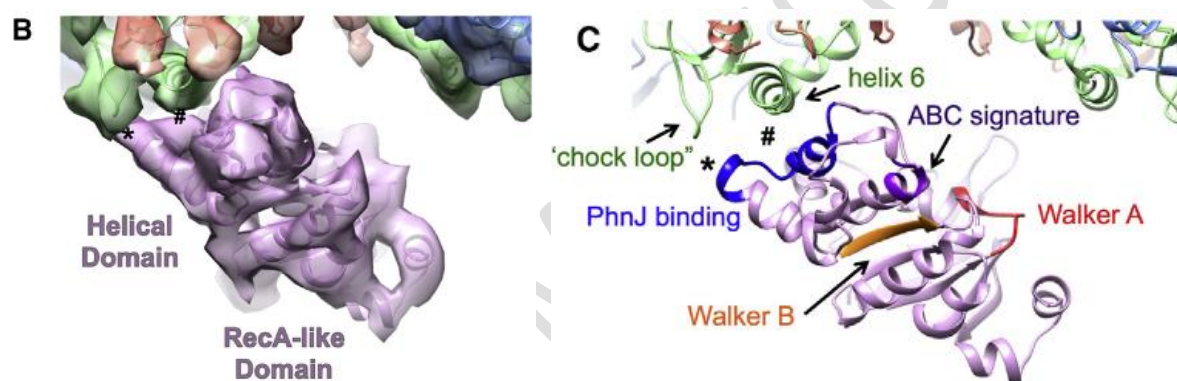
Figure 64. PhnK is an NBD-like Protein and Interacts with PhnJ; (B) One PhnK binds to the core complex with the models fitted in the map; (C) The same view as (B) with the NBD motifs color labeled. Reproduced with permission from ref [583]. Copyright 2016 CelPress.

Besides herbicides, malathion organophosphates are considered as a major constituent of pesticides and insecticides. Extensively used in agricultural, horticultures and for numerous household applications, malathion is among the major organic pollutants, having leading antagonistic effects on human health and environment [584]. Detoxification of malathion from these contaminated sites has also been achieved by the Carboxylesterase produced by several bacterial species, including Bacillus thuringiensis MOS-5 and Sphingobium yanoikuyae strain P4.

Aromatic oxyphenoxypropionic acid ester herbicides are widely used with detrimental environmental effects as well [585]. Besides aromatic oxyphenoxypropinate esters Methylobacterium populi YC-XJ1 exhibits a diverse degrading ability towards phthalate esters, organophosphorus flame retardants, or chlorpyrifos. This activity is related to the activity of

hydrolases secreted by these bacteria. Hydrolysis takes place through successive steps, but without a complete removal of the aromatic compounds (Figure 65).
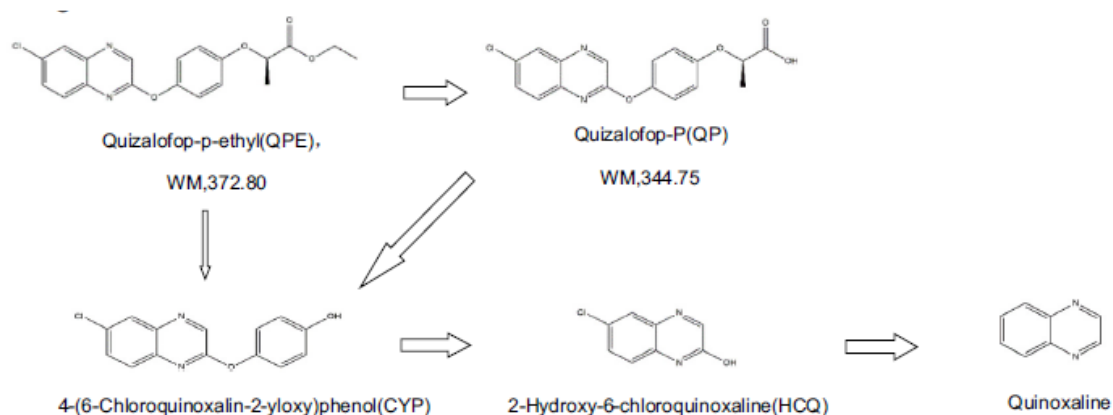
Figure 65. Biodegradation of an oxyphenoxypropionic acid ester herbicide. Reproduced with permission from ref [585]. Copyright 2020 MDPI.
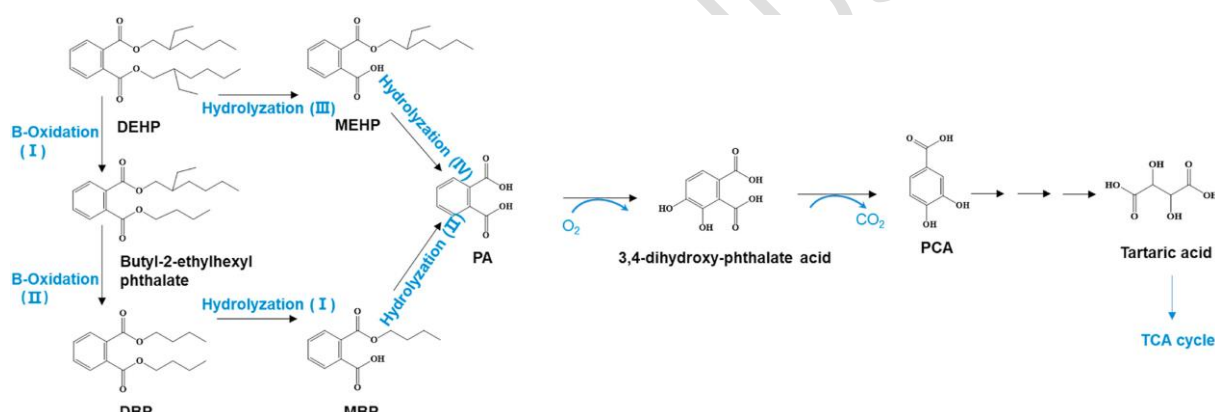
Figure 66. The primary pathway of PAEs biodegradation by the isolated strain E3. Reproduced with permission from ref [586]. Copyright 2021 Elsevier.

Phenoxyalkanoic acid herbicides are compounds in which 2,4-dichlorophenoxy or 4-chloro-2-methylphenoxy groups are substituted on the second carbon of acetic (2-[2,4-dichlorophenoxy]acetic acid [2,4-D] and 2-[4-chloro-2-methylphenoxy] acetic acid) or propionic acid ([2R]-2-[2,4-dichlorophenoxy] propanoic acid, 2-[4-chloro-2-methylphenoxy] propanoic acid [mecoprop], and [2R]-2-[4-chloro-2-methylphenoxy]propanoic acid) or on the 4th carbon of butyric acid (4-[2,4-dichlorophenoxy]butanoic acid [2,4-DB] and 4-[4-chloro-2-methylphenoxy]butanoic acid). In commercial formulations, the above phenoxyalkanoic acid herbicides are present mainly as acids and sodium or potassium salts [587].

These herbicides are mainly metabolized by microorganisms in soils, but the microorganisms that perform well under alkaline environments are rarely considered. The

degradation process occurs through hydrolysis in the presence of hydrolases (Figure 66). Three modules of tfd gene clusters involved in 2,4-dichlorophenoxyacetic acid catabolism and genes encoding monovalent cation/proton antiporters involved in alkali tolerance were putatively identified. Thus, Cupriavidus oxaliticus strain X32 showed encouraging degradation abilities, tolerance, and even alkali tolerance and could be a promising candidate for the bioremediation of PAA-contaminated sites, especially in alkaline surroundings [588].

3.3.2.4. Biodegradation of insecticides

Synthesized early in 1874 [589] (1,1,1-trichloro-2,2-bis(*p*-chlorophenyl)ethane) DDT has been proposed as an insecticide and after that largely utilized in agriculture [590]. However, its pollutant effects were unanimously recognized only after several decades of utilization when Stockholm Convention on Persistent Organic Pollutants proposed in 2004 a global ban on several persistent organic pollutants that also included DDT derivatives (*p,p'*-DDT, *p,p'*-DDT) and its co-synthesis side-products (*p,p'*-DDD and *p,p'*-DDE). This decision has also been accompanied by efforts of bioremediation of waters that accumulated these compounds by considering several types of microorganisms [591-594].

The mechanistic investigations related to these studies revealed a quite complex process occurring through a consistent number of new pollutant intermediates [595] (Figure 67). The elimination of chlorine is not trivial and the process is slow enough that results in the persistence of these partially dechlorinated intermediates in water.

Common insecticides have been identified in surface and drinking waters together with other herbicides including atrazine, chlorotriazines, terbuthylazine, simazine, 2,4-dichlorophenoxyacetic acid, 2-methyl-4-chlorophenoxyacetic acid, and bentazon [596]. Organic insecticides, extensively used for crop protection, cover a wide range of chemical structures, including hydrocarbons, carboxylic acid derivatives, alcohols, aldehydes, ketones, amines, nitro compounds, quinones, thiocyanates, mercaptans, heterocyclic compounds, etc [597].

Fipronil is a broad-spectrum insecticide that belongs to the phenylpyrazole chemical family. Microorganisms reported to be active in remediation of this insecticide were Bacillus species (secreting proteases, amylases, and xylanases; proteases are enzymes which break down proteins and peptides, amylase catalyses the hydrolysis of starch into sugars and xylanases break down hemicellulose, i.e. the linear polysaccharide xylan into xylose) with the main contribution from proteases able to disrupt the C-N bonds [598], and Klebsiella pneumoniae by 16S rRNA bacteria (secreting proteolytic and pullulanase enzymes) [599].
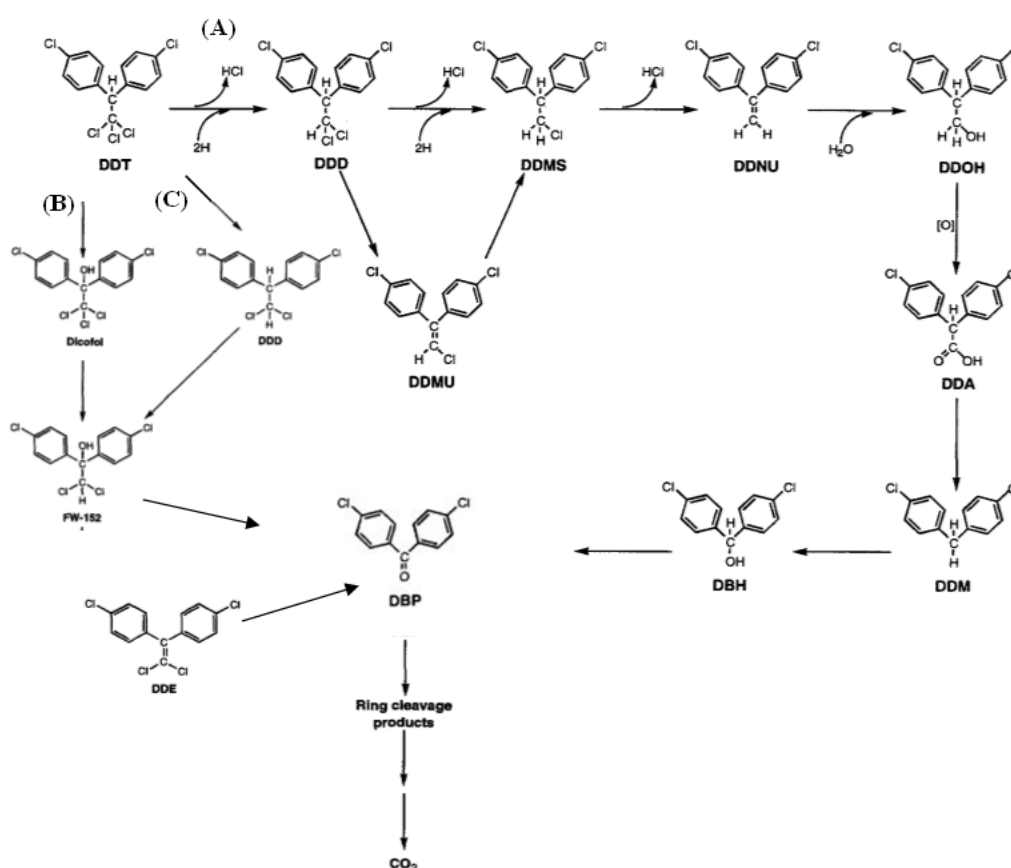
Figure 67. Proposed pathway for bacterial metabolism of DDT via (A): reductive dechlorination; DDT = 1,1,1-trichloro- 2,2-bis(*p*-chloropenyl)ethane; DDD = l,l-dichloro-2,2-bis(*p*-chlorophenyl)ethane; DDMU = l-chloro-2,2-bis(*p*-chlorophenyl)ethylene; DDMS = 1 -chloro-2,2-bis(*p*-chlorophenyl)ethane; DDNU = 2,2-bis(*p*-chlorophenyl)ethylene; DDOH = 2,2-bis(*p*-chlorophenyl)ethanol; DDA = bis(*p*-chlorophenyl)-acetic acid; DDM = bis(*p*-chlorophenyl) methane; DBH=4,4'-dichlorobenzhydrol; DBP = 4,4' dichlorobenzophenone, and PCPA = *p*-chlorophenylacetic; Dicofol = 2,2,2-Trichloro-1,1-bis(4-chlorophenyl)ethanol; FW-152= 2,2,-Dichloro-1,1-bis(4-chlorophenyl)ethanol; DDE = 1,1 -dichloro-2,2-bis(4-chlorophenyl)ethene by *Phanerochaete chrysosporium*. Adapted from ref [595]. Copyright 2010 the Royal Society Te Aparangi.

Chlorpyrifos is an insecticide extensively used to control various insect pests and its long time utilization [600] led to significant quantities of this compound accumulated in water together with its major metabolite intermediate 3,5,6-trichloropyridinol [601]. Its bioremediation is based on enzymes secreted by a variety of bacterial and fungal species. Among these enzymes, agarose and redox-active molecules degrade α or β linkages in agarose and showed activity in a large type of other catalytic reactions (from Shewanella sp. BT05 Bacteria) [602].

Organophosphorus pesticides are predominantly used in agriculture due to their broad-spectrum insecticidal activity and chemical stability. Accordingly, their biodegradation is of current interest and Profenofos and Quinalphos are among these insecticides. Culture media using bacterium isolated from wetland paddy rhizosphere containing Kosakinia oryzae and its

strain VITPSCQ3 showed rather high pesticide tolerance, efficient biofilm formation and capability of synthesizing organophosphate degrading enzymes [603].

3.3.2.5 Biodegradation of fungicides

Carbendazim is a widely used, systemic, broad-spectrum benzimidazole fungicide and a metabolite of benomyl. It is also employed as a casting worm control agent in amenity turf situations such as golf greens, tennis courts and to control plant diseases in cereals and fruits, including citrus, bananas, strawberries, pineapples, and pomes [604]. *Dioxygenases*, as part of *oxidoreductase enzymes*, secreted by *Rhodococcus,* a genus of aerobic, nonmotile gram-positive bacteria, catalyze the degradation of such molecules [605]. Genomic analysis hypothesized that this enzyme is also capable of hydrolyzing carbendazim.

Azole fungicides are another group of chemicals currently found in wastewaters and surface water, with potential implications for agriculture. The biodegradation pathway of climbazole was proposed to involve oxidative dehalogenation, side chain oxidation and azole ring loss [606]. A similar pathway was also applied to triazole fungicide fluconazole. Bifonazole and clotrimazole are other fungicide active compounds. The mycoremediation capacity of these pesticides has been demonstrated by using hydrolytic and oxidative enzymes responsible for degradation of organic substrates produced by mycelia of *Lentinula edodes* [607]. The degradation process was found to affect primarily the imidazole moiety of both investigated azole compounds.

Azoles such as imazalil or tebuconazole have been shown to exhibit a synergetic effect with pyrethroid insecticides like α-cypermethrin through inhibition of *cytochrome P450 monooxygenase* responsible for pyrethroid detoxification. However, *cytochrome P450 enzymes* are not enantioselective for imazalil [608]. Phytoremediation of realistic environmental concentrations of these chiral pesticides was demonstrated by the catalytic contribution of several enzymes such as *superoxide dismutase*, *peroxidases, catalase, ascorbate peroxidase, dehydroascorbate reductase* and *glutathione S-transferase* secreted by *Phragmites australis* wetland plant species [609]. Degradation of tebuconazole occurs through (5-(4-Chlorophenyl)-2,2-dimethyl-3-(1H-1,2,4-triazol-1-ylmethyl)-1,3-pentanediol and 5-(3-((1H-1,2,4-Triazol-1-yl)methyl)-3-hydroxy-4,4-dimethylpentyl)-2-chlorophenol), while imazalil degradation occurs through (α-(2,4-Dichlorophenyl)-1H-imidazole-1-ethanol and 3-[1-(2,4-Dichlorophenyl)-2-(1H-imidazol-1-yl)ethoxy]-1,2-propanediol) [610].

Ipconazole is an asymmetric triazole fungicide for treating rice seed (Table S2 in SI). Its degradation has been achieved by secreted enzymes of isolated microorganisms including bacterial, actinomycetous (Kitasatospora species and Streptomyces species), and fungal (Mucor species and Penicillium species) strains [611].

These microorganisms produce a cocktail on enzymes such as amylolitic enzymes (including α-amylase and amyloglucosidase [612], keratinases and amylases commonly used to break down starch [613], proteases, lipases, phytase, and polygalacturonase [614], cellulases and pectinases [615]. The degradation is not total and metabolites of the Ipconazole degradation are still large molecules (1*RS*, 2*SR*, 5*RS*)-2-[(4-chlorophenyl)-hydroxymethyl]-5-(1-hydroxy-1-methyl-ethyl)-1-(1*H*-1,2,4-triazol-1-ylmethyl)-cyclopentanol, (1*RS*, 2*RS*, 5*RS*)-5-[(4-chlorobenzyl)-2-(1-hydroxy-1-methylethyl)-3-hydroxy-1-(1*H*-1,2,4-triazol-1-ylmethyl)-cyclopentanol, and (1*RS*, 2*SR*, 5*RS*)-5-(4-chlorobenzyl)-3-hydroxy-2-isopropyl-1-(1*H*-1,2,4-triazol-1-ylmethyl) cyclopentanol (Figure 68). Thus, the primary metabolic reaction is dominated by oxidation at either the carbon of the methine in the isopropyl group, the carbon of the benzylmethylene or the carbon of the methyl portion of the isopropyl group as well as that of the methylene portion of the cyclopentane ring.
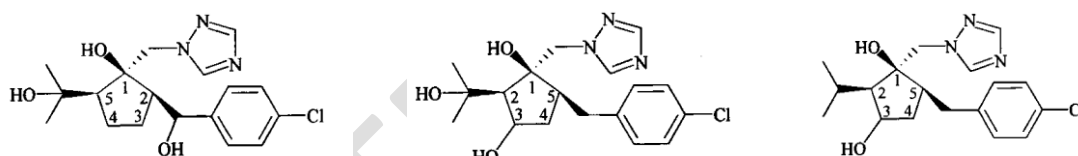
Figure 68. Metabolites of Ipconazole degradation

3.3.2.6 Biodegradation of plasticizers

Bisphenols are common synthetic ingredients of the polycarbonate plastics and epoxy resins and potent endocrine disrupting compounds. Phenol itself is only slightly persistent in water, with a half-life between 2 to 20 days, so it is less dangerous than bisphenols. The bioremediation of waters containing these molecules is catalyzed by Phenol oxidases such as laccases [479,616-619] and less effective tyrosinases [620]. Differently to steroids, under a control of the pH and the temperature (best at a temperature of 50 °C) it is possible a complete removal of bisphenol A and nonylphenol that is associate to enzymatic initiated radical polymerization. The polymerization produced dimers, trimers and tetramers which have larger molecular weights of 454, 680 and 906 amu resulting in the sedimentation of such molecules from water

[479]. Bisphenol A oxidation products catalyzed by Trametes villosa laccase have also been reported as oligomers as large as a heptamer in an insoluble fraction of the reaction mixture. However, jointly to these, the degradation of the phenolic oligomers to 4-isopropenylphenol that persists as a waste compound has been as well identified [621]. While the oxidation activity of laccases is related to the presence of a specific copper-trimer, for the tyrosinases the biocatalytic activity is associated to the presence of dimeric copper (Figure 69). It is worth to notice that in spite of the numerous efforts, to-date such both dimeric and trimeric species have not been really synthesized using reproducible synthetic routes. Peroxidases can be as well effective in these processes [622]. The main products of such processes are oxidized compounds containing an additional phenolic group that are also non innocent molecules [616,623]. Investigations carried out for the degradation of Bisphenol A by laccases suggested that the process follows the pathways indicated in Figure 70. The first step corresponds to its dimerization via an oxidative condensation pathway generating oligomers with C-O and C-C bonds bridging the phenolic groups [624]. Further these dimers suffer successive transformations resulting in the compounds 1-13. The process involves the generation of a radical at the phenolic hydroxyl and formation of oligomers via radical coupling outside the enzyme active site [619]. Although the action of these enzymes resulted in a consistent diminution of toxicity, several degradation products such as *p*-hydroxyacetophenone, *p*-hydroxybenzaldehyde, *p*-hydroxybenzoic acid, hydroquinone, *p-iso*-propylphenol, 2-phenylpropenal or phenol are known to be more toxic than the starting Bisphenol A [624].

However, the intermediate products of the degradation of Bisphenol A may suffer other additional parallel transformations (Figure 71) such as *i)* the alkylation of *p-iso*-propylphenol to 1-methyl-4-isopropenyl-2-cyclohexenol or ii) the successive reductive degradation of Bisphenol A leading to p-xylene, toluene, ethylbenzene, and cyclohexanone [625]. This pathway also reveals the role of the nature of the laccase in this process. With laccases from Trametes versicolor the transformation starts from the C atoms between two benzene rings that connects Bisphenol A. Noteworthy, a high purity of enzyme is not mandatory. Accordingly, compared with expensive pure enzymes, the crude laccase solution showed greater efficiency in the Bisphenol A degradation [625].
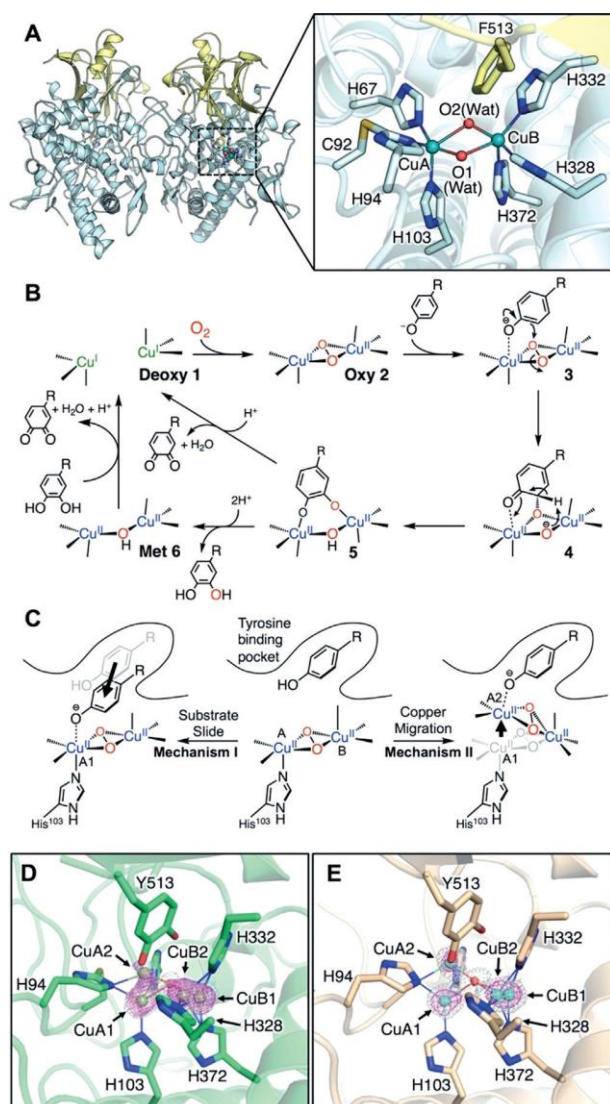
Figure 69. A) Homodimeric structure [chain A (left) and chain B (right)] of the pro-form of wild type tyrosinase (pro-WT, PDB code: 3W6W). Expanded view shows the copper center. The copper-binding domain is indicated in light-blue and C-terminal domain is indicated in yellow. B) Schematic representation of the catalytic cycle of tyrosinase. C) Two mechanistic models for the step coordinating phenol substrate to the copper ion in the hydroxylation reaction. D), E) The copper-binding sites of pro-F513Y (D) and pro-C92A/F513Y (E). Reproduced with permission from ref [626]. Copyright 2020 Wiley-VCH GMBH.
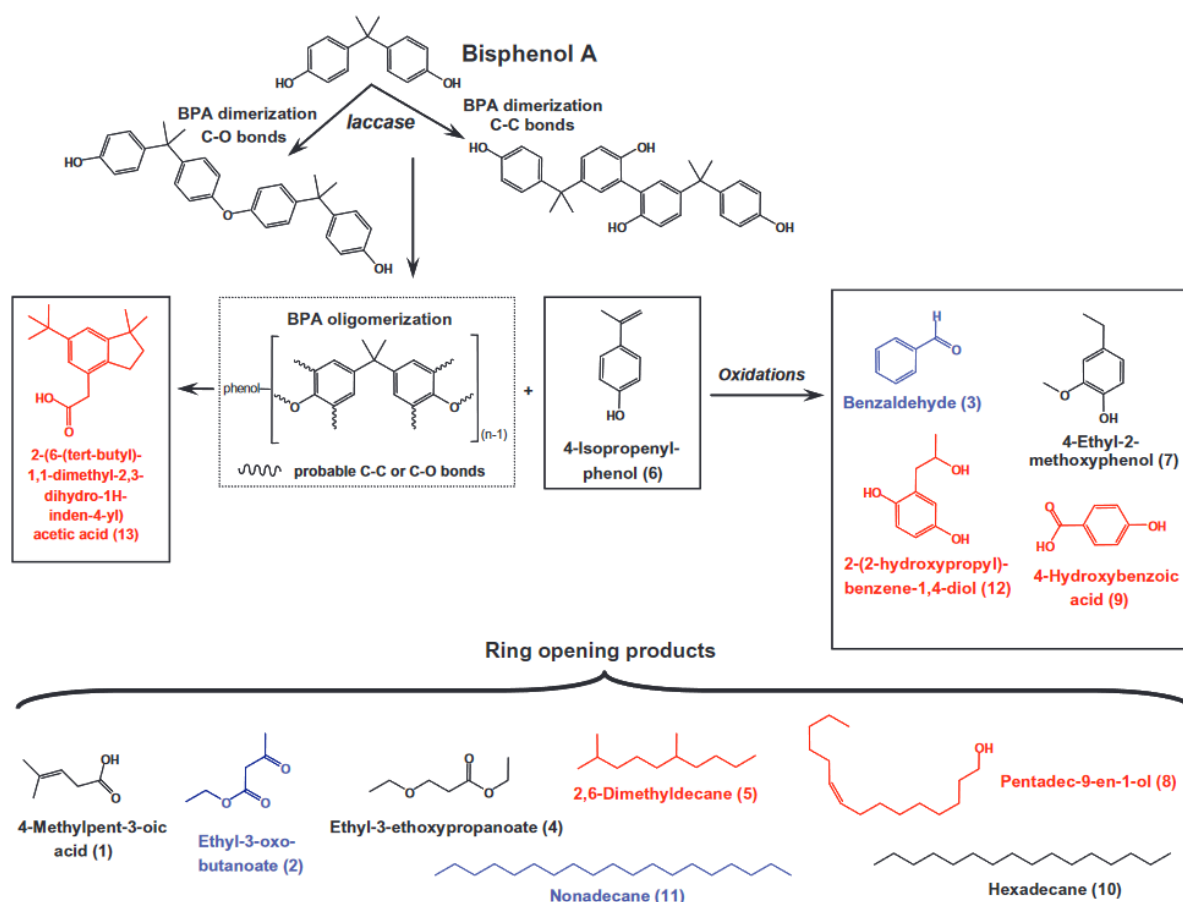
Figure 70. Possible pathways for the degradation of Bisphenol A by *laccase* of *Pleurotus ostreatus* and *Pleurotus pulmonarius* with its degradation products. Compounds numbered 1, 4, 6, 7 and 10 were formed by both laccases, 2, 3 and 11 only by *Pleurotus ostreatus* while 5, 8, 9, 12 and 13 only by *Pleurotus pulmonarius*. Reproduced with permission from ref [624]. Copyright 2017 Elsevier.

Experiments carried out with laccases from Coriolopsis polyzona also showed that the pH and the temperature are statistically significant factors in the removal of these plasticizers [627]. Optimal results corresponded to temperatures higher than 40 ºC, and pH values near 5. Even more, the addition of a non-green compound such as 2,2'-azino-bis(3-ethylbenzthiazoline-6-sulfonic acid in the laccase/mediator system significantly increased the efficiency of the enzymatic treatment.
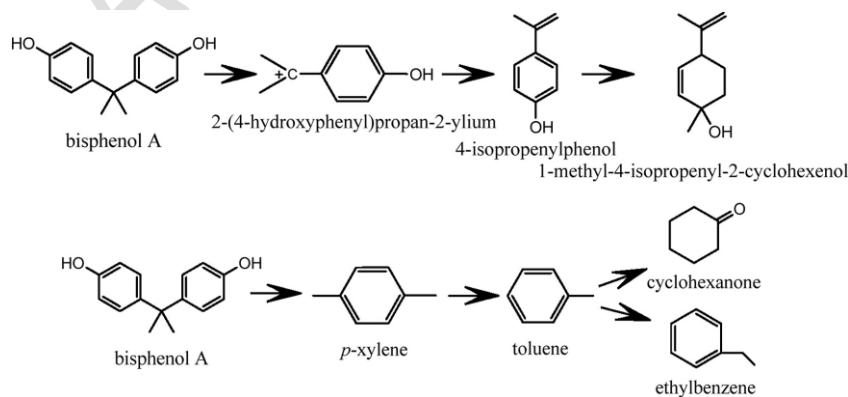
Figure 71. Partial intermediate reaction diagram of <u>bisphenol</u> A degradation. Reproduced with permission from ref [625]. Copyright 2019 Elsevier.
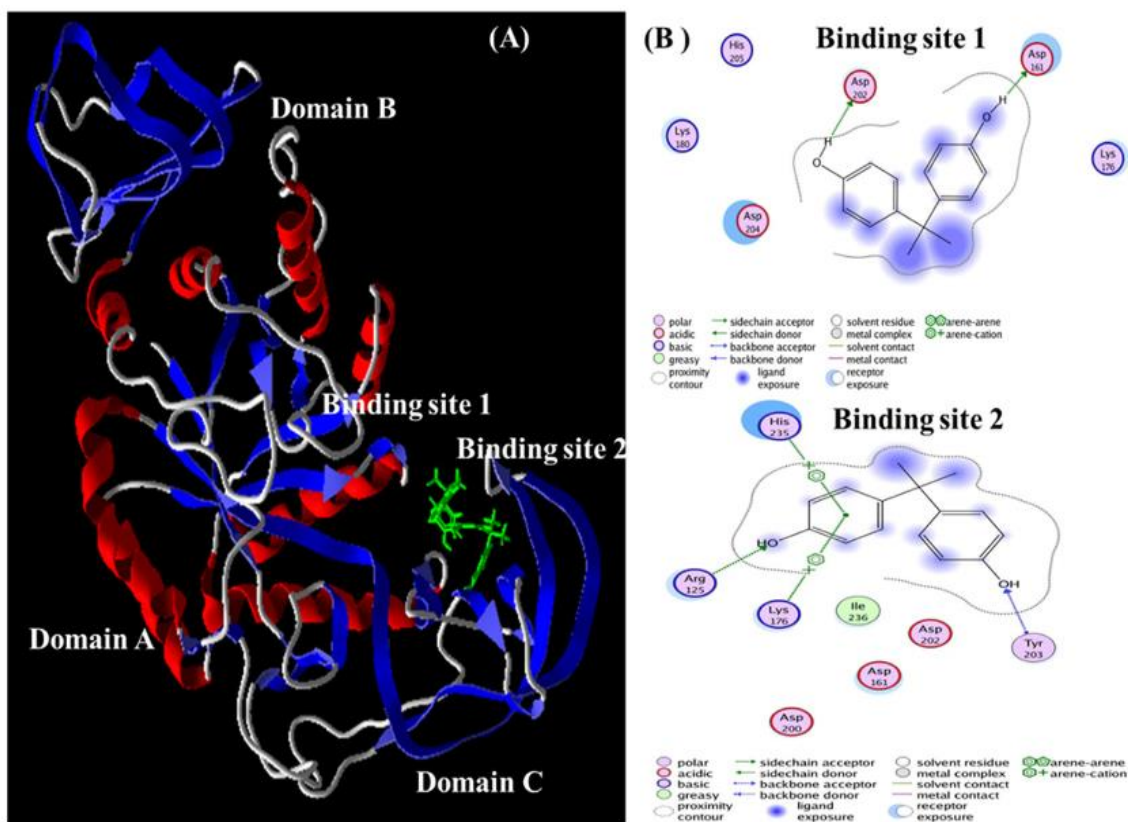
Figure 72. The interaction of amylase with Bisphenol A. Reproduced with permission from ref [628]. Copyright 2017 Elsevier.

Bisphenol A may also play an inhibiting bioremediation effect due to the denaturation of enzymes. This is associated to its phenolic groups as an effect of hydrophobic interactions and hydrogen bonds occurring upon association with hydrolases. This inhibition of bioremediation has been well confirmed from the investigation with α-Amylase (a model of hydrolase in sludge that hydrolyses alpha bonds of large, alpha-linked polysaccharides, such as starch and glycogen, yielding glucose and maltose) (Figure 72) [628].

Phthalic acid esters or phthalates are another class of refractory organic compounds showing endocrine-disrupting effects. These compounds are widely used to enhance flexibility to plastics and, since they are not covalently bound to polymers, are continuously released into the environment during production, leaching or abrasion [629]. The biodegradation of these plastizers was mainly centered on the use of various fungi (Fusarium oxysporum [630] and culmorum [631], Neurospora crassa and Trichoderma harzianum [632], Pleurotus ostreatus [633], Polyporum brumalis [634], Saccharomyces cerevisiae [635], Coriolopsis polyzona [627] or Pleurotus

ostreatus, <u>Phanerochaete</u> chrysosporium [636] since all of them are quite efficient microorganisms to secrete esterase to degrade phthalates.
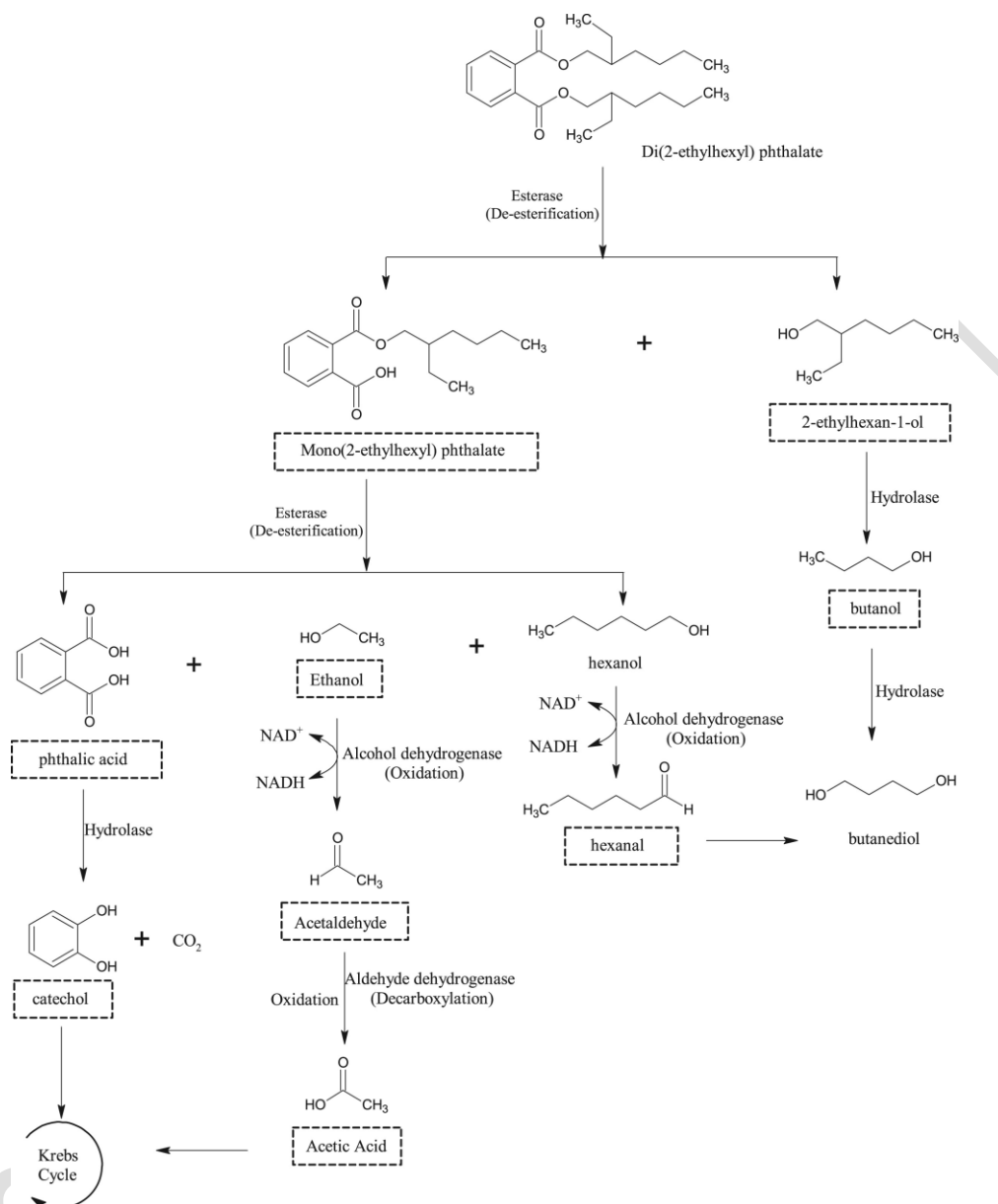
Figure 73. Proposed pathway for the metabolism of DEHP by F. culmorum. The dashed line shows compounds identified by GC/MS. Reproduced with permission from ref [629]. Copyright 2019 Elsevier.

According to the mechanism proposed by González-Márquez *et al.* [629] (Figure 73) di(2-ethylhexyl) phthalate (DEHP) is enzymatically hydrolyzed to mono (2-ethylhexyl) phthalate and 2-ethylhexan-1-ol that is further metabolized into butanol. Then, mono (2-ethylhexyl) phthalate suffers an additional hydrolysis to form phthalic acid, ethanol and hexanol, while phtalic acid is hydrolyzed to catechol and CO_2 and ethanol is oxidized firstly to acetaldehyde, which also undergoes oxidation to acetic acid. Finally, catechol and acetic acid is supposed to

enter into the Krebs cycle where they would be mineralized to CO_2 and H_2O [637], while butanol and hexanal would be transformed into butanediol.

Like for the case of Bisphenol A these transformations are rather slow in terms of the reaction rates, and the produced intermediates (phenols and acids) are not really innocent in aquatic environment.

Oxidoreductases, hydrolases (proteases, esterases and cellulases) and lyases have been also reported for such wastewater treatment applications. Hydrolases can treat biological wastes, while *oxidoreductases* are good candidates for the detoxification of textile effluents or wastewaters containing phenols, aromatic compounds or hormones [638].
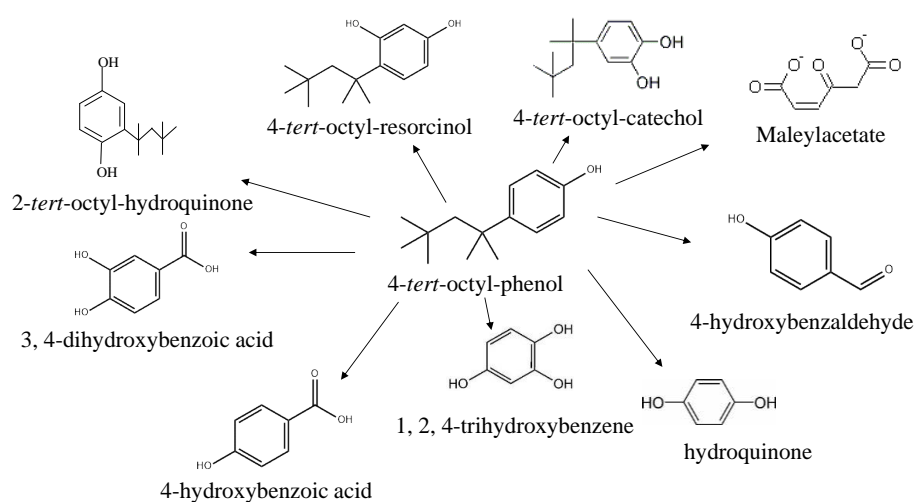
Scheme 10. Products identified in the bioremediation of waters containing the endocrine disrupter *4-tert*-octylphenol catalyzed by yeast strain Candida rugopelliculosa RRKY5. Reproduced with permission from ref [639]. Copyright 2017 Elsevier.

The bioremediation of waters containing the endocrine disrupter 4-tert-octylphenol has also been reported to be catalyzed by the yeast strain Candida rugopelliculosa RRKY5. The process takes place through phenolic ring hydroxylation and alkyl chain oxidation pathways with the production of the molecules indicated in Scheme 10 [639]. Typically, Candida produces multiple lipase isoenzymes (CRLs) with distinct differences in substrate specificity, in particular with regard to selectivity, able to catalyze both the hydrolysis and the synthesis of ester groups in insoluble substrates [640]. However, it was already demonstrated that lipases may also act as biocatalysts for the epoxidation of fatty acids and phenolic compounds [641]. Particularly, the yeast Strain Candida rugopelliculosa RRKY5 may afford biodegradation of the endocrine disrupter 4-*tert*-octylphenol *via* phenolic ring hydroxylation and alkyl chain oxidation pathways, resulting in the products indicated in Scheme 9. From the chemical point of view such a process changes the structure of the initial pollutant, but from a toxicological

point of view it does not provide a progress since one phenol derivative is multiplied to a family of phenols.

3.3.2.7 Bioremediation of waters polluted with dyes (Decolorization of waters)

Paper and pulp mills, textiles and dyestuff industries, distilleries and tanneries are some of the industries which release highly colored wastewaters [642] and most of the compounds inside are recalcitrant to microbial degradation. Such pollutants, besides causing aesthetic damage to sites, are also toxic and carcinogenic. Among others, azo dyes released into the environment in effluents from textile and dyestuff industries are structurally the most diverse [643].

Experiments carried out in a low nitrogen medium with a series fungi and mushrooms secreting different enzymes showed their capability to degrade such molecules [644-645]. The list includes the following fungi: Sordaria fimicola (catalase, laccase, superoxide dismutase), Halosarpheia ratnagiriensis (Pleurotus ostreatus) and Flavodon flavus (oxidative (laccase, manganese peroxidase and lignin peroxidase) the former two belonging to the Ascomycota and the third to the Basidiomycotas isolated from mangrove sediment (glucose oxidase and glyoxal oxidase) (S. fimicola), Coriolus versicolor (manganese peroxidase and laccase), and hydrolytic enzymes (cellulases, xylanases and tanases)), Ganodermalucidum (cellulase and hemicellulase lignocellulolytic enzymes), Agaricus brasiliensis (manganese peroxidase).

The most toxic dyes are those containing *p*-diphenylenediamine and benzidine moieties while the substitution of the *p*-diphenylenediamine hydrogen or complexation of benzidine with copper ions reduces mutagenicity [646]. Phanerochaete chrysosporium, Streptomyces chromofuscus and Trametes versicolor (lignin peroxidase and manganese-dependent peroxidase), Corrollospora maritima (cellulases, hemicellulases and pectinases) were able to decolorize and even to mineralize several synthetic dyes with different chemical structures. The possible structures of degradable dyes include: azo, sulfonated-azo, triphenylmethane, heterocyclic, and polymeric ones (Azo-dyes, Azure B, Brilliant green, Bromphenol blue, Congo red, Cresol red, Crystal violet, Orange II, Remazol Brilliant Blue R, Tropaeolin O, etc.) [647-649]. Total degradation of these dyes was merely achieved by using a combined anaerobic–aerobic treatment with a bacterial consortium.

Investigations carried out with archetypal white-rot fungus Phanerochaete chrysosporium confirmed the necessity of combining the activity of laccases, cellobiose dehydrogenase, cellulases, hemicellulases, pectinases, etc. in conjunction with the H_2O_2-producing enzymes (oxidases and peroxidases) for the remediation of waters polluted with recalcitrant

compounds (Figure 74) [650]. Thus, laccases (as a Cu^{2+}- phenol oxidase) may catalyze the oxidation of phenolic substrates by O_2, but can also oxidize nonphenolic lignin model compounds in the presence of a suitable redox mediator, while cellobiose dehydrogenase (as member of the family of <u>oxidoreductases</u>, acting on the CH-OH group of donor with other acceptors) can directly reduce nitro groups as for example in the munitions 2,4,6-trinitro-toluene and hexahydro-1,3,5-trinitro-1,3,5-triazine [650]. Laccase is also responsible for the effective decolorization reaction of coal-derived humic acids through the oxidation to fulvic acid and of anthraquinone-type dyes, where the peroxidase has no activity [651]. However, the laccase has as a disadvantage the sensitivity to lignite [652]. Partial decolorization of azo dyes (orange G and amaranth) and a complete decolorization of triphenylmethane dyes (bromophenol blue and malachite green) was achieved by Pycnoporus sanguineus cultures in submerged liquid culture producing laccase as the sole phenol oxidase [653].
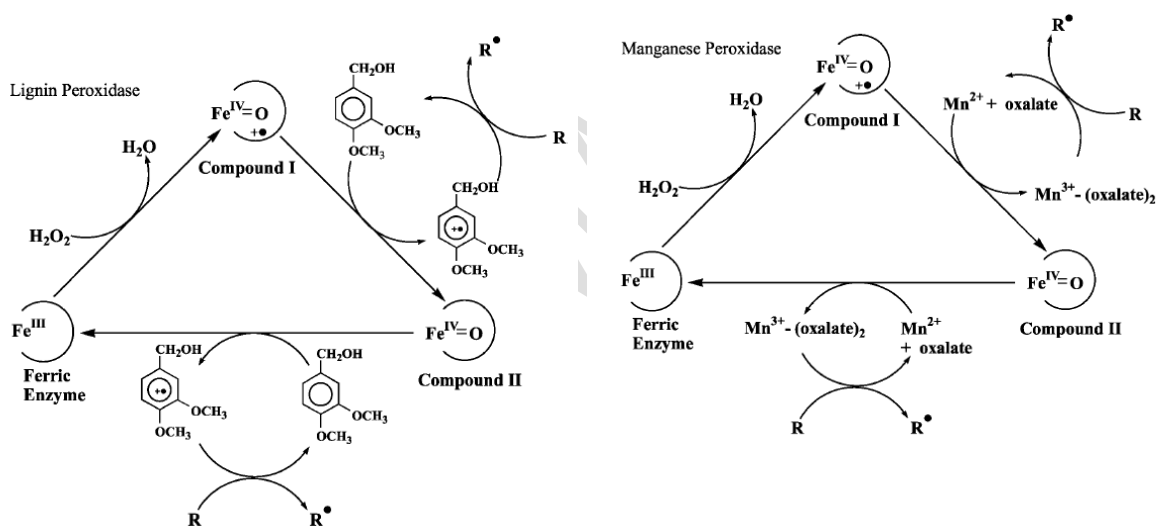
Figure 74. Catalysis and mediation by lignin and manganese peroxidases. Reproduced with permission from ref [650]. Copyright 2000 Springer Nature.

The mechanism of advanced color removal involves two successive one-electron oxidations of the phenolic ring by the hydrogen peroxide-oxidized forms of the enzyme producing a carbonium ion [646]. Water molecule reacts with the phenolic carbon bearing the azo linkage, resulting an unstable hydroxyl intermediate breaking down into a quinone and an amidophenyldiazine. The latter compound is then oxidized by oxygen into the corresponding phenyldiazene radical which after elimination of nitrogen gives a phenyl radical finally oxidized by oxygen.

The position of the substituent was also reported to be important. Compounds containing a methyl group in position 3 were not substrate for the laccase. Similarly, those compounds

substituted with dimethyl and dimethoxy groups in positions 2,6 and 2,3 were substrates, while those containing the same groups in position 3,5 were not. Consequently, *laccase*-mediated oxidation of phenolic-azo dyes seems to depend both on the electronic character and the position of the substituent on the phenolic ring [654].

The presence of adjuvants like veratryl alcohol which is a secondary metabolite of white-rot fungi like Phanerochaete chrysosporium or Trametes versicolor that produce the ligninolytic enzyme lignin peroxidase enhances the activity of both laccase and manganese-dependent peroxidase [655].

Similar fungi and mushrooms were utilized for the decolorization of distillery wastewaters [656].

3.3.3 Biodegradation of micotoxins

The biodegradation of micotoxins present in waters is still in an infancy stage. Oxygenases, secreted by Aspergillus niger produced rather high biomass yields. These oxygenases have no specificity difference for aliphatic hydrocarbons (linear and nonlinear), appearing for aromatic substrates with increasing amount as the complexity of the ring increases [657].

Free-metal enzymes have also been considered for this application. Mechanistic investigations of the degradation of Zearalenone, a potent estrogenic metabolite produced by some Fusarium and Gibberella species, also known as RAL and F-2 mycotoxin [658] at the atomic level indicated that the degradation process involves two concerted reaction pathways. These pathways rely on a proton transfer and a nucleophilic-substituted ring opening with the formation of a hydroxyl product [659].

3.3.4 Biodegradation of other chemical compounds

Decabromodiphenyl ether (DBDE) is part of the polybrominated diphenyl ethers (PBDE) congeners commonly used as a flame retardant in numerous commercial products [660]. Although with a low solubility in water, due to an uncontrolled disposal of the products, they have been also identified as wastewater compounds. Bioremediation of PBDE and its derivatives has been indicated to be catalyzed by catechol 2,3-oxygenase genes, produced by a series of Gemmatimonas, Pseudomonas, Staphylococcus, Cupriavidus, Ensifer, and Hydrogenophaga spores which are able to promote meta-cleavage at specific unbrominated locations in carbon backbones [661]. These enzymes are also active for the benzene cleavage of the PBDE congeners,

but with the formation of a series of byproducts, including brominated products, dihydroxydiphenyl ether, and others that still preserve toxicity.

3.3.5 Immobilisation of the enzymes

During the past several years, considerable progress has been made in the development of immobilized oxidative enzymes with focus on finding new support materials, improving the immobilization methods and their applications. Among all oxidative enzymes, *laccases* and *peroxidase* are general oxidative enzymes with ability to oxidize various types of compounds. These enzymes have been the subject of extensive research due to their potential applications in various bioremediation fields during the last decades and therefore can be considered as reference for this topic. Immobilized *laccase* or *peroxidase* have shown better stability, and reusability as well as easy separation from reaction mixture, making them more convenient and economic in comparison to free enzymes [662].

The immobilization protocol is crucial for the stability and catalytic behavior of the enzyme and, therefore, several approaches have been reported considering both the characteristics of the enzyme and the support [663-666]. The most frequently reported immobilization procedures to date are: *i)* adsorption occurring through hydrophobic and van der Waals interactions (on glass, alumina, silica gel, molecular sieves, graphite, cellulose, chitosan, sepharose, nylon-66, resins, soil, etc); *ii)* ionic or covalent binding that are much stronger; these procedures offer the advantage of limiting the leaching from the surface and the disadvantage of rendering unusable the deactivated catalyst (biopolymers sepharose, agarose, silica, zeolites, membranes, etc.); *iii)* cross-linking between enzyme and matrix. This protocol avoids the dilution of activity, especially owing to the introduction of a large portion of non-catalytic ballast leading to a loss of more than 50% from the native activity. This procedure can be applied through: a) covalent glutaraldehyde approach (on glass, alumina, silica gel, molecular sieves, graphite, cellulose, chitosan, carbon, etc), or b) via enzyme cross-linking by multifunctional reagents (i.e. like (3-aminopropyl) triethoxysilane approach on glass, ceramics, kaolin, montmorillonite, carbon, dextran, etc.); *iv)* enzyme immobilization by physical entrapment reverse micelle that considers inclusion of an enzyme in a polymer network (gel lattice) such as an organic polymer or a silica sol-gel, or a membrane device such as a hollow fiber or a microcapsule (gelatin, polyacrylamidic gel, etc.). To make clear the difference between entrapment and support binding Sheldon defined support binding as the binding of an

enzyme to a prefabricated support and entrapment the synthesis of the polymeric network in the presence of the enzyme [667].

The immobilization of laccases onto mono-aminoethyl-N-aminoethyl (MANAE)–agarose polysaccharide occurring via the interaction of the amino-groups with the acidic functionalities of the enzyme led to a biocatalyst preserving 90% of the initial activity of the enzyme after 15 cycles. Besides this relative improvement, the slight alteration produced in the geometry of the enzyme also enhances its activity compared to the free enzyme [618].

Comparison of the activity between the free and immobilized laccases extracted from *Trametes versicolor* deposited via various routes, i.e.: i) deposition on TiO_2 sol–gel coated PVDF membranes [668]; ii) deposition on hybrid membrane with TiO_2 based bio-catalytic nanoparticle suspension [669]; iii) deposition on electrospun fibrous membranes [670]; iv) deposition on Hippospongia communis sponging scaffolds [671]; v) deposition onto polyamide 6/chitosan nanofibers modified using bovine serum albumin and hexamethylenediamine as spacers and glutaraldehyde as a cross-linker [672] showed that indeed the deposition protocol and nature of the support exert an influence on the activity, and the thermal and storage stabilities of the enzyme due to the degree of alteration of the enzyme tridimensional structure. The activity and stability of these immobilized enzyme were examined under different immobilization process parameters (e.g. pH, temperature, molar strength) and under different operational conditions for enzymatic degradation of selected EDCs (bisphenol A and 17α-ethinylestradiol).

Additional improvements are, however, still essential such as the development of the new materials for immobilization with higher capacity, easy preparation, and cheaper price. Moreover, immobilization methods still need improvement to become more efficient and avoid enzyme wasting during immobilization and enzyme leakage in working cycles.

A novel and simple immobilization approach is to synthesize self-assembled enzyme-inorganic hybrid materials with flowe-like morphology [673]. Such hybrid materials having flower-like shapes (nanoflowers) were more active and stable than conventionally immobilized enzymes owing to their large surface area and to the effective confinement of enzyme molecules in their interior [674-675]. Some examples also evidenced that nanoflowers composed of *laccase* and copper phosphate were not only more stable but also more active compared to free *laccases* [674,676].

The association of recyclable enzyme-inorganic nanoflowers with the magnetic nanoparticles adds several other advantages to these catalysts such as easier separation, simple operation, and low cost (Figure 75) [677-678].
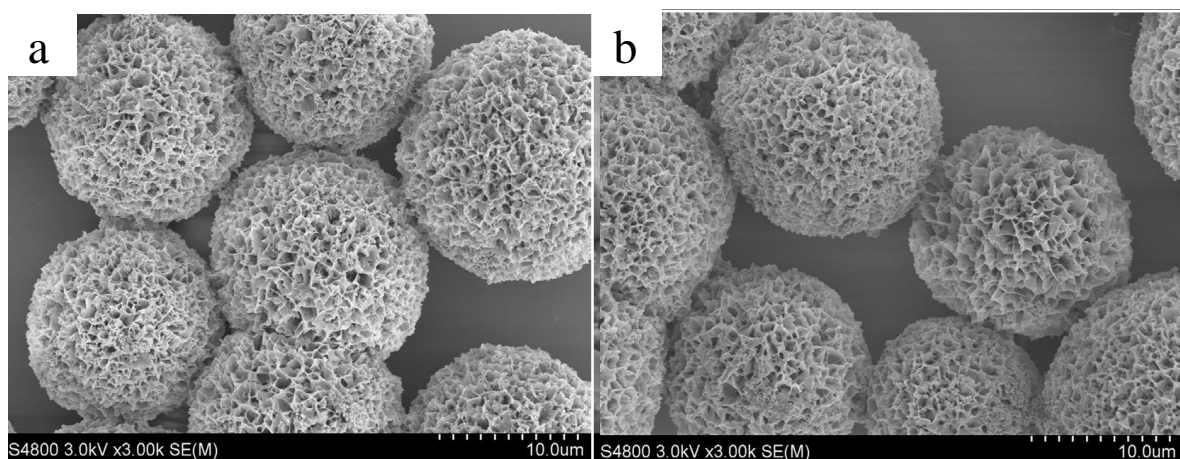
Figure 75. Magnetic nanoflowers (a) and laccase-loaded magnetic nanoflowers (b). Reproduced with permission from ref [679]. Copyright 2019 Elsevier.

The immobilization procedure may also combine the catalytic properties of the enzyme with those of the support. These may correspond to acid-base [680-683] or metal catalytic functionalities [684].

Trametes hirsuta and a purified laccase from this organism were able to degrade triarylmethane, indigoid, azo, and anthraquinonic dyes. Immobilization of the Trametes hirsuta *laccase* on alumina enhanced the thermal stability of the enzyme and its tolerance against some enzyme inhibitors, such as halides, copper chelators, and dyeing additives. Thus, free laccase losses 50 % of its activity at 50 mM NaCl, while the 50 % inhibitory NaCl concentration of the immobilized enzyme was 85 mM. Even more, the effluents decolorized by immobilized laccase could be used for dyeing with acceptable color quality [685]. The same laccase immobilized in a polyacrylamide gel converts 4-methyl-3-hydroxyanthranilic acid to 2-amino-4,6-dimethyl-3-phenoxazinone-1,9-carboxylic acid (actinocin), a phenoxazinone chromophore occurring in actinomycins [686].

Immobilization of laccase and tyrosinase following a diazotization process involving the absence of the phenolic group of tyrosine residues in the catalytic site led to a different behavior. Polyacrylonitrile beads were pretreated with glutaraldehyde aqueous solution as the coupling agent and then with a phenylendiamine solution to obtain aminoaryl derivatives that were coupled with a buffer solution containing laccase [687]. Besides the common drawbacks associated with the use of soluble enzymes, such as poor catalytic stability, non-recyclability, and biocatalyst inactivation, a significant difference of this protocol is that at pH=3.0 the immobilized enzyme retains more than 70% of its maximum activity, while the free form retains only 20%. Similarly, at pH=8.0, the immobilized laccase has 70% of its maximum activity, while free laccase is almost inactive.
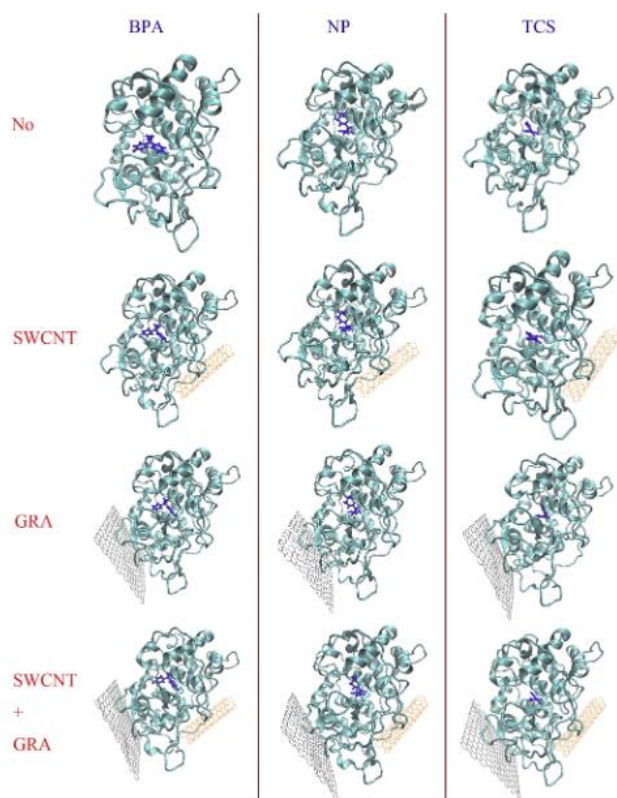
Figure 76. Initial conformations of Bisphenol A (BPA), nonylphenol (NP) and riclosan (TCS) with manganese peroxidase (MnP) in the absence and presence of nanomaterials at 0 ns. "No" indicates that no nanomaterials are presented; "SWCNT", "GRA" and "SWCNT+GRA" corresponds to only SWCNT, only GRA and both SWCNT and GRA are presented, respectively. The substrates are in blue. Reproduced with permission from ref [636]. Copyright 2017 Elsevier.

The deposition of the enzyme on a magnetic recoverable solid makes easier the separation of the enzyme, but it has only a little influence on the activity [688]. Laccase-loaded magnetic nanoflowers were prepared by attaching amino-functionalized magnetic nanoparticles onto the *laccase*-inorganic hybrid nanoflowers. These hybrid materials exhibited excellent catalytic activity for bisphenol A degradation under room temperature in the presence of 2,2'-azino-bis(3-ethylbenzothiazoline-6-sulfonic acid, preserving over 92% of its initial activity after 60 days of storage at 4 °C [679]. Recycling and reuse was also possible with an only small loss of activity. Recovery is the most important advantage provided by the association of enzymes with the magnetic recoverable solids.

The influence of the support on the behavior of an immobilized enzyme has been studied for manganese peroxidase deposited onto graphene (GRA) and single-walled carbon nanotube (SWCNT) (Figure 76) [636]. While GRA tended to decrease the overall stability of the binding between manganese peroxidase and its substrates, SWCNT and also SWCNT+GRA generally caused only a minor impact on the mean binding energy between enzyme and its substrates.

Thus, the native biodegradation processes may be indeed influenced by these carbon nanomaterials by changing the interactions of the substrates and their enzymes. These studies also demonstrated that water behavior and H-bond interactions between *manganese peroxidase* and substrates changed in these materials [636].
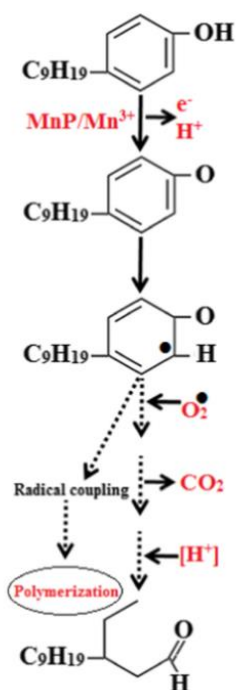
Scheme 11. Hypothetical reaction/breakdown pathway of nonylphenol, as a model EDCs degradation by MnP. Reproduced with permission from ref [689]. Copyright 2017 Springer Nature.

Manganese peroxidase (MnP from white-rot fungus Ganoderma lucidum IBL-05) has been insolubilized in the form of cross-linked enzyme aggregates (CLEAs) using various aggregating agents, *i.e.* acetone, ammonium sulfate, ethanol, 2-propanol, and tert-butanol, followed by glutaraldehyde (GA) cross-linking [689]. The recovered CLEAs activity depended both on the precipitant type and GA concentrations with a highest recovered activity of 47 %. The biocatalytic capacity of these enzymes checked for removing endocrine disrupting chemicals such as nonylphenol and triclosan, in a packed bed reactor system showed the capability to destroy the aromatic cycle with the formation of functionalized alkanes and polymers. Scheme 11 depicts the steps proposed for the bioremediation of nonylphenol [689].

Like for free enzymes, the operation time of the immobilized biocatalysts is quite limited. Utilization of whole cells from the edible mushroom Agaricus bisporus offered another simple concept of immobilization because it excludes the need for enzyme purification [690]. These cells

were entrapped in chitosan and alginate matrix. Further modification of the alginate with colloidal silica enhanced the activity due to retention of both cells and *tyrosinase* from fractured cells, which otherwise leached from matrix capsules. Such a treatment preserved the activity of the mushroom cells in water keeping 73% of their initial activity after 30 days [690]. However, this is still not satisfactory from an efficiency point of view because the deactivated biocatalyst is a waste.

The immobilization of enzymes on membranes provides another opportunity to recycle these catalysts. The erythromycin esterase checked for the degradation of p-nitro-phenyl-butyrate has been immobilized on membranes following two different routes: *i)* covalent grafting, and *ii)* adsorption through hydrophobic and hydrophilic parts on ceramic membrane supports [691-693].

3.3.6 Biotreatment of sludges

Anaerobic digestion of sludges provides a rather green route for their treatment. It mainly consists of four successive biochemical processes, ie hydrolysis, acidogenesis, acetogenesis and methanogenesis [694] where large biopolymers such as polysaccharides, proteins, starches, free oil and grease are firstly hydrolyzed into smaller entities followed by acido- and acetogenesis down into shorter chain volatile fatty acids, ammonia, H2, CO_2 and H_2S [695] Various bacteria such as Clostridium, Cellulomonas, Bacteroides, Succinivibrio, Prevotella, Ruminococcus, Fibrobacter, Firmicutes, Erwinia, Acetovibrio, Microbispora, Syntrophobacter, Pelotomaculum, Methanobacterium and Methanoculleus species were reported to be involved in these steps [696].

However, besides organic molecules heavy metals are other toxic components of the sludge. Differently to organic molecules, toxic heavy metals cannot be degraded but in the presence of these biocatalysts can change the oxidation state and thus can be complexate to less toxic compounds. With this aim microorganisms associated to the use of green plants may remove or render toxic environmental contaminants harmless [697]. The combination of different biological strategies could lead to an improvement in the remediation performance as demonstrated for different micro-, vermi- and phyto-remediations applied in a sewage sludge polluted landfill [698]. Experiments placing earthworms, bacteria, and plants led to removal rates around 20–25% for heavy metals (Cd 15%–35%; Ni 24%–37%; Pb 15%–33%; Cr 7%–39%), 19.5–28% for benzo(a)pyrene and 50-78% for organochloride insecticide dieldrin in dual and triple treatments. Recent examples indicated the phytoremediation of As, Ba, Cd, Cu, Cr, Ni,

Pb, Se and Zn in sewage sludge-based substrates demonstrating the efficiency of Catharanthus roseus for which the translocation process was progressive in the treatment [699].

The microbial population present in activated sludge provides the chemical energy required by these processes. Thus, bioelectrochemical or microbial electrochemical systems are capable of converting chemical energy into electrical energy while employing microbes as catalysts. These are energy-generating bioremediation processes. Electron donors are oxidized generating electrons, H^+ ions, and CO_2, while the reducible substrates are reduced accepting electrons while the toxic products become less-toxic or value-added products [700]. Synergistic effects between iron and microbes on the contaminant degradation make the role of iron beyond that of a nutritional necessity. Iron may assist biological wastewater treatments, including anaerobic digestion, S and Cl reduction, N and P removal, heavy metal immobilization, aromatic and halogenated hydrocarbon compounds degradation, and sludge granulation. Numerous types of microbes in water, soils and sediments are involved in the transformation of iron, such as sulfate-reducing bacteria, dissimilatory metal-reducing bacteria, hydrogen-consuming methanogens and denitrifiers and the synergistic effects between iron and microbes have been used to successfully enhance various types of microbial metabolic activities and environmental contaminant removal, including anaerobic digestion [701]. The iron-bearing sludge is usually produced in the iron-oxidizing process with amorphous or crystalline iron minerals as final products leading to the contaminant removal by adsorption and/or coprecipitation but also to iron-containing some risks associated to the sludge aggregates because of the adsorbed contaminants [701]. Also, soil microbes aid in many metabolic reactions associated with biogeochemical cycling of nutrients, enhance detoxification of pollutants and maintain soil microbial structure [702]. Thus, the microorganisms may increase the availability of nutrients and limit the negative effects of heavy metals on plants. Bacteria may also contain plasmids that ensure resistance against some metalloids [703].

Based on these, recent achievements recommended an environmentally friendly and cost-effective disposal of sewage sludge affording its conversion into biochar as an efficient catalyst for the environmental photo-degradation of the organic pollutants [694]. Such catalysts are recyclable and ensure negligible metal leaching. Also high-temperature carbonized sludge produce low-cost sludge biochar-based electrodes that exhibits excellent electrical conductivity for environmental pollution remediation and harmful metals immobilization. However, the control synthesis route for desired physiochemical properties (e.g., surface area, porosity, functional groups, and metal phase structure), dynamic catalytic reaction and mechanisms, and applications in the broad field of catalysis are still in the early stage. For the large-scale

industrial application and environmental sustainability, considerable efforts should be made in future research to solve the existing scientific and technological challenges. Firstly, more attention should be given to elucidate the underlying mechanisms of sludge biochar formation through thermal conversion. Detail investigation required to reveal the effects of the heating-operating condition on their physiochemical properties. Also, the inorganic species of sludge have catalytic effects on the thermal conversion process and resultant products [704].

Sludge has been as well proposed to be activated through cultures of aquatic plants and worms for waste recovery and biomass production. Such an approach associated to the increase of the carbon dioxide concentrations and dissolved phosphorus binding metals (zinc, iron, aluminum and manganese) stimulated the growth of floating aquatic ferns thus demonstrating a strong potential of the biocascade for combined sludge waste reduction and phosphorus recovery (until 45%) [705].

3.3.7 Bioremediation by combined processes

An advanced bioremediation can be achieved by combining bioenzymatic degradation of wastes in water with other treatments. Combination of biological and electrochemical processes to mineralize organic compounds have been reported in several studies [706] [707]. Only electrochemical processes have as main limitation a rather high energy consumption to obtain a complete mineralization that is in the range of 100–$150\,kWhkg^{-1}$ COD [708] and therefore it has relatively high associated economic costs. Taking as an example a pesticide, oxyfluorfen was firstly biodegraded reaching up to 90% removal, and then oxidized by electrolysis using boron-doped diamond as the anode with a complete mineralization of the residual pollutants [706]. Following a similar approach, endocrine disruptor bisphenol A was first exposed to remediation to Bacillus subtilis HV-3 and then electrochemically degraded (close to 98%) [707].

Electrobioremediation couples electrokinetics and bioremediation [709]. According to this, by applying electro-biostimulation the activity of already present microorganisms is enhanced. Experiments taking a microbial consortium acclimated to 2,4-dichlorophenoxyacetic acid biodegradation showed that such strategy afforded an increased pollutant removal efficiency reaching up almost 100%.

Bioremediation of waters has been also combined with photocatalytic processes. Coupling *lacasses* with organometallic complexes offers an elegant route to enhance the bioremediation efficiency. The lysine-free laccase allows a precise engineering of the enzyme surface by post-functionalization of different areas of its surface by reductive alkylation without compromising

the enzyme core function, therefore preserving the activity for the intramolecular electron-transfer and dioxygen reduction [710]. Adding a ruthenium photo-sensitizer it was demonstrated the occurrence of an electron transfer between the enzyme surface and both the T1 and the TNC copper centres located in its interior. As an example of such a catalytic system the [Ru(bpy)$_3$]$^{2+}$–laccase bimolecular system affords the photo-oxidation of olefins coupled to the light-driven reduction of O$_2$ [711] through a radical mechanism in which O$_2$ acts both as a renewable electron acceptor and as O atom donor (Figure 77). Theoretical calculations taking the Ru(II)-to-Cu(II) centre distances showed a good correlation with the photoreducibility and the reactivity of the grafted enzymes.
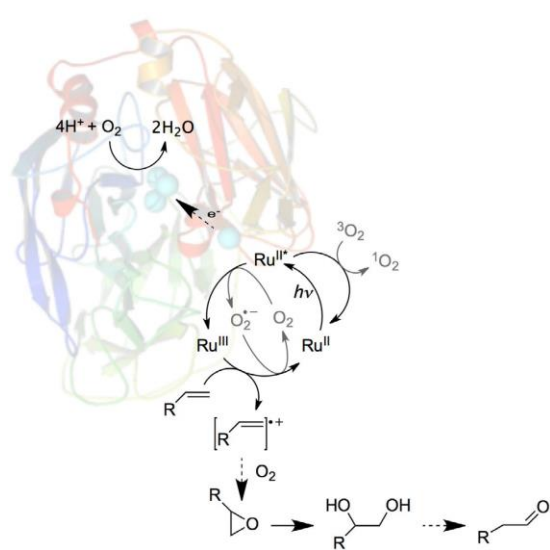
Figure 77. Photo-oxidation of olefins coupled to the light-driven reduction of O$_2$ by a Ru–polypyridyl complex–laccase. The paths depicted in grey do not lead to product formation in the absence of enzyme. Ribbon model of *laccase*: Cu ions are depicted as cyan spheres. Reproduced with permission from ref [710]. Copyright 2017 Wiley-VCH GMBH.

3.2.8. Engineering the process

Antibiotics with phenolic groups such as tetracycline, chlortetracycline, doxycycline, oxytetracycline and sulfamethoxazole were typically degraded by free and immobilized enzymes in aqueous solutions in continuous stirred tank reactors [450].

Immobilization of the enzymes with the scope to recover and recycle the catalyst is less efficient than the enzyme itself because such a process may drastically affect their tridimensional structure. A solution is the use of free enzyme membrane reactors, where the membrane is used to keep the biocatalyst confined within the reactor that operates in

recirculation loop. Using such a set-up the enzymes can be recirculated with the reaction medium while the reaction products in the permeate are continuously removed [712]. This approach is especially effective for industrial wastewaters that come from pharmaceutical production. While at the exit from the industrial plants these waters present the highest pollutant content between 10^{-1} and $10^4 \, \mu g \cdot L^{-1}$, raw surface waters from rivers, lakes and ponds in a close proximity accumulate lower concentrations of these (between 10^{-4} and $10^3 \, \mu g \cdot L^{-1}$) [450].

Microbial fuel cells and biochar have emerged as promising biodegradation processes due to low cost, energy efficient and environmental benignity. With higher removal rate (20–50%) combined hybrid processes seems to be more efficient for permanent and sustainable elimination of reluctant antibiotics [443-444].

4. Innovative combined solar driven technologies: Advantages and drawbacks

Catalysis makes possible the transformation of substrates into products by increasing the reaction rate and overcoming the energy barriers encountered in the mechanism using a substance (the "*catalyst*") that opens new reaction pathways [713]. In most of the examples of catalytic processes known so far, particularly in the chemical industry,[714] heat is the energy that is provided to the system to overcome the activation barrier.

However, besides conventional thermal catalysis, there is an increasing interest in the use of other types of energy to promote reactions and accelerate their rates (Scheme 12). Part of this interest derives from the on-going shift in the energy sector,[715-716] moving from fossil fuels that provide heat by combustion, to renewable electricity (*electrocatalysis* [717] and *plasma catalysis* [718]) or the use of solar light as primary energy (*photocatalysis* [719]).
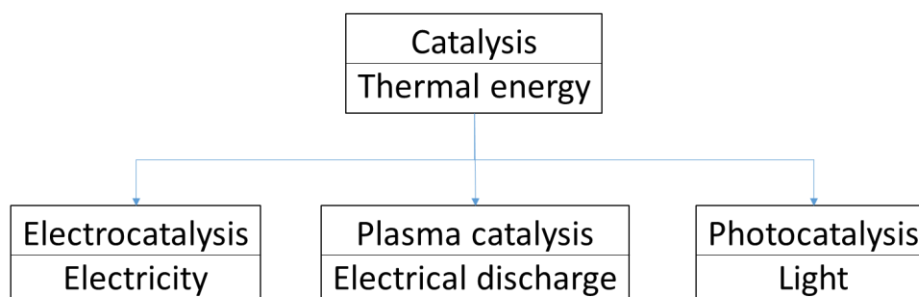
Scheme 12. Alternative catalysis types based on the energy used to overcome activation barriers.

After the description and discussion of the specific features of photocatalysis in terms of mechanism, reactor design and materials, the second part of this chapter will be dedicated to the growing interest in coupling photocatalysis with biocatalysis, electrocatalysis and sonocatalysis by examining the balance between advantages and drawbacks. Up to date, such exploration is essentially restricted to lab-scale and an important question arises on their scale-up.

4.1 Photocatalysis: Fundamentals and strategies to improve efficiency.

In photocatalysis, photons of sufficiently high energy are absorbed by a material or molecular compound and the energy of the photon transformed in the generation of a transient state derived from the electronic excitation from occupied to unoccupied orbitals or from electronic states [720] These transient states of the photocatalysts, typically living in the microsecond time scale, can promote chemical reactions of substrates and other compounds.

In molecular substances these electronic excited states involve the HOMO-LUMO transition [721], but in the most common photocatalysis by semiconducting solids photon absorption produces a transient charge separate state with electrons in the conduction band and positive electron holes in the valence band [722] If electrons and holes become separate and move to different points of the surface of the material, they can promote independently in substrates a chemical reduction by conduction band electrons and a chemical oxidation by the valence band holes.[8] Electron-hole recombination, either at the site where charge separation has taken place or after charge migration and random recombination, is the main energy waste process that decreases the efficiency of the photocatalytic process [723]. Scheme 13 illustrates the elementary steps encountered in photocatalysis by semiconducting particles.
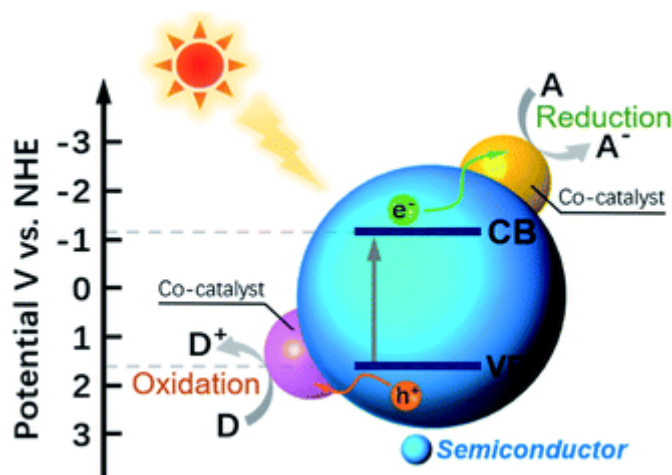
Scheme 13. General elementary steps in photocatalysis promoted by semiconductors. Adapted with permission from ref. [724]. Copyright 2021 Royal Society of Chemistry. *i*) light excitation and electron promotion; *ii*) Charge carrier migration to the particle surface; *iii*) Chemical reduction and oxidation of substrates in contact with the semiconductor particle. These chemical processes can occur at special sites on the semiconductor surface denoted as co-catalysts. Electron-hole recombination can occur at any time, decreasing the efficiency of the photocatalytic process.

The potential of photocatalysis using semiconductors, particularly TiO_2, to remove pollutants from the environment,[725-727] atmosphere,[728] water [729-736] and soils,[271,737-738] was recognized in the early 80s of the XXth and has remained as an active broad research area since then. [727-728] [729-730] [271,731-738] [739] The reason behind the use of photocatalysis for environmental remediation was the well-proven ability of photocatalysts exposed to the ambient to generate reactive oxygen species triggering a general unspecific mechanism resulting in the oxidation of a very wide range of chemical compounds, including most of the organic pollutants.[740] As the final end-products of the complete photocatalytic oxidation of organic compounds would be innocuous CO_2 and H_2O, this ideal complete photocatalytic process would correspond to the mineralization or combustion of diluted organic compounds at near ambient temperature even in aqueous phase.[741] The general mechanism of photocatalytic pollutant degradation, involving reactive oxygen species, fits within the broad field of advanced oxidation techniques,[742-746] except that in the photocatalytic process no oxidizing chemicals others than air and/or moisture are necessarily employed and that the photocatalytic process requires photons to occur. It should be stressed that photons can be considered as the cleanest chemical reagent making unnecessary additional treatments to remove any byproduct, as it may be the case of other advanced oxidation processes. Thus, the Fenton-treated wastewaters require separation of Fe^{3+} or other transition metal salts after the reaction and subsequent appropriate management of the resulting metal-containing sludge.

Not surprisingly in view of the general scope in the nature of pollutants that can be degraded by reactive oxygen species, the field of photocatalysis applied to water treatment has attracted an immense interest. A search in the Web of Science database in January 2021 using as keywords "photocatalysis" and "water treatment" or "water purification" retrieved over 35 000 items. About 1500 of these entries were classified as reviews covering many aspects related to the nature of the photocatalyst, degradation of certain types of recalcitrant pollutants at various concentrations, photoreactor design, combination of photocatalysis and other purification techniques and many others. Thus, the reader is referred to this extensive literature for a comprehensive coverage of the state of the art of photocatalysis for water treatment and for a detailed description of special subtopics. To give an idea of the breadth of the area, some of the most recent reviews focus on the use of photocatalysis for the removal of specific industrial, agricultural and pharmaceutical pollutants in waters, the most researched being dyes of relevance for the textile industry and as a pigments, [747-758] pesticides,[737,759-761] antibiotics,[449,762-766] halogenated organic compounds,[767-769] and heavy metals,[770-771] just to name a few. In general, these reviews reflect the growing concern of certain types of compounds and metabolites of anthropogenic origin with recently discovered negative activity in human health,[772] such as hormone equivalents,[2,773] endocrine disruptors,[774] and other biological effects even at low or ultra-low concentration.

Regarding water disinfection by photocatalysis [775] and considering the dramatic impact of SARS-COV-2 pandemic on human life and society and that this virus is present in urban wastewaters, special attention has been paid to the use of photocatalysis as the most appropriate technique for its deactivation.[776-778] Photocatalysis is being considered as a very efficient treatment particularly for wastewater treatment at hospitals [779] and other source points of high COVID-10 virus concentration.[780]

The following paragraphs of this section are intended to provide a short summary of the main directions, achievements and current state of the art on several of the main points related to application of photocatalysis for water treatment. Emphasis is made on the present limitations that have to be overcome for general implementation of this technology in water treatment. These limitations are related to the residence time and light power needed to achieve the wanted level of pollutant degradation at high water flow rates. In general, photocatalysis is a slow process compared to filtration techniques, requiring hours of irradiation times to reach significant levels of pollutant degradation. Also, the use of artificial UV light to activate certain photocatalysts is a drawback, since it requires adequate lamps and equipment and the process has associated a high maintenance and operation cost. Solar light, on the other hand, has the

drawback of daily intermittence, dependence on weather conditions and precautions to avoid algae growth. Since photocatalysis implies light penetration in the wastewater, problems related to lack of transparency and water turbidity may require some pretreatment by precipitation, flocculation or filtration prior to application of the photocatalytic process.

4.1.1 General photodegradation mechanisms.

As mentioned earlier, the advantage of photocatalysis for environment remediation and pollutant degradation is that in the charge separation state of a semiconductor in contact with the ambient, reactive oxygen species can be generated provided that electrons and holes have sufficient energy to react with these species. This is due to the fact that exposed to the air and water or humidity, the charge separate state of most semiconductors prefers to react almost universally with O_2 as the best electron acceptor of conduction band electrons and with H_2O as the best electron donor for valence band holes. In this way, starting both from O_2 (by reduction) or H_2O (by oxidation), highly reactive radicals with O atoms in the formal intermediate (–I) oxidation state are generated. [740] These oxygen radicals can interconvert among them through proton, or proton and electron transfer processes. Scheme 14 summarizes the reaction network resulting in the generation of reactive oxygen species.

Scheme 14. Reactive oxygen species generated on the photocatalyst surface, diffusing to the surrounding aqueous medium. These reactive oxygen species are formed from the reduction of oxygen and oxidation of water and can interconvert among them. Reproduced with permission from ref. [740] Copyright 2017 American Chemical Society.

Among the reactive oxygen species with (–I) oxidation state, hydroxyl radical is considered as the most aggressive chemical that can be generated in aqueous media.[781-782] Hydroxyl radicals can react by three different mechanisms, including electron transfer, hydrogen atom abstraction and electrophilic addition.[781,783] The thermodynamic standard value of oxidation potential for $^{.}OH_g/^{-}OH_{aq}$ is +1.98 V vs. RHE,[784] meaning that they can abstract one electron of many organic molecules having lone electron pairs or other electron-rich functional groups, resulting in the generation from neutral molecules of organic radical cations that are highly reactive against molecular oxygen or can decompose in other ways.[785] Besides, due to the high value of the O-H bond energy (about 467 kJ.mol^{-1}) that is higher than most C-H bond energy values (average energy value for C^{sp3}-H bonds 413 kJ.mol^{-1}) and the low activation barrier for the atom exchange, $^{•}OH$ radicals can abstract a hydrogen atom from virtually any organic molecule, generating C centered radicals.[781] Carbon centered radicals are known to react again with molecular oxygen resulting in instable hydroperoxyls prone to decompose by C-C bond cleavage, the key step in the way to oxidative degradation of a pollutant. A third common reactivity pattern of $^{•}OH$ radicals is electrophilic addition to multiple bonds. Scheme 15 summarizes the general reactivity of $^{•}OH$ radicals and some of the subsequent steps leading to the oxidative cleavage of C-C bonds. Similarly, other reactive oxygen species, such as superoxide or hydroperoxyl radicals, can trigger also the formation of C centered radicals or radical cations that are the key intermediates in the way to degradation.
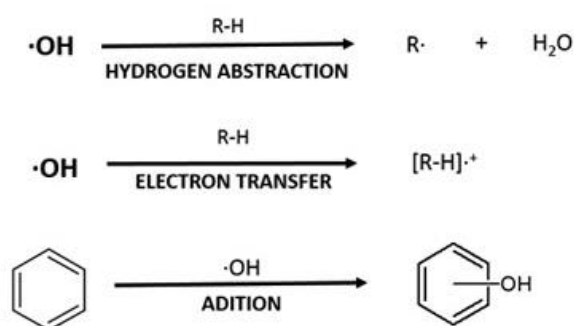
Scheme 15. General reactivity of $^{.}OH$ radicals. Drawing adapted with permission from ref. [786]. Copyright 2013 Chilean Chemical Society.

Although less reactive than $^{•}OH$ radicals, superoxide and hydroperoxyl radicals are also highly reactive, promoting hydrogen abstraction from specific positions and participating in electron transfer processes.[740]

The above considerations serve to justify why irradiation of a semiconductor under ambient conditions is a general methodology to promote the oxidative degradation of organic pollutants through the generation of reactive oxygen species. The complete degradation process would occur through multiple attacks of reactive oxygen species, combined with trapping by molecular O_2 from the ambient and C-C bond breaking, resulting in intermediates with smaller number of molecules. In these bond ruptures and due to the increasing number of O atoms, CO_2 may evolve. Final products, reluctant to undergo further oxidation, are carboxylic acid, polycarboxylic acids and hydroxylated carboxylic acids, such as acetic and propionic acids.

Besides reactive oxygen species other degradation mechanisms can also occur concomitantly. Thus, highly toxic oxidized metal oxo anions, like Cr(VI) species, can undergo reduction by the photogenerated conduction band electrons. Similarly, electron rich organic molecules can react directly with valence band holes and forming organic radical cations that, similarly to those generated by the intermediacy of $^\bullet$OH, would react with ambient oxygen.

Organic dyes may also have specific photocatalytic degradation mechanisms. Since organic dyes have strong absorption bands in the visible region, photoexcitation by photons in this range can lead to the generation of transient singlet or excited states localized in the dye. These electronic excited states can transfer electrons to or from the semiconductor resulting in charge separation involving the dye and the photocatalyst. This process is generally known as photosensitization and can be very efficient, particularly considering that dyes are frequently ions or highly polar, bulky molecules that adsorb strongly to the photocatalyst surface. Charge separation through photosensitization occurring upon dye irradiation with visible light and generation of radical ions of the dye favors the oxidative attack and results in decolorization of the dye. Note that this photosensitization mechanism is particularly important for wide bandgap semiconductors that do not absorb visible light, but can participate in photosensitized electron transfer process due to light absorption by the dye. Scheme 16 illustrates the degradation mechanism specific for dyes based on photosensitization.

It should be commented that frequently the effect wanted in the photocatalytic treatment of dyes is wastewater decolorization and this visual effect can be achieved by disruption of the conjugated bonds of the chromophore, even though most of the molecular structure still remains intact. In this sense, dye decolorization easily followed by UV-Vis spectroscopy may not really correspond to the occurrence of molecular degradation with oxidative cleavage of the initial structure and possible CO_2 evolution, but only to the alteration of the chromophoric system.
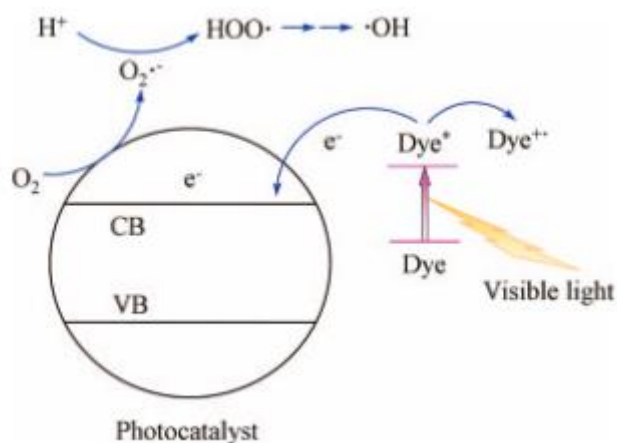
Scheme 16. Mechanism of dye decolorization upon visible light irradiation of a wide bandgap semiconductor through a photosensitization mechanism leading to the generation of the dye radical cation. This radical cation intermediate reacts with ambient oxygen disrupting the chromophore responsible for the color. Reproduced with permission from ref. [787]. Copyright 2012 Taylor & Francis.

This variety of mechanisms based on the generation of reactive oxygen species or in the direct oxidation or reduction of substrates are very general and can be applicable to numerous pollutants, either organic or inorganic. Therefore, photocatalysis in aqueous media was recognized since the beginning as a very powerful technique for wastewater treatment and environment remediation, particularly suited when the concentration of pollutants is low in the range of a few mg/L or below or when the wanted effect is wastewater decolorization.

4.1.2. Photocatalysts

The photocatalyst is the key component converting light into chemical energy. The most widely used photocatalysts are inorganic semiconductors. [788]Considerable effort has been made in testing the performance of any possible semiconductor in water treatment. Due to their intrinsic photocatalytic stability, semiconducting metal oxides such as TiO_2, ZnO, CuO, Fe_2O_3, WO_3, CeO_2 or oxo salts like perovskites have been widely studied.

Most of these metal oxides are wide bandgap semiconductors with absorption onset in the UV region. Since natural sunlight has almost a negligible energy in the UV ($\lambda > 380$ nm), the use of metal oxides in photocatalysis is generally associated to employing lamps as photon source. One point to be reminded is that light penetration correlates inversely with light wavelength, meaning that the penetration of UV light into an aqueous solution, particularly below 300 nm, is lesser than that of the visible light. This means that in the photoreactor design

the distance from the lamps to the photocatalyst has to take into consideration the irradiation wavelength.

TiO₂ as photocatalyst

Regarding semiconductors, there is no doubt that TiO$_2$ still continues to be the most important photocatalyst and a considerable research is focused on enhancing its activity. Thus, about 19 000 items are retrieved in the Web of Science database in January 2021 by combining the words of photocatalysis, water treatment and TiO$_2$. More than 10 000 items have been published since 2015, indicating that the field is currently very active with over 1 500 publications on the activity of TiO$_2$ for water treatment consistently in the last five years. Thus, the number of publications using TiO$_2$ is over one-half of the total number of items dealing with photocatalysis for water treatment, giving an idea of the relevance of TiO$_2$ in the field in spite of its limitations. The main reason for this prevalence is the combination of high efficiency under UV light irradiation, availability, chemical and photochemical stability and lack of toxicity.

However, while TiO$_2$ can exhibit high photocatalytic activity under UV light, the onset of anatase photoresponse (about 380 nm corresponding to 3.2 eV) is just on the limit of the solar emission spectrum reaching the Earth surface and, therefore, a complete lack of photocatalytic activity under sunlight exposure is commonly observed. This lack of sunlight activation and the high charge carrier recombination rates, meaning that most of the absorbed photons are useless, are the main drawbacks of TiO$_2$ and, therefore, of photocatalysis in general.

To overcome these two important limitations, much effort has been made to modify TiO$_2$ photoresponse and enhance the efficiency. Thus, the photocatalytic activity of TiO$_2$ in different phases and prepared from various procedures has been amply reported since the starting of photocatalysis for wastewater treatment.[734,789] However, the need of UV light for activation and its low efficiency due to the large extent of charge carrier recombination have determined a continued research to improve the efficiency of this metal oxide semiconductor. Doping by metal and non-metallic elements,[735,790] surface amorphization to render "*black titania*",[791-792] preferential crystallographic facet growth,[793] spatial structuring at the nanoscale[794-796] and formation of heterojunctions with other semiconductors and co-catalysts[797-799] have been general strategies that have been used to increase the photocatalytic TiO$_2$ efficiency in general and in the field of water treatment in particular.[800]

Beyond TiO₂.

Besides TiO$_2$, there are other semiconducting metal oxides that have also been studied as photocatalysts for wastewater treatment. Probably, ZnO is the second most studied photocatalyst.[801-802] ZnO also a wide bandgap semiconductor with similar conduction and valence band potentials as TiO$_2$ and exhibiting a large active under UV light. One of the main problems is the stability of this metal oxide under even mild acid conditions. It should be reminded that many oxides of di- and tri- positive metal cations dissolve in acid media and this happens in this case. ZnO is also not stable under strong basic conditions. Thus, it can be concluded that there is no much gain using ZnO as alternative of TiO$_2$. Similar conclusions about stability or lack of clear advantages respect to TiO$_2$ also apply for other metal oxides.

Besides oxides, chalcogenides have also been explored as photocatalysts.[93] Metal chalcogenides are characterized by a narrower bandgap than the corresponding oxide, meaning that, in contrast to metal oxides that are wide bandgap semiconductors, most metal chalcogenides exhibit visible light absorption.[803] Although metal chalcogenides have generally a remarkable photocatalytic activity, their lower photochemical stability and their tendency to undergo photocorrosion limit considerably their real applicability.[804] Photocorrosion occurs when one of the charge carriers reacts slower than the other and it results in accumulation of one charge carrier on the particle, producing the dissolution of the corresponding ion.[805-806] In the case of metal chalcogenides, this photocorrosion is usually minimizing by the presence of sulfide or polysulfides in the medium,[807] but this is not generally possible in wastewater treatment. In addition, typical metal chalcogenide photocatalysts have highly toxic metals, like Cd. All these drawbacks make metal chalcogenides of low use.

As commented earlier, most photoresponsive materials have been tested as photocatalysts for wastewater remediation. The list includes many novel 2D nanomaterials like MXenes [808] whose synthesis has been recently reported by Gogotsi in 2011 and that have also been tested as photocatalysts for water purification. Particularly, the probably most widely studied 2D MXene, Ti$_3$C$_2$ carbide obtained by HF etching or other exfoliation technique of the Ti$_3$AlC$_2$ phase and characterized by having negative charged sheets in aqueous suspensions is able to adsorb positively charged dyes such as methylene blue, promoting their subsequent photocatalytic degradation. Figure 78 illustrates MXene synthesis. Since MXenes are mostly conductive materials, they are most generally used in combination with a semiconductor, such as TiO$_2$,[809-812] graphitic carbon nitride,[813] 2D metal-organic frameworks[814] and other photocatalyts.[815]
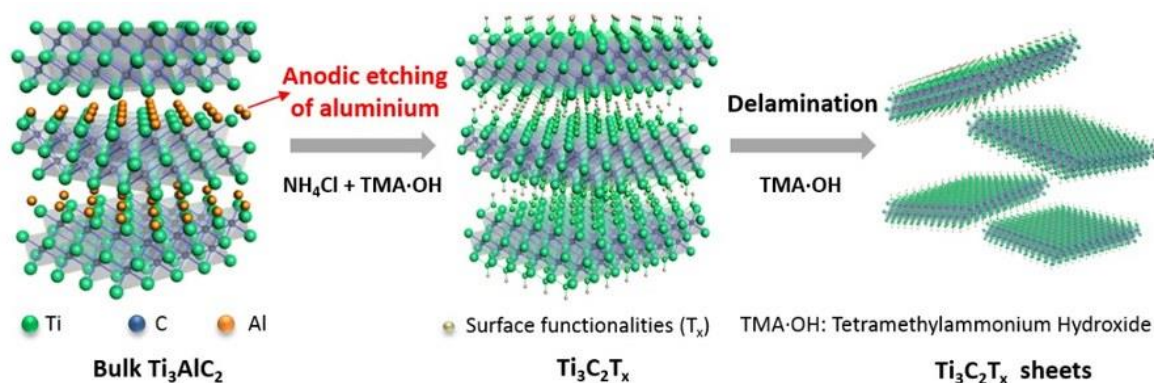
Figure 78. Preparation of single layers of Ti$_3$C$_2$ from Ti$_3$AlC$_2$ by anodic etching and subsequent exfoliation. Reproduced with permission from ref. [816] Copyright 2018 Wiley-VCH GMBH.

Due to the space limitation, in the next sections we will focus on two different types that have been under the spotlight in recent years, due to the potential advantages in comparison with oxides and chalcogenides. The aim is to illustrate the breadth of the field by presenting the use of metal organic frameworks and non-metallic graphitic carbide as photocatalysts for wastewater treatment.

Metal-organic frameworks (MOFs) as photocatalysts.

MOFs in which metal clusters are connected to rigid multipodal organic linkers forming a crystalline porous lattice are in many respects like molecular transition metal complexes, but holding these metal complexes in fixed position in an open network, making them accessible to pollutants through the crystal pores. [817-820] High surface area and large pore sizes and volumes together with a considerable flexibility in composition and structures are the main positive features of MOFs. MOFs allow a large degree of design by considering the coordination geometry around the metal nodes and binding directionality of the organic linkers. Scheme 17 illustrates the main structural characteristic of MOFs and their advantages respect to other materials.
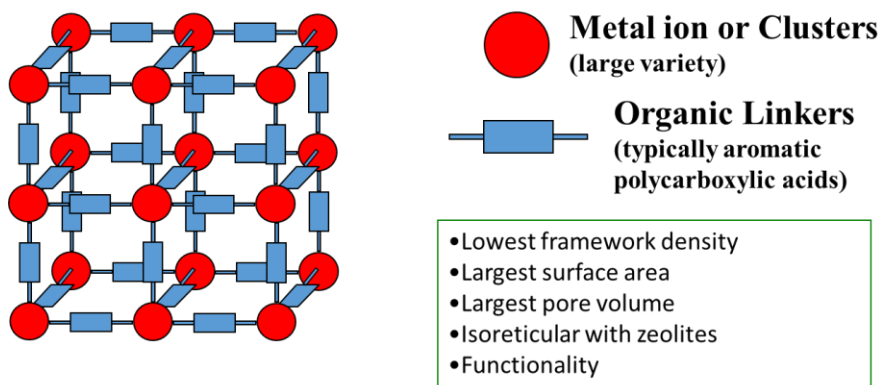
Scheme 17. Cartoon representing MOFs structure with metal ions or clusters at nodal positions coordinated by rigid bipodal organic linkers. The main structural properties of MOFs have also been indicated.

Since molecular transition metal complexes, such as for instance ruthenium polypyridyls, are among the best studied soluble photocatalysts and photosensitizers, it derives that MOFs can be considered as the heterogeneous counterparts of these soluble metal complexes. The use of MOFs as photocatalysts, including wastewater treatment, has been recently reviewed, summarizing strategies to enhance their photocatalytic activity.[821] Not surprisingly, dye decolorization has been a preferred test reaction to evaluate their photocatalytic activity.[752,822-829] MOFs are especially suited as visible light photocatalysts.[121]

Besides as-prepared materials, MOFs can also be subjected to post-synthetic modification to adapt the structure to their role as photocatalyst. A common post-synthetic treatment is the incorporation or metal nanoparticles that have the role of co-catalyst favoring the charge carrier trapping and their transfer to substrates. In one of the examples trimetallic Cu-Co-Ni nanoparticles were uniformly incorporated inside MIL-101(Fe)-NH_2 and the resulting material exhibit visible-light photocatalytic activity for removal of cationic methylene blue and anionic crystal violet dyes using a trace amount of H_2O_2.[830] Scheme 18 illustrates the process. Although Cu-Co-Ni/MIL-101(Fe)-NH_2 exhibits an enhanced photocatalytic activity in comparison with the parent MOF and other control materials, the decay, even moderate, observed in the performance of Cu-Co-Ni/MIL-101(Fe)-NH_2 upon reuse certainly hampers any possible real application of this material. Since MOF structure is based on metal-ligand coordination bonds that are weaker than covalent bonds, MOFs have also been carefully surveyed for stability, providing convincing evidence of structural robustness.
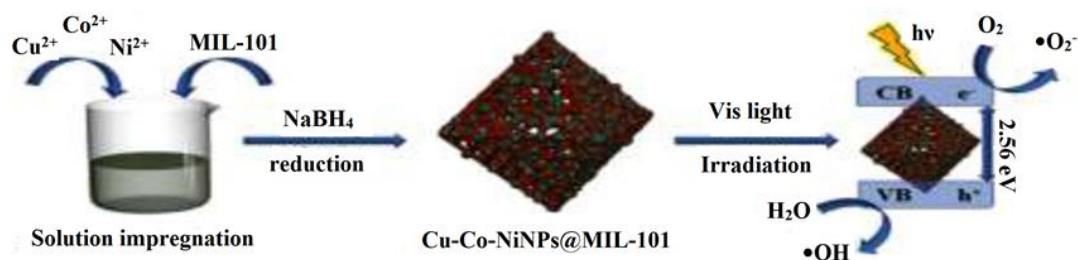
Scheme 18. Preparation and photocatalytic activity of Cu-Co-Ni/MIL-101(Fe)-NH$_2$. Reproduced with permission from ref. [830]. Copyrigth 2020 Elsevier.

The photocatalytic activity of MOFs for water treatment relies at least three possible centers, including active metal nodes, linkers or occluded guests. In one of the examples using the internal void space to include a photoactive guest, atomic clusters, such as PW12 heteropolyoxometallate, have also been incorporated inside MOFs and the resulting guest-host material used as photocatalyst for the degradation of pharmaceuticals in water.[831]

Besides metal and metal oxides nanoparticles, carbon dots are attracting considerable attention in photocatalysis as light harvesters and as charge trapping agents. Carbon dots have been incorporated inside MOFs, such as MIL-88B(Fe)-NH$_2$ and the resulting composite used as visible light photocatalyst for Cr(VI) reduction and methylene blue oxidation.[832] The carbon dot-MIL-88B(Fe)-NH$_2$ material was prepared in a single step and it is proposed that the enhanced photocatalytic activity derives from the role of carbon dots as electron acceptors increasing the efficiency of photoinduced charge separation.[832] Scheme 19 illustrates the preparation procedure, structure and band alignment of the carbon dot-MIL-88B(Fe)-NH$_2$ material.
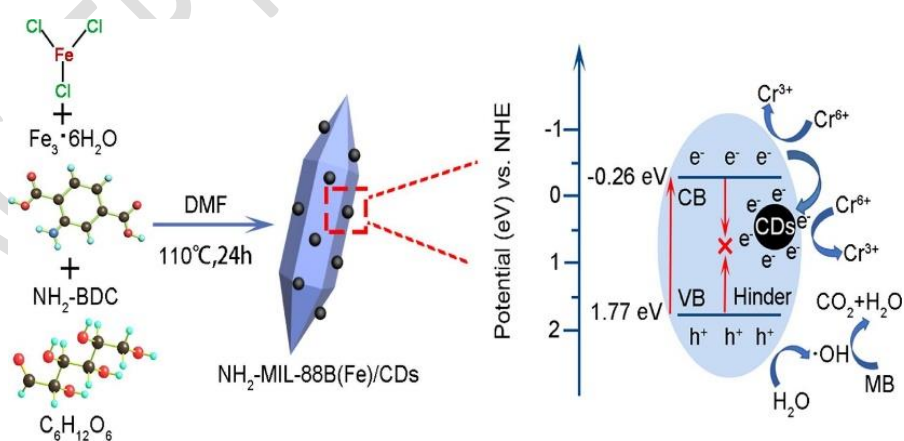
Scheme 19. Precursors, structure and band alignment of carbon dot-MIL-88B(Fe)-NH$_2$. BDC and CD corresponds to 1,4-benzenedicarboxylate and carbon dots, respectively. Reproduced with permission from ref. [832]. Copyrigth 2020 Elsevier.

177

2D MOFs in which the thickness of the crystallites are a few nanometers are currently under intense investigation due to their potential in electro- and in photocatalysis.[833]The nanometric thin nanosheets offer high substrate accessibility and favorable diffusion, in addition to optical advantages derived from light excitation on the material. These 2D MOFs have also been explored as photocatalysts for dye degradation in the absence of H_2O_2.[750]

Frequently the photocatalytic activity increases upon the combination of two or more semiconductors. These systems are generally denoted as "heterojunctions" and depending on the band energy alignment of the two components, various possibilities can appear (Scheme 20). These heterojunctions have also been reported using MOFs as components. For instance, it has been found that the heterojunction of $AgVO_4$ and ZIF-8 is more efficient for Rhodamine B degradation than the individual components.[834] In other example, it has been recently reported that incorporation of red phosphorous inside MIL-101(Fe) exhibits an excellent activity for tetracycline degradation, the composite being stable and reusable.[835] A related version of red phosphorous inside ZIF-67 has photocatalytic activity for Cr(VI) salts reduction and rhodamine B oxidation.[836]
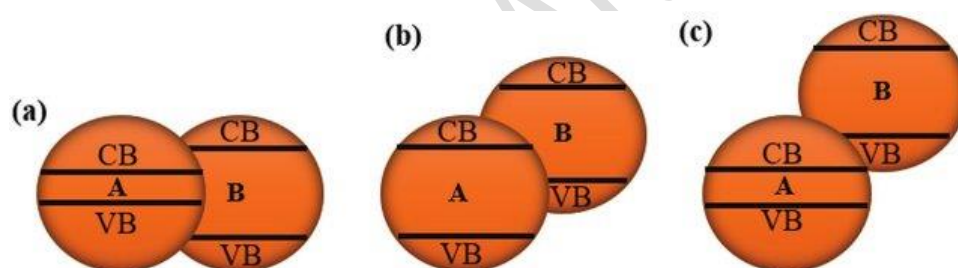
Scheme 20. Types of heterojunction of two semiconductors depending on the conduction and valence band alignment. a) Type I or straddled, b) Type II heterojunction or Z-scheme, and c) Type III or broken gap. Reproduced with permission from ref. [837]. Copyrigth 2017 Wiley-VCH GMBH.

Ultrathin 2D nanosheets are especially suited as components in heterojunctions, since the surface to volume ratio is larger and the percentage of atoms exposed to the heterojunction in 2D MOFs is higher. One particular case of this heterojunction with 2D MOF is the case of BiOBr and ultrathin MOF nanosheets to form a Z-scheme photocatalyst.[838] Mixed metal MOFs can exhibit enhanced light harvesting properties and in a heterojunction these MOFs can act as photosensitizers. One illustrative example is Ce-doped MIL-101-NH_2 forming a heterojunction with Ag_3PO_4 that exhibits high photocatalytic activity for decolorization of methylene blue.[839]

MOFs can also be used as precursor of advanced metal oxide photocatalysts and their heterojunctions.[840]In one of study, porous TiO_2/ZrO_2 photocatalyst was prepared by depositing TiO_2 on UiO-66 and the resulting TiO_2-UiO-66 composited submitted to calcination. The

porous TiO_2/ZrO_2 on UiO-66 exhibits enhanced visible light photocatalytic activity for dye decolorization.[841] Scheme 21 illustrates the band alignment on this multicomponent photocatalyst and show a TEM image of the resulting composite. More elaborated multicomponent MOF-containing materials have also been developed as advanced,[823] multifunctional adsorbent-disinfectant photocatalyst.[842]
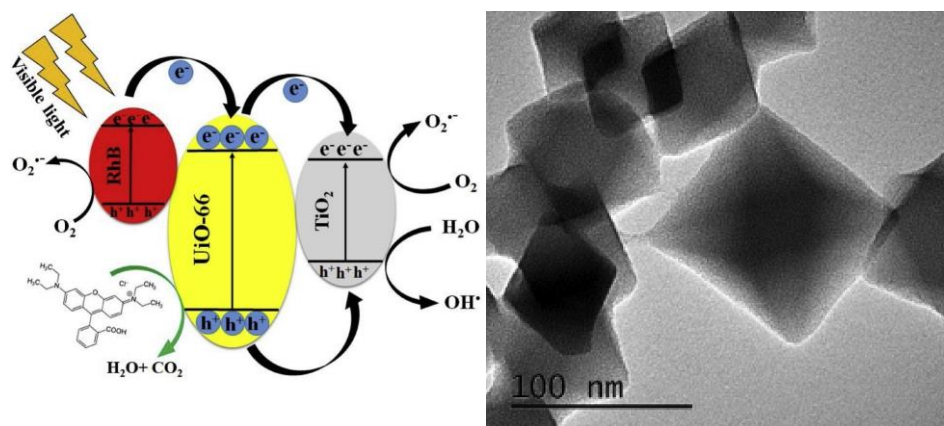
Scheme 21. Band alignment and TEM image of the TiO_2/ZrO_2/UiO-66 photocatalyst. Adapted with permission from ref. [841]. Copyrigth 2019 Elsevier.

Carbon nitride

As commented earlier, besides TiO_2, metal oxides, metal chalcogenides and MOFs, graphitic carbon nitride (g-CN) has emerged as one of the most-studied metal-free photocatalyst.[843] The ideal structure of graphitic carbon nitride is a polymer of s-triazin and s-heptazine unit with melon substructures. Scheme 22 shows an ideal structure of g-CN.[844]
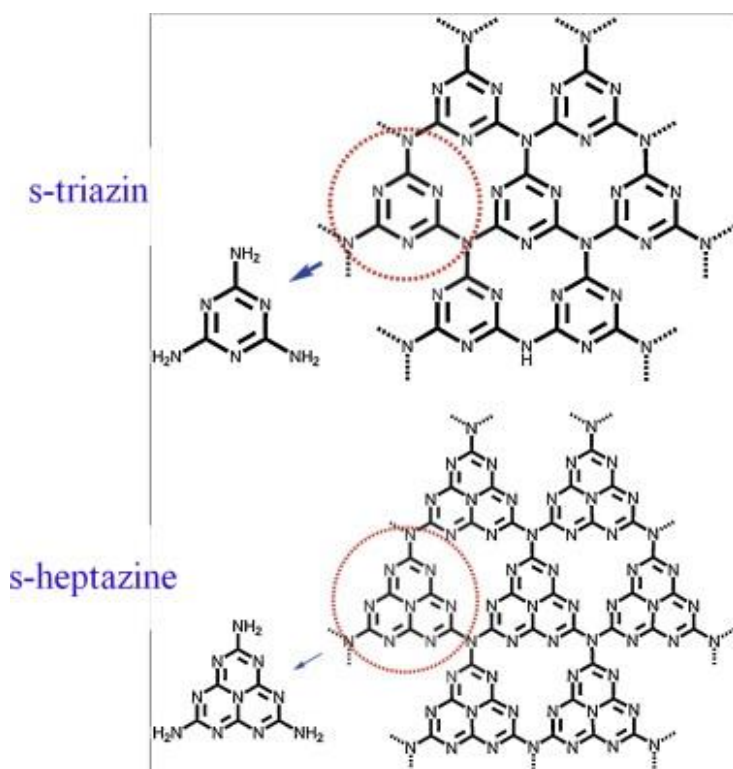
Scheme 22. Structures of ideal graphitic carbon nitride. Reproduced with permission from ref. [844]. Copyrigth 2014 Elsevier.

It appears that the exact preparation procedure determines the quality of g-CN and its photocatalytic performance and photostability. A recent study has shown that downshifting the valence band oxidation potential and increasing g-CN surface area increases g-CN self-degradation by photogenerated reactive oxygen species.[845] It was also found that the presence of aromatic humic acids probably acting as a quencher diminishes the photocatalytic degradation of diclofenac by g-CN.[845] This effect of polyphenolic humic acids quenching charge separation is probably general and should decrease the efficiency of most semiconductors.

As in the case of graphene, the optical properties and photocatalytic activity of g-CN for water treatment can be enhanced by doping with nitrogen, boron,[846]sulfur,[847] phosphorous[848] and other elements. A fully bio-based oxygenated g-CN supported on polyester has been prepared and used for water treatment.[849] g-CN was formed by microwave thermal treatment of guanidine hydrochloride and tris(hydroxymethyl)aminomethane. The polyester obtained by solvent-free condensation of glycerol and a mixture oil-based dimer and citric acids.[849] Besides on polyesters based on glycerol, g-CN has also been supported on pickering cellulose foams,[850] carbon nanotubes[848] and many other substrates, allowing easier recovery or immobilization.

The use of natural, renewable feedstocks in the preparation of supported photocatalysts represents an advance towards sustainability and better use of resources.

g-CN has also been used as one component in heterojunctions and multicomponent photocatalyst for water treatment.[847] Among the various systems those combining g-CN and TiO$_2$ as well as MOFs have been intensively investigated.[851]

4.1.3 Comparison among different photocatalysts and conditions.

The current state of the art can be summarized indicating that issues of sunlight efficiency and stability of modified TiO$_2$ forms have not been yet satisfactorily solved and there is ample room for improvement. Therefore, beyond TiO$_2$, virtually every known photocatalyst in their various modifications has also been tested for water treatment. Several reviews are focused on describing the state of the art regarding these more novel photocatalysts beyond TiO$_2$, such as graphenes,[852-856] carbon nitride,[843,857-859] bismuth oxyhalides,[860] bismuth vanadate,[861-863] metal-organic frameworks,[758,864-866] covalent organic frameworks[867-868] or diamond nanoparticles,[869-870] among others.

Regarding elaboration of a ranking of photocatalyst efficiency, one of the main problems that is common for all the photocatalytic reactions is the difficulty to define some absolute numbers that could allow comparison among different materials. The photocatalytic activity depends on multitude of variables, including the mass of photocatalyst in a volume and how the photocatalyst is exposed to the light, the intensity of the light and its spectral range, the photoreactor design, nature of pollutants, presence of oxygen and other natural products acting as promoters or inhibitors. The influence of all these parameters makes frequently impossible to draw conclusions on the relative activity. On top of this variability of experimental conditions, there are also issues related to photocatalyst stability, activity decay and costs that are also very important and generally not sufficiently addressed. Photocatalyst stability is generally supported by a low number of reuses under batch conditions, but no realistic continuous flow long-term (weeks or months) tests are performed. In many of the cases, ready implementation of these photocatalysts seems not possible due to various reasons, like the lack of proven stability, poor efficiency, high cost or toxicity.

Therefore, at the present, it is evident that testing and evaluation of new materials as photocatalysts for water purification and pollutant degradation will continue to attract much research effort in the next years. However, the field will benefit enormously of definition and acceptance of efficiency parameters and even certain common standard experimental protocols

that could serve to advance in a confident photocatalyst activity comparison and the quest a definitive photocatalyst.

In this regard, the IUPAC proposed phenol and anionic alkylsulfate surfactant as probes to check the activity of advanced oxidation techniques to promote degradation of aromatic and aliphatic compounds [871] and these model compounds could also be used to evaluate the photocatalytic activity of different materials, describing experimental procedures to follow the course of the reaction. Besides substrate disappearance, product analysis and decrease of total organic and inorganic carbon are parameters to be considered. In the case of dyes, rhodamine B, methylene blue and recalcitrant azo compounds are also preferred models.

Besides the performance against probe molecules, efficiency parameters borrowed from other photocatalytic reactions could also be used to rank the photocatalytic activity. Thus, energy efficiency parameters such as those used in advanced oxidation techniques,[872] water splitting[873] or photocatalytic CO_2 reduction, in which light-to-chemical conversion efficiency is the figure of merit. Collector surface for direct sunlight irradiation is also related to energy used in the process.[872] In the present case of wastewater remediation, the efficiency in which the light energy is converted into the generation of reactive oxygen species or the degradation of key pollutants, like phenol, could be also a valuable figure of merit to rank the various photocatalysts and clarify the field.

It is clear that these efficiency values are also function of the operation conditions and photoreactor design. For this reason, the research should also address which are the best conditions in terms of photocatalyst concentration, photocatalyst immobilization, illuminated area, flow rates, etc. In any case, it is clear that the field will benefit enormously for some agreement in benchmark probes and efficiency data that could be widely employed to establish photocatalyst performance, allowing comparison among photocatalysts, conditions and photoreactors.

4.1.4. Photoreactors

Regarding photoreactors, it should be commented that most of the studies in the area have been carried out under batch conditions. However, implementation of photocatalytic water purification would most likely require almost universally the use of continuous flow. Issues like photocatalyst stability are better study in a continuous flow reactor in which it is possible to determine deactivation as a function of the operation time. In continuous flow reactors,

suspended photocatalysts are difficult to maintain and deposition of the photocatalyst as a thin layer in the irradiated region is preferable (see chapter 2.3.4).

In this regard, suspended particulate materials are widely employed as photocatalysts, particularly for batch reactions in which there is not a continuous flow. They offer the advantage of a better light adsorption throughout the whole reactor volume, but the concentration of suspended photocatalyst has to be optimized for a maximum efficiency.

However, separation of these particles after the process is complicate, since in most of the cases the best photocatalytic activity is achieved for nanoparticles that do not sediment easily by gravity and whose presence in the treated water is unwanted. One elegant solution to this dilemma, higher activity for nanoparticles and difficult recovery and separation after the process, could be the use of magnetically responsive photocatalysts.[874-876] However, for continuous flow it is always more convenient to deposit a thin film of the photocatalyst in the illuminated region of the photoreactor. Photocatalyst immobilization raises, however, the issue of how to design the reactor to ensure sufficient contact between the irradiated photocatalyst and the pollutants in water.

One important point to be also considered is the light source. At first sight, the use of natural solar light is very appealing, since it would reduce considerably the capital investment required for lamps and ballasts, minimizing energy consumption of the process. There are in market commercially available solar photoreactors. Scheme 23 illustrates a simple model of these solar photoreactors. However, the use of sunlight has several drawbacks to be considered, including night intermittency and dependence on weather conditions. In addition, since solar spectrum reaching the Earth surface has only a small fraction, about 4 %, of the total energy in the ultraviolet region, the use of natural sunlight to promote the photocatalytic water treatment requires of visible-light responsive photocatalysts. This limits considerably the materials that can be used as photocatalysts or alternatively makes necessary modification of conventional, stable metal oxides in such a way that they become photo responsive under visible light irradiation. As commented earlier, strategies to render TiO_2 and other metal oxides as efficient visible light photocatalysts are still not satisfactory. Therefore, the selection of available visible light photocatalysts, particular with photo response in the red side of the visible spectrum, corresponding to narrow bandgap semiconductors (about 2.0 eV), is limited in comparison with those that respond into the UV zone.
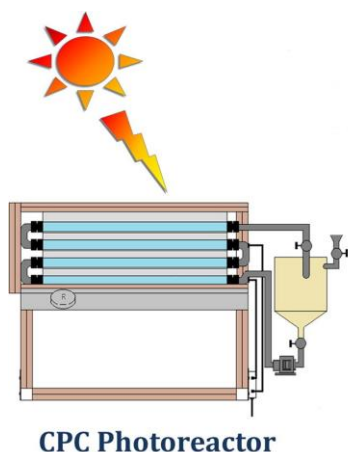
CPC Photoreactor

Scheme 23. Illustration of a continuous flow solar photoreactor constituted by parabolic mirrors and a recirculating solution. Adapted with permission from ref. [877]. Copyrigth 2015 Elsevier.

4.1.5 Photocatalysis: Related practical developments

Due to the long treatment times and the need of transparency and low turbidity, photocatalysis cannot be the preferred wastewater treatment technique when the pollutant concentration is high. When pollutant concentration or the total organic carbon content is in the range of 1 mg.L^{-1} or below photocatalysis is possibly the technique of choice, since other alternatives, particularly advanced oxidation processes, are more costly in this concentration range. Thus, photocatalysis together with membrane filtration are especially suited as secondary treatment for removal or deactivation of micro- and ultra-low concentration pollutants in waters, but photocatalysis has the advantage to degrade or deactivate the micropollutant, while membranes have to be disposed after losing their permeability.[878]

This field of photocatalytic micropollutant degradation is attracting much current interest due to the large public concern on the negative effects of antibiotics and other therapeutic drugs can have in humans and aquatic environments, even at low concentrations. The field of photocatalysis for treatment of low concentration pollutants has been recently reviewed.[879] When pollutant concentration is low photocatalytic irradiation can be done using sunlight[878] or artificial UV light and the process can be carried out under continuous flow.[880-881] Besides TiO_2 and its heterojunctions,[799,811] other photocatalysts such as carbon nitride have also been tested to tackle with these low concentration of emerging pollutants and found more efficient than other alternatives.[882]

Considering the low concentration of micropollutants, one interesting issue is the possible influence that other organic compounds naturally present in fresh waters at similar or higher concentrations can exert on the efficacy of degradation. Particularly, humic and fulvic acids and other organic matter of natural or anthropogenic nature can influence adversely the performance of the photocatalytic degradation of micropollutants. To address this issue, besides model aqueous solutions, it is necessary to perform experiments in which these possible quenchers are also present.

For wastewaters in which pollutant concentration is higher than 1 mg.L^{-1} or the wanted quality of treated water is high, then, it is more convenient to combine photocatalysis with other compatible technique. While the target of many of the studies in advanced oxidation processes is the complete mineralization of the pollutant, a cost-effective approach could be the combination of a mild photocatalytic process with a subsequent biological treatment. As summarized in Scheme 24, the rationale behind the success of this two-step process is that photocatalysis is an oxidative treatment that increases the oxygen percentage in the pollutant, decreasing its molecular mass and these two effects are generally positive to increase the biodegradability of organic compounds. One clear example that can take as a model of other cases is phenol, a non-biodegradable organic molecule. Mild, incomplete, photocatalytic processes increase biodegradability of model phenol aqueous solutions as determined by the comparison of the biological oxygen demand and final total organic carbon of phenol solutions, before and after photocatalytic treatment.[883]
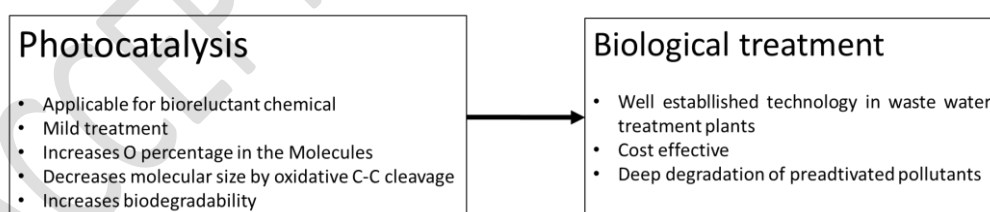
Scheme 24. Combination of photocatalysis and biological degradation resulting in a combined cost-effective treatment.

Combination of photocatalysis with biodegradation, photocatalysis with ultrasounds, photocatalysis with electrocatalysis (photoelectrocatalysis) and different various complementary treatment techniques is also well described in the state of the art (Scheme 25). The advances in three of these combinations (photocatalysis and biodegradation,

sonophotocatalysis and photoelectrocatalysis) are briefly described below in the corresponding sections of Chapter 3.
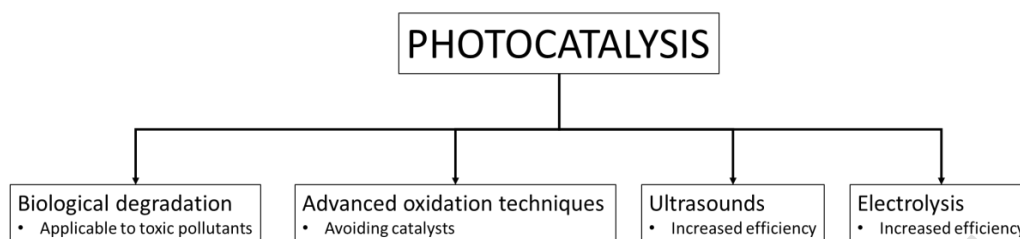
Scheme 25. Photocatalysis as a technique compatible with other wastewater treatment processes.

Combination of photocatalysis and other purification techniques increases the efficiency of water treatment in comparison with only one of the two treatments independently. As commented earlier, a key issue is the removal of byproducts formed in the photocatalytic degradation that are present in very low concentrations, but that could still exhibit adverse effects at this concentration range. Combining photocatalysis with other complementary technique can diminish further the residual concentration after the treatment.

Photocatalysis has been extensively researched and used as a complement to dark methodologies for advanced oxidation purification processes. There is in the literature an extensive number of books and reviews dealing on advanced oxidation techniques and most of them contain a section dealing on the photocatalytic enhancement of these advanced oxidations.[9,742,744-746,787,884-889] The target of advanced oxidation processes is the use of a chemical reagent to generate reactive oxygen species that can promote unspecific oxidation in aqueous media for a large variety of organic and inorganic pollutants. The nature of some these reactive oxygen species has been previously commented, but their formation, as well as other oxygen-centered radicals is achieved by using hydrogen peroxide, monoperoxysulfate, persulfate, ozone and other chemical oxidizing reagents. Typically, these oxidants require of a catalyst such as Fe^{2+} salts in the Fenton reaction or Co^{2+} for monoperoxysulfate. Scheme 26 indicates some types of advance oxidation techniques.
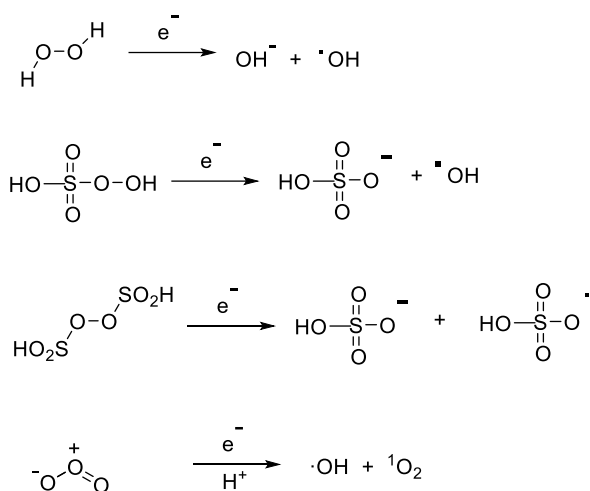
Scheme 26. Reactive oxygen radical species generated from peroxy chemicals

One of the main issues in some advanced oxidation techniques is how to separate the catalyst, typically transition metal ions, from the aqueous solution after the treatment and, for this reason, there is a logical interest in developing heterogeneous catalysts for advanced oxidation processes.[890] In this context, light can also activate the oxidizing reagent either directly by excitation of the chemical agent or by means of a photocatalyst that promotes electron donation to the oxidizing chemical triggering the formation of oxygen-centered radicals. The concept is shown in Scheme 27.
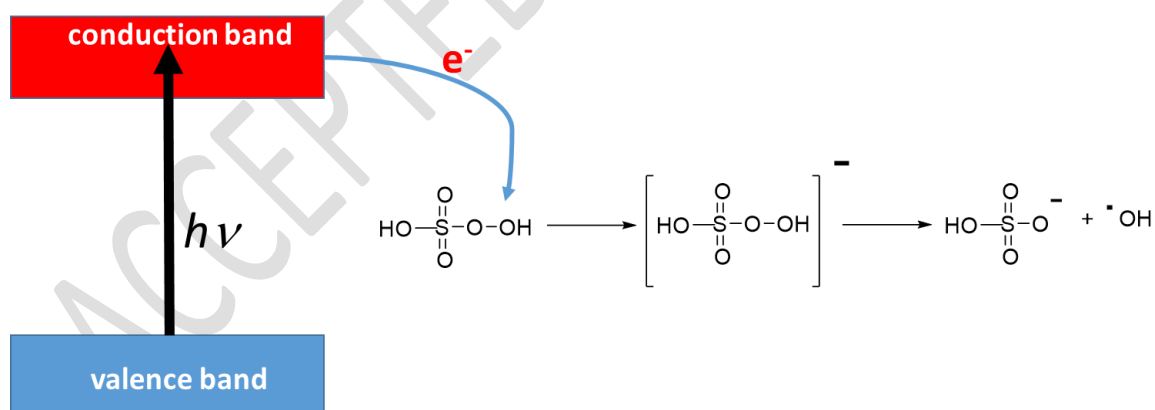
Scheme 27. Photocatalytic activation of peroxy reagents through one electron transfer from conduction band electrons of a photocatalyst.

Direct photon absorption by the oxidizing reagent requires typically deep UV photons of wavelength about 254 nm or lower. This is because most of the oxidants compatible with water treatment, such as hydrogen peroxide or ozone, do not have any chromophore in the UVA

187

(λ>380 nm) or even UVB region (λ >300 nm). This short UV wavelength not only makes necessary irradiation with artificial light, but also more energy-efficient LED illumination technologies do not reach this UV range. Furthermore, the low molar absorptivity of these oxidizing reagents makes necessary a high photon intensity and high transparency of the aqueous phase, something that does not always happen in wastewaters.

The use of a photocatalyst, harvesting longer wavelength photons circumvent this problem and by generation of high energy conduction band electrons and valence band holes promote the decomposition of the oxidizing reagent. However, although the action of photocatalysis is promoted by oxidants and the advanced oxidation techniques can use photocatalysts to trigger the process as indicated in Scheme 26, the main drawback is the capital cost of the irradiation equipment together with the operation cost caused by the addition of a chemical reagent. This cost makes the combination of photocatalysis and advanced oxidation less appealing that development of only one of the two techniques.

One of the major limitations, among others commented above, regarding the use of photocatalysis for water treatment is that the complete pollutant degradation generally requires multiple attacks of reactive oxygen species and that in the way to complete mineralization, as the by-products become more oxidized they tend to be increasingly reluctant to undergo further oxidation. Not surprisingly short chain carboxylic acids, such as acetic, propionic and oxalic acids are commonly the final products of the deep photocatalytic degradation of pollutants. Some of these carboxylic acids are only selectively further degraded by hydroxyl radicals, while other reactive oxygen species are not able to activate them. This means that irradiation times for complete degradation can be too long to have practical interest and a compromise between the decrease in the total or organic carbon content and duration of the photocatalytic treatment has to be reached.

It should be commented at this point that most photocatalytic processes follow a first-order kinetics. Accordingly, while the time corresponding to one half-life decreases the concentration of pollutant by one half and two and three half-life times by 75 and 87.5 %, respectively, the relative decrease in pollutant concentration by increasing further the irradiation time is becoming lesser and lesser.

Therefore, in photocatalysis a compromise should be reached between a reasonable irradiation time and maximum pollutant concentration decrease. Optimization of the irradiation time is particularly important considering the cost of artificial light and the photoreactor volume and design.

In other words, while photocatalysis following a first-order kinetics could be an efficient treatment to diminish pollutant concentration, it appears too costly for complete mineralization of pollutants. Validated mathematical models appear as the most convenient tool to establish at which point photocatalysis has lost most of its value as a pollutant degradation technique depending on how the photocatalyst is placed and the type of photoreactor employed.[768,881,891-896] Modelling is particularly useful at industrial or pilot plant scale [768] and for special photoreactor designs with immobilized thin films photocatalysts[891-892]or using three dimensional monolith reactors.[881]

From these considerations, it can be concluded that the combination of photocatalysis with other complementary techniques, such as micro-/ultrafiltration, biodegradation, electrodialysis or others can be more cost effective and advantageous. Several of the most studied combinations coupling photocatalysis and other techniques are discussed in the following sections.

4.2 Photobiocatalysis treatment of waste waters

The development of photobiocatalyst processes is emerging. However, the interest is such coupling is growing and has been already pointed out.[896] The benefit of such coupling lies in two different activation modes where the substrate can be photoexcited and then react on the biocatalyst or the photons can modify the electronic structure of active sites.[897] In practice, the photobiocatalytic systems are basically composed of photocatalytic materials, porous carriers and biofilm. Advantages provided by these coupled technologies lye in the efficiency gain in the removal of recalcitrant pollutants and mineralization. Hence, lower operating cost would be expected. However, this assumption rests on many questions related to the location of active enzymes in the porous substrate and the nature of their intimate contact with the photocatalyst. Other points to consider are a better utilization efficiency of photons and an enhanced diffusion inside the porous structure of the photocatalysts.[898]

Photobiocatalysis combines the general degradation capabilities of semiconductors upon light irradiation with the catalytic power of biology.[899] It provides a hybrid approach, merging abilities of inorganic materials with the high activity and low cost with self-replicating biocatalysts represented by bacteria, enzymes, microbes, etc. Concomitant production of hydrogen, oxygen or hydrogen peroxide that could play a role in the water remediation may constitute a further pivotal feature of this combined approach.

Studies focused on the photocatalytic H₂ production using bio-hybrid assemblies composed of clostridium acetobutylicum [FeFe]-hydrogenase (CAI) and mercaptopropionic acid-capped CdS already demonstrated the interaction of CdS with the enzyme upon hole-transfer (Figure 79). The increased TOF values were attributed to a rapid electron transfer facilitated by the enzyme.[900]However, the long-term stability of such hybrid systems was affected by the photooxidative corrosion of capped−CdS.
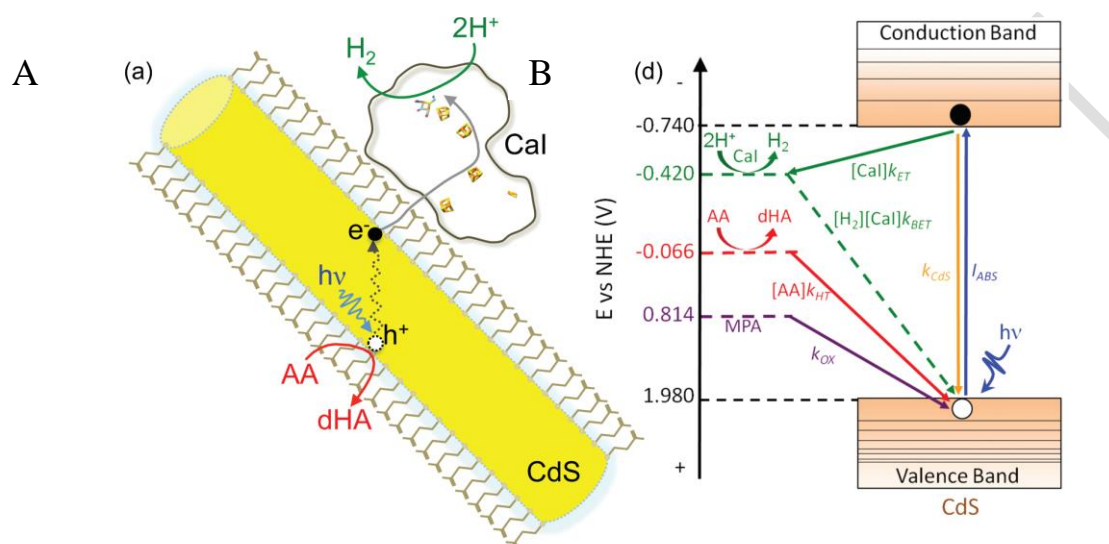
Figure 79. Properties of CdS nanorods and CdS:CaI aggregates. (a) The proposed scheme for photocatalytic H₂ production by the CdS:CaI assembly. Electron-transfer [FeS]-clusters and the catalytic H-cluster are shown in yellow (sulfur) and orange (iron). CdS and CaI are drawn to scale, while MPA molecules are enlarged by a factor of ∼5. (b) Energy level diagram showing processes in photoexcited CdS that are relevant to H₂ production. (Abbreviations: AA, ascorbic acid; dHA, dehydroascorbate; CaI, [FeFe]-hydrogenase; E_g, band gap energy; k_{ET}, rate constant for ET from CdS to CaI; k_{HT}, rate constant for HT from CdS to AA; MPA, mercaptopropionic acid; k_{OX}, rate of photo-oxidation of surface-bound MPA ligands; k_{BET}, rate constant for ET from CaI to CdS (H₂ uptake); I_{ABS}, flux of absorbed photons; k_{CdS}, rate of excited state decay in CdS, including both radiative and non-radiative pathways (e.g., electron−hole recombination, carrier trapping). Potentials are shown vs NHE (pH=7, 1 bar H₂). Reproduced with permission from ref [900]. Copyrigth 2012 American Chemical Society.

Water oxidation may also be coupled with water treatment. Photocatalytic O₂ generation can be catalyzed by enzymes possessing an appropriate inorganic cluster such as Mn_4CaO_5 that is conserved in protein complexes.[901] Its hypothesized precursor is an anoxygenic photobacterium containing a type II photosynthetic reaction center as photo-oxidant (bRC2, iron–quinone type) (Figure 80). Such a bRC2 complex can catalyze the photo-oxidation of Mn^{2+} to Mn^{3+}, but only in the presence of bicarbonate that makes possible the formation of (bRC2)Mn^{2+}(bicarbonate) complexes. Figure 80 depicts a model for the origin of the water oxidation catalyst and chemically feasible steps in the evolution of oxygenic photosystem.
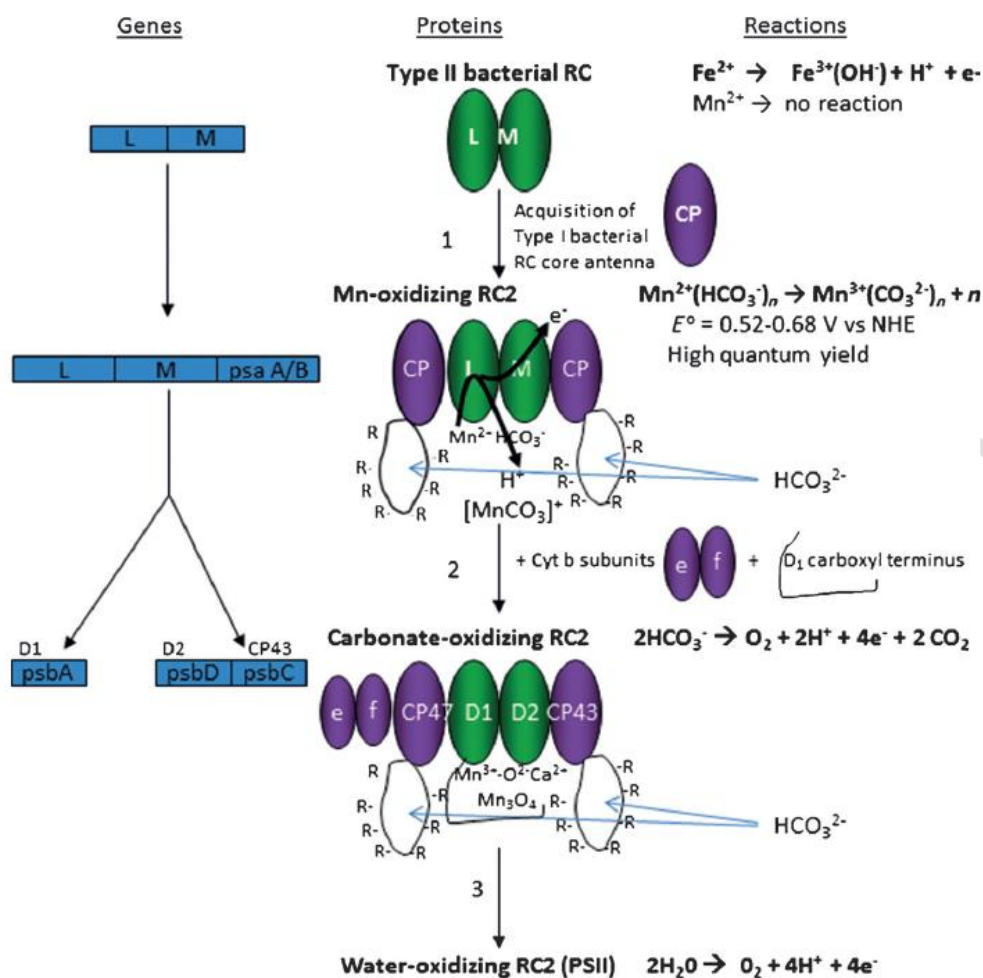
Figure 80. The chemically feasible steps in the evolution of the water oxidation complex of oxygenic photosystem II from the bacterial reaction center. Reproduced with permission from ref. [901]. Copyrigth 2013 Wiley-VCH GMBH.

Further, the concept has been expanded to other applications as wastewater oxidation for water purification, or oxidative biomass conversion, but also for the sequestration of heavy metals.

4.2.1 Biocatalysts associated to organo-photocatalysts for water remediation

Dead algal cells and chlorophyll could accelerate under visible light irradiation the photo-transformation of benzo[a]pyrene (BaP), a ubiquitous and persistent pollutant with potently mutagenic and carcinogenic toxicity. Chlorophyll *a* extracted from *Selenastrum capricornutum* was found to be the major active substance in dead algal cells, and generated a high level of singlet oxygen able to catalyze the photo-transformation of BaP, thus offering a possible remediation strategy of organic pollutants in natural water environment (Figure 81).[902] After absorbing light, chlorophyll reaches its triplet state that can transfer its energy to the ground

state oxygen, resulting in the formation of $^1O_2$ by spin flip in O_2. However, $^1O_2$ only affords the formation of BaP quinones without leading to a deeper degradation.
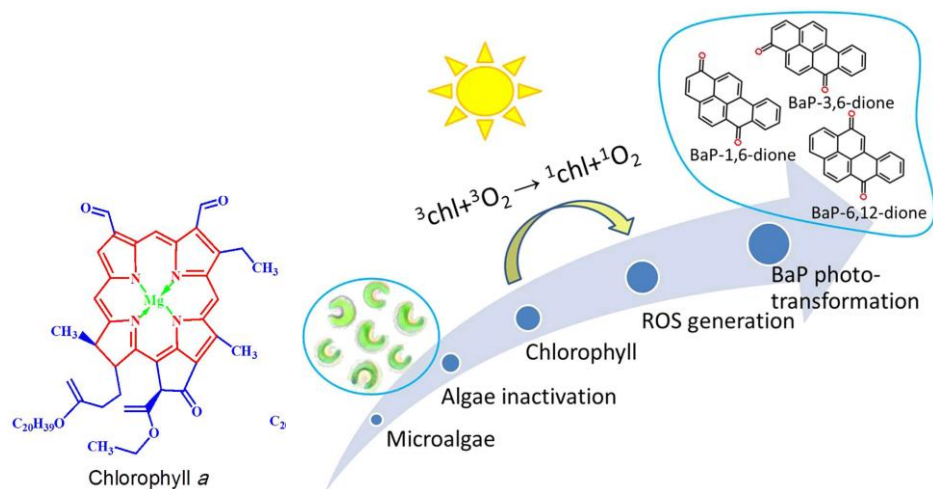
Figure 81. Mechanism of dead algal cells accelerating the photo-transformation of BaP. Chl, chlorophyll. Reproduced with permission from ref [902]. Copyrigth 2015 Springer Nature.

Cyanobacteria are a group of photosynthetic bacteria that lives in a wide variety of moist soils, water and obtaining energy via photosynthesis. Most cyanobacteria are oxygenic photoautotrophs, and thus their growth and survival is highly dependent on effective utilization of incident light.[903] These microorganisms produce various phytochromes and cyanobacteriochromes that allow these cells to respond to light in the range from 300 to 750 nm with photosynthetic enzymes comprising, among others, oxidoreductases allowing to photooxidize water. Thus, cyanobacterial species, such as *Microcystis aeruginosa* are able to remove the widely used drug, tetracycline, even at high concentrations. Similar behavior has been observed for chlorophyte alga *Chlorella pyrenoidosa*.[904]Other pharmaceutical water contaminants such as doxylamine,[905] carbamazepine[906] and also microplastics[907] have also been treated with photosynthetic cyanobacteria under illumination.

The effect of the light in the photobiodegradation of the various compounds has been demonstrated in the debromination of polybrominated diphenyl ethers on cyanobacterium *Microcystis flos-aquae*.[908] where 5 to 11 times more debromination products were measured at a light intensity of 100 μmol photons m^{-2}s^{-1} than at 20 μmol photons m^{-2}s^{-1}. Living cultures of *Microcystis flos-aquae* transformed the polybrominated ethers at a rate of 0.22 day^{-1} while no transformation was observed in the respective autoclaved cultures. Also, the cyanobacterium led to an additional hydroxylation of the aromatic ring (Figure 82).
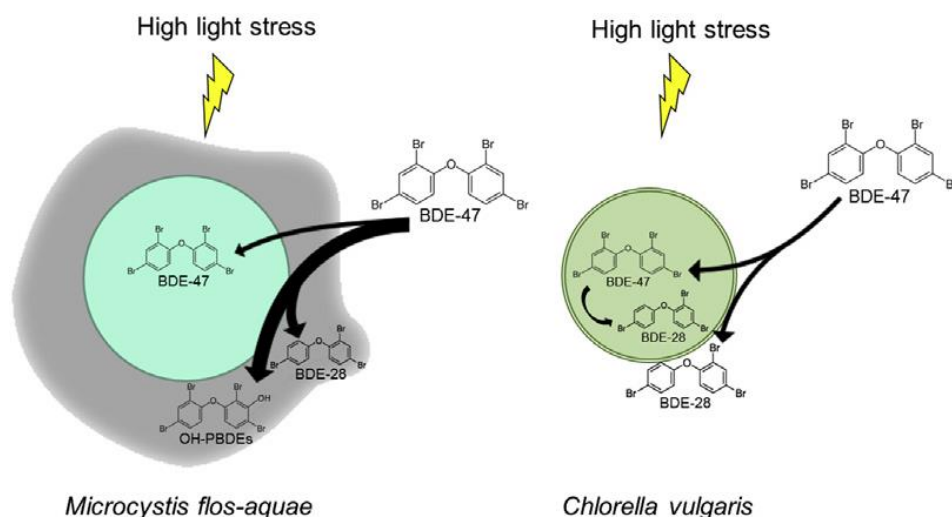
Figure 82. Comparative debromination of polybrominated diphenyl ethers in the presence of *Microcystis flos-aquae* and *Chlorella vulgaris*. Reproduced with permission from ref [908]. Copyrigth 2019 Elsevier.

4.2.2 Heterogeneous photocatalysis in tandem with biocatalysis

The association of fungal membrane bioreactor (FMBR) and photocatalytic semiconductor membrane reactor (PMR) (Figure 83) offers an example of integrated fungal biodegradation and photocatalytic degradation of textile wastewater from reactive washing processes.[909] In the integrated system, the photocatalytic degradation was employed as a post-treatment application after the fungal biodegradation process (working with *Coriolus versicolour*, *Trametes versicolor* or *Phanerochaete chrysosporium*). The tandem process led to higher removal efficiency expressed through color removal and chemical oxygen demand (93 and 99%, respectively) compared to simple photocatalytic degradation on TiO_2 (88 and 53%) or ZnO (53 and 21%) photocatalysts, or to independent fungal biodegradation using Phanerochaete chrysosporium efficiencies (56 and 60%), respectively.[909]
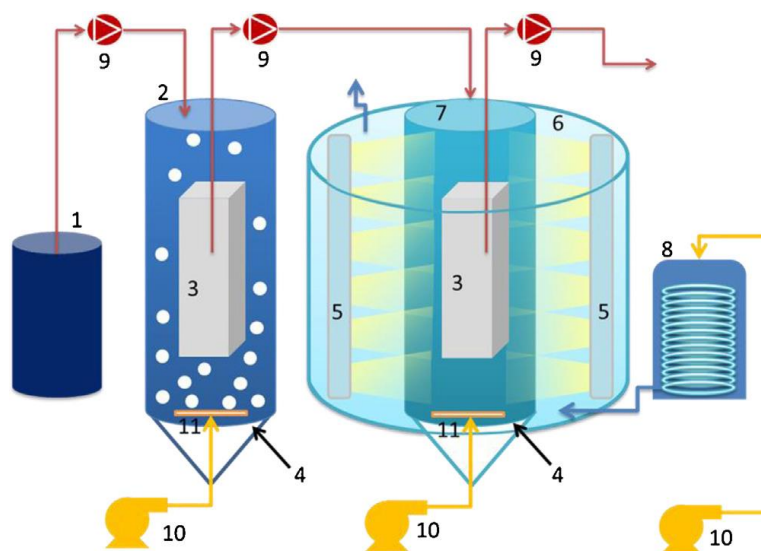
Figure 83. Experimental setup of the sequential photocatalytic membrane reactor and fungal membrane bioreactor integrated process: 1. Stock waste-water; 2. Pyrex glass reactor; 3. Membrane module; 4. Fritz filter; 5. UVA lamps; 6. Reflecting lid for keeping the light in; 7. Pyrex glass reactor; 8. Ice vessel; 9. Peristaltic pump; 10,11. Air blower. Reproduced with permission from ref [909]. Copyrigth 2016 Elsevier.

Coupling powder photocatalysts with homogeneous biocatalysts represents another route to achieve photobiodegradation. Copper modified g-C$_3$N$_4$ as photocatalysts could effectively improve the dehydrogenase activity, which indicated that the biocompatibility of these catalysts had a very good protective effect on activated sludge. Thus, the presence of Cu-g-C$_3$N$_4$ could effectively alleviate the inhibition of residual nitrobenzene on microbial activity in simulated waste-water, effectively improving the dehydrogenase activity.[910] While ambient conditions indicated a certain inhibitory effect of nitrobenzene on dehydrogenase, the addition of Cu-g-C$_3$N$_4$ had a positive effect on the activity reducing in a large extent the toxicity of nitrobenzene. The process has been described through consecutive reactions in which after photocatalytic degradation of nitrobenzene, part of it was mineralized, while another part was decomposed into small molecules that were degraded by the living microorganisms as nutrient substrates for growth, so the growth and metabolism of activated sludge showed a strong trend.

4.2.3 *In-situ* production of H$_2$O$_2$ in the context of water treatment

The combination of light, photocatalyst and enzyme can be useful for *in-situ* production of H$_2$O$_2$. Under UV or visible light irradiated, the photocatalyst can be excited and abstract an electron from ethylenediaminetetraacetic acid (EDTA) acting as electron donor. Afterwards, the reduction of oxygen to hydrogen peroxide can occur. Once formed, H$_2$O$_2$ serves as substrate

to catalyze an enzyme reaction (Figure 84).[911] The slow step of the process is photoactivation process which can be speed up by increasing light intensity and/or the amount of the photocatalyst.[912] Such concept can be powerful due to its simplicity and cost-efficiency. On the other hand, some limitations have been identified related to the use of EDTA. Indeed, harmful environmental side products, such as formaldehyde and ethylene diamine can form, but the substitution by formate can avoid such deleterious effects.[913] Another important drawback can be related to the stability and the robustness of enzyme. As aforementioned, increasing the light intensity and temperature have a benefit in terms of rate in conversion, but this one can be counter balanced by the degradation of the enzyme. Future studies should explore enzymes from more thermophilic organisms that also have some tolerance to UV light.
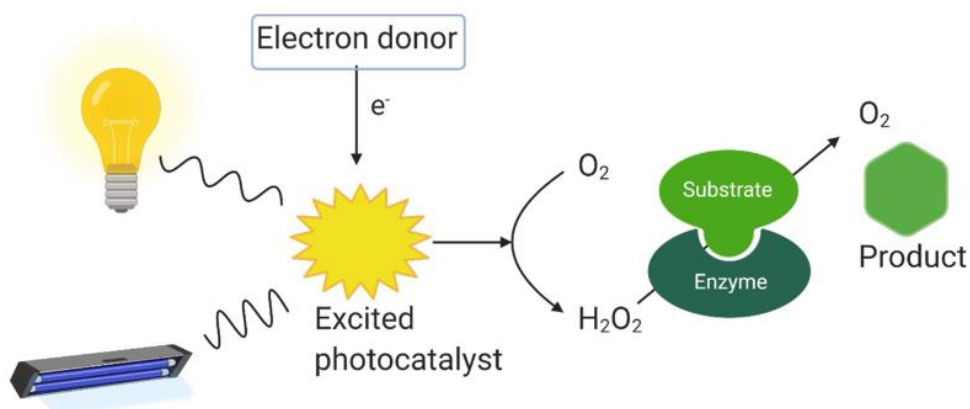
Figure 84. *In-situ* production of hydrogen peroxide by combining photocatalyst irradiated by UV or visible light. Once reduced by an electron donor, oxygen is reduced to hydrogen peroxide. Afterwards, H_2O_2 is used to catalyze an enzyme reaction. Reproduced with permission from ref [911]. Copyrigth 2021 Elsevier.

4.2.4 Metal sequestration in waste waters through hybrid photo and biocatalysis

Tandem microbe-photocatalyst systems, which behave as a semi-artificial photosynthetic system, have been considered to treat organic contamination in water and for the sequestration of heavy metals as well.[914] These combined treatment systems integrates microbial cells with artificial photocatalysts for solar-to-chemical conversion (Figure 85).
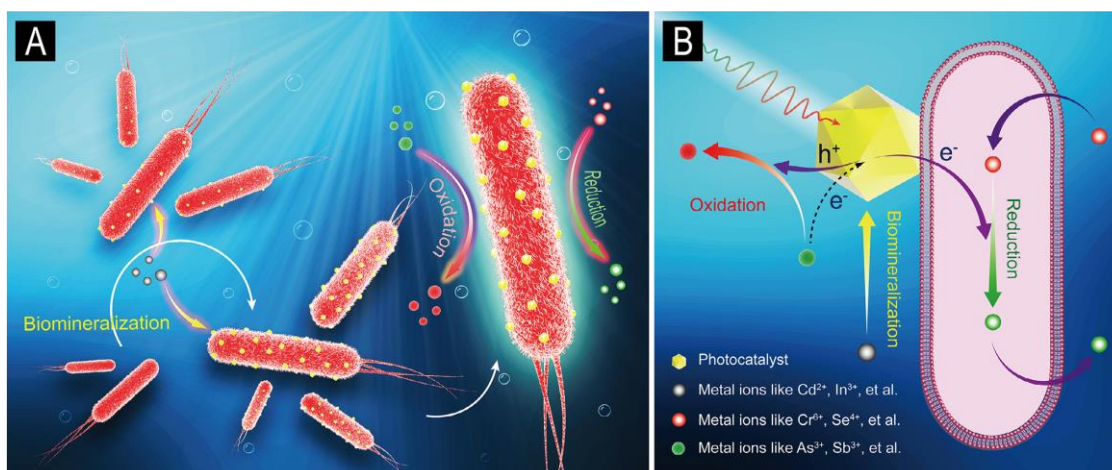
Figure 85. (A) Schematic diagram of the synthesis of microbe-photocatalyst hybrids (MPH) based on the mineralization ability of microorganism; (B) Mechanism of the directional transfer of electrons between different metal ions in the hybrid system driven by light. Reproduced with permission from ref [914]. Copyrigth 2021 Elsevier.

This concept is applicable to the simultaneous remediation of multiple heavy metal pollutants in wastewater such as Cd^{2+}, Pb^{2+}, Cu^{2+}, Zn^{2+} or In^{3+} by microbial mineralization (taking Bacillus thuringiensis HM-311 as biocatalyst) and the formation of metallic mineral particles with photocatalytic activity on the surface of the microorganisms.[914] The synthesized photocatalytic nanomaterials generate electrons under illumination, and transfer these electrons into the microbial cells with several positive effects: i) promote the intracellular enzymatic reduction of metals that are toxic as high-valence ions (such as Cr^{6+}, Se^{4+}) in the wastewater; and ii) maintain the continuous operation of the MPH, whereby these metal ions are simultaneously oxidized and detoxified (Figure 85).

4.2.5 Prerequisites to optimize photobiocatalytic processes: From sequential to intimate coupling.

In case of sequential approaches, photocatalytic and biocatalytic processes have to occur together for a simple optimization to get complete mineralization and biodegradation as prerequisite to downsize to installation. In this configuration, photocatalytic process can transform recalcitrant water contaminants into molecules that will be more readily converted during the biocatalytic step. Previous investigations revealed that operating parameters such the light wavenumber, catalyst, residence time can be easily tuned for efficient biodegradation of phenolic compounds (2,4,5-trichlorophenol as representative compound) in steady-state conditions.[915] It has been shown that dechlorinated and aliphatic compounds lead to highest

efficiency during the biological post-treatment. Nevertheless, particular attention must be paid in the presence of very low concentration of chlorinated and aromatic molecules which intensify the inhibitory effect leading to deactivation. Accordingly, optimal conditions are requested to avoid a quasi-complete dechlorination during the first step to preserve the efficiency of enzyme.

Intimate coupling of photo and biocatalytic treatment needs careful precautions to take advantage of possible synergy effect. Indeed, the sensitivity to enzymes and bio-organisms to UV light, toxic substrates, and OH radical attack in case of advance oxidation catalytic process can lead to their deterioration. Some advantages have been pointed out in the development of hierarchical materials.[759]Ordered macro/mesoporous SiO_2-TiO_2. The biofilm can be located inside the porous structure of the materials offering a better protection while open pores (macropores) can improve light diffusion and the hydrodynamics of the systems (Figure 86)
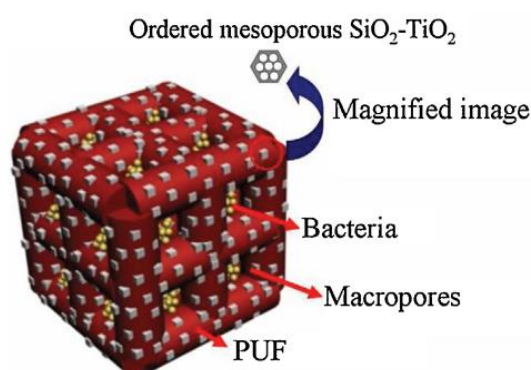
Figure 86. Schematic view of the floating macro/mesoporous SiO_2–TiO_2/PUF carrier. Reproduced with permission from ref [916]. Copyrigth 2016 Elsevier.

4.3. Photoelectrocatalysis

4.3.1. Principle

The coupling of photocatalysis with electrocatalysis processes is an interesting way to increase hole lifetime by hindering the recombination of electron-hole pairs. Consequently, light and electrical energy are necessary for this process, which allows separating the e^-/h^+ pairs photogenerated at the surface of a semiconductor by applying a small bias potential on a conductive surface on which the semi-conductor is deposited. Compared to electrocatalysis, much lower potential is required to reach the complete mineralization of the pollutants due to

the participation of photons from light source to the process. For n-type semi-conductors, the photogenerated electrons at the anode are extracted by the external electrical circuit, concentrated in the cathode and cannot recombine with the holes. Thus, only holes at the surface of the anode remain available for surface reaction either with water to produce strongly oxidizing hydroxyl radical species or directly with pollutants to degrade them (Figure 87). It is also important to specify that, even if the studies of the oxidation of water pollutants are mainly focused on the photoanode[917], photogenerated electrons transferred to the cathode can be used to increase the degradation efficiency of organic pollutants, since solubilized O_2 can be reduced in the reactor leading to reactive oxygen species, of which the nature depends on the composition of the cathode[13,917]. The electrons can also be collected, and photocatalytic fuel cells are able to produce electricity energy while treating wastewater under solar light[918]. Electrons may also be used for water splitting for generating another energy vector, H_2[919].
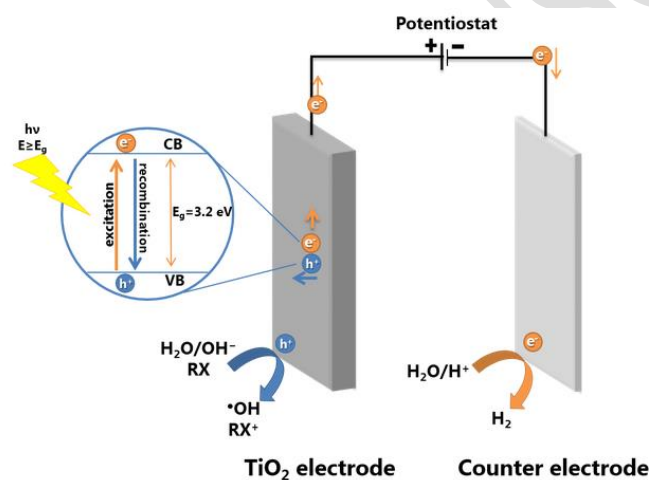
Figure 87. Scheme of the Photoelectrocatalysis process for a n-type semiconductor deposited on a photoanode. Reproduced from ref. [920]. Copyrigth 2019 IntechOpen.

For photoelectrocatalysis, the semiconductor must be deposited on a conductive substrate, the ensemble constituting the photoelectrode. As a consequence, photoelectrocatalysis involves at minimum two interfaces, one between the semiconductor and the conductive substrate and the second one between the semiconductor and the electrolyte. Thus, the performance of the photoelectrocatalytic process depends on all the constituents, not only on the electrolyte (Temperature, pH value, presence of dissolved oxidants, the electrolyte ions) and the nature and morphology of the semiconductor, as for photocatalysis, but also on the nature of the substrate[921]. To improve the process, and especially the charge transfer to the reactants, cocatalysts may be introduced between the semi-conductor and the electrolyte, as well as an

interlayer between the semi-conductor and the cocatalyst to better improve the charge separation and transfer and protect the photoanode from corrosion[922]. On the other hand, the conductive substrate-semiconductor interface is of major importance for the electron collection process to avoid a "back electron-hole recombination"[923], and various interlayers may be inserted between the semiconductor and the conductive substrate to improve the electron extraction[922,924].

4.3.2. Photoelectrocatalysts for water treatment

The first studies on photoelectrocatalytic water treatment were performed in the earlier 1990's[925] on an usual photocatalyst, TiO$_2$, in the form of film of low porosity obtained by depositing TiO$_2$ powders on various conductive substrates such as conductive transparent glasses, such as Fluorine doped tin oxide (FTO) or indium tin oxide (ITO) glass, or on Ti plates. It was demonstrated as efficient photoelectrocatalyst for degrading a wide range of pollutants such as chlorophenol, various dyes or bisphenol A[919]. As for photocatalysis, improvements in photoelectrocatalysis were reached by nanostructuring TiO$_2$ in the form of nanotubes, nanorods and nanowires, leading to an increase in the surface area, thus enlarging the semiconductor/electrolyte interface, reducing light-scattering loss and improving the charge transfer. The first TiO$_2$ nanofibers were synthesized in the form of powder by hydrothermal dehydration[926] and thereafter various sol-gel and hydrothermal routes were successfully applied to generate nanorods or nanotubes[919]. The main drawback of these synthesis methods is a wide distribution of tube geometries obtained in solution, which form arbitrary organized tubes or bundles when compacted to the conductive substrate [927]. One solution arose with the use of templates to orientate the growth of TiO$_2$ nanotubes but the most significant enhancement in that domain was gained with the synthesis of self-organized TiO$_2$ nanotube arrays by electrochemical anodization of metallic Ti plates. This synthesis method presents many advantages such as an easy control of the growth properties by adjustment of the applied potential, anodization time and electrolyte composition, and the direct obtaining of a photoanode[13,919] while the self-alignment improves the photoelectrocatalytic performance. Various types of nanostructured TiO$_2$, reviewed in [919], demonstrated their efficiency for the photoelectrocatalytic degradation of many pollutants. As for photocatalysis, various metal (Cr, Fe, Cu etc.) and non-metal (B, N) were added as dopants to TiO$_2$, or TiO$_{2-x}$ composites were synthesize, with X = metals (Ag, Pd, Au etc.), oxides (SiO$_2$, WO$_3$ etc.), sulfides (CdS, etc.) or carbon in order (i) to shift its optical response from ultraviolet towards visible light by

199

decreasing the band gap energy or (ii) to favor the separation of e-/h+ charges; some examples may be found in [13,919875] Apart from TiO_2-based photocatalytic materials, other photoanodes, based on W (WO_3, Bi_2WO_6, $ZnWO_4$), α-Fe_2O_3, Sb-SnO_2 or ZnO have demonstrated their high efficiency for the photoelectrocatalytic removal of pollutants as reviewed in [13].

p-n heterojunction photoanodes also constitute promising materials for photoelectrocatalysis. When two semiconductors with different Fermi levels are put in contact, photogenerated e- and h+ are exchanged until the thermodynamic equilibrium is reached, giving rise to two regions with opposite charges, e- on the one side, h+ on the other side. This kind of materials allows tuning the oxidative power of holes of the photoanode for limiting the formation of undesired by-products. For example, ammonia oxidation may be enhanced by using chlorine radicals but generating toxic nitrate and chlorate species. By associating WO_3 to $BiVO_4$, it was possible to tune the valence band position and consequently to regulate the oxidizing ability of photogenerated holes, avoiding the over-oxidation of ammonia and chloride[928]. Conducting polymers such as polyaniline (PANI), polypyrrole (PPy) or poly(3,4 ethylenedioxythiophene) (PEDOT) can also serve as electron acceptors, electron donors and photosensitisers that can be deposited on inorganic semiconductors such as TiO_2 by spin-coating or electropolymerization, to improve their photoelectrocatalytic properties. Thus, TiO_2 nanotube arrays modified by PPy (Figure 88), considered as a p semiconductor, constituted an efficient p-n heterojunction for the decolorization of methylene blue by photoelectrocatalysis, with an improved degradation rate under UV or visible light compare to not modified TiO_2 nanotube array (Figure 88a)[929]. The presence of PPy not only increases the photocurrent density under UV irradiation but enlarge the light adsorption range of the photoelectrode to visible light (Figure 88b).
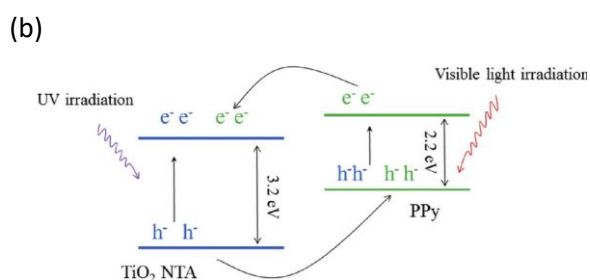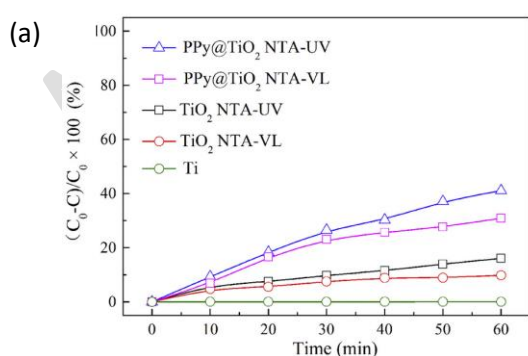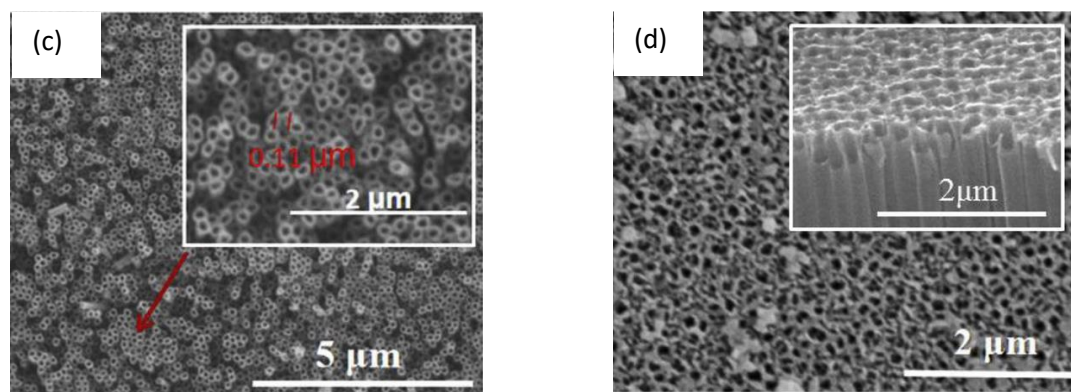
Figure 88. Conversion of methylene blue as a function of time in the presence of TiO$_2$ plate, TiO$_2$ nanotube array (TiO$_2$ NTA) alone or modified by electrodeposition of PPy (PPy@TiO$_2$ NTA) by photoelectrocatalysis under UV or visible light (VL) irradiation and applied voltage (15V) (a) photocurrent of TiO$_2$ NTA and PPy@TiO2 NTA under visible light irradiation (b). SEM image of TiO$_2$ NTA (c) and PPy@TiO$_2$ NTA (d). Adapted with permission from ref. [929]. Copyrigth 2020 Elsevier.

Beyond the fact that photoelectrocatalysis constitutes an interesting way to avoid e$^-$/h$^+$ recombination and thus enhance the oxidation efficiency, the electrons collected at the cathode can be valorized for reduction reactions or to generate electricity or H$_2$ energy vector, which gives another additional value to this process compared to photocatalysis or electrocatalysis.

4.3.3. Combination of photoelectrocatalysis and electroreduction

The main application of the combination of photoelectrocatalysis and electroreduction in wastewater treatment concerns the simultaneous removal of organic pollutants by photoelectrocatalytic oxidation and of heavy metals by electroreduction. In addition to the use of the photogenerated electrons for reducing polluting metals, a synergy between the two processes may occur, accelerating the removal of the two types of pollutants compared to the single processes[930]. A small external bias potential or current is generally applied to enhance the separation of photoinduced e$^-$/h$^+$ at the photoanode, where the oxidation of the organic pollutants happens, while heavy metals are reduced at the cathode. On the one hand, this combined process may be applied to complete treatment of wastewater containing both types of pollutant. Thus, a large part of the studies are devoted to the reduction of Cr(VI) into much less toxic Cr(III), while many organic pollutants are degraded using this combined process, as for example methylene blue, tetracycline or phenol[930]. An enhancement of the Cr(VI) reduction rate by the presence of the phenol has been observed, attributed to the role of the organic pollutant as a hole trapping, while the reduction of Cr(VI) consumes the photogenerated electrons that cannot recombine with holes, promoting phenol degradation[930].

p-n heterojunction can also be used for the photoanode material to enhance the oxidative properties due to the better separation of the photogenerated e^-/h^+. Figure 89 shows an example of combined removal of an organic pollutant and a heavy metal, Cr(VI). A sophisticated photoanode made of 1D nanowires of Co_3O_4 deposited on a 2D surface of NiFe-LDH supported on 3D Ni foam constituted very efficient p-n heterojunction allowing the removal of bisphenol A (BPA) by photoelectrocatalytic process, in parallel with the reduction of Cr(VI) at the cathode, with more than 95% BPA and Cr(VI) removal at 0.7 V of applied voltage using visible light, while only 40-45% of removal for both pollutants is reached by photocatalysis and 13% for BPA and 5% for Cr(VI) by electrocatalysis[931].
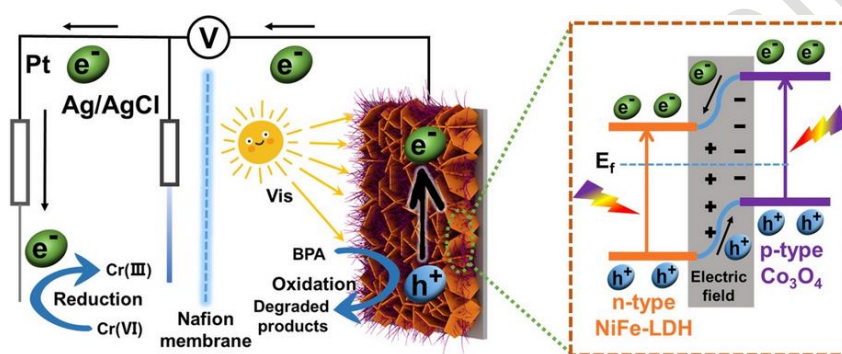
Figure 89. Scheme of a combine system allowing the photoelectrocatalytic oxidation of bisphenol A at the photoanode (a p-n heterojunction NiFe-LDH/Co_3O_4) and the simultaneous reduction of Cr(VI) at the cathode by the photogenerated electrons. Reproduced with permission from [931]. Copyrigth 2021 Elsevier.

On this other hand, the coupling of photoelectrocatalysis and electroreduction allows solving one important problem of wastewater treatment due to the possible interaction between heavy metals, and chelating agents, which is the main limitation of the removal of metal ions by conventional precipitation processes. So, the destruction of the chelating agents, such as tartrate, citrate or ethylenediaminetetracetic acid (EDTA) is possible at the photoanode, favoring the recovery of the liberated metal ions at the cathode. The removal of many complexes were studied, among which mainly Cu(II)-EDTA, Ni(II)-EDTA and Cr(VI)-EDTA[930].

4.4.4. Photoelectrocatalytic pollutant degradation coupled with energy production

Photocatalytic fuel cell (PFC) is a promising process aiming at combining a wastewater photoelectrocatalytic treatment to a simultaneous energy production. In this process, the

photoanode, made of a photocatalyst, is immersed in solution containing the pollutant and the cathode is in contact with an electrolyte solution in another compartment. Upon irradiation, e^-/h^+ are produced at the photoanode and the electrons are transferred to the cathode via an external circuit to generate electricity, while the holes oxidize water and other compounds present in the wastewater. The main advantage of this process is that there is no need to apply an external bias for the photoelectrocatalytic pollutants degradation, which reduces the overall energy consumption of the process. The performance of such combined system depends on the nature of both the photoanode and the cathode, but the PFC performance is primarily determined by the capacity of the photoanode for absorbing visible light and efficiently separating e^-/h^+. Many water pollutants, such as alcohols (methanol, ethanol, propanol), polyols and sugars (glycerol, xylitol, sorbitol, glucose etc.) or other pollutants (Ammonia, urea, surfactants etc.) can be thus degraded by light conversion at the photoanode while producing electricity at the cathode[932]. TiO_2 based photoanodes were successfully used for this type of application, but rapidly replaced by visible light-responsive photoanodes and more recently heterojunction advanced materials as $BiVO_4$/WO_3/W, $BiVO_4$/TiO_2 or WO_3/ZnO/Zn. For example WO_3 loaded on hexagonal rod-like ZnO/Zn constituted a very efficient photoanode not for converting phenol, not only in a model solution but also for treating for the first time an actual food wastewater of high COD concentration with an abatement of 63.6% of the COD while generating a power density P_{max} of 0.498 μW cm^{-2}.[933]

Photoelectrocatalytic water splitting for H_2 production, a storable, clean and renewable energy vector, is another attractive approach for energy recovery when it is coupled with wastewater treatment. At the photoanode, the photooxidation of the organic pollutant takes place according to equation (96):

$$C_xH_yO_z + (2x - z)H_2O + 2 (2x - z + y/2)h^+ \rightarrow xCO_2 + 2(2x - z + y/2)H^+$$

(96)
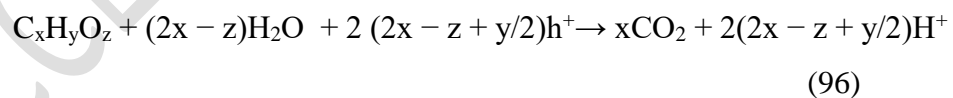
and the hydrogen is produced at the cathode from the electrons according to equation (97):

$$2H^+ + 2e^- \rightarrow H_2 \tag{97}$$

corresponding to the overall reaction:

$$C_xH_yO_z + (2x - z)H_2O \rightarrow xCO_2 + (2x - z + y/2)H_2 \tag{98}$$
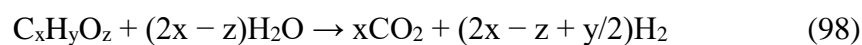
which in turns corresponds to a reforming reaction.

Materials developed for the photoanode for the oxidation of organic pollutants coupled with production of hydrogen were reviewed by Lianos in 2011[934]. Since then, doped TiO_2 nanotubes arrays have been continuing to be the most studied materials for this kind of process[935-936]. Recent progresses were made in that domain when new kind of photoelectrocatalysts emerged able to store the electrons photogenerated under light illumination, and to release them in the dark. Thus light harvesting materials, based on WO_3 or MoO_3 that can store and release electrons, are very promising materials developed for this application. For example, dual-photoelectrodes solar-charged photoelectrochemical wastewater fuel cell (scPEWFC) made up of WO_3 at the anode and Cu_2O nanowire arrays at the cathode were not only able to produce *ca.* 3 times more H_2 than that of pure photocatalytic water splitting while removing phenol by photoelectrocatalytic oxidation under visible light without additional bias, but also to continue to produce H_2 under the dark.[937].

Other systems, presenting triple functions, are able to generate both hydrogen and electricity at the cathode while degrading organic pollutants at the photoanode[938].

Finally, in the domain of photoelectrocatalytic conversion of pollutants coupled with valorization processes, the recent progress concerns the production of syngas by reducing the CO_2 produced at the photoanode into CO at the cathode, in parallel to the reduction of water into H_2 thus producing syngas[939] or methane.

4.3.5. Other type of coupling for photoelectrocatalytic pollutant degradation

As in the photoelectrocatalytic process, the efficiency of the pollutants degradation is mainly dependent on the photoanode, other ways may be used to improve the efficiency of the process by enhancing the production of reactive radicals, especially for the removal of recalcitrant pollutants. This can be achieved by coupling for example photoelectrocatalytic oxidation of the pollutants at the anode with a photoelectron-Fenton process.

Photoelectro-Fenton (PEF) is an interesting process for degrading herbicides, pharmaceuticals and textile dyes[940], which consists of producing continuously hydrogen peroxide at a carbonaceous cathode by reduction of O_2 gas by the following reaction (equation (99)):

$$O_2 + 2H^+ + 2e^- \rightarrow H_2O_2 \qquad\qquad (99)$$

In the presence of Fe^{2+}, for example, in acidic solution, a reaction occurs between H_2O_2 and Fe^{2+} leading to the production of hydroxyl radicals according the Fenton reaction (equation (100)):

$$Fe^{2+} + H_2O_2 + H^+ \rightarrow Fe^{3+} + \bullet OH + H_2O \qquad (100)$$
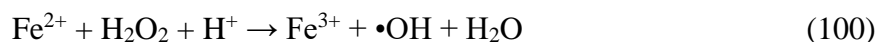
$[Fe(OH)]^{2+}$ species may be also produced that are easily converted into Fe^{2+} and $\bullet OH$ by photolysis, while H_2O_2 may be also decomposed into $\bullet OH$ by photolysis.

It is an electrocatalytic reaction since Fe^{2+} are regenerated by reduction at the cathode of Fe^{3+} into Fe^{2+}. A more interesting way consists in using a cathode able to participate directly to the Fenton reaction instead of soluble ions. Thus, a CuO/Cu_2O cathode favors the formation of $\bullet OH$ by reaction between $Cu(I)$ and H_2O_2, and an increase of the pollutant removal efficiency was observed compared to a single photoelectrocatalytic process[941].

Other types of efficient coupling were recently reported in the literature as the coupling of photoelectrocatalysis and reverse osmosis[942], which is in fact a two-steps process allowing to complete the mineralization of the pollutants after a partial conversion by the photoelectrocatalytic process, or the coupling with electroenzymatic process[943].

4.4 Sono- and sonophotocatalysis for the purification of waste waters

Ultrasonication has been regularly used for oxidative destruction of organic compounds [944-949].Ultrasonication can produce cavitation that can induce chemical reactions due to the release of a high amount of energy within the micro-sized bubbles during their formation, growth, and subsequent collapse in a short fraction of time, producing shock waves of high temperatures and pressure of about 2000 bar in few microseconds [950-951] (Figure 90) Due to such high temperatures, cavitation and hot spots produced by ultrasounds can promote water decomposition and oxygen reduction to form hydroxyl radicals and other oxidative species, as well as the degradation of volatile and hydrophobic molecules.
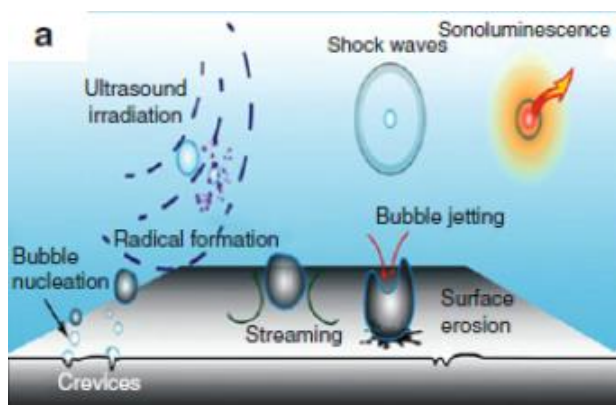
Figure 90. Schematic diagram of the cavitation effect induced by the ultra sound waves. Reproduced with permission from ref [951]. Copyrigth 2016 Springer.

Taking advantage of the ultrasound energy, cavitational reactors, either as an individual treatment method or in combination with other purification processes, have shown considerable promise for wastewater treatment applications in recent years [952]. Furthermore, the application of ultrasound as a source of agitation and activation for other oxidation processes such as those promoted photocatalytically has been reported and this combination gives beneficial results as compared to the results achieved in individual treatments [953].

4.4.1 Sonocatalytic purification of wastewater

The degradation of bisphenol A has been enhanced by a heterogeneous ultrasound-sludge biochar catalyst/persulfate approach that corresponded to a positively synergistic effect between sonochemistry and catalytic chemistry [954]. Breaking down sludge flocks (sonodyspergation effect) and destruction of the cell membranes of microorganisms forming flocks is a direct effect of ultrasonic disintegration of sludge excess affording therelease of organic material by liquid sludge (the sonolysis effect) [955-956]. While coexisting Cl^-, SO_4^{2-} and NO_3^- exerted no inhibition on the degradation, HCO_3^- and humic acid have a significant quenching effect. Both $SO_4^{\cdot-}$ and $HO\cdot$ participate in this degradation process, but $SO_4^{\cdot-}$ have a predominant role. The possible pathway includes five intermediate products resulting through hydroxylation and demethylation processes (Figure 91).
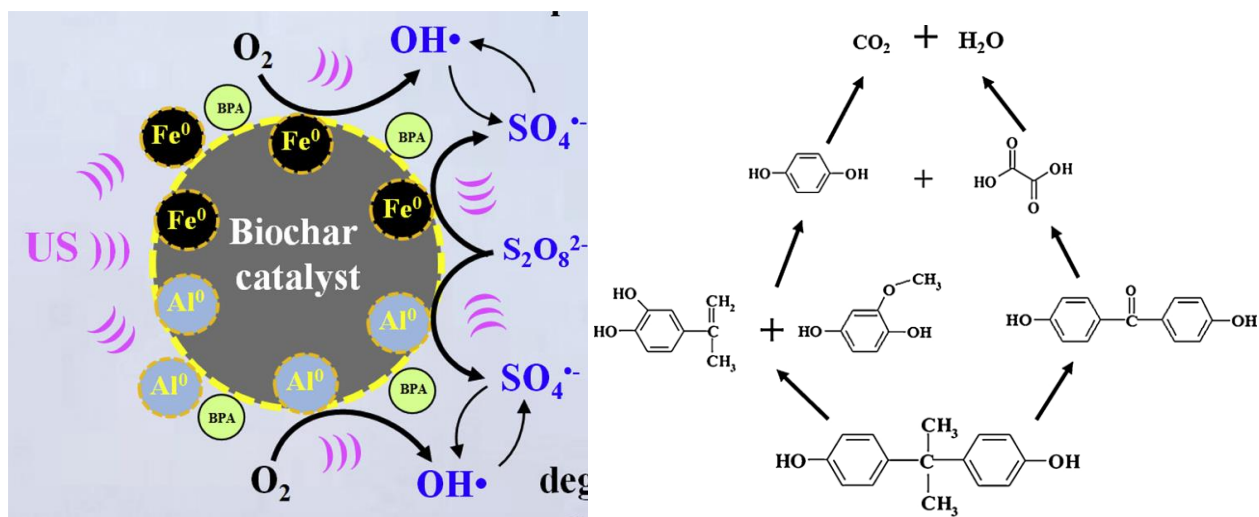
Figure 91. Reaction mechanism of bisphenol (BPA) degradation by biochar catalyst in a persulfate/ultrasound process. Adapted from ref [954]. Copyrigth 2020 Elsevier.

The system of persulfate as oxidizing reagent and Zn(0) as catalyst has been activated by low frequency ultrasound generated from an ultrasonic bath for the degradation of nitrobenzene. The synergistic effect in the ultrasound/Zn(0)/persulfate is associated to the formation of free radicals [957].

$$Zn^0 + S_2O_8^{2-} \rightarrow Zn^{2+} + 2SO_4^{\bullet-} \qquad (101)$$

$$SO_4^{\bullet-} + H_2O \rightarrow HSO_4^- + {}^{\bullet}OH \qquad (102)$$

Bromate is a potential carcinogenic compound that can form during the disinfection of drinking water. A study on the influence of the ultrasound frequency on the sonocatalytic reduction of BrO_3^- on TiO_2 has observed the occurrence of sonoluminescence at an ultrasound frequency of 500 kHz. Ultrasound cavitation enhanced the H_2 production and increased BrO_3^- reduction rate by increasing the number of TiO_2 conduction band electrons [958].

$$TiO_2 \rightarrow e^- + h^+ \qquad (103)$$

$$h^+ + OH^- \rightarrow {}^{\bullet}OH \qquad (104)$$

$$2 \, {}^{\bullet}OH \rightarrow H_2O_2 \qquad (105)$$

$$BrO_3^- + 6H^+ + 6e^- \rightarrow Br^- + 3H_2O \qquad (106)$$
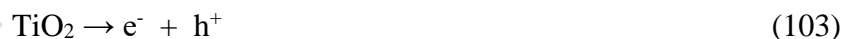
Catalytic ultrasonication using Ce-based catalysts has been often reported in advanced oxidation processes for organic wastewater treatment. Its association with MnO_2 homogeneously dispersed onto the surface of CeO_2, MnO_2/CeO_2 catalyst, enhanced the oxidation ability of

ultrasound and realized complete decolorization of methyl orange [959]. The main active species was $^\bullet OH$, which was produced by the decomposition of H_2O_2 by leached Mn^{3+} and Ce^{3+} cations (Figure 92). Noteworthy, the mechanism of methyl orange degradation is quite different compared to that in the ultrasound-MnO_2 system.
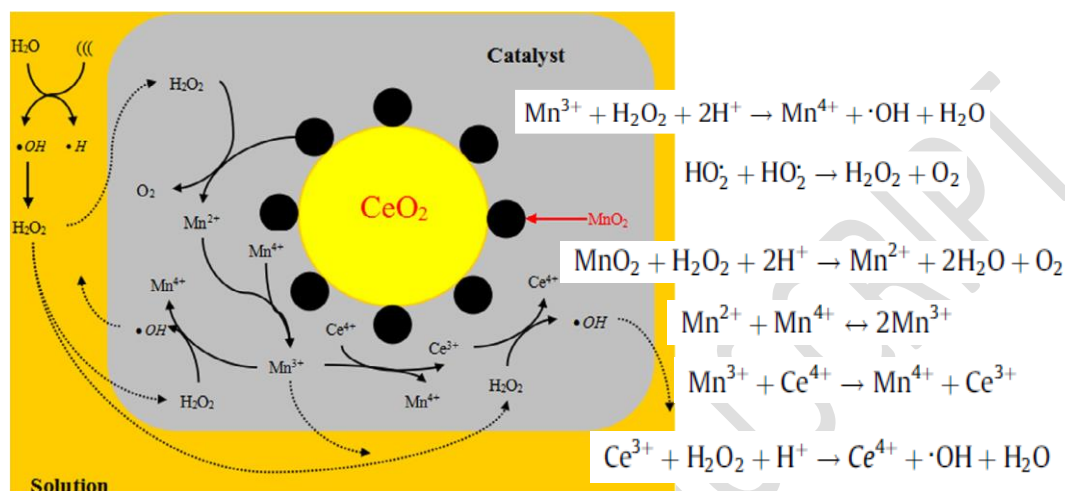
Figure 92. Schematic reaction mechanism in the catalytic ultrasonic oxidation over MnO_2/CeO_2. Adapted from ref [959]. Copyrigth 2015 Elsevier.

Degradation of diclofenac by combining $FeCeO_x$ with ultrasounds follows a similar mechanism, the redox Mn^{3+}/Mn^{4+} being replaced by a Fenton Fe^{2+}/Fe^{3+} catalyst. According to the author's proposal, the produced H_2O_2 is further transformed into reactive $^\bullet OH$, $^\bullet OOH$ and $^1O_2$ radical species [960-961]. The formation of these radical species correlates with the presence of abundant oxygen vacancies on $FeCeO_x$ surface. The degradation process includes hydroxylation, decarboxylation, dehydrogenation, and C-N cleavage of the diclofenac molecule (Figure 93).
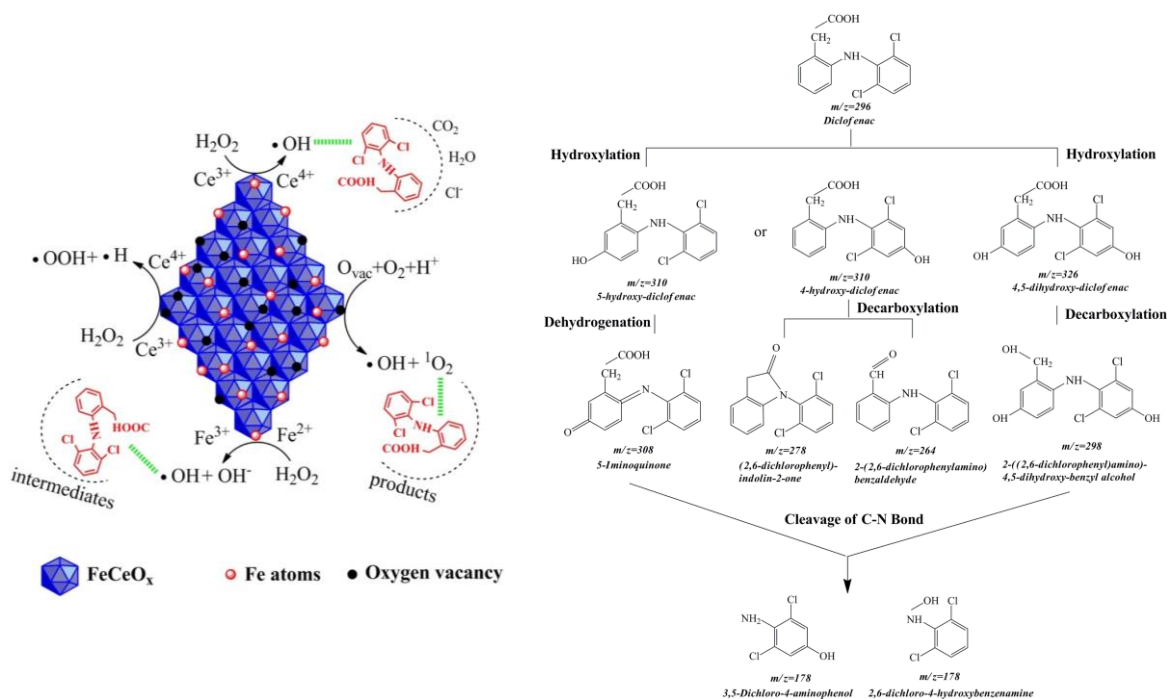
Figure 93. Diclofenac reaction mechanism in a $FeCeO_x$-H_2O_2 Fenton-like process, and b) its degradation pathways. Adapted from ref [961]. Copyrigth 2017 Elsevier.

Overall, the degradation rate only by combining ultrasonication with catalysis is slow compared to other established methods. Enhancing the efficiency of sonocatalysis could be only achieved by combination with other advanced oxidation processes such as photocatalysis.

4.4.2 Sono-photocatalysis

A sonophotocatalytic reaction has been defined as a photocatalytic reaction with ultrasonic irradiation or the simultaneous irradiation of light and ultrasound in the presence of a photocatalyst [962-964]. The association of sono-, photo- and catalysis into sonophotocatalysis provides favorable conditions to enhance the formation and participation of reactive oxygen species like $^\bullet OH$, $^\bullet HO_2$, $^\bullet O_2$, H_2O_2, etc. Among these, H_2O_2 is the most stable but it may serve as a precursor for the reactive free radicals. Thus, hybrid photocatalysis and sonolysis allows chemical processes difficult or even not possible to be promoted by photocatalytically or by ultrasounds independently, such as the decomposition of water to H_2 and O_2 [965]. As a photocatalytic requirement, the combined process needs a light-sensitive material prone to induce an O_2 evolution in water. TiO_2, ZnO and various mixed oxides such as $BiVO_4$ are among the most common and investigated materials as photocatalysts [951,966].

Besides optical properties, to be effective, the catalyst should present a suitable particle size. In this regard, ultrasound may enhance the rate of photocatalytic degradation by promoting photocatalyst disaggregation, by inducing the desorption of organic substrates and degradation intermediates from the photocatalyst surface and, mainly, by favoring the scission of the photocatalytically and sonolytically produced H_2O_2, with a consequent increase of oxidizing species in the aqueous phase [967]. The phase composition of TiO_2 and particle size are important parameters, as demonstrated for TiO_2 photocatalysts with an optimized anatase/rutile ratio. These samples were obtained by modification with polyethylene glycol and exhibited a satisfactory activity and stability for the degradation of rhodamine B. The most efficient catalysts was the sample having an optimal crystallite and particle size [968].

Sonophotocatalytic degradation of wastewaters with TiO$_2$ photocatalysts

As described in previous sections, photocatalysis over TiO_2 or other semiconductors [969]is definitely useful in advanced oxidation process for wastewater treatment. Photoexcitation of semiconductor TiO_2 promotes valence band electrons to the conduction band, thus, leaving an electron deficiency or hole in the valence band. Holes can react with water molecules to form OH radicals, which subsequently can attack the pollutant [969]. The synergistic effect of photocatalysis with sonolysis is also the result of the enhancement of mass transfer rate of contaminants and intermediates between the liquid phase and the solid phase of catalyst [970]. The synergism is particularly notable at the low concentration characteristic of emerging contaminants as demonstrated for the sonochemical degradation of rhodamine B, for which intensification studies demonstrated a 93% removal rhodamine B of a very low concentration (10 ppm) [948]. In a lesser extent, grafting titanium onto a mesoporous SBA-15 silica support afforded Eriochrome Black T decolorization (ca 89 %) through a sonophotocatalytic degradation under visible light irradiation [971].

The combination of sonocatalytic, photocatalytic and sonophotocatalytic processes taking TiO_2 as catalyst has been investigated for the degradation in aqueous solutions of many water pollutant molecules such as phenol [972], 2-chlorophenol, gasoline additives such as *tert*-butyl ether [973-974], building block chemicals for the production of polyesters [975], polymer plasticizers [976], numerous azo dyes [977] as acid orange 8, acid red 1 [967], reactive brilliant orange K-R [978], congo-red and methyl-orange [923], endocrine-disrupting chemicals as bisphenol, diethylstilbestrol, or pentachlorophenol [979], pesticides as methyl 1-[(butylamino)carbonyl]-1H-benzimidazol-2-ylcarbamate (benomyl) [980] and herbicides as isoproturon [981], and complex pharmaceutical wastes [982] as the antiepileptic carbamazepine or diclofenac [970]. It was

demonstrated that, the occurrence of synergy effects during sonocatalytic, photocatalytic and sonophotocatalytic degradation of hydroquinone depend on the amount and size of microbubbles. [983] The size of the bubbles and cavitation hole also influence the efficacy in H_2O_2 formation.

The disposal of the TiO_2 nanoparticles may also be associated to the sonophotocatalytic degradation of phenol wastes [984]. Accordingly, the deposition of these nanoparticles on a hexafluoropropylene tetrafluoroethylene microtube under mild conditions using ultrasound technique occured with changes in the polymer surface resulting in the formation of thin layer of TiO_2 nanoparticles in the inner walls of the microtube with increased photocatalytic activity.

No important differences have been observed in the nature of degradation intermediates formed for different substrates under similar conditions, indicating the involvement of similar reaction mechanisms. The degradation pathway of ibuprofen included mainly decarboxylation, demethylation and hydroxylation reactions, while the oxidation of diclofenac, mainly proceeded by oxidation and hydroxylation reactions between chloroaniline and phenylacetic acid [985].

For such complex molecules sonophotocatalysis provided good reaction rates, while the degree of removal was below 50%. However, acute toxicity tests showed an increase in toxicity over the time-course of the studied treatments [970]. Experiments carried out directly with pharmaceutical industry wastewaters confirmed the limitations of this approach [986].

Coupling of sonolysis and solar photocatalysis using titanium dioxide, two complementary advanced oxidation synergistic processes were identified for the degradation of bisphenol A as model organic pollutant [987]. Thus, ultrasound irradiation was mostly participating in the disappearance of the target pollutant, while photocatalysis proved to be more efficient for reaching mineralization. However, depending on the catalyst loading the synergistic effect may be inhibited by an effect of the titanium dioxide on the cavitational processes. Also, a luminescent device producing a piezoelectric effect enhanced the synergetic effect of sonolysis and photocatalysis with TiO_2 [988].

The pH of the waste solution is an important parameter in these processes. Ultrasound exposure cumulated with the photocatalytic effect of TiO_2 suggested that a neutral pH as 7 is favorable for an enhanced degradation [989].

An advanced degradation of the water pollutants could be achieved by the addition of H_2O_2 or ozone. This allowed the decomposition of herbicide propyzamide in aqueous solution (Figure 94) [990]. However, for the degradation of reactive black 5 dye in aqueous solutions a simple combination of photocatalysis with the addition of H_2O_2 hindered the process due to

scavenging of the photogenerated holes and hydroxyl radicals [991]. TiO_2 photocatalysis has been also enhanced in the presence of low doses of peracetic acid affording the inactivation of *E. coli* aqueous suspensions at relatively short contact times [992].
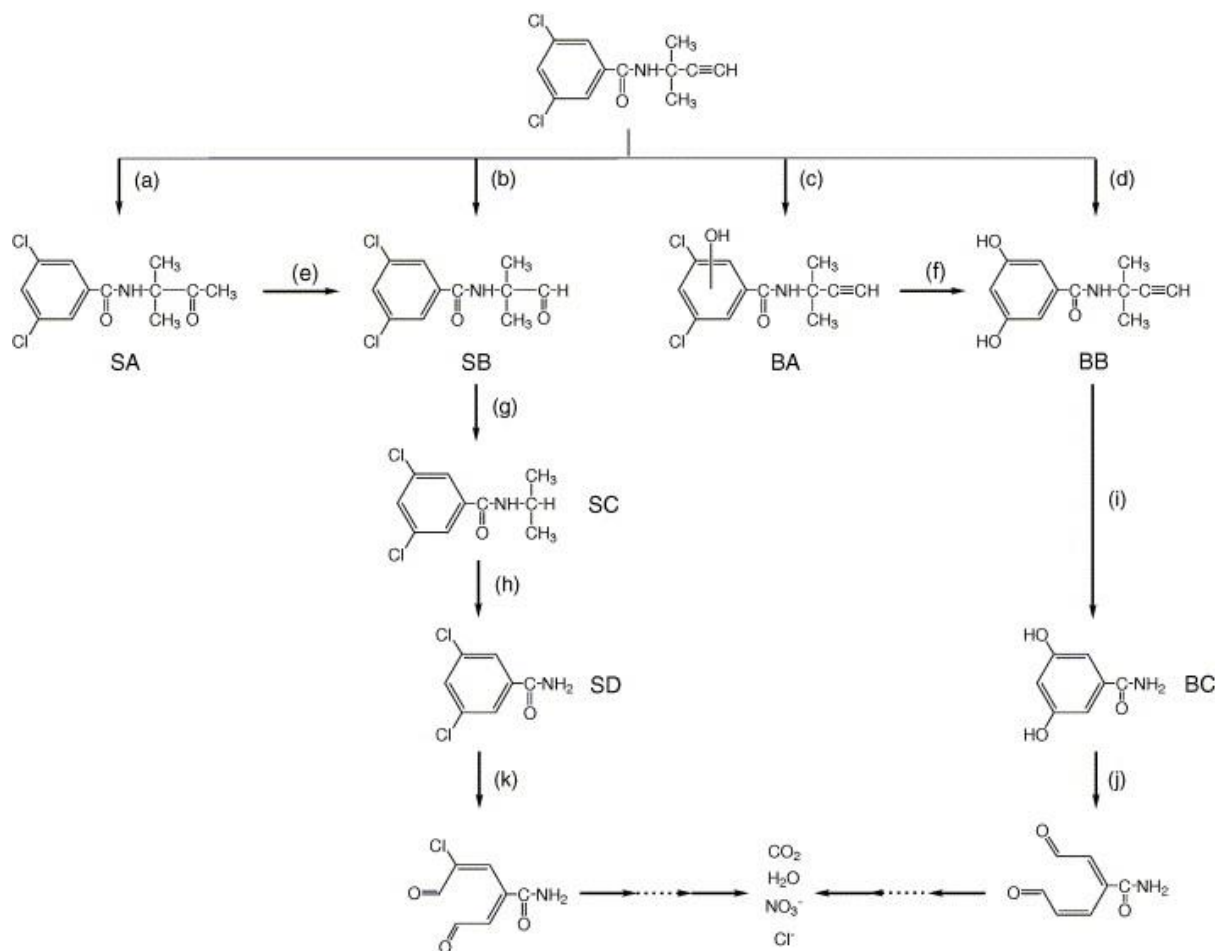
Figure 94. Decomposition of 3,5-dichloro-N-(3-methyl-1-butyn-3-yl)benzamide (propyzamide herbicide) by a concerted effect of sono- and photocatalysis with addition of H_2O_2. Reproduced with permission from ref [990]. Copyrigth 2005 Elsevier.

Ultrasound irradiation and its combination with heterogeneous TiO_2 has also been coupled with homogeneous photo-Fenton catalysis for the degradation of malachite green in water [993]. The addition of H_2O_2 and $FeCl_3$ favored indeed dye decomposition, but the mineralization was slower due to the formation of stable by-products accompanied by the release of nitrates to the solution. Additional experiments carried out with bisphenol A as pollutant showed that ultrasound has the principal role of eliminating the initial substrate and providing hydrogen peroxide for the photocatalytic systems, while photo-Fenton and TiO_2 photocatalysis are mainly responsible for the transformation of the intermediates in CO_2 and water [994]. More complex catalysts resulted from the association of iron with TiO_2-Ce catalysts [995]. As an effect

the band gap energies decreased from 2.50 eV for TiO_2 to 2.40 eV for TiO_2-Ce that corresponded to an increased degradation yield of the Reactive Yellow 84 dye.

The synergistic effects between ultrasound and UV irradiation depends on several factors also including the chemical properties and concentration of not only the substances initially present, but also their decomposition intermediates [996]. Thus, the iron catalytic activity, as demonstrated for the degradation of the biorecalcitrant pharmaceutical micropollutant ibuprofen, was only slightly enhanced by the ultrasonic irradiation [997-998] while there was no effect for Monocrotophos organophosphate insecticide removal [999].

Besides, the essential parameters such as solution temperature, concentrations of initial pollutant and catalyst, initial pH, dosages of Fenton's reagent and hydrogen peroxide, ultrasonic power density, gas sparging, presence of radical scavenger, the addition of a cosolvent may influence the process. The implementation of doping elements and supports may enhance the degradation rate of pollutants [1000]. Also, an enhancement of the photocatalytic activity towards the visible light spectrum could be achieved by doping with noble metals, narrow band gap semiconductors such as Bi_2O_3 or rare-earth dopants such as Gd^{3+}, Nd^{3+} or Y^{3+} (Figure 95) [1000].
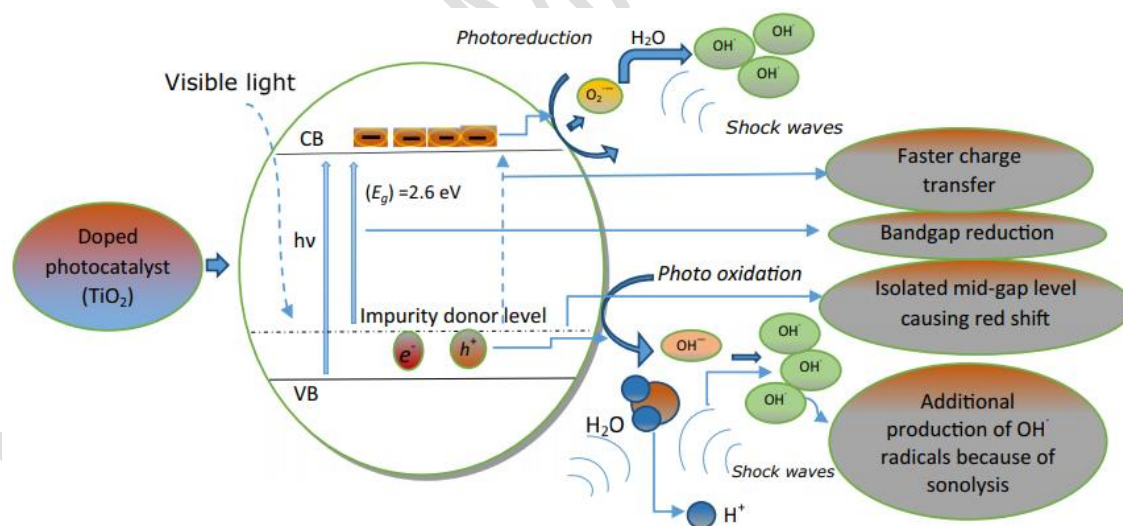
Figure 95. The difference between a sonophotocatalytic and a doped-sonophotocatalytic process for the treatment of recalcitrant hazardous organic water pollutants. Reproduced with permission from ref [1000]. Copyrigth 2017 Elsevier.

Following this approach an enhancement has been reported for the degradation in aqueous solutions of methyl orange over metal-nanosized Ag/TiO_2 [1001] and nonylphenol ethoxylate surfactant over Au/TiO_2 photocatalysts [1002]. However, while all of these photocatalysts were

efficient for the degradation of organic compounds, the presumed synergism through the sonophotocatalysis were not enough documented.

After co-doping with nitrogen, biphasic TiO_2/Bi_2WO_6 heterojunction photocatalysts [1003]. present better sonophotocatalytic activity for the removal of different pollutants, such as methylene blue, *p*-nitrophenol, rhodamine B, and levofloxacin, compared with pure constituents where superoxide radical (O_2^-) was found to dominate the process. This behavior has been attributed to a synergic effect among doping, heterophase junction, and heterojunctions as well as between sonocatalysis and photocatalysis [1004]. (Figure 96). Composites of TiO_2 nanoparticles modified with MWCNTs and CdS [1005] or iron [1006] were as well investigated in the degradation of rhodamine B and methylene blue, respectively, via a cooperative participation of the photocatalyst nanoparticles and CNT.
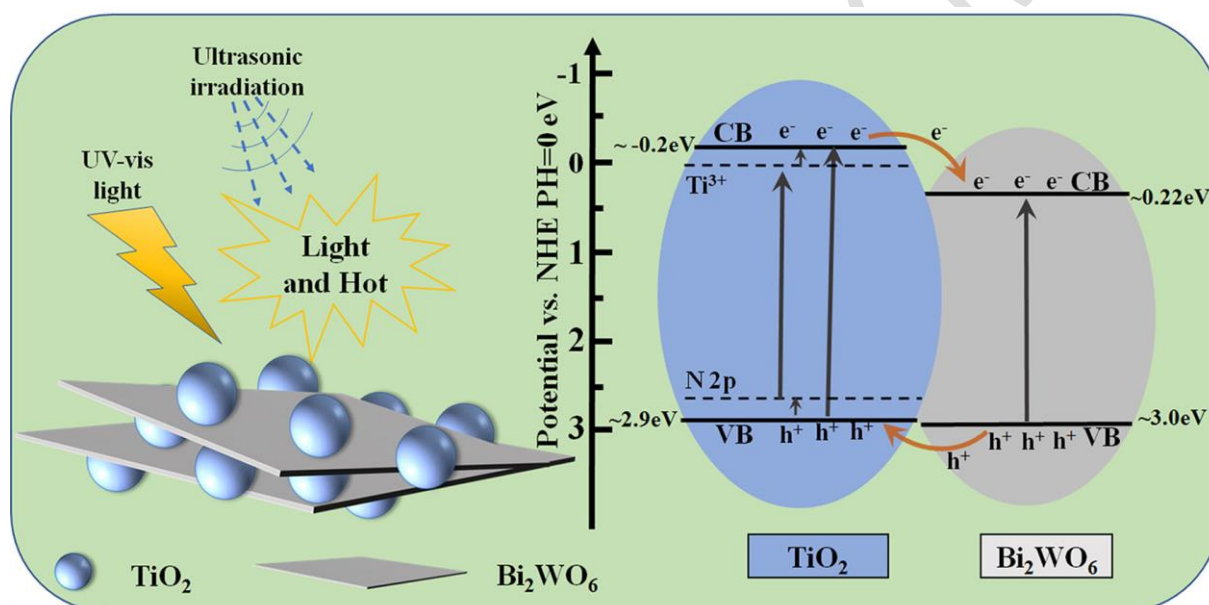
Figure 96. Possible mechanism for the sonophotocatalytic degradation of organic contaminants over N/Ti^{3+} co-doping biphasic TiO_2/Bi_2WO_6 heterojunctions. Reproduced with permission from ref [1004]. Copyrigth 2019 Elsevier.

The degradation of the Acid Red B dye over $Er^{3+}:YAlO_3/TiO_2$-ZnO and $Er^{3+}:YAlO_3/TiO_2$–SnO_2 composites occurs through an up-conversion luminescence mechanism where the absorbed visible light is emitted as ultraviolet light, producing in both semiconductors electron excitation from the valence to the conduction band [1007-1008]. Then, the highly oxidative holes on valence band of TiO_2 not only directly decompose the dye molecules adsorbed on the surface of $Er^{3+}:YAlO_3/TiO_2$-ZnO composite particles, but also oxidize H_2O or OH^- to produce hydroxyl radicals with high activity and indirectly degrade the dye molecules in aqueous solution. In addition, the electrons on the conduction band of ZnO may then react with oxygen adsorbed on the surface, yielding radicals such as $\cdot OH$ and O_2^-. These radicals can also degrade

214

the surrounding organic dye molecules, leading to volatile degradation by-products or entire mineralization into CO_2, H_2O and mineral acids

The oxidative degradation of 4-chlorophenol by sonolytic, photocatalytic and sonophotocatalytic processes was studied in aqueous solutions using $Bi_2O_3/TiZrO_4$ as a visible light driven photocatalyst. The results reveal that this photocatalyst is capable of degrading 4-CP. Both sono- and photocatalytic processes led to the formation of a number of intermediate products that were not formed during the sonophotocatalytic degradation [1009].

Corona pre-treated colloidal TiO_2 deposited on pre-treated polypropylene followed by the deposition of Ag nanoparticles were investigated in order to remove dye C.I. Acid Orange 7 from an aqueous solution. Although sonophotocatalytic degradation of dye ensured a fast decolorization, most prominent in acidic conditions, but TOC values of water measured after sonophotocatalysis were still not satisfactory [1010].

The association of TiO_2 sonophotocatalytic degradation with a porous support may lead to some additional advantages [1011]. Besides preventing coagulation of the photocatalyst some benefits like i) pore entrapment of titania avoiding evolution towards an opaque substrate, increasing photocatalyst efficiency; ii) diminution of UV irradiation blocking due high particle concentration; and iii) enhanced synergy of UV and ultrasonic irradiation in wastewater treatment with production of higher fluxes of hydroxyl radicals, further complementing the adsorptive capacity of supports like activated carbon to adsorb the generated intermediate by-products. Similar effects were also reported utilizing nanocomposites composed of porous Ni−Ti layered double hydroxides (LDH) nanoparticles and hierarchical $g-C_3N_4$ nanosheets that were employed for the sonophotocatalytic removal of amoxicillin, as a model antibiotic, from aqueous solutions [1012]. According to the proposed mechanism (Figure 97), and the total organic content data of the examined solutions, the degradation is the effect of the generation of different active species, e.g., ·OH radicals and holes by sonophotocatalysis that can further oxidize and even mineralize the fragmented molecules from amoxicillin. These composites were also indicated as reusable and stable catalysts.
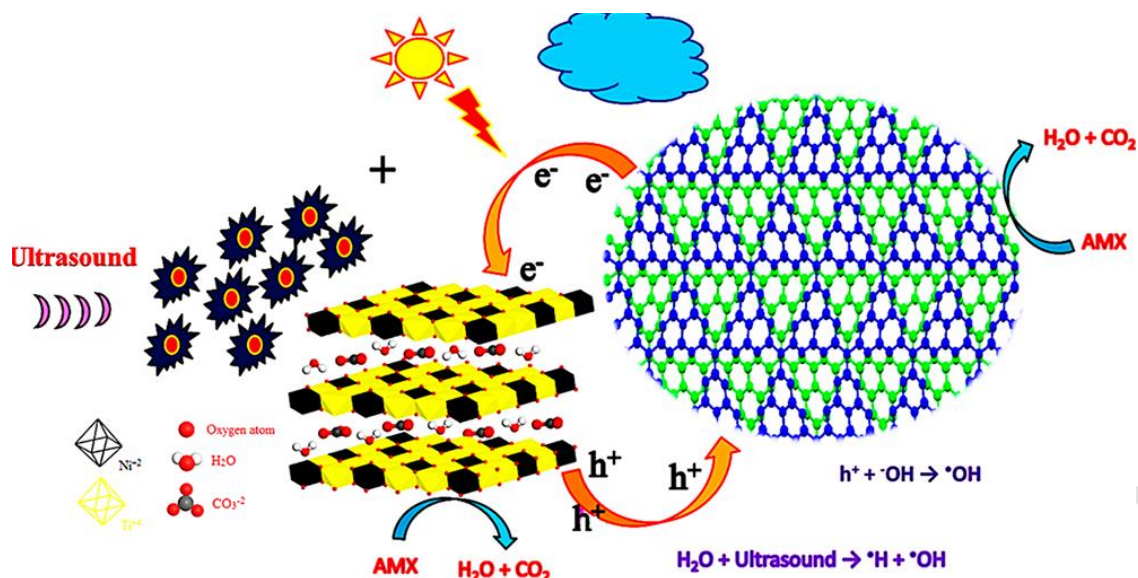
Figure 97. Sonophotocatalytic effects in the degradation of amoxicillin over porous Ni−Ti LDH nanoparticles/hierarchical g-C$_3$N$_4$ nanosheets nanocomposites. Reproduced with permission from ref [1012]. Copyrigth 2019 American Chemical Society.

The separation of the sonophotocatalyst nanoparticles from the aqueous phase can be improved using a magnetic core (Fe$_3$O$_4$@SiO$_2$@TiO$_2$). It may be used for the pre-treatment of organophosphate pesticide wastewaters, increasing their biodegradability for a subsequent biological treatment [1013].

Sonophotocatalytic degradation of wastewaters with ZnO photocatalysts

Investigations on the ZnO mediated sonophotocatalytic degradation of phenol in water revealed that H$_2$O$_2$ formed *in-situ* cannot be quantitatively correlated with the degradation of this pollutant. It is an intermediate which undergoes concurrent formation and decomposition resulting in a stabilization for the case of sonophotocatalysis [1014]. Various reaction parameters such as catalyst loading, substrate concentration, pH, or presence of air/O$_2$ influence the maxima and minima in its oscillation curve. However, the sonophotocatalytic degradation of phenol showed that ZnO is more active than TiO$_2$ [1015]. Like for TiO$_2$, anions such as chloride and sulphate inhibit the activity of ZnO [1016].

The atmosphere in which the sonophoto-degradation is carried out exerts an important effect as well. Experiments carried out in sonophotocatalytic degradation of *E. coli* in different environments showed that the inactivation efficiency of ZnO nanofluids under purging with nitrogen, oxygen, argon and their mixtures led to different inactivation efficiency being correlated to the production of hydroxyl radicals and the inactivation mechanism [1017]. It varied

216

in the following order: no aeration < nitrogen < argon < oxygen < $Ar/O_2(3:7)$ < $Ar/O_2(7:3)$ < $Ar/O_2(5:5)$.

The deposition of ZnO nanoparticles onto multi-walled carbon nanotubes afforded an increased absorbance of photocatalyst in the visible-light region that correlates with an enhanced degradation of Rhodamine B dye [1018]. Accordingly, the sonophotocatalysis was faster than the respective individual processes due to the formation of higher amounts of reactive radicals as well as the increase of the active surface area of the composite.

ZnO nanoparticles were also considered for the degradation of more complex molecules such as antibiotic-resistant gastrointestinal pathogens in water. Taking ABR Salmonella Typhimurium as reference model, sonophotocatalytic processes with Fe-doped ZnO nanoparticles was able to achieve disinfection upon visible-LED light illumination [1019]. Iron doped ZnO nanoparticles were found to be more effective than ZnO while a complete disinfection was not achieved with TiO_2 [1020]. Fe-doped ZnO nanoparticles impregnated on Kaolinite were also active for the disinfection of *Enterobacter* sp [1021] and for the degradation of dyes from real textile effluents [1022]. Other cations such as Gd^{3+} [1023], Pr^{3+} [1024] or Ni^{2+} [1025] were found to have the same promotional effect on ZnO for the degradation of various textile dyes

Also, the impregnation of ZnO with Ni allowed the sonophotocatalytic degradation of textile dyes such as Acid Violet 49 and Acid Blue 45 [1026]. Synergy effect on the sonocatalytic activity of Na-doped and C-doped ZnO nanostructures towards the degradation of methylene-blue and methyl orange has been assigned to a lowering of the band gap, nanorod morphology with more active crystal facet (0001), and efficient separation of photogenerated electron-hole pairs under visible light and ultrasound irradiation. Hydroxy radicals produced by sonolysis in induce a loss of sonophotocatalytic activity in the presence of isopropyl alcohol which plays the role of hole scavenger [1027].

Sonophotocatalytic degradation of wastewaters with other photocatalysts

Comparative experiments for the degradation of rhodamine 6G under ultrasound activation indicated a superior activity of CuO compared to TiO_2. However, under sonophotocatalytic conditions its behavior was inferior to that of TiO_2 [1028]. Studies in the presence of radical scavengers such as methanol (CH_3OH) and n-butanol (C_4H_9OH) indicated lower degradation levels confirming the dominance of radical mechanism. Other studies dealing with the treatment of real industrial wastewater containing a copper phthalocyanine pigment taking CuO and TiO_2 catalysts showed a different order. In this case, with or without various additives like H_2O_2 and ozone, TiO_2 was slightly superior to CuO [1029].

Fenton-type catalysts also led to encouraging results. CeO_2-Fe_3O_4 has been investigated for the decolorization of azo dyes Red DR16, direct orange 26, and organic pollutants in water such as benzotriazole, bisphenol A, or 2,4,6-trichlophenol in an accelerated hybrid-ultrasound Fenton-coupled and ultraviolet irradiation process generated in the presence of sulfate radicals produced through decomposition of persulfate and peroxymonosulfate anions [1030].

Its activity derives from an acceleration of the cycle of Fe(III)/Fe(II) and Ce(IV)/Ce(III) in CeO_2-Fe_3O_4 that resulted in generation of hydroxyl and sulfate radicals as main agents for destruction (not mineralization) of dye molecule.

Fe-doped Bi_2O_3 catalysts were investigated for the sonophotocatalytic treatment of synthetic Basic Brown 1 dye and real textile wastewater in the presence of oxidants such as H_2O_2 and peroxymonosulfate dye with good decolorization effects (color removal of 99 %) [1031].

The advantages of utilizing advanced two-dimensional semiconductor materials in sonophotocatalytic water remediation have been recently reviewed [1032]. These 2D catalysts include graphene, transition metal chalcogenides, carbides, nitrides, phosphides and were investigated for the degradation of various antibiotics and dyes in wastewater. The addition of iron also exerts a positive effect. A similar behavior has also been demonstrated for the degradation of Basic Blue 41 over $NiFe_2O_4$/RGO nanocomposite with efficiencies around 97 % [1033] and of Malachite Green by nanocrystalline chitosan-ascorbic acid@$NiFe_2O_4$ spinel ferrite [1034].

Composite 3D core-shell urchin-like MoS_2/carbon photocatalyst allows a large increase of the electrical conductivity of MoS_2 that accelerates the electron transfer efficiency and provides more active sites for the degradation of the pharmaceutical residues in water [1035]. The effect of the pollutant concentration, the initial pH, co-existing anions, peroxymonosulfate dose and ultrasonic intensity has been demonstrated in a sonophotocatalytic coupling system for levofloxacin degradation under visible light irradiation (Figure 98).

MnO_2 has also been identified as a sonophotocatalyst for the degradation of very small concentrations of Indigo carmine dye pollutant from water. The investigations demonstrated a complex effect of anions/salts on the degradation that ranges from 'inhibition' (PO_4^{3-}, CO_3^{2-}, HCO_3^-) and 'no effect' (SO_4^{2-}, Cl^-) to 'enhancement' (NO_3^-, CH_3COO^-) [1036]. H_2O_2 scavenging the *in-situ* formed ·OH radicals exerts a negative effect with such catalyst.

Silver polyphosphate catalysts such as $Ag_5P_3O_{10}$ and $(AgPO_3)_6$ microspheres promote the sonocatalytically degradation of Rhodamine B due their capability to produce of OH radicals in the reaction system [1037-1038].
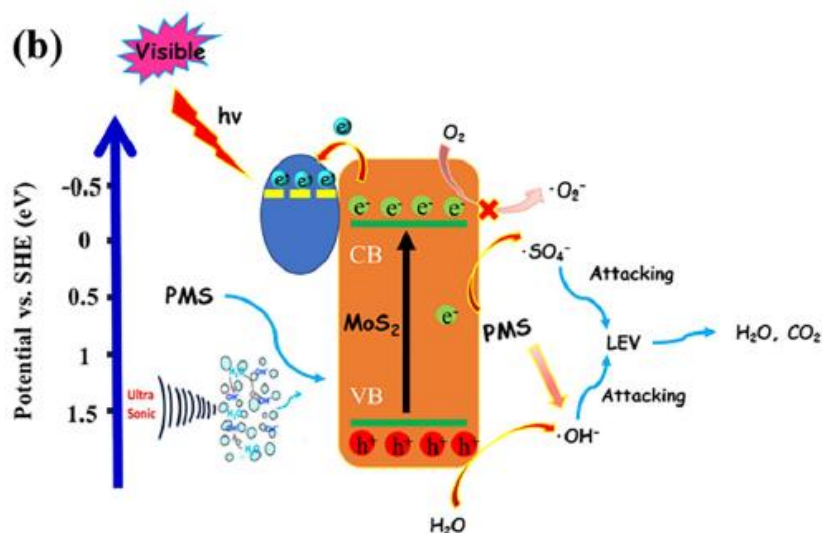
Figure 98. Band energy diagram and separation mechanism of photo-generated electron–hole pairs at the interface between MoS_2 and carbon layer under visible-light driven. Reproduced with permission from ref [1035]. Copyrigth 2019 Elsevier.

Technological limitations in utilization of sono- and sonophotocatalytic processes

The comparison of batch recirculating systems hosting an ultrasound/hydrodynamic cavitation reactor with immobilized photoreactor in series indicated a superior performance of the former in terms of the degradation yields [1039].

Batch reactors were also investigated considering the effect of the operational conditions [948]. These studies identified a series of important operational parameters controlling the efficiency of the sonophotocatalytical process such as i) the waste concentration and operating pH; ii) the addition of a secondary oxidant (such as H_2O_2 or O_3) and its concentration; or iii) the addition of some additives such as CCl_4 and its concentration. The quantitative influence of these parameters was fitted to a mathematical model.

However, even if the sonophotocatalysis may provide an improvement compared to simple sono- and photocatalysis from the applied point of view it imposes some problems that are mainly related with the type of the reactor. Batch reactors achieve rather small productivities and are associated to catalyst losses. However, the association of these reactors with a ceramic membrane microfiltration process may limit these disadvantages, although at the cost of a further decrease of the productivity [1040]. Ceramic membrane microfiltration could efficiently recover TiO_2 photocatalyst with a mean granular size of 0.33 μm from slurry reactor, achieving 99.9% recovery rate [1040]. An obvious but not significant enhancement effect of ultrasonic irradiation for ceramic membrane microfiltration has been found, which could be closely

related with the low conversion efficiency of ultrasonic energy. Contrary to polymeric membranes, the ceramic membrane showed good stability under ultrasonic irradiation.

To overcome some of these disadvantages, synergistic degradation of waste organic molecules in an ultrasound intensified photocatalytic reactor has been as well proposed [1041]. However, the progress in this direction is still not satisfactory and further research and development is necessary to bring the combined treatment closer to any possible application.

5. Challenges in new strategies for predicting or investigating the catalyst at nanoscale close to real working conditions.

5.1 Context and challenges

In the light of all research investigations discussed in this review, the complexity of heterogeneous systems clearly appears. Firstly, this level of complexity in inherently related to the existence of different gas-liquid-solid interfaces poorly described yet. Secondly the remaining discrepancies on the reaction mechanisms despite of the wide number of papers dealing with kinetics of radical and non radical reactions in catalytic water treatment probably slower subsequent discovery towards efficient systems [40]. This later point could be crucial because in the first case textural properties and catalyst functionalities could play a minor role reduced to ROS production, while in the second scenario, textural and adsorptive properties would participate significantly. Presently, rational quantitative evaluations of radical and non radical pathways are missing while it likely represents a key issue regarding a faster development of catalytic processes for water treatment.

In most case academic researches are restricted to model operating conditions taking a single pollutant into account. The reactor design and the integration of catalysts with optimized functionalities are clearly crucial parameters. However, they could not be decisive for further upscaling. In the few examples representative of real conditions with water containing multiple pollutants the contribution of the catalyst is not correctly defined and deactivation through poisoning effect could be the major drawback limiting the development of catalytic technologies. The hydrophilicity/hydrophobicity as well as pH conditions that monitore the surface charges and related interactions with the adsorbates must be also taken into account. Some predictions at molecular level towards practical applications cannot be mature if all these

aspects are not correctly taken into account. Up to now molecular modelling, as potential prediction tool, has mostly considered the interactions of one pollutant on a model surface which is not really representative of the real surface with water as solvent neglected in this approach (see chapter 2.2.4). The predictive models form molecular modelling are in some extent useful to get reliable mechanistic insights but are restricted to model surface and in many cases do not account for the competition with water for adsorption. The main objective of this chapter is to go beyond the existing through the identification of scientific challenges but also to inventories novel scientific approaches not specifically developped initially for water treament but that could stimulate new useful orientations by taking intrinsic pecularities of catalytic water treatment systems into account, related to the extreme low concentration of pollutants for their removal.

A grand challenge in basic researches in heterogeneous catalysis lies in the relationship between computational chemistry, which can lead to precise information at atomic level, and the development of methodologies for the preparation of catalyst materials [1042] associated to their characterization in working conditions at this level of precision. Indeed, if we are able to correlate and anticipate changes in electronic structures with catalytic properties, then one could expect the development of new generation of catalysts. To comply with this requirement important efforts are needed towards: – the development of tools with atomic level precision that can match with computational approaches – The implementation of advance characterizations that can probe the catalyst surface at atomic level under working conditions – The development of accurate model reactions at working conditions from computational approaches.[1043].

However, such approaches and their usefulness at the lab-scale may have no future if we are not able to value them on the largest scales. The emergence of artificial intelligence could lead to faster decision in the development of catalytic processes integrating reduction cost. Indeed, multiple parameters must be taken into account for their optimization, in batch reactor, *i.e.* optimal catalyst-to-contaminant ratio, purity of the catalyst, time, pH conditions, temperature, etc. At first glance AI could be suited to predict useful technology in case of multiple pollutants and the development of continuous flow technology [1044]. However, this novel approach is infancy and and must overcome some limitations lying in the selection of reliable data, the use of hybrid AI tools and increase investigations at the scale of pilot.

5.2 Computational approaches combined with artificial intelligence

5.2.1 Add-value for predicting and developing more active catalysts by using methodology from computational calculations and artificial intelligence

As depicted in chapter 3.3 the immobilization of bio-enzymes on solid substrates and/or their substitution by synthetic systems represents a useful option especially for further transfer to continuous flow reactor. Despite the sharp gain in power of supercomputers, computational calculations are in most cases restricted to model systems that cannot reflect the complexity of real catalytic systems. Regarding enzymes the tremendous size of proteins is a critical issue and it is not evident that the full potential of computational techniques will be able to offer useful insights to produce new generation of proteins. The growth of protein database simultaneously to the development of high throughput screening methods thanks to artificial intelligence and more particularly machine learning could be more powerful and speed up the engineering of new enzymes as well as the elaboration of synthetic nanomaterials that could mimic their kinetic behavior.[1045] Other factors stimulated the development of fast methodologies, including statistical and machine learning approaches likely because of their high sensitivity to inhibiting effects in the presence of wide range of organics. Presently huge efforts are dedicated to the methodologies which will allow to bridge the gap between technologies *in vitro* and *in vivo* close to the real operating conditions. Today, novel approaches arise for engineering new generations of catalysts through the development of machine learning algorithms and the selection of appropriate algorithms to create efficient artificial enzymes. As described in chapter 3.1, the immobilization of enzyme faces too important issues related to a full understanding of the description of the aqueous-substrate interface and biomolecule-substrate interactions according to their intrinsic features. It is obvious that these parameters govern the catalytic performance of immobilized enzymes. Presently, tools for simulation cannot be enough powerful to distinguish undefined interfaces between solid substrate-biomolecule, substrate-water and water-biomolecules. The computational approaches using advanced force-fields simulation tools can better match experimental observations. Nevertheless, model structured surfaces for current solid substrate, such as TiO_2, conventionally used differ from amorphous surfaces including defective sites and various degree of hydroxylation and charge according to pH conditions.[1046] An alternative approach would consist in the development of cost-effective nanomaterials capable to mimic the kinetic behavior of enzymes with improved stability and higher efficiency in broader operating conditions.

Machine learning is an emerging approach which benefits to an exponential growth of scientific papers published in this branch of computer science in the last decades (Figure 99).[1047] The usefulness of this approach to predict the effectiveness and cost-efficiency in the removal of phenol from industrial wastewater by using photo-Fenton process has been recently emphasized.[1046] The best accuracy obtained for deep neural network shows that pH, light intensity, amount of H_2O_2 and specific level of impurities are relevant parameters while the concentration of Fe^{3+} and TiO_2 as catalyst plays a minor role. The growing interest of machine learning for developing new materials has been also illustrated in the development of perovskites for photocatalytic applications, but the statistical significance implies management of accurate experimental data and broader generalization would need the implementation of combinatorial procedures.
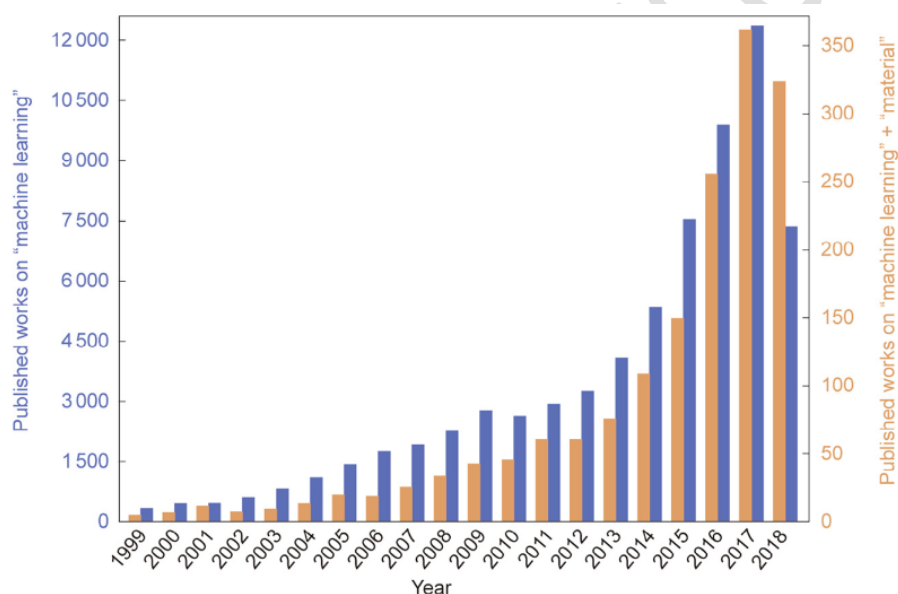
Figure 99. Number of paper combining the key words machine learning and machine learning + material from 1999 to 2018. Reproduced with permission from ref [1047]. Copyrigth 2019 Elsevier.

Modeling the functionalities of catalysts cannot be an easy task according to the catalyst composition. A rapid screening can be achieved from bimetallic and multi-metallic catalysts exhibiting high activities by using accessible descriptors associated to intrinsic physicochemical properties of element in multimetallic catalytic systems, *i.e.* ionic potential, electron affinity, coordination geometry.[1048] This strategy can provide rapidly precise information on the physicochemical properties of materials at a resolution that could not be obtained from experimental and *ab initio* methods. The development of decision tree and data-

driven approaches leads to significant achievements[1049] using, particle size diameter of platinum particles, surface area from dataset and sphericity from DFT calculations to predict the catalytic properties of Pt nanoparticles. This approach is also suitable for homogeneous catalysts especially organometallic catalysts with electronic properties of the transition metal bonded to ligands predicted from spin-state ordering and specific bond lengths.[1050]

Machine learning and data management are useful where massive experimental data can be inventoried. In case of this preprequisite could not be fulfilled then the resulting consequence can be the lack of clear guidance that could lead rapidly to the synthesis of an efficient catalytic system. High-throughput DFT calculations are also powerful to investigate a wide number of catalytic materials to identify relevant descriptors that influence their intrinsic properties.[1051] Photocatalysis is probably an excellent example because tremendous number of publications for a wide range of reactions can be found in the literature. These studies pointed out the relevance of perovskites, but there is no clear consensus regarding the most efficient catalysts as well as the most important descriptors that govern their efficiency. Furthermore, those materials are also remarkable in PMS activation.[969] Perovskites with a structure ABO_3 are recognized for their versatility due to their ease to accommodate a wide number of elements in A and B site leading to multiple substitutions. An optimization of structural distortions induced by substitutions in A and B-sites as well as the stabilization of unusual valence states for cations in B-site are quite challenging. Results from Decision tree analysis used data base composed of 151 experimental results during the period 2005-2017. They account for visible as UV light irradiation of perovskite type structures in order to identify the most important parameters leading to a high production of hydrogen from photocatalytic water splitting.[1052] These authors classified catalysts systems in three categories as low, medium and high production rate. Data mining analysis reveals that ion doping in B-site is the most determining parameter to change the band-gap but this factor could not be directly related to H_2 production. Co-catalyst for charge separation and the use of sacrificial agent have not been considered as sound solutions. Returning to high-throughput DFT calculations to discriminate relevant composition, Figure 104 summarizes the investigation of 5,329 cubic and distorted structures taking their thermal stability and the energy requested to form oxygen vacancy recognized as critical parameters for improving their properties in thermochemical water splitting reaction. From these calculations, data in Figure 100 offer an overview emphasizing that a greater stability corresponds to orthorhombic structure with preferentially rare-earth in A-site and transition metals in B-site. 139 structures have been identified as potential candidates for the selected catalytic application. Nonetheless, structural features are not the unique factors which

can govern the catalytic properties of these materials. Their textural properties and preparation methods must be closely associated in determining the best option. Indeed, it has been reported that the preparation method is also an important parameter [1052] likely due to the fact that it can influence both the specific surface area and surface segregation process in connection with their stability. Based on these considerations, it seems obvious that the combination of high-throughput molecular calculations combined with machine learning could be a suitable approach to get faster discoveries.
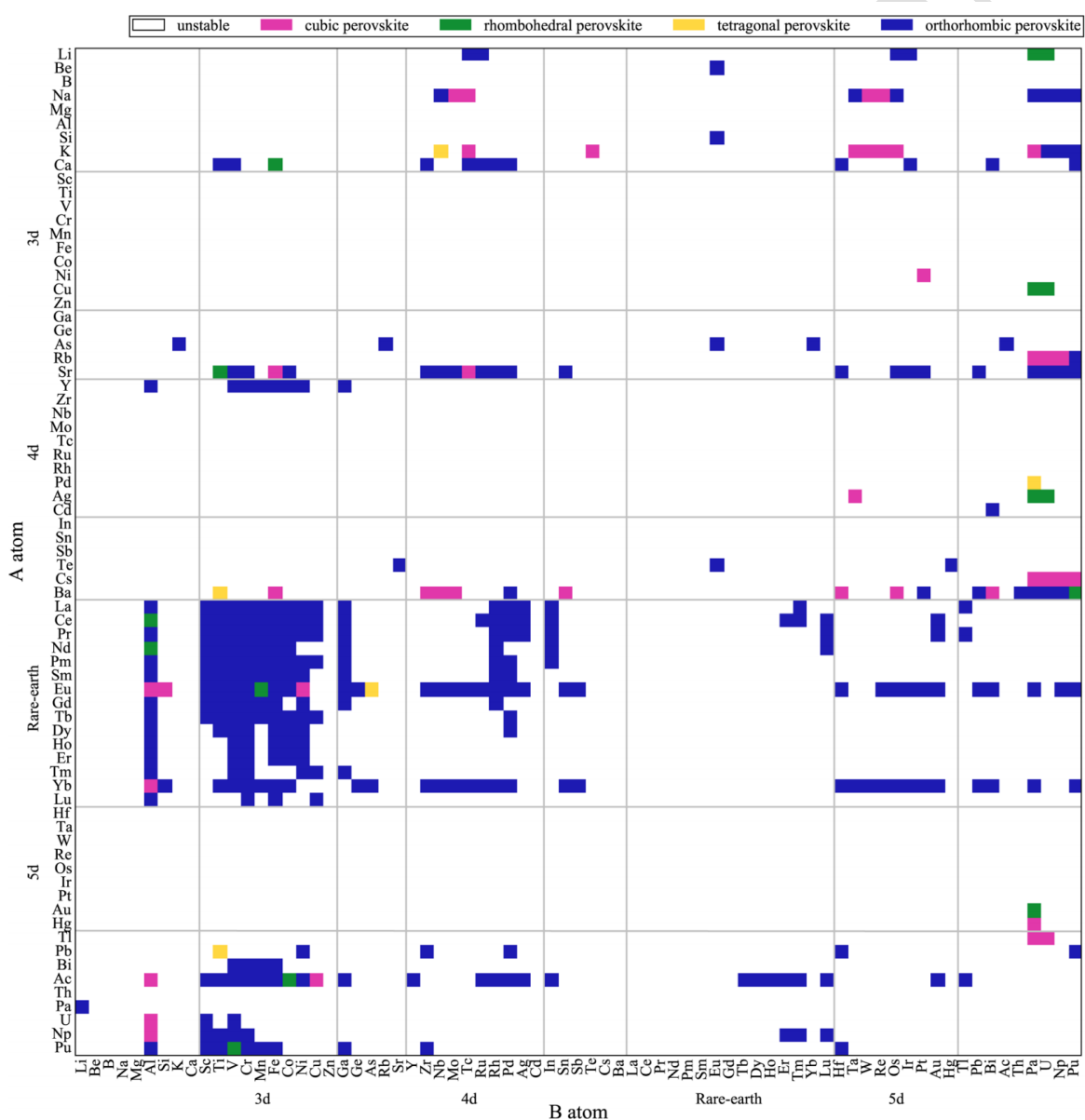
Figure 100. Map of perovskite composition representing structural feature and stability from High-throughput DFT calculation. 5,329 stoichiometric composition are reported including 389 perovskites that predicted as stable according to the phases in the A−B−O phase diagram. The atoms on the x- and y-axes are ordered by atomic number. The colors show which distortions are stable. Reprinted with permission from ref [1051]. Copyrigth 2016 American Chemical Society.

A fast accessibility of reliable quantitative structural information of active sites from *in-situ, operando* and spectroscopic measurements can speed up surface optimization of functional groups of heterogeneous catalysts. Some examples have been recently given for the determination of the local structure of Ni^{2+} cations in a MOF.[1053] The main objective was the determination of the structure of several adsorbates on Ni^{2+} from experimental XANES spectra. The optimization of experimental and predicted XANES spectra have taken into account several parameters, such as the Ni-adsorbate distance; two angles reflecting the position of the adsorbate with respect to Ni center (α_1 and α_2) and two angles which represent the bending of the molecule (β_1 and β_2) (Figure 101). The analysis of the calculated standard deviation values shows that the main parameters which affect XANES spectra are the Ni-adsorbate distance and β_1 angle. This example corresponds to a gas phase reaction, but it can widen the scope of application to more complex aqueous media when the solvent through the formation of hydrogen bonding can strengthen the adsorption bond and then induce structural deformations and changes in bond length.
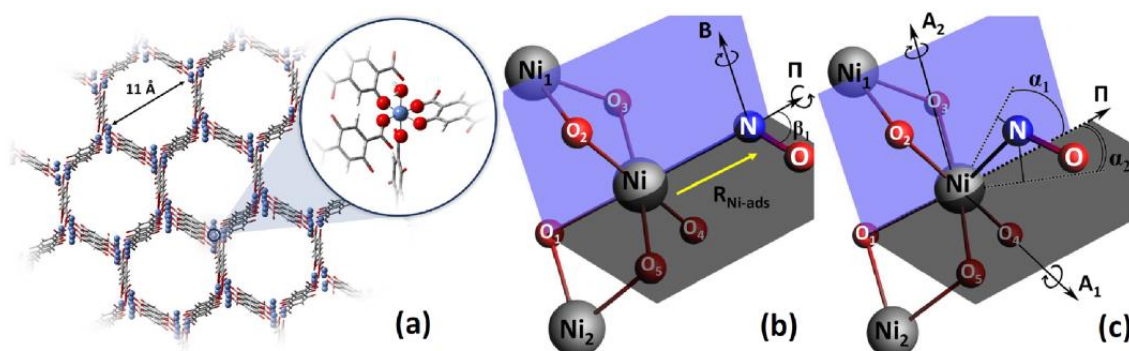
Figure 101. (a) 3D representation of a dehydrated CPO-27-Ni structure. The C atom is colored in grey, white for H, red for O and blue for Ni. (b) and (c) structural parameters used for the refinement of the geometry of the adsorbate position relative to Ni center in the CPO-17-Ni structure. NO has been considered in this figure as adsorbate. The molecule is placed on the polar axis π. Two planes appear and 4 axes for the molecular rotation are used. β_1 angle specifies the bending angle of the NO molecule compared to the polar axis. β_2 (not shown) refers to the rotation of the molecule around the polar axis. α_1 angle represents the whole rotation of NO around A_1 and α_2 angle the whole rotation around A_2. Reprinted with permission from ref [1053]. Copyrigth 2019 Elsevier.

5.2.2 Molecular modeling of water-solid interface: a step forward to a better understanding of reaction mechanisms and surface stability?

In practice, most theoretical calculations dealt with model metallic of metallic oxide surfaces to predict reaction paths and reaction intermediates that could explain experimental observations in terms of rate measurements and selectivity previously illustrated in chapter 1.2. Most of them dealt with gas phase catalytic reactions which partially account for the complexity of heterogeneous catalyst surface exposed to a condensed phase. In general, two implicit and explicit methods are developed to model the interaction between aqueous phase and the catalyst surface. In case, of explicit models, water interaction is treated as individual molecules whereas the behavior of many water molecules requires implicit models. The superiority of one model over another is presently not proven.

Saleheen and Heyden [1054] gave their viewpoint which explain the slow progress to model accurately at molecular scale the solid-liquid interface due to the fact that the current harmonic approximation in the estimation of partition functions and free energies is no longer valid. Another specific requirement must be also kept into consideration related to wider configurations for space sampling (approximately 1 order of magnitude more atoms) which cannot be depicted by empirical potentials but need a quantum chemical description in the particular case of transition metal catalysts. Hence, numerous molecular models for heterogeneous catalysts do not account for solvent effects and will neglect support and coverage effects. The complexity in understanding the role of the liquid-solid interface lies in various interactions between the solvent, the solid and the reactant giving rise to dispersion forces, hydrogen bonding and chemical bonding, which can change the energies and the entropies of the reactant intermediates. It is obvious that the development of more specific approaches could be useful to gain more insights into the elucidation of reaction mechanisms and also crystallographic orientations.

In practice, the main challenge lies in the development of robust computational tools which account for a reduction of computation cost keeping a high accuracy on the estimates of kinetic and thermodynamic parameters. In some extent, by considering ice-film able to simulate the increase ordering of water molecules, a solid-like behavior can simplify the calculations of the partition functions. Nevertheless, one question arises regarding if adsorbate could be able to induce explicit perturbations based on this model of description that could mimic those involved at the solid-liquid interface. Alternative isotropic continuum solvation models have been already examined which reduce the number of parameters for charactering the solvent by homogeneous constant dielectric continuum. Based on this methodology, shorter computation times comparable to gas-phase interface models can be obtained.[1055] Nevertheless, some limitations have been identified specially to model accurately hydrogen bonding.

Microsolvation models were also found unsuitable to reproduce boundary conditions at the liquid-solid interface [1056] and evaluate accurately entropic effects.[1057] Among the different theoretical approaches, some of them are now ready to tackle more complex phenomena than those found for instance in electro-photocatalysis at the solid-liquid interface. Significant breakthroughs could be possibly envisioned to elucidate photocatalytic reactions and the clues to find out new materials. Recent developments of a classical force field to investigate the interfaces between iron oxy-hydroxide and water could serve as background for numerous catalytic processes as aforementioned. According to this model, it is possible to compute at nanosecond scale systems composed of thousand atoms.[1058] For enzyme and homogeneous catalysis, hybrid model combining quantum mechanical and molecular mechanical could be more suited to describe bond scission/formation.[1059] Calculations dealing with the interface between adsorbed water on stoichiometric, defect-free (110) rutile oxide surfaces of TiO_2, RuO_2, and IrO_2 are reported elsewhere.[1060] The authors investigated the impact of water on the stabilities of the intermediates during electro-reduction of oxygen. In their model the water was considered as adsorbed H_2O molecules which can form two-dimensional water chains. Reaction encountered in the activation of light alcohols such as glycol emphasize the competition in the C-H and C-O bond cleavage showing that water through the creation of hydrogen bonding can make easier the O-H bond breakage.[1061] Water is also able to act as co-catalyst.

Recent investigations asked themselves the question if conventional vacuum computations can properly estimate microsolvation effects at the H_2O/Pt(111) interface.[1062] It was found that the reaction scheme in alcohol decomposition at the Pt(111)/water interface differs from that established in gas phase at the Pt(111)/gas phase interface.

The relevance to include one water molecule in the simulation has been demonstrated because the formation of hydrogen bond can modify the reactivity of intermediate and change the reaction pathways. Indeed, a greater stabilization of intermediates can modify the competition with water for adsorption preventing significant poisoning effect.[1063] The formation of hydrogen bond leads also to stabilization of ads-NH_2 in ammonia electrooxidation on Pt(100) electrode.[1064] A second aspect lies in the high dielectric constant of water with electrostatic effects represented by continuum models. According to this model the pH as explicit criteria in water treatment could be considered through modification of the charge of the surface.

Presently, modeling the interaction between water and functionalized surfaces is essentially performed on model surfaces[1065-1067] and essentially metallic surface for which

water can be weakly bonded and its desorption further facilitated. Recent advance using force field algorithms on Pt(111) show that the fine structure of the interface is driven by the competition between Pt-water and water-water interactions.[1068] The literature is scarce regarding bimetallic systems and only few examples dealing with Ag/Cu and Au/Pt alloys can be found which served as solid substrate for novel developments in force field approaches to model the interface water-alloy surface.[1069] Random distribution of the atoms has been considered. The selected alloys have been chosen because Ag and Cu exhibit comparable adsorption properties towards water but differ from lattice parameters with interatomic distance of 25.6 nm for Cu vs. 29.2 nm for Ag. By contrast, Pt and Au have comparable lattice parameters, but their adsorption energies are significantly different with a much stronger water adsorption on Pt. An interface composed of two layers has been chosen. The first layer is built up with water mostly adsorbed flat on top sites, while the second layer is less structured. It has been found that water binds more strongly on Cu diluted in Ag, because it is no longer restricted by shorter Cu-Cu bond distance in monometallic system. In that case Ag is protected to water adsorption and available for interaction with reaction intermediates. The same trend also characterizes water adsorption on Au in Au/Pt alloy. Nevertheless, Figure 102 clearly emphasizes a preferential adsorption on Pt top sites with total coverage reflecting the adsorptive properties. Pt surrounding Au surface atoms limits the accessibility of water molecules to surface Au atoms. In this specific case, Pt tune the behavior of Au(111) surface from disordered to ordered water interface.

Quite similar spectral features have been observed on amorphous SiO_2 exposed to water.
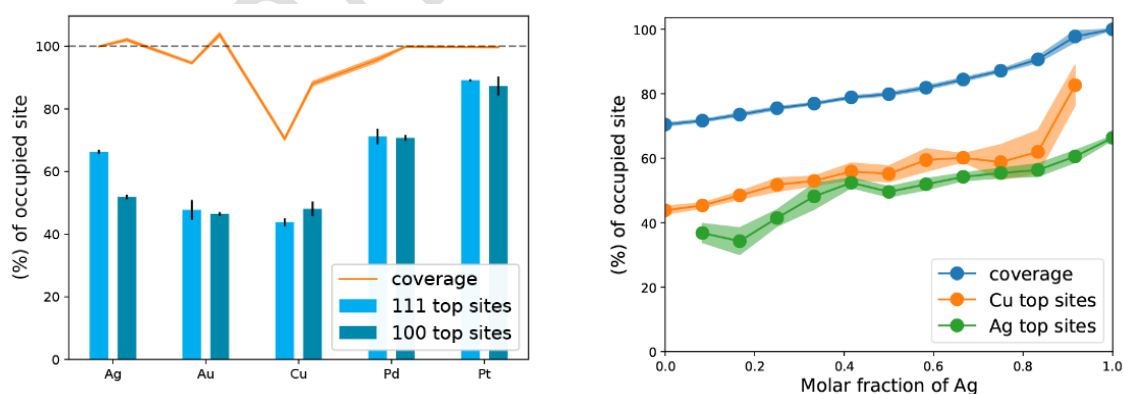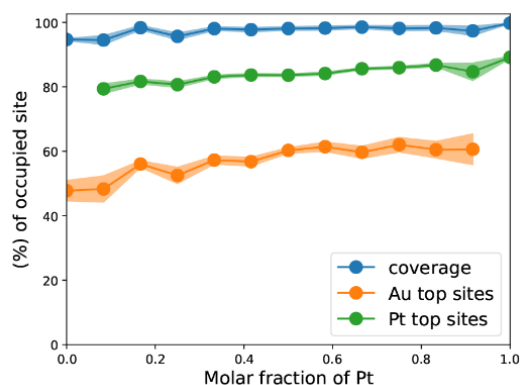
Figure 102. (a) Distribution of the top sites covered by adsorbed water and global coverage for multiple facets. (b) Distribution of the top sites of copper and silver covered by adsorbed water and global coverage for multiple alloy composition of Cu/Ag. (c) Distribution of the top sites of gold and platinum covered by adsorbed water and global coverage for multiple alloy composition of Au/Pt. Reprinted with permission from ref [1069]. Copyrigth 2020 American Chemical Society.

Different scenarios characterize metal oxide surfaces where water can adsorb dissociatively involving oxygen and the coordinated metal site acting as acid sites. Numerous investigations refers to TiO_2 likely due to its extensive use in photochemistry and electrochemistry leading at the beginning strong debates. Nevertheless, a consensus seems to be found which emphasize different behaviors on stoichiometric and defective $TiO_2(110)$ surface. In the former case water adsorb molecularly while dissociation is promoted on kinks, steps and oxygen vacancies.[1070] In practice, the formation of multilayers can occur which can be distinguished by the nature of bond strength. As explained the first monolayer in direct interaction with the solid substrate can be coordinated through Ti and O atoms while the second layer can form according to weaker bond. Similar questions repeat for other transition metal oxides. Siahrostami and Vojvodic[1060] computed water adsorption on $TiO_2(110)$, RuO_2 and IrO_2. They described the formation of three different water chains. The first one strongly bonded to the metal. Weak interactions characterize the second and third water chains forming a film with features similar to bulk water. Such film has only minor effect and do not hinder the accessibly of the reactants/intermediates to the surface.

Another important parameter is related to the water structure in interaction with hydrophilic or hydrophobic surface.[1071] Some examples have been illustrated in the particular case of nitrate reduction to check the benefit on diffusion phenomena when hydrophilic and hydrophobic surfaces coexist.[148] Fundamentally these two surfaces differ from the density of water molecules at their vicinity. In principle, the presence of multiple organics of inorganic pollutants, usually in trace amount which can compete for adsorption and/or inhibitors could

take advantage of resulting attractive and repulsive properties with hydrophobic surface by minimizing inhibiting effect and/or locally enhanced concentration and the related reaction rates.[22]

5.3 Prospects *in operando* and *in-situ* spectroscopic techniques: Toward better mechanistic insights into complex media

The development of powerful spectroscopic tools to investigate the response given by a catalytic surface exposed to a reactive environment probably contributed in the understanding of dynamic surface reconstructions. Thus, it is possible to get more insights into changes in geometrical and electronic structures of the surface and interface leading to the building of active sites close to operating conditions as well as the elucidation of real intermediates. All these discoveries mostly obtained for gas-solid systems provided significant breakthroughs that lead to improve the properties of existing technologies or to suggest alternative ones. It is also worthy to note that even technologies investigating the catalyst under UHV conditions went beyond this limitation to get more relevant information.

In the particular case of gas-liquid-solid systems the target seems more challenging to reach especially in the particular case of diluted systems with trace amount of soluble contaminant. As explained several questions arose in a better description and integration of the gas-liquid and solid liquid interface. For liquid samples different approaches to generate a liquid jet in UHV conditions have been experienced for XAS and XPS analysis. Up to now the characterization of solid/liquid interface provided key information for various applications especially the development of novel electrochemical flow cells which make possible soft X-ray absorption study to probe the behavior of electrodes under working conditions.[1072] As earlier found,[1073] such a discovery and related advanced instrumentation developments broadened the panel of investigations for the removal of soluble contaminants in aqueous phase through water splitting with *in-situ* oxygen and hydrogen generation as well as biological processes. These previous developments also advice inherent problems linked to soft X-rays irradiations inducing samples damage which contributed flow liquid cell which could be *a priori* more relevant than static cells from a practical viewpoint. Some relevant examples are illustrated in the literature especially with liquid phase containing halogenated compound which illustrated the interaction between cobalt and the halogenated molecule.[1074] Presently, only few examples are dedicated to water treatment with trace amount of pollutant which

probably emphasizes the predominant role played by water and the rigorous methodology which much be implemented for elucidating the role of water in the stabilization of reactive intermediate at the surface.

Electrocatalytic reduction of nitrates on transition metals was found as promising approach but electrocatalysts suffer from weak performances in terms of selectivity and stability. As describe the first reduction of nitrates to nitrites is recognized as the slow step of the process and the rate of this reaction would depend on the strength of nitrate adsorption under acidic medium. The benefit of strategies consisting in alloying two metals has been proven with substantial gain in activity and enhanced selectivity towards nitrogen production (see chapter 1.2.). Nevertheless, fundamental questions remain unanswered related to the nature and abundance of reactive intermediates and the influence of the applied potential on the nature of the rate determining step in the course of their electroreduction.[1075] Relevant mechanistic insights need more relevant semi-quantitative comparisons between surface coverages predicted by computational and microkinetic approaches with experimental observations at nanoscale of catalysts in working conditions. *In-situ* XANES and EXAFS were found useful to describe the catalytic behavior of Pt/C vs. potential and electrolyte environment. XANES signal in the range 11565-11575 eV has been assigned to adsorbed H atoms on Pt with intensity sensitive to the coverage. The authors observed its attenuation after nitrates addition to the reaction medium. Jointly, the formation of oxidized Pt species is visualized on XANES spectra. The applied potential allows a careful monitoring of the adsorbate coverage showing competitive adsorption of hydrogen and nitrates at positive potential whereas negative potential leads to a complete coverage by ads-H species even in the presence of nitrates

The development of time-resolved spectroscopic tools can be useful especially to get direct insights which could help in solving divergences. By way of illustration, it is sometimes difficult to relate the facets of crystals to catalytic efficiency. Ag$_3$PO$_4$ used as photocatalyst in the degradation of antibiotics is a representative example.[1076] Indeed, some controversies arose regarding the most efficient facets of the crystal assigned to the (111) surface exhibiting the highest surface energy.[1077] On the contrary, Hsieh et al. reported that (100) was the most efficient facet resulting in more extensive production of ROS whereas the (111) facilitates charge recombination.[1078] Time-resolved spectroscopic tools can be useful to get direct evidences of the dynamics of this recombination providing a relevant comparison between the surface structure and the photocatalytic activity. He et al.[1076] found a higher mobility of holes on (111) surface as active species in the photodegradation process.

5.3.1. *In-situ* techniques to probe bulk and surface catalysts features

Surface science studies have shown their potential to probe the surface of model systems under UHV conditions. Indeed, they brought important mechanistic insights for gas phase reactions but far from usual operating conditions in catalytic conditions taking into account the impact of coverage on kinetic parameters. Lowering the temperature to get higher coverages of adsorbates would not be appropriate. UHV techniques, thanks to significant technical advancements can work today near ambient pressure.[1073] First example can be devoted to near-ambient pressure X-ray Photoelectron spectroscopy with technical progresses earlier detailed.[1079] Useful examples of interest for environmental concern point out the usefulness of this technique to investigate water films on substrates such as $TiO_2(111)$[1080] extensively used in photocatalytic oxidation reactions or amorphous SiO_2.[1081] As exemplified in Figure 103, three components on the O1s photopeak appear when $TiO_2(111)$ is exposed to weak water pressure. At the lowest partial pressure of water, H_2O can dissociate giving rise to the formation of two surface OH species one refilling vacancies while the second one forms from H when binds surface oxygen species. A rise in the water pressure leads to molecular adsorption (534 eV) which has been explained through the formation of hydrogen bonding between H and O from water molecules.
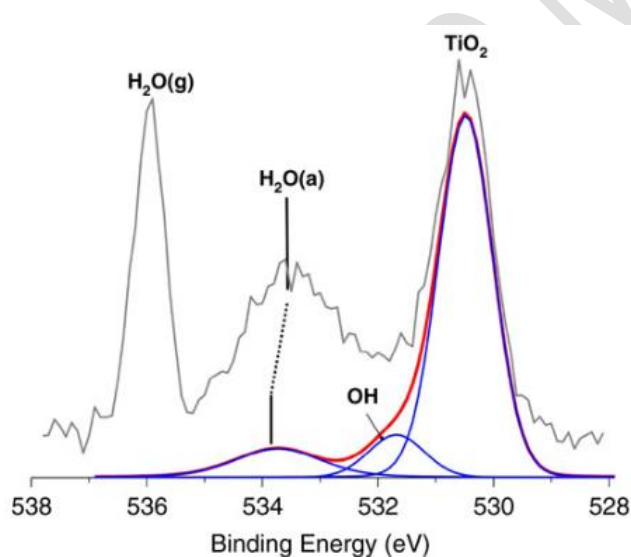
Figure 103. O1s photopeak recorded on $TiO_2(111)$ exposed to 2.25 Pa H_2O at 25°C (bottom curve) and to 133 Pa at -3°C (top curve). The components at 534 eV and 531.7 eV were assigned to molecular water and OH adsorbed species. Reprinted with permission from ref [1079]. Copyrigth 2008 Elsevier.

From this study the thickness of the film has been estimated to ~3 monolayers with relative humidity (RH) in the range 20 and 50% but shifts near 8 monolayers for 95% RH. Such changes

observed in binding structure of the water film is also accompanied to change in the enthalpy of adsorption from -70 kJ/mol to -45 kJ/mol with a rise in coverage from 0.2 ML to 0.5 ML. Change in the strength of water adsorption is discernible on the O1s photopeak with a slight shift observed on the 534 eV signal to lower values.[1079] Complementary experiments from AFM in the Kelvin probe mode have examined preferential orientations of the water dipoles according to the thickness of the film. The authors explain the results summarized in Figure 104 to a random orientation of water bonded to SiO_2 at low coverage and low humidity which corresponds to invariance of the surface potential. Above 4-5 layers, the water film exhibits a liquid-like behavior. The orientation of water bonded to OH groups would no longer exist beyond the second layer.
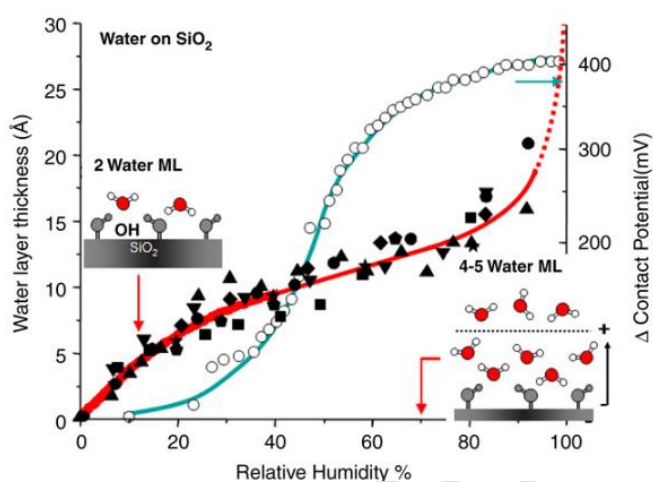
Figure 104. Plot of the water film thickness vs. the relative humidity (RH). A thickness of 0.3 nm was assumed to correspond to one monolayer of water. The right y-axis (open symbols): correspond the potential measurements et 21°C from AFM operating in the Kelvin probe mode at 21°C vs RH. Reprinted with permission from ref [1079]. Copyrigth 2008 Elsevier.

Such spectroscopic features seem in rather good agreement with theoretical calculations where water was considered as adsorbed H_2O molecules which can form two-dimensional water chains. As earlier discussed, strong adsorption is limited to the first water layer, the second layer being more disordered.[1069]

In case of thin film electro- or photocatalysts. The development of spatially resolved Near-ambient pressure XPS can open to high-throughput approaches. Some illustrations come from the investigation in working conditions of ceria thin film as working electrode. Yttria-stabilized zirconia as electrolyte separates the working electrode and the Pt counter electrode. Spatially resolved XPS can lead to surface potential mapping which allows the visualization of electrochemically active region according to the chemical environment.[1082] This study

illustrates the potentiality of mapping from Near-ambient pressure XPS as a high throughput combinatorial approach. Probably the gap with more representative water-solid interface is significant. Nonetheless, the potentiality to probe the surface under working conditions and access to a spatial distribution of active elements could be helpful in the elaboration of supported catalysts.

Regarding functionalized catalysts the exploitation of X-ray absorption techniques can be more useful than XPS offering advantages to investigate in working conditions the evolution of the oxidation state of transition metals. Nevertheless, the main disadvantage is related to the bulk sensitivity of this technique. Advantages and limitations have been earlier compared for the investigation of Pt electrodes in fuel cell applications, *i.e.* Pt/C.[1083] In practice XAS measurements are usually performed using synchrotron radiation and two modes of acquisition can be selected using either transmission or fluorescence. Time acquisition in closely related to the power of the detection, a complete spectra being recorded within few minutes by using a Quick EXAFS monochromatic or even less in case of energy dispersive monochromatic which can drastically increase the domain of application of this techniques to investigate the transition chemical processes. As a consequence more reliable information can be obtained regarding the fast kinetics of valence changes of transition metals during *in-situ* redox processes. In some extent perturbations of the XAS spectra induced by adsorbates can be also visualized.[1084] As example, on normalized XAS spectra recorded at the Pt L_3 edge, the sensitivity of an adsorbate will depend on the accessible Pt atoms of the particle, i.e. the metal dispersion. Accordingly, getting insights into the restructuring of Pt particles could be envisioned. This has been exploited to investigate the underpotential Cu deposition on Pt/C electrode. Changes observed at the Pt L_3 edge have been ascribed to charge transfer from Cu to the Pt. Presently, the comparison between experimental and theoretical approaches on bimetallic systems are relatively scarce. Electron transfer as a function of electronic affinity characterizing the two metals in bimetallic particles could in some extent explain their different behavior towards water adsorption. Such features have been underlined from computational studies since a strengthening of the metallic character would weaken the metal-water adsorption bond considered as a key factor in developing their catalytic efficiency.

XAS techniques have been profitably used for electrochemical applications with a typical liquid cell for *in-situ* experiments (Figure 105). The powerful of this technique was found appropriate to investigate structural changes of unstable nanosized bimetallic particles under reaction which can reach thermodynamic equilibrium much faster than bulk materials. More recent investigations emphasized the usefulness of this technique to get more relevant

structure-activity relationships that could allow a sharp reduction of Pt loading in electrocatalysts.[1085-1086] Even though the applications are scarce for environmental applications the data already obtained from these *in-situ* approach in aqueous phase could serve to understand the benefit obtained in bimetallic systems or by the intrinsic nature or the support materials to change structural and electronic properties of nanoparticles of active phases. By way of illustration, Pt and Rh in PtRhSnO$_2$/C remains essentially at the metallic state during electroxidation and the metal-metal coordination from EXAFS analysis agrees with homogeneous distribution without significant restructuring effects. This reveals the key role played by SnO$_2$ that would weaken the interaction between water and the noble metals. The stability of small Pt nanoparticles can be directly visualized during electro chemical oxidation by using *in-situ* high-energy-resolution X-ray absorption spectroscopy.[1086] According, to the potential regime, Pt can bind hydrogen or oxygen more strongly on small nanoparticles recognized as more sensitive to oxidation then leading to partial dissolution. In-situ XAS measurements also provide direct information on restructuring of bimetallic particles with reversible changes on NiPt particle shifting from Ni- to Pt-terminated surface which emphasize the difficile challenge in controlling the stability according the reactive medium.[1087]
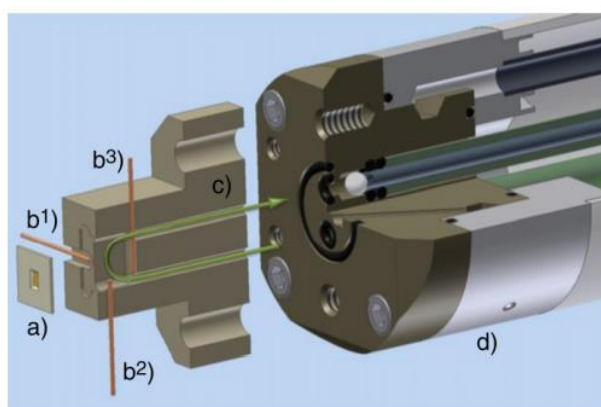
Figure 105. Scheme of electrochemical cell for in-situ X-ray absorption spectroscopy. a) Si$_3$N$_4$ window, b1) electrical connection to Si$_3$N$_4$ (working electrode), b2) reference electrode, b3) counter electrode, c) PEEK body, d) support green assembly. The green arrow indicates the liquid flow. Reproduced with permission from ref [1088]. Copyrigth 2010 Elsevier.

5.3.2. From solid to adsorbates and reactive intermediates

Infrared spectroscopy is widely used, quasi routinely, essentially for gas phase reactions in order to identify surface functional groups of heterogeneous catalysts and the interaction

between these groups with probe molecules and/or adsorbates generated in the course of reactions in the particular case of *operando* spectroscopic investigations. Technical aspects must be considered for designing specific IR cell to heat uniformly and irradiate completely the sample in case of catalytic and photocatalytic reactions respectively. Water interaction usually complexifies data treatment due to the strong adsorption of water and loss of resolution caused by significant IR band overlapping. Successful achievements have been recently reported thanks to the implementation of multivariate curve resolution alternating least squares analysis.[1089] Even though advance time-resolved methodologies have been mostly developed for gas-phase catalytic reactions to identify relevant species with a time resolution of the microsecond order, their potentiality for probing solid-water interfaces would probably bring original insights. Indeed, previous investigations[1090] report outstanding achievements which underline the potentiality of this methodology to investigate hydrogen bonding in liquid phase. It is clear the impact of hydrogen bonding on the configuration of adsorbate and strength of adsorption is still an open question with predictions which have not been supported by experimental evidences.

In case of *in-situ* liquid phase reactions Time resolved reflectance Fourier transformed spectroscopic measurements on Pt/TiO_2 photocatalysts coupled to multivariable analysis is a powerful approach to elucidate reaction intermediates and mechanisms.[1091] Basically, the photo-induced response given by a laser pulse irradiation can provide significant information of short life-time of photoregenerate charges and radicals.[1092] Clearly, this method allow the detection of radical oxygen species as key intermediate in catalytic oxidation reaction.

Finally, in introduction of this chapter a relevant example has been described related to the catalytic degradation of antibiotics by using Ag_3PO_4 as photocatalysts. This an offers the opportunities to established reliable structure-activity correlations since previous observations demonstrated the structure-sensitivity of this reaction. Nevertheless, some controversies arose from these studies regarding the most active exposed facet among (100) and (111) predominantly formed on cubic and tetrahedral Ag_3PO_4 structures respectively.[1093] Femtosecond time-resolved diffuse reflectance experiments on different Ag_3PO_4 morphologies irradiated under 400 nm excitation lead to more insights into the dynamics of charges carriers.[1076] The transient absorption profiles in Figure 106 in the range 825-1175 nm reflect electron trapping and subsequent decrease can be ascribed to charge recombination. The charge carrier dynamics can be modeled by a two exponential function according to equation (107) where A and τ_1 stands for the amplitude and the lifetime. The different values for the lifetime

(Table 5) highlight a slower recombination of charge carrier for cubic morphology characterized predominantly by (100) facets. Accordingly, the highest performance in antibiotic photodegradation has been explained by a higher mobility of electrons and holes in tetrahedral Ag_3PO_4 crystal which can be transported and then involve redox reactions

$$\Delta A = \Delta A_0 + \sum_i A_i e^{-\tau/\tau_1} \tag{107}$$
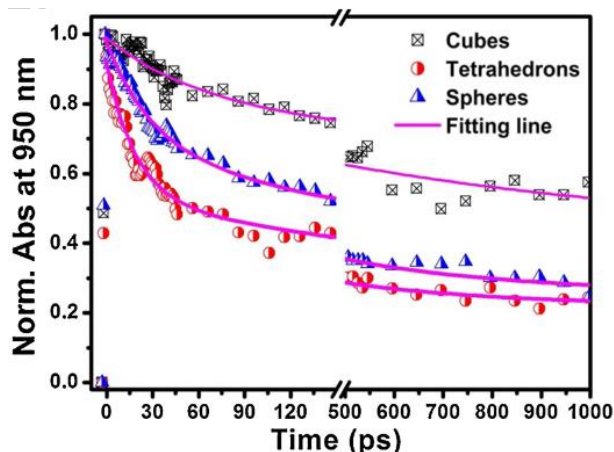
Figure 106. Temporal response of transient absorption by Ag_3PO_4 tetrahedrons, cubes and spheres from femtosecond time-resolved diffuse reflectance infrared spectroscopic experiments. Reprinted with permission from ref. [1076]. Copyrigth 2021 Elsevier.

Table 5. Lifetime of TDR decay for Ag_3PO_4 crystals calculated from time profile at 950 nm. Reprinted with permission from ref [1076].

Sample (Ag_3PO_4)	τ_1 (ps)	τ_2 (ps)	$\tau_{average}$ (ps)
Tetrahedrons	18.9 (67.9%)	327 (67.9%)	118
Cubes	58.8 (54.2%)	801 (54.2%)	399
Sphere	30.1 (50.2%)	350 (50.2%)	189

6. Conclusion and outlook

This review emphasizes some peculiarities of catalytic processes as potential substitutes to current technologies for water treatment. While oxidative and reductive treatments can be implemented and have been documented in this review, most of examples considers emerging pollutants such as phenolic compounds, antibiotics, pesticides, etc. recognized for their

recalcitrance. Advanced oxidation process (AOP) is a powerful technique but can fail to completely mineralize these recalcitrant contaminants. The basic idea in the various examples described in this review is linked to the introduction of catalysts, mainly heterogeneous catalysts, and checking if this idea can be relevant based on the balance between advantages and drawbacks. This comparison could open some prospects in their development at short or medium terms. Particular attention was also paid to fundamentals because academic viewpoint is undoubtedly linked to further successful practical developments and the controversies that exist actually on the reaction mechanisms[1094] and related identification of catalyst functionalities can be serious limitations and slow down their development.

Some important aspects have been devoted to non-solar, *i.e.* plasma, microwave and bio-catalysis as well as solar driven catalytic technologies with a particular attention in coupling with other catalytic technologies, *i.e.* biocatalysis, sonocatalysis and electrocatalysis. Hybrid solutions are actually emerging with promising achievements at lab-sale but not really yet optimized for development at pilot or industrial scale at short and medium terms. An important aspect lies in the add-value of such coupling not fully established. Indeed, the development of synergies implies important prerequisites such as enhancing the performance of each single catalytic technologies before their further coupling. This is not trivial because, at first glance, some questions may arise regarding the exact level at which a catalytic process should be investigated, *i.e.* from nanoscale to pilot reactor. As a matter of fact, this review clearly emphasizes that a multiscale approach is probably necessary and among the huge number of review papers dedicated to catalytic water treatment, a review dealing with strategies tackling different scales and levels of expertise from catalyst at nanoscale to reactor design was missing. But this could be not enough because most of the investigations up to date missed a critical parameter of capital importance: Indeed, the presence of water and the interface with the solid catalyst, which can interfere on the stability and reactivity of intermediates, has not been investigated in detail and is not fully understood. As a matter of fact, the importance of this parameter has been already pointed in the early 2010s but we must confess that the standpoints given by the authors have not attracted a great interest despite the fact that water adsorption cannot be neglected compared to contaminants characterized by extremely low concentration [1095-1096] and no direct answer has been really addressed to these previous challenges. This specific point is closely related to the optimization of the solid-liquid-gas interphase and the intimate contact between these three phases is not strictly dependent on the catalyst itself but also concerns the strategy selected for the reactor design. It is true that this peculiarity leads to

apparent controversies first on reaction mechanisms and unfortunately no clear consensus arises up to date.

Lack of basic knowledges whith still divergences on the reaction mechanisms

Taking the example of catalytic ozonation treatment, the implementation of heterogeneous catalysis led to several contradictions first on the effective role of the catalyst in the production of ROS through ozone decomposition and from this first step the successive reactions which can take place at the surface of the catalysts, *i.e. (i)* adsorption of ozone and subsequent production of ROS, – *(ii)* the adsorption of the organic contaminant with subsequent reactions with ozone and/or ROS – *(iii)* coadsorption of ozone and the organic contaminants in competition on the same sites or on different sites. In addition, pH conditions are crucial influencing the rate of production of ROS typically favored in basic conditions. We should emphasize that this parameter is not be systematically controlled in the course of the reaction. Based on this the precise quantification of the homogeneous or heterogeneous processes can fluctuate in the course of the reaction with changes of their relative contribution. Modifications in pH conditions can also alter the charges at the surface and then modify adsorptive properties and the affinity towards poisoning effects.

Catalyst stability as a point of discussion to establish robust prediction models

The catalyst stability is a key point and literature is scarce. A careful examination of this parameters is related to the development of continuous flow reactors. Indeed, sub-processes can occur in case of partial lixiviation of the heterogeneous catalyst releasing active elements in solution. Some illustrations gave examples where homogeneous and heterogeneous catalysis can coexist. Their respective contribution is not clearly quantified because current *in-situ* techniques, namely EPR spectroscopy as suitable technique for monitoring the production of ROS is unable to distinguish HO• radicals at the surface and dispersed in solution. In addition, improper methods for quenching tests can induce undesired reactions between the spin trapping agent and radicals. This can be one of the reasons explaining the few tentative of quantitative approaches to correlate the detection of ROS to apparent rate constant inducing weaknesses on the development of robust kinetic models capable to integrate deactivation.

Most of kinetic models are developed at lab-scale in simulated conditions taking simple reaction media into account usually far from the compositions of real wastewater stream containing several unstable contaminants and/or refractory molecules. Generalized lumped kinetic models are usually preferred. Only few examples can illustrate this point but important

question remains unsolved regarding the specific role of the catalyst as promoter of ROS from O_3 decomposition or active adsorbed intermediates in real operating conditions. The implementation of sophisticated kinetic models cannot be purely justified and empirical approaches are generally preferred to fit experimental and predict kinetic measurements by adding or neglecting in the reaction rate the term $k_{catal}[C]$. Presently, deactivation phenomena are not correctly apprehended while the consequence of poisoning effect could be more significant than physical processes associated to mass and heat transfers. The loss of active phase through lixiviation process is also of major concern because of the release of soluble metallic ions in treated water. But some recent developments on the catalyst design illustrated in chapter 2 have been achieved both to promote active surface species and to enhance their resistance to deactivation through encapsulation or confinement of the catalyst in porous substrates of various structures or by synthesizing core-shell structures. Confinement can be a useful strategy in combination with the utilization of inorganic membranes, porous assembly and hierarchical porous materials to immobilize the catalytic active phases can reduce the distance between the catalytic surface and the reactants. Accordingly, this confinement could also locally increase the concentration of the soluble contaminant at the vicinity of the active site and then speed up the kinetics of its transformation. Core-shell or yolk-shell structures with the active catalyst in the core or yolk and a carbon shell have been developed offering a better protection towards leaching and sintering in addition to the ability of carbon to enhance the adsorption and activation of the oxidizing agent and the redox properties of the catalysts.

How to get more reliable surface-reactivity relationship? A step forward more rational experimental approaches

In parallel, these improvements on the catalyst design, the development of more relevant *operando* spectroscopic investigations, *i.e.* coupling catalytic and spectroscopic information, could solve the existing discrepancies on the reaction mechanisms and also offer some guideline towards a better integration of the catalyst to the reactor design. The development of miniaturized reactors could be more suited for *operando* spectroscopic studies. In connection to this methodology, the implementation of such devices developing high surface to volume ratio favoring lower heat and mass transfer perturbations could *a priori* lead to better correlation between catalytic measurements and the surface functionalities. The immobilization of active species on the microchannels from nanoparticles to enzymes can illustrate the high flexibility of miniaturized reactors. This option can be useful for developing highly appreciable combined high-throughput approaches to get more reliable kinetic

information and to screen a huge number of catalysts. This approach is actually not really prioritized while it could accelerate the search for a consensus substituting unsuccessful incremental approaches. More efficient catalytic processes for water treatment being more energy-efficient also refers to safer and sustainable technological developments and it is obvious that such small catalytic devices could also largely match to this objective and attract practical applications.

Biocatalysis : Towards more robust enzymes and the development of hybrid systems

A renewal of biocatalysis is related to the weak capability of enzymes to completely mineralize recalcitrant water contaminants. As a consequence, a large panel of organics can coexist. Even though, their ultralow concentration can have a limited eco-toxicological impact, strong inhibiting effects can occur and then deteriorate the efficacy of enzymes. This has probably stimulated the development of membrane bioreactors with preferential permeation preventing undesired sub-reaction and deactivation. Two ideas have emerged which in fact are intimately linked in connection with the development of single and hybrid systems, *i.e.* biocatalysis and photobiocatalysis. The first one concerns the immobilization of enzyme over inorganic systems for the degradation of antibiotics. Conceptually this a good idea, *laccase* or *peroxidase* immobilization improved their stability, and reusability. The second ideas concern the development of membrane reactors playing the role of substrate. However, the predictions from mathematical simulation emphasize the low competitiveness of this process because of membrane conditioning costs. As a matter of fact, prospects could be expected if cost efficiency in lifetime of the enzymatic reactors and/or regeneration costs and membrane conditioning can be improved. Recent advances in the development of photoinduced biocatalytic systems likely represent a novelty but remains at the state of proof of concept up to date. The interest of this approach is growing because of the impact of such coupling could produce at large industrial scale for the development of new generation of chemical processes for the conversion of bioresources to add-value chemicals. This is also true for water remediation but probably in lesser importance. Future benefits need the development of more robustness enzymes and more thermophilic organisms with improved tolerance to UV light. More fundamental insights into the mechanism of electron transfer from the photocatalyst and the biofilm are prerequisites to develop efficient systems. Optimal catalyst architecture with improved light reflection and broader operating pH conditions can contribute also to significant improvement in efficacy.

Photocatalytic reactors have been widely developed and attractivity is still growing by considering the number of published papers per year up to date and their high visibility towards the readership. Nevertheless, a huge variability of experimental conditions unables to draw reliable conclusions that would able to intensify practical developments. The efficiency of such processes depends on numerous parameters, *i.e.* the mass of photocatalyst in the reactor volume, the exposition to the light, the intensity of the light and its spectral range, the photoreactor design, the nature of pollutants, the presence of oxygen and other natural products acting as promoters or inhibitors. As already emphasized, the catalyst stability is also of prime importance in the capital cost for the development of such processes. Some similarities, with biocatalysis and other hybrid catalytic systems are essentially related to the lack of standard procedures which could allow their ranking and accelerate the discovery towards more efficient systems. Despite this variability, new generations of photocatalyst have emerged such as graphene, MOF, carbon nitride, diamond nanoparticles as potential substitutes of the benchmark TiO_2. Recent recommendations from IUPAC to use probe molecules for the evaluation of catalytic efficiency could be a first step towards the implementation of standardized procedures. The substitution of batch reactors, composed of suspended nanoparticles difficult to separate by simple sedimentation, by continuous fixed bed flow reactor, open different challenges in the architecture design for facilitating light diffusion in the catalyst bed and more commonly light penetration as conventional drawback in case of low transparency and turbidity. This would imply the set-up of upstream separation processes. In practice, the incorporation of materials able to absorb NIR absorption into photocatalysts could promote photothermal effect and make full use of the solar spectrum. Presently, significant advances in mathematical models based on validated kinetic models are able to explain the discrepancies on the measurements from solar simulators and under natural sunlight. This can offer helpful guidelines for the conceptualization of efficient catalytic systems for the abatement of new recalcitrant organic pollutants

Emerging coupled photoinduced technology : what could we expect at short terms?

Sonophotocatalysis combines ultrasonic sound waves, ultraviolet radiation and a semiconductor material as a photocatalyst. The profitable use visible light irradiation can be also implemented. The usefulness of ultrasound lies in slower photogenerated electron-hole recombination. A linear rate enhancement in the degradation rates of pollutant as a function of

the acoustic power was observed assigned to an increase in the number of cavitation bubbles resulting in the production of higher amount of reactive HO• radicals. Accordingly, synergistic effect can be obtained underlining the benefit of this coupling. However, some drawbacks must be solved prior to large-scale applications. Indeed, the selection of continuous flow reactor would be the best option in terms of productivities and present developments mostly refer to preferential batch reactors utilization characterized by small productivity and loss of catalyst. Probably, further improvement related to this type of reactor could be envisioned by using preferentially ceramic membrane microfiltration process, because of their better resistance to degradation compared to polymeric counterparts. Presently, this approach is at the stage of proof of concept and the cost-efficiency will be probably a key parameter for further exploitation at large scale.

The coupling of photocatalysis with electrocatalysis processes also offers some advantages increasing the holes lifetime by hindering the recombination of electron-hole pairs. A complete mineralization of the pollutants is reached at lower potential due to the participation of photons from light source emphasizing a synergy through this coupling. The principle lies in the improved production of reactive •OH radical through the electroreduction of oxygen. In addition to this general feature; photocatalytic fuel cells are able to produce electricity energy and the collected electrons may also promote water splitting to produce hydrogen as energy vector. Presently most of the application dealt with the simultaneous removal of organic pollutants by photoelectrocatalytic oxidation and of heavy metals by electroreduction. Let us note that *in-situ* production of hydrogen can be also profitably used for reduction reaction as envisioned for nitrates removal. Similarly to sonophotocatalysis and photobiocatalysis, inherent major drawbacks are related to extensive use of batch reactors. Continuous efforts towards the development of continuous flow reactor and the development of materials exhibiting improved light activity and more efficient and stable near-infrared irradiation.

Alternative to light-driven catalytic technologies

The development of non-solar driven technology could be an alternative. The combination of plasma with catalysis has been extensively investigated. Plasma is an efficient energy source to generate electrons, ions, radicals and photons with an electric field that can further lead to the production of reactive oxygen, nitrogen species with UV irradiation and/or pulsed electric field. But plasma itself is not enough efficient to insure a complete mineralization and the combination with heterogeneous catalysts is relevant. Both offer a powerful technology but

some challenges are still remaining to a complete industrial scale-up. Some issues in the complete mineralization of complex organics, *i.e.* pharmaceuticals, pesticides or insecticides, and undesirable homogeneous catalytic process should pay more attention to avoid serious damages to ecosystems after rejection of treated wastewater. The stability and separation are still under investigation. Indeed, such treatment present some limitations to remove with high efficacy insecticides, pesticides, etc. Reactive species generated by plasma (O_3, H_2O_2, $O^\bullet$ or $HO^\bullet$) can deteriorate the long-term stability of heterogeneous catalysts.

The combination of an electromagnetic wave with solid catalytic materials provide a more efficient heating than conventional thermal heating insuring much higher heating rates, and correlatively enhanced reaction rates. MW radiation, can be profitably use for wastewater treatments. Indeed, the beneficial thermal induced effect can create hot spots and/or electron/holes pairs, for producing ROS directly from water, O_2 or additional oxidants such as hydrogen peroxide or persulfates. In addition, a non-thermal effect of microwaves can improve the intra-particle diffusion and mass transfer coefficients porous materials thanks to the molecular excitation of organic molecules exhibiting a higher dielectric loss than the aqueous solution. This technology is emerging and promising because extrapolation to continuous flow reactor seems feasible. However, some questions are arising on the potential scale-up of this technology, which probably needs a careful attention on the physicochemical properties of the catalytic materials especially in terms of stability.

What do we still need for a step forward to industrial realization?

As final remarks, it seems obvious that the development of catalytic technologies is growing and the expected practical achievements are still infancy. Clearly, multiple hybrid approaches have been explored and large parts have exploited the assistance of photons or not. Most of them emphasized practical limitations but also the need get better insight into the characteristic of catalytic materials especially in working conditions. Probably, key information at nanoscale are missing and the prevalent incremental trial and error approaches will never lead to these key information. More rational approaches must be developed which should speed up future research through the elaboration of standardized procedures and the selection probe organic molecules as refractory contaminant that could lead to ranking and selection of the best technologies or practical approaches. High-throughput approaches could be an alternative. Fast acquisition of computational and experimental data should accelerate and improve the reliability in the discovery novel catalytic materials and/or prioritized existing

245

findings based on statistical analysis and machine learning techniques. The introduction of computer sciences for developing of smart systems capable to mimic human intelligence could help to predict the performances in more realistic conditions, *i.e.* multiple pollutants and continuous flow technology, leading to a faster decision integrating a reduction cost.

The modelling of the liquid/solid interface represents a grand challenge. Up to date, the molecular scale structures of adsorbed water on metals and metal oxides is still unclear while water-solid interfacial interactions directly impact the stability and reactivity of intermediates. *Ab initio* calculations recently started, mostly in connection with the development catalytic systems for biomass conversion and also electrochemical applications, but the conclusion drawn from these investigations could be also helpful for water treatment. The implementation of theoretical calculations could ease the full description and understanding the aqueous-substrate interface and biomolecule-substrate according to their intrinsic features once immobilized on a solid substrate. An open question is related to the development of cost-effective nanomaterials capable to mimic the kinetic behavior of enzymes with improved stability and higher efficiency in broader operating conditions.

Modeling the interaction between water and functionalized surfaces is presently mostly restricted to model surfaces. However, some improvements in force field algorithms can lead to fine structure of the interface driven by the competition between solid-water and water-water interactions. However, some limitations on the initial assumption to build up the model could not be strictly representative because the pH as experimental parameter can play a key role on the charges at the surface. Consequently, some questions might arise on the reliability of molecular model to induce explicit perturbations that could mimic those involved at the solid-liquid interface

Despite some technical limitations, convincing comparisons with *in-situ* exploration using XPS and XAS techniques emphasized the relevance of modeling approaches even though they can lie on assumptions that could be point of debate. The development of time-resolved spectroscopic experiments can lead to useful information to discriminate among the most active facet of crystals. Hence, coupling this approach to theoretical calculation could provide guideline in an appropriate preparation method. Clearly, all these remark are none exhaustive.

Hence, one can expect that investigation on catalytic water treatment will intensify in the near future as a key environmental concern worldwide. However, the efficacy to find a suitable catalytic technology at short terms requires concerted action and a closer interaction between

experimentalists and theoreticians to identify and solve the limiting steps in the development of industrial solution at large scale.

AUTHOR INFORMATION

Corresponding Author

Vasile I. Parvulescu - *University of Bucharest, Faculty of Chemnistry, Department of Organic Chemistry, Biochemistry and Catalysis, B-dul Regina Elisabeta 4-12, Bucharest 030016, Romania;* *https://orcid.org/0000-0002-5519-3423* *; Phone: +40 745 502 052; Email:* *vasile.parvulescu@chimie.unibuc.ro*

Authors

Florence Epron - *Université de Poitiers, CNRS UMR 7285, Institut de Chimie des Milieux et Matériaux de Poitiers (IC2MP), 4 rue Michel Brunet, TSA 51106, 86073 Poitiers Cedex 9, France;* *https://orcid.org/0000-0002-7720-1578* *; Phone: +33 549 454 832; Email:* *florence.epron@univ-poitiers.fr*

Hermenigildo Garcia - *Instituto Universitario de Tecnología Química, Universitat Politecnica de Valencia-Consejo Superior de Investigaciones Científicas, Universitat Politencia de Valencia, Av. de los Naranjos s/n, 46022 Valencia, Spain;* *https://orcid.org/0000-0002-9664-493X* *; Phone: +34 963 877 807; Email:* *hgarcia@upv.es*

Pascal Granger - *Univ. Lille, CNRS, Centrale Lille, Univ. Artois, UMR 8181 - UCCS - Unité de Catalyse et Chimie du Solide, F-59000 Lille, France;* *https://orcid.org/0000-0002-8333-4246* *; Phone: +33 320 434 938; Email:* *pascal.granger@univ-lille.fr*

Author Contributions

All authors contributed equaly.

Notes

The authors declare no competing financial interest.

Biographies

Vasile I. Parvulescu is Professor and Director of the Centre of Catalysts and Catalytic Processes of the University of Bucharest. He graduated and received the PhD both at the Polytechnic Institute of Bucharest under the supervision of Prof. Dr. Doc. I.V. Nicolescu, the founder of heterogeneous catalysis school in Romania. After a research stage in the Institute of Inorganic Chemistry, Rare and Non-Ferrous Metals he joined the Faculty of Chemistry of the University of Bucharest where he became Full Professor in 1999. He is among the founders of the Centre of Catalysts and Catalytic Processes of which he became director in 2006. His main

research interests include synthesis and investigation of catalytic materials for selective organic reactions, environmental catalysis, biomass valorization, energy production or catalytic processes under photo and plasma activation. Prof. Parvulescu is co-founder of the Romanian Catalysis Society in 1992 of which he also serves as president since 2005. Between 2011-2015 he acted as secretary of the European Federation of Catalysis Societies. He is also member of the editorial Boards of several journals (Applied Catalysis A General, Applied Catalysis B Environmental, ChemCatChem, Chemistry, Catalysts, Revue Roumaine de Chimie) and of the board of several International Conferences. He is co-author of more than 420 papers, 38 review articles and book chapters, 10 books (Wiley, RSC, Elsevier, Romanian Academy), and 28 patents.

Florence Epron is CNRS Research Director at the Institute of Chemistry of Poitiers (IC2MP), France. She obtained her Ph.D. degree in Materials Chemistry in 1991 from Pierre and Marie Curie University in Paris. In 1992, she joined the Laboratory of Catalysis in Organic Chemistry of Poitiers University as a post-doc, where she was recruited as CNRS Associate Researcher in 1994. She was promoted Research Director in 2015. She was the head of the group "Catalysis by metals" (2009-2012) and then of the SAMCat group ("From the active site to the catalytic material", more than 35 permanent staff) from 2012, when the IC2MP was created. She will be deputy director of the IC2MP from 2022. She is specialist in heterogeneous catalysis and more specifically in catalysis by metals. After having focused her research work on water treatment, mainly on nitrate reduction, she extended her background in the development of monometallic and bimetallic catalysts for various applications such as catalytic reforming and H_2 production from biomass.

Hermenegildo García is full Professor at the Instituto de Tecnología Química of the Technical University of Valencia and Honorary Adjunct Professor at the Center of Excellence in Advanced Materials Research of King Abdullaziz University. Prof. Garcia has been active in the field of heterogeneous catalysis working with porous catalysts and NPs, as well as in the photocatalytic production of solar fuels. Prof. Garcia is doctor Honoris Causa from the University of Bucharest, the recipient of the 2011 Janssen-Cilag award given by the Spanish Royal Society of Chemistry, the 2016 Jaume I prize for Novel Technologies, the Lifetime achievement award by the VDGOOD Professional Association, Trivandrum in 2021, the 2021 Yueqi Award by the Chinese University of Mining Technology, Xuzhou, Medal Lecturer in 2021 awarded by the International Association for Advanced Materials, elected member of the ChemPubSoc in 2018 and Lee Hsun Lecturer of the Chinese Academy of Science at Shenyang in 2015. Prof. Garcia is currently elected President of the Editorial Board of ChemCatChem

(Wiley). Member of the editorial board of scientific journals: Energy Environmental Science (RSC), Chemistry-An European Journal (Wiley), EnergyChem (Elsevier), Photochem. Photobiol. Sci. (RSC), J. Mol. Catal. A (Elsevier), Nanomaterials (MDPI), Molecules (MDPI) and International Journal of Molecular Science (MDPI). Professor Garcia has appeared in the list of Highly-Cited Researchers in the years 2015-2020. He has published over 850 research articles and has acted as guest editor in two books for the Royal Society of Chemistry and Wiley.

Pascal Granger is born in 1964. He graduated the University of Poitiers (France) and obtained the PhD degree in applied chemistry in 1992 in the same university. His professional activity continued at the Laboratory of Homogeneous and Heterogeneous Catalysis of Lille (CNRS), firstly in a postdoctoral stage, then as Lecturer (1994) and full professor (2003). He is presently Distinguished professor and head of an international laboratory bridging the Unité de Catalyse et Chimie du Solide (CNRS) and the National Chemical Laboratory of Pune (CSIR – India). His fields of expertise focus the kinetics of heterogeneous catalytic reactions for environmental applications and related mechanisms, correlations between spectral and kinetic investigations, and "operando" understanding of ageing processes. Pascal Granger co-authored more than 150 papers, 7 book chapters and served as guest editor of 4 books.

Aknowledgements

ABBREVIATIONS

ACF:	activate carbon fiber
AFM:	atomic force microscope
AI:	Artificial Intelligence
AOP:	advanced Oxidation Processes
4-AP:	4-aminophenol
APR:	aqueous phase reforming
ATP:	adenosine Triphosphate
ATR:	attenuated total reflectance
BPA :	bisphenol A
CFD:	computational fluid dynamic
CLEA:	cross-linked enzyme aggregate

g-CN:	graphitic carbon nitride
CNT:	carbon nanotube
COD:	chemical oxygen demand
4-CP:	4-chlorophenol
CSTR:	continuous stirred tank reactor
CWAO:	catalytic wet air oxidation
DBD:	dielectric-barrier discharge
DBDE:	decabromodiphenylether
DC:	corona discharge
2,4-DCP:	2,4-dichlorophenol
DCPMU:	3-(3,4-cichlorophenyl)-1-hydroxymethyl-1-methyurea
DDT:	1,1,1-trichloro-2,2-bis(p-chlorophenyl)ethane
DDE:	1,1,1-trichloro-2,2-bis(p-chlorophenyl)ethene
DEA:	desethylatrazine
DEHP:	diethylhexyl phthalate
DFT:	density functional theory
DIA:	desisopropylatrazine
DMPO:	5,5-dimethyl-1-pyrroline-N-oxide
DNA:	deoxyribonucleic acid
DT50:	half-life in soil
EDC:	endochrine disruptor chemical
EDS:	energy dispersive spectroscopy
EDTA:	ethylenediaminetatraacetic acid
EPR:	electron paramagnetic resonance
EXAFS:	X-ray absorption spectroscopic analysis
FAD:	flavin adenine dinucleotide
FMN:	flavin mononucleotide in the H form
FTIR:	Fourier transform infrared spectroscopy
FTO:	fluorine tin oxide
GADP:	gliding arc discharge plasm
GC/MS:	gas chromotagraphy/mass spectrometry
GDP:	glow discharge plasma
G-L-S:	gas-liquid-solid
rGO:	reduced graphene oxide
HAADF:	high-angle annular dark-field imaging
HBT:	1-hydroxybenzotriazole
HOMO-LUMO:	molecular orbitals
HOPC:	3D hierarchically-ordered porous carbon materials (HOPC)
HTC:	hydrothermal carbon
IR:	infrared
ITO:	iridium tin oxide
IUPAC:	international union of pure and applied chemistry
LAS:	Lewis acid sites (LAS)
LDH:	layered double hydroxide
MANAE:	mono-aminoethyl-N-aminoethyl
MFC :	microbial fuel cell

MICP :	microbially induced carbonate precipitation (MICP)
MIL :	abbreviation for MOF from matériaux de l′institut Lavoisier
MOF :	metal-organic frameworks
MOx :	metal oxides
MPUVL:	microwave-UV plasma
MW:	microwave
MWCT:	multi-walled carbon nanotube
NADH	nicotinamide adenine dinucleotide
NIR:	near infrared light
4-NP:	4-nitrophenol
PAA:	phenoxyalkanoic acid
PANI:	polyaniline
PBDE:	polybrominated diphenyl ether
PDA:	polydopamine
PEF:	photo-electro Fenton
PFC:	photocatalytic fuel cell
PDOR:	phthalate dioxygenase reductase
PDS:	Peroxydisulfate
PEDOT:	poly(3,4-ethylenedioxythiophene)
PMS:	peroxymonosulfate
PNP:	p-nitrophenol
PPy:	polypyrrole
PVDF:	polyvinylidene fluoride
PZC:	point zero charge
RH:	relative humidity
ROS:	reactive oxygen species
TA:	tartaric acid
SAC:	single atom catalysts
SARS-COV-2:	severe acute respiratory syndrome coronavirus 2
STEM:	scanning transmission electron microscope
SWCNT:	single-walled carbon nanotube
TEM:	Transition electron microscopy
TNT:	TiO_2 nanotube
TOF:	turn-over frequency
TrzN:	triazine hydrolase or atrazine chlorohydrolase
UHV:	ultra-high vacuum
US:	high intensity ultrasound
UV:	ultraviolet
UV-VIS:	ultraviolet-visible
WAO:	wet air oxidation
XANES:	X-ray absorption near edge structure
XAS:	X-ray absorption spectroscopy
XPS:	X-ray photoelectron spectroscopy
ZVI:	zero-valent iron

REFERENCES

(1) Villarín, M. C.; Merel, S. Paradigm shifts and current challenges in wastewater managements, *J. Hazard. Mater.* **2020**, *390*, 122139.

(2) Cheng, D.; Ngo, H. H.; Guo, W.; Chang, S. W.; Nguyen, D. D.; Liu, Y.; Wei, Q.; Wei, D. A critical review on antibiotics and hormones in swine wastewater: Water pollution problems and control approaches, *Journal of hazardous materials* **2020**, *387*, 121682.

(3) Mousset, E.; Dionysiou, D. D. Photoelectrochemical reactors for treatment of water and wastewater: a review *Environ. Chem. Lett.* **2020**, *18*, 1301-1318.

(4) Corominas, L.; Byrne, D. M.; Guest, J. S.; Hospido, A.; Roux, P.; Shaw, A.; M.D., S. The application of life cycle assessment (LCA) to wastewater treatment: A best practice guide and critical review, *Water Res.* **2020**, *184*, 116058.

(5) Serrão Sousa, V.; Ribau Teixeira, M. Metal-based engineered nanoparticles in the drinking water treatment systems: A critical review, *Sci. Total Environ.* **2020**, *707*, 13607.

(6) Weissbrodt, D. G.; Winkler, M. K. H.; Wells, G. F. Water resource recovery and circularity Responsible science, engineering and educationfor water resource recovery and circularity, *Environ. Sci.: Water Res.Technol.* **2020**, *6*, 1952-1966.

(7) Nieto-Sandoval, J.; Munoz, M.; de Pedro, Z. M.; Casas, J. A. Catalytic hydrodechlorination as polishing step in drinking water treatment for the removal of chlorinated micropollutants, *Separation Purification Technol.* **2019**, *227*, 115717.

(8) Nagar, A.; Pradeep, T. Clean Water through Nanotechnology: Needs, Gaps, and Fulfillment, *ACS Nano* **2020**, *14*, 6420-6435.

(9) Miklos, D. B.; Remy, C.; Jekel, M.; Linden, K. G.; Drewes, J. E.; Huebner, U. Evaluation of advanced oxidation processes for water and wastewater treatment - A critical review, *Water Research* **2018**, *139*, 118-131.

(10) Van Aken, P.; Lambert, N.; Van den Broeck, R.; Degrève, J.; Dewil, R. Advance in ozonation and biodegradation processes to enhance chlorophenol abatement in multisubstrate wastewaters: a review, *Environ. Sci.: Water Res.Technol.* **2019**, *5*, 444-481.

(11) Lee, J.; Kim, I. S.; Hwang, M.-H.; Chae, K.-J. Atomic layer deposition and electrospinning as membrane surface engineering methods for water treatment: a short review, *Environ. Sci.: Water Res.Technol.* **2020**, *6*, 1765-1785.

(12) Yu, G.; Wang, Y.; Cao, H.; Zhao, H.; Xie, Y. Reactive oxygen species and catalytic active sites in heterogeneous catalytic ozonation for water purification, *Environ. Sci. Technol.* **2020**, *54*, 5931-5946.

(13)   Garcia-Segura, S.; Brillas, E. Applied photoelectrocatalysis on the degradation of organic pollutant in wastewaters, *J. Photochem. Photobiol. C* **2017**, *31*, 1-35.

(14)   Gagol, M.; Przyjazny, A.; Boczkaj, G. Wastewater treatment by means of advanced oxidation processes based on cavitation: a review, *Chem. Eng. J.* **2018**, *338*, 599-627.

(15)   Xue, C.; Mao, Y.; Wang, W.; Song, Z.; Zhao, X.; Sun, J.; Wang, Y. Current status of applying microwave-associated catalysis for the degradation of organics in aqueous phase - a review, *J. Environ. Sci.* **2019**, *81*, 119-135.

(16)   Bhargava, S. K.; Tardio, J.; Prasad, J.; Föger, K.; Akolekar, D. B.; Grocott, S. C. Wet oxidation and catalytic wet oxidation, *Ind. Eng. Chem. Res.* **2006**, *45*, 1221-1258.

(17)   Glaze, W. H.; Kang, J. W.; Chaplin, D. H. The chemistry of water treatment processes involving ozone, hydrogen peroxide and UV-radiation, *Ozone: Sci. Eng.* **1987**, *9*, 335-352.

(18)   Trojanowicz, M. Removal of persistent organic pollutants (POPs) from waters and wastewaters by the use of ionizing radiation, *Sci Total Environ.* **2020**, *718*, 134425.

(19)   Hodges, B. C.; Cates, E. L.; Kim, J.-H. Challenges and prospects of advanced oxidation water treatment processes using catalytic nanomaterials, *Nature Technol.* **2018**, *13*, 642-650.

(20)   Armstrong, D. A.; Huie, R. E.; Koppenol, W. H.; Lymar, S. V.; Merényi, G.; Neta, P.; Ruscic, B.; D.M., S.; Steenken, S.; Wardman, P. Standard electrode potentials involving radicals in aqueous solution: inorganic radicals (IUPAC Technical Report), *Pure Appl. Chem.* **2015**, *87*, 1139-1150.

(21)   Zhang, B.-T.; Y., Z.; Teng, Y.; Fan, M. Sulfate radical and its application in decontamination technologies, *Crit. Rev. Environ. Sci. Technol.* **2015**, *45*, 1759-1800.

(22)   Tokazhanov, G.; Ramazanova, E.; Hamid, S.; Bae, S.; Lee, W. Advances in the catalytic reduction of nitrate by metallic catalysts for high efficiency and N2 selectivity: A review, *Chem. Eng. J.* **2020**, *384*, 123252.

(23)   Keane, M. A. Supported transition metal catalysts for hydrodechlorination reactions, *ChemCatChem* **2011**, *3*, 800-821.

(24)   Zhu, Y.; Zhu, R.; Xi, Y.; Zhu, J.; Zhu, G.; He, H. Strategies for enhancing the heterogeneous Fenton catalytic reactivity: A review, *Appl. Catal. B: Environ.* **2019**, *255*, 117739.

(25)   Vorontsov, A. V. Advancing Fenton and photo-Fenton water treatment through the catalyst design, *Materials* **2019**, *372*, 103-112.

(26)   Zhu, R.; Zhu, Y.; Xian, H.; Yan, L.; Fu, H.; Zhu, G.; Xi, Y.; Zhu, J.; He, H. CNTs/ferrihydrite as a highly efficient heterogeneous Fenton catalyst for the degradation of

Bisphenol A: The important role of CNTs in accelerating Fe(III)/Fe(II) cycling, *Appl. Catal. B: Environ.* **2020**, *270*, 118891.

(27)   Lu, S.; Liu, L.; Demissie, H.; An, G.; Wan, D. Design and application of metal-organic frameworks and derivatives as heterogeneous Fenton-like catalysts for organic wastewater treatment: A review, *Environ. Int.* **2021**, *146*, 106273.

(28)   Li, T. G., L.; Peng, X. ; Wang, W.; Zhang, W. . ,, Enhanced degradation of sulfamethoxazole by a novel Fenton-like system with significantly reduced consumption of H_2O_2 activated by g-C_3N_4/MgO composite, *Water Res.* **2021**, *190*, 116777.

(29)   Hill, G. R. Kinetics, mechanism, and activation energy of the cobaltous ion catalyzed decomposition of ozone, *J. Am. Chem. Soc.* **1948**, *70*, 1306-1307.

(30)   Wang, J.; Chen, H. Catalytic ozonation for water and wastewater treatment: Recent advances and perspective, *Sci. Total Environ.* **2020**, *704*, 135249.

(31)   Jeirani, Z.; Soltan, J. Improved formulation of Fe-MCM-41 for catalytic ozonation of aqueous oxalic acid, *Chem. Eng. J.* **2017**, *307*, 756-765.

(32)   Xu, Y.; Wang, Q.; Yoza, B. A.; Li, Q. X.; Kou, Y.; Tang, Y.; Ye, H.; Li, Y.; Chen, C. Catalytic Ozonation of Recalcitrant Organic Chemicals in Water Using Vanadium Oxides Loaded ZSM-5 Zeolites, *Front. Chem.* **2019**, *7*, 384.

(33)   Chen, H.; Fang, C.; X., G.; Jiang, G.; Wang, X.; Sun, S.-P.; Wu, W. D.; Wu, Z. Sintering- and oxidation-resistant ultrasmall Cu(I)/(II) oxides supported on defect-rich mesoporous alumina microspheres boosting catalytic ozonation, *J. Colloid Interface Sci.* **2021**, *581 B*, 964-978.

(34)   Nawrocki, J. Catalytic ozonation in water: Controversies and questions. Discussion paper, *Appl. Catal. B. Environ.* **2013**, *142-143*, 465-471.

(35)   Wang, Y.; Duan, X.; Xie, Y.; H., S.; Wang, S. Nanocarbon-Based Catalytic Ozonation for Aqueous Oxidation: Engineering Defects for Active Sites and Tunable Reaction Pathways, *ACS Catal.* **2020**, *10*, 13383-13414.

(36)   Lee, J.; von Gunten, U.; Kim, J.-H. Persulfate-Based Advanced Oxidation: Critical Assessment of Opportunities and Roadblocks, *Environ. Sci. Technol.* **2020**, *384*, 123265.

(37)   Huang, D.; Zhang, G.; Yi, J.; Cheng, M.; Lai, C.; Xu, P.; Zhang, C.; Liu, Y.; Zhou, C.; Xue, W.; Wang, R.; Li, Z.; Chen, S. Progress and challenges of metal-organic frameworks-based materials for SR-AOPs applications in water treatment, *Chemosphere* **2021**, *263*, 127672.

(38)   Xia, X.; Zhu, F.; Li, J.; Yang, H.; Wei, L.; Li, Q.; J., J.; G., Z.; Zhao, Q. A Review Study on Sulfate-Radical-Based Advanced Oxidation Processes for Domestic/Industrial

Wastewater Treatment: Degradation, Efficiency, and Mechanism, *Front. Chem.* **2020**, doi: 10.3389/fchem.2020.592056

(39)   Yang, X.; Ding, X.; Zhou, L.; Zhao, Q.; Ji, Y.; Wang, X.; Chovelon, J.-M.; Xiu, G. Direct oxidation of antibiotic trimethoprim by unactivated peroxymonosulfate via a non radical transformation mechanism, *Chemosphere* **2021**, *263*, 128194.

(40)   Duan, X.; Sun, H.; Shao, Z.; Wang, S. Nonradical reactions in environmental remediation processes: Uncertainty and challenges, *Appl. Catal. B. Environ.* **2018**, *224*, 973-982.

(41)   Yun, E.-T.; Yoo, H. Y.; Bae, H.; Kim, H.-I.; Lee, J. Exploring the role of persulfate in the activation process: radical precursor versus electron acceptor, *Environ. Sci. Technol.* **2017**, *51*, 10090-10099.

(42)   Zhang, T.; Chen, Y.; Wang, Y.; Le Roux, J.; Yang, Y.; Croué, J.-P. Efficient peroxydisulfate activation process not relying on sulfate radical mechanism for water pollutant degradation, *Environ. Sci. Technol.* **2014**, *48*, 5868-5875.

(43)   Guo, F. R.; Wang, K. J.; Lu, J. H.; Chen, J. C.; Dong, X. W.; Xia, D. S.; Zhang, A. Q.; Q., W. Activation of peroxymonosulfate by magnetic carbon supported prussian blue nanocomposite for the degradation of organic contaminants with singlet oxygen and superoxide radicals, *Chemosphere* **2019**, *218*, 1071-1081.

(44)   Garcia-Rodriguez, O.; Mousset, E.; Olvera-Vargas, H.; Lefebvre, O. Electrochemical treatment of highly concentrated wastewater: A review of experimental and modeling approaches from lab- to full-scale, *Crit. Rev. Environ. Sci. Technol.* **2020**, doi: 10.1080/10643389.10642020.11820428.

(45)   Bampos, G.; Frontistis, Z. Sonocatalytic degradation of butylparaben in aqueous phase over Pd/C nanoparticles, *Environ. Sci. Pollut. Res.* **2019**, *26*, 11905-11919.

(46)   Qiu, P.; Park, B.; Choi, J.; Thockchom, B.; Pandit, A. B.; Khim, J. A review on heterogeneous sonocatalyst for treatment of organic pollutants in aqueous phase based on catalytic mechanism, *Ultrason. Sonochem.* **2018**, *45*, 29-49.

(47)   Wang, J.; Chu, L. Irradiation treatment of pharmaceutical and personal care products (PPCPs) in water and wastewater: An overview, *Radiat. Phys. Chem.* **2016**, *125*, 56-64.

(48)   Kolaczkowski, S. T.; Plucinski, P.; Rivas, F. J.; McLurgh, D. B. Wet oxidation : a review of process technologies and aspects in reactor design, *Chem. Eng. J.* **1999**, *73*, 143-160.

(49)   Sushma; Kumari, M.; Saroha, A. K. Performance of various catalysts on treatment of refractory pollutants in industrial wastewater by catalytic wet air oxidation: A review, *J. Environ. Manage.* **2018**, *228*, 169-188.

(50) Barbier, J. J.; Oliviero, L.; Renard, B.; Duprez, D. Role of ceria-supported noble metal catalysts (Ru, Pd, Pt) in wet airoxidation of nitrogen and oxygen containing compounds, *Top. Catal.* **2005**, *33*, 77-86.

(51) De los Monteros, A. E.; Lafaye, G.; Cervantes, A.; Del Angel, G.; Barbier, J.; Torres, G. Catalytic wet air oxidation of phenol over metal catalyst (Ru,Pt) supported on TiO2-CeO2 oxides, *Catal. Today.* **2015**, *258*, 564-569.

(52) Martin-Hernandez, M.; Carrera, J.; Suarez-Ojeda, M.-E.; Besson, M.; Descorme, C. Catalytic wet air oxidation of a high strength p-nitrophenol wastewater over Ru and Pt catalysts: Influence of the reaction conditions on biodegradability enhancement, *Appl. Catal. B. Environ.* **2012**, *123-124*, 141-150.

(53) Sushma; Saroha, A. K. Biodegradability enhancement of industrial organic raffinate containing pyridine and its derivatives by CWAO using ceria promoted MnOx/Al2O3 catalyst at atmospheric pressure, *Chem. Eng. J.* **2018**, *334*, 985-994.

(54) Oliveira, A. S.; Baeza, J. A.; Saenz de Miera, B.; Calvo, L.; Rodriguez, J. J.; Gilarranz, M. A. Aqueous phase reforming coupled to catalytic wet air oxidation for the removal and valorisation of phenolic compounds in wastewater, *J. Environ. Management.* **2020**, *274*, 111199.

(55) Liu, Y.; Wang, J. L. Reduction of nitrate by zero valent iron (ZVI)-based materials: A review, *Sci. Total Environ.* **2019**, *671*, 388-403.

(56) Epron, F.; Gauthard, F.; Pineda, C.; Barbier, J. Catalytic reduction of nitrate and nitrite on Pt-Cu/Al2O3 catalysts in aqueous solution: Role of the interaction between copper and platinum in the reaction, *J. Catal.* **2001**, *198*, 309-318.

(57) Bradu, C.; Capat, C.; Papa, F.; Frunza, L.; Olaru, E.-A.; Crini, G.; Morin-Crini, N.; Euvrard, E.; Balint, I.; Zgura, I.; Munteanu, C. Pd-Cu catalysts supported on anion exchange resin for the simultaneous catalytic reduction of nitrate ions and reductive dehalogenation of organochlorinated pollutants from water, *Appl. Catal. A. General.* **2019**, *570*, 120-129.

(58) Garron, A.; Epron, F. Use of formic acid as reducing agent for application in catalytic reduction of nitrate in water, *Water Res.* **2005**, *39* 3073-3081.

(59) Huang, N.; Wang, W. L.; Xu, Z. B.; Lee, M. Y.; Wu, Q. Y.; Hu, H. Y. A study of synergistic oxidation between ozone and chlorine on benzalkonium chloride degradation pathway, *Chem. Eng. J.* **2020**, *382*, 122856.

(60) Sun, J.; Wei, B.; Mei, Q.; An, Z.; Wang, X.; Han, D.; Xie, J.; Zhan, J.; Zhang, Q.; Wang, W.; M., H. Theoretical investigation on the degradation of dibutyl phtlatate initiated by

˙OH and SO4˙- in aqueous solution : Mechanisms, kinetics and ecotoxicity assesment, *Chem. Eng. J.* **2020**, *382*, 122791.

(61)   Yao, Y.; Xie, Y.; Zhao, B.; Zhou, L.; Shi, Y.; Wang, Y.; Sheng, Y.; Zhao, H.; Sun, J.; Cao, H. N-dependent ozonation efficiency over nitrogen-containing heterocyclic contaminants : A combined density functional theory study on the reaction kinetics and degradation pathways, *Chem. Eng. J.* **2020**, *382*, 122708.

(62)   Huber, M. M.; Cononica, S.; Park, G. Y.; von Gunten, U. Oxidation of pharmaceuticals during ozonation and advanced oxidation process, *Environ. Sci. Technol.* **2003**, *37*, 1016-1024.

(63)   Kasprzyk-Hordern, B.; Ziólek, M.; Nawrocki, J. Catalytic ozonation and methods of enhancing molecular ozone reactions in water treatment, *Appl. Catal. B* **2003**, *46*, 639-669.

(64)   de Vera, G. A.; Gernjak, W.; Weinberg, H.; Farré, M. J.; Keller, J.; von Gunten, U. Kinetics and mechanism of nitrates and ammonium formation during ozonation of dissolved organic pollutants, *Water Res.* **2017**, *108*, 451-461.

(65)   Berger, P.; Leitner, N. K. V.; Doré, M.; Legube, B. Ozone and hydroxyl radicals induced oxidation of glycine, *Water Res.* **1999**, *33*, 433-441.

(66)   Leitner, N. K. V.; Bergé, N.; Legube, B. Oxidation of aminogroups by hydroxyradicals in relation to the oxidation degree of the α carbon, *Env. Sci. Technol.* **2002**, *36*, 3083-3089.

(67)   Brillas, E.; Cabot, P. L.; Rodríguez, R. M.; Arias, C.; Garrido, J. A.; Oliver, R. Degradation of the herbicide 2,4-DP by catalyzed ozonation using the O3/Fe2+/UVA system, *Appl. Catal. B* **2004**, *51*, 117-127.

(68)   Skoumal, M.; Cabot, P. L.; Centellas, F.; Arias, C.; Rodríguez, R. M.; Garrido, J. A.; Brillas, E. Mineralization of paracetamol by ozonation catalyzed with Fe2+, Cu2+ and UVA light, *Appl. Catal. B* **2006**, *66*, 228-240.

(69)   Monteagudo, J. M.; Carmona, M.; Durán, A. Photo-Fenton-assisted ozonation of p-Coumaric acid in aqueous solution, *Chemosphere* **2005**, *60*, 1103-1110.

(70)   Beltran-Heredia, J.; Torregrosa, J.; Dominguez, J. R.; Peres, J. A. Comparison of the degradation of p-hydroxybenzoic acid in aqueous solution by several oxidation processes, *Chemosphere* **2001**, *42*, 351-359.

(71)   Pillai, K. C.; Kwon, T. O.; Moon, I. S. Degradation of wastewater from terephthalic acid manufacturing process by ozonation catalyzed with Fe2+, H2O2 and UV light : Direct versus indirect ozonation reactions, *Appl. Catal. B* **2009**, *91*, 319-328.

(72)   Kusic, H.; Koprivanac, N.; Bozic, A. L. Minimization of organic pollutant content in aqueous solutionby means of AOPs: UV- and ozone-based technologies, *Chem. Eng. J.* **2006**, *123*, 127-137.

(73)   Legube, B.; Leitner, N. K. V. Catalytic ozonation : A promising advance oxidation technology for water treatment, *Catal. Today.* **1999**, *53*, 61-72.

(74)   Zhao, W.; Wu, Z.; Wang, D. Ozone direct oxidation kinetics of Cationic Red X-GRL in aqueous solution, *J. Hazard. Mater.* **2006**, *137*, 1859-1865.

(75)   Pestovsky, O.; Bakac, A. Reactivity of aqueous Fe(IV) in hydride and hydrogen atom transfer reactions, *J. Am. Chem. Soc.* **2004**, *126*, 13757−13764.

(76)   Eberhardt, M. K.; Ramirez, G.; Ayala, E. Does the reaction of copper (I) with hydrogen peroxide give hydroxyl radicals? A study of aromatic hydroxylation, *J. Org. Chem.* **1989**, *54*, 5922−5926.

(77)   Johnson, G. R. A.; Nazhat, N. B.; Saadalla-Nazhat, R. A. Reaction of the aqua copper (I) ion with hydrogen peroxide. Evidence for a Cu(III) (cupryl) intermediate, *J. Chem. Soc., Faraday Trans.* **1988**, *84*, 501−510.

(78)   Pham, A. N.; Xing, G.; Miller, C. J.; Waite, T. D. Fenton-like copper redox chemistry revisited: Hydrogen peroxide and superoxide mediation of copper-catalyzed oxidant production, *J. Catal.* **2013**, *301*, 54-64.

(79)   Yi, Q.; Ji, J.; Shen, B.; Dong, C.; Liu, J.; Zhang, J.; Xing, M. Singlet oxygen triggered by superoxide radicals in a molybdenum cocatalytic Fenton reaction with enhanced redox activity in the environnment, *Environ. Sci. Technol.* **2019**, *53*, 9725-9733.

(80)   Ren, Y.; Dong, Q.; Feng, J.; Ma, J.; Wen, Q.; M., Z. Magnetic porous ferrospinel $NiFe_2O_4$: A novel ozonation catalyst with strong catalytic property for degradation of di-n-butyl phtalate and convenient separation from water, *J. Colloid Interface Sci.* **2012**, *382*, 90-96.

(81)   Sun, W.; Wei, H.; An, L. Y.; Jin, C.; Wu, H.; Xiong, Z.; Pu, C.; Sun, C. Oxygen vacancy medited $La_{1-x}Ce_xFeO_3$ perovskite oxides as efficient catalysts for CWAO of acrylic acid by A-site Ce doping, *Appl. Catal. B* **2019**, *245*, 20-28.

(82)   Nekouei, F.; Nekouei, S.; Kargarzadeh, H. Enhanced adsorption and catalytic oxidation of ciprofloxacin on hierarchical CuS hollow nanospheres@N-doped cellulose nanocrystals hybrid composites: Kinetic and radical generation mechanism studies, *Chem. Eng. J.* **2018**, *335*, 567-578.

(83)   Ben Hammouda, S.; Zhao, F.; Safaei, Z.; Babu, I.; Ramasamy, D. L.; Sillanpää, M. Reactivity of novel ceria-perovskite composites CeO2-LaMO3 (M=Cu, Fe) in the catalytic wet peroxidative oxidation of the new emergent pollutant 'bisphenol F': characterization, kinetic and mechanism studies, *Appl. Catal. B* **2017**, *218*, 119-136.

(84)   Munoz, M.; de Pedro, Z. M.; Casas, J. A.; Rodriguez, J. J. Combining efficiency catalytic hydrodechnlorination and wet peroxide oxidation (HDC-CWPO) for the abatement of organochlorinated water pollutants, *Appl. Catal. B* **2014**, *150-151*, 197-203.

(85)   Wang, B.; An, B.; Su, Z.; Li, L.; Liu, Y. A novel strategy for sequential reduction of nitrate into nitrogen by CO2 anion radical: Experimental study and DFT calculation, *Chemosphere* **2021**, *269*, 128754.

(86)   Kim, H.; Lim, J.; Lee, S.; Kim, H.-H.; Lee, C.; Lee, J.; Choi, W. Spontaneous generation of H2O2 and hydroxyl radicals through O2 reduction on copper phosphide under ambient aqueous conditions, *Environ. Sci. Technol.* **2019**, *53*, 2918-2925.

(87)   Yuan, I.; Shen, J.; Chen, Z.; Guan, X. Role of Fe/pumice composition and structure in promoting the ozonation reaction, *Appl. Catal. B* **2016**, *180*, 707-714.

(88)   Zhang, H.; He, Y.; Lai, L.; Yao, G.; Lai, B. Catalytic ozonation of Bisphenol A in aqueous solution by Fe_3O_4-MnO_2 magnetic composites : Performance, transformation pathways and mechanism, *Separation and purification technol.* **2020**, *245*, 116449.

(89)   Yuan, Y.; Xing, G.; Garg, S.; Ma, J.; Kong, X.; Dai, P.; Waite, T. D. Mechanistic insights into the catalytic ozonation process using iron oxide-impregnated activated carbon, *Water Res.* **2020**, *177*, 115785.

(90)   Bing, J.; Hu, C.; Nie, Y.; Yang, M.; Qu, J. Mechanism of catalytic ozonation in Fe2O3/Al2O3@SBA-15 aqueous suspension for destruction of Ibuprofen, *Environ. Sci. Technol.* **2015**, *49*, 1690-1697.

(91)   Zhang, T.; Li, W.; Croué, J.-P. Catalytic ozonation of oxalate with a cerium supported palladium oxide: An efficient degradation not relying on hydroxyl radical oxidation, *Environ. Sci. Technol.* **2011**, *45*, 9339-9346.

(92)   Wu, Q.; Hu, X.; Yu, P. L. Kinetics on catalytic wet air oxidation of phenol, *Chem. Eng. J.* **2003**, *58*, 923-928.

(93)   Zhang, Y.; Fan, J.; Yang, B.; Ma, L. Synergistic effect of ferrous ion and copper oxide on the oxidative degradation of aqueous acetaminophen at acid conditions : A mechanism investigation, *Chem. Eng. J.* **2017**, *326*, 612-619.

(94)   Chen, W.; Li, X.; Tang, Y.; Zhou, J.; Wu, D.; Wu, Y.; Li, L. Mechanim insight of pollutant degradation and bromate inhibition by Fe-Cu-MCM-41 catalyzed ozonation, *J. Hazard. Mater.* **2018**, *346*, 226-233.

(95)   Granger, P.; Troncea, S.; Dacquin, J. P.; Trentesaux, M.; Gardoll, O.; Nuns, N.; Parvulescu, V. I. Peculiar kinetic properties of Cu-doped Pd/CexZr1-xO2 in water

denitrification : Impact of Pd-Cu interaction vs structural properties of $Ce_xZr_{1-x}O_2$, *Appl. Catal. B* **2019**, *253*, 391-400.

(96)   Granger, P.; Troncéa, S.; Dacquin, J. P.; Parvulescu, V. I. Support-induced effect on the catalytic properties of Pd particles in water denitrification : Impact of the preparation on surface and structural features of $Ce_{0.5}Zr_{0.5}O_2$, *Appl. Catal. B* **2018**, *224*, 648-659.

(97)   Al Bahri, M.; Calvoa, L.; Gilarranz, M. A.; Rodriguez, J. J.; F., E. Activated carbon supported metal catalysts for reduction of nitrate in water with high selectivity towards N_2, *Appl. Catal. B* **2013**, *138-139*, 141-148.

(98)   Gauthard, F.; Epron, F.; Barbier, J. Palladium and platinum-based catalysts in the catalytic reduction of nitrate in water: effect of copper, silver, or gold addition, *J. Catal.* **2003**, *220*, 182-191.

(99)   Zhao, Y.; Baeza, J. A.; Rao, N. K.; Calvo, L.; Gilarranz, M. A.; Li, Y. D.; Lefferts, L. Unsupported PVA- and PVP-stabilized Pd nanoparticles as catalyst for nitrite hydrogenation in aqueous phase, *J. Catal.* **2014**, *318*, 162-169.

(100)   Martínez, J.; Ortiz, A.; Ortiz, I. State-of-the-art and perspectives of the catalytic and electrocatalytic reduction of aqueous nitrates, *Appl. Catal. B* **2017**, *207*, 42-59.

(101)   Pintar, A.; Batista, J.; Levee, J.; T., K. Kinetics of the catalytic liquid-phase hydrogenation of aqueous nitrate solutions, *Appl. Catal. B* **1996**, *11*, 81-98.

(102)   Wärna, J.; Turunen, I.; Salmi, T.; Manula., T. Kinetics of nitrate reduction in monolith reactor, *Chem. Eng. Sci.* **1994**, *49*, 5763-5773.

(103)   Xu, P.; Agarwal, S.; Lefferts, L. Mechanism of nitrite hydrogenation over Pd/g-Al2O3 according a rigorous kinetic study, *J. Catal.* **2020**, *383*, 124-134.

(104)   Oliviero, L.; Barbier, J., J.; Duprez, D. Wet air oxidation of nitrogen-containing organic compounds and ammonia in aqueous media, *Appl. Catal. B* **2003**, *40*, 163-184.

(105)   Lousteau, C.; Ayadi, H.; Descorme, C. Aqueous phase catalytic wet air oxidation of ammonia : thermodynamic considerations, *Appl. Catal. B* **2017**, *202*, 12-20.

(106)   Qin, J.; Aika, K. I. Catalytic wet air oxidation of ammonia over alumina supported metals, *Appl. Catal. B* **1998**, *16*, 261-268.

(107)   Lee, D. K.; Cho, J. S.; Yoon, W. L. Catalytic wet oxidation of ammonia: Why is N2 formed preferentially against NO^{3-}, *Chemosphere* **2005**, *61*, 573-578.

(108)   Wang, Y.; Sun, W.; Wei, H.; Sun, C. Extended study of ammonia conversion to N2 using a Ru/0.2TiZrO4 catalyst via catalytic wet air oxidation, *Catal. Sci. Technol.* **2016**, *6*, 6144-6151.

(109) Gai, H.; Liu, X.; Feng, B.; Gai, C.; Huang, T.; Xiao, M.; Song, H. An alternative scheme of biological removal of ammonia nitrogen from waste-highly dispersed Ru cluster @mesoporous TiO2 for the catalytic wet oxidation of low-concentration of ammonia, *Chem. Eng. J.* **2021**, *407*, 127082.

(110) Zhao, H.; Gao, J.; Zhou, W.; Wang, Z.; Wu, S. Quantitative detection of hydroxyl radicals in Fenton system by UV-vis spectroscopy, *Anal. Methods* **2015**, *7*, 5447-5453.

(111) Xianq, Q.; Yu, J.; Wong, P. K. Quantitative characterization of hydroxyl radicals produced by various photocatalysts, *J. Colloid Interface Sci.* **2011**, *357*, 163-167.

(112) Utsumi, H.; Y.H., H.; Ichikawa, K. A. Kinetic study of 3-chlorophenol enhanced hydroxyl radical generation during ozonation, *Water Res.* **2003**, *37*, 4924-4928.

(113) Pei, S.; You, S.; Ma, J.; Chen, X.; Ren, N. Electron Spin Resonance Evidence for Electro-generated Hydroxyl Radicals, *Environ. Sci. Technol.* **2020**, *54*, 13333-13343.

(114) Fontmorin, J. M.; Burgos Castillo, R. C.; Tang, W. Z.; Sillanpää, M. Stability of 5,5-dimethyl-1-pyrroline-N-oxide as spin-trap for quantification of hydroxyl radicals in processes based on Fenton reaction, *Water Res.* **2016**, *99*, 24-32.

(115) Han, S. K.; Ichiwaka, K.; H., U. Quantitative analysis for the enhancement of hydroxyl radical generation by phenols during ozonation of water, *Water Res.* **1998**, *32*, 3261-3266.

(116) Song, Z.; Wang, M.; Wang, Z.; Wang, Y.; Li, R.; Zhang, Y.; Liu, C.; Liu, B.; Xu, B.; Qi, F. Insight into heteroatom-doped graphene for catalytic ozonation : active centers, reactive oxygen species evolution, and catalytic mechanism, *Environ. Sci. Technol.* **2019**, *53*, 5337-5348.

(117) den Hartog, S.; Samanipour, M.; Ching, H. Y. V.; Van Doorslaer, S.; Breugelmans, T.; Hubin, A.; Ustarroz, J. Reactive oxygen species formation at Pt nanoparticles revisited by electron paramagnetic resonance and electrochemical analysis, *Electrochem. Commun.* **2021**, *122*, 106878.

(118) Lazaro-Martinez, J. M.; Lombardo Lupano, L. V.; Piehl, L. L.; Rodriguez-Castellon, E.; Campo Dall' Orto, V. New Insights about the Selectivity in the Activation of Hydrogen Peroxide by Cobalt or Copper Hydrogel Heterogeneous Catalysts in the Generation of Reactive Oxygen Species, *J. Phys. Chem. C* **2016**, *120*, 29332-29347.

(119) Karthikeyan, S.; Sekaran, G. I. In situ generation of a hydroxyl radical by nanoporous activated carbon derived from rice husk for environmental applications: kinetic and thermodynamic constants, *Phys. Chem. Chem. Phys.* **2014**, *16*, 3924-3933.

(120) Bulanin, K. M.; Lavalley, J. C.; Tsyganenko, A. A. IR spectra of adsorbed ozone, *Colloïds Surf. A* **1995**, *101*, 153-158.

(121)   Ebbesen, S. D.; Mojet, B. L.; L., L. In situ ATR-IR study of nitrite hydrogenation over Pd/Al$_2$O$_3$., *J. Catal.* **2008**, *256*, 15-23.

(122)   Ebbesen, S. D.; Mojet, B. L.; L., L. In Situ Attenuated Total Reflection Infrared (ATR-IR) Study of the adsorption of NO^{2-},NH$_2$OH, and NH^{4+} on Pd/Al$_2$O$_3$ and Pt/Al$_2$O$_3$, *Langmuir* **2008**, *24*, 869-879.

(123)   Rosca, V.; Beltramo, G. L.; Koper, M. T. M. Reduction of NO adlayers on Pt(110) and Pt(111) in acidic media: evidence for adsorption site-specific reduction, *Langmuir* **2005**, *21*, 1448-1456.

(124)   Casero, E.; Alonso, C.; Martin-Gago, J. A.; Borgatti, F.; Felici, R.; Renner, F.; Lee, T. L.; Zegenhagen, J. Nitric-oxide adsorption and oxidation on Pt(111) in electrolyte solution under potential control., *Surf. Sci.* **2002**, *507-510* 688-694.

(125)   Gao, Y.; Zhu, Y.; Lyu, L.; Zeng, Q.; Xing, X.; Hu, C. Electronic structure modulation of graphitic carbon nitride by oxygen doping for enhanced catalytic degradation of organic pollutants through peroxymonosulfate activation, *Environ. Sci. Technol.* **2018**, *52*, 14371−14380.

(126)   Li, H.; Shang, J.; Yang, Z.; Shen, W.; Ai, Z.; Zhang, L. Oxygen vacancy associated surface fenton chemistry: Surface structure dependent hydroxyl radicals generation and substrate dependent reactivity, *Environ. Sci. Technol.* **2017**, *51*, 5685−5694.

(127)   Li, H.; Shang, H.; Cao, X.; Yang, Z.; Ai, Z.; Zhang, L. Oxygen vacancies mediated complete visible light NO oxidation via side-on bridging superoxide radicals, *Environ. Sci. Technol.* **2018**, *52*, 8659−8665.

(128)   Zhu, G.; Zhu, J.; Jiang, W.; Zhang, Z.; Wang, J.; Zhu, Y.; Zhang, Q. Surface oxygen vacancy induced-MnO2 nanofiber for highly efficient ozone elimination, *Appl. Catal. B* **2017**, *209*, 729-737.

(129)   Ma, Y.; Wu, X.; G., Z. Core-shell Ag@Pt nanoparticles supported on sepiolite nanofibers for the catalytic reduction of nitrophenols in water: Enhanced catalytic performance and DFT study, *Appl. Catal. B* **2017**, *205*, 262-270.

(130)   Chen, C.; Zhang, H.; Lia, K.; Tanga, Q.; Bian, X.; Gu, J.; Cao, Q.; Zhong, L.; Russell, C. K.; Fan, M.; Jia, J. Cu$^+$ based active sites of different oxides supported Pd-Cu catalysts and electrolytic in-situ H2 evolution for high-efficiency nitrate reduction reaction, *J. Catal.* **2020**, *392*, 231-243.

(131)   Shin, H.; Jung, S.; Bae, S.; Lee, W.; Kim, H. Nitrite Reduction Mechanism on a Pd Surface, *Environ. Sci. Technol.* **2014**, *48*, 12768−12774.

(132) Belkacemi, K.; Larachi, F.; Sayari, A. Lumped Kinetics for Solid-Catalyzed Wet Oxidation: A Versatile Model, *J. Catal.* **2000**, *193*, 224-237.

(133) Guo, Y.; Zhu, S.; Wang, B.; Huang, J.; Deng, S.; Yu, G.; Wang, Y. Modelling of merging contaminant removal during heterogeneous catalytic ozonation using chemical kinetic approaches, *J. Hazard. Mater.* **2019**, *380*, 120888.

(134) Pintar, A.; Berčič, G.; Besson, M.; Gallezot, P. Catalytic wet-air oxidation of industrial effluent: total mineralization of organics and lumped kinetic modelling, *Appl. Catal. B* **2004**, *47*, 143-152.

(135) Palomares, A. E.; Franch, C.; Corma, A. Nitrates removal from polluted aquifers using (Sn or Cu)/Pd catalysts in a continuous reactor, *Catal. Today.* **2010**, *149*, 348-351.

(136) Hagen, J. *Industrial Catalysis*; Ed. Wiley-VCH Verlag GmbH & Co.KGaA, 2006.

(137) Gómez-Quero, S.; Cárdenas-Lizana, F.; Keane, M. A. Liquid phase catalytic hydrodechlorination of 2,4-dichlorophenol over Pd/Al$_2$O$_3$: Batch vs. continuous operation, *Chem. Eng. J.* **2011**, *166*, 1044-1051.

(138) Monteil, H.; Pechaud, Y.; Oturan, N.; Trellu, C.; Oturan, M. A. Pilot scale continuous reactor for water treatment by electrochemical advanced oxidation processes : Development of a new hydrodynamic/reactive combined model, *Chem. Eng. J.* **2021**, *404*, 127048.

(139) Lopes, R. J. G.; Quinta-Ferreira, R. M. Assessment of CFD Euler-Euler method for trickle-bed reactor modelling in the catalytic wet oxidation of phenolic wastewaters, *Chem. Eng. J.* **2010**, *160*, 293-301.

(140) Chander, A.; Kundu, A.; Bej, S. K.; Dalai, A. K.; Vohra, D. K. Hydrodynamic characteristics of cocurrent upflow and downflow of gas and liquid in a fixed bed reactor, *Fuel* **2001**, *80*, 1043-1053.

(141) Van Klinken, J.; Van Dongen, R. H. Catalyst dilution for improved performance of laboratory trickle-flow reactors, *Chem. Eng. Sci.* **1980**, *35*, 59-66.

(142) Li, C.; Sun, W.; Lu, Z.; Ao, X.; Li, S. Ceramic nanocomposite membranes and membrane fouling: A review, *Water Res.* **2020**, *175*, 115674.

(143) Zhang, W.; Ding, L.; Luo, J.; Jaffrin, M. Y.; Tang, B. Membrane fouling in photocatalytic membrane reactors (PMRs) for water and wastewater treatment: A critical review, *Chem. Eng. J.* **2016**, *302*, 446-458.

(144) Jiang, H.; Jiang, X.; She, F.; Wang, Y.; Xing, W.; Chen, R. Insights into membrane fouling of a side-stream ceramic membranereactor for phenol hydroxylation over ultrafine TS-1, *Chem. Eng. J.* **2014**, *239*, 373-380.

(145) Franch, C.; Lammertink, R. G. H.; Lefferts, L. Partially hydrophobized catalyst particles for aqueous nitrite hydrogenation, *Appl. Catal. B* **2014**, *156-157*, 166-172.

(146) Wada, K.; Hirata, T.; Hosokawa, S.; Iwamoto, S.; Inoue, M. Effect of supports on Pd-Cu bimetallic catalysts for nitrate and nitrite reduction in water, *Catal. Today.* **2012**, *185*, 81-87.

(147) Xu, P. Three-Phase Catalytic reactions in aqueous solutions, PhD Thesys, *Twente University* **2020**, *ISBN : 978-90-365-5047-5*.

(148) Quintanilla, A.; Bakker, J. J. W.; Kreutzer, M. T.; Moulijn, J. A.; F., K. Tuning the support adsorption properties of Pd/SiO2 by silylation to improve the selective hydrogenation of aromatic ketones, *J. Catal.* **2008**, *257*, 55-63.

(149) Rostam, A. B.; Taghizadeh, M. Advanced oxidation processes integrated by membrane reactors and bioreactors for various wastewater treatments: A critical review, *J. Environ. Chem. Eng.* **2020**, *8*, 104566.

(150) Coronas, J.; Santamaría, J. Catalytic reactors based on porous ceramic membranes, *Catal. Today.* **1999**, *51*, 377-389.

(151) Aran, H. C.; Pacheco Benito, S.; Luiten-Olieman, M. W. J.; Er, S.; Wessling, M.; Lefferts, L.; Benes, N. E.; Lammertink, R. G. H. Carbon nanofibers in catalytic membrane microreactors, *J. Membrane Sci.* **2011**, *381*, 244-250.

(152) Ravnjak, M.; Vrtovšek, J.; Pintar, A. Denitrification of drinking water in a two-stage membrane bioreactor by using immobilized biomass, *Bioresource Technol.* **2013**, *128*, 804-808.

(153) Vospernik, M.; Pintar, A.; Berčič, G.; Batista, J.; Levec, J. Potentials of ceramic membranes as catalytic three-phase reactors, *Chem. Eng. Research Design* **2004**, *82*, 659-666.

(154) Randal, M.; Seaman, J.; Kim, J.; K., D. Activity and stability of the catalytic hydrogel membrane reactor for treating oxidized contaminants, *Water Res.* **2020**, *174*, 115593.

(155) Julbe, A.; Farrusseng, D.; Guizard, C. Porous ceramic membranes for catalytic reactors-overview and new ideas, *J. Membr. Sci.* **2001**, *181*, 3-20.

(156) Aran, H. C.; Chinthaginjala, J. K.; Groote, R.; Roelofs, T.; Lefferts, L.; Wessling, M.; R.G.H., L. Porous ceramic mesoreactors: A new approach for gas-liquid contacting in multiphase microreaction technology, *Chem. Eng. J.* **2011**, *169*, 239-246.

(157) Ho, H. L.; Chan, W. K.; Blondy, A.; Yeung, K. L.; Schrotter, J. C. Experiment and modeling of advance ozone membrane reactor for tretament of organic endocrine disrupting pollutants in water, *Catal. Today.* **2012**, *193*, 120-127.

(158) Petrova, I. V.; Anokhina, T. S.; Borisov, R. S.; Volkov, V. V.; A.B., Y. Removal of trichloroethylene from water in the catalytic membrane reactor, *Catal. Today.* **2016**, *268*, 150-155.

(159) Wu, Y.; Zhang, H.; Yan, Y. Effect of copper ion-exchange on catalytic wet peroxide oxidation of phenol over ZSM-5 membrane, *J. Environ. Management* **2020**, *270*, 110907.

(160) Osegueda, O.; Dafinov, A.; Llorca, J.; Medina, F.; J., S. Heterogeneous catalytic oxidation of phenol by in situ generated hydrogen peroxide applying novel catalytic membrane reactors, *Chem. Eng. J.* **2015**, *262*, 344-355.

(161) Mansas, C.; Mendret, J.; Brosillon, S.; A., A. Coupling catalytic ozonation and membrane separation: A review., *Separation and Purification Technology* **2020**, *236*, 116221.

(162) Sannino, D.; Vaiano, V.; Ciambelli, P.; Isupova, L. A. Mathematical modelling of the heterogeneous photo-Fenton oxidation of acetic acid on structured catalysts, *Chem. En. J.* **2013**, *224*, 53-58.

(163) Sannino, D.; Vaiano, V.; Isupova, L. A.; Ciambelli, P. Heterogeneous photo-Fenton oxidation of organic pollutants on structured catalysts, *J. Adv. Oxid. Technol.* **2012**, *15* 294-300.

(164) Sannino, D.; Vaiano, V.; Isupova, L. A.; Ciambelli, P. Photo-Fenton oxidation of acetic acid on supported LaFeO3 and Pt/LaFeO3 perovskites, *Chem. Eng. Trans.* **2011**, *25*, 1013-1018.

(165) Keil, F. J. Process intensification, *Rev. Chem. Eng.* **2018**, *34*, 135-200.

(166) Costantini, F.; Bula, W. P.; Salvio, R.; Huskens, J.; Gardeniers, H. J. G. E.; Reinhoudt, D. N.; Verboom, W. Nanostructure based on polymer brushes for efficient heterogeneous catalysis in microreactors, *J. Am. Chem. Soc.* **2009**, *131*, 1650-1651.

(167) Kashid, M. N.; Kiwi-Minsker, L. Microstructured reactors for multiphase reactions: state of the art, *Ind. Eng. Chem. Research* **2009**, *48*, 6465-6485.

(168) Gavriilidis, A.; Angeli, P.; Cao, E.; Yeong, K. K.; Wan, Y. S. S. Technology and applications of micro engineered reactors, *Chem. Eng. Res. Des.* **2002**, *80*, 3-30.

(169) Mason, B. P.; Price, K. E.; Steinbacher, J. L.; Bogdan, A. R.; McQuade, D. T. Greener approaches to organic synthesis using microreactor technology, *Chem. Rev.* **2007**, *107*, 2300-2318.

(170) deMello, A. J. Control and detection of chemical reactions, *Nature* **2006**, *442*, 394-402.

(171) Constantini, F.; Benetti, E. M.; Tiggelaar, R. M.; Gardeniers, H. J. G. E.; Reinhoudt, D. N.; Huskens, J.; Vancso, G. J.; Verboom, W. A brush-gel/metal nanoparticle hybrid film as an efficient supported catalyst in glass microreactor, *Chem. Eur. J.* **2010**, *16*, 12406-12411.

(172)   Myazaki, M.; Maeda, H. Microchannel enzyme reactors and their applications for processing, *Trends Biotechnol.* **2006**, *24*, 463-470.

(173)   Zhang, L.; Liu, Z.; Wang, Y.; Xie, R.; Ju, X.-J.; Wang, W.; Lin, L.-G.; Chu, L.-Y. Facile immobilization of Ag nanoparticles on microchannel walls in microreactors for catalytic applications, *Chem. Eng. J.* **2017**, *309*, 691-699.

(174)   Losey, M. W.; Schmidt, M. A.; Jensen, K. F. Microfabricated multiphase packed-bed reactors : characterization of mass transfer and reactions, *Ind. Eng. Chem. Res.* **2001**, *40*, 2555-2562.

(175)   Gorges, R.; Meyer, S.; Kreisel, G. Photocatalysis in microreactors, *J. Photochem. Photobiol. A, Chem.* **2004**, *A167*, 95-99.

(176)   Qiu, B.; Xing, M.; Zhang, J. Stöber-like method to synthesize ultralight, porous, stretchable Fe_2O_3/graphene aerogels for excellent performance in photo-Fenton reaction and electrochemical capacitors, *J. Mater. Chem. A.* **2015**, *3*, 12820-12827.

(177)   Wang, N.; Zhu, L.; Lei, M.; She, Y.; Cao, M.; Tang, H. Ligand-Induced Drastic Enhancement of Catalytic Activity of Nano-BiFeO3 for Oxidative Degradation of Bisphenol A, *ACS Catal.* **2011**, *1*, 1193-1202.

(178)   Hou, X.; Huang, X.; Jia, F.; Ai, Z.; Zhao, J.; Zhang, L. Hydroxylamine Promoted Goethite Surface Fenton Degradation of Organic Pollutants, *Environ. Sci. Technol.* **2017**, *51*, 5118-5126.

(179)   Shi, J.; Ai, Z.; Zhang, L. $Fe@Fe_2O_3$ core-shell nanowires enhanced Fenton oxidation by accelerating the Fe(III)/Fe(II) cycles, *Water Res.* **2014**, *59*, 145-153.

(180)   Dong, C.; Ji, J.; Shen, B.; Xing, M.; Zhang, J. Enhancement of H_2O_2 Decomposition by the Co-catalytic Effect of WS_2 on the Fenton Reaction for the Synchronous Reduction of Cr(VI) and Remediation of Phenol, *Environ. Sci. Technol.* **2018**, *52*, 11297-11308.

(181)   Huang, M.; Wang, X.; Liu, C.; Fang, G.; Gao, J.; Wang, Y.; Zhou, D. Mechanism of metal sulfides accelerating Fe(II)/Fe(III) redox cycling to enhance pollutant degradation by persulfate: Metallic active sites vs. reducing sulfur species, *J. Hazard Mater.* **2021**, *404 B*, 124175.

(182)   Wang, K.; Liu, X.; Tang, J.; Wang, L.; Sun, H. Ball milled Fe0@FeS hybrids coupled with peroxydisulfate for Cr(VI) and phenol removal: Novel surface reduction and activation mechanisms, *Sci Total Environ.* **2020**, *739*, 139748.

(183)   Zhang, N.; Tsang, E. P.; Chen, J.; Fang, Z.; Zhao, D. Critical Role of Oxygen Vacancies in Heterogeneous Fenton Oxidation over Ceria-Based Catalysts, *J. Colloid Interface Sci.* **2020**, *558*, 163−172.

(184) Huang, Y.; Luo, M.; Li, S.; Xia, D.; Tang, Z.; Hu, S.; Ye, S.; Sun, M.; He, C.; Shu, D. Efficient catalytic activity and bromate minimization over lattice oxygen-rich MnOOH nanorods in catalytic ozonation of bromide-containing organic pollutants: Lattice oxygen-directed redox cycle and bromate reduction, *J. Hazard Mater.* **2021**, DOI: 10.1016/j.jhazmat.2020.124545.

(185) Chen, X. X.; Yang, H.; Au, C. T.; Tian, S. H.; Xiong, Y.; Chang, Y. Efficiency and mechanism of pollutant degradation and bromate inhibition by faceted CeO2 catalyzed ozonation: experimental and theoretical study, *Chem. Eng. J.* **2020**, *390*, 124480.

(186) Hu, J.; Zeng, X.; Wang, G.; Qian, B.; Liu, Y.; Hu, X.; He, B.; Zhang, L.; Zhang, X. Modulating mesoporous Co3O4 hollow nanospheres with oxygen vacancies for highly efficient peroxymonosulfate activation, *Chem. Eng. J.* **2020**, *400*, 125869.

(187) Jing, Q.; Li, H. Hierarchical nickel cobalt oxide spinel microspheres catalyze mineralization of humic substances during wet air oxidation at atmospheric pressure, *Appl. Catal. B. Environ.* **2019**, *256*, 117858.

(188) Lu, S.; Wang, G.; Chen, S.; Yu, H.; Ye, F.; Quan, X. Heterogeneous activation of peroxymonosulfate by LaCo1-xCuxO3 perovskites for degradation of organic pollutants, *J. Hazard. Mater.* **2018**, *353*, 401-409.

(189) Zhao, Y.; An, H.; Dong, G.; Feng, J.; Wei, T.; Ren, Y.; Ma, J. Oxygen vacancies induced heterogeneous catalysis of peroxymonosulfate by Ni-doped AgFeO2 materials: Evolution of reactive oxygen species and mechanism, *Chem. Eng. J.* **2020**, *388*, 124371.

(190) Zhang, S.; Sun, M.; Hedtke, T.; Deshmukh, A.; Zhou, X.; Weon, S.; Elimelech, M.; Kim, J.-H. Mechanism of heterogeneous Fenton reaction kinetics enhancement under nanoscale spatial confinement, *Environ. Sci. Technol.* **2020**, *54*, 10868-10875.

(191) Qian, J.; Gao, X.; Pan, B. Nanoconfinement-mediated water treatment: from fundamental to application, *Environ. Sci. Technol.* **2020**, *54*, 8509-8526.

(192) Li, X.; Wang, J.; Zhang, X.; Hou, X.; Xu, H.; Yao, Z.; Jiang, Z. A High-Efficient Carbon-Coated Iron-Based Fenton-Like Catalyst with Enhanced Cycle Stabilityand Regenerative Performance, *Catalysts* **2020** *10*, 1486.

(193) Zhuang, Y.; Yuan, S.; Liu, J.; Zhang, Y.; Du, H.; Wu, C.; Zhao, P.; Chen, H.; Pei, Y. Synergistic effect and mechanism of mass transfer and catalytic oxidation of octane degradation in yolk-shell Fe3O4@C/Fenton system., *Chem.Eng. J.* **2020**, *379*, 122262.

(194) Qin, H.; Cheng, H.; Li, H.; Wang, Y. Degradation of ofloxacin, amoxicillin and tetracycline antibiotics using magnetic core-shell MnFe2O4@C-NH2 as a heterogeneous Fenton catalyst., *Chem. Eng. J* **2020**, *396*, 125304.

(195)   Zeng, T.; Yu, M.; Zhang, H.; He, Z.; Chen, J.; Song, S. Fe/Fe3C@N-doped porous carbon hybrids derived from nano-scale MOFs: robust and enhanced heterogeneous catalyst for peroxymonosulfate activation., *Catal. Sci. Technol.* **2017**, *7*, 396-404.

(196)   Yang, W.; Lu, Z.; Vogler, B.; Wu, T.; Lei, Y. Enhancement of Copper Catalyst Stability for Catalytic Ozonation in Water Treatment Using ALD Overcoating, *ACS Appl. Mater. Interfaces* **2018**, *10*, 43323-43326.

(197)   Otor, H. O.; Steiner, J. B.; Garcia-Sancho, C.; Alba-Rubio, A. C. Encapsulation Methods for Control of Catalyst Deactivation: A Review., *ACS Catal* **2020**, *10*, 4630-7656.

(198)   Zaki, A.; Wastiaux, M.; Casale, S.; Mussi, A.; Dhenin, J. F.; Lancelot, C.; Dacquin, J. P.; Granger, P. Nano-engineered hierarchical porous silicas for enhanced catalytic efficiency in the liquid phase., *Catal. Sci. Technol.* **2018**, *8*, 4604-4608.

(199)   Shwetharani, R.; Sakar, M.; Fernando, C. A. N.; Binas, V.; Geetha Balakrishna, R. Recent advances and strategies to tailor the energy levels, active sites and electron mobility in titania and its doped/composite analogues for hydrogen evolution in sunlight. , *Catal. Sci. Technol.* **2019**, *9*, 12-46.

(200)   Yang, X. Y.; Chen, L. H.; Li, Y.; Rooke, J. C.; Sanchez, C.; Su, B. L. Hierarchically porous materials: synthesis strategies and structure design., *Chem. Soc. Rev.* **2017**, *46*, 481-558.

(201)   Soler-Illia, G. J. D.; Sanchez, C.; Lebeau, B.; Patarin, J. Chemical strategies to design textured materials: From microporous and mesoporous oxides to nanonetworks and hierarchical structures, *Chem. Rev* **2002**, *102*, 4093-4135.

(202)   Zhou, X. L.; Zhang, H.; Shao, L. M.; He, P. J. Preparation and Application of Hierarchical Porous Carbon Materials from Waste and Biomass: A Review, *Waste Biomass Valor.* **2021**, *12*, 1699-1724.

(203)   Chu, C.; Yang, J.; Huang, D.; Li, J.; Wang, A.; Alvarez, P. J. J.; Kim, J.-H. Cooperative Pollutant Adsorption and Persulfate-Driven Oxidation on Hierarchically Ordered Porous Carbon, *Environ. Sci. Technol.* **2019**, *53*, 10352-10360.

(204)   Yang, S.; Duan, X.; Liu, J.; Wu, P.; Li, C.; Dong, X.; Zhu, N.; Dionysiou, D. D. Efficient peroxymonosulfate activation and bisphenol A degradation derived from mineral-carbon materials: Key role of double mineral-templates. , *Appl. Catal. B.* **2020**, *267*, 118701.

(205)   Yang, Z.; Duan, X. G.; Wang, J.; Li, Y.; Fan, X. B.; Zhang, F. B.; Zhang, G. L.; Peng, W. C. Facile Synthesis of High-Performance Nitrogen-Doped Hierarchically Porous Carbon for Catalytic Oxidation., *ACS Sustain. Chem. Eng.* **2020**, *8*, 4236-4243.

(206) Lu, K.; Min, Z.; Qin, J.; Shi, P.; Wu, J.; Fan, J.; Min, Y.; Xu, Q. Preparation of nitrogen self-doped hierarchical porous carbon with rapid-freezing support for cooperative pollutant adsorption and catalytic oxidation of persulfate., *Sci. Total Environ.* **2021**, *752*, 142282.

(207) Makhotkina, O. A.; Preis, O. A.; Parkhomchuk, E. V. Water delignification by advanced oxidation processes: Homogeneous and heterogeneous Fenton and H2O2 photo-assisted reactions., *Appl. Catal. B.* **2008**, *51*, 821-826.

(208) Shamzhy, M.; Opanasenko, M.; Concepcion, P.; Martinez, A. New trends in tailoring active sites in zeolite-based catalysts, *Chem. Soc. Rev.* **2019**, *48*, 1095-1149.

(209) Sashkina, K. A.; Labko, V. S.; Rudina, N. A.; Parmon, V. N.; Parkhomchuk, E. V. Hierarchical zeolite FeZSM-5 as a heterogeneous Fenton-type catalyst., *J. Catal.* **2013**, *299*, 44-52.

(210) Yuan, S.; Wang, M.; Liu, J.; Guo, B. Recent advances of SBA-15-based composites as the heterogeneous catalysts in water decontamination: A mini-review., *J. Environ. Manag.* **2020**, *254*, 109787.

(211) Li, H.; Wang, H.; Gao, Q.; Han, B.; Xia, K.; Zhou, C. Hierarchical flower-like Co2TiO4 nanosheets with unique structural and compositional advantages to boost peroxymonosulfate activation for degradation of organic pollutants., *J. Mater. Chem. A* **2020**, *8*, 20953-20962.

(212) Sunil Sekhar, A. C.; Zaki, A.; Troncea, S.; Casale, S.; Vinod, C. P.; Dacquin, J. P.; Granger, P. Enhanced selectivity of 3-D ordered macroporous Pt/Al2O3 catalysts in nitrites removal from water, *Appl. Catal.A* **2018**, *564*, 26-32.

(213) Huang, B.; Wu, Z.; Zhou, H.; Li, J.; Zhou, C.; Xiong, Z.; Pan, Z.; Yao, G.; Lai, B. Recent advances in single-atom catalysts for advanced oxidation processes in water purification. , *J. Hazard. Mater.* **2021**, *412*, 125253.

(214) Xu, J.; Zheng, X.; Feng, Z.; Lu, Z.; Zhang, Z.; Huang, W.; Li, Y.; Vuckovic, D.; Li, Y.; Dai, S.; Chen, G.; Wang, K.; Wang, H.; Chen, J. K.; Mitch, W.; Cui, Y. Organic wastewater treatment by a single-atom catalyst and electrolytically produced H2O2., *Nat. Sustain.* **2020**, doi: 10.1038/s41893-41020-00635-w.

(215) Li, X.; Huang, X.; Xi, S.; Miao, S.; Ding, J.; Cai, W.; Liu, S.; Yang, X.; Yang, H.; Gao, J.; Wang, J.; Huang, Y.; Zhang, T.; Liu, B. Single Cobalt Atoms Anchored on Porous N-Doped Graphene with Dual Reaction Sites for Efficient Fenton-like Catalysis., *J. Am. Chem. Soc.* **2018**, *140*, 12469-12475.

(216) Yin, Y.; Shi, L.; Li, W.; Li, X.; Wu, H.; Ao, Z.; Tian, W.; Wang, S.; Sun, H. Boosting Fenton-Like Reactions via Single Atom Fe Catalysis., *Environ. Sci. Technol.* **2019**, *53*, 11391-11400.

(217) Barsoum, M. W. *MAX Phases: Properties of Machinable Ternary Carbides and Nitrides*; Wiley-VCH Verlag GmbH & Co.: Weinheim, Germany, 2013.

(218) Benchakar, M.; Bilyk, T.; Garnero, C.; Loupias, L.; Marais, C.; Pacaud, J.; Canaff, C.; Chartier, P.; Morisset, S.; Guignard, N.; Mauchamp, V.; Célérier, S.; A., H. MXene supported cobalt layered double hydroxide nanocrystals: facile synthesis route for a synergistic oxygen evolution reaction electrocatalyst., *Adv. Mater. Interfaces.* **2019**, *6*, 1901328.

(219) Tran, N. M.; Ta, Q. T. H.; Sreedhar, A.; Noh, J. S. Ti3C2Tx MXene playing as a strong methylene blue adsorbent in wastewater., *Appl. Surf. Sci* **2021**, *537*, 148006.

(220) Liu, Y.; Luo, R.; Qi, J.; Wang, C.; Sun, X.; Wang, L. Sandwich-like Co3O4/MXene composite with enhanced catalytic performance for Bisphenol A degradation., *Chem. Eng. J.* **2018**, *347*, 731-740.

(221) Ding, M.; Chen, W.; Xu, H.; Shen, Z.; Lin, T.; Hu, K.; Lu, C.; Xie, Z. Novel alpha-Fe2O3/MXene nanocomposite as heterogeneous activator of peroxymonosulfate for the degradation of salicylic acid. , *J. Hazard. Mater.* **2020**, *382*, 121064.

(222) Fayyaz, A.; Saravanakumar, K.; Talukdar, K.; Kim, Y.; Yoon, Y.; Park, C. M. Catalytic oxidation of naproxen in cobalt spinel ferrite decorated Ti3C2Tx MXene activated persulfate system: Mechanisms and pathways., *Chem. Eng. J.* **2021**, *407*, 127842.

(223) Fu, K.; Liu, X.; Yu, D.; Luo, J.; Wang, Z.; Crittenden, J. C. Highly Efficient and Selective Hg(II) Removal from Water UsingMultilayered Ti3C2Ox MXene via Adsorption Coupled with Catalytic Reduction Mechanism., *Environ. Sci. Technol.* **2020**, *54*, 16212-16220.

(224) Zimmerman, J. B.; Anastas, P. T.; Erythropel, H. C.; Leitner, W. Designing for a green chemisty future., *Science* **2020**, *367*, 397-400.

(225) Leonel, A. G.; Mansur, A. A. P.; Mansur, H. S. Advanced Functional Nanostructures based on Magnetic Iron Oxide Nanomaterials for Water Remediation: A Review, *Water research* **2021**, *190*, 116693.

(226) Nasrollahzadeh, M.; Sajjadi, M.; Iravani, S.; Varma, R. S. Green-synthesized nanocatalysts and nanomaterials for water treatment: Current challenges and future perspectives. , *J. Hazard. Mater.* **2021**, *401*, 123401.

(227) Chen, M.; Zhou, S.; Zhu, Y.; Sun, Y.; Zeng, G.; Yang, C.; Xu, P.; Yan, M.; Liu, Z.; Zhang, W. Toxicity of carbon nanomaterials to plants, animals and microbes: Recent progress from 2015-present., *Chemosphere* **2018**, *2016*, 255-264.

(228) Becker, S. A.; Truskewycz, A.; Cole, I.; Ball, A. S. Green synthesis of Opuntia-derived carbon nanodots for the catalytic decolourization of cationic dyes. , *New J. Chem.* **2020**, *44*, 20001-20012.

(229)   Chen, Y. D.; Duan, X.; Zhang, C.; Wang, S.; Ren, N.; Ho, S. H. Graphitic biochar catalysts from anaerobic digestion sludge for nonradical degradation of micropollutants and disinfection., *Chem. Eng. J.* **2020**, *384*, 123244.

(230)   Liang, J.; Xu, X.; Zhong, Q.; Xu, Z.; Zhao, L.; Qiu, H.; Cao, X. Roles of the mineral constituents in sludge-derived biochar in persulfate activation for phenol degradation. , *J. Hazard. Mat.* **2020**, *398*, 122861.

(231)   Nasrollahzadeh, M.; Sajjadi, M.; Iravani, S.; Varma, R. S. Starch, cellulose, pectin, gum, alginate, chitin and chitosan derived (nano)materials for sustainable water treatment: A review., *Carbohydr. Polym.* **2021**, *251*, 116986.

(232)   Bihanic, C.; Diliberto, S.; Pelissier, F.; Petit, E.; Boulanger, C.; Grison, C. Eco-CaMnOx: A Greener Generation of Eco-catalysts for Eco-friendly Oxidation Processes. , *ACS Sustainable Chem. Eng.* **2020**, *8*, 4044-4057.

(233)   Wang, N.; Wang, P. Study and application status of microwave in organic wastewater treatment - A review., *Chem. Eng. J* **2016**, *283*, 193-214.

(234)   Epron, F.; Henry, F.; Sagnes, O. Chemical synthesis and dielectric characterization in microwave domain of polypyrrole latexes, *Makromol. Chem. Macromol. Symp* **1990**, *6*, 527-533.

(235)   Mishra, R. R.; Sharma, A. K. Microwave-material interaction phenomena: Heating mechanisms, challenges and opportunities in material processing, *Compos. Pt A- Appl. Sci. Manuf.* **2016**, *81*, 78-97.

(236)   Chen, L. F.; Ong, C. K.; Neo, C. P.; Varadan, V. V.; Varadan, V. K. In *Microwave Electronics*, 2005; Vol. John Wiley & Sons Ltd.

(237)   Wei, R.; Wang, P.; G., Z.; Wang, N.; Zheng, T. Microwave-responsive catalysts for wastewater treatment: A review. , *Chem. Eng. J.* **2020**, *382*, 122781.

(238)   Galinada, W. A.; Kaczmarski, K.; Guiochon, G. Influence of Microwave Irradiation on the Mass-Transfer Kinetics of Propylbenzene in Reversed-Phase Liquid Chromatography, *Ind. Eng. Chem. Res.* **2005**, *44*, 8368-8376.

(239)   Costa, C.; Santos, W. H. S.; Araujo, P. H. H.; Sayer, C.; Santos, A. F.; Fortuny, M. Microwave-assisted rapid decomposition of persulfate, *Eur. Polym. J.* **2009**, *45*, 2011−2016.

(240)   Hu, L.; Zhang, G.; Wang, Q.; Wang, X.; Wang, P. Effect of Microwave Heating on Persulfate Activation for Rapid Degradation and Mineralization of p-Nitrophenol., *ACS Sustainable Chem. Eng.* **2019**, *7*, 11662-11671.

(241)   Hu, L.; Wang, P.; Shen, T.; Wang, Q.; Wang, X.; Xu, P.; Zheng, Q.; Zhang, G. The application of microwaves in sulfate radical-based advanced oxidation processes for environmental remediation: A review., *Sci. Total Environ.* **2020**, *722*, 137831.

(242)   Qi, C.; Liu, X.; Lin, C.; Zhang, H.; Li, X.; Ma, J. Activation of peroxymonosulfate by microwave irradiation for degradation of organic contaminants., *Chem.Eng. J.* **2017**, *315*, 201-209.

(243)   Antoniou, M. G.; A., d. l. C. A.; Dionysiou, D. D. Degradation of microcystin-LR using sulfate radicals generated through photolysis, thermolysis and e− transfer mechanisms, *Appl. Catal. B.* **2010**, *96*, 290-298.

(244)   Bo, L. L.; Zhang, Y. B.; Quan, X.; Zhao, B. Microwave assisted catalytic oxidation of p-nitrophenol in aqueous solution using carbon-supported copper catalyst, *J. Hazard. Mater.* **2008**, *153*, 1201-1206.

(245)   Quan, X.; Zhang, Y.; Chen, S.; Zhao, Y.; Yang, F. Generation of hydroxyl radical in aqueous solution by microwave energy using activated carbon as catalyst and its potential in removal of persistent organic substances, *J. Mol. Catal. A-Chem.* **2007**, *263*, 216-222.

(246)   Yu, J. G.; Zhao, X. H.; Yang, H.; Chen, X. H.; Yang, Q.; Yu, L. Y.; Jiang, J. H.; Chen, X. Q. Aqueous adsorption and removal of organic contaminants by carbon nanotubes., *Sci. Total Environ.* **2014**, *482-483*, 241-251.

(247)   Sun, Y.; Yu, I. K. M.; Tsang, D. C. W.; Fan, J.; Clarck, J. H.; Luo, G.; Zhang, S.; Khan, E.; Graham, N. J. D. Tailored design of graphitic biochar for high-efficiency and chemical-free microwave-assisted removal of refractory organic contaminants, *Chem. Eng. J.* **2020**, *398*, 125505.

(248)   Chen, J.; Xue, S.; Song, Y.; Shen, M.; Zhang, Z.; Yuan, T.; Tian, F.; Dionysiou, D. D. Microwave-induced carbon nanotubes catalytic degradation of organic pollutants in aqueous solution. , *J. Hazard. Mater.* **2016**, *310*, 226-234.

(249)   Mishra, S.; Sahu, T. K.; Verma, P.; Kumar, P.; K., S. S. Microwave-Assisted Catalytic Degradation of Brilliant Green by Spinel Zinc Ferrite Sheets., *ACS Omega.* **2019**, *4*, 10411-10418.

(250)   Qi, C.; Chen, H.; Xu, C.; Xu, Z.; Chen, H.; Yang, S.; Li, S.; He, H.; Sun, C. Synthesis and application of magnetic materials-barium ferrite nanomaterial as an effective microwave catalyst for degradation of brilliant green. , *Chemosphere* **2020**, *260*, 127681.

(251)   Qiu, Y.; Zhou, J.; Cai, J.; Xu, W.; You, Z.; Yin, C. Highly efficient microwave catalytic oxidation degradation of p-nitrophenol over microwave catalyst of pristine α-Bi2O3., *Chem. Eng. J.* **2016**, *306*, 667-675.

(252) Wang, Y.; Wang, Y.; Yu, L.; Wang, R.; Zhang, X. Highly effective microwave-induced catalytic degradation of Bisphenol A in aqueous solution using double-perovskite intercalated montmorillonite nanocomposite. , *Chem. Eng. J.* **2020**, *390*, 124550.

(253) Bi, X.; Wang, P.; Jiang, H.; Xu, H.; Shi, S.; Huang, J. Treatment of phenol wastewater by microwave-induced ClO2-CuOx/Al2O3 catalytic oxidation process., *J. Eur. Ceram. Soc.* **2002**, *22*, 93-99.

(254) Hu, E.; Cheng, H. Impact of surface chemistry on microwave-induced degradation of atrazine in mineral micropores., *Environ. Sci. Technol.* **2013**, *47*, 533-541.

(255) Hu, E.; Cheng, H. Catalytic effect of transition metals on microwave-induced degradation of atrazine in mineral micropores., *Water Res.* **2014**, *57*, 8-19.

(256) Zhang, B.; Li, J.; Sun, J.; Zhang, S.; Zhai, H.; Du, Z. Nanometer silicon carbide powder synthesis and its dielectric behavior in the GHz range. , *Journal of the European Ceramic Society* **2002**, *22*, 93-99.

(257) Yin, J.; Cai, J.; Yin, C.; Gao, L.; Zhou, J. Degradation performance of crystal violet over CuO@AC and CeO2-CuO@AC catalysts using microwave catalytic oxidation degradation method. , *J. Environ. Chem. Eng.* **2016**, *4*, 958-964.

(258) Chen, J.; Pan, H.; Hou, H.; Li, H.; Yang, J.; Wang, L. High efficient catalytic degradation of PNP over Cu-bearing catalysts with microwave irradiation., *Chem. Eng. J.* **2017**, *323*, 444-454.

(259) Wang, N.; Zheng, T.; Jiang, J.; Lung, W. S.; Miao, X.; Wang, P. Pilot-scale treatment of p-Nitrophenol wastewater by microwave-enhanced Fenton oxidation process: Effects of system parameters and kinetics study, *Chem. Eng. J.* **2014**, *239*, 351-359.

(260) Yao, T.; Qi, Y.; Mei, Y.; Yang, Y.; Aleisa, R.; Tong, X.; Wu, J. One-step preparation of reduced graphene oxide aerogel loaded with mesoporous copper ferrite nanocubes: A highly efficient catalyst in microwave-assisted Fenton reaction., *J. Hazard. Mater.* **2019**, *378*, 120712.

(261) Qi, Y.; Zuo, Q.; Mei, Y.; Yao, T.; Wu, J. Porous NiCo2O4 Sheet Catalysts for the Microwave Assisted Fenton Reaction., *ACS Appl. Nano Mater.* **2020**, *3*, 7152-7160.

(262) Horikoshi, S.; Hidaka, H.; N., S. Environmental remediation by an integrated microwave/UV-illumination method II. Characteristics of a novel UV-VIS-microwave integrated irradiation device in photodegradation processes, *J. Photochem. Photobiol.* **2002**, *153*, 185-189.

(263) Ferrari, C.; Chen, H.; Lavezza, R.; Santinelli, C.; Longo, I.; Bramanti, E. Photodegradation of Rhodamine B Usingthe Microwave/UV/H2O2: Effect of Temperature., *Int. J. Photoenergy* **2013**, 854857.

(264)   Gromboni, C. F.; Kamogawa, M. Y.; Ferreira, A. G.; Nobrega, J. A.; Nogeira, A. R. A. Microwave-assisted photo-Fenton decomposition of chlorfenvinphos and cypermethrin in residual water., *J. Photochem. Photobiol.* **2007**, *185*, 32-37.

(265)   Satoshi, H.; Hisao, H.; Nick, S. Environmental remediation by an integrated microwave/UV-illumination method. 1. Microwave-assisted degradation of rhodamine-B dye in aqueous TiO2 dispersions. , *Environ. Sci. Technol.* **2002**, *36*, 1357-1366.

(266)   Ling, L.; Feng, Y.; Li, H.; Chen, Y.; Wen, J.; Zhu, J.; Bian, Z. Microwave induced surface enhanced pollutant adsorption and photocatalytic degradation on Ag/TiO2., *Appl. Surf. Sci.* **2019**, *483*, 772-779.

(267)   Zhao, G.; Gao, J.; Shi, W.; Liu, M.; Li, D. Electrochemical incineration of high concentration azo dye wastewater on the in situ activated platinum electrode with sustained microwave radiation. , *Chemosphere* **2009**, *77*, 188-193.

(268)   Wu, Z. L.; Ondruschka, B.; Cravotto, G. Degradation of Phenol under Combined Irradiation of Microwaves and Ultrasound., *Environ. Sci. Technol.* **2008**, *42*, 8083-8087.

(269)   Chen, B.; Zhu, C.; Fei, J.; Jiang, Y.; Yin, C.; Su, W.; He, X.; Lid, Y.; Chen , Q.; Ren, Q.; Chen, Y. Reaction kinetics of phenols and p-nitrophenols in flowing aerated aqueous solutions generated by a discharge plasma jet, *J. Hazard. Mater.* **2019**, *363*, 55-63.

(270)   Giwa, A.; Yusuf, A.; Balogun, H. A.; Sambudi, N. S.; Bilad, M. R.; Adeyemi, I.; Chakraborty, S.; Curcio, S. Recent advances in advanced oxidation processes for removal of contaminants from water: a comprehensive review, *Process Saf. Environ. Prot.* **2021**, *146*, 220-256.

(271)   Cheng, M.; Zeng, G.; Huang, D.; Lai, C.; Xu, P.; Zhang, C.; Liu, Y. Hydroxyl radicals based advanced oxidation processes (AOPs) for remediation of soils contaminated with organic compounds: a review, *Chemical Engineering Journal* **2016**, *284*, 582-598.

(272)   Bruggeman, M. J.; Kushner, B. J.; Locke, B. R.; Gardeniers, J. G. E.; Graham, W. G.; Graves, D. B.; Hofman-Caris, R. C. H. M.; Maric, D.; Reid, J. P.; Ceriani, E.; Fernandez Rivas, D.; Foster, J. E.; Garrick, S. C.; Gorbanev, Y.; Hamaguchi, S.; Iza, F.; Jablonowski, H.; Klimova, E.; Kolb, J.; Krcma, F.; Lukes, P.; Machala, Z.; Marinov, I.; Mariotti, D.; Mededovic Thagard, S.; Minakata, D.; Neyts, E. C.; Pawlat, J.; Petrovic, Z. L.; Pflieger, R.; Reuter, S.; Schram, D. C.; Schröter, S.; Shiraiwa, M.; Tarabová, B.; Tsai, P. A.; Verlet, J. R. R.; Woedtke, T.; von, W., K.R.; Yasui, K.; Zvereva, G. Plasma-liquid interactions: a review and roadmap, *Plasma Sources Sci. Technol.* **2016**, *25*, 053002.

(273) Chen, B.; Zhu, C.; Fei, J.; He, X.; Yin, C.; Wang, Y.; Jiang, Y.; Chen, L.; Gao, Y.; Han, Q. Water content effect on oxides yield in gas and liquid phase using DBD arrays in mist spray, *Plasma Sci. Technol.* **2016**, *18*, 41-50.

(274) Lu, X.; Naidis, G. V.; Laroussi, M.; Reuter, S.; Graves, D. B.; Ostrikov, K. Reactive species in non-equilibrium atmospheric-pressure plasmas: generation, transport, and biological effects, *Phys. Rep.* **2016**, *630*, 1-84.

(275) Adamovich, I.; Baalrud, S.; Bogaerts, A.; Bruggeman, P. J.; Cappelli, M.; Colombo, V.; Czarnetzki, U.; Ebert, U.; Eden, J. G.; Favia, P.; Graves, D. B.; Hamaguchi, S.; Hieftje, G.; Hori, M.; Kaganovich, I. D.; Kortshagen, U.; Kushner, M. J.; Mason, N. J.; Mazouffre, S.; Mededovic Thagard, S.; Metelmann, H.-R.; Mizuno, A.; Moreau, E.; Murphy, A. B.; Niemira, B. A.; Oehrlein, G. S.; Petrovic, Z. L.; Pitchford, L. C.; Pu, Y.-K.; Rauf, S.; Sakai, O.; Samukawa, S.; Starikovskaia, S.; Tennyson, J.; Terashima, K.; Turner, M. M.; van de Sanden, M. C. M.; Vardelle, A. The 2017 Plasma Roadmap: low temperature plasma science and technology, *J. Phys. D: Appl. Phys.* **2017**, *50*, 323001.

(276) Shang, K.; Li, J.; Morent, R. Hybrid electric discharge plasma technologies for water decontamination: a short review, *Plasma Sci. Technol.* **2019**, *21*, 043001.

(277) Fan, J.; Wu, H.; Liu, R.; Meng, L.; Sun, Y. Review on the treatment of organic wastewater by discharge plasma combined with oxidants and catalysts, *Environ. Sci. Pollut. Res. Int.* **2020**, *28*, 2522-2548.

(278) Ansari, M.; Sharifian, M.; Ehrampoush, M. H.; Mahvi, A. H.; Salmani, M. H.; Fallahzadeh, H. Dielectric barrier discharge plasma with photocatalysts as a hybrid emerging technology for degradation of synthetic organic compounds in aqueous environments: a critical review, *Chemosphere* **2021**, *263*, 128065.

(279) Hijosa-Valsero, M.; Molina, R.; Schikora, H.; Müller, M.; Bayona, J. M. Removal of priority pollutants from water by means of dielectric barrier discharge atmospheric plasma, *J. Hazard. Mater.* **2013**, *262*, 664-673.

(280) Tang, S.; Li, X.; Zhang, C.; Liu, Y.; Zhang, W.; Yuan, D. Strengthening decomposition of oxytetracycline in DBD plasma coupling with Fe-Mn oxide-loaded granular activated carbon, *Plasma Sci. Technol.* **2019**, *21*, 025504.

(281) Merouani, D. R.; Abdelmalek, F.; Ghezzar, M. R.; Semmoud, A.; Addou, A.; Brisset, J.-L. Influence of peroxynitrite in gliding arc discharge treatment of Alizarin Red S and post-discharge effects, *Ind. Eng. Chem. Res.* **2013**, *52*, 1471-1480.

(282) Magureanu, M.; Bradu, C.; Piroi, D.; Mandache, N. B.; Parvulescu, V. I. Pulsed corona discharge for degradation of methylene blue in water., *Plasma Chem. Plasma Process.* **2013**, *33*, 51-64.

(283) Berardinelli, A.; Hamrouni, A.; Dirè, S.; Ceccato, R.; Camera-Roda, G.; Ragni, L.; Palmisano, L.; Parrino, F. Features and application of coupled cold plasma and photocatalysis processes for decontamination of water, *Chemosphere* **2021**, *262*, 128336.

(284) Turner, M. In *Cold plasma in food and agriculture: fundamentals and applications*; Misra, N. N., Schlüter, O., Cullen, P. J., Eds.; Elsevier, 2016.

(285) Lu, P.; Cullen, P. J.; Ostrikov, K. In *Cold plasma in food and agriculture: fundamentals and applications*; Misra, N. N., Schlüter, O., Cullen, P. J., Eds.; Elsevier, 2016.

(286) Ollegott, K.; Wirth, P.; Oberste-Beulmann, C.; Awakowicz, P.; Muhler, M. Fundamental Properties and Applications of Dielectric Barrier Discharges in Plasma-Catalytic Processes at Atmospheric Pressure, *Chem. Ing. Tech.* **2020**, *92*, 1-18.

(287) Kogelschatz, U.; Eliasson, B.; Egli, W. From ozone generators to flat television screens: history and future potential of dielectric-barrier discharges, *Pure Appl. Chem.* **1999**, *71*, 1819-1828.

(288) Kraus, M.; Eliasson, B.; Kogelschatz, U.; Wokaun, A. CO2 reforming of methane by the combination of dielectric-barrier discharges and catalysis, *Phys. Chem. Chem. Phys.* **2001**, *3*, 294-300.

(289) Eliasson, B.; Kogelschatz, U. Nonequilibrium volume plasma chemical processing, *IEEE Trans. Plasma Sci.* **1991**, *19*, 1063-1077.

(290) Muhlisin, Z.; Rahmawati, I.; Arianto, F.; Triadyaksa, P. Characterization of negative corona plasma discharge reactor using point-to-plane electrode configuration in atmospheric pressure and its application in the treatment of woven natural silk, *J. Phys. Conf. Series* **2020**, *152*, 012031.

(291) Wang, X. Y.; Zhou, M. H.; Jin, X. L. Application of glow discharge plasma for wastewater treatment, *Electrochimica Acta* **2012**, *83*, 501-512.

(292) Wen, Y. Z.; Shen, C. S.; Ni, Y. Y.; Tong, S. P.; Yu, F. Glow discharge plasma in water: a green approach to enhancing ability of chitosan for dye removal, *J. Hazard. Mater.* **2012**, *201*, 162-169.

(293) Al-Shamma'a, A. I.; Pandithas, I.; Lucas, J. Low- pressure microwave plasma ultraviolet lamp for water purification and ozone applications, *J. Phys. D: Appl. Phys.* **2001**, *34*, 2775-2781.

(294)   Shen, C.; Wu, S.; Chen, H.; Rashid, S.; Wen, Y. Phthalate degradation by glow discharge plasma enhanced with pyrite in aqueous solution, *Water Sci. Technol.* **2016**, *74*, 1365-1375.

(295)   Richard, F.; Cormier, J. M.; Pellerin, S.; Chapelle, J. Physical study of a gliding arc discharge, *J. Appl. Phys.* **1996**, *79*, 2245-2250.

(296)   *Plasma Chemistry and Catalysis in Gases and Liquids*; Parvulescu, V. I.; Magureanu, M.; Lukes, P., Eds.; Wiley: Weinheim, 2012.

(297)   Lukes, P.; Locke, B. R.; Brisset, J. L. In *Plasma Chemistry and Catalysis in Gases and Liquids*; Parvulescu, V. I., Magureanu, M., Lukes, P., Eds.; Wiley Weinheim, 2012.

(298)   Jiang, B.; Zheng, J.; Qiu, S.; Wu, M.; Zhang, Q.; Yan, Z.; Xue, Q. Review on electrical discharge plasma technology for wastewater remediation, *Chem. Eng. J.* **2014**, *236*, 348-368.

(299)   Grinevich, V. I.; Kvitkova, E. Y.; Plastinina, N. A.; Rybkin, V. V. Application of dielectric barrier discharge for waste water purification, *Plasma Chem. Plasma Process.* **2011**, *31*, 573-583.

(300)   Russo, M.; Iervolino, G.; Vaiano, V.; Palma, V. Non-Thermal Plasma Coupled with Catalyst for the Degradation of Water Pollutants: a Review, *Catalysts* **2020**, *10*, 1438.

(301)   Urashima, K.; Uchida, Y. Characteristics of Pulsed Arc Electrohydraulic Discharges and Their Application to Water Treatment, *Res. Rep., Tokyo Denki Univ.* **2002**, *50*.

(302)   De Giacomo, A.; Dell'Aglio, M.; De Pascale, O.; Capitelli, M. From single pulse to double pulse ns-laser induced breakdown spectroscopy under water: elemental analysis of aqueous solutions and submerged solid samples, *Spectrochim. Acta, Part B* **2007**, *62*, 721-738.

(303)   Kušic, H.; Koprivanac, N.; Locke, B. R. Decomposition of phenol by hybrid gas/liquid electrical discharge reactors with zeolite catalysts, *J. Hazard. Mater.* **2005**, *125*, 190-200.

(304)   Mao, D.; Yan, X.; Wang, H.; Shen, Z.; Yi, C. Catalysis of rGO-WO3 nanocomposite for aqueous bisphenol A degradation in dielectric barrier discharge plasma oxidation process, *Chemosphere* **2021**, *262*, 128073.

(305)   Ren, J.; Jiang, N.; Shang, K.; Lu, N.; Li, J.; Wu, Y. Synergistic degradation of trans-ferulic acid by water falling film DBD plasma coupled with cobalt oxyhydroxide: performance and mechanisms, *Chem. Eng. J.* **2019**, *372*, 321-331.

(306)   Caro, H. Badische Anilin- und Sodafabrik [BASF], "Verfahren zur Darstellung blauer Farbstoffe aus Dimethylanilin und anderen tertiaren aromatischen Monaminen" (Method for preparation of blue dyes from dimethylaniline and other tertiary aromatic monoamines), Deutsches Reich Patent no. 1886, **1877**.

(307)   In *London: Pharmaceutical Press. From Medicines Complete website*, 2012.

(308) Houas, A.; Lachheb, H.; Ksibi, M.; Elaloui, E.; Guillard, C.; Herrmann, J. M. Photocatalytic degradation pathway of methylene blue in water, *Appl. Catal. B: Environ.* **2001**, *31*, 145-157.

(309) Wang, J.; Sun, Y.; Feng, J.; Xin, L.; Ma, J. Degradation of triclocarban in water by dielectric barrier discharge plasma combined with TiO2/activated carbon fibers: Effect of operating parameters and byproducts identification., *Chem. Eng. J.* **2016**, *300*, 36-46.

(310) Mahmood, A.; Mahmood Ramay, S.; Al-Zaghayer, Y. S.; Atiq, S.; Ansari, S. H. Thermal/plasma treatment effect on photocatalytic degradation of aqueous solution of methylene blue using Au-doped Fe/TiO2 photocatalyst., *Desalination Water Treat.* **2015**, *57*, 5183-5192.

(311) Gong, S.; Sun, Y.; Zheng, K.; Jiang, G.; Li, L.; Feng, J. Degradation of levofloxacin in aqueous solution by non-thermal plasma combined with Ag3PO4/activated carbon fibers: Mechanism and degradation pathways, *Separ. Purif. Technol.* **2020**, *250*, 117264.

(312) Magureanu, M.; Piroi, D.; Mandache, N. B.; David, V.; Medvedovici, A.; Bradu, C.; Parvulescu, V. I. Degradation of antibiotics in water by non-thermal plasma treatment., *Water Res.* **2011**, *45*, 3407-3410.

(313) Reddy, P. M. K.; Raju, B. R.; Karuppiah, J.; Reddy, E. L.; Subrahmanyam, C. Degradation and mineralization of methylene blue by dielectric barrier discharge non-thermal plasma reactor, *Chem. Eng. J.* **2013**, *217*, 41-47.

(314) Xua, Z.; Xue, X.; Hu, S.; Li, Y.; Shen, J.; Lan, Y.; Zhou, R.; Yang, F.; Chen, C. Degradation effect and mechanism of gas-liquid phase dielectric barrier discharge on norfloxacin combined with H_2O_2 or Fe^{2+}, *Sep.Purif. Technol.* **2020**, *230*, 115862.

(315) Krupež, J.; Kovačević, V. V.; Jović, M.; Roglić, G. M.; Natić, M. M.; Kuraica, M. M.; Obradović, B. M.; Dojčinović, B. P. Degradation of nicotine in water solutions using a water falling film DBD plasma reactor: direct and indirect treatment, *J. Phys. D: Appl. Phys.* **2018**, *51*, 174003.

(316) Marković, M.; Jović, M.; Stanković, D.; Kovačević, V.; Roglić, G.; Gojgić-Cvijović, G.; Manojlović, D. Application of non-thermal plasma reactor and Fenton reaction for degradation of ibuprofen, *Sci. Total Environ.* **2015**, *505*, 1148-1155.

(317) Aggelopoulos, C. A.; Meropoulis, S.; Hatzisymeon, M.; Lada, Z. G.; Rassias, G. Degradation of antibiotic enrofloxacin in water by gas-liquid nsp-DBD plasma: Parametric analysis, effect of H2O2 and CaO2 additives and exploration of degradation mechanisms, *Chem. Eng. J.* **2020**, *398*, 125622.

(318) Reddy, P. M. K.; Subrahmanyam, C. Catalytic Plasma Reactor for Degradation and Mineralization of Pharmaceuticals and Personal Care Product, *J. Adv. Oxid. Technol.* **2015**, *18*, 161-166.

(319) Reddy, P. M. K.; Dayamani, A.; Mahammadunnisa, S.; Subrahmanyam, C. Mineralization of phenol in water by catalytic non-thermal plasma reactor - an eco-friendly approach for wastewater treatment, *Plasma Proc. Polym.* **2013**, *10*, 1010-1017.

(320) Korichi, N.; Aubry, O.; Rabat, H.; Cagnon, B.; Hong, D. Paracetamol degradation by catalyst enhanced non-thermal plasma process for a drastic increase in the mineralization rate, *Catalysts* **2020**, *10*, 959.

(321) Guo, H.; Li, Z.; Xie, Z.; Song, J.; Xiang, L.; Zhou, L.; Li, C.; Liao, L.; Li, J.; Wang, H. Accelerated Fenton reaction for antibiotic ofloxacin degradation in discharge plasma system based on graphene-Fe_3O_4 nanocomposites, *Vacuum* **2021**, *185*, 110022.

(322) Deng, R.; He, Q.; Yang, D.; Dong, Q.; Wu, J.; Yang, X.; Chen, Y. Enhanced synergistic performance of nano-Fe^0-CeO_2 composites for the degradation of diclofenac in DBD plasma, *Chem. Eng. J.* **2021**, *406*, 126884.

(323) Cheng, J.; Wang, D.; Wang, B.; Ning, H.; Zhang, Y.; Li, Y.; An, J.; Gao, P. Plasma-catalytic degradation of ciprofloxacin in aqueous solution over different MnO2 nanocrystals in a dielectric barrier discharge system, *Chemosphere* **2020**, *253*, 126595.

(324) Li, S.; Liu, L.; Ma, X.; Li, Y. Degradation of Thiamethoxam in Wastewater by Low Temperature Plasma, *J. Adv. Oxid. Technol.* **2016**, *19*, 347-357.

(325) Li, S. P.; Jiang, Y. Y.; Cao, X. H.; Dong, Y. W.; Dong, M.; Xu, J. Degradation of nitenpyram pesticide in aqueous solution by low-temperature plasma, *Environ. Technol.* **2013**, *34*, 1609-1616.

(326) Li, C.; Rao, Y.; Zhang, B.; Huang, K.; Cao, X.; Peng, D.; Wu, J.; Xiao, L.; Huang, Y. Extraordinary catalysis induced by titanium foil cathode plasma for degradation of water pollutant, *Chemosphere* **2019**, *214*, 341-348.

(327) Chen, G.; Hu, W.; Yu, J.; Chen, W.; Huang, J. Exploring the cooperation effect of DBD byproducts and Ag/TiO2 catalyst for water treatment in an APPJ system, *Plasma Sci. Technol.* **2016**, *19*, 015503.

(328) Iervolino, G.; Vaiano, V.; Pepe, G.; Campiglia, P.; Palma, V. Degradation of Acid Orange 7 Azo dye in aqueous solution by a catalytic-assisted, non-thermal plasma process., *Catalysts* **2020**, *10*, 888.

(329) Tao, X.; Yuan, X.; Huang, L. Effects of Fe(II)/Fe(III) of Fe-MOFs on catalytic performance in plasma/fenton-like system, *Colloids Surf. A Physicochem. Eng. Asp.* **2021**, *610*, 125745.

(330) Marković, M. D.; Dojčinović, B. P.; Obradović, B. M.; Nešić, J.; Natić, M. M.; Tosti, T. B.; Kuraica, M. M.; Manojlović, D. D. Degradation and detoxification of the 4-chlorophenol by non-thermal plasma-influence of homogeneous catalysts, *Sep. Purif. Technol* **2015**, *154*, 246-254.

(331) Reddy, P. M. K.; Subrahmanyam, C. Green approach for wastewater treatment-degradation and mineralization of aqueous organic pollutants by discharge plasma, *Ind. Eng. Chem. Res.* **2012**, *51*, 11097-11103.

(332) Bobkova, E. S.; Grinevich, V. I.; Ivantsova, N. A.; Rybkin, V. V. A study of sulfonol decomposition in water solutions under the action of dielectric barrier discharge in the presence of different heterogeneous catalysts, *Plasma Chem. Plasma Process.* **2012**, *32*, 97-107.

(333) Al Momani, F.; Smith, D. W.; Gamal El-Din, M. Degradation of cyanobacteria toxin by advanced oxidation processes, *J. Hazard. Mater.* **2008**, *150*, 238-249.

(334) Xin, Q.; Zhang, Y.; Li, Z.; Lei, L.; Yang, B. Mn/Ti-doped carbon xerogel for efficient catalysis of microcystin-LR degradation in the water surface discharge plasma reactor, *Environ. Sci. Pollut. Res.* **2015**, *22*, 17202-17208.

(335) Namihira, T.; Yamaguchi, T.; Yamamoto, K.; Choi, J.; Kiyan, T.; Sakugawa, T.; Katsuki, S.; Akiyama, H. Characteristics of pulsed discharge plasma in water, *IEEE International Pulsed Power Conference* **2005**, 1013-1016.

(336) Zhang, Y.; Zhang, R.; Ma, W.; Zhang, X.; Wang, L.; Guan, Z. Purification of water by bipolar pulsed discharge plasma combined with TiO_2 catalysis, *J. Phys. Conf. Ser.* **2013**, *418*, 012125.

(337) Li, X.; Wang, T.; Qu, G.; Liang, D.; Hu, S. Enhanced degradation of azo dye in wastewater by pulsed discharge plasma coupled with MWCNTs-TiO2/γ-Al2O3 composite photocatalyst, *J. Environ. Manage.* **2016**, *172*, 186-192.

(338) Hsieh, K.; Wang, H.; Locke, B. R. Analysis of a gas-liquid film plasma reactor for organic compound oxidation, *J. Hazard. Mater.* **2016**, *317*, 188-197.

(339) He, D.; Sun, Y.; Li, S.; Feng, J. Decomposition of tetracycline in aqueous solution by corona discharge plasma combined with a Bi2MoO6 nanocatalyst, *J. Chem. Technol. Biotechnol.* **2014**, *90*, 2249-2256.

(340) Guo, H.; Jiang, N.; Wang, H.; Shang, K.; Lu, N.; Li, J.; Wu, Y. Degradation of flumequine in water by pulsed discharge plasma coupled with reduced graphene oxide/TiO_2 nanocomposites, *Sep. Purif. Technol.* **2019**, *218*, 206-216.

(341) Li, Z.; Lin, S.; Li, D.; Jiang, N.; Wang, H.; Han, J.; Li, J. Multi-catalysis induced by pulsed discharge plasma coupled with graphene-Fe_3O_4 nanocomposites for efficient removal of ofloxacin in water: Mechanism, degradation pathway and potential toxicity, *Chemosphere* **2021**, *265*, 129089.

(342) Guo, H.; Jiang, N.; Wang, H.; Lu, N.; Shang, K.; Li, J.; Wu, Y. Pulsed discharge plasma assisted with graphene-WO3 nanocomposites for synergistic degradation of antibiotic enrofloxacin in water, *Chem. Eng. J.* **2019**, *372*, 226-240.

(343) Guo, H.; Jiang, N.; Wang, H.; Lu, N.; Shang, K.; Li, J.; Wu, Y. Degradation of antibiotic chloramphenicol in water by pulsed discharge plasma combined with TiO2/WO3 composites: mechanism and degradation pathway, *J. Hazard. Mater.* **2019**, *371*, 666-676.

(344) Marouf-Khelifa, K.; Abdelmalek, F.; Khelifa, A.; Addou, A. TiO_2-assisted degradation of a perfluorinated surfactant in aqueous solutions treated by gliding arc discharge, *Chemosphere* **2008**, *70*, 1995-2001.

(345) Ghezzar, M. R.; Abdelmalek, F.; Belhadj, M.; Benderdouche, N.; Addou, A. Enhancement of the bleaching and degradation of textile wastewaters by Gliding arc discharge plasma in the presence of TiO_2 catalyst, *J. Hazard. Mater.* **2009**, *164*, 1266-1274.

(346) Hijosa-Valsero, M.; Molina, R.; Montràs, A.; Müller, M.; Bayona, J. M. Decontamination of waterborne chemical pollutants by using atmospheric pressure nonthermal plasma: a review, *Environ. Technol. Rev.* **2014**, *3*, 71-91.

(347) Locke, B. R.; Sato, M.; Sunka, P.; Hoffmann, M. R.; Chang, J. S. Electrohydraulic Discharge and Nonthermal Plasma for Water Treatment, *Ind. Eng. Chem. Res.* **2006**, *45*, 882-905.

(348) Duan, S.; Liu, X.; Wang, Y.; Meng, Y.; Alsaedi, A.; Hayat, T.; Li, J. Plasma surface modification of materials and their entrapment of water contaminant: a review, *Plasma Process. Polym.* **2017**, *14*, 1-30.

(349) Cui, Y.; Cheng, J.; Chen, Q.; Yin, Z. The Types of Plasma Reactors in Wastewater Treatment, *IOP Conference Series: Earth & Environ. Sci.* **2018**, *208*, 012002.

(350) Zhou, R.; Zhou, R.; Alam, D.; Zhang, T.; Li, W.; Xia, Y.; Mai-Prochnow, A.; An, H.; Lovell, E. C.; Masood, H.; Amal, R.; Ostrikov, K.; Cullen, P. J. Plasma-catalytic bubbles using CeO2 for organic pollutant degradation, *Chem. Eng. J.* **2021**, *403*, 126413.

(351) Reddy, P. M. K.; Mahammadunnisa, S.; Subrahmanyam, C. Catalytic non-thermal plasma reactor for mineralization of endosulfan in aqueous medium: a green approach for the treatment of pesticide contaminated water, *Chem. Eng. J.* **2014**, *238*, 157-163.

(352) Wang, B. A novel dielectric-barrier-discharge loop reactor for cyanide water treatment, *Plasma Chem. Plasma Process.* **2017**, *37*, 1121-1131.

(353) Alvarez, P. J. J.; Illman, W. A. In *Bioremediation and Natural Attenuation: Process Fundamentals and Mathematical Models*; John Wiley & Sons, 2006.

(354) Basu, S.; Rabara, R. C.; Negi, S.; Shukla, P. Engineering PGPMOs through gene editing and systems biology: a solution for phytoremediation?, *Trends Biotechnol.* **2018**, *36*, 499-510.

(355) Huang, D. L.; Xue, W. J.; Zeng, G. M.; Wan, J.; Chen, G. M.; Huang, C.; Zhang, C.; Cheng, M.; Xu, P. Immobilization of Cd in river sediments by sodium alginate modified nanoscale zero-valent iron: impact on enzyme activities and microbial community diversity, *Water Res.* **2016**, *106*, 15-25.

(356) Khan, F. I.; Husain, T.; Hejazi, R. An overview and analysis of site remediation technologies, *J. Environ. Manag.* **2004**, *71*, 95-122.

(357) Rafael, J. 5th edition of the International Conference Wastes: Solutions, Treatments and Opportunities, Portugal, 2019; p 93-98.

(358) Wei, Z.; Van Le, Q.; Peng, W.; Yang, Y.; Yang, H.; Gu, H.; Lam, S. S.; Sonne, C. A review on phytoremediation of contaminants in air, water and soil and amendment, *J. Hazard. Mater.* **2021**, *403*, 123658.

(359) Godlewska, P.; Ok, Y. S.; Oleszczuk, P. The dark side of black gold: Ecotoxicological aspects of biochar and biochar-amended soils, *J. Hazard. Mater.* **2021**, *403*, 123833.

(360) Liu, S. J.; Liu, Y. G.; Tan, X. F.; Zeng, G. M.; Zhou, Y. H.; Liu, S. B.; Yin, Z. H.; Jiang, L. H.; Li, M. F.; Wen, J. The effect of several activated biochars on Cd immobilization and microbial community composition during in-situ remediation of heavy metal contaminated sediment, *Chemosphere* **2018**, *208*, 655-664.

(361) Chien, S.-W. C.; Wang, H.-H.; Chen, Y.-M.; Wang, M.-K.; Liu, C.-C. Removal of heavy metals from contaminated paddy soils using chemical reductants coupled with dissolved organic carbon solutions, *J. Hazard. Mater.* **2021**, *403*, 123549.

(362) Yu, Y. H.; Su, J. F.; Shih, Y.; Wang, J.; Wang, P. Y.; Huang, C. P. Hazardous wastes treatment technologies, *Water Environ. Res.* **2020**, *92*, 1833-1860.

(363) El-sayed, M. E. A. Nanoadsorbents for water and wastewater remediation, *Sci. Total Environ.* **2020**, *739*, 139903.

(364) Chen, L.; Wang, Y.; Wan, Y.; Cai, Y.; Xiong, Y.; Fan, Z.; Conradson, S. D.; Fu, H.; Yuan, L.; Feng, W. Highly efficient and selective pillararene-based organic materials for Hg^{2+} and CH_3Hg^+ extraction from aqueous solution, *Chem. Eng. J.* **2020**, *387*, 124087.

(365) Azubuike, C. C.; Chikere, C. B.; Okpokwasili, G. C. Bioremediation techniques-classification based on site of application: principles, advantages, limitations and prospects, *World J. Microbiol. Biotechnol.* **2016**, *32*, 180.

(366) Jaiswal, S.; Shukla, P. Alternative Strategies for Microbial Remediation of Pollutants via Synthetic Biology, *Frontiers in Microbiology* **2020**, *11*, 808.

(367) Dangi, A. K.; Sharma, B.; Hill, R. T.; Shukla, P. Bioremediation through microbes: systems biology and metabolic engineering approach, *Crit. Rev. Biotechnol.* **2019**, *39*, 79-98.

(368) Hermanova, S.; Pumera, M. Biocatalytic Micro- and Nanomotors, *Chem. Eur. J.* **2020**, *26*, 11085 - 11092.

(369) Yin, Z.; Song, L.; Lin, Z.; Hui, K.; Wang, Q.; Song, H.; Xuan, L.; Wang, Z.; Gao, W. Granular activated carbon-supported titanium dioxide nanoparticles as an amendment for amending copper-contaminated sediments: Effect on the pH in sediments and enzymatic activities, *Ecotoxicol. Environ. Saf.* **2020**, *206*, 111325.

(370) Konhauser, K. O. Diversity of bacterial iron mineralization, Earth-Science Reviews, **1998**, *43*, 91-121.

(371) Rawlings, D. E.; Dew, D.; du Plessis, C. Biomineralization of metal-containing ores and concentrates, *Trends Biotechnol.* **2003**, *21*, 38-44.

(372) Liu, L.; Li, W.; Song, W.; Guo, M. Remediation techniques for heavy metalcontaminated soils: principles and applicability, *Sci. Total Environ.* **2018**, *633*, 206-219.

(373) Li, Q.; Csetenyi, L.; Gadd, G. M. Biomineralization of metal carbonates by Neurospora crassa, *Environ. Sci. Technol.* **2014**, *48*, 14409-14416.

(374) Qian, X.; Fang, C.; Huang, M.; Achal, V. Characterization of fungal-mediated carbonate precipitation in the biomineralization of chromate and lead from an aqueous solution and soil, *J. Clean. Prod.* **2017**, *164*, 198-208.

(375) Kumari, D.; Qian, X.-Y.; Pan, X.; Achal, V.; Li, Q.; Gadd, G. M. Microbially induced carbonate precipitation for immobilization of toxic metals, *Adv. Appl. Microbiol.* **2016**, *94*, 79-108.

(376) *Electronic Code of Federal Regulations* **1995**, *58 FR 9387, Feb. 19, 1993, as amended at 58 FR 9099, Feb. 25, 1994; 60 FR 54769, Oct. 25, 1995*.

(377) *The World Health Organization* **2011**, *Data Guidelines for Drinking-water Quality4th ed., Geneva*.

(378) He, M.; Li, X.; Guo, L.; Miller, S. J.; Rensing, C.; Wang, G. Characterization and genomic analysis of chromate resistant and reducing Bacillus cereus strain SJ1, *BMC Microbiol.* **2010**, *10*, 221.

(379) He, M.; Li, X.; Liu, H.; Miller, S. J.; Wang, G.; Rensing, C. Characterization and genomic analysis of a highly chromate resistant and reducing bacterial strain Lysinibacillus fusiformis ZC1, *J. Hazard Mater.* **2011**, *185*, 682-688.

(380) Xia, X.; Wu, S.; Li, N.; Wang, D.; Zheng, S.; Wang, G. Novel bacterial selenite reductase CsrF responsible for Se(IV) and Cr(VI) reduction that produces nanoparticles in Alishewanella sp. WH16-1, *J. Hazard Mater.* **2018**, *342*, 499-509.

(381) Chen, F.; Cao, Y.; Wei, S.; Li, Y.; Li, X.; Wang, Q.; Wang, G. Regulation of arsenite oxidation by the phosphate two-component system PhoBR in Halomonas sp. HAL1, *Front. Microbiol.* **2015**, *6*, 923.

(382) Fan, X.; Nie, L.; Shi, K.; Wang, Q.; Xia, X.; Wang, G. Simultaneous 3-/4-hydroxybenzoates biodegradation and arsenite oxidation by Hydrogenophaga sp. H7, *Front. Microbiol.* **2019**, *10*, 1346.

(383) Marinho, B. A.; Cristovao, R. O.; Boaventura, R. A. R.; Vilar, V. J. P. As(III) and Cr(VI) oxyanion removal from water by advanced oxidation/reduction processes-a review, *Environ. Sci. Pollut. Res. Int.* **2019**, *26*, 2203-2227.

(384) dos Santos Alves Figueiredo, B.; de Siqueira, F. G.; Chan Salum, T. F.; Zanette, C. M.; Rigon Spier, M. Microalgae and cyanobacteria as enzyme biofactories, *Algal Res.* **2017**, *25*, 76-89.

(385) Gollapudi, U. K.; Knutson, C. L.; Bang, S. S.; Islam, M. R. A new method for controlling leaching through permeable channels, *Chemosphere* **1995**, *30*, 695-705.

(386) Castanier, S.; Le Métayer-Levrel, G.; Perthuisot, J.-P. Ca-carbonates precipitation and limestone genesis - the microbiogeologist point of view, *Sediment. Geol.* **1999**, *126*, 9-23.

(387) Dhami, N. K.; Mukherjee, A.; Watkin, E. L. J. Microbial diversity and mineralogical-mechanical properties of calcitic cave speleothems in natural and in vitro biomineralization conditions, *Front. Microbiol.* **2018**, paper 40.

(388) Holm, L.; Sander, C. An evolutionary treasure: unification of a broad set of amidohydrolases related to urease, *Proteins* **1997**, *28*, 72-82.

(389) Park, I.-S.; Hausinger, R. P. Requirement of Carbon Dioxide for in Vitro Assembly of the Urease Nickel Metallocenter, *Science* **1995**, *267*, 1156-1158.

(390) Sumner, J. B. The isolation and crystallization of the enzyme urease, *J. Biol. Chem.* **1926**, *69*, 435-441.

(391) Jabri, E.; Carr, M. B.; Hausinger, R. P.; Karplus, P. A. The Crystal Structure of Urease from Kiebsiella aerogenes, *Science* **1995**, *268*, 998-1004.

(392) Mulrooney, S. B.; Hausinger, R. P. Klebsiella aerogenes urease genes and evidence for accessory proteins facilitating nickel incorporation, *J. Bacteriol.* **1990**, *172*, 5837-5843.

(393) Lauchnor, E. G.; Schultz, L. N.; Bugni, S.; Mitchell, A. C.; Cunningham, A. B.; Gerlach, R. Bacterially Induced Calcium Carbonate Precipitation and Strontium Coprecipitation in a Porous Media Flow System, *Environ. Sci. Technol.* **2013**, *47*, 1557-1564.

(394) Warren, L. A.; Maurice, P. A.; Parmar, N.; Ferris, F. G. Microbially mediated calcium carbonate precipitation: Implications for interpreting calcite precipitation and for solid-phase capture of inorganic contaminants, *Geomicrobiol. J.* **2001**, *18*, 93-115.

(395) Peng, D.; Qiao, S.; Luo, Y.; Ma, H.; Zhang, L.; Hou, S.; Wu, B.; Xu, H. Performance of microbial induced carbonate precipitation for immobilizing Cd in water and soil, *J. Hazard. Mater.* **2020**, *400*, 123116.

(396) Fujita, Y.; Redden, G. D.; Ingram, J. C.; Cortez, M. M.; Ferris, F. G.; Smith, R. W. Strontium incorporation into calcite generated by bacterial ureolysis, *Geochim. Cosmochim. Ac.* **2004**, *68*, 3261-3270.

(397) Li, M.; Cheng, X.; Guo, H. Heavy metal removal by biomineralization of urease producing bacteria isolated from soil, *Int. Biodeterior. Biodegrad.* **2013**, *76*, 81-85.

(398) Jiang, N.-J.; Liu, R.; Du, Y.-J.; Bi, Y.-Z. Microbial induced carbonate precipitation for immobilizing Pb contaminants: Toxic effects on bacterial activity and immobilization efficiency, *Sci. Total Environ.* **2019**, *672*, 722-731.

(399) Ivanov, V.; Chu, J. Applications of microorganisms to geotechnical engineering for bioclogging and biocementation of soil in situ, *Rev. Environ. Sci. Bio/Technol.* **2008**, *153*, 139-153.

(400) Hoffman, M.; Deccho, A. W. In *Microbial Extracellular Polymeric Substances: Characterization, Structure and Function*; Wingender, J., Neu, T. R., Flemming, H.-C., Eds.; Springer, 1999.

(401) Wang, S.; Lee, M. H.; Hausinger, R. P.; Clark, P. A.; Wilcox, D. E.; Scott, R. A. Structure of the Dinuclear Active Site of Urease. X-ray Absorption Spectroscopic Study of Native and 2-Mercaptoethanol-Inhibited Bacterial and Plant Enzymes, *Inorg. Chem.* **1994**, *33*, 1589-1593.

(402) Hammes, F.; Verstraete, W. Key roles of pH and calcium metabolism in microbial carbonate precipitation, *Rev. Environ. Sci. Biotechnol.* **2002**, *1*, 3−7.

(403)   Ferris, F. G.; Fyfe, W. S.; Beveridge, T. J. Bacteria as nucleation sites for authigenic minerals in a metal-contaminated lake sediment, *Chem. Geol.* **1987**, *63*, 225−232.

(404)   Fujita, Y.; Ferris, E. G.; Lawson, R. D.; Colwell, F. S.; Smith, R. W. Calcium carbonate precipitation by ureolytic subsurface bacteria, *Geomicrobiol. J.* **2000**, *17*, 305−318.

(405)   Shi, K.; Dai, X.; Fan, X.; Zhang, Y.; Chen, Z.; Wang, G. Simultaneous removal of chromate and arsenite by the immobilized Enterobacter bacterium in combination with chemical reagents, *Chemosphere* **2020**, *259*, 127428.

(406)   Fujita, Y.; Taylor, J. L.; Gresham, T. L. T.; Delwiche, M. E.; Colwell, F. S.; McLing, T. L.; Petzke, L. M.; Smith, R. W. Stimulation of Microbial Urea Hydrolysis in Groundwater to Enhance Calcite Precipitation, *Environ. Sci. Technol.* **2008**, *42*, 3025-3032.

(407)   Chaudhary, P.; Beniwal, V.; Umar, A.; Kumar, R.; Sharma, P.; Kumar, A.; Al-Hadeethi, Y.; Chhokar, V. In vitro microcosm of co-cultured bacteria for the removal of hexavalent Cr and tannic acid: A mechanistic approach to study the impact of operational parameters, *Ecotoxicol. Environ. Saf.* **2021**, *208*, 111484.

(408)   Eswaramoorthy, S.; Poulain, S.; Hienerwadel, R.; Bremond, N.; Sylvester, M. D.; Zhang, Y.-B.; Berthomieu, C.; Van Der Lelie, D.; Matin, A. Crystal structure of ChrR-a quinone reductase with the capacity to reduce chromate, *PLoS One* **2012**, *7*, e36017.

(409)   Saha, R.; Saha, I.; Nandi, R.; Ghosh, A.; Basu, A.; Ghosh, S. K.; Saha, B. Application of Chattim tree (devil tree, Alstonia scholaris) saw dust as a biosorbent for removal of hexavalent chromium from contaminated water, *Can. J. Chem. Eng.* **2013**, 814-821.

(410)   Seo, H.; Roh, Y. Biotransformation and Its Application: Biogenic Nano-Catalyst and Metal-Reducing-Bacteria for Remediation of Cr(VI)-Contaminated Water, *J. Nanosci. Nanotechnol* **2015**, *15*, 5649-5652.

(411)   Liu, H.; Guo, L.; Liao, S.; Wang, G. Reutilization of immobilized fungus Rhizopus sp. LG04 to reduce toxic chromate, *J. Appl. Microbiol.* **2012**, *112*, 651-659.

(412)   Macur, R. E.; Jackson, C. R.; Botero, L. M.; McDermott, T. R.; Inskeep, W. P. Bacterial populations associated with the oxidation and reduction of arsenic in an unsaturated soil, *Environ. Sci. Technol.* **2004**, *38*, 104-111.

(413)   Fan, H.; Su, C.; Wang, Y.; Yao, J.; Zhao, K.; Wang, Y.; Wang, G. Sedimentary arsenite-oxidizing and arsenate-reducing bacteria associated with high arsenic groundwater from Shanyin, Northwestern China, *J. Appl. Microbiol.* **2008**, *105*, 529-539.

(414)   Santini, J. M.; vanden Hoven, R. N. Molybdenum-containing arsenite oxidase of the chemolithoautotrophic arsenite oxidizer NT-26, *J. Bacteriol.* **2004**, *186*, 1614-1619.

(415) vanden Hoven, R. N.; Santini, J. M. Arsenite oxidation by the heterotroph Hydrogenophaga sp. str. NT-14: the arsenite oxidase and its physiological electron acceptor, *Biochim. Biophys. Acta* **2004**, *1656*, 148-155.

(416) Weiss, S.; Carapito, C.; Cleiss, J.; Koechler, S.; Turlin, E.; Coppee, J. Y.; Heymann, M.; Kugler, V.; Stauffert, M.; Cruveiller, S.; Medigue, C.; Van Dorsselaer, A.; Bertin, P. N.; Arsene-Ploetze, F. Enhanced structural and functional genome elucidation of the arsenite-oxidizing strain Herminiimonas arsenicoxydans by proteomics data, *Biochimie* **2009**, *91*, 192-203.

(417) Sawaya, M. R.; Cannon, G. C.; Heinhorst, S.; Tanaka, S.; Williams, E. B.; Yeates, T. O.; Kerfeld, C. A. The structure of beta-carbonic anhydrase from the carboxysomal shell reveals a distinct subclass with one active site for the price of two, *J. Biol. Chem.* **2006**, *281*, 7546-7555.

(418) Kerfeld, C. A.; Sawaya, M. R.; Tanaka, S.; Nguyen, C. V.; Phillips, M.; Beeby, M.; Yeates, T. O. Protein Structures Forming the Shell of Primitive Bacterial Organelles, *Science* **2005**, *309*, 936-938.

(419) Yeates, T. O.; Kerfeld, C. A.; Heinhorst, S.; Cannon, G. C.; Shively, J. M. Protein-based organelles in bacteria: carboxysomes and related microcompartments, *Nature Rev. Microbiol.* **2008**, *6*, 681-691.

(420) Giri, A.; Banerjee, U. C.; Kumar, M.; Pant, D. Intracellular carbonic anhydrase from Citrobacter freundii and its role in bio-sequestration, *Bioresour. Technol.* **2018**, *267*, 789-792.

(421) Van Den Hendea, S.; Rodriguesb, A.; Hamaekersf, H.; Sonnenholznerc, S.; Vervaeren, H.; Boona, B. Microalgal bacterial flocs treating paper mill effluent: A sunlight-based approach for removing carbon, nitrogen, phosphorus, and calcium, *N. Biotechnol.* **2017**, *39*, 1-10.

(422) Chen, P.-H.; Liu, H.-L.; Chen, Y.-J.; Cheng, Y.-H.; Lin, W.-L.; Yeh, C.-H.; Chang, C.-H. Enhancing CO_2 bio-mitigation by genetic engineering of cyanobacteria, *Energy Environ. Sci.* **2012**, *5*, 8318-8327.

(423) Dhami, N. K.; Quirin, M. E. C.; Mukherjee, A. Carbonate biomineralization and heavy metal remediation by calcifying fungi isolated from karstic caves, *Ecol. Eng.* **2017**, *103*, 106-117.

(424) Huang, S.; Jia, X.; Zhao, Y.; Bai, B. Elevated CO_2 benefits the soil microenvironment in the rhizosphere of Robinia pseudoacacia L. seedlings in Cd- and Pb-contaminated soils, *Chemosphere* **2017**, *168*, 606-616.

(425) Schultz, L.; Pitts, B.; Mitchell, A. C.; Cunningham, A. B.; Gerlach, R. Imaging biologically induced mineralization in fully hydrated flow systems, *Microsc. Today* **2011**, *19*, 12−15.

(426) Allen, R. M.; Bennetto, H. P. Microbial fuel cells: Electricity production from carbohydrates, *Appl. Biochem. Biotechnol.* **1993**, *39-40*, 27-40.

(427) Pant, D.; Van Bogaert, G.; Diels, L.; Vanbroekhoven, K. A review of the substrates used in microbial fuel cells (MFCs) for sustainable energy production, *Bioresour. Technol.* **2010**, *101*, 1533-1543.

(428) Potter, M. C. Electrical Effects Accompanying the Decomposition of Organic Compounds, *Proc. Royal Soc. B* **1911**, *84*, 260-276.

(429) Fang, C.; Achal, V. The Potential of Microbial Fuel Cells for Remediation of Heavy Metals from Soil and Water-Review of Application, *Microorganisms* **2019**, *7*, 697.

(430) Liu, N.; Liao, P.; Zhang, J.; Zhou, Y.; Luo, L.; Huang, H.; Zhang, L. Characteristics of denitrification genes and relevant enzyme activities in heavy-metal polluted soils remediated by biochar and compost, *Sci. Total Environ.* **2020**, *739*, 139987.

(431) Zhou, Z.; Zheng, Y.; Shen, J.; Zhang, L.; Liu, Y.; He, J. Responses of activities, abundances and community structures of soil denitrifiers to short-term mercury stress, *J. Environ. Sci.* **2012**, *24*, 369-375.

(432) Escher, B. I.; Eggen, R. I. L.; Schreiber, U.; Schreiber, Z.; Vye, E.; Wisner, B.; Schwarzenbach, R. P. Baseline Toxicity (Narcosis) of Organic Chemicals Determined by In Vitro Membrane Potential Measurements in Energy-Transducing Membranes, *Environ. Sci. Technol.* **2002**, *36*, 1971-1979.

(433) Cajthaml, T. Biodegradation of endocrine disrupting compounds by ligninolytic fungi: mechanisms involved in the degradation, *Environ. Microbiol.* **2015**, *17*, 4822-4834.

(434) Santos, L. H. M. L. M.; Gros, M.; Rodriguez-Mozaz, S.; Delerue-Matos, C.; Pena, A.; Barcelo, D.; Montenegro, M. C. B. S. M. Contribution of hospital effluents to the load of pharmaceuticals in urban wastewaters: identification of ecologically relevant pharmaceuticals, *Sci. Total Environ.* **2013**, *461-462*, 302-316.

(435) Frédéric, O.; Yves, P. Pharmaceuticals in hospital wastewater: Their ecotoxicity and contribution to the environmental hazard of the effluent, *Chemosphere* **2014**, *115*, 31-39.

(436) Bergheim, M.; Gminski, R.; Spangenberg, B.; Debiak, M.; Bürkle, A.; Mersch-Sundermann, V.; Kümmerer, K.; Gieré, R. Antibiotics and sweeteners in the aquatic environment: biodegradability, formation of phototransformation products, and in vitro toxicity, *Environ. Sci. Pollut. Res. Int.* **2015**, *22*, 18017-18030.

(437) Chu, H.-Q.; Tan, X.-B.; Zhang, Y.-L.; Yang, L.-B.; Zhao, F.-C.; Guo, J. Continuous cultivation of Chlorella pyrenoidosa using anaerobic digested starch processing wastewater in the outdoors, *Bioresour. Technol.* **2015**, *185*, 40-48.

(438) Panja, S.; Sarkar, D.; Datta, R. Removal of antibiotics and nutrients by Vetiver grass (Chrysopogon zizanioides) from secondary wastewater effluent, *Int. J. Phytoremediation* **2020**, *22*, 764-773.

(439) Copete-Pertuz, L. S.; Placido, J.; Serna-Galvis, E. A.; Torres-Palma, R. A.; Mora, A. Elimination of Isoxazolyl-Penicillins antibiotics in waters by the ligninolytic native Colombian strain Leptosphaerulina sp. considerations on biodegradation process and antimicrobial activity removal, *Sci. Total Environ.* **2018**, *630*, 1195-1204.

(440) Panja, S.; Sarkar, D.; Li, K.; Datta, R. Uptake and transformation of ciprofloxacin by vetiver grass (Chrysopogon zizanioides), *Int. Biodeterior Biodegradation* **2019**, *142*, 200-210.

(441) Khan, N. A.; Ahmed, S.; Farooqi, I. H.; Ali, I.; Vambol, V.; Changani, F.; Yousefi, M.; Vambol, S.; Khan, S. U.; Khan, A. H. Occurrence, sources and conventional treatment techniques for various antibiotics present in hospital wastewaters: A critical review, *Trends Analyt. Chem.* **2020**, *129*, 115921.

(442) Goosens, H.; Ferech, M.; Vander Stichele, R.; Elseviers, M.; Group, E. P. Outpatient antibiotic use in Europe and association with resistance: a crossnational database study, *Lancet* **2005**, *365*, 579-587.

(443) Russell, J. N.; Yost, C. K. Alternative, environmentally conscious approaches for removing antibiotics from wastewater treatment systems, *Chemosphere* **2021**, *263*, 128177.

(444) Chaturvedi, P.; Giri, B. S.; Shukla, P.; Gupta, P. Recent advancement in remediation of synthetic organic antibiotics from environmental matrices: Challenges and perspective, *Bioresour. Technol.* **2021**, *319*, 124161.

(445) Du, Y.; Wang, J.; Li, H.; Mao, S.; Wang, D.; Xiang, Z.; Guo, R.; Chen, J. The dual function of the algal treatment: Antibiotic elimination combined with CO2 fixation, *Chemosphere* **2018**, *211*, 192-201.

(446) Quinn, B.; Gagné, F.; Blaise, C. An investigation into the acute and chronic toxicity of eleven pharmaceuticals (and their solvents) found in wastewater effluent on the cnidarian, Hydra attenuate, *Sci. Total Environ.* **2008**, *2-3*, 306-314.

(447) Liu, Z. H.; Kanjo, Y.; Mizutani, S. Removal mechanisms for endocrine disrupting compounds (edcs) in wastewater treatment-Physical means, biodegradation, and chemical advanced oxidation: A review, *Sci. Total Environ.* **2009**, *407*, 731-748.

(448)   Silva, C. P.; Otero, M.; Esteves, V. Processes for the elimination of estrogenic steroid hormones from water: A review., *Environ. Pollut.* **2012**, *165*, 38-58.

(449)   Homem, V.; Santos, L. Degradation and removal methods of antibiotics from aqueous matrices-A review, *J. Environ. Manag.* **2011**, *92*, 2304-2347.

(450)   de Cazes, M.; Abejón, R.; Belleville, M.-P.; Sanchez-Marcano, J. Membrane bioprocesses for pharmaceutical micropollutants removal from waters, *Membranes* **2014**, *4*, 692-729.

(451)   Zainab, S. M.; Junaid, M.; Xu, N.; Malik, R. N. Antibiotics and antibiotic resistant genes (ARGs) in groundwater: A global review on dissemination, sources, interactions, environmental and human health risks, *Review Water Res.* **2020**, *187*, 116455.

(452)   De Gunzburg, J.; Bensoussan, C. Methods for the Inactivation of Antibiotics, **2012**, *WO 2012007536 A1*.

(453)   Suda, T.; Hata, T.; Kawai, S.; Okamura, H.; Nishida, T. Treatment of tetracycline antibiotics by laccase in the presence of 1-hydroxybenzotriazole, *Bioresour. Technol.* **2012**, *103*, 498-501.

(454)   Wen, X.; Jia, Y.; Li, J. Enzymatic degradation of tetracycline and oxytetracycline by crude manganese peroxidase prepared from phanerochaete chrysosporium, *J. Hazard. Mater.* **2010**, *177*, 924-928.

(455)   Li, X.; Xu, Q.; Cheng, J.; Yuan, Y. Improving the bioremoval of sulfamethoxazole and alleviating cytotoxicity of its biotransformation by laccase producing system under coculture of Pycnoporus sanguineus and Alcaligenes faecalis, *Bioresour. Technol.* **2016**, *220*, 333-340.

(456)   Zhang, Y.; Chen, Q.; Ji, J.; Zhao, L.; Zhang, L.; Qiu, J.; He, J. Complete Genome Sequence of Alcaligenes Faecalis Strain JQ135, a Bacterium Capable of Efficiently Degrading Nicotinic Acid, *Curr. Microbiol.* **2018**, *75*, 1551-1554.

(457)   Homlok, H.; Kiskó, G.; Kovács, A.; Tótha, T.; Takács, E.; Mohácsi-Farkas, C.; Wojnárovits, L.; Szabó, L. Antibiotics in a wastewater matrix at environmentally relevant concentrations affect coexisting resistant/sensitive bacterial cultures with profound impact on advanced oxidation treatment, *Sci. Total Environ.,* **2021**, *754*, 142181.

(458)   Sodhi, K. K.; Kumar, M.; Singh, D. K. Insight into the amoxicillin resistance, ecotoxicity, and remediation strategies, *J. Water Process. Eng.* **2021**, *39*, 101858.

(459)   Mitchell, S. M.; Ullman, J. L.; Teel, A. L.; Watts, R. J. Hydrolysis of amphenicol and macrolide antibiotics: Chloramphenicol, florfenicol, spiramycin, and tylosin, *Chemosphere* **2015**, *134*, 504-511.

(460) Qiu, M.; Hu, A.; Huang, Y.-m. M.; Zhao, Y.; He, Y.; Xu, J.; Lu, Z. Elucidating degradation mechanisms of florfenicol in soil by stable-isotope assisted nontarget screening, *J. Hazard. Mater.* **2021**, *403*, 123974.

(461) Cycon, M.; Mrozik, A.; Piotrowska-Seget, Z. Antibiotics in the soil environmentdegradation and their impact on microbial activity and diversity, *Front. Microbiol.* **2019**, *10*, 338.

(462) Shi, Y.; Lin, H.; Ma, J.; Zhu, R.; Sun, W.; Lin, X.; Zhang, J.; Zheng, H.; Zhang, X. Degradation of tetracycline antibiotics by Arthrobacter nicotianae OTC-16, *J. Hazard. Mater.* **2021**, *403*, 123996.

(463) Wen, X.; Jia, Y.; Li, J. Degradation of tetracycline and oxytetracycline by crude lignin peroxidase prepared from phanerochaete chrysosporium-A white rot fungus, *Chemosphere* **2009**, *75*, 1003-1007.

(464) Zhang, Y. J.; Geissen, S. U. In vitro degradation of carbamazepine and diclofenac by crude lignin peroxidase, *J. Hazard. Mater.* **2010**, *176*, 1089-1092.

(465) Margot, J.; Maillard, J.; Rossi, L.; Barry, D. A.; Holliger, C. Influence of treatment conditions on the oxidation of micropollutants by trametes versicolor laccase, *New Biotechnol.* **2013**, *30*, 803-813.

(466) Lloret, L.; Eibes, G.; Lú-Chau, T. A.; Moreira, M. T.; Feijoo, G.; Lema, J. M. Laccase-catalyzed degradation of anti-inflammatories and estrogens, *Biochem. Eng. J.* **2010**, *51*, 124-131.

(467) Hata, T.; Shintate, H.; Kawai, S.; Okamura, H.; Nishida, T. Elimination of carbamazepine by repeated treatment with laccase in the presence of 1-hydroxybenzotriazole, *J. Hazard. Mater.* **2010**, *181*, 1175-1178.

(468) Suzuki, K.; Hirai, H.; Murata, H.; Nishida, T. Removal of estrogenic activities of 17 beta-estradiol and ethinylestradiol by ligninolytic enzymes from white rot fungi, *Water Res.* **2003**, *37*, 1972-1975.

(469) Tamagawa, Y.; Yamaki, R.; Hirai, H.; Kawai, S.; Nishida, T. Removal of estrogenic activity of natural steroidal hormone estrone by ligninolytic enzymes from white rot fungi, *Chemosphere* **2006**, *65*, 97-101.

(470) Auriol, M.; Filali-Meknassi, Y.; Adams, C. D.; Tyagi, R. D.; Noguerol, T. N.; Pina, B. Removal of estrogenic activity of natural and synthetic hormones from a municipal wastewater: Efficiency of horseradish peroxidase and laccase from trametes versicolor, *Chemosphere* **2008**, *70*, 445-452.

(471)   Li, M.; Zhu, X.; Wilkinson, S.; Huang, M.; Achal, V. Complete Genome Sequence of Carbonic Anhydrase Producing Psychrobacter sp. SHUES1 1, *Front. Microbiol.* **2016**, *7*, 1442.

(472)   Wang, S.; Huang, W.; Fang, G.; Zhang, Y.; Qiao, H. Analysis of steroidal estrogen residues in food and environmental samples, *Int. J. Environ. Anal. Chem.* **2008**, *88*, 1-25.

(473)   Nussey, S. S.; Whitehead, S. A. *Endocrinology - An integrated approach*; Taylor & Francis: London, 2001.

(474)   Hakulinen, N.; Kiiskinen, L.-L.; Kruus, K.; Saloheimo, M.; Paanen, A.; Koivula, A.; Rouvinen, J. Crystal structure of a laccase from melanocarpus albomyces with an intact trinuclear copper site, *Nat. Struct. Biol.* **2002**, *9*, 601-605.

(475)   Czajka, C. P.; Londry, K. L. Anaerobic biotransformation of estrogens, *Sci. Total Environ.* **2006**, *367*, 932-941.

(476)   Garcia-Morales, R.; Rodríguez-Delgado, M.; Gomez-Mariscal, K.; Orona-Navar, C.; Hernandez-Luna, C.; Torres, E.; Parra, R.; Cárdenas-Chávez, D.; Mahlknecht, J.; Ornelas-Soto, N. Biotransformation of Endocrine-Disrupting Compounds in Groundwater: Bisphenol A, Nonylphenol, Ethynylestradiol and Triclosan by a Laccase Cocktail from Pycnoporus sanguineus CS43, *Water, Air, Soil Pollut.* **2015**, *226*, 251.

(477)   Lloret, L.; Eibes, G.; Moreira, M. T.; Feijoo, G.; Lema, J. M. Removal of estrogenic compounds from filtered secondary wastewater effluent in a continuous enzymatic membrane reactor. Identification of biotransformation products, *Environ. Sci. Technol.* **2013**, *47*, 4536-4543.

(478)   Dean, J. F. D.; LaFayette, P. R.; Rugh, C.; Tristram, A. H.; Hoopes, J. T.; Eriksson, K.-E. L.; Merkle, S. A. In *Lignin and Lignan Biosynthesis. ACS Symposium Series 697*; Lewis, N. G., Sarkanen, S., Eds.; American Chemical Society,: Washington, DC, 1998.

(479)   Torres-Duarte, C.; Viana, M. T.; Vazquez-Duhalt, R. Laccase-mediated transformations of endocrine disrupting chemicals abolish binding affinities to estrogen receptors and their estrogenic activity in zebrafish, *Appl. Biochem. Biotechnol.* **2012**, *168*, 864-876.

(480)   Carballa, M.; Omil, F.; Ternes, T.; Lema, J. M. Fate of pharmaceutical and personal care products (ppcps) during anaerobic digestion of sewage sludge, *Water Res.* **2007**, *41*, 2139-2215.

(481)   Ye, X.; Peng, T.; Feng, J.; Yang, Q.; Pratush, A.; Xiong, G.; Huang, T.; Hu, Z. A novel dehydrogenase 17β-HSDx from Rhodococcus sp. P14 with potential application in bioremediation of steroids contaminated environment, *J. Hazard. Mater.* **2019**, *362*, 170-177.

(482) Chakrabarty, S.; Austin, R. N.; Deng, D.; Groves, J. T.; Lipscomb, J. D. Radical Intermediates in Monooxygenase Reactions of Rieske Dioxygenases, *J. Am. Chem. Soc.* **2007**, *129*, 3514-3515.

(483) Tsang, H. T.; Batie, C. J.; Ballou, D. P.; Penner-Hahn, J. E. X-ray absorption spectroscopy of the [2-iron-2-sulfur] Rieske cluster in Pseudomonas cepacia phthalate dioxygenase. Determination of core dimensions and iron ligation, *Biochemistry* **1989**, *28*, 7233-7240.

(484) Correll, C. C.; Batie, C. J.; Ballou, D. P.; Ludwig, M. L. Phthalate dioxygenase reductase: a modular structure for electron transfer from pyridine nucleotides to [2Fe-2S], *Science* **1992**, *258*, 1604-1610.

(485) Karlsson, A.; Beharry, Z. M.; Eby, D. M.; Coulter, E. D.; Neidle, E. L.; Kurtz Jr, D. M.; Eklund, H.; Ramaswamy, S. X-ray Crystal Structure of Benzoate 1,2-Dioxygenase Reductase from Acinetobacter sp. Strain ADP1, *J. Mol. Biol.* **2002**, *318*, 261-272.

(486) Toräng, L.; Nyholm, N.; Albrechtsen, H.-J. Shifts in biodegradation kinetics of the herbicides MCPP and 2,4-D at low concentrations in aerobic aquifer materials, *Environ. Sci. Technol.* **2003**, *37*, 3095-3103.

(487) de Lipthay, J. R.; Sørensen, S. R.; Aamand, J. Effect of herbicide concentration and organic and inorganic nutrient amendment on the mineralization of mecoprop, 2,4-D and 2,4,5-T in soil and aquifer samples, *Environ. Pollut.* **2007**, *148*, 83-93.

(488) Carboneras, B.; Villaseñor, J.; Fernandez-Morales, F. J. Modelling aerobic biodegradation of atrazine and 2,4-dichlorophenoxy acetic acid by mixed-cultures, *Bioresour. Technol.* **2017**, *243*, 1044-1050.

(489) Orrego, R.; Guchardi, J.; Hernandez, V.; Krause, R.; Roti, L.; Armour, J.; Ganeshakumar, M.; Holdway, D. Pulp and paper mill effluent treatments have differential endocrine disrupting effects on rainbow trout, *Environ. Toxicol. Chem.* **2009**, *28*, 181-188.

(490) Ryokkynen, A.; Nieminen, P.; Mustonen, A.-M.; Pyykonen, T.; Askikainen, J.; Hanninen, S.; Mononen, J.; Kukkonen, J. V. K. Phytoestrogens alter the reproductive organ development in the mink (Mustela vison), *Toxicol. Appl. Pharmacol.* **2005**, *202*, 132-139.

(491) Buckland, B. C.; M.D., L.; Dunnill, P. The kinetics of cholesterol oxidase synthesis by Nocardia rhodocrous, *Biotechnol. Bioeng.* **1976**, *XVIII*, 601-621.

(492) Dykstra, C. M.; Giles, H. D.; Banerjee, S.; Pavlostathis, S. G. Biotransformation of phytosterols under aerobic conditions, *Water Res.* **2014**, *58*, 71-81.

(493) Uhía, I.; Galán, B.; Morales, V.; García, J. L. Initial step in the catabolism of cholesterol by Mycobacterium smegmatis mc2155, *Environ. Microbiol.* **2011**, *13*, 943-959.

(494) Auriol, M.; Filali-Meknassi, Y.; Adams, C. D.; Tyagi, R. D. Natural and synthetic hormone removal using the horseradish peroxidase enzyme: Temperature and pH effects, *Water Res.* **2006**, *40*, 2847-2856.

(495) Auriol, M.; Filali-Meknassi, Y.; Tyagi, R. D.; Adams, C. D. Oxidation of natural and synthetic hormones by the horseradish peroxidase enzyme in wastewater, *Chemosphere* **2007**, *68*, 1830-1837.

(496) Gelo, P. M.; Kim, H. H.; Butlin, N. G.; Palmore, G. T. R. Electrochemical studies of a truncated laccase produced in Pichia pastoris, *Appl. Environ. Microbiol.* **1999**, *65*, 5515-5521.

(497) Glaberman, S.; Kiwiet, J.; Aubee, C. B. Evaluating the role of fish as surrogates for amphibians in pesticide ecological risk assessment, *Chemosphere* **2019**, *235*, 952-958.

(498) Choudri, B. S.; Charabi, Y.; Al-Nasiri, N.; Al-Awadhi, T. Pesticides and herbicides, *Water Environ. Res.* **2020**, *92*, 1425-1432.

(499) García-Galán, M. J.; Monllor-Alcaraz, L. S.; Postigo, C.; Uggetti, E.; López de Alda, M.; Díez-Montero, R.; García, J. Microalgae-based bioremediation of water contaminated by pesticides in peri-urban agricultural areas, *Environ. Pollut.* **2020**, *265*, 114579.

(500) Khan, M. A.; Costa, F. B.; Fenton, O.; Jordan, P.; Fennell, C.; Mellander, P.-E. Using a multi-dimensional approach for catchment scale herbicide pollution assessments, *Sci. Total Environ.* **2020**, *747*, 141232.

(501) Muszyński, P.; Brodowska, M. S.; Paszko, T. Occurrence and transformation of phenoxy acids in aquatic environment and photochemical methods of their removal: a review, *Environ. Sci. Pollut. Res.* **2020**, *27*, 1276-1293.

(502) Magnoli, K.; Carranza, C. S.; Aluffi, M. E.; Magnoli, C. E.; Barberis, C. L. Herbicides based on 2,4 D: its behavior in agricultural environments and microbial biodegradation aspects. A review, *Environ. Sci. Pollut. Res.* **2020**, *27*, 38501-38512.

(503) Holland, N. T.; Duramad, P.; Rothman, N.; Figgs, L. W.; Blair, A.; Hubbard, A.; Smith, M. T. Micronucleus frequency and proliferation in human lymphocytes after exposure to herbicide 2,4-dichlorophenoxyacetic acid in vitro and in vivo, *Mutat. Res. Genet. Toxicol. Environ. Mutagen.* **2002**, *521*, 165-178.

(504) Islam, F.; Farooq, M. A.; Gill, R. A.; Wang, J.; Yang, C.; Ali, B.; Wang, G.-X.; Zhou, W. 2,4-D attenuates salinity-induced toxicity by mediating anatomical changes, antioxidant capacity and cation transporters in the roots of rice cultivars, *Sci Rep.* **2017**, *7*, 10443.

(505) Pileggi, M.; Pileggi, S. A. V.; Sadowsky, M. J. Herbicide bioremediation: from strains to bacterial communities, *Heliyon* **2020**, *6*, e05767.

(506) Müller, M. D.; Buser, H.-R. Conversion reactions of various phenoxyalkanoic acid herbicides in soil. Enantiomerization and enantioselective degradation of the chiral 2-phenoxypropionic acid herbicides, *Environ Sci Technol.* **1997**, *31*, 1953-1959.

(507) de Lipthay, J. R.; Aamand, J.; Barkay, T. Expression of tfdA genes in aquatic microbial communities during acclimation to 2,4-dichlorophenoxyacetic acid, *FEMS Microbiol. Ecol.* **2002**, *40*, 205-214.

(508) Batıoglu-Pazarbas, M.; Milosevic, N.; Malaguerra, F.; Binning, P. J.; Albrechtsen, H.-J.; Bjerg, P. L.; Aamand, J. Discharge of landfill leachate to streambed sediments impacts the mineralization potential of phenoxy acid herbicides depending on the initial abundance of tfdA gene classes, *Environ. Pollut.* **2013**, *176*, 275-283.

(509) González, A. J.; Gallego, A.; Gemini, V. L.; Papalia, M.; Radice, M.; Gutkind, G.; Planes, E.; Korol, S. E. Degradation and detoxification of the herbicide 2,4-dichlorophenoxyacetic acid (2,4-D) by an indigenous Delftia sp. strain in batch and continuous system, *Int. Biodeterior. Biodegrad.* **2012**, *66*, 8-13.

(510) Lopes, R. D. O.; Pereira, P. M.; Pereira, A. R. B.; Fernandes, K. V.; Carvalho, J. F.; França, A. D. S. D.; Valente, R. H.; da Silva, M.; Ferreira-Leitão, V. S. Atrazine, desethylatrazine (DEA) and desisopropylatrazine (DIA) degradation by Pleurotus ostreatus INCQS 4031, *Biocatal. Biotransformation* **2020**, *38*, 415-430.

(511) Zaya, R.; Amini, Z.; Whitaker, A.; Kohler, S.; Ide, C. Atrazine exposure affects growth, body condition and liver health in Xenopus laevis tadpoles, *Aquat. Toxicol.* **2011**, *104*, 243-253.

(512) Baxter, L.; Brain, R.; Lissemore, L.; Solomon, K.; Hanson, M.; Prosser, R. Influence of light, nutrients, and temperature on the toxicity of atrazine to the algal species Raphidocelis subcapitata: implications for the risk assessment of herbicides, *Ecotoxicol. Environ. Saf.* **2016**, *132*, 250-259.

(513) Murphyam, M.; Heck, M.; Coady, K.; Tompsett, A.; Jones, P.; Du Preez, L.; Everson, G.; Solomon, K.; Carr, J.; Smith, E.; Kendall, R.; Van Der Kraak, G.; Giesy, J. Atrazine concentrations, gonadal gross morphology and histology in ranid frogs collected in Michigan agricultural areas, *Aquat. Toxicol.* **2006**, *76*, 230-245.

(514) Zhou, N.; Wang, J.; Wang, W.; Wu, X. Purification, characterization, and catalytic mechanism of N-Isopropylammelide isopropylaminohydrolase (AtzC) involved in the degradation of s-triazine herbicides, *Environ. Pollut.* **2021**, *268*, 115803.

(515) Ofaim, S.; Zarecki, R.; Porob, S.; Gat, D.; Lahav, T.; Kashi, Y.; Aly, R.; Eizenberg, H.; Ronen, Z.; Freilich, S. Genome-scale reconstruction of Paenarthrobacter aurescens TC1 metabolic model towards the study of atrazine bioremediation, *Sci. Rep.* **2021**, *10*, 13019.

(516) Hsieh, H.-Y.; Lin, C.-H.; Hsu, S.-Y.; Stewart, G. C. A Bacillus spore-based display system for bioremediation of atrazine, *Appl. Environ. Microbiol.* **2020**, *86*, e01230.

(517) Liu, X.; Hui, N.; Kontro, M. H. Improved short-term microbial degradation in circulating water reducing high stagnant atrazine concentrations in subsurface sediments, *Water* **2020**, *12*, 2507.

(518) Szewczyk, R.; Różalska, S.; Mironenka, J.; Bernat, P. Atrazine biodegradation by mycoinsecticide Metarhizium robertsii: Insights into its amino acids and lipids profile, *J. Environ. Manage.* **2020**, *262*, 110304.

(519) Campbell, J. J. R.; Hogg, L. A.; Strasdine, G. A. Enzyme distribution in Pseudomonas Aeruginosa, *J. Bacteriol.* **1962**, *83*, 1155-1160.

(520) Cao, D.; He, S.; Li, X.; Shi, L.; Wang, F.; Yu, S.; Xu, S.; Ju, C.; Fang, H.; Yu, Y. Characterization, genome functional analysis, and detoxification of atrazine by Arthrobacter sp. C2, *Chemosphere* **2021**, *264*, 128514.

(521) Seffernick, J. L.; Reynolds, E.; Fedorov, A. A.; Fedorov, E.; Almo, S. C.; Sadowsky, M. J.; Wackett, L. P. X-ray Structure and Mutational Analysis of the Atrazine Chlorohydrolase TrzN, *J. Biol. Chem.* **2010**, *285*, 30606-30614.

(522) Nardini, M.; Ridder, I. S.; Rozeboom, H. J.; Kalk, K. H.; Rink, R.; Janssen, D. B.; Dijkstra, B. W. The X-ray Structure of Epoxide Hydrolase from Agrobacterium radiobacter AD1. An enzyme to detoxify harmful epoxides, *J. Biol. Chem.* **1999**, *274*, 14579-14586.

(523) Henn, C.; Monteiro, D. A.; Boscolo, M.; Da Silva, R. Biodegradation of atrazine and ligninolytic enzyme production by basidiomycete strains, *BMC Microbiol.* **2020**, *20*, 01950.

(524) Tao, Y.; Han, S.; Zhang, Q.; Yang, Y.; Shi, H.; Akindolie, M. S.; Jiao, Y.; Qu, J.; Jiang, Z.; Han, W.; Zhang, Y. Application of biochar with functional microorganisms for enhanced atrazine removal and phosphorus utilization, *J. Clean. Prod.* **2020**, *257*, 12053.

(525) Yu, T.; Wang, L.; Ma, F.; Wang, Y.; Bai, S. A bio-functions integration microcosm: Self-immobilized biochar-pellets combined with two strains of bacteria to remove atrazine in water and mechanisms, *J. Hazard. Mater.* **2020**, *384*, 121326.

(526) Aguiar, L. M.; Souza, M. D. F.; de Laia, M. L.; de Oliveira Melo, J.; da Costa, M. R.; Gonçalves, J. F.; Silva, D. V.; dos Santos, J. B. Metagenomic analysis reveals mechanisms of atrazine biodegradation promoted by tree species, *Environ. Pollut.* **2020**, *267*, 115636.

(527) Dhiman, N.; Jasrotia, T.; Sharma, P.; Negi, S.; Chaudhary, S.; Kumar, R.; Mahnashi, M. H.; Umar, A.; Kumar, R. Immobilization interaction between xenobiotic and Bjerkandera adusta for the biodegradation of atrazine, *Chemosphere* **2020**, *257*, 127060.

(528) Pouilly, N.; Mitchell, C. G. The enzymes of β-oxidationm Rhodococcus ruber, *Biochem. Soc. Trans.* **1994**, *22*, 223S-223S.

(529) Xu, X.; Zarecki, R.; Medina, S.; Ofaim, S.; Liu, X.; Chen, C.; Hu, S.; Brom, D.; Gat, D.; Porob, S.; Eizenberg, H.; Ronen, Z.; Jiang, J.; Freilich, F. Modeling microbial communities from atrazine contaminated soils promotes the development of biostimulation solutions, *ISME J.* **2019**, *13*, 494-508.

(530) Jiang, Z.; Zhang, X.; Wang, Z.; Cao, B.; Deng, S.; Bi, M.; Zhang, Y. Enhanced biodegradation of atrazine by Arthrobacter sp. DNS10 during coculture with a phosphorus solubilizing bacteria: Enterobacter sp. P1, *Ecotoxicol. Environ. Saf.* **2019**, *172*, 159-166.

(531) Chan-Cheng, M.; Cambronero-Heinrichs, J. C.; Masís-Mora, M.; Rodríguez-Rodríguez, C. E. Ecotoxicological test based on inhibition of fungal laccase activity: Application to agrochemicals and the monitoring of pesticide degradation processes, *Ecotoxicol. Environ. Saf.* **2020**, *195*, 110419.

(532) Gao, N.; Zhang, J.; Pan, Z.; Zhao, X.; Ma, X.; Zhang, H. Biodegradation of Atrazine by Mixed Bacteria of Klebsiella variicola Strain FH-1 and Arthrobacter sp. NJ-1, *Bull. Environ. Contam. Toxicol.* **2020**, *105*, 481-489.

(533) Zhang, N.; Xie, F.; Guo, Q. N.; Yang, H. Environmental disappearance of acetochlor and its bioavailability to weed: A general prototype for reduced herbicide application instruction, *Chemosphere* **2021**, *265*, 129108.

(534) Liu, J.; Zhang, X.; Xu, J.; Qiu, J.; Zhu, J.; Cao, H.; He, J. Anaerobic biodegradation of acetochlor by acclimated sludge and its anaerobic catabolic pathway, *Sci. Total Environ.* **2020**, *748*, 141122.

(535) Chen, Q.; Wang, C. H.; Deng, S. K.; Wu, Y. D.; Li, Y.; Yao, L.; Jiang, J. D.; Yan, X.; He, J.; Li, S. P. Novel three-component rieske non-heme iron oxygenase system catalyzing the N-dealkylation of chloroacetanilide herbicides in Sphingomonads DC-6 and DC-2, *Appl. Environ. Microbiol.* **2014**, *80*, 5078-5085.

(536) Chu, C.; Liu, B.; Liu, J.; He, J.; Lv, L.; Wang, H.; Xie, X.; Tao, Q.; Chen, Q. Phytoremediation of acetochlor residue by transgenic Arabidopsis expressing the acetochlor N-dealkylase from Sphingomonas wittichii DC-6, *Sci. Total Environ.* **2020**, *728*, 138687.

(537) Jakoncic, J.; Jouanneau, Y.; Meyer, C.; Stojanoff, V. The crystal structure of the ring-hydroxylating dioxygenase from Sphingomonas CHY-1, *FEBS J.* **2007**, *274*, 2470-2481.

(538) Duc, H. D.; Thuy, N. T. D.; Truc, H. T. T.; Nhu, N. T. H.; Oanh, N. T. Degradation of butachlor and propanil by Pseudomonas sp. Strain But2 and Acinetobacter baumannii strain DT, *FEMS Microbiol. Lett* **2020**, *367*, 151.

(539) Sorensen, S. R.; Bending, G. D.; Jacobsen, C. S.; Walker, A.; Aamand, J. Microbial degradation of isoproturon and related phenylurea herbicides in and below agricultural fields, *FEMS Microbiol. Ecol.* **2003**, *45*, 1-11.

(540) Giacomazzi, S.; Cochet, N. Environmental impact of diuron transformation: a review, *Chemosphere* **2004**, *56*, 1021-1032.

(541) You, I.-S.; Bartha, R. Metabolism of 3,4-dichloroaniline by Pseudomonas putida, *J. Agric. Food Chem.* **1982**, *30*, 274-277.

(542) Dejonghe, W.; Goris, J.; Dierickx, A.; De Dobbeleer, V.; Crul, K.; De Vos, P.; Verstraete, W.; Top, E. M. Diversity of 3-chloroaniline and 3,4-dichloroaniline degrading bacteria isolated from three different soils and involvement of their plasmids in chloroaniline degradation, *FEMS Microbiol. Ecol.* **2002**, *42*, 315-325.

(543) Rajmohan, S.; Dodd, C. E. R.; Waites, W. M. Enzymes from isolates of Pseudomonas fluorescens involved in food spoilage, *J. Appl. Microbiol.* **2002**, *93*, 205-213.

(544) Zhao, Z.; Hou, S.; Lan, D.; Wang, X.; Liu, J.; Khan, F. I.; Wang, Y. Crystal structure of a lipase from Streptomyces sp. Strain W007 - implications for thermostability and regiospecificity, *FEBS J.* **2017**, *284*, 3506-3519.

(545) Da Silva Coelho-Moreira, J.; Bracht, A.; da Silva de Souza, A. C.; Oliveira, R. F.; de Sá-Nakanishi, A. B.; de Souza, C. G. M. Degradation of diuron by Phanerochaete chrysosporium: role of ligninolytic enzymes and cytochrome P450, *BioMed Res. Int.* **2013**, *2013*, 1-9.

(546) Kučić Grgić, D.; Ocelić Bulatović, V.; Cvetnić, M.; Dujmić Vučinić, Ž.; Vuković Domanovac, M.; Markić, M.; Bolanča, T. Biodegradation kinetics of diuron by Pseudomonas aeruginosa FN and optimization of biodegradation using response surface methodology, *Water Environ. J.* **2020**, *34*, 61-73.

(547) Hu, K.; Torán, J.; López-García, E.; Barbieri, M. V.; Postigo, C.; de Alda, M. L.; Caminal, G.; Sarrà, M.; Blánquez, P. Fungal bioremediation of diuron-contaminated waters: Evaluation of its degradation and the effect of amendable factors on its removal in a trickle-bed reactor under non-sterile conditions, *Sci. Total Environ.* **2020**, *743*, 140628.

(548) Shah, M. B.; Jang, H.-H.; Zhang, Q.; Stout, C. D.; Halpert, J. R. X-ray crystal structure of the cytochrome P450 2B4 active site mutant F297A in complex with clopidogrel: Insights

into compensatory rearrangements of the binding pocket, *Arch. Biochem. Biophys.* **2013**, *530*, 64-72.

(549) Yang, Y.; Pratap Singh, R.; Song, D.; Chen, Q.; Zheng, X.; Zhang, C.; Zhang, M.; Li, Y. Synergistic effect of Pseudomonas putida II-2 and Achromobacter sp. QC36 for the effective biodegradation of the herbicide, *Ecotoxicol. Environ. Saf.* **2020**, *188*, 109826.

(550) Niks, D.; Hille, R. Molybdenum- and tungsten-containing formate dehydrogenases and formylmethanofuran dehydrogenases: structure, mechanism and cofactor insertion, *Protein Sci.* **2019**, *28*, 111-122.

(551) Cherney, M. M.; Zhang, Y.; Solomonson, M.; Weiner, J. H.; James, M. N. G. Crystal Structure of Sulfide:Quinone Oxidoreductase from Acidithiobacillus ferrooxidans: Insights into Sulfidotrophic Respiration and Detoxification, *J. Mol. Biol.* **2010**, *398*, 292-305.

(552) Kisker, C.; Schindelin, H.; Rees, D. C. MOLYBDENUM-COFACTOR-CONTAINING ENZYMES:Structure and Mechanism, *Annu. Rev. Biochem.* **1997**, *66*, 233-267.

(553) Kletzin, A.; Adams, M. W. Tungsten in biological systems, *FEMS Microbiol.Rev.* **1996**, *18*, 5-63.

(554) White, H.; Strobl, G.; Feicht, R.; Simon, H. Carboxylic acid reductase: a new tungsten enzyme catalyses the reduction of non-activated carboxylic acids to aldehydes, *Eur. J. Biochem.* **1989**, *184*, 89-96.

(555) Nykiel-Szymańska, J.; Bernat, P.; Słaba, M. Biotransformation and detoxification of chloroacetanilide herbicides by Trichoderma spp. with plant growth-promoting activities, *Pestic. Biochem. Physiol.* **2020**, *163*, 216-226.

(556) Loessner, M. J.; Kramer, K.; Ebel, F.; Scherer, S. C-terminal domains of Listeria monocytogenes bacteriophage murein hydrolases determine specific recognition and high-affinity binding to bacterial cell wall carbohydrates, *Molecular Microbiology.* **2002**, *44*, 335-491.

(557) Pérez-Dorado, I.; Campillo, N. E.; Monterroso, B.; Hesek, D.; Lee, M.; Páez, J. A.; García, P.; Martínez-Ripoll, M.; García, J. L.; Mobashery, S.; Menéndez, M.; Hermoso, J. A. Elucidation of the molecular recognition of bacterial cell wall by modular pneumococcal phage endolysin CPL-1, *J. Biol. Chem.* **2007**, *282*, 24990-24999.

(558) Loffredo, E.; Castellana, G.; Senesi, N. Decontamination of a municipal landfill leachate from endocrine disruptors using a combined sorption/bioremoval approach, *Environ. Sci. Pollut. Res.* **2014**, 2654-2662.

(559) Xiao, P.; Kondo, R. Biodegradation and biotransformation of pentachlorophenol by wood-decaying white rot fungus Phlebia acanthocystis TMIC34875, *J. Wood. Sci.* **2020**, *66*, 2.

(560) Aregbesola, O. A.; Mokoena, M. P.; Olaniran, A. O. Biotransformation of pentachlorophenol by an indigenous Bacillus cereus AOA-CPS1 isolated from wastewater effluent in Durban, South Africa, *Biodegradation* **2020**, *31*, 369-383.

(561) Zang, H.; Wang, H.; Miao, L.; Cheng, Y.; Zhang, Y.; Liu, Y.; Sun, S.; Wang, Y.; Li, C. Carboxylesterase, a de-esterification enzyme, catalyzes the degradation of chlorimuron-ethyl in Rhodococcus erythropolis D310-1, *J. Hazard. Mater.* **2020**, *387*, 121684.

(562) Cheng, Y.; Zang, H. L.; Wang, H. L.; Li, D. P.; Li, C. Y. Global transcriptomic analysis of Rhodococcus erythropolis D310-1 in responding to chlorimuron-ethyl., *Ecotox. Environ. Safe.* **2018**, *157*, 111-120.

(563) Zhang, S.; Zhang, C.; Sun, F.; Zhang, Z.; Zhang, X.; Pan, H.; Sun, P.; Zhang, H. Glutathione-S-transferase (GST) catalyzes the degradation of Chlorimuron-ethyl by Klebsiella jilinsis 2N3, *Sci. Total Environ.* **2020**, *729*, 139075.

(564) Udomsinprasert, R.; Pongjaroenkit, S.; Wongsantichon, J.; Oakley, A. J.; Prapanthadara, L. A.; Wilce, M. C.; Ketterman, A. J. Identification, characterization and structure of a new Delta class glutathione transferase isoenzyme, *Biochem. J.* **2005**, *388*, 763-771.

(565) Heidarrezaei, M.; Shokravi, H.; Huyop, F.; Koloor, S. S. R.; Petrů, M. Isolation and characterization of a novel bacterium from the marine environment for trichloroacetic acid bioremediation, *Appl. Sci. (Switzerland)* **2020**, *10*, 4593.

(566) Franken, S. M.; Rozeboom, H. J.; Kalk, K. H.; Dijkstra, B. W. Crystal structure of haloalkane dehalogenase: an enzyme to detoxify halogenated alkanes, *EMBO J.* **1991**, *10*, 1297-1302.

(567) Samadi, A.; Sharifi, H.; Ghobadi Nejad, Z.; Hasan-Zadeh, A.; Yaghmaei, S. Biodegradation of 4-Chlorobenzoic Acid by Lysinibacillus macrolides DSM54T and Determination of Optimal Conditions, *Int. J. Environ. Res.* **2020**, *14*, 145-154.

(568) Coleman, N. V.; Rich, D. J.; Tang, F. H. M.; Vervoort, R. W.; Maggi, F. Biodegradation and Abiotic Degradation of Trifluralin: A Commonly Used Herbicide with a Poorly Understood Environmental Fate, *Environ. Sci. Technol.* **2020**, *54*, 10399-10410.

(569) Hu, T.; Xiang, Y.; Chen, Q.; Shang, N.; Xu, M.; Huang, X. A novel esterase LanE from Edaphocola flava HME-24 and the enantioselective degradation mechanism of herbicide lactofen, *Ecotoxicol. Environ. Saf.* **2020**, *205*, 111141.

(570) Mougin, C.; Boyer, F. D.; Caminade, E.; Rama, R. Cleavage of the diketonitrile derivative of the herbicide isoxaflutole by extracellular fungal oxidases, *J. Agric. Food Chem.* **2000**, *48*, 4529-4534.

(571) Zhang, B.; Ni, Y.; Liu, J.; Yan, T.; Zhu, X.; Li, Q. X.; Hua, R.; Pan, D.; Wu, X. Bead-immobilized Pseudomonas stutzeri Y2 prolongs functions to degrade s-triazine herbicides in industrial wastewater and maize fields, *Sci. Total Environ.* **2020**, *731*, 139183.

(572) Zhu, J.; Zhao, Y.; Fu, L.; Liu, Z.; Li, X.; Meng, Z. Application of a simazine degrading bacterium, Arthrobacter ureafaciens XMJ-Z01 for bioremediation of simazine pollution, *Water Environ J.* **2020**, *34*, 561-572.

(573) Zhang, C.; Chen, L.; Si, H.; Gao, W.; Liu, P.; Zhang, J. Study on the characteristics and mechanisms of nicosulfuron biodegradation by Bacillus velezensis CF57, *J. Basic Microbiol.* **2020**, *60*, 649-658.

(574) Chen, L.; Gu, W.; Xu, H. y.; Yang, G. L.; Shan, X. F.; Chen, G.; Wang, C. F.; Qian, A. D. Complete genome sequence of Bacillus velezensis 157 isolated from Eucommia ulmoides with pathogenic bacteria inhibiting and lignocellulolytic enzymes production by SSF, *3 Biotech* **2018**, *8*, 114.

(575) García-Vara, M.; Hu, K.; Postigo, C.; Olmo, L.; Caminal, G.; Sarrà, M.; López de Alda, M. Remediation of bentazone contaminated water by Trametes versicolor: Characterization, identification of transformation products, and implementation in a trickle-bed reactor under non-sterile conditions, *J. Hazard. Mater.* **2020**, 124476.

(576) Mazurkewich, S.; Helland, R.; Mackenzie, A.; Eijsink, V. G. H.; Pope, P. B.; Brändén, G.; Larsbrink, J. Structural insights of the enzymes from the chitin utilization locus of Flavobacterium johnsoniae, *Sci. Rep.* **2020**, *10*, 13775.

(577) Ramasubbu, N.; Paloth, V.; Luo, Y.; Brayer, G. D.; Levine, M. J. Structure of human salivary alpha-amylase at 1.6 Å resolution:implications for its role in the oral cavity, *Acta Crystallogr. D* **1996**, *52*, 435-446.

(578) Singh, S.; Kumar, V.; Gill, J. P. K.; Datta, S.; Singh, S.; Dhaka, V.; Kapoor, D.; Wani, A. B.; Dhanjal, D. S.; Kumar, M.; Harikumar, S. L.; Singh, J. Herbicide glyphosate: Toxicity and microbial degradation, *Int. J. Environ. Res. Public Health* **2020**, *17*, 1-18.

(579) Madureira Barroso, G.; dos Santos, J. B.; de Oliveira, I. T.; Rocha Nunes, T. K. M.; Alves Ferreira, E.; Marinho Pereira, I.; Valadão Silva, D.; de Freitas Souza, M. Tolerance of Bradyrhizobium sp. BR 3901 to herbicides and their ability to use these pesticides as a nutritional source, *Ecol. Indic.* **2020**, *119*, 106783.

(580) Gattás, F.; Espinosa, M.; Babay, P.; Pizarro, H.; Cataldo, D. Invasive species versus pollutants: Potential of Limnoperna fortunei to degrade glyphosate-based commercial formulations, *Ecotoxicol. Environ. Saf.* **2020**, *201*, 110794.

(581) la Cecilia, D.; Porta, G. M.; Tang, F. H. M.; Riva, M.; Maggi, F. Probabilistic indicators for soil and groundwater contamination risk assessment, *Ecol. Indic.* **2020**, *115*, 106424.

(582) Stosiek, N.; Talma, M.; Klimek-Ochab, M. Carbon-Phosphorus Lyase-the State of the Art, *Appl. Biochem. Biotechnol.* **2020**, *190*, 1525-1552.

(583) Yang, K.; Ren, Z.; Raushel, F. M.; Zhang, J. Structures of the Carbon-Phosphorus Lyase Complex Reveal the Binding Mode of the NBD-like PhnK, *Structure* **2016**, *24*, 37-42.

(584) Sirajuddin, S.; Khan, M. A.; Qader, S. A. U.; Iqbal, S.; Sattar, H.; Ansari, A. A comparative study on degradation of complex malathion organophosphate using of Escherichia coli IES-02 and a novel carboxylesterase, *Int. J. Biol. Macromol.* **2020**, *145*, 445-455.

(585) Li, X.; Wang, J.; Jia, Y.; Reheman, A.; Yan, Y. The genome analysis of methylobacterium populi yc-xj1 with diverse xenobiotics biodegrading capacity and degradation characteristics of related hydrolase, *Int. J. Mol. Sci.* **2020**, *21*, 1-18.

(586) Chen, F.; Li, X.; Dong, Y.; Li, J.; Li, Y.; Li , H.; Chen, L.; Zhou, M.; Hou, H. Biodegradation of phthalic acid esters (PAEs) by Cupriavidus oxalaticus strain E3 isolated from sediment and characterization of monoester hydrolases, *Chemosphere* **2021**, *266*, 129061.

(587) Paszko, T.; Muszyński, P.; Materska, M.; Bojanowska, M.; Kostecka, M.; Jackowska, I. Adsorption and degradation of phenoxyalkanoic acid herbicides in soils: A review, *Environ. Toxicol. Chem.* **2016**, *35*, 271-286.

(588) Xiang, S.; Lin, R.; Shang, H.; Xu, Y.; Zhang, Z.; Wu, X.; Zong, F. Efficient Degradation of Phenoxyalkanoic Acid Herbicides by the Alkali-Tolerant Cupriavidus oxalaticus Strain X32, *J. Agric. Food Chem.* **2020**, *68*, 3786-3795.

(589) Zeidler, O. Verbindungen von Chloral mit Brom- und Chlorbenzol, *Ber. Dtsch. Chem. Ges.* **1874**, *7*, 1180-1181.

(590) Müller, P. H. Über Zusammenhänge zwischen Konstitution und insektizider Wirkung, *Helv. Chim. Acta* **1946**, *29*, 1560-1580.

(591) Bumpus, J. A.; Aust, S. D. Biodegradation of DDT [1,1,1-Trichloro-2,2-Bis(4-Chlorophenyl)Ethane] by the White Rot Fungus Phanerochaete chrysosporium, *Appl. Environ. Microbiol.* **1987**, *53*, 2001-2008.

(592) Bumpus, J. A.; Powers, R. H.; Sun, T. Biodegradation of DDE (1,1 -dichloro-2,2-bis(4-chlorophenyl)ethene) by Phanerochaete chrysosporium *Mycological research* **1993**, *97*, 95-98.

(593) Nadeau, L. J.; Menn, F.; Breen, A.; Sayler, G. S. Aerobic Degradation of 1,1,1-Trichloro-2,2-Bis(4-Chlorophenyl)Ethane (DDT) by Alcaligenes eutrophus A5, *Appl. Environ. Microbiol.* **1994**, *60*, 51-55.

(594) Corona-Cruz, A.; Gold-Bouchot, G.; Gutierrez-Rojas, M.; Monroy-Hermosillo, O.; Favela, E. Anaerobic-Aerobic Biodegradation of DDT (Dichlorodiphenyl Trichloroethane) in Soils, *Bull. Environ. Contam. Toxicol.* **1999**, *63*, 219-225.

(595) Aislabie, J. M.; Richards, N. K.; Boul, H. L. Microbial degradation of DDT and its residues-a review, *N.Z.J. Agric. Res.* **2010**, *40*, 269-282.

(596) Wan, Y.; Tran, T. M.; Nguyen, V. T.; Wang, A.; Wang, J.; Kannan, K. Neonicotinoids, fipronil, chlorpyrifos, carbendazim, chlorotriazines, chlorophenoxy herbicides, bentazon, and selected pesticide transformation products in surface water and drinking water from northern Vietnam, *Sci. Total Environ.* **2021**, *750*, 141507.

(597) Bloomquist, J. R. In *Radcliffe's IPM World Textbook*; University of Minnesota 1999.

(598) Bhatt, P.; Sharma, A.; Rene, E. R.; Kumar, A. J.; Zhang, W. Bioremediation of fipronil using Bacillus sp. FA3: Mechanism, kinetics and resource recovery potential from contaminated environments, *J. Water Proc. Eng.* **2021**, *39*, 101712.

(599) Sayi, D. S.; Vinod Kumar, K.; Jijitha, P.; Sachithanandam, V.; Narayanan, J. K. Isolation and molecular identification of pesticide (fipronil) degrading bacteria from mangrove soil, *Res. J. Chem. Environ.* **2020**, *24*, 125-128.

(600) King, C. In *U.S.D.A, Agriculture Hand book No. 69*; U.S. Govt. Printing Office, 1954

(601) Huang, Y.; Zhang, W.; Pang, S.; Chen, J.; Bhatt, P.; Mishra, S.; Chen, S. Insights into the microbial degradation and catalytic mechanisms of chlorpyrifos, *Environ. Res.* **2021**, *194*, 110660.

(602) Marsili, E.; Baron, D. B.; Shikhare, I. D.; Coursolle, D.; Gralnick, J. A.; Bond, D. R. Shewanella secretes flavins that mediate extracellular electron transfer, *PNAS* **2008**, *105*, 3968-3973.

(603) Dash, D. M.; Osborne, W. J. Rapid biodegradation and biofilm-mediated bioremoval of organophosphorus pesticides using an indigenous Kosakonia oryzae strain -VITPSCQ3 in a Vertical-flow Packed Bed Biofilm Bioreactor, *Ecotoxicology and Environmental Safety* **2020**, *192*, 110290.

(604) Wight, A. Two-headed fish mystery deepens, *Stock & Land* **2009**.

(605) Bai, N.; Wang, S.; Abuduaini, R.; Zhang, M.; Zhu, X.; Zhao, Y. Rhamnolipid-aided biodegradation of carbendazim by Rhodococcus sp. D-1: Characteristics, products, and phytotoxicity, *Sci. Total Environ.* **2017**, *590-591*, 343-351.

(606) Cai, W.; Ye, P.; Yang, B.; Shi, Z.; Xiong, Q.; Gao, F.; Liu, Y.; Zhao, J.; Ying, G. Biodegradation of typical azole fungicides in activated sludge under aerobic conditions, *J. Environ. Sci.* **2021**, *103*, 288-297.

(607) Kryczyk-Poprawa, A.; Żmudzki, P.; Maślanka, A.; Piotrowska, J.; Opoka, W.; Muszyńska, B. Mycoremediation of azole antifungal agents using in vitro cultures of Lentinula edodes, *3 Biotech* **2019**, *9*, 207.

(608) Kuhlmann, J.; Kretschmann, A. C.; Bester, K.; Bollmann, U. E.; Dalhoff, K.; Cedergreen, N. Enantioselective mixture toxicity of the azole fungicide imazalil with the insecticide α-cypermethrin in Chironomus riparius: Investigating the importance of toxicokinetics and enzyme interactions, *Chemosphere* **2019**, *225*, 166-173.

(609) Carias, C. C.; Novais, J. M.; Martins-Dias, S. Are Phragmites australis enzymes involved in the degradation of the textile azo dye acid orange 7?, *Bioresour. Technol.* **2008**, *99*, 243-251.

(610) Lv, T.; Carvalho, P. N.; Casas, M. E.; Bollmann, U. E.; Arias, C. A.; Brix, H.; Bester, K. Enantioselective uptake, translocation and degradation of the chiral pesticides tebuconazole and imazalil by Phragmites australis, *Environ. Pollut.* **2017**, *229*, 362-370.

(611) Eizuka, T.; Ito, A.; Chida, T. Degradation of ipconazole by microorganisms isolated from paddy soil, *J. Pestic. Sci.* **2003**, *28*, 200-207.

(612) Montenegro Stamford, T. L.; Montenegro Stamford, T. C.; Stamford, N. P.; Silva Santos, C. E. R.; do Carmo Catanho Pereira de Lyra, M.; Ha-Park, Y.; Bae, J.-W.; Araujo, J. M. Interspecies variation of Kitasatospora recifensis endophytic from yam bean producing thermostable amylases in alternative media, *World J. Microbiol. Biotechnol.* **2007**, *23*, 1719-1724.

(613) Chitte, R.; Dey, S. Production of a fibrinolytic enzyme by thermophilic Streptomyces species, *World J. Microbiol. Biotechnol.* **2002**, *18*, 289-294.

(614) Thompson, D. P.; Eribo, B. Extracellular enzyme production by Rhizopus and Mucor species on solid media, *Can. J. Microbial.* **1984**, *30*, 126-128.

(615) Naraian, R.; Gautam, R. L. In *New and Future Developments in Microbial Biotechnology and Bioengineering, Penicillum System Properties and Applications*; Elsevier B.V., 2018.

(616) Fukuda, T.; Uchida, H.; Takashima, Y.; Uwajima, T.; Kawabata, T.; Suzuki, M. Degradation of bisphenol A by purified laccase from Trametesvillosa, *Biochem. Biophys. Res. Commun.* **2001**, *284*, 704- 706.

(617)   Saito, T.; Kato, K.; Yokogawa, Y. Detoxification of bisphenol A and nonylphenol by purified extracellular laccase from a fungus isolated from soil, *J. Biosci. Bioeng.* **2004**, *98*, 64-66.

(618)   Brugnari, T.; Pereira, M. G.; Bubna, G. A.; de Freitas, E. N.; Contato, A. G.; Corrêa, R. C. G.; Castoldi, R.; de Souza, C. G. M.; de MoraesPolizeli, M. L. T.; Bracht, A.; Peralta, R. M. A highly reusable MANAE-agarose-immobilized Pleurotus ostreatus laccase for degradation of bisphenol A, *Sci. Total Environ.* **2018**, *634*, 1346-1351.

(619)   Beck, S.; Berry, E.; Duke, S.; Milliken, A.; Patterson, H.; Prewett, D. L.; Rae, T. C.; Sridhar, V.; Wendland, N.; Gregory, B. W.; Johnson, C. M. Characterization of Trametes versicolor laccase-catalyzed degradation of estrogenic pollutants: Substrate limitation and product identification, *Int. Biodeterior. Biodegradation* **2018**, *127*, 146-159.

(620)   Bilal, M.; Iqbal, H. M. N.; Barceló, D. Mitigation of bisphenol A using an array of laccase-based robust bio-catalytic cues - A review, *Sci Total Environ* **2019**, *689*, 160-177.

(621)   Uchida, H.; Fukuda, T.; Miyamoto, H.; Kawabata, T.; Suzuki, M.; Uwajima, T. Polymerization of bisphenol A by purified laccase from Trametes villosa, *Biochem. Biophy. Res. Commun.* **2001**, *287*, 355-358.

(622)   Tsutsumi, Y.; Haneda, T.; Nishida, T. Removal of estrogenic activities of bisphenol A and nonylphenol by oxidative enzymes from lignin-degrading basidiomycetes, *Chemosphere* **2001**, *42*, 271-276.

(623)   Diano, N.; Mita, D. G. In *Einschlag, F.S.G., Waste Water - Treatment and Reutilization, InTech (Croatia) Part 1*, 2011.

(624)   de Freitas, E. N.; Bubna, G. A.; Brugnari, T.; Kato, C. G.; Nolli, M.; Rauen, T. G.; Moreira, R. d. F. P. M.; Peralta, R. A.; Bracht, A.; de Souza, C. G. M.; Peralta, R. M. Removal of bisphenol A by laccases from Pleurotus ostreatus and Pleurotus pulmonarius and evaluation of ecotoxicity of degradation products, *Chem. Eng. J.* **2017**, *330*, 1361-1369.

(625)   Hongyan, L.; Zexiong, Z.; Shiwei, X.; He, X.; Yinian, Z.; Haiyun, L.; Zhongsheng, Y. Study on transformation and degradation of bisphenol A by Trametes versicolor laccase and simulation of molecular docking, *Chemosphere* **2019**, *224*, 743-750.

(626)   Fujieda, N.; Umakoshi, K.; Ochi, Y.; Nishikawa, Y.; Yanagisawa, S.; Kubo, M.; Kurisu, G.; Itoh, S. Copper-Oxygen Dynamics in the Tyrosinase Mechanism, *Angew. Chem. Int. Ed.* **2020**, *59*, 13385-13390.

(627)   Cabana, H.; Jiwan, J.-L. H.; Rozenberg, R.; Elisashvili, V.; Penninckx, M.; Agathos, S. N.; Jones, J. P. Elimination of endocrine disrupting chemicals nonylphenol and bisphenol A

and personal care product ingredient triclosan using enzyme preparation from the white rot fungus Coriolopsis polyzona, *Chemosphere* **2007**, *67*, 770-778.

(628) Hou, G.; Zhang, R.; Hao, X.; Liu, C. An exploration of the effect and interaction mechanism of bisphenol A on waste sludge hydrolysis with multi-spectra, isothermal titration microcalorimetry and molecule docking, *J. Hazard. Mater.* **2017**, *333*, 32-41.

(629) González-Márquez, A.; Loera-Corral, O.; Santacruz-Juárez, E.; Tlécuitl-Beristain, S.; García-Dávila, J.; Viniegra-González, G.; Sánchez, C. Biodegradation patterns of the endocrine disrupting pollutant di(2-ethyl hexyl) phthalate by Fusarium culmorum, *Ecotoxicol. Environ. Saf.* **2019**, *170*, 293-299.

(630) Kim, Y. H.; Lee, J.; Moon, S. H. Degradation of an endocrine disrupting chemical, DEHP [di-(2-ethylhexyl)-phthalate], by Fusarium oxysporum f. sp. pisi cutinase, *Appl. Microbiol. Biotechnol.* **2003**, *63*, 75-80.

(631) Ahuactzin-Pérez, M.; Tlecuitl-Beristain, S.; García-Dávila, J.; González-Pérez, M.; Gutiérrez-Ruíz, M. C.; Sánchez, C. Degradation of di (2-ethyl hexyl) phthalate by Fusarium culmorum: kinetics, enzymatic activities and biodegradation pathway based on quantum chemical modeling, *Sci. Total. Environ.* **2016**, *566-567*, 1186-1193.

(632) Aguilar-Alvarado, Y.; Báez-Sánchez, M. R.; Martínez-Carrera, D.; Ahuactzin-Pérez, M.; Cuamatzi-Muñoz, M.; Sánchez, C. Mycelial growth and enzymatic activities of fungi isolated from recycled paper wastes grown on di (2-ethylhexyl) phthalate, *Pol. J. Environ. Stud.* **2015**, *24*, 1897-1902.

(633) Ahuactzin-Pérez, M.; Tlecuitl-Beristain, S.; García-Dávila, J.; González-Pérez, M.; Gutiérrez-Ruíz, M. C.; Sánchez, C. A novel biodegradation pathway of the endocrine-disruptor di(2-ethyl hexyl) phthalate by Pleurotus ostreatus based on quantum chemical investigation, *Ecotoxicol. Environ. Saf.* **2018**, *147*, 494-499.

(634) Lee, S. M.; Lee, J. W.; Koo, B. W.; Kim, M. K.; Choi, D. H.; Choi, I. G. Dibutyl phthalate biodegradation by the white rot fungus, *Polyporus brumalis. Biotechnol. Bioeng.* **2007**, *97*, 1516-1522.

(635) Begum, A.; Katsumata, H.; Kaneco, S.; Suzuki, T.; Ohta, K. Biodegradation of phthalic acid esters by bakery yeast Saccharomyces cerevisiae, *Bull. Environ. Contam. Toxicol.* **2003**, *70*, 255-261.

(636) Chen, M.; Zeng, G.; Lai, C.; Zhang, C.; Xu, P.; Yan, M.; Xiong, W. Interactions of carbon nanotubes and/or graphene with manganese peroxidase during biodegradation of endocrine disruptors and triclosan, *Chemosphere* **2017**, *184*, 127-136.

(637) Holms, W. H. In *Biochem. Soc. Symp. No.54, Krebs' citric acid cycle: half a century and still turning*; Kay, J., Weitzman, P. D., Eds.; Biochemical Society: London, 1987.

(638) Nyanhongo, G. S.; Gubitz, G.; Sukyai, P.; Leitner, C.; Haltrich, D.; Ludwig, R. Oxidoreductases from trametes spp. In biotechnology: A wealth of catalytic activity, *Food Technol. Biotech.* **2007**, *45*, 250-268.

(639) Rajendran, R. k.; Huang, S.-L.; Lin, C.-C.; Kirschner, R. Biodegradation of the endocrine disrupter 4-tert-octylphenol by the yeast strain Candida rugopelliculosa RRKY5 via phenolic ring hydroxylation and alkyl chain oxidation pathways, *226* **2017**, *Bioresour. Technol.*, 55-64.

(640) Brocca, S.; Secundo, F.; Ossola, M.; Alberghina, L.; Carrea, G.; Lotti, M. Sequence of the lid affects activity and specificity of Candida rugosa lipase isoenzymes, *Protein Sci.* **2003**, *12*, 2312-2319.

(641) Aouf, C.; Durand, E.; Lecomte, J.; Figueroa-Espinoza, M.-C.; Dubreucq, E.; Fulcrand, H.; Villeneuve, P. The use of lipases as biocatalysts for the epoxidation of fatty acids and phenolic compounds, *Green Chem.* **2014**, *16*, 1740-1754.

(642) Archibald, F. S.; Paice, M. G.; Jurasek, L. Decolorization of Kraft bleachery effluent chromophores by Coriolus (Trametes) versicolor, *Enzyme Microb. Technol.* **1990**, *12*, 846-853.

(643) Raghukumar, C. Fungi from marine habitats: an application in bioremediation, *Mycol. Res.* **2000**, *104*, 1222-1226.

(644) Afiya, H.; Ahmet, E. E.; Manjur, M. S. Environmental science enzymatic decolorization of remazol brilliant blue royal (RB 19) textile dye by white rot fungi, *J. App. Advanc. Res.* **2019**, *4*, 11-15.

(645) Dayi, B.; Duishemambet, K.; Hatice, K.; Akdogan, A. Characterization of recuperating talent of white-rot fungi cells to dye-contaminated soil/water, *Chin. J. Chem. Eng.* **2019**, *27*, 634-638.

(646) Torres, E.; Bustos-Jaimes, I.; Le Borgne, S. Potential use of oxidative enzymes for the detoxification of organic pollutants, *Appl. Catal. B: Environ.* **2003**, *46*, 1-15.

(647) Rodriguez, E.; Pickard, M. A.; Vazquez, D. R. Industrial dye decolorization by laccases from ligninolytic fungi, *Curr. Microbiol.* **1999**, *38*, 27-32.

(648) Raghukumar, C. In *Marine Microbiology: Facets & Opportunities*; Ramaiah, N., Ed.; National Institute of Oceanography Dona-Paula: Goa, India, 2004.

(649) Mohandass, C.; Kamat, S.; Shailaja, M. S. Simultaneous detoxification and decolourization of molasses spent wash by the immobilized white-rot fungus Flavodon flavus isolated from a marine habitat, *Enzyme Microb. Technol.* **2004**, *35*, 197-202.

(650) Cameron, M. D.; Timofeevski, S.; Aust, S. D. Enzymology of Phanerochaete chrysosporium with respect to the degradation of recalcitrant compounds and xenobiotics, *Appl. Microbiol. Biotechnol.* **2000**, *54*, 751-758.

(651) Soares, G. M. B.; Costa-Ferreira, M.; de Amorim, M. T. P. Decolorization of an anthraquinone-type dye using a laccase formulation, *Bioresour. Technol.* **2001**, *79*, 171-177.

(652) Fakoussa, R. M.; Frost, P. J. In vivo-decolorization of coal-derived humic acids by laccase-excreting fungus Trametes versicolor, *Appl. Microbiol. Biotechnol.* **1999**, *52*, 60-65.

(653) Pointing, S. B.; Vrijmoed, L. L. P. Decolorization of azo and triphenylmethane dyes by Pycnoporus sanguineus producing laccase as the sole phenoloxidase, *World J. Microbiol. Biotechnol.* **2000**, *16*, 317- 318.

(654) Reyes, P.; Pickard, M. A.; Vazquez-Duhalt, R. Hydroxybenzotriazole increases the range of textile dyes decolorized by immobilized laccase, *Biotechnol. Lett.* **1999**, *2*, 875-880.

(655) Maceiras, R.; Rodriguez, C. S.; Sanroman, A. Influence of several activators on the extracellular laccase activity and in vivo decolourization of poly R-478by semi-solid-state cultures of Trametes versicolor, *Acta Biotechnol.* **2001**, *21*, 255-264.

(656) Rajasundari, K.; Murugesan, R. Decolourization of Distillery Waste Water - Role of Microbes and their Potential Oxidative Enzymes (Review), *J. Appl. Environ. Biol. Sci.* **2011**, *1*, 54-68.

(657) Flores-Flores, T. C.; Gutiérrez-Rojas, M.; Revah, S.; Favela-Torres, E. Comparative study for oxygenases produced by Aspergillus Niger, ATCC 9642, in solid-state and submerged fermentation, *Rev. Mex. Ing. Quim.* **2011**, *10*, 189-207.

(658) Hui, R.; Hu, X.; Liu, W.; Liu, W.; Zheng, Y.; Chen, Y.; Guo, R. T.; Jin, J.; Chen, C.-C. Characterization and crystal structure of a novel zearalenone hydrolase from Cladophialophora bantiana, *Acta Crystallogr. F. Struct. Biol. Commun.* **2017**, *73*, 515-519.

(659) Zhou, J.; Zhu, L.; Chen, J.; Wang, W.; Zhang, R.; Li, Y.; Zhang, Q.; Wang, W. Degradation mechanism for Zearalenone ring-cleavage by Zearalenone hydrolase RmZHD: A QM/MM study, *Sci. Total Environ.* **2019**, *709*, 135897.

(660) Chou, H.-L.; Hwa, M.-Y.; Lee, Y.-C.; Chang, Y.-J.; Chang, Y.-T. Microbial degradation of decabromodiphenyl ether (DBDE) in soil slurry microcosms, *Environ. Sci. Pollut. Res.* **2016**, *23*, 5255-5267.

(661) Yang, C. W.; Huang, H. W.; Chao, W. L.; Chang, B. V. Bacterial communities associated with aerobic degradation of polybrominated diphenyl ethers from river sediments, *Environ. Sci. Pollut. Res.* **2015**, *22*, 3810-3819.

(662)   Shakerian, F.; Zhao, J.; Li, S.-P. Recent development in the application of immobilized oxidative enzymes for bioremediation of hazardous micropollutants-A review, *Chemosphere* **2020**, *239*, 124716.

(663)   Bryjak, J.; Kolarz, B. N. Immobilisation of trypsin on acrylic copolymers, *Process Biochem.* **1998**, *33*, 409 -417.

(664)   Duran, N.; Rosa, M. A.; D'Annibale, A.; Gianfreda, L. Applications of laccases and tyrosinases (phenoloxidases) immobilized on different supports: a review, *Enzyme Microb. Technol.* **2002**, *31*, 907-931.

(665)   Sheldon, R. A. Enzyme immobilization: The quest for optimum performance, *Adv Syn. Catal.* **2007**, *349*, 1289-1307.

(666)   Ba, S.; Arsenault, A.; Hassani, T.; Jones, J. P.; Cabana, H. Laccase immobilization and insolubilization: from fundamentals to applications for the elimination of emerging contaminants in wastewater treatment, *Crit. Rev. Biotechnol.* **2012**, *33*, 404-418.

(667)   Sheldon, R. Cross-linked enzyme aggregates as industrial biocatalysts, *Org. Process. Res. Develop.* **2011**, *15*, 213-223.

(668)   Hou, J.; Dong, G.; Ye, Y.; Chen, V. Enzymatic degradation of bisphenol-A with immobilized laccase on TiO2 sol-gel coated PVDF membrane, *J. Membr. Sci.* **2014**, *469*, 19-30.

(669)   Hou, J.; Dong, G.; Luu, B.; Sengpiel, R. G.; Ye, Y.; Wessling, M., , , Hybrid membrane with TiO_2 based bio-catalytic nanoparticle suspension system for the degradation of bisphenol-A. Bioresour. Technol., **2014**, *169*, 475-483.

(670)   Dai, J.; Wang, H.; Chi, H.; Wang, Y.; Zhao, J. Immobilization of laccase from Pleurotus ostreatus on magnetic separable SiO2 support and excellent activity towards azo dye decolorization, *J. Environ. Chem. Eng.* **2016**, *4*, 2585-2591.

(671)   Zdarta, J.; Antecka, K.; Frankowiski, R.; Zgola-Grzeskowiak, A.; Ehrlich, H.; Jesionowski, T. The effect of operational parameters on the biodegradation of bisphenols by Trametes versicolor laccase immobilized on Hippospongia communis sponging scaffolds, *Sci. Total Environ.* **2018**, *615*, 784-795.

(672)   Maryšková, M.; Ardao, I.; García-González, C. A.; Martinová, L.; Rotková, J.; Ševců, A. Polyamide 6/chitosan nanofibers as support for the immobilization of Trametes versicolor laccase for the elimination of endocrine disrupting chemicals, *Enzyme Microb. Technol.* **2016**, *89*, 31-38.

(673)   Ge, J.; Lei, J.; Zare, R. N. Protein-inorganic hybrid nanoflowers, *Nat. Nanotechnol.* **2012**, *7*, 428-432.

(674) Altinkaynak, C.; Tavlasoglu, S.; Ozdemir, N.; Ocsoy, I. A new generation approach in enzyme immobilization: organic-inorganic hybrid nanoflowers with enhanced catalytic activity and stability, *Enzym. Microb. Technol* **2016**, *93-94*, 105-112.

(675) Rong, J.; Zhang, T.; Qiu, F.; Zhu, Y. Preparation of efficient, stable, and reusable laccase-$Cu_3(PO_4)_2$ hybrid microspheres based on copper foil for decoloration of Congo red, *ACS Sustain. Chem. Eng.* **2017**, *5*, 4468-4477.

(676) Patel, S. K. S.; Otari, S. V.; Li, J. L.; Kim, D. R.; Kim, S. C.; Cho, B. K.; Kaliag, V. C.; Kangh, Y. C.; Lee, J.-K. Synthesis of crosslinked protein-metal hybrid nanoflowers and its application in repeated batch decolorization of synthetic dyes, *J. Hazard. Mater.* **2018**, *347*, 442-450.

(677) Fu, S.; Wang, S.; Zhang, X.; Qi, A.; Liu, Z.; Yu, X.; Chen, C.; Li, L. Structural effect of Fe3O4 nanoparticles on peroxidase-like activity for cancer therapy, *Colloids Surf. B: Biointerfaces* **2017**, *154*, 239-245.

(678) Gao, X. J.; Fan, X. J.; Chen, X. P.; Ge, Z. Q. Immobilized β-lactamase on Fe_3O_4 magnetic nanoparticles for degradation of β-lactam antibiotics in wastewater, *Int. J. Environ. Sci. Technol.* **2018**, *15*, 2203-2212.

(679) Fu, M.; Xing, J.; Ge, Z. Preparation of laccase-loaded magnetic nanoflowers and their recycling for efficient degradation of bisphenol A, *Sci. Total Environ.* **2019**, *651*, 2857-2865.

(680) Bautista, F. M.; Bravo, M. C.; Campelo, J. M.; Garcia, A.; Luna, D.; Marinas, J. M.; Romero, A. A. Covalent immobilization of acid phosphatase on amorphous $AlPO_4$ support, *J. Mol. Catal. B: Enzymatic* **1999**, *6*, 473-481.

(681) Tian, C.; Xu, X.; Zhang, H.; Mehio, N.; Guo, Y.; Ma, L.; Dai, S. Incorporating Lanthanum into Mesoporous Silica Foam Enhances Enzyme Immobilization and the Activity of Penicillin G Acylase Due to Lewis Acid-Base Interactions, *ChemBioChem* **2020**, *21*, 2143-2148.

(682) Jiang, Y.; Guo, C.; Xia, H.; Mahmood, I.; Liu, C.; Liu, H. Magnetic nanoparticles supported ionic liquids for lipase immobilization: Enzyme activity in catalyzing esterification, *J. Mol. Catal. B: Enzymatic* **2009**, *58*, 103-109.

(683) Macario, A.; Giordano, G.; Setti, L.; Parise, A.; Campelo, J. M.; Marinas, J. M.; Luna, D. Study of lipase immobilization on zeolitic support and transesterification reaction in a solvent free-system, *Biocatal. , Biotransformation* **2007**, *25*, 328-335.

(684) Garcia, L. F.; Lacerda, M. F. A. R.; Thomaz, D. V.; de Souza Golveia, J. C.; Pereira, M. D. G. C.; de Souza Gil, E.; Schimidt, F.; Santiago, M. F. Optimization of laccase-alginate-

chitosan-based matrix toward 17 α-ethinylestradiol removal, *Prep. Biochem. Biotechnol.* **2019**, *49*, 375-383.

(685)   Abadulla, E.; Tzanov, T.; Costa, S.; Robra, K. H.; Cavaco, P. A.; Guebitz, G. M. Decolorization and detoxification of textile dyes with a laccase from Trametes hirsute, *Appl. Environ. Microbiol.* **2000**, *66*, 3357-3362.

(686)   Osiadacz, J.; Al Adhami, A. J. H.; Bjraszewska, D.; Fischer, P.; Peczyniska, C. W. On the use of Trametes versicolor laccase for the conversion of 4-methyl-3-hydroxyanthranilic acid to actinocin chromophore, *J. Biotechnol.* **1999**, *72*, 141-149.

(687)   Nicolucci, C.; Rossi, S.; Menale, C.; Godjevargova, T.; Ivanov, Y.; Bianco, M.; Mita, L.; Bencivenga, U.; Mita, D. G.; Diano, N. Biodegradation of bisphenols with immobilized laccase or tyrosinase on polyacrylonitrile beads, *Biodegradation* **2011**, *22*, 673-683.

(688)   Lin, J.; Liu, Y.; Chen, S.; Le, X.; Zhou, X.; Zhao, Z.; Ou, Y.; Yang, J. Reversible immobilization of laccase onto metal-ion-chelated magnetic microspheres for bisphenol A removal, *Int. J. Biol. Macromol.* **2016**, *84*, 189-199.

(689)   Bilal, M.; Asgher, M.; Iqbal, H. M. N.; Hu, H.; Zhang, X. Bio-based degradation of emerging endocrine-disrupting and dye-based pollutants using cross-linked enzyme aggregates, *Environ. Sci. Pollut. Res.* **2017**, *24*, 7035-7041.

(690)   Kampmann, M.; Boll, S.; Kossuch, J.; Bielecki, J.; Uhl, S.; Kleiner, B.; Wichmann, R. Efficient immobilization of mushroom tyrosinase utilizing whole cells from Agaricus bisporus and its application for degradation of bisphenol A, *Water Res.* **2014**, *57*, 295-303.

(691)   Mazzei, R.; Giorno, L.; Piacentini, E.; Mazzuca, S.; Drioli, E. Kinetic study of abiocatalytic membrane reactor containing immobilized beta-glucosidase for the hydrolysis of oleuropein, *J. Membr. Sci.* **2009**, *339*, 215-223.

(692)   Belleville, M. P.; Lozano, P.; Iborra, J. L.; Rios, G. M. Preparation of hybrid membranes for enzymatic reaction, *Sep. Purif. Technol.* **2001**, *25*, 229-233.

(693)   Magnan, E.; Catarino, I.; Paolucci-Jeanjean, D.; Preziosi-Belloy, L.; Belleville, M. P. Immobilization of lipase on a ceramic membrane: activity and stability, *J. Membr. Sci.* **2004**, *241*, 161-166.

(694)   Liew, C. S.; Yunus, N. M.; Chidi, B. S.; Lam, M. K.; Goh, P. S.; Mohamad, M.; Sin, J. C.; Lam, S. M.; Lim, J. W.; Lam, S. S. A review on recent disposal of hazardous sewage sludge via anaerobic digestion and novel composting, *J. Hazard. Mater.* **2022**, *4235*, 126995.

(695)   Zhen, G.; Lu, X.; Kato, H.; Zhao, Y.; Li, Y. Y. Overview of pretreatment strategies for enhancing sewage sludge disintegration and subsequent anaerobic digestion: current advances, full-scale application and future perspectives., *Renew. Sustain Energy Rev.* **2017**, *69*, 559-577.

(696) Cai, M.; Wilkins, D.; Chen, J.; Ng, S. K.; Lu, H.; Jia, Y.; Lee, P. K. Metagenomic reconstruction of key anaerobic digestion pathways in municipal sludge and industrial wastewater biogas-producing systems., *Front. Microbiol.* **2016**, *7*, 1-12.

(697) Das, P. K. Phytoremediation and Nanoremediation : Emerging Techniques for Treatment of Acid Mine Drainage Water, *Def. Life Sci. J.* **2018**, *3*, 190-196.

(698) Urionabarrenetxea, E.; Garcia-Velasco, N.; Anza, M.; Artetxe, U.; Lacalle, R.; Garbisu, C.; Becerril, T.; Soto, M. Application of in situ bioremediation strategies in soils amended with sewage sludges., *Sci. Total Environ.* **2021**, *766* 144099.

(699) Barbosa, E. S.; Cacique, A. P.; de Pinho, G. P.; Silverio, F. O. Catharanthus roseus potential for phyto-stabilizing metals in sewage sludge., *J. Environ. Health Sci. Eng., Part A* **2019**, 1093-4529.

(700) Bagchi, S.; Behera, M. Assessment of Heavy Metal Removal in Different Bioelectrochemical Systems: A Review., *J. Hazard. Toxic Radioact. Waste* **2020**, *24*, 04020010

(701) Tian, T.; Yu, H. Q. Iron-assisted biological wastewater treatment: Synergistic effect between iron and microbes., *Biotechnol. Adv.* **2020**, *44*, 107610.

(702) Khan, S.; Hesham, A. E. L.; Qiao, M.; Rehman, S.; He, J. Z. Effects of Cd and Pb on soil microbial community structure and activities., *Environ. Sci. Pollut. Res.* **2010**, *17*, 288-296.

(703) Radziemska, M.; Gusiatin, Z. M.; Cydzik-Kwiatkowska, A.; Cerd, A.; Pecina, V.; Bes, A.; Datta, R.; Majewski, G.; Mazur, Z.; Dziecioł, J.; Danish, S.; Brtnický, M. Insight into metal immobilization and microbial community structure in soil from a steel disposal dump phytostabilized with composted, pyrolyzed or gasified wastes., *Chemosphere* **2021**, *272*, 129576.

(704) Mian, M. M.; Liu, G.; Fu, B. Conversion of sewage sludge into environmental catalyst and microbial fuel cell electrode material: A review., *Sci. Total Environ.* **2019**, *666*, 525-539.

(705) Schuijt, L. M.; van Bergen, T. J. H. M.; Lamers, L. P. M.; Smolders, A. J. P.; Verdonschot, P. F. M. Aquatic worms (Tubificidae) facilitate productivity of macrophyte Azolla filiculoides in a wastewater biocascade system., *Sci. Total Environ.* **2021**, *787*, 147538.

(706) Carboneras, M. B.; Rodrigo, M. A.; Canizares, P.; Villasenor, J.; Fernandez-Morales, F. J. Removal of oxyfluorfen from polluted effluents by combined bio-electro processes, *Chemosphere* **2020**, *240*, 124912.

(707)   Mohan, H.; Lim, J.-M.; Lee, S.-W.; Cho, M.; Park, Y.-J.; Seralathan, K.-K.; Oh, B.-T. Enhanced removal of bisphenol A from contaminated soil by coupling Bacillus subtilis HV-3 with electrochemical system, *Chemosphere* **2020**, *249*, 126083.

(708)   Ganzenko, O.; Huguenot, D.; Van Hullebusch, E. D.; Esposito, G.; Oturan, M. A. Electrochemical advanced oxidation and biological processes for wastewater treatment: a review of the combined approaches, *Environ. Sci. Pollut. Res.* **2014**, *21*, 8493-8524.

(709)   Barba, S.; Villaseñor, J.; Rodrigo, M. A.; Cañizares, P. Biostimulation versus bioaugmentation for the electro-bioremediation of 2,4-dichlorophenoxyacetic acid polluted soils, *J. Environ. Manage.* **2021**, *277*, 111424.

(710)   Robert, V.; Monza, E.; Tarrago, L.; Sancho, F.; De Falco, A.; Schneider, L.; Npetgat Ngoutane, E.; Mekmouche, Y.; Pailley, P. R.; Simaan, A. J.; Guallar, V.; Tron, T. Probing the Surface of a Laccase for Clues towards the Design of Chemo-Enzymatic Catalysts, *ChemPlusChem* **2017**, *82*, 607-614.

(711)   Schneider, L.; Mekmouche, Y.; Rousselot-Pailley, P.; Simaan, A. J.; Robert, V.; Reglier, M.; Aukauloo, A.; Tron, T. *ChemSusChem* **2015**, *8*, 3048 - 3051.

(712)   de Cazes, M.; Belleville, M.; Petit, E.; Salomo, M.; Bayer, S.; Czaja, R.; De Gunzburg, J.; Sanchez-marcano, J. Erythromycin degradation by esterase (EreB) in enzymatic membrane reactors, *Biochem. Eng. J.* **2016**, *114*, 70-78.

(713)   Masel, R. I. *Chemical kinetics and catalysis*; Wiley-Interscience New York, 2001.

(714)   Hagen, J. *Industrial catalysis: a practical approach*; John Wiley & Sons, 2015.

(715)   Garcia, H. Revolutionary Times, *Chemistry–A European Journal* **2020**, *26*, 14-18.

(716)   Renn, J.; Schlögl, R.; Rosol, C.; Steininger, B. A rapid transition of the world's energy systems, *Nature Outlook* **2017**, 133-180.

(717)   Wieckowski, A.; Savinova, E. R.; Vayenas, C. G. *Catalysis and electrocatalysis at nanoparticle surfaces*; cRc Press, 2003.

(718)   Xu, S.; Chansai, S.; Stere, C.; Inceesungvorn, B.; Goguet, A.; Wangkawong, K.; Taylor, S. R.; Al-Janabi, N.; Hardacre, C.; Martin, P. A. Sustaining metal–organic frameworks for water–gas shift catalysis by non-thermal plasma, *Nature Catalysis* **2019**, *2*, 142-148.

(719)   Serpone, N. In *Kirk-Othmer Encyclopedia of Chemical Technology*, 2000.

(720)   Zhang, J.; Tian, B.; Wang, L.; Xing, M.; Lei, J. In *Photocatalysis*; Springer, 2018.

(721)   Arques, A.; Amat, A.; Santos-Juanes, L.; Vercher, R.; Marin, M.; Miranda, M. 2, 4, 6-Triphenylthiapyrylium cation as homogeneous solar photocatalyst, *Catalysis today* **2007**, *129*, 37-42.

(722)   Serpone, N.; Emeline, A. V. *Semiconductor Photocatalysis: Past, Present, and Future Outlook*; ACS Publications, 2012.

(723)   Ohtani, B. Titania photocatalysis beyond recombination: a critical review, *Catalysts* **2013**, *3*, 942-953.

(724)   Lei, Q.; Yang, S.; Ding, D.; Tan, J.; Liu, J.; Chen, R. Local-interaction-field-coupled semiconductor photocatalysis: recent progress and future challenges, *Journal of Materials Chemistry A* **2021**, *9*, 2491-2525.

(725)   Dong, F.; Zhang, Y.; Zhang, S. Photocatalysis for environmental applications, *Frontiers in chemistry* **2019**, *7*, 303.

(726)   Chen, D.; Sivakumar, M.; Ray, A. K. Heterogeneous photocatalysis in environmental remediation, *Developments in Chemical Engineering and Mineral Processing* **2000**, *8*, 505-550.

(727)   Di Paola, A.; García-López, E.; Marcì, G.; Palmisano, L. A survey of photocatalytic materials for environmental remediation, *Journal of hazardous materials* **2012**, *211*, 3-29.

(728)   Ifang, S.; Gallus, M.; Liedtke, S.; Kurtenbach, R.; Wiesen, P.; Kleffmann, J. Standardization methods for testing photo-catalytic air remediation materials: problems and solution, *Atmospheric Environment* **2014**, *91*, 154-161.

(729)   Legrini, O.; Oliveros, E.; Braun, A. M. PHOTOCHEMICAL PROCESSES FOR WATER-TREATMENT, *Chemical Reviews* **1993**, *93*, 671-698.

(730)   Chong, M. N.; Jin, B.; Chow, C. W. K.; Saint, C. Recent developments in photocatalytic water treatment technology: A review, *Water Research* **2010**, *44*, 2997-3027.

(731)   Malato, S.; Fernandez-Ibanez, P.; Maldonado, M. I.; Blanco, J.; Gernjak, W. Decontamination and disinfection of water by solar photocatalysis: Recent overview and trends, *Catalysis Today* **2009**, *147*, 1-59.

(732)   Mills, A.; Davies, R. H.; Worsley, D. WATER-PURIFICATION BY SEMICONDUCTOR PHOTOCATALYSIS, *Chemical Society Reviews* **1993**, *22*, 417-425.

(733)   Xu, P.; Zeng, G. M.; Huang, D. L.; Feng, C. L.; Hu, S.; Zhao, M. H.; Lai, C.; Wei, Z.; Huang, C.; Xie, G. X.; Liu, Z. F. Use of iron oxide nanomaterials in wastewater treatment: A review, *Science of the Total Environment* **2012**, *424*, 1-10.

(734)   Lee, S.-Y.; Park, S.-J. TiO2 photocatalyst for water treatment applications, *Journal of Industrial and Engineering Chemistry* **2013**, *19*, 1761-1769.

(735)   Lazar, M. A.; Varghese, S.; Nair, S. S. Photocatalytic Water Treatment by Titanium Dioxide: Recent Updates, *Catalysts* **2012**, *2*, 572-601.

(736) Al-Mamun, M. R.; Kader, S.; Islam, M. S.; Khan, M. Z. H. Photocatalytic activity improvement and application of UV-TiO2 photocatalysis in textile wastewater treatment: A review, *Journal of Environmental Chemical Engineering* **2019**, *7*.

(737) Higarashi, M. M.; Jardim, W. F. Remediation of pesticide contaminated soil using TiO2 mediated by solar light, *Catalysis Today* **2002**, *76*, 201-207.

(738) Zhu, X.; Zhou, D.; Wang, Y.; Cang, L.; Fang, G.; Fan, J. Remediation of polychlorinated biphenyl-contaminated soil by soil washing and subsequent TiO 2 photocatalytic degradation, *Journal of Soils and Sediments* **2012**, *12*, 1371-1379.

(739) Fujishima, A.; Rao, T. N.; Tryk, D. A. Titanium dioxide photocatalysis, *Journal of photochemistry and photobiology C: Photochemistry reviews* **2000**, *1,* 1-21.

(740) Nosaka, Y.; Nosaka, A. Y. Generation and detection of reactive oxygen species in photocatalysis, *Chemical reviews* **2017**, *117*, 11302-11336.

(741) Herrmann, J.-M. Heterogeneous photocatalysis: fundamentals and applications to the removal of various types of aqueous pollutants, *Catalysis today* **1999**, *53*, 115-129.

(742) Andreozzi, R.; Caprio, V.; Insola, A.; Marotta, R. Advanced oxidation processes (AOP) for water purification and recovery, *Catalysis today* **1999**, *53*, 51-59.

(743) Coleman, H.; Vimonses, V.; Leslie, G.; Amal, R. Removal of contaminants of concern in water using advanced oxidation techniques, *Water science and technology* **2007**, *55*, 301-306.

(744) Kanakaraju, D.; Glass, B. D.; Oelgemöller, M. Advanced oxidation process-mediated removal of pharmaceuticals from water: A review, *Journal of Environmental Management* **2018**, *219*, 189-207.

(745) Parsons, S. *Advanced oxidation processes for water and wastewater treatment*; IWA publishing, 2004.

(746) Stefan, M. I. *Advanced oxidation processes for water treatment: fundamentals and applications*; IWA publishing, 2017.

(747) Akpan, U. G.; Hameed, B. H. Parameters affecting the photocatalytic degradation of dyes using TiO2-based photocatalysts: A review, *Journal of Hazardous Materials* **2009**, *170*, 520-529.

(748) Anwer, H.; Mahmood, A.; Lee, J.; Kim, K.-H.; Park, J.-W.; Yip, A. C. K. Photocatalysts for degradation of dyes in industrial effluents: Opportunities and challenges, *Nano Research* **2019**, *12*, 955-972.

(749) Chaudhuri, R. G.; Chaturvedi, A.; Iype, E. Visible light active 2D C3N4-CdS hetero-junction photocatalyst for effective removal of azo dye by photodegradation, *Mater. Res. Express* **2018**, *5*, 036202/036201-036202/036209.

(750) Dong, J.-P.; Shi, Z.-Z.; Li, B.; Wang, L.-Y. Synthesis of a novel 2D zinc(II) metal-organic framework for photocatalytic degradation of organic dyes in water, *Dalton Trans.* **2019**, *48*, 17626-17632.

(751) Hu, F.; Luo, W.; Hu, Y.; Dai, H.; Peng, X. Insight into the kinetics and mechanism of visible-light photocatalytic degradation of dyes onto the P doped mesoporous graphitic carbon nitride, *J. Alloys Compd.* **2019**, *794*, 594-605.

(752) Mahata, P.; Madras, G.; Natarajan, S. Novel photocatalysts for the decomposition of organic dyes based on metal-organic framework compounds, *J. Phys. Chem. B* **2006**, *110*, 13759-13768.

(753) Rajeshwar, K.; Osugi, M. E.; Chanmanee, W.; Chenthamarakshan, C. R.; Zanoni, M. V. B.; Kajitvichyanukul, P.; Krishnan-Ayer, R. Heterogeneous photocatalytic treatment of organic dyes in air and aqueous media, *Journal of Photochemistry and Photobiology C-Photochemistry Reviews* **2008**, *9*, 171-192.

(754) Rauf, M. A.; Ashraf, S. S. Fundamental principles and application of heterogeneous photocatalytic degradation of dyes in solution, *Chemical Engineering Journal* **2009**, *151*, 10-18.

(755) Rauf, M. A.; Meetani, M. A.; Hisaindee, S. An overview on the photocatalytic degradation of azo dyes in the presence of TiO2 doped with selective transition metals, *Desalination* **2011**, *276*, 13-27.

(756) Reza, K. M.; Kurny, A. S. W.; Gulshan, F. Parameters affecting the photocatalytic degradation of dyes using TiO2: a review, *Applied Water Science* **2017**, *7*, 1569-1578.

(757) Singh, K.; Arora, S. Removal of Synthetic Textile Dyes From Wastewaters: A Critical Review on Present Treatment Technologies, *Critical Reviews in Environmental Science and Technology* **2011**, *41*, 807-878.

(758) Wu, Z.; Yuan, X.; Zhang, J.; Wang, H.; Jiang, L.; Zeng, G. Photocatalytic decontamination of wastewater containing organic dyes by metal–organic frameworks and their derivatives, *ChemCatChem* **2017**, *9*, 41-64.

(759) Ahmed, S.; Rasul, M. G.; Brown, R.; Hashib, M. A. Influence of parameters on the heterogeneous photocatalytic degradation of pesticides and phenolic contaminants in wastewater: A short review, *Journal of Environmental Management* **2011**, *92*, 311-330.

(760) Burrows, H. D.; Canle, M.; Santaballa, J. A.; Steenken, S. Reaction pathways and mechanisms of photodegradation of pesticides, *Journal of Photochemistry and Photobiology B-Biology* **2002**, *67*, 71-108.

(761) Chiron, S.; Fernandez-Alba, A.; Rodriguez, A.; Garcia-Calvo, E. Pesticide chemical oxidation: state-of-the-art, *Water Research* **2000**, *34*, 366-377.

(762) Daghrir, R.; Drogui, P. Tetracycline antibiotics in the environment: a review, *Environmental Chemistry Letters* **2013**, *11*, 209-227.

(763) Lei, J.; Chen, B.; Zhou, L.; Ding, N.; Cai, Z.; Wang, L.; In, S.-I.; Cui, C.; Zhou, Y.; Liu, Y.; Zhang, J. Efficient degradation of antibiotics in different water matrices through the photocatalysis of inverse opal K-g-C3N4: insights into mechanism and assessment of antibacterial activity, *Chem. Eng. J. (Amsterdam, Neth.)* **2020**, *400*, 125902.

(764) Moreira, N. F.; Sousa, J. M.; Macedo, G.; Ribeiro, A. R.; Barreiros, L.; Pedrosa, M.; Faria, J. L.; Pereira, M. F. R.; Castro-Silva, S.; Segundo, M. A. Photocatalytic ozonation of urban wastewater and surface water using immobilized TiO2 with LEDs: Micropollutants, antibiotic resistance genes and estrogenic activity, *Water research* **2016**, *94*, 10-22.

(765) Tang, H.; Shang, Q.; Tang, Y.; Yi, X.; Wei, Y.; Yin, K.; Liu, M.; Liu, C. Static and continuous flow photoelectrocatalytic treatment of antibiotic wastewater over mesh of TiO2 nanotubes implanted with g-C3N4 nanosheets, *J. Hazard. Mater.* **2020**, *384*, 121248.

(766) Yuan, X.; Chen, H.; Yu, H.; Zhang, J.; Guo, J. Photocatalyst for degrading antibiotics and its preparation method and application in wastewater treatment, **2020**, CN111790405A.

(767) Pera-Titus, M.; Garcia-Molina, V.; Banos, M. A.; Gimenez, J.; Esplugas, S. Degradation of chlorophenols by means of advanced oxidation processes: a general review, *Applied Catalysis B-Environmental* **2004**, *47*, 219-256.

(768) Tatti, L.; Niego, D.; Rota, F.; Bruzzi, P.; Moroni, A.; Bellobono, I. R.; Bonardi, M.; Bianchi, M.; Muntau, H. Mathematical modelling of pilot-plant photomineralization of chlorophenols in aqueous solution, by photocatalytic membranes immobilizing titanium dioxide, *Chemosphere* **1997**, *34*, 41-49.

(769) Zada, A.; Qu, Y.; Ali, S.; Sun, N.; Lu, H.; Yan, R.; Zhang, X.; Jing, L. Improved visible-light activities for degrading pollutants on TiO2/g-C3N4 nanocomposites by decorating SPR Au nanoparticles and 2,4-dichlorophenol decomposition path, *J. Hazard. Mater.* **2018**, *342*, 715-723.

(770) Azimi, A.; Azari, A.; Rezakazemi, M.; Ansarpour, M. Removal of Heavy Metals from Industrial Wastewaters: A Review, *Chembioeng Reviews* **2017**, *4*, 37-59.

(771)   Tang, W.-W.; Zeng, G.-M.; Gong, J.-L.; Liang, J.; Xu, P.; Zhang, C.; Huang, B.-B. Impact of humic/fulvic acid on the removal of heavy metals from aqueous solutions using nanomaterials: A review, *Science of the Total Environment* **2014**, *468*, 1014-1027.

(772)   Schwarzenbach, R. P.; Egli, T.; Hofstetter, T. B.; Von Gunten, U.; Wehrli, B. Global water pollution and human health, *Annual review of environment and resources* **2010**, *35*, 109-136.

(773)   Johnson, A.; Williams, R.; Matthiessen, P. The potential steroid hormone contribution of farm animals to freshwaters, the United Kingdom as a case study, *Science of the Total Environment* **2006**, *362*, 166-178.

(774)   Snyder, S. A.; Westerhoff, P.; Yoon, Y.; Sedlak, D. L. Pharmaceuticals, personal care products, and endocrine disruptors in water: implications for the water industry, *Environmental engineering science* **2003**, *20*, 449-469.

(775)   Foster, H. A.; Ditta, I. B.; Varghese, S.; Steele, A. Photocatalytic disinfection using titanium dioxide: spectrum and mechanism of antimicrobial activity, *Applied microbiology and biotechnology* **2011**, *90*, 1847-1868.

(776)   Kweinor Tetteh, E.; Opoku Amankwa, M.; Armah, E. K.; Rathilal, S. Fate of COVID-19 Occurrences in Wastewater Systems: Emerging Detection and Treatment Technologies—A Review, *Water* **2020**, *12*, 2680.

(777)   Vicenzi, E. "SEVERE ACUTE RESPIRATORY SYNDROME CORONAVIRUS 2 (SARS-COV-2) QUANTIFICATION AFTER TUNGSTEN TRIOXIDE BASED (WO3) PHOTOCATALYST TREATMENT," Viral Pathogenesis and Biosecurity Unit, San Raffaele Hospital, Milano, Italy, 2020.

(778)   Ghezzi, S.; Pagani, I.; Poli, G.; Pal, S.; Licciulli, A.; Perboni, S.; Vicenzi, E. Rapid Inactivation of SARS-CoV-2 by Coupling Tungsten Trioxide (WO3) Photocatalyst with Copper Nanoclusters, *Journal of Nanotechnology and Nanomaterials* **2020**, *1*.

(779)   Ghernaout, D.; Elboughdiri, N. Urgent proposals for disinfecting hospital wastewaters during COVID-19 pandemic, *Open Access Library Journal* **2020**, *7*, 1-18.

(780)   Vaidya, P. N.; Shivanand, G. Degradation of COVID–19 by the Root of Photocatalysis: A Review, *population*, *10*, 11.

(781)   Dorfman, L. M.; Adams, G. E. Reactivity of the hydroxyl radical in aqueous solutions, **1973**.

(782)   Berndt, T.; Richters, S.; Jokinen, T.; Hyttinen, N.; Kurtén, T.; Otkjær, R. V.; Kjaergaard, H. G.; Stratmann, F.; Herrmann, H.; Sipilä, M. Hydroxyl radical-induced formation of highly oxidized organic compounds, *Nature communications* **2016**, *7*, 1-8.

(783) Anbar, M.; Meyerstein, D.; Neta, P. The reactivity of aromatic compounds toward hydroxyl radicals, *The Journal of Physical Chemistry* **1966**, *70*, 2660-2662.

(784) Koppenol, W.; Liebman, J. F. The oxidizing nature of the hydroxyl radical. A comparison with the ferryl ion (FeO2+), *The journal of physical chemistry* **1984**, *88*, 99-101.

(785) Schmittel, M.; Burghart, A. Understanding reactivity patterns of radical cations, *Angewandte Chemie International Edition in English* **1997**, *36*, 2550-2589.

(786) SALGADO, P.; MELIN, V.; CONTRERAS, D.; MORENO, Y.; MANSILLA, H. D. FENTON REACTION DRIVEN BY IRON LIGANDS, *Journal of the Chilean Chemical Society* **2013**, *58*, 2096-2101.

(787) Wang, J. L.; Xu, L. J. Advanced Oxidation Processes for Wastewater Treatment: Formation of Hydroxyl Radical and Application, *Critical Reviews in Environmental Science and Technology* **2012**, *42*, 251-325.

(788) Gaya, U. I. *Heterogeneous photocatalysis using inorganic semiconductor solids*; Springer Science & Business Media, 2013.

(789) Friedmann, D.; Mendive, C.; Bahnemann, D. TiO2 for water treatment: parameters affecting the kinetics and mechanisms of photocatalysis, *Applied Catalysis B: Environmental* **2010**, *99*, 398-406.

(790) Qian, W.; Greaney, P. A.; Fowler, S.; Chiu, S.-K.; Goforth, A. M.; Jiao, J. Low-temperature nitrogen doping in ammonia solution for production of N-doped TiO2-hybridized graphene as a highly efficient photocatalyst for water treatment, *ACS Sustainable Chemistry & Engineering* **2014**, *2*, 1802-1810.

(791) Han, C.; Pelaez, M.; Likodimos, V.; Kontos, A. G.; Falaras, P.; O'Shea, K.; Dionysiou, D. D. Innovative visible light-activated sulfur doped TiO2 films for water treatment, *Applied Catalysis B: Environmental* **2011**, *107*, 77-87.

(792) Ullattil, S. G.; Narendranath, S. B.; Pillai, S. C.; Periyat, P. Black TiO2 nanomaterials: a review of recent advances, *Chemical Engineering Journal* **2018**, *343*, 708-736.

(793) Ong, W. J.; Tan, L. L.; Chai, S. P.; Yong, S. T.; Mohamed, A. R. Facet-dependent photocatalytic properties of TiO2-based composites for energy conversion and environmental remediation, *ChemSusChem* **2014**, *7*, 690-719.

(794) Kamat, P. V. TiO2 nanostructures: recent physical chemistry advances, *J. Phys. Chem. C* **2012**, *116*, 11849-11851.

(795) Grover, I. S.; Singh, S.; Pal, B. The preparation, surface structure, zeta potential, surface charge density and photocatalytic activity of TiO2 nanostructures of different shapes, *Applied surface science* **2013**, *280*, 366-372.

(796) Khan, S. B.; Hou, M.; Shuang, S.; Zhang, Z. Morphological influence of TiO2 nanostructures (nanozigzag, nanohelics and nanorod) on photocatalytic degradation of organic dyes, *Applied Surface Science* **2017**, *400*, 184-193.

(797) Luan, S.; Qu, D.; An, L.; Jiang, W.; Gao, X.; Hua, S.; Miao, X.; Wen, Y.; Sun, Z. Enhancing photocatalytic performance by constructing ultrafine TiO2 nanorods/g-C3N4 nanosheets heterojunction for water treatment, *Science Bulletin* **2018**, *63*, 683-690.

(798) Jia, Y.; Yu, X.-Y.; Luo, T.; Jin, Z.; Sun, B.; Liu, J.-H.; Huang, X.-J. Necklace-like mesoporous MgO/TiO2 heterojunction structures with excellent capability for water treatment, *Dalton Transactions* **2014**, *43*, 2348-2351.

(799) Guo, N.; Zeng, Y.; Li, H.; Xu, X.; Yu, H.; Han, X. Novel mesoporous TiO2@ g-C3N4 hollow core@ shell heterojunction with enhanced photocatalytic activity for water treatment and H2 production under simulated sunlight, *Journal of hazardous materials* **2018**, *353*, 80-88.

(800) Pichat, P. *Fundamentals of TiO2 Photocatalysis. Consequences for Some Environmental Applications Chapter 10*, 2016.

(801) Lee, K. M.; Lai, C. W.; Ngai, K. S.; Juan, J. C. Recent developments of zinc oxide based photocatalyst in water treatment technology: A review, *Water Research* **2016**, *88*, 428-448.

(802) Roy, N.; Chakraborty, S. ZnO as photocatalyst: An approach to waste water treatment, *Materials Today: Proceedings* **2020**.

(803) Wang, J.; Meng, J.; Li, Q.; Yang, J. Single-layer cadmium chalcogenides: promising visible-light driven photocatalysts for water splitting, *Physical Chemistry Chemical Physics* **2016**, *18*, 17029-17036.

(804) Nie, L.; Zhang, Q. Recent progress in crystalline metal chalcogenides as efficient photocatalysts for organic pollutant degradation, *Inorganic Chemistry Frontiers* **2017**, *4*, 1953-1962.

(805) Ning, X.; Zhen, W.; Wu, Y.; Lu, G. Inhibition of CdS photocorrosion by Al2O3 shell for highly stable photocatalytic overall water splitting under visible light irradiation, *Applied catalysis B: environmental* **2018**, *226*, 373-383.

(806) Tang, Y.; Hu, X.; Liu, C. Perfect inhibition of CdS photocorrosion by graphene sheltering engineering on TiO 2 nanotube array for highly stable photocatalytic activity, *Physical Chemistry Chemical Physics* **2014**, *16*, 25321-25329.

(807)   Davis, A. P.; Huang, C. The photocatalytic oxidation of sulfur-containing organic compounds using cadmium sulfide and the effect on CdS photocorrosion, *Water Research* **1991**, *25*, 1273-1278.

(808)   Gogotsi, Y.; Anasori, B. The rise of MXenes, *ACS Nano* **2019**, *13*, 8491-8494.

(809)   Hieu, V. Q.; Phung, T. K.; Nguyen, T.-Q.; Khan, A.; Doan, V. D.; Tran, V. A. Photocatalytic degradation of methyl orange dye by Ti3C2-TiO2 heterojunction under solar light, *Chemosphere* **2021**, 130154.

(810)   Gao, Y.; Wang, L.; Zhou, A.; Li, Z.; Chen, J.; Bala, H.; Hu, Q.; Cao, X. Hydrothermal synthesis of TiO2/Ti3C2 nanocomposites with enhanced photocatalytic activity, *Materials Letters* **2015**, *150*, 62-64.

(811)   Quyen, V. T.; Thanh, D. M.; Le Van, Q.; Viet, N. M.; Nham, N. T.; Thang, P. Q. Advanced synthesis of MXene-derived nanoflower-shaped TiO2@ Ti3C2 heterojunction to enhance photocatalytic degradation of Rhodamine B, *Environmental Technology & Innovation* **2020**, 101286.

(812)   Wang, X.; Yang, Y.; Lu, G.; Shi, G.; Wang, Y.; Wang, R.; Xie, X.; Sun, J. In-situ preparation of Ti3C2/Ti3+-TiO2 composites with mosaic structures for the adsorption and photo-degradation of flowing acetaldehyde under visible light, *Applied Surface Science* **2020**, *531*, 147101.

(813)   Wu, Z.; Liang, Y.; Yuan, X.; Zou, D.; Fang, J.; Jiang, L.; Yang, H.; Xiao, Z. MXene Ti3C2 derived Z–scheme photocatalyst of graphene layers anchored TiO2/g–C3N4 for visible light photocatalytic degradation of refractory organic pollutants, *Chemical Engineering Journal* **2020**, *394*, 124921.

(814)   Cheng, L.; Tang, Y.; Xie, M.; Sun, Y.; Liu, H. 2D ultrathin NiMOF decorated by Ti3C2 MXene for highly improved photocatalytic performance, *Journal of Alloys and Compounds* **2021**, *864*, 158913.

(815)   Fang, H.; Pan, Y.; Yan, H.; Qin, X.; Wang, C.; Xu, L.; Pan, C. Facile preparation of Yb3+/Tm3+ co-doped Ti3C2/Ag/Ag3VO4 composite with an efficient charge separation for boosting visible-light photocatalytic activity, *Applied Surface Science* **2020**, *527*, 146909.

(816)   Yang, S.; Zhang, P.; Wang, F.; Ricciardulli, A. G.; Lohe, M. R.; Blom, P. W. M.; Feng, X. Fluoride-Free Synthesis of Two-Dimensional Titanium Carbide (MXene) Using A Binary Aqueous System, *Angewandte Chemie International Edition* **2018**, *57*, 15491-15495.

(817)   Kitagawa, S. Metal–organic frameworks (MOFs), *Chemical Society Reviews* **2014**, *43*, 5415-5418.

(818)   Zhou, H.-C.; Long, J. R.; Yaghi, O. M. Introduction to metal–organic frameworks, *Chemical reviews* **2012**, *112*, 673-674.

(819)   Dhakshinamoorthy, A.; Li, Z.; Garcia, H. Catalysis and photocatalysis by metal organic frameworks, *Chemical Society Reviews* **2018**, *47*, 8134-8172.

(820)   Maurin, G.; Serre, C.; Cooper, A.; Férey, G. The new age of MOFs and of their porous-related solids, *Chemical Society Reviews* **2017**, *46*, 3104-3107.

(821)   Li, S.; Luo, P.; Wu, H.; Wei, C.; Hu, Y.; Qiu, G. Strategies for improving the performance and application of MOFs photocatalysts, *ChemCatChem* **2019**, *11*, 2978-2993.

(822)   Liang, Y.; Huang, H.; Kou, L.; Li, F.; Lu, J.; Cao, H.-L. Synthesis of Metal-Organic Framework Materials by Reflux: A Faster and Greener Pathway to Achieve Super-Hydrophobicity and Photocatalytic Application, *Cryst. Growth Des.* **2018**, *18*, 6609-6616.

(823)   Cui, S.; Ye, Z.; Qian, C.; Liu, J.; Jin, J.; Liang, Q.; Liu, C.; Xu, S.; Li, Z. Construction of ternary Ag/AgBr@UIO-66(NH2) heterojunctions with enhanced photocatalytic performance for the degradation of methyl orange, *J. Mater. Sci.: Mater. Electron.* **2018**, *29*, 15138-15146.

(824)   Tabatabaei, N.; Dashtian, K.; Ghaedi, M.; Sabzehmeidani, M. M.; Ameri, E. Novel visible light-driven Cu-based MOFs/Ag2O composite photocatalysts with enhanced photocatalytic activity toward the degradation of orange G: their photocatalytic mechanism and optimization study, *New J. Chem.* **2018**, *42*, 9720-9734.

(825)   Zhang, M.; Wang, L.; Zeng, T.; Shang, Q.; Zhou, H.; Pan, Z.; Cheng, Q. Two pure metal-organic framework-photocatalysts readily prepared for the degradation of methylene blue dye under visible light, *Dalton Trans.* **2018**, *47*, 4251-4258.

(826)   Tilgner, D.; Kempe, R. A Plasmonic Colloidal Photocatalyst Composed of a Metal-Organic Framework Core and a Gold/Anatase Shell for Visible-Light-Driven Wastewater Purification from Antibiotics and Hydrogen Evolution, *Chem. - Eur. J.* **2017**, *23*, 3184-3190.

(827)   Tilgner, D.; Friedrich, M.; Verch, A.; de Jonge, N.; Kempe, R. A Metal-Organic Framework Supported Nonprecious Metal Photocatalyst for Visible-Light-Driven Wastewater Treatment, *ChemPhotoChem* **2018**, *2*, 349-352.

(828)   Xu, W.-T.; Ma, L.; Ke, F.; Peng, F.-M.; Xu, G.-S.; Shen, Y.-H.; Zhu, J.-F.; Qiu, L.-G.; Yuan, Y.-P. Metal-organic frameworks MIL-88A hexagonal microrods as a new photocatalyst for efficient decolorization of methylene blue dye, *Dalton Trans.* **2014**, *43*, 3792-3798.

(829)   Zhao, Y.; Li, L.; Ding, B.; Wang, X.-G.; Liu, Z.-Y.; Yang, E.-C.; Zhao, X.-J. Encapsulated anion-dominated photocatalytic and adsorption performances for organic dye

degradation and oxoanion pollutant capture over cationic Cu(i)-organic framework semiconductors, *Dalton Trans* **2021**, *50*, 197-207.

(830) Chen, J.; Xing, Z.; Han, J.; Su, M.; Li, Y.; Lu, A. Enhanced degradation of dyes by Cu-Co-Ni nanoparticles loaded on amino-modified octahedral metal-organic framework, *J. Alloys Compd.* **2020**, *834*, 155106.

(831) Li, G.; Zhang, K.; Li, C.; Gao, R.; Cheng, Y.; Hou, L.; Wang, Y. Solvent-free method to encapsulate polyoxometalate into metal-organic frameworks as efficient and recyclable photocatalyst for harmful sulfamethazine degrading in water, *Appl. Catal., B* **2019**, *245*, 753-759.

(832) Shao, L.; Yu, Z.; Li, X.; Li, X.; Zeng, H.; Feng, X. Carbon nanodots anchored onto the metal-organic framework NH2-MIL-88B(Fe) as a novel visible light-driven photocatalyst: Photocatalytic performance and mechanism investigation, *Appl. Surf. Sci.* **2020**, *505*, 144616.

(833) Dhakshinamoorthy, A.; Asiri, A. M.; Garcia, H. 2D metal–organic frameworks as multifunctional materials in heterogeneous catalysis and electro/photocatalysis, *Advanced Materials* **2019**, *31*, 1900617.

(834) Zhai, B.; Chen, Y.; Liang, Y.; Gao, Y.; Shi, J.; Zhang, H.; Li, Y. Modifying Ag3VO4 with metal-organic frameworks for enhanced photocatalytic activity under visible light, *Mater. Chem. Phys.* **2020**, *239*, 122078.

(835) Lei, X.; Wang, J.; Shi, Y.; Yao, W.; Wu, Q.; Wu, Q.; Zou, R. Constructing novel red phosphorus decorated iron-based metal organic framework composite with efficient photocatalytic performance, *Appl. Surf. Sci.* **2020**, *528*, 146963.

(836) Ma, Y.; Tuniyazi, D.; Ainiwa, M.; Zhu, E. Confined amorphous red phosphorus in metal-organic framework as a superior photocatalyst, *Mater. Lett.* **2020**, *262*, 127023.

(837) Opoku, F.; Govender, K. K.; van Sittert, C. G. C. E.; Govender, P. P. Recent progress in the development of semiconductor-based photocatalyst materials for applications in photocatalytic water splitting and degradation of pollutants, *Advanced Sustainable Systems* **2017**, *1*, 1700006.

(838) Chen, Z.; Lin, B.; Wang, X. BiOBr/ultrathin metal-organic framework nanosheet Z-type photocatalyst and preparation method and application in photocatalytic degradation of pollutants, **2020**, CN112058316A.

(839) Zhao, D.; Cai, C. Adsorption and photocatalytic degradation of pollutants on Ce-doped MIL-101-NH2/Ag3PO4 composites, *Catal. Commun.* **2020**, *136*, 105910.

(840) Sanati, S.; Abazari, R.; Albero, J.; Morsali, A.; García, H.; Liang, Z.; Zou, R. Metal–Organic Framework Derived Bimetallic Materials for Electrochemical Energy Storage, *Angewandte Chemie International Edition* **2021**, *60*, 11048-11067.

(841) Abdi, J.; Yahyanezhad, M.; Sakhaie, S.; Vossoughi, M.; Alemzadeh, I. Synthesis of porous TiO2/ZrO2 photocatalyst derived from zirconium metal organic framework for degradation of organic pollutants under visible light irradiation, *J. Environ. Chem. Eng.* **2019**, *7*, 103096.

(842) Mohaghegh, N.; Faraji, M.; Abedini, A. Highly efficient multifunctional Ag/TiO2 nanotubes/Ti plate coated with MIL-88B(Fe) as a photocatalyst, adsorbent, and disinfectant in water treatment, *Appl. Phys. A: Mater. Sci. Process.* **2019**, *125*, 1-10.

(843) Cao, S.; Low, J.; Yu, J.; Jaroniec, M. Polymeric Photocatalysts Based on Graphitic Carbon Nitride, *Advanced Materials* **2015**, *27*, 2150-2176.

(844) Dong, G.; Zhang, Y.; Pan, Q.; Qiu, J. A fantastic graphitic carbon nitride (g-C3N4) material: Electronic structure, photocatalytic and photoelectronic properties, *Journal of Photochemistry and Photobiology C: Photochemistry Reviews* **2014**, *20*, 33-50.

(845) Wang, Y.-D.; Lee, T.-W.; Lo, Y.-C.; Hong, W.-J.; Chen, C. Insights into photochemical stability of graphitic carbon nitride-based photocatalysts in water treatment, *Carbon* **2021**, *175*, 223-232.

(846) Lei, L.; Wang, W.; Wang, C.; Zhang, M.; Zhong, Q.; Fan, H. In situ growth of boron doped g-C3N4 on carbon fiber cloth as a recycled flexible film-photocatalyst, *Ceram. Int.* **2021**, *47*, 1258-1267.

(847) Hasija, V.; Raizada, P.; Hosseini-Bandegharaei, A.; Singh, P.; Nguyen, V.-H. Synthesis and photocatalytic activity of Ni-Fe layered double hydroxide modified sulphur doped graphitic carbon nitride (SGCN/Ni-Fe LDH) photocatalyst for 2,4-dinitrophenol degradation, *Top. Catal.* **2020**, *63*, 1030-1045.

(848) Sudhaik, A.; Raizada, P.; Thakur, S.; Saini, R. V.; Saini, A. K.; Singh, P.; KumarThakur, V.; Nguyen, V.-H.; Khan, A. A. P.; Asiri, A. M. Synergistic photocatalytic mitigation of imidacloprid pesticide and antibacterial activity using carbon nanotube decorated phosphorus doped graphitic carbon nitride photocatalyst, *J. Taiwan Inst. Chem. Eng.* **2020**, *113*, 142-154.

(849) Dutta, G. K.; Karak, N. Bio-based waterborne polyester supported oxygeneous graphitic carbon nitride nanosheets as a sustainable photocatalyst for aquatic environment remediation, *J. Cleaner Prod.* **2021**, *285*, 124906.

(850) Anusuyadevi, P. R.; Riazanova, A. V.; Hedenqvist, M. S.; Svagan, A. J. Floating Photocatalysts for Effluent Refinement Based on Stable Pickering Cellulose Foams and Graphitic Carbon Nitride (g-C3N4), *ACS Omega* **2020**, *5*, 22411–22419.

(851) Safaralizadeh, E.; Mahjoub, A. R.; Fazlali, F.; Bagheri, H. Facile construction of C3N4-TE@TiO2/UiO-66 with double Z-scheme structure as high performance photocatalyst for degradation of tetracycline, *Ceram. Int.* **2021**, *47*, 2374-2387.

(852) Ali, I.; Basheer, A. A.; Mbianda, X. Y.; Burakov, A.; Galunin, E.; Burakova, I.; Mkrtchyan, E.; Tkachev, A.; Grachev, V. Graphene based adsorbents for remediation of noxious pollutants from wastewater, *Environment International* **2019**, *127*, 160-180.

(853) Perreault, F.; de Faria, A. F.; Elimelech, M. Environmental applications of graphene-based nanomaterials, *Chemical Society Reviews* **2015**, *44*, 5861-5896.

(854) Singh, P.; Shandilya, P.; Raizada, P.; Sudhaik, A.; Rahmani-Sani, A.; Hosseini-Bandegharaei, A. Review on various strategies for enhancing photocatalytic activity of graphene based nanocomposites for water purification, *Arabian Journal of Chemistry* **2020**, *13*, 3498-3520.

(855) Upadhyay, R. K.; Soin, N.; Roy, S. S. Role of graphene/metal oxide composites as photocatalysts, adsorbents and disinfectants in water treatment: a review, *Rsc Advances* **2014**, *4*, 3823-3851.

(856) Zhang, N.; Zhang, Y.; Xu, Y.-J. Recent progress on graphene-based photocatalysts: current status and future perspectives, *Nanoscale* **2012**, *4*, 5792-5813.

(857) Hasija, V.; Raizada, P.; Sudhaik, A.; Sharma, K.; Kumar, A.; Singh, P.; Jonnalagadda, S. B.; Thakur, V. K. Recent advances in noble metal free doped graphitic carbon nitride based nanohybrids for photocatalysis of organic contaminants in water: A review, *Applied Materials Today* **2019**, *15*, 494-524.

(858) Mousavi, M.; Habibi-Yangjeh, A.; Pouran, S. R. Review on magnetically separable graphitic carbon nitride-based nanocomposites as promising visible-light-driven photocatalysts, *Journal of Materials Science-Materials in Electronics* **2018**, *29*, 1719-1747.

(859) Zhang, C.; Li, Y.; Shuai, D.; Shen, Y.; Xiong, W.; Wang, L. Graphitic carbon nitride (g-C3N4)-based photocatalysts for water disinfection and microbial control: A review, *Chemosphere* **2019**, *214*, 462-479.

(860) Jin, X.; Ye, L.; Xie, H.; Chen, G. Bismuth-rich bismuth oxyhalides for environmental and energy photocatalysis, *Coordination Chemistry Reviews* **2017**, *349*, 84-101.

(861) Nagabhushana, G.; Nagaraju, G.; Chandrappa, G. Synthesis of bismuth vanadate: its application in H 2 evolution and sunlight-driven photodegradation, *Journal of Materials Chemistry A* **2013**, *1*, 388-394.

(862) Wang, W.; Yu, Y.; An, T.; Li, G.; Yip, H. Y.; Yu, J. C.; Wong, P. K. Visible-light-driven photocatalytic inactivation of E. coli K-12 by bismuth vanadate nanotubes: bactericidal performance and mechanism, *Environmental science & technology* **2012**, *46*, 4599-4606.

(863) Monfort, O.; Plesch, G. Bismuth vanadate-based semiconductor photocatalysts: a short critical review on the efficiency and the mechanism of photodegradation of organic pollutants, *Environmental Science and Pollution Research* **2018**, *25*, 19362-19379.

(864) Deng, X.; Li, Z.; García, H. Visible Light Induced Organic Transformations Using Metal-Organic-Frameworks (MOFs), *Chemistry–A European Journal* **2017**, *23*, 11189-11209.

(865) Bedia, J.; Muelas-Ramos, V.; Peñas-Garzón, M.; Gómez-Avilés, A.; Rodríguez, J. J.; Belver, C. A review on the synthesis and characterization of metal organic frameworks for photocatalytic water purification, *Catalysts* **2019**, *9*, 52.

(866) Gautam, S.; Agrawal, H.; Thakur, M.; Akbari, A.; Sharda, H.; Kaur, R.; Amini, M. Metal oxides and metal organic frameworks for the photocatalytic degradation: A review, *Journal of Environmental Chemical Engineering* **2020**, *8*, 103726.

(867) Chen, W.; Yang, Z.; Xie, Z.; Li, Y.; Yu, X.; Lu, F.; Chen, L. Benzothiadiazole functionalized D–A type covalent organic frameworks for effective photocatalytic reduction of aqueous chromium (VI), *Journal of Materials Chemistry A* **2019**, *7*, 998-1004.

(868) Wang, H.; Wang, H.; Wang, Z.; Tang, L.; Zeng, G.; Xu, P.; Chen, M.; Xiong, T.; Zhou, C.; Li, X. Covalent organic framework photocatalysts: structures and applications, *Chemical Society Reviews* **2020**, *49*, 4135-4165.

(869) Espinosa, J. C.; Catalá, C.; Navalón, S.; Ferrer, B.; Álvaro, M.; García, H. Iron oxide nanoparticles supported on diamond nanoparticles as efficient and stable catalyst for the visible light assisted Fenton reaction, *Applied Catalysis B: Environmental* **2018**, *226*, 242-251.

(870) Manickam-Periyaraman, P.; Espinosa, J. C.; Ferrer, B.; Subramanian, S.; Álvaro, M.; García, H.; Navalón, S. Bimetallic iron-copper oxide nanoparticles supported on nanometric diamond as efficient and stable sunlight-assisted Fenton photocatalyst, *Chemical Engineering Journal* **2020**, *393*, 124770.

(871) Primo, A.; García, H. In *New and Future Developments in Catalysis*; Suib, S. L., Ed.; Elsevier Inc. Chapters, 2013.

(872) Bolton, J. R.; Bircher, K. G.; Tumas, W.; Tolman, C. A. Figures-of-merit for the technical development and application of advanced oxidation technologies for both electric-

and solar-driven systems (IUPAC Technical Report), *Pure and Applied Chemistry* **2001**, *73*, 627-637.

(873) Hisatomi, T.; Kubota, J.; Domen, K. Recent advances in semiconductors for photocatalytic and photoelectrochemical water splitting, *Chemical Society Reviews* **2014**, *43*, 7520-7535.

(874) Zielińska-Jurek, A.; Bielan, Z.; Dudziak, S.; Wolak, I.; Sobczak, Z.; Klimczuk, T.; Nowaczyk, G.; Hupka, J. Design and application of magnetic photocatalysts for water treatment. The effect of particle charge on surface functionality, *Catalysts* **2017**, *7*, 360.

(875) Gómez-Pastora, J.; Dominguez, S.; Bringas, E.; Rivero, M. J.; Ortiz, I.; Dionysiou, D. D. Review and perspectives on the use of magnetic nanophotocatalysts (MNPCs) in water treatment, *Chemical Engineering Journal* **2017**, *310*, 407-427.

(876) Almeida, F.; Grzebielucka, E. C.; Antunes, S. R. M.; Borges, C. P. F.; Andrade, A. V. C.; Souza, É. C. F. Visible light activated magnetic photocatalysts for water treatment, *Journal of Environmental Management* **2020**, *273*, 111143.

(877) Quiñones, D. H.; Álvarez, P. M.; Rey, A.; Contreras, S.; Beltrán, F. J. Application of solar photocatalytic ozonation for the degradation of emerging contaminants in water in a pilot plant, *Chemical Engineering Journal* **2015**, *260*, 399-410.

(878) Prieto-Rodriguez, L.; Miralles-Cuevas, S.; Oller, I.; Agüera, A.; Puma, G. L.; Malato, S. Treatment of emerging contaminants in wastewater treatment plants (WWTP) effluents by solar photocatalysis using low TiO2 concentrations, *Journal of hazardous materials* **2012**, *211*, 131-137.

(879) Yang, W.; Zhou, H.; Cicek, N. Treatment of organic micropollutants in water and wastewater by UV-based processes: a literature review, *Critical Reviews in Environmental Science and Technology* **2014**, *44*, 1443-1476.

(880) Carbonaro, S.; Sugihara, M. N.; Strathmann, T. J. Continuous-flow photocatalytic treatment of pharmaceutical micropollutants: activity, inhibition, and deactivation of TiO2 photocatalysts in wastewater effluent, *Applied Catalysis B: Environmental* **2013**, *129*, 1-12.

(881) Hossain, M. M.; Raupp, G. B.; Hay, S. O.; Obee, T. N. Three-dimensional developing flow model for photocatalytic monolith reactors, *AIChE Journal* **1999**, *45*, 1309-1321.

(882) Li, X.; Chen, D.; Li, N.; Xu, Q.; Li, H.; He, J.; Lu, J. Silver bromide-loaded hollow porous carbon nitride with ultrahigh activity as visible light photocatalysts for water remediation, *Appl. Catal., B* **2018**, *229*, 155-162.

(883) Navalon, S.; Martin, R.; Alvaro, M.; Garcia, H. Sunlight-assisted Fenton reaction catalyzed by gold supported on diamond nanoparticles as pretreatment for biological degradation of aqueous phenol solutions, *ChemSusChem* **2011**, *4*, 650-657.

(884) Asghar, A.; Raman, A. A. A.; Daud, W. M. A. W. Advanced oxidation processes for in-situ production of hydrogen peroxide/hydroxyl radical for textile wastewater treatment: a review, *Journal of Cleaner Production* **2015**, *87*, 826-838.

(885) Babu, D. S.; Srivastava, V.; Nidheesh, P. V.; Kumar, M. S. Detoxification of water and wastewater by advanced oxidation processes, *Science of the Total Environment* **2019**, *696*, 133961.

(886) Boczkaj, G.; Fernandes, A. Wastewater treatment by means of advanced oxidation processes at basic pH conditions: A review, *Chemical Engineering Journal* **2017**, *320*, 608-633.

(887) Klavarioti, M.; Mantzavinos, D.; Kassinos, D. Removal of residual pharmaceuticals from aqueous systems by advanced oxidation processes, *Environment International* **2009**, *35*, 402-417.

(888) Oturan, M. A.; Aaron, J.-J. Advanced Oxidation Processes in Water/Wastewater Treatment: Principles and Applications. A Review, *Critical Reviews in Environmental Science and Technology* **2014**, *44*, 2577-2641.

(889) Ribeiro, A. R.; Nunes, O. C.; Pereira, M. F. R.; Silva, A. M. T. An overview on the advanced oxidation processes applied for the treatment of water pollutants defined in the recently launched Directive 2013/39/EU, *Environment International* **2015**, *75*, 33-51.

(890) Nidheesh, P. Heterogeneous Fenton catalysts for the abatement of organic pollutants from aqueous solution: a review, *Rsc Advances* **2015**, *5*, 40552-40577.

(891) Chang, H. T.; Wu, N.-M.; Zhu, F. A kinetic model for photocatalytic degradation of organic contaminants in a thin-film TiO2 catalyst, *Water research* **2000**, *34*, 407-416.

(892) Puma, G. L.; Yue, P. L. Modelling and design of thin-film slurry photocatalytic reactors for water purification, *Chemical engineering science* **2003**, *58*, 2269-2281.

(893) Peill, N. J.; Hoffmann, M. R. Mathematical model of a photocatalytic fiber-optic cable reactor for heterogeneous photocatalysis, *Environmental science & technology* **1998**, *32*, 398-404.

(894) Rota, F.; Cavassi, M.; Niego, D.; Gorlani, R.; Vianelli, L.; Tatti, L.; Bruzzi, P.; Moroni, A.; Bellobono, I. R.; Bianchi, M. Mathematical modelling of photomineralization of phenols in aqueous solution, by photocatalytic membranes immobilizing titanium dioxide, *Chemosphere* **1996**, *33*, 2159-2173.

(895) Sannino, D.; Vaiano, V.; Sacco, O.; Ciambelli, P. Mathematical modelling of photocatalytic degradation of methylene blue under visible light irradiation, *Journal of Environmental Chemical Engineering* **2013**, *1*, 56-60.

(896) Meyer, L. E.; Eser, B. E.; Kara, S. Coupling light with biocatalysis for sustainable synthesis - very recent developments and future perpectives., *Curr. Opinion Green Sustainable Chem.* **2021**, https://doi.org/10.106/j. cogsc.2021.100496.

(897) Hong, B. C. Enantioselective sysnthesis enabled by visible light photocatalysis. , *Org. Biomol. Chem.* **2020**, https://doi.org/10.1039/d1030.ob007759e.

(898) Yua, M.; Wanga, J.; Tang, L.; Feng, C.; Liu, H.; Zhang, H.; Peng, B.; Z., C.; Xi, Q. Intimate coupling of photocatalysis and biodegradation for wastewater treatment: mechanisms, recent advances and environmental applications. , *Water Res.* **2020**, *175*, 115673.

(899) Sakimoto, K. K.; Wong, A. B.; Yang, P. Self-photosensitization of non-photosynthetic bacteria for solar-to-chemical production. , *Science* **2016**, *351*, 74-77.

(900) Brown, K. A.; Wilker, M. B.; Boehm, M.; Dukovic, G.; King, P. W. Characterization of Photochemical processes for H2 production by CdS nanorod-[FeFe] hydrogenase complexes., *J. Am. Chem. Soc.* **2012**, *134*, 5627-5636.

(901) Khorobrykh, A.; Dasgupta, J.; Kolling, D. R. J.; Terentyev, V.; Klimov, V. V.; Dismukes, G. C. Evolutionary origins of the photosynthetic water oxidation cluster: bicarbonate permits Mn2+ photo-oxidation by anoxygenic bacterial reaction centers., *ChemBioChem* **2013**, *14*, 1725-1731.

(902) Luo, L.; Lai, X.; Chen, B.; Lin, L.; Fang, L.; Tam, N. F. Y.; Luan, T. Chlorophyll catalyse the photo-transformation of carcinogenic benzo[a]pyrene in water. , *Sci. Rep.* **2015**, *5*, 12776.

(903) Ho, M. Y.; Soulier, N. T.; Canniffe, D. P.; Shen, G.; Bryant, D. A. Light regulation of pigment and photosystem biosynthesis in cyanobacteria., *Current Opinion in Plant Biology* **2017**, *37*, 24-33.

(904) Pan, M.; Lyu, T.; Zhan, L.; Matamoros, V.; Angelidaki, I.; Cooper, M.; Pan, G. Mitigating antibiotic pollution using cyanobacteria: removal efficiency, pathways and metabolism., *Water Res.* **2020**, *190*, 116735.

(905) Xiong, J. Q.; Cui, P.; Ru, S.; Govindwar, S. P.; Kurade, M. B.; Jang, M.; Kim, S. H.; Jeon, B. H. Unravelling metabolism and microbial community of a phytobed co-planted with Typha angustifolia and Ipomoea aquatica for biodegradation of doxylamine from wastewater. , *J. Hazard. Mater.* **2021**, *401*, 123404.

(906)   Wang, Q.; Liu, W.; Li, X.; Wang, R.; Zhai, J. Carbamazepine toxicity and its co-metabolic removal by the cyanobacteria Spirulina platensis., *Sci. Total Environ.* **2020**, *706*, 135686.

(907)   Shabbir, S.; Faheem, M.; Ali, N.; Kerr, P. G.; Wang, L. F.; Kuppusamy, S.; Li, Y. Periphytic biofilm: an innovative approach for biodegradation of microplastics., *Sci. Total Environ.* **2020**, *717*, 137064.

(908)   Chalifour, A.; Chin, W. Y.; Leung, P. Y.; Cheung, S. G.; Fung-Yee Tam, N. Effect of light on the transformation of BDE-47 by living and autoclaved cultures of Microcystis flos-aquae and Chlorella vulgaris., *Chemosphere* **2019**, *233*, 140-148.

(909)   Deveci, E. Ü.; Dizge, N.; Yatmaz, H. C.; Aytepe, Y. Integrated process of fungal membrane bioreactor and photocatalytic membrane reactor for the treatment of industrial textile wastewater., *Biochem. Eng. J.* **2016**, *105*, 420-427.

(910)   Hou, F.; Liu, J.; Zhang, Y.; Zhao, C.; Xiao, X.; Zou, J.; Wang, H.; Jiang, B. Synthesis of Metallic Copper Modified g-C3N4 by Molecular Self-assembly Structure and Its Combined Catalytic Performance with Activated Sludge., *J. Hazard. Mater.* **2020**, *388*, 121754.

(911)   Wapshott-Stehli, H. L.; Grunden, A. M. In situ H2O2 generation methods in the context of enzyme biocatalysis., *Enzyme Microb. Technol.* **2021**, *145*, 109744.

(912)   Mandpe, P.; Prabhakar, B.; Gupta, H.; Shende, P. Glucose oxidase-based biosensor for glucose detection from biological fluids., *Sens. Rev.* **2020**, *40*, https://doi. org/10.1108/SR-1101-2019-0017.

(913)   Perez, D. I.; Grau, M. M.; Arends, I. W. C. E.; Hollmann, F. Visible light-driven and chloroperoxidase-catalyzed oxygenation reactions., *Chem. Commun.* **2009**, 6848-6850.

(914)   Zuo, W.; Yu, Y.; Huang, H. Making waves: Microbe-photocatalyst hybrids may provide new opportunities for treating heavy metal polluted wastewater., *Water Res.* **2021**, *195*, 116984.

(915)   Marsolek, M. D.; Kiritsits, M. J.; Gray, K. A.; Rittmann, B. E. Coupled photocatalytic-biodegradation of 2,4,5-trichlorophenol: Effects of photolytic and photocatalytic effluent composition on bioreactor process performance, community diversity, and resistance and resilience to perturbation., *Water Res.* **2014**, *50*, 59-69.

(916)   Zhang, L.; Xing, Z.; Zhang, H.; Li, Z.; Wu, X.; Zhang, X.; Zhang, Y.; Zhou, W. High thermostable ordered mesoporous SiO2-TiO2 coated circulating-bed biofilm reactor for unpredictable photocatalytic and biocatalytic performance., *Appl. Catal. B* **2016**, *180*, 521-529.

(917) Xu, Y.; Zhong, D.; Jia, J.; Li, K.; Li, J.; Quan, X. Dual slant-placed electrodes thin film photocatalytic reactor : Enhanced dye degradation efficiency by self-generated electric field. , *Chem. Eng. J.* **2013**, *225*, 138-143.

(918) Ammar, S. H.; Shafi, R. F.; Ali, A. D. A novel airlift photocatalytic fuel cell (APFC) with immobilized CdS coated zerovalent iron (Fe@CdS) and d-C3N4 photocatalysts film as photoanode for power generation and organic degradation., *Colloid surface A* **2020**, *602*, 125164.

(919) Bessegato, G. G.; Guaraldo, T. T.; de Brito, J. F. J.; F., B. M.; Zanoni, M. V. B. Achievements and trends in photoelectrocatalysis : from environmental to energy applications., *Electrocatal.* **2015**, *6*, 415-441.

(920) Bessegato, G. G.; Guaraldo, T. T.; Zanoni, M. V. B. *Enhancement of Photoelectrocatalysis Efficiency by Using Nanostructured Electrodes*, 2014.

(921) Meng, X.; Zhang, Z.; Li, X. Synergetic photoelectrocatalytic reactors for environmental remediation: a review., *J. Photoc. Photobio C* **2015**, *24*, 83-101.

(922) Ding, C.; Shi, J.; Wang, Z.; Li, C. Photoelectrocatalytic water splitting: significance of cocatalysts, electrolyte, and interfaces., *ACS Catal* **2017**, *7*, 675-688.

(923) Le Formal, F.; Pendlebury, S. R.; Cornuz, M.; Tilley, S. D.; Gratzel, M.; Durrant, J. R. Back Electron-Hole Recombination in Hematite Photoanodes for Water Splitting., *J. Am. Chem. Soc.* **2014**, *136*, 2564−2574.

(924) Din, C.; Wang, Z.; Shi, J.; Yao, T.; Li, A.; Yan, P.; Huang, B.; Li, C. Substrate-Electrode Interface Engineering by an Electron-Transport Layer in Hematite Photoanode. , *ACS Appl. Mater. Interfaces.* **2016**, *8*, 7086-7091.

(925) Vinodgopal, K.; Hotchandani, S.; Kamat, P. V. Electrochemically assisted photocatalysis - TiO2 particulate film electrodes for photocatalytic degradation of 4-chlorophenol., *J. Phys. Chem.* **1993**, *97*, 9040-9044.

(926) Oota, T.; Saito, H.; Yamai, I. Synthesis of potassium hexatitanate fibers by the hydrothermal dehydration method. , *J. Crystal Growth* **1979**, *46*, 331-338.

(927) Paramasivam, I.; Jha, H.; Liu, N.; Schmuki, P. A Review of Photocatalysis using Self-organized TiO2 Nanotubes and Other Ordered Oxide Nanostructures., *Small* **2012**, *8*, 3073-3103.

(928) Zhang, Y.; Ji, Y.; Li, J.; Bai, J.; Chen, S.; Li, L.; Wang, J.; Zhou, T.; Jiang, P.; Guan, X.; Zhou, B. Efficient ammonia removal and toxic chlorate control by using BiVO4/WO3 heterojunction photoanode in a self-driven PEC-chlorine system., *J. Haz. Mater.* **2021**, *402*, 123725.

(929) Zhang, J.; Pang, Z.; Sun, Q.; Chen, X.; Zhu, Y.; Li, M.; Wang, J.; Qiu, H.; Li, X.; Chronakis, I. S. TiO2 nanotube aray modified with polypyrrole for efficient photoelectrocatalytic decolorization of methylene blue., *J. Alloy Compd.* **2020**, *820*, 153128.

(930) Ye, S.; Chen, Y.; Yao, X.; Zhang, J. Simultaneous removal of organic pollutants and heavy metals in wastewater by photoelectrocatalysis: A review, *Chemosphere* **2021**, *273*, 128503.

(931) Fei, W.; Gao, J.; Li, N.; Chen, D.; Xu, Q.; Li, H.; He, J.; Lu, J. A visible-light active p-n heterojunction NiFe-LDH/Co$_3$O$_4$ supported on Ni foam as photoanode for photoelectrocatalytic removal of contaminants, *J. Haz. Mater.* **2021**, *402*, 123515.

(932) Antoniadou, M.; Lianos, P. Photoelectrochemical oxidation of organic substances over nanocrystalline titania: Optimization of the photoelectrochemical cell, *Catal. Today.* **2009**, *144* 166-171.

(933) Lam, S.-M.; Sin, J.-C.; Lin, H.; Li, H.; Lim, J. W.; Zeng, H. A Z-scheme WO$_3$ loaded-hexagonal rod-like ZnO/Zn photocatalytic fuel cell for chemical energy recuperation from wastewater treatment, *Appl. Surf. Sci.* **2020**, *514*, 145945.

(934) Lianos, P. Production of electricity and hydrogen by photocatalytic degradation of organic wastes in a photoelectrochemical cell: The concept of the Photofuelcell: A review of a re-emerging research field, *J. Hazard Mater.* **2011**, *185* 575-590.

(935) Jia, Y.; Liu, P.; Wang, Q.; Wu, Y.; Cao, D.; Quiao, Q.-A. Construction of Bi$_2$S$_3$-BiOBr nanosheets on TiO$_2$ NTA as the effective photocatalysts: Pollutant removal, photoelectric conversion and hydrogen generation, *J. Colloid Interf. Sci.* **2021**, *585*, 459-469.

(936) Peerakiatkhajohn, P.; Yun, J. H.; Butburee, T.; Chen, H. J.; Thaweesak, S.; Lyu, M. Q.; Wang, S. C.; Wang, L. Z. Bifunctional photoelectrochemical process for humic acid degradation and hydrogen production using multi-layered p-type Cu2O photoelectrodes with plasmonic Au@TiO$_2$, *J Hazard Mater.* **2021**, *402*, 123533.

(937) Zhou, Z.; Wu, Z.; Xu, Q.; Zhao, G. A solar-charged photoelectrochemical wastewater fuel cell for efficient and sustainable hydrogen production, *J. Mater. Chem. A.* **2017**, 25450-25459.

(938) Chang, S.; Hu, C.; Beyhaqi, A.; Wang, M.; Zeng, Q. Highly Efficient Hydrogen and Electricity Production Combined with Degradation of Organics Based on a Novel Solar Water-Energy Nexus System, *ACS Appl. Mater. Interfaces.* **2020**, *12*, 2505-2515.

(939) Cui, R.; Shen, Q.; Guo, C.; Tang, B.; Yang, N.; Zhao, G. Syngas electrosynthesis using self-supplied CO2 from photoelectrocatalytic pollutant degradation, *Appl. Catal. B: Environm.* **2020**, *261*, 118253.

(940)   Almeida, L. C.; Silva, B. F.; Zanoni, M. V. B. Combined photoelectrocatalytic/electro-Fenton process using a Pt/TiO2NTs photoanode for enhanced degradation of an azo dye: A mechanistic study, *J. Electroanal. Chem.* **2014**, *734*, 43-52.

(941)   Li, X.; Liu, S.; Cao, D.; Mao, R.; Zhao, X. Synergetic activation of H2O2 by photo-generated electrons and cathodic Fenton reaction for enhanced self-driven photoelectrocatalytic degradation of organic pollutants, *Appl. Catal. B: Environm.* **2018**, *235*, 1-8.

(942)   Sheydaei, M.; Karimi, M.; Vatanpour, V. Continuous flow photoelectrocatalysis/reverse osmosis hybrid reactor for degradation of a pesticide using nano N-TiO2/Ag/Ti electrode under visible light, *J. Photoc. Photobiol. A.* **2019**, *384*, 112068.

(943)   Cheng, L.; Liu, L.; Zhang, J. Visible light-driven photoelectrocatalysis coupling with electroenzymatic process for degradation of chloramphenicol, *Chem. Eng. J.* **2017**, *330*, 1380-1389.

(944)   Petrier, C.; Lamy, M. F.; Francony, A.; Benahcene, A.; David, B.; Renaudin, V.; Gondrexon, N. Sonochemical degradation of phenol in dilute aqueous solutions: comparison of the reaction rates at 20 and 487 kHz, *J. Phys. Chem. A.* **1994**, *98*, 10514-10520.

(945)   Francony, A.; Petrier, C. Sonochemical degradation of carbon tetrachloride in aqueous solution at two frequencies: 20 kHz and 500 kHz, *Ultrason. Sonochem.* **1999**, *3*, S77-S82.

(946)   Gogate, P. R. Treatment of wastewater streams containing phenolic compounds using hybrid techniques based on cavitation: a review of Current Status and the way Forward, *Ultrason. Sonochem.* **2008**, *15*, 1-15.

(947)   Chand, R.; Ince, N. H.; Gogate, P. R.; Bremner, D. H. Phenol degradation using 20, 300 and 520 kHz ultrasonic reactors with hydrogen peroxide, ozone and zero valent metals, *Sep. Purif. Tech.* **2009**, *67*, 103-109.

(948)   Mishra, K. P.; Gogate, P. R. Intensification of degradation of aqueous solutions of rhodamine B using sonochemical reactors at operating capacity of 7 L, *J. Environ. Manage.* **2011**, *92*, 1972-1977.

(949)   Tijani, J. O.; Fatoba, O. O.; Madzivire, G.; Petrik, L. F. A Review of Combined Advanced Oxidation Technologies for the Removal of Organic Pollutants from Water, *Water Air Soil Pollut.* **2014**, *225*, 2102

(950)   Adewuyi, Y. G. Sonochemistry: Environmental Science and Engineering Applications, *Ind. Eng. Chem. Res.* **2001**, *40*, 4681-4715.

(951)   Theerthagiri, J.; Senthil, R. A.; Thirumalai, D.; Madhavan, J. In *Handbook of Ultrasonics and Sonochemistry*; Ashokkumar, M., Ed.; Springer, 2016.

(952) Gogate, P. R.; Pandit, A. B. A review of imperative technologies for wastewater treatment II: hybrid methods, *Adv. Env. Res.* **2004**, *8*, 553-597.

(953) Gogate, P. R.; Pandit, A. B. Sonophotocatalytic reactors for wastewater treatment: a critical Review, *AIChE J.* **2004**, *50*, 1051-1079.

(954) Diao, Z.-H.; Donga, F.-X.; Yana, L.; Chen, Z.-L.; Qian, W.; Kong, L.-J.; Zhang, Z.-W.; Zhang, T.; Tao, X.-Q.; Du, J.-J.; Jiang, D.; Chu, W. Synergistic oxidation of Bisphenol A in a heterogeneous ultrasoundenhanced sludge biochar catalyst/persulfate process: Reactivity and mechanism, *J. Hazard. Mater.* **2020**, *384*, 121385.

(955) Zielewicz, E. Effects of ultrasonic disintegration of excess sewage sludge, *Top. Curr. Chem.* **2016**, *374*, 67.

(956) Chatel, G.; Colmenares, J. C. Sonochemistry: from Basic Principles to Innovative Applications, *Top. Curr. Chem.* **2017**, *375*, 8.

(957) Guo, J.; Zhu, L.; Sun, N.; Lan, Y. Degradation of nitrobenzene by sodium per- sulfate activated with zero-valent zinc in the presence of low frequency ultra- sound, *J. Taiwan. Inst. Chem.* **2017**, *78*, 137-143.

(958) Cui, M.; Choi, J.; Lee, Y.; Ma, J.; Kim, D.; Choi, J.; Jang, M.; Khim, J. Significant enhancement of bromate removal in drinking water: Implications for the mechanism of sonocatalytic reduction, *Chem. Eng. J.* **2017**, *317*, 404-412.

(959) Zhao, H.; Zhang, G.; Chong, S.; Zhang, N.; Liu, Y. MnO_2/CeO_2 for catalytic ultrasonic decolorization of methyl orange: process parameters and mechanisms, *Ultrason. Sonochem.* **2015**, *27*, 474-479.

(960) Chong, S.; Zhang, G.; Zhang, N.; Liu, Y.; Zhu, J.; Huang, T. Preparation of $FeCeO_x$ by ultrasonic impregnation method for heterogeneous Fenton degradation of diclofenac, *Ultrason. Sonochem.* **2016**, *32*, 231-240.

(961) Chong, S.; Zhang, G.; Zhang, N.; Liu, Y.; Huang, T.; Chang, H. Diclofenac degradation in water by FeCeOx catalyzed H2O2: influencing factors, mechanism and pathways, *J. Hazard. Mater.* **2017**, 150-159.

(962) Harada, H. Sonophotocatalytic reaction of sodium chloride solution: Comparison of reaction products from sodium chloride solution with those from pure water and influence of insoluble photocatalyst on sonochemical reaction, *Jpn. J. Appl. Phys.* **2000**, *39(Part 1, 5B)*, 2974-2977.

(963) Harada, H.; Hosoki, C.; Ishikane, M. Sonophotocatalysis of water in a CO2-Ar atmosphere, *J. Photochem. Photobiol. A: Chem.* **2003**, *160*, 11-17.

(964)   Joseph, C. G.; Puma, G. L.; Bono, A.; Krishnaiah, D. Sonophotocatalysis in advanced oxidation process: A short review, *Ultrason. Sonochem.* **2009**, *16*, 583-589.

(965)   Harada, H. Sonophotocatalytic decomposition of water using TiO_2 photocatalyst, *Ultrason. Sonochem.* **2001**, *8*, 55-58.

(966)   Harada, H.; Hosoki, C.; Kudo, A. Overall water splitting by sonophotocatalytic reaction: The role of powdered photocatalyst and an attempt to decompose water using a visible-light sensitive photocatalyst, *J. Photochem. Photobiol. A, Chem.* **2001**, *141*, 219-224.

(967)   Mrowetz, M.; Pirola, C.; Selli, E. Degradation of organic water pollutants through sonophotocatalysis in the presence of TiO2, *Ultrason. Sonochem.* **2003**, *10*, 247-254.

(968)   Hu, X.; Zhu, Q.; Gu, Z.; Zhang, N.; Liu, N.; Stanislaus, M. S.; Li, D.; Yang, Y. Wastewater treatment by sonophotocatalysis using PEG modified TiO2 film in a circular Photocatalytic-Ultrasonic system, *Ultrason. Sonochem.* **2017**, *36*, 301-308.

(969)   Hoffmann, M. R.; Martin, S. T.; Choi, W.; Bahnemann, D. W. Environmental applications of semiconductor photocatalysis, *Chem. Rev.* **1995**, *95*, 69-96.

(970)   Jelic, A.; Michael, I.; Achilleos, A.; Hapeshi, E.; Lambropoulou, D.; Perez, S.; Petrovic, M.; Fatta-Kassinos, D.; Barcelo, D. Transformation products and reaction pathways of carbamazepine during photocatalytic and sonophotocatalytic treatment, *J. Hazard. Mater.* **2013**, *263*, 177-186.

(971)   Gobara, H. M.; Elsalamony, R. A.; Hassan, S. A. Sonophotocatalytic degradation of eriochrome black-T dye in water using Ti grafted SBA-15, *J. Porous Mater.* **2016**, *23*, 1311-1318.

(972)   Wu, C. D.; Zhang, J. Y.; Wu, Y.; Wu, G. Z. Degradation of phenol in water by the combination of sonolysis and photocatalysis, *Desalin. Water Treat.* **2013**, *52*, 1911-1918.

(973)   Bertelli, M.; Selli, E. Kinetic analysis on the combined use of photocatalysis, H_2O_2 photolysis, and sonolysis in the degradation of methyl tert-butyl ether, *Appl. Catal. B: Environ.* **2004**, *52*, 205-212.

(974)   Selli, E.; Bianchi, C. L.; Pirola, C.; Bertelli, M. Degradation of methyl tert-butyl ether in water: effects of the combined use of sonolysis and photocatalysis, *Ultrason. Sonochem.* **2005**, *12*, 395-400.

(975)   Naruke, Y.; Tanaka, H.; Harada, H. The Effects of Coupling Photocatalysis and Sonolysis on Malonic Acid Solution, *Electrochem* **2011**, *79*, 826-830.

(976)   Na, S.; Ahn, Y.-G.; Cui, M.; Khim, J. Significant diethyl phthalate (DEP) degradation by combined advanced oxidation process in aqueous solution, *J. Environ. Manage.* **2012**, *101*, 104-110.

(977)   Zewde, A. A.; Zhang, L.; Li, Z.; Odey, E. A. A review of the application of sonophotocatalytic process based on advanced oxidation process for degrading organic dye, *Rev. Environ. Health* **2019**, *34*, 365-375.

(978)   An, T.; Gu, H.; Xiong, Y.; Chen, W.; Zhu, X.; Sheng, G.; Fu, J. Decolourization and COD removal from reactive dye-containing wastewater using sonophotocatalytic technology, *J. Chem. Technol. Biotechnol.* **2003**, *78*, 1142-1148.

(979)   Tokumoto, T.; Ishikawa, K.; Furusawa, T.; Ii, S.; Hachisuka, K.; Tokumoto, M.; Tsai, H.-J.; Uchida, S.; Maezawa, A. Sonophotocatalysis of endocrine-disrupting chemicals, *Mar. Environ. Res.* **2008**, *66*, 372-377.

(980)   Park, J.-H. Photochemical degradation and toxicity reduction of methyl 1-[(butylamino)carbonyl]-1H-benzimidazol-2-ylcarbamate in agricultural wastewater: Comparative study of photocatalysis and sonophotocatalysis, *Desalination* **2009**, *249*, 480-485.

(981)   Schieppati, D.; Galli, F.; Peyot, M. L.; Yargeau, V.; Bianchi, C. L.; Boffito, D. C. An ultrasound-assisted photocatalytic treatment to remove an herbicidal pollutant from wastewaters, *Ultrason. Sonochem.* **2019**, *54*, 302-310.

(982)   Hussein Abdurahman, M.; Zuhairi Abdullah, A.; Fazliani Shopware, N. A comprehensive review on sonocatalytic, photocatalytic, and sonophotocatalytic processes for the degradation of antibiotics in water: Synergistic mechanism and degradation pathway, *Chem. Eng. J.* **2021**, *413*, 127412.

(983)   Rahimi, S.; Ayati, B.; Rezaee, A. Optimization of reaction parameters for the sonophotocatalytic degradation of hydroquinone, *Res. Chem. Intermed.* **2016**, *43*, 1935-1956.

(984)   Colmenares, J. C.; Nair, V.; Kuna, E.; Lomot, D. Development of photocatalyst coated fluoropolymer based microreactor using ultrasound for water remediation, *Ultrason. Sonochem.* **2018**, *41*, 297-302.

(985)   Michael, I.; Achilleos, A.; Lambropoulouc, D.; Osorio Torrens, V.; Pérez, S.; Petrovic, M.; Barcelóe, D.; Fatta-Kassinos, D. Proposed transformation pathway and evolution profile of diclofenac and ibuprofen transformation products during (sono)photocatalysis, *Appl. Catal. B: Environ.* **2014**, *147*, 1015-1027.

(986)   Verma, A.; Chhikara, I.; Dixit, D. Photocatalytic treatment of pharmaceutical industry wastewater over TiO_2 using immersion well reactor: synergistic effect coupling with ultrasound, *Desalination Water Treat.* **2013**, *52*, 6591-6597.

(987) Torres, R. A.; Nieto, J. I.; Combet, E.; Petrier, C.; Pulgarin, C. Influence of TiO$_2$ concentration on the synergistic effect between photocatalysis and high-frequency ultrasound for organic pollutant mineralization in water, *Appl. Catal. B: Environ.* **2008**, *80*, 168-175.

(988) Hayashi, N.; Yasutomi, R.; Kasai, E. Development of dispersed-type sonophotocatalytic process using piezoelectric effect caused by ultrasonic resonance, *Ultrason. Sonochem.* **2010**, *17*, 884-891.

(989) Sandoval González, A.; Silva Martínez, S. Study of the sonophotocatalytic degradation of basic blue 9 industrial textile dye over slurry titanium dioxide and influencing factors, *Ultrason. Sonochem.* **2008**, *15*, 1038-1042.

(990) Yano, J.; Matsuura, J.-i.; Ohura, H.; Yamasaki, S. Complete mineralization of propyzamide in aqueous solution containing TiO2 particles and H2O2 by the simultaneous irradiation of light and ultrasonic waves, *Ultrason. Sonochem.* **2005**, *12*, 197-203.

(991) Kritikos, D. E.; Xekoukoulotakis, N. P.; Psillakis, E.; Mantzavinos, D. Photocatalytic degradation of reactive black 5 in aqueous solutions: Effect of operating conditions and coupling with ultrasound irradiation, *Water Res.* **2007**, *41*, 2236- 2246.

(992) Drosou, C.; Coz, A.; Xekoukoulotakis, N. P.; Moya, A.; Vergara, Y.; Mantzavinos, D. Peracetic acid-enhanced photocatalytic and sonophotocatalytic inactivation of E. coli in aqueous suspensions, *J. Chem. Technol. Biotechnol.* **2010**, *85*, 1049-1053.

(993) Berberidou, C.; Poulios, I.; Xekoukoulotakis, N. P.; Mantzavinos, D. Sonolytic, photocatalytic and sonophotocatalytic degradation of malachite green in aqueous solutions, *Appl. Catal. B: Environ.* **2007**, *74*, 63-72.

(994) Torres-Palma, R. A.; Nieto, J. I.; Combet, E.; Petrier, C.; Pulgarin, C. An innovative ultrasound, Fe2+ and TiO2 photoassisted process for bisphenol a mineralization, *Water Res.* **2010**, *44*, 2245-2252.

(995) Dönmez, Ö.; Dükkancı, M.; Gündüz, G. Effects of catalyst preparation method and reaction parameters on the ultrasound assisted Photocatalytic oxidation of reactive yellow 84 dye, *J. Environ. Health. Sci. Engineer.* **2020**, *18*, 835-851.

(996) Sekiguchi, K.; Sasaki, C.; Sakamoto, K. Synergistic effects of high-frequency ultrasound on photocatalytic degradation of aldehydes and their intermediates using TiO$_2$ suspension in water, *Ultrason. Sonochem.* **2011**, *18*, 158-163.

(997) Méndez-Arriaga, F.; Torres-Palma, R. A.; Pétrier, C.; Esplugas, S.; Gimenez, J.; Pulgarin, C. Mineralization enhancement of a recalcitrant pharmaceutical pollutant in water by advanced oxidation hybrid processes, *Water Res.* **2009**, *43*, 3984-3991.

(998) Madhavan, J.; Grieser, F.; Ashokkumar, M. Combined advanced oxidation processes for the synergistic degradation of ibuprofen in aqueous environments, *J. Hazard. Mater.* **2010**, *178*, 202-208.

(999) Madhavan, J.; Sathish Kumar, P. S.; Anandan, S.; Grieser, F.; Ashokkumar, M. Sonophotocatalytic degradation of monocrotophos using TiO_2 and Fe^{3+}, *J. Hazard. Mater.* **2010**, *177*, 944-949.

(1000) Panda, D.; Manickam, S. Recent advancements in the sonophotocatalysis (SPC) and doped-sonophotocatalysis (DSPC) for the treatment of recalcitrant hazardous organic water pollutants, *Ultrason. Sonochem.* **2017**, *36*, 481-496.

(1001) Wang, H.; Niu, J.; Long, X.; He, Y. Sonophotocatalytic degradation of methyl orange by nano-sized Ag/TiO2 particles in aqueous solutions, *Ultrason. Sonochem.* **2008**, *15*, 386-392.

(1002) Anandan, S.; Ashokkumar, M. Sonochemical synthesis of Au-TiO2 nanoparticles for the sonophotocatalytic degradation of organic pollutants in aqueous environment, *Ultrason. Sonochem.* **2009**, *16*, 316-320.

(1003) Jia, Y.; Zhan, S.; Ma, S. Fabrication of TiO_2-Bi_2WO_6, Binanosheet for Enhanced Solar Photocatalytic Disinfection of E. coli: Insights on the Mechanism, *ACS Appl. Mater. Interfaces* **2016**, *8*, 6841-6851.

(1004) Sun, M.; Yao, Y.; Ding, W.; Anandan, S. N/Ti^{3+} co-doping biphasic TiO_2/Bi_2WO_6 heterojunctions: Hydrothermal fabrication and sonophotocatalytic degradation of organic pollutants, *J.Alloys Compd.* **2019**, *820*, 153172.

(1005) Zhu, L.; Meng, Z.-D.; Park, C.-Y.; Ghosh, T.; Oh, W.-C. Characterization and relative sonocatalytic efficiencies of a new MWCNT and CdS modified TiO2 catalysts and their application in the sonocatalytic degradation of rhodamine B, *Ultrason. Sonochem.* **2013**, *20*, 478-484.

(1006) Zhang, K.; Oh, W. C. Kinetic study of the visible light-induced sonophotocatalytic degradation of MB solution in the presence of Fe/TiO2-MWCNT catalyst, *Bull. Korean. Chem. Soc.* **2010**, *31*, 1589-1595.

(1007) Gao, J.; Jiang, R.; Wang, J.; Kang, P.; Wang, B.; Li, Y.; LI, K.; Zhang, X. The investigation of sonocatalytic activity of Er^{3+}:$YAlO_3$/TiO2-ZnO composite in azo dyes degradation, , *Ultrason. Sonochem.* **2011**, *18*, 541-548.

(1008) Zhai, Y.; Li, Y.; Wang, J.; Wang, J.; Yin, L.; Kong, Y.; Han, G.; Fan, P. Effective sonocatalytic degradation of organic dyes by using Er3+:YAlO3/TiO2-SnO2 under ultrasonic irradiation, *J. Mol. Catal. A: Chem.* **2013**, *366*, 282-287.

(1009) Neppolian, B.; Ciceri, L.; Bianchi, C. L.; Grieser, F.; Ashokkumar, M. Sonophotocatalytic degradation of 4-chlorophenol using Bi2O3/TiZrO4 as a visible light responsive photocatalyst, *Ultrason. Sonochem.* **2011**, *18*, 135-139.

(1010) Markovic, D.; Šaponjic, Z.; Radoic, M.; Radetic, T.; Vodnik, V.; Potkonjak, B.; Radetic, M. Sonophotocatalytic degradation of dye C.I. Acid Orange 7 by TiO2 and Ag nanoparticles immobilized on corona pretreated polypropylene non-woven fabric, *Ultrason. Sonochem.* **2015**, *24*, 221-229.

(1011) Puma, L. G.; Bono, A.; Krishnaiah, D.; Collin, J. G. Preparation of titanium dioxide photocatalyst loaded onto activated carbon support using chemical vapor deposition: A review paper, *J. Hazard. Mater.* **2008**, *157*, 209-219.

(1012) Abazari, R.; Mahjoub, A. R.; Sanati, S.; Rezvani, Z.; Hou, Z.; Dai, H. Ni-Ti layered double hydroxide@graphitic carbon nitride nanosheet: a novel nanocomposite with high and ultrafast sonophotocatalytic performance for degradation of antibiotics, *Inorg. Chem.* **2019**, *58*, 1834-1849.

(1013) Lirong, M.; Jianjun, S.; Ming, Z.; Jie, H. Synthesis of Magnetic Sonophotocatalyst and its Enhanced Biodegradability of Organophosphate Pesticide, *Bull. Korean Chem. Soc.* **2014**, *35*, 3521-3526.

(1014) Jyothi, K. P.; Yesodharan, S.; Yesodharan, E. P. Ultrasound (US), Ultraviolet light (UV) and combination (US + UV) assisted semiconductor catalysed degradation of organic pollutants in water: Oscillation in the concentration of hydrogen peroxide formed in situ, *Ultrason. Sonochem.* **2014**, *21*, 1787-1796.

(1015) Anju, S. G.; Yesodharan, S.; Yesodharan, E. P. Zinc oxide mediated sonophotocatalytic degradation of phenol in water, *Chem. Eng. J.* **2012**, *189-190*, 84- 93.

(1016) Talebian, N.; Nilforoushan, M. R.; Mogaddas, F. J. Comparative study on the sonophotocatalytic degradation of hazardous waste, *Ceram. Int.* **2013**, *39*, 4913-4921.

(1017) Yan, Z.; Zhang, L.; Zhao, Z.; Qi, H.; Li, Y.; Cang, D. *Enhanced antimicrobial activity of ZnO nanofluids in sonophotocatalysis and its mechanism, Ultrason. Sonochem* **2018**, *47*, 133-140.

(1018) Ahmad, M.; Ahmed, E.; Hong, Z. L.; Ahmed, W.; Elhissi, A.; Khalid, N. R. Photocatalytic, sonocatalytic and sonophotocatalytic degradation of Rhodamine B using ZnO/CNTs composites photocatalysts, *Ultrason. Sonochem.* **2014**, *21*, 761-773.

(1019) Rahman, P. H.; Misra, A. J.; Panda, S.; Das, B.; Bhol, P.; Mohanty, P. S.; Tamhankar, A. J.; Mishra, A.; Lundborge, C. S.; Tripathy, S. K. Sonophotocatalysis-mediated

morphological transition modulates virulence and antibiotic resistance in Salmonella Typhimurium, *Environ. Sci.-Water Res. Technol.* **2020**, *6*, 1917-1930.

(1020) Habeeb Rahman, A. P.; Misra, A. J.; Das, S.; Das, B.; Jayabalan, R.; Suar, M.; Mishra, A.; Tamhankar, A. J.; Lundborg, C. S.; Tripathy, S. K. Mechanistic insight into the disinfection of Salmonella sp. by sun-light assisted sonophotocatalysis using doped ZnO nanoparticles, *Chem. Eng. J.* **2018**, *336*, 476-488.

(1021) Misra, A. J.; Das, S.; Habeeb Rahman, A. P.; Das, B.; Jayabalan, R.; Behera, S. K.; Suar, M.; Tamhankar, A. J.; Mishra, A.; Lundborg, C. S.; Tripathy, S. K. Doped ZnO nanoparticles impregnated on Kaolinite (Clay): A reusable nanocomposite for photocatalytic disinfection of multidrug resistant Enterobacter sp. under visible light, *J. Colloid Interface Sci.* **2018**, *530*, 610-623.

(1022) Dinesh, G. K.; Anandan, S.; Sivasankar, T. Synthesis of Fe/ZnO composite nanocatalyst and its sonophotocatalytic activity on acid yellow 23 dye and real textile effluent, *Clean Techn. Environ. Policy* **2016**, *18*, 1889-1903.

(1023) Khataee, A.; Soltani, R. D. C.; Karimi, A.; Joo, S. W. Sonocatalytic degradation of a textile dye over Gd-doped ZnO nanoparticles synthesized through sonochemical process, *Ultrason. Sonochem.* **2015**, *23*, 219-230.

(1024) Khataee, A.; Karimi, A.; Oskoui, S. A.; Soltani, R. D. C.; Hanifehpour, Y.; Soltani, B.; Joo, S. W. Sonochemical synthesis of Pr-doped ZnO nanoparticles for sonocatalytic degradation of Acid Red 17, *Ultrason. Sonochem.* **2015**, *22*, 371-381.

(1025) Saharan, P.; Chaudhary, G. R.; Lata, S.; Mehta, S. K.; Mor, S. Ultra fast and effective treatment of dyes from water with the synergistic effect of Ni doped ZnO nanoparticles and Ultrasonication, *Ultrason. Sonochem.* **2015**, *22*, 317-325.

(1026) Khitab, F.; Jan, M. R.; Shah, J. Removal of hazardous textile dyes from water using Ni impregnated ZnO through sonophotocatalytic degradation, *Desalin. Water Treat.* **2020**, *205*, 357-372.

(1027) Sharma, S.; Dutta, V.; Singh, P.; Raizada, P.; Rahmani-Sani, A.; Hosseini-Bandegharaei, A.; Thakur, V. K. Carbon quantum dot supported semiconductor photocatalysts for efficient degradation of organic pollutants in water: A review, *Journal of Cleaner Production* **2019**, *228*, 755-769.

(1028) Bokhale, N. B.; Bomble, S. D.; Dalbhanjan, R. R.; Mahale, D. D.; Hinge, S. P.; Banerjee, B. S.; Mohod, A. V.; Gogate, P. R. Sonocatalytic and sonophotocatalytic degradation of rhodamine 6G containing wastewaters, *Ultrason. Sonochem.* **2014**, *21*, 1797-1804.

(1029) Ayare, S. D.; Gogate, P. R. Sonophotocatalytic oxidation based treatment of phthalocyanine pigment containing industrial wastewater intensified using oxidising agents, *Sep. Purif. Technol.* **2020**, *233*, 115979.

(1030) Ghanbari, F.; Ahmadi, M.; Gohari, F. Heterogeneous activation of peroxymono-sulfate via nanocomposite CeO_2-Fe_3O_4 for organic pollutants removal: the effect of UV and US irradiation and application for real wastewater, *Sep. Purif. Technol.* **2019**, *228*, 115732

(1031) Dinesh, G. K.; Anandan, S.; Sivasankar, T. Synthesis of Fe-doped Bi_2O_3 nanocatalyst and its sonophotocatalytic activity on synthetic dye and real textile wastewater, *Environ. Sci. Pollut. Res.* **2016**, *23*, 20100-20110.

(1032) Theerthagiri, J.; Lee, S. J.; Karuppasamy, K.; Arulmani, S.; Ashokkumar, M.; Choi, M. Y. Application of advanced materials in sonophotocatalytic processes for the remediation of environmental pollutants, *J. Hazard. Mater.* **2021**, *412*, 125245.

(1033) Bazgir, A.; Khorshidi, A.; Kamani, H.; Asharafi, A. D.; Naghipour, D. Modeling of azo dyes adsorption on magnetic NiFe2O4/RGO nanocomposite using response surface methodology, *J. Environ. Health. Sci. Engineer.* **2019**, *17*, 931-947.

(1034) Hasan, I.; Bassi, A.; Alharbi, K. H.; BinSharfan, I. I.; Khan, R. A.; Alslame, A. Sonophotocatalytic Degradation of Malachite Green by Nanocrystalline Chitosan-Ascorbic Acid@$NiFe_2O_4$ Spinel Ferrite, *Coatings* **2020**, *10*, 1200.

(1035) Zeng, L.; Li, S.; Li, X.; Li, J.; Fan, S.; Chen, X.; Yin, Z.; Tadé, M.; Liu, S. Visible-light-driven Sonophotocatalysis and Peroxymonosulfate Activation over 3D Urchin-like MoS2/C Nanoparticles for Accelerating Levofloxacin Elimination: Optimization and Kinetic Study, *Chem. Eng. J.* **2019**, *378*, 122039.

(1036) Vidya Lekshmi, K. P.; Yesodharan, S.; Yesodharan, E. P. MnO_2 efficiently removes indigo carmine dyes from polluted water, Heliyon, **2018**, *4*, e00897.

(1037) Song, L.; Zhang, S.; Wu, X.; Zhang, S.; Tian, H.; Ye, J. Preparation, characterization and sonodegradation properties of silver tyipolyphosphate catalyst, *Catal. Commun.* **2013**, *30*, 27-31.

(1038) He, P.; Song, L.; Wu, X.; Tian, H.; Wei, Q.; Ye, J.; Zhang, L.; Cui, Y.; Wang, Y. Fabrication and sonocatalytic property of AgPO3 microsphere, *Ultrason. Sonochem.* **2014**, *21*, 136-141.

(1039) De-Nasri, S.; Nagarajan, S.; Robertson, P. K. J.; Ranade, V. V. Cavitation and immobilised photo-catalysis for effluent treatment: A comparative study of individual and combined operations, *Environmental Division - Core Programming Area at the 2018 AIChE Annual Meeting, Pittsburg, PA, USA* **2018**, 2-4.

(1040) Cui, P.; Chen, Y.; Chen, G. Degradation of Low Concentration Methyl Orange in Aqueous Solution through Sonophotocatalysis with Simultaneous Recovery of Photocatalyst by Ceramic Membrane Microfiltration, *Ind. Eng. Chem. Res.* **2011**, *50*, 3947-3954.

(1041) Cheng, Z.; Quan, X.; Xiong, Y.; Yang, L.; Huang, Y. Synergistic degradation of methyl orange in an ultrasound intensified photocatalytic reactor, *Ultrason. Sonochem.* **2012**, *19*, 1027-1032.

(1042) Dacquin, J. P.; Granger, P.; Zaki, A.; Casale, S.; Mussi, A.; Dhenin, J. F.; Lancelot, C. Nano-engineered hierarchical porous silicas for enhanced catalytic efficiency in liquid phase, *Catal. Sci. Technol.* **2018**, *8*, 4604-4608.

(1043) Spivey, J. J.; Krishna, K. S.; Kumar, C. S. S. R.; Dooley, K. M.; Flake, J. C.; Haber, L. H.; Xu, Y.; Janik, M. J.; Sinnott, S. B.; Cheng, Y.-T.; Liang, T.; Sholl, D. S.; Manz, T. A.; Diebold, U.; Parkinson, G. S.; Bruce, D. A.; de Jongh, P. Synthesis, characterization, and computation of catalysts at the center for atomic-level catalyst design, *J. Phys. Chem. C* **2014**, *118*, 20043-20069.

(1044) Adam, G.; Isanullah, I.; Naushad, M.; Sillanpää, M. Application of artificial intelligence in water treatment for optimization and automation of adsorption processes: Recent advance and prospect, *Chem. Eng. J.* **2002**, *427*, 130011.

(1045) Siedhoff, N. E.; Schwaneberg, U.; Davari, M. D. *Machine learning-assisted enzyme engineering, Methods in Enzymology* **2020**, *643*, 281-315.

(1046) Ali, Y.; Shreemali, J.; Chakrabarti, T.; Chakrabarti, P.; Poddar, S. Prediction of reaction parameters on reaction kinetics for treatment of industrial wastewater: A machine learning perspective, *Mater. Today : Proceeding* **2020** https://doi.org/10.1016/j.matpr.2020.1009.1702.

(1047) Zhou, T.; Song, Z.; Sundmacher, K. Big Data Creates New Opportunities for Materials Research: A Review onMethods and Applications of Machine Learning for Materials Design, *Engineering* **2019**, *5*, 1017-1026.

(1048) Li, Z.; Ma, X.; H., X. Feature engineering of machine-learning chemisorptionmodels for catalyst design, *Catal. Today* **2017**, *280*, 232-238.

(1049) Fernandez, M.; Barron, H.; Barnard, A. S. Artificial neural network analysis of the catalytic efficiency of platinum nanoparticles, *RSC Adv.* **2017**, *2*, 48962-48971.

(1050) Janet, J. P.; Kulik, H. J. Predicting electronic structure properties of transition metal complexes with neural networks, *Chem. Sci.* **2017**, *8*, 5137-5152.

(1051) Emery, A. A.; Saal, J. E.; Kirklin, S.; Hegde, V. I.; Wolverton, C. High-Throughput Computational Screening of Perovskites for Thermochemical Water Splitting Applications, *Chem. Mater.* **2016**, *28*, 5621−5634.

(1052) Can, E.; Yildirim, R. Data mining in photocatalytic water splitting over perovskites literature for higher hydrogen production, *Appl. Catal. B* **2019**, *242*, 267-283.

(1053) Guda, A. A.; Guda, S. A.; Lomachenko, K. A.; Soldatov, M. A.; Pankin, I. A.; Soladatov, A. V.; Braglia, L.; Bugaev, A. L.; Martini, A.; Signorile, M.; Groppo, E.; Piovano, A.; Borfecchia, E.; Lamberti, C. Quantitative structural determination of active sites from in situ and operando XANES spectra: from standard ab ignition to chemometric and machine learning approaches, *Catal. Today* **2019**, *336*, 3-21.

(1054) Saleheen, M.; Heyden, A. Liquid-Phase modelling in heterogeneous catalysis, *ACS Catal.* **2018**, *8*, 2188-2194.

(1055) Zhang, J.; Zhang, H.; Wu, T.; Wang, Q.; van der Spoe, D. Comparison of Implicit and Explicit Solvent Models for the Calculation of Solvation Free Energy in Organic Solvents, *J. Chem. Theory Comput.* **2017**, *13*, 1034−1043.

(1056) Im, W.; Roux, B. Brownian dynamics simulations of ions channels: A general treatment of electrostatic reaction fields for molecular pores of arbitrary geometry, *J. Phys. Chem.* **2001**, *115*, 4850-4861.

(1057) Taylor, C. D.; Neurock, M. Theoretical insights into the structure and reactivity of the aqueous/metal interface, *Curr. Opin. Solid State Mater. Sci.* **2005**, *9*, 49-65.

(1058) Fogarty, J. C.; Aktulga, H. M.; Grama, A. Y.; van Diun, A. C. T.; Pandit, S. A. A reactive molecular dynamics simulation of the silica-water interface, *J. Phys. Chem.* **2010**, *132*, 174704.

(1059) Svensson, M.; Humbel, S.; Froese, R. D. J.; Matsubara, T.; Sieber, S.; Morokuma, K. ONIOM: A Multilayered Integrated MO + MM Method for Geometry Optimizations and Single Point Energy Predictions. A Test for Diels−Alder Reactions and Pt(P(t-Bu)3)2 + H2 Oxidative Addition, *J. Phys. Chem.* **1996**, *100*, 19357-19363.

(1060) Siahrostami, S.; Vojvodic, A. Influence of Adsorbed Water on the Oxygen Evolution Reaction on Oxides, *J. Phys. Chem. C* **2015**, *119*, 1032-1037.

(1061) Zhang, X.; Sewell, T. E.; Glatz, B.; Sarupri, S.; Getman, R. On the water structure at hydrophobic interfaces and the roles of water on transitient-metal catalyzed reactions: a short review, *Catal. Today* **2017**, *285*, 57-64.

(1062) Schweitzer, B.; Steinman, S. N.; C., M. Can microsolvation effects be estimated from vacuum computations? A case-study of alcohol decomposition the H2O/Pt(111) interface, *Phys. Chem. Chem. Phys.* **2019**, *21*, 5368-5377.

(1063) Réocreux, R.; Michel, C. Rational design of heterogeneous catalysts for biomass conversion - Inputs from computational chemistry, *Curr. Opinion Green Sustain. Chem.* **2018**, *10*, 51-59.

(1064) Skachkov, D.; Rao, C. V.; Ishikawa, Y. Combined first principles molecular dynamics/density functional theory study of ammonia electrooxidation on Pt(100) electrode, *J. Phys. Chem. C* **2013**, *177*, 25451-25466.

(1065) Lin, X.; Grob, A. First-principle study of the water structure on flat and stepped gold surface, *Surf. Sci.* **2012**, *606*, 886-891.

(1066) Feibelman, P. J. Partial dissociation of water on Ru(0001), *Science* **2002**, *295*, 99-102.

(1067) Michaelides, A.; Hu, P. A density functional theory study of hydroxyl and the intemediate in the water formation on Pt., *J. Chem. Phys.* **2001**, *114*, 513-519.

(1068) Steinmann, S. N.; De Morais, R. F.; Götz, A. W.; Fleurat-Lessard, P.; Iannuzzi, M.; Sautet, P.; Michel, C. Force field for water over Pt(111): development, assessment, and comparison, *J. Chem. Theory Comput.* **2018**, *14*, 3238-3251.

(1069) Clabaut, P.; Fleurat-Lessard, P.; Michel, C.; Steinmann, S. N. Ten facets, one force field: the GAL 19 force field for water-noble metal interfaces, *J. Chem. Theory Comput.* **2020**, *16*, 4565-4578.

(1070) Sun, C.; Liu, L.-M.; Lu, G. Q.; Smith, S. C. Titania-water interactions : a review of theoretical studies, *J. Mater. Chem.* **2010**, *20*, 10319.

(1071) Patel, A. J.; Varilly, P.; Chandler, D. Fluctuations of water near extended hydrophobic and hydrophilic surfaces, *J. Phys. Chem. B* **2010**, *114*, 1632-1637.

(1072) Jiang, P.; Chen, J.-L.; Borondics, F.; Glans, P.-A.; West, M. W.; Chang, C.-L.; Salmeron, M.; Guo, J. In situ soft X-ray absorption spectroscopy investigation of electrochemical corrosion of copper in aqueous $NaHCO_3$ solution, *Electrochem. Commun.* **2010**, *12*, 820-822.

(1073) Escudero, C.; Salmeron, M. From solid-vacuum to solid-gas and solid-liquid interfaces : in situ studies of structure and dynamics under relevant conditions, *Surf. Sci.* **2013**, *607*, 2-9.

(1074) Liu, H.; Guo, J.; Yin, Y.; Augustsson, A.; Dong, C.; Nordgren, J.; Chang, C.; Alivisatos, P.; Thornton, G.; Ogletree, D. F.; Requejo, F. G.; de Groot, F.; Salmeron, M. Electronic Structure of CobaltNanocrystals Suspended in Liquid, *Nano Lett.* **2007**, *7*, 1919-1922.

(1075) Liu, J. X.; Richards, D.; Singh, N.; Goldsmith, B. R. Activity and selectivity trends in electrocatalytic nitrate reduction on transition metals, *ACS Catal.* **2019**, *9*, 7052-7064.

(1076) He, S.; Zhai, C.; Fujitsuka, M.; Kim , S.; Zhu, M.; Yin, R.; Zeng, L.; Majima, T. Femtosecond time-resolved diffuse reflectance study on facet engineered charge-carrier dynamics in Ag3PO4 for antibiotics photodegradation, *Appl. Catal. B* **2021**, *281*, 119479.

(1077) Zheng, B.; Wang, X.; Liu, C.; Tan, K.; Xie, Z.; Zheng, L. High-efficiency visible light responsive photocatalysts : Ag3PO4 tetrahedral microcrystals with exposed (111) facets of high surface energy, *J. Mater. Chem. A* **2013**, *1*, 12635-12640.

(1078) Hsieh, M. S.; Su, H. J.; Hsieh, P. L.; Chiang, Y. W.; Huang, M. H. Synthesis of Ag3PO4 crystal with tunable shapes for facet-dependent optical property, photocatalytic, and electrical conductivity examinations, *ACS Appl. Mater. Interface* **2017**, *9*, 39086-39093.

(1079) Salmeron, M.; Schlögl, R. Ambient pressure photoelectron spectroscopy: A new tool for surfacescience and nanotechnology, *Surf. Sci. Rep.* **2008**, *63*, 169-199.

(1080) Ketteler, G.; Yamamoto, S.; Bluhm, H.; Andersson, K.; Starr, D. E.; Ogletree, D. F.; Ogasawara, H.; Nilsson, A.; Salmeron, M. Polarization-resolved broad-bandwidth sum-frequency generation spectroscopy of monolayer relaxation, *J. Phys. Chem. C* **2007**, *111*, 8278-8282.

(1081) Verdaguer, A.; Weis, C.; Oncins, G.; Ketteler, G.; Bluhm, H.; Salmeron, M. Growth and structure of water on SiO2 films on Si investigated by Kelvin probe microscopy and in situ X-ray spectroscopies, *Langmuir* **2007**, *23*, 9699-9703.

(1082) Zhang, C.; Grass, M. E.; Yu, Y.; Gaskell, K. J.; DeCaluwe, S. C.; Chang, R.; Jackson, G. S.; Hussain, Z.; Bluuhm, H.; Eichhorn, B. W.; Liu, Z. Multielement activity mapping and potential mapping in solid oxide electrochemical cells through the use of operando XPS, *ACS Catal.* **2012**, *2*, 2297-2304.

(1083) Russell, A. E.; Rose, A. X-ray Absorption Spectroscopy of Low Temperature Fuel Cell Catalysts, *Chem. Rev.* **2004**, *104*, 4613-4635.

(1084) McBreen, J.; Ogrady, W. E.; Tourillon, G.; Dartyge, E.; Fontaine, A. XANES study of underpotential deposited copper on carbon-supported platinum, *J. Electroanal. Chem.* **1991**, *307*, 229-240.

(1085) Kowal, A.; Li, M.; Shao, M.; Sasaki, K.; Vukmirovic, M. B.; Zhang, J.; Marinkovic, N. S.; Liu, P.; Frenkel, A. I.; Adzic, R. R. Ternary Pt/Rh/SnO$_2$ electrocatalysts for oxidizing ethanol to CO$_2$, *Nat. Mater.* **2009**, *8*, 325-330.

(1086) Merte, L. R.; Behafarid, F.; Miller, D. J.; Friebel, D.; Cho, S.; Mbuga, F.; Sokaras, D.; Alonso-Mori, R.; Weng, T.-C.; Nordlund, D.; Nilsson, A.; Roldan Cuenya, B. E. lectrochemical oxidation of size-selcted Pt nanoparticles studied unsing high-energy-resolution X-ray absorption spectroscopy, *ACS Catal.* **2012**, *2*, 2371-2376.

(1087) Tupy, S. A.; Karim, A. M.; Bagia, C.; Deng, W.; Huang, Y.; Vlachos, D. G.; Chen, J. G. Correlation ethylene glycol reforming activity with in situ EXAFS detection of Ni segregation in supported NiPt bimetallic catalysts, *ACS Catal.* **2012**, *2*, 2290-2296.

(1088) Jiang, P.; Chen, J.-L.; Borondics, F.; Glans, P. A.; West, M. W.; Chang, C. L.; Salmeron, M.; Guo, J. In situ soft X-ray absorption spectroscopy investigation of electrochemical corrosion of copper in aqueous NaHCO3 solution, *Electrochem. Comm.* **2010**, *12*, 820-822.

(1089) Rasmussen, S. B.; Portela, R.; Bazin, P.; Avila, P.; Bañares, M. A.; Daturi, M. Transient operando study on the NH_3/NH^{4+} interplay in V-SCR monolithic catalysts, *Appl. Catal. B 2018* **2018**, 109-115.

(1090) Bruijn, J. R.; van der Loop, T. H.; Woutersen, S. Changing hydrogen bon structure during an aqueous liquid-lisuid transition investigated with time-resolved and two-dimensional vibrational spectrocopy, *J. Phys. Lett.* **2016**, *7*, 795-799.

(1091) Haselmann, G. M.; Baumgartner, B.; Wang, J.; Wieland, K.; Gupta, T.; Herzig, C.; Limbeck, A.; Lendl, B.; Eder, D. In situ photodeposition and methanol photooxidation on Pt/TiO2 : Pt-loadingdependent photocatalytic reaction pathways studied by liquid-phase infrared spectroscopy, *ACS Catal.* **2020**, *10*, 2964-2977.

(1092) Pichat, P. Representative examples of infrared spectroscopy uses in semiconductor photocatalysis, *Catal. Today* **2014**, *224*, 251-257.

(1093) Martin, D. J.; Umezawa, N.; Chen, X.; Ye, J.; Tang, J. Facet engineered Ag3PO4 for efficient water oxidation, *Energy Env. Sci.* **2013**, *6*, 3380-3386.

(1094) Duan, X.; Sun, H.; Shao, Z.; Wang, S. Nonradical reactions in environmental remediation processes: Uncertainty and challenges, *Appl. Catal. B* **2018**, *224*, 973-982.

(1095) Nawrocki, J. Catalytic ozonation in water : controversies and questions. discussion paper, *Appl. Catal. B* **2013**, *142-143*, 465-471.

(1096) Nawrocki, J.; Kasprzyk-Horden, B. The efficiency and mechanisms of catalytic ozonation, *Appl. Catal. B* **2010**, *99*, 27-42.